Russian-German Cooperation SYSTEM LAPTEV SEA
The Expedition LENA 2002

Edited by
Mikhail N. Grigoriev, Volker Rachold, Dmitry Yu. Bolshiyanov,
Eva-Maria Pfeiffer, Lutz Schirrmeister, Dirk Wagner
and Hans-Wolfgang Hubberten

Ber. Polarforsch. Meeresforsch. 466 (2003)
ISSN 1618 - 3193

Mikhail N. Grigoriev, Permafrost Institute, Russian Academy of Sciences
677018 Yakutsk, Yakutia, Russia

Volker Rachold, Lutz Schirrmeister, Dirk Wagner and Hans-Wolfgang Hubberten, Alfred-Wegener-Institute for Polar and Marine Research, Research Department Potsdam, PO Box 60 01 49, D-14401 Potsdam, Germany

Dmitry Yu. Bolshiyanov, Arctic and Antarctic Research Institute (AARI), Bering St. 38, 199397 St. Petersburg, Russia

Eva-Maria Pfeiffer, Institute for Soil Science, Hamburg University, Allende-Platz 2, D-20146 Hamburg, Germany

Russian-German Cooperation SYSTEM LAPTEV SEA:

The Expedition LENA 2002

by the participants of the expedition

edited by Mikhail N. Grigoriev, Volker Rachold, Dmitry Yu. Bolshiyanov, Eva-Maria Pfeiffer, Lutz Schirrmeister, Dirk Wagner and Hans-Wolfgang Hubberten

Contents

1 Introduction

Volker Rachold and Mikhail N. Grigoriev

Our knowledge of the Arctic climate system has been significantly improved through multi-disciplinary investigations carried out in the Siberian Arctic during previous Russian-German projects, such as THE LAPTEV SEA SYSTEM (1994-1997), TAYMYR (1994-1997) and LAPTEV SEA 2000 (1998-2001). The results have been presented in two collections of papers published by Kassens et al. (1999) and Rachold (2002) and in numerous other articles.

Detailed climatic reconstructions of the late Quaternary and important information concerning the complex modern system were obtained and form the basis for the prediction of future climate changes. The investigations documented that the closely coupled land-ocean system of the Laptev Sea with the East Siberian hinterland and its complex connections, such as the Lena Delta, represent a key region for understanding environmental changes. Our present knowledge indicates that environmental changes in this area not only affect the Arctic Ocean but also contribute to variations in the global system.

Within the framework of the project SYSTEM LAPTEV SEA 2000 terrestrial expeditions to the Lena Delta and the Laptev Sea coastal region were performed 1998 (Rachold and Grigoriev, 1999), 1999 (Rachold and Grigoriev, 2000), 2000 (Rachold and Grigoriev, 2001) and 2001 (Pfeiffer and Grigoriev 2002). Based on the experiences and results of these expeditions, the fifth expedition, LENA 2002, was carried out from June 23 to September 11, 2002. A multi-disciplinary, Russian-German team of 27 scientists worked in the Lena Delta, in the surroundings of the city of Tiksi and on the New Siberian Archipelago (Figure 1-1). The scientific program of the expedition focused on terrestrial and coastal research fields, i.e.:

A. Permafrost soils and ecosystems (☞ Chapter 3: *Ecological studies on permafrost soils and landscapes of the central Lena Delta*)

B. Recent periglacial environments (☞ *Chapter 4: Periglacial features around Tiksi*

C. Quaternary environmental changes based on the study of permafrost sequences (☞ *Chapter 5.2: Permafrost, periglacial and paleo-environmental studies on the New Siberian Islands*)

D. Arctic coastal dynamics (☞ *Chapter 5.3: Coastal studies on the New Siberian Islands*)

Acknowledgments

The success of the expedition LENA 2002 would have not been possible without the support by several Russian, Yakutian, and German institutions and authorities. In particular, we would like to express our appreciation to the Tiksi Hydrobase and the Lena Delta Reserve, special thanks to D. Melnichenko and

D. Gorokhov. The members of the expedition wish to thank the captains and crewmembers of the vessels "Pavel Bashmakov" and "Neptun" and the staff of the biological station Samoylov.

The coastal studies presented here are a direct contribution to Arctic Coastal Dynamics (ACD), which is a project of the International Arctic Science Committee (IASC), the International Permafrost Association (IPA) and IGBP-LOICZ. Additional financial support by INTAS (project numbers INTAS 2001-2329 and INTAS 2001-2332) is highly appreciated.

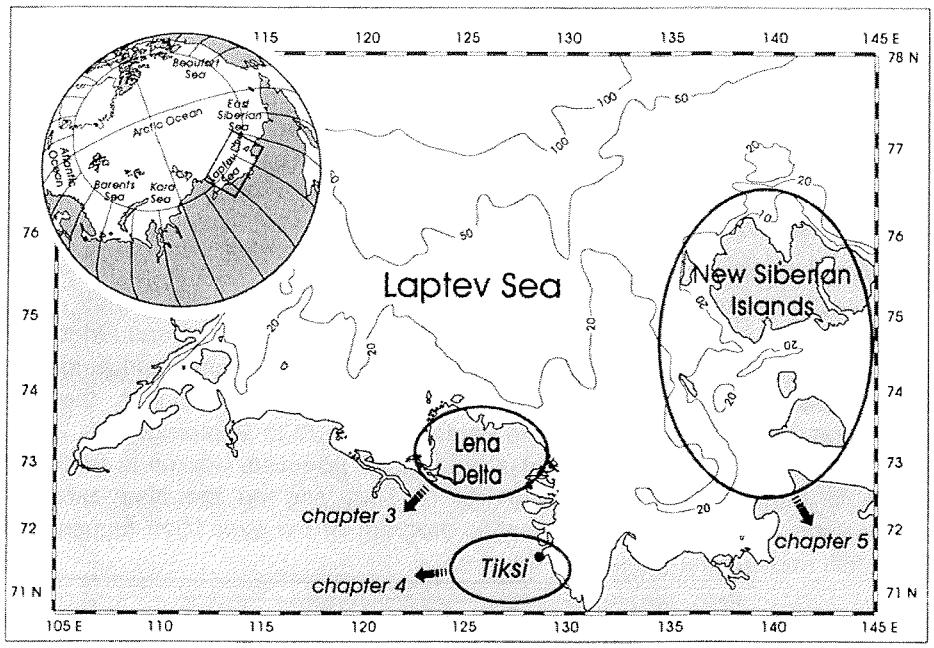

Figure 1-1: Map showing the location of the working area of the expedition LENA 2002.

References

Kassens, H., Bauch, H., Dmitrenko, I., Eicken, H., Hubberten, H.-W., Melles, M., Thiede, J. and Timokhov, L. (1999), Land-Ocean systems in the Siberian Arctic: dynamics and history. Springer, Berlin, 711pp.

Pfeiffer E.-M. and Grigoriev, M.N. (2002): Russian-German Cooperation SYSTEM LAPTEV SEA 2000: The Expedition LENA 2001. Reports on Polar and Marine Research 426.

Rachold, V. and Grigoriev, M.N. (1999): Russian-German Cooperation SYSTEM LAPTEV SEA 2000: The Lena Delta 1998 Expedition. Reports on Polar and Marine Research 316.

Rachold, V. and Grigoriev, M.N. (2000): Russian-German Cooperation SYSTEM LAPTEV SEA 2000: The Expedition Lena 1999 Expedition. Reports on Polar and Marine Research 354.

Rachold, V. and Grigoriev, M.N. (2001): Russian-German Cooperation SYSTEM LAPTEV SEA 2000: The Expedition LENA 2000. Reports on Polar and Marine Research 388.

Rachold, V.(2002): The modern and ancient terrestrial and coastal environment of the Laptev Sea region, Siberian Arctic - A preface, Polarforschung 70

2 Expedition itinerary and general logistics

Volker Rachold and Mikhail N. Grigoriev

With respect to the scientific program, the expedition group had been divided into three teams prior to the expedition. For each team specific working areas, shown in Figure 1-1, had been selected.

Team 1 was based on a biological station of the Lena Delta Reserve on the Island Samoylov in the central part of the Lena Delta. The team concentrated on modern processes of permafrost-affected soils, i. e. the balance of greenhouse gases (CH_4 and CO_2) and microbial process studies regarding the CH_4 cycle and carried out additional biological studies. Two sub-teams (team 1a: 26 June – 28 July and team 1b: 30 July – 7 September) with a total number of 16 participants worked on the island Samoylov.

☞ ***Chapter 3: Ecological studies on permafrost soils and landscapes of the central Lena Delta***

Team 2 concentrated on the investigation of periglacial features in the surroundings of the city of Tiksi. The team consisting of 4 participants was based in Tiksi from 30 July to 12 August.

☞ ***Chapter 4: Periglacial features around Tiksi***

Team 3 was based onboard the ice-going research vessel Pavel Bashmakov and combined the working groups concentrating on (1) Quaternary environmental changes based on the study of permafrost sequences and (2) Arctic coastal dynamics. From 14 August to 2 September the team comprising 14 participants visited several pre-selected locations along the coast of the New Siberian Archipelago.

☞ ***Chapter 5: Cruise to the New Siberian Islands onboard RV Pavel Bashmakov***

The general logistics of the LENA 2002 Expedition were jointly organized by the Permafrost Institute (Yakutsk), the Arctic and Antarctic Research Institute (St. Petersburg) and the Research Unit Potsdam of the Alfred Wegener Institute. Logistic operations in Tiksi (rent of busses, trucks, helicopters etc.) were organized by the Tiksi Hydrobase.

The list of participants and the addresses of the institutions involved are presented in Table 2.1 and Table 2.2.

Table 2-1. List of participants.

Name	email	Institution	Team
Ekatarina Abramova	abramova-katya@mail.ru	LDR	1a, 1b
Felix Are	fare@peterlink.ru	PSUMOC	3b
Dmitry Bolshiyanov	bolshiyanov@aari.nw.ru	AARI	3a
Alexander Derevyagin	dereviag@online.ru	MGU	2, 3a
Antje Eulenburg	eulenbur@awi-potsdam.de	AWI	3a, 3b
Irina Fyedorova	bolshiyanov@aari.nw.ru	AARI	1b
Mikhail Grigoriev	grigoriev@mpi.ysn.ru	PIY	1a, 3b
Guido Grosse	ggrosse@awi-potsdam.de	AWI	2, 3a
Hans-Wolfgang Hubberten	hubbert@awi-potsdam.de	AWI	3b
Svenja Kobabe	skobabe@awi-potsdam.de	AWI	1b
Victor Kunitsky	kunitsky@mpi.ysn.ru	PIY	2, 3a
Anna Kurtshatova	kurtshatova@mpi.ysn.ru	PIY	1a
Svetlana Kuzmina	skuz@orc.ru	SIEE	1b
Tatyana Kuznetsova	esin@sgm.ru	MGU	3a
Lars Kutzbach	lkutzbach@awi-potsdam.de	AWI	1a, 1b
Hanno Meyer	hmeyer@awi-potsdam.de	AWI	1b, 3a
Eva-Maria Pfeiffer	E.M.Pfeiffer@ifb.uni-hamburg.de	IFB	1a
Volker Rachold	vrachold@awi-potsdam.de	AWI	3b
Sergey Rasumov	rasumov@mpi.ysn.ru	PIY	3b
Lutz Schirrmeister	lschirrmeister@awi-potsdam.de	AWI	2, 3a
Waldemar Schneider	wschneider@awi-potsdam.de	AWI	1a, 3b
Oliver Spott	oliver_spott@yahoo.de	AWI	1a, 1b
Günter Stoof	gstoof@awi-potsdam.de	AWI	1a, 1b
Mikhail Tretiakov	tretiakov@aari.nw.ru	AARI	1b
Dirk Wagner	dwagner@awi-potsdam.de	AWI	1a
Sebastian Wetterich	swetterich@awi-potsdam.de	AWI	1b
Christian Wille	cwille@awi-potsdam.de	AWI	1a, 1b

Table 2-2. List of participating institutions.

AARI	Arctic and Antarctic Research Institute Bering St. 38, 199397 St. Petersburg, Russia
LDR	Lena Delta Reserve 28 Academician Fyodorov St., Tiksi 678400, Yakutia, Russia
MGU	Moscow State University, Faculty of Paleontology 119899 Moscow, Russia
PIY	Permafrost Institute, Russian Academy of Science 677018 Yakutsk, Yakutia, Russia
PSUMOC	St. Petersburg State University of Means of Communications 9 Moskovskii, 190031 St. Petersburg, Russia
SIEE	Severtsov Institute of Ecology and Evolution, Russian Academy of Sciences 33 Leninskiy Prospect, 117071 Moscow, Russia
AWI	Alfred Wegener Institute, Research Unit Potsdam PO Box 60 0149, D-14401 Potsdam, Germany
IFB	Institute for Soil Science, Hamburg University Allende-Platz 2, D-20146 Hamburg, Germany

3 Ecological studies on permafrost soils and landscapes of the central Lena Delta

Dirk Wagner, Lars Kutzbach, Christian Wille, Svenja Kobabe, Oliver Spott, Anna Kurchatova, Mikhail N. Grigoriev, Günther Stoof, Waldemar Schneider, Ekatarina N. Abramova, Hanno Meyer, Svetlana Kuzmina, Sebastian Wetterich, Dmitry Bolshiyanov, Irina Fedórova, Mikhail Tretiakov and Eva-Maria Pfeiffer

Wet tundra environments of the Arctic influence the global climate by the release of methane and other radiatively active trace gases into the atmosphere. Methane contributes to the enhanced greenhouse effect with a portion of approx. 20 % (Wuebbles and Hayhoe, 2002). The world-wide wetland area has a size of about 5.5 x 10^6 km^2 (Aselman and Crutzen, 1989), about half of it is located in high-latitudes of the northern hemisphere (> 50°N). The atmospheric input of methane from tundra soils of this region has been estimated between 20-40 Tg CH_4 yr^{-1} (Christensen et al. 1996), corresponding to about 25 % of the methane emission from natural sources (Fung et al. 1991). However, the strength of tundra environments as a methane source and the sensitivity of permafrost to potential changes in climate are still uncertain.

Approximately 14 % of the global carbon are stored in permafrost soils and sediments (Post et al., 1982). Due to this carbon pool, tundra environments play a major role in the global carbon cycle, even more since current climate models predict significant changes in temperature and precipitation patterns in these regions (Hansen et al., 1988; Kattenberg et al., 1996).

The interdisciplinary soil and microbiological studies are focused on the seasonal variability of the modern carbon fluxes (CH_4, CO_2), the quantification of microbial processes as well as the thermal and hydrological dynamics of permafrost affected soils of the Lena Delta.

During the fifth Lena Delta Expedition the investigations of the methane and carbon dioxide emission from different polygonal tundra sites and tundra lakes could be continued by closed chamber measurements. Furthermore, fluxes of methane, carbon dioxide, water vapour, sensible heat and momentum was analysed on the ecosystem scale by eddy covariance measurements for the first time. The microbial methane production and oxidation of permafrost soils was studied by additional field experiments. For further microbial ecological studies permafrost sediments of late Pleistocene age were drilled and transported in frozen conditions to Germany.

In addition to the investigation of the carbon dynamic, which pertain to an ongoing long-term study of trace gas fluxes from permafrost soils, research to the following topics were carried out during the expedition 2002: recent cryogenesis, botanical diversity, recent insects and freshwater ostracodes, paleo-climate and the hydrology of the central delta.

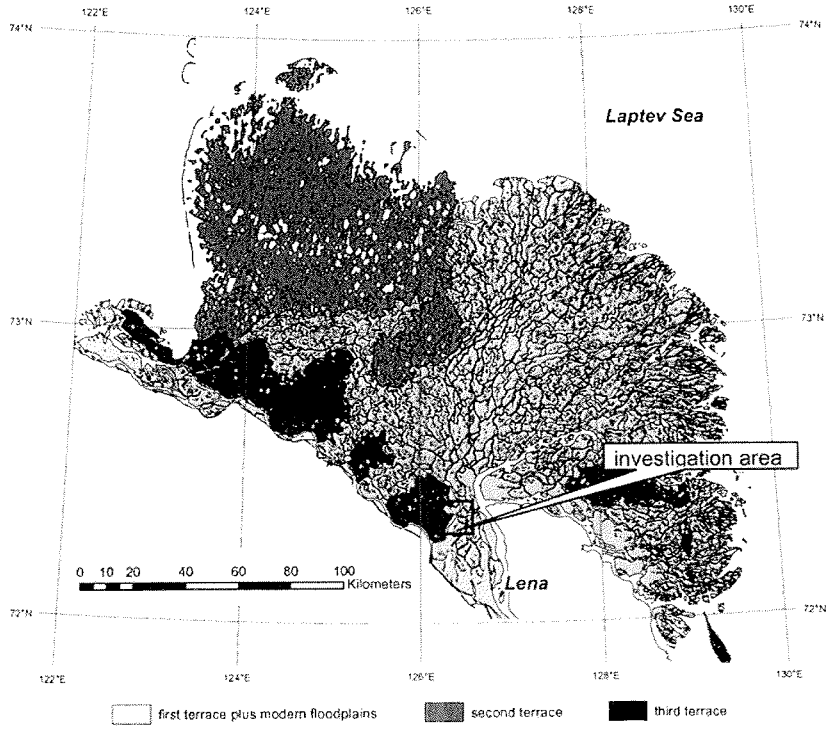

Figure 3-1. Map of the Lena Delta with location of the investigation area Samoylov / Kurungnakh. Geomorphological units are according to Grigoriev (1993).

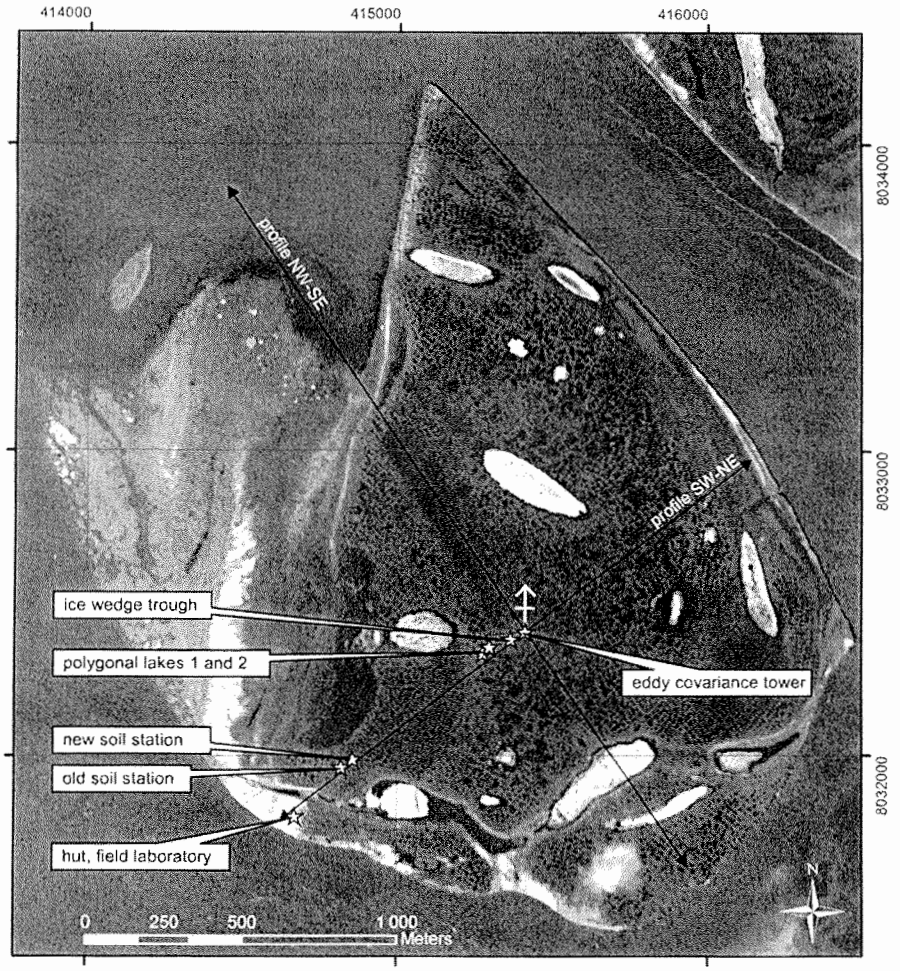

Figure 3-2. Site map Samoylov Island. – Positions of investigation sites, instruments, and geodetic elevation profiles. Coordinate system: UTM Zone 52N, WGS84. Satellite image: CORONA June 22, 1964.

3.1 Heat, water and carbon exchange between arctic tundra and the atmospheric boundary layer – the eddy covariance method

Lars Kutzbach, Christian Wille and Eva-Maria Pfeiffer

3.1.1 Introduction

An eddy covariance measurement system (ECS) was installed in June 2002 on Samoylov Island. The ECS was designed to determine simultaneously the turbulent fluxes of CH_4, CO_2, H_2O, sensible heat, and momentum that are representative on the ecosystem scale. The advantages of the eddy covariance technique are:

(1) It inherently averages the small-scale variability of fluxes over a surface area that increases with measurement height (ha to km^2, ecosystem scale).

(2) Measurements are continuous and in high temporal resolution (intervals of 15 to 30 min).

(3) Fluxes are determined without disturbing the surface being monitored.

(4) Fluxes of carbon, energy, and water are measured parallelly, by the same method, and in the same scale. Thus, a good basis for analysing interactions between the individual fluxes is provided.

Almost all vertical transport of air constituents in the atmospheric boundary layer happens by turbulence. The micrometeorological eddy covariance technique analyses the properties of turbulent moving air parcels - the eddies- to determine the vertical fluxes of air constituents, such as energy, water vapour, CO_2, or CH_4. The eddy flux F_c of any scalar quantity c is computed as the covariance of the density of the scalar quantity ρ_c and the vertical wind velocity w.

$$F_c = \overline{w' \rho_c'}$$

The primes indicate the fluctuation about the mean value, and the overbar represents the mean of the product over a sampling interval.

The spatially extended eddies are leaded past a stationary sensor by the mean horizontal wind u_{mean}. Thus, measurements at one point in space over a time period provide a spatially-integrated flux value, that is representative for a specific footprint area depending on sensor height and micrometeorological conditions.

Because the eddy covariance technique considers the very small fluctuations about the mean, it requires a high resolution of sensors (0.5 % of mean). To resolve the important small-scaled eddies adequately, the frequency response of the ECS has to be high (10 Hz).

3.1.2 Experimental set-up

The ECS tower was established in the centre of the terrace plain in the east part of Samoylov Island at 72°22.44' N, 126°29,80' E (UTM: Zone 52 415417E 8032409N, Figure 3-2). The Holocene river terrace is characterised by wet polygonal tundra with very poor drainage. The macrorelief of the terrace is level with slope gradients less than 0.2 % (Figure 3-3). Only at scarps along ancient river channels, abrupt elevation differences of up to 2.5 m are present. The surface of the terrace is structured by a regular microrelief with elevation differences of about 0.5 m (Figure 3-5), which is caused by the genesis of low-centred ice wedge polygons. The fetch of polygonal tundra, which is considered a homogenous landscape, extended at least 870 m in all directions from the tower, except for the sector from southwest to west. With a typical wind speed for the region of 5 m s^{-1}, more than 90 % of the measured flux originated within this footprint area.

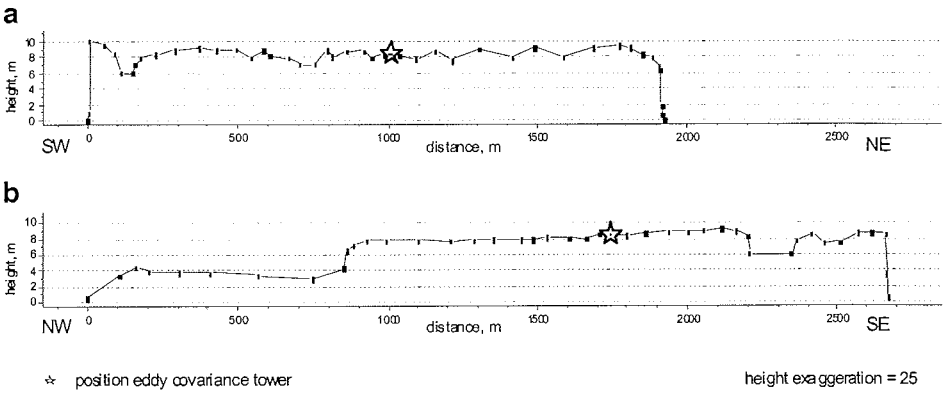

Figure 3-3. Relief of the island Samoylov and position of the eddy covariance tower. – a elevation profile from south-west to north-east, b elevation profile from north-west to south-east. Positions of profiles are shown in Figure 3-2.

To minimise perturbation, instruments were set up in a line to the southwest (Figure 3-4), which is the least frequent wind direction. Data gathered during periods with winds from southwest to west will be excluded from the flux analyses.

Parallelly to the ECS measurements, barometric pressure, air temperature, air humidity, radiation, and soil temperature (at two sites in a polygon adjacent to the ECS tower) were recorded automatically. Complementary meteorological data was provided by the automatic meteorological station on Samoylov Island (see Chapter 3.2).

In addition to the automatic measurements, active layer depth, water level depth, soil moisture, and soil temperature profiles were measured manually in intervals of 1 to 3 days at a transect of 14 soil survey sites. At three of these sites (S1, S2, S7), CH_4 emission was determined daily by a closed-chamber

technique for comparison between methods. For characterisation of the vegetation at the investigation site, the species composition was studied at 5 vegetation survey sites. The spatial arrangement of instruments, soil and vegetation survey sites, and elevation profiles is shown in Figure 3-4. A short characterisation of soil survey sites is given in Table 3-2.

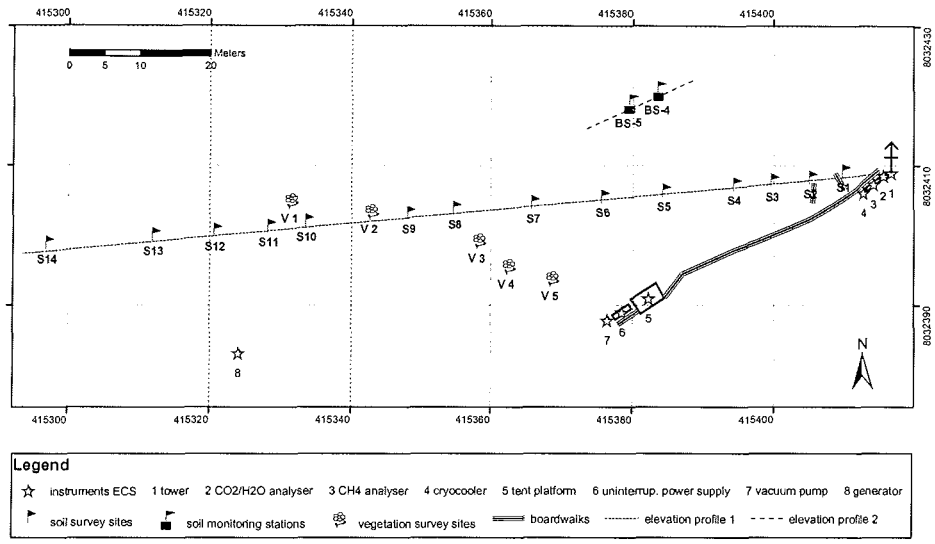

Figure 3-4. Site map eddy covariance measurement system. – Positions of instruments, soil survey sites, soil monitoring stations, vegetation survey sites, and elevation profiles. Coordinate system: UTM Zone 52N, WGS84.

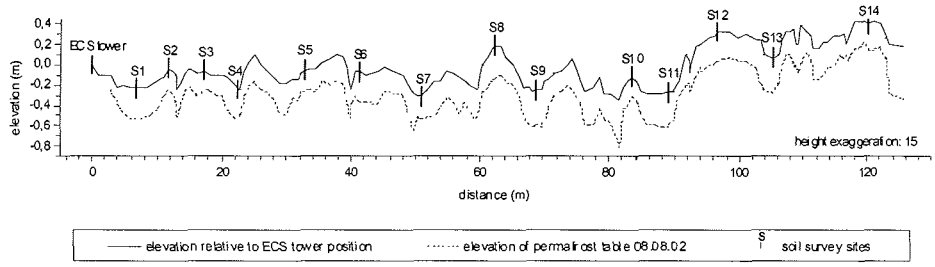

Figure 3-5. Elevation profile 1 with positions of soil survey sites S1 to S14. – The straight line indicates the soil surface, the dashed line indicates the permafrost table. Distances and elevations are measured relative to the soil surface position at the ECS tower.

The ECS was composed of commercially available instruments assembled according to our objectives (Fig. 3-6, Fig. 3-7). The technical set-up included a three-axis sonic anemometer, an infrared CO_2/H_2O analyser, and a CH_4 analyser based on tuneable laser infrared spectroscopy. Both gas analysers were closed-path instruments and were arranged in series in the sample gas line. Accuracy of concentration measurements was 20 ppm for H_2O, 0.3 ppm for CO_2, and 0.007 ppm for CH_4. The anemometer and the sample air intake were mounted on a 3.6 m high tower while the gas analysers were installed at the base of the tower. Sample air was drawn through the system by a vacuum pump with a flow rate of 19 slpm. Various filters and needle valves provided a pressure drop inside the system. Pressure was 820...850 hPa inside the CO_2/H_2O analyser and 75 hPa inside the CH_4 analyser. All signals were digitised at 10 Hz by the anemometer. Data were logged and processed by the software EdiSol running on a portable PC. Autonomous and continuous operation was ensured by a generator and an uninterruptible power supply. Further information on instruments is given in Table 3-1.

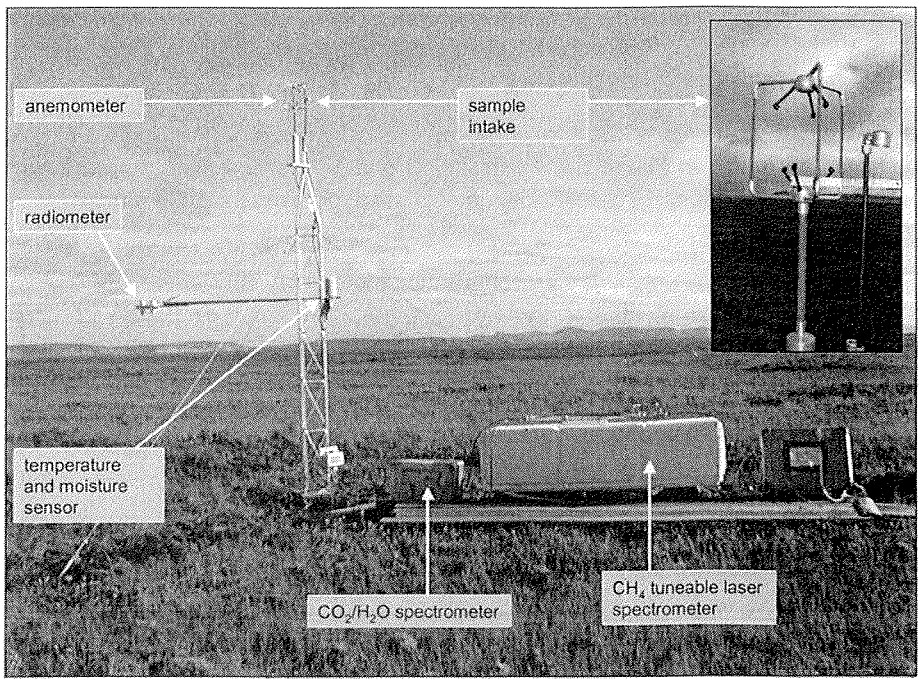

Figure 3-6. Photograph of the ECS in the field.

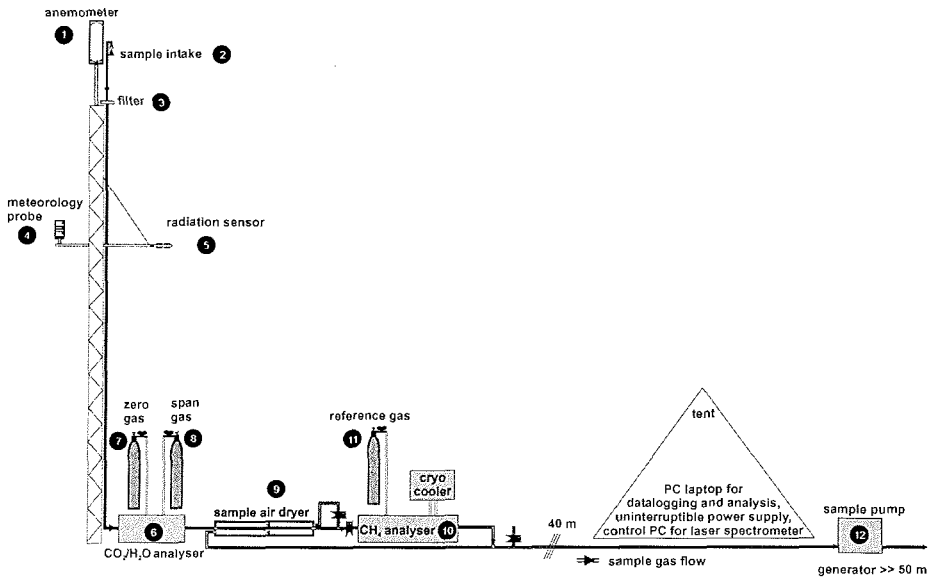

Figure 3-7. Technical set-up of the ECS.

Table 3-1. Components of ECS and related measurements. – Positions 1-12 are numbered according to Figure 3-7. Positions 13 and 14: sensors used for automatic measurements; positions 15 and 16: instruments used for manual measurements.

Pos.	Sensor Type
1	Gill Instruments Ltd., Ultrasonic anemometer 1210 R3
2	PE tubing 3/8" OD 1/4" ID
3	Schleicher & Schuell, Membranfilter 1µm TE 37
4	Rotronic Meßgeräte GmbH, Meteorological probe for humidity and temperature MP103A
5	Kipp & Zonen B.V., Net radiometer CNR 1
6	LI-COR LI-7000, Differential infrared CO_2/H_2O analyzer
7	Zero gas: pure N_2
8	Span gas: 480ppm CO_2 in N_2
9	Perma Pure Inc., Gas dryer PD-200T-48 SS
10	Campbell Scientific Inc., Tunable diode laser CH_4 analyzer TGA100
11	Reference gas: 0.5% CH_4 in N_2
12	Busch Inc., Rotary vacuum pump RB0021
13	Druck Messtechnik GmbH, Barometric pressure sensor RPT 410
14	Campbell Scientific Ltd., Thermistor soil temperature probe 107
15	UIT GmbH Dresden, Soil temperature probe ET, Pt 1000
16	Delta-T Devices Ltd., Moisture meter HH2, soil moisture probe ML2, profile soil moisture probe PR1

Table 3-2. Characterisation of soil survey sites adjacent to the ECS.

ID	soil material	soil type	situation in microrelief
S1	complete profile peat	*Typic Fibristel*	polygon centre, wet, swampy
S2	0...11 cm peat; 11...16 cm Sl3; 16...28 cm Slu	*Typic Aquiturbel*	polygon rim, relatively flat, not much elevated
S3	0...6 cm peat; 6...13 cm Sl3; 13...25 cm Slu	*Typic Aquiturbel*	polygon centre, degraded polygon, moist
S4	complete profile peat	*Typic Glacistel*	polygon crack, swampy, vegetated, about 0.6m wide
S5	0...11 cm peat; 11...26 cm Slu	*Typic Aquiturbel*	polygon rim, flat, polygon strongly degraded, drained
S6	0...9 cm peat; 9...15 cm Sl3; 15...36 cm Slu...Lu	*Typic Aquiturbel*	slope of raised polygon rim, direction crack
S7	complete profile peat	*Typic Glacistel*	polygon crack, 1m wide, swampy, vegetated
S8	0..6 cm peat; 6...19 cm Slu; 19...41 cm Lu	*Typic Aquiturbel*	polygon rim, strongly raised, dry
S9	complete profile peat	*Typic Fibristel*	polygon centre, wet, swampy
S10	0...11 cm peat; 11...25 cm Slu	*Typic Aquiturbel*	polygon rim, relatively flat, not much raised
S11	complete profile peat	*Typic Fibristel*	polygon centre, wet, swampy
S12	0...7 cm peat; 7...15 cm Slu; 15...35 cm Lu	*Typic Aquiturbel*	polygon rim, strongly raised
S13	complete profile peat	*Typic Fibristel*	polygon centre, wet, swampy
S14	0...5 cm peat; 5...14 cm Sl3; 14...23 cm Lu; 23...30 cm Lu	*Typic Aquiturbel*	polygon rim, strongly raised, dry

3.1.3 First Results

Some exemplary datasets of the eddy covariance flux calculations and the supporting soil and meteorological measurements are shown in Figure 3-9 and Figure 3-8, respectively.

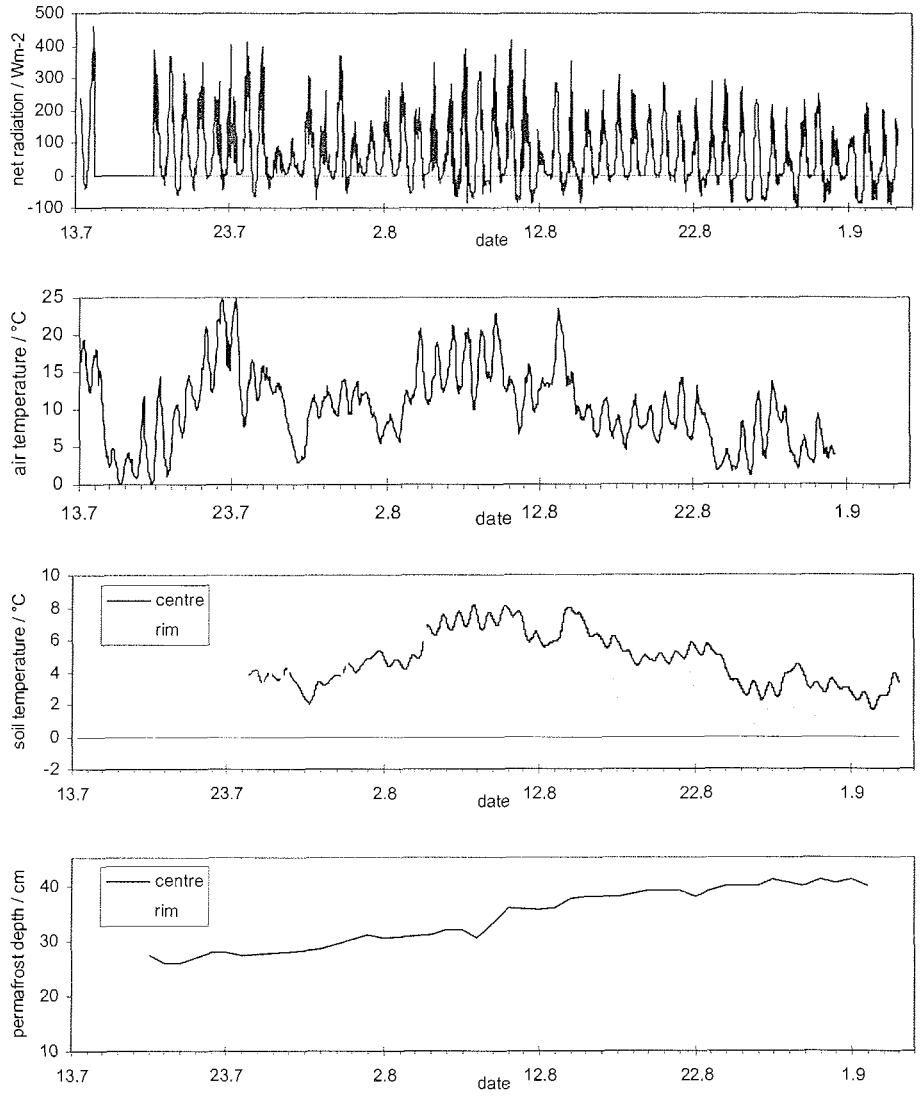

Figure 3-8. Results of ECS supporting measurements. – From top to bottom: net radiation, air temperature 0.5 m above ground (data from meteorological station), soil temperature at 10 cm below surface and depth of the permafrost table. Soil temperature and permafrost depth were measured in the centre and the rim of a polygon adjacent to the ECS tower.

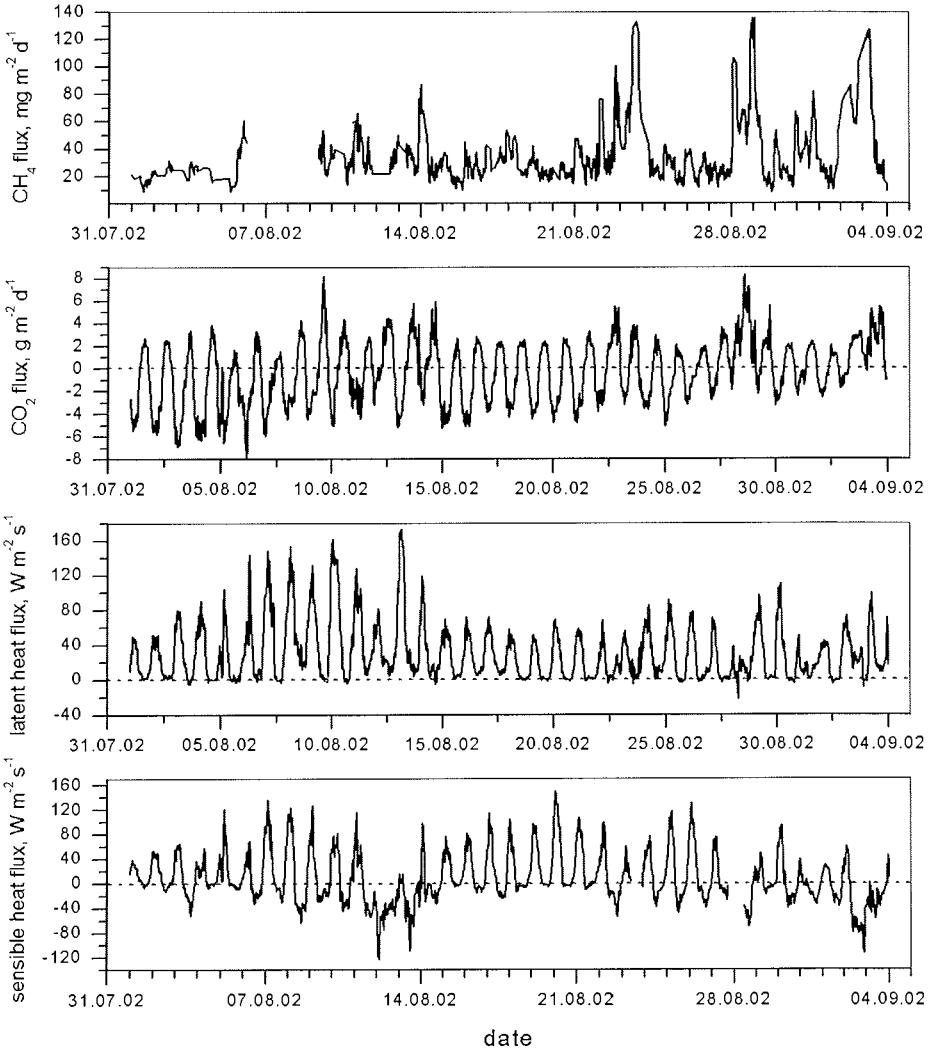

Figure 3-9. Preliminary calculations of eddy covariance fluxes August 2002. – From top to bottom: fluxes of methane, carbon dioxide, latent heat, sensible heat.

3.1.4 Perspectives

The presented measurement campaign will make available the first data of ecosystem-representative CH_4 and CO_2 fluxes for permafrost landscapes of the Siberian Arctic. The experimental set-up provides data sets that allow the coupling of the water and energy budget of permafrost soils with the carbon exchange processes between permafrost soils, tundra vegetation, and the atmospheric boundary layer. This kind of data is necessary for the improvement of soil-vegetation-atmosphere models able to assess the impact of climatic change on arctic ecosystems.

Based on the experiences made during these expeditions, the option of using the ECS during further campaigns in cooperation with other working groups will be evaluated. Due to its rugged and autonomous design, the ECS can be used in remote areas and under severe climatic conditions. Most interesting would be the installation on aircrafts or research vessels to investigate spatial variability of trace gas fluxes on the large scale.

3.2 Energy and water budget of permafrost soils – long time soil survey station on Samoylov Island

Christian Wille, Svenja Kobabe and Lars Kutzbach

3.2.1 Survey station 1998...2002

The automatic soil and meteorology measurement station on Samoylov Island was installed in July of 1998. It was situated in direct vicinity to the emission measurement site on the first terrace about 150 meters northeast of the Lena Delta reserve station building. The data recorded by the measurement station are as shown Table 3-3.

Table. 3-3. Data and sensors of Samoylov measurement station 1998...2002.

Pos.	Data Measured	Sensor Type
1	Air Temperature and Relative Humidity	Rotronic Meßgeräte GmbH Meteorological Probe for Humidity and Temperature MP340
2	Wind Speed & Direction	R M Young Company Anemometer 05103
3	Net Radiation	Kipp & Zonen B.V. Net Radiometer NR-Lite
4	Precipitation (liquid, i.e. Rain)	R M Young Company Tipping Bucket Rain Gauge 52203
5	Snow Height	Campbell Scientific Ltd. Sonic Ranging Sensor SR 50
6	Soil Temperature	Campbell Scientific Ltd. Thermistor Soil Temperature Probe 107
7	Soil Bulk Electrical Conductivity	Campbell Scientific Ltd. TDR Soil Moisture System
8	Soil Volumetric Water Content	Campbell Scientific Ltd. TDR Soil Moisture System
9	Heat Flux out of / into Soil	Hukseflux Thermal Sensors Heat Flux Sensor HFP01SC

Measurements of air temperature and relative humidity were made at 0.5 and 2.0 meters above ground. The measurement of soil bulk electrical conductivity and soil water content were made by time domain reflectometry (TDR). Soil temperature and TDR measurements were carried out along two vertical profiles in the polygon centre and the polygon rim respectively. Soil heat flux was recorded at two different depths in the polygon rim.

Due to technical problems there exist several gaps in the data. Table 3-4 shows the time periods during which data was collected by the station. As an example, Figure 3-10 shows a one year period of soil temperature data collected at the polygon rim site together with air temperature (0.5 m above ground) data from the same time period.

Table 3-4. Existing data series 1998...2002.

Data	Existing Data Series
Meteorological Data (Pos. 1-4 of Table 3-3)	28.07.98...10.05.00 17.08.00...20.10.00 18.03.01...25.08.02
Soil Data (Pos. 5-9 of Table 3-3)	30.07.98...18.12.99 06.02.00...25.05.00 25.07.00...12.11.00 14.02.01...05.06.01 22.07.01...25.08.02

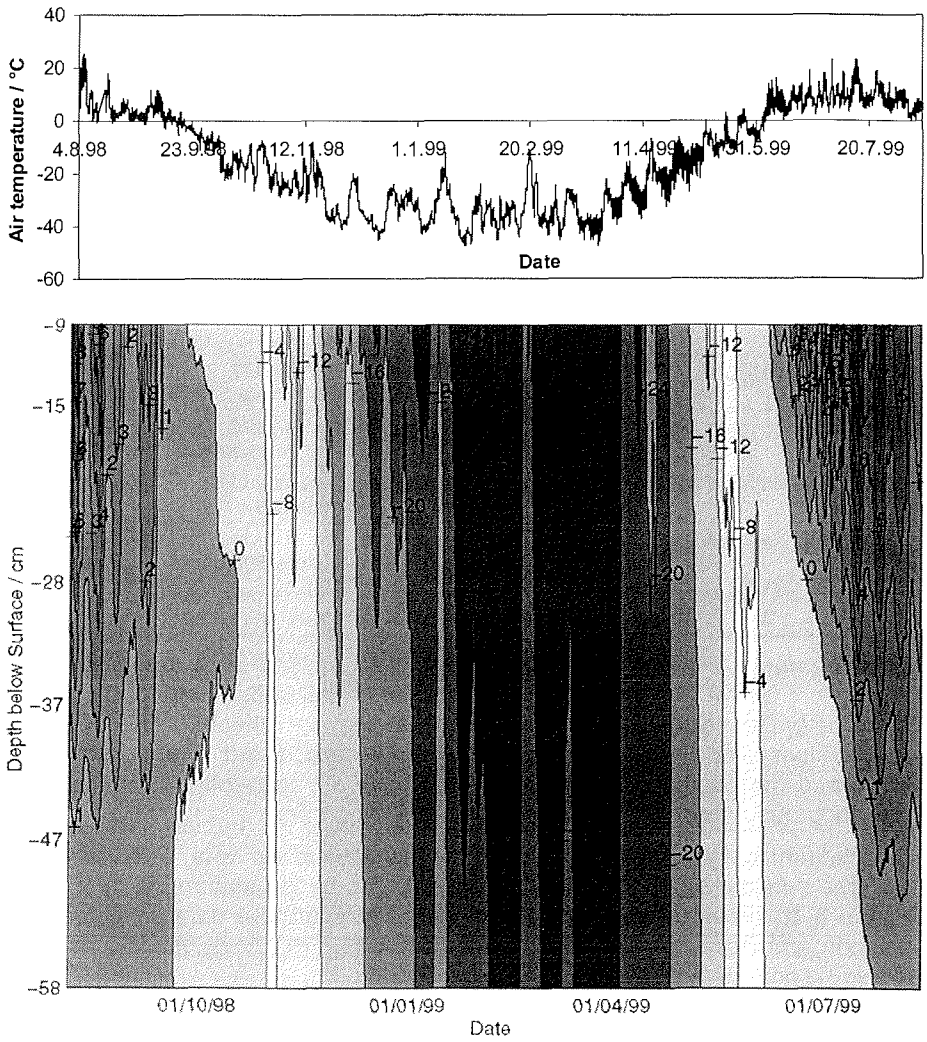

Figure 3-10. Air temperature at 0.5 m above ground (top) and Soil temperature profile from polygon rim (bottom) during period 04.08.98...12.08.99. Depth labels in soil temperature chart indicate position of sensors.

3.2.2 New long time survey station

During the Lena 2002 expedition two new measurement stations were set up on Samoylov Island. The first station which serves as the new permanent meteorology and soil survey station is situated about 30 m northeast of the old measurement site as shown in Figure 3-11. The station was put in operation in August of 2002.

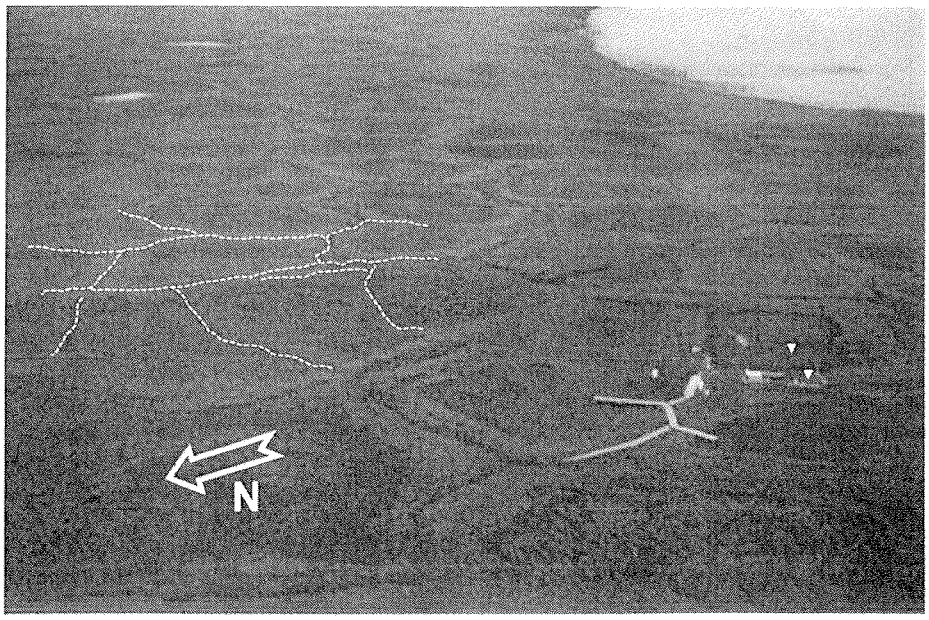

Figure 3-11. Arial view of the old measurement station in 2001. The white triangles indicate the position of the old soil measurement profiles. The dashed line encircles the polygon in which the new soil profiles were installed.

For the new measurement station 3 profile pits were dug through the active layer and into the permafrost at the summit and the slope of the elevated polygon rim (BS-1, BS-2) and in the depressed centre (BS-3) of the designated polygon. Figure 3-12 shows a 3D-model of the polygon and the position of the profiles.

Soils were described and classified according to *Soil Taxonomy* (USDA1998, 8th edition) and the German field book for describing soils *Bodenkundliche Kartieranleitung* (AG Boden 1994, 4th edition). Additionally, soils were classified according to the *World Reference Base for Soil Resources* (FAO 1998) and the Russian system of Elovskaya (1987). The soil descriptions are given in Tables 3-5...3-7. Three different sample types were collected from each horizon: moist and deep frozen samples for microbiological analyses, air-dried bulk samples to investigate soil chemistry, and undisturbed soil density cores to analyze soil physics. A complete sample list is provided in Appendix 3-1.

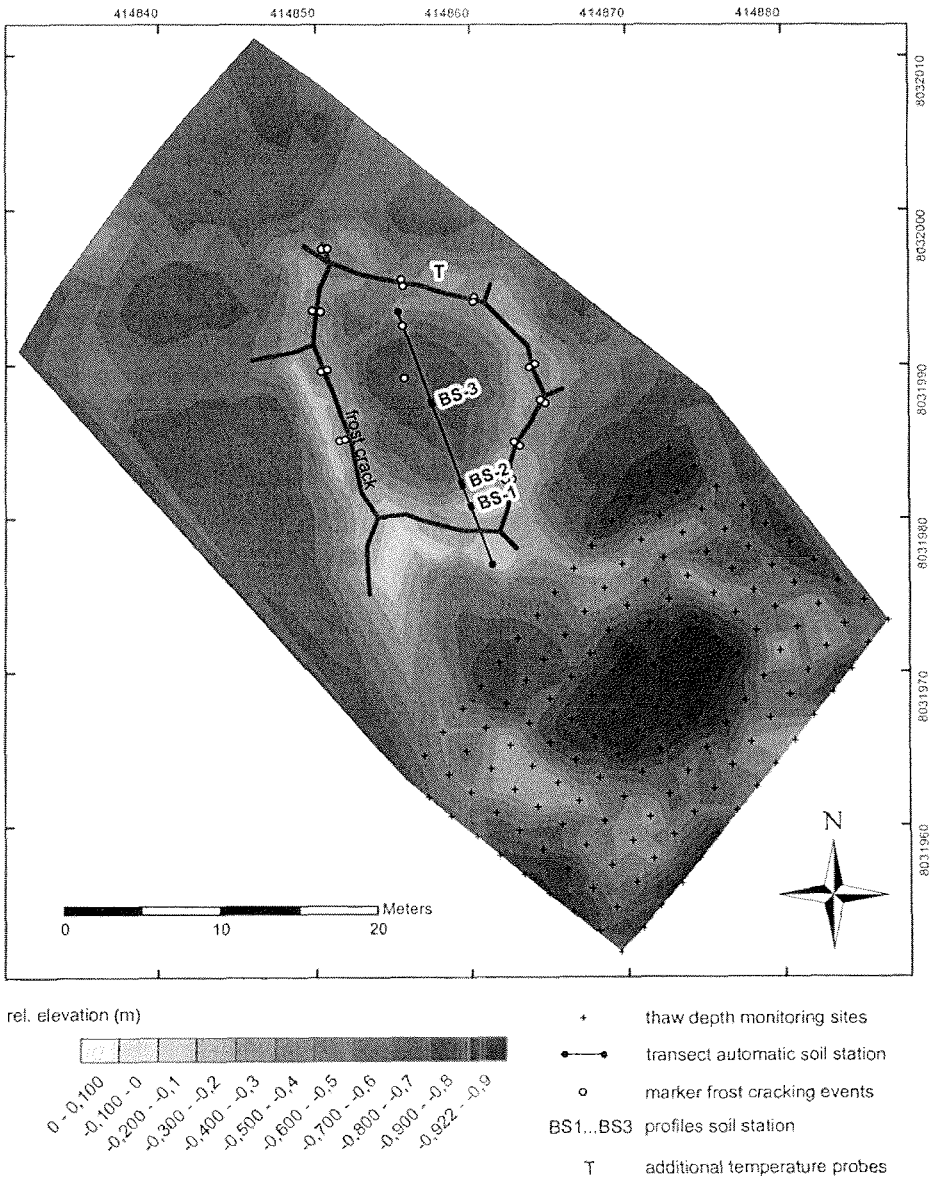

Figure 3-12. Site map new longtime soil survey station. – Positions of thaw depth monitoring sites (manual measurements), polygon transect (see Figure 3-13), markers for frost cracking events, soil profiles BS-1...BS-3, and additional temperature probes. The 3D-model is based on a triangulated irregular network (TIN; 482 measuring points). Elevation values are measured relatively to the heighest point. Coordinate system: UTM Zone 52N, WGS84.

Table 3-5. Description of soil profile BS-1 (summit of polygon rim).

profile ID: **LD02-BS-1** location: Samoylov, Lena-Delta date: 16.08.02
altitude a.s.l.: 12.0 m UTM: Zone 52, 414860E, 8031981N

relief situation: 1. main delta terrace, summit of elevated polygon rim
substrate: fluviatile (+aeolian) stratified sands and loams, peat layers

profile depth: 100 cm permafrost depth: 40 cm water level depth: --

vegetation: mosses total 95%, height 1...2 cm, *Hylocomium splendens* 90%; lichens 1%; vascular plants total 25%, height 20 cm, *Carex aquatilis* 15%, *Dryas octopetala* 4%, *Astragalus frigidus* 3%, *Hedysarum hedysaroides* 3%, *Lagotis glauca* r, *Valeriana capitata* r, *Saxifraga punctata* r

depth (cm)	horizon[1] (cm)	sample ID LD02-	properties
0...3	Oi	6983	organic material, slightly decomposed moss fibers, >30% org. matter, few fine roots, 7.5YR2/2, inclusions of aeolian sand
3...7	Ajj1	6984	loamy sand, granular to single grain, 2...4% org. matter, many fine roots, 10YR3/2
7...15	Ajj2	6985	sandy loam, subangular blocky to coherent, 2...4% org. matter, many fine roots, 10YR3/2
15...23	Bjjg1	6986	sandy loam, granular to coherent (compressed), 2...4% org. matter, common fine roots, very many dead fine roots (fossil A horizon), 2.5YR4/1, irregular band of redoximorphic concretions: 30...40% (7.5YR4/4)
23...29	Bjjg2	6987	silt loam, platy to coherent, stratified, peat layers, 4...8% org. matter, common fine roots, 2.5Y4/2, peat: root residues, sedge leave sheaths, wood
29...34	Bjjg3	6988	sand, coherent, <1% org. matter, very few fine roots, 2.5Y4/2, α,α-dipyridyl reaction positive
34...40	Bjjg4	6989	sandy loam/silt loam, coherent, stratified, peat layers, 8...15% org. matter. no roots, 10YR2/2, α,α-dipyridyl reaction positive
40...55	Bjjgf1	6990	permafrost, alternating peat and sediment layers, peat layers narrow (<0.5cm), horizontal ice veins, high ice content in peat layers
55...65	Bjjgf2	6991	similar to Bjjgf1
65...100	Bjjgf3	6992	similar to Bjjgf1

remarks: sediments stratified; wavy to irregular horizon boundaries: cryoturbation

Soil Taxonomy: **Typic Aquiturbel**
World Reference Base for Soil Resources: **Gleyi-Turbic Cryosol (Fluvic)**
Russian Classification (Elovskaya): **Permafrost Turfness Gley**

1) symbols according to Soil Taxonomy 8th edition (USDA 1998)

Table 3-6. Description of soil profile BS-2 (slope of polygon rim).

profile ID: **LD02-BS-2** location: Samoylov, Lena-Delta date: 20.08.02
altitude a.s.l.: 11.8 m UTM: Zone 52, 414859E, 8031982N

relief situation: 1. main delta terrace, slope of elevated polygon rim
substrate: shallow moss and sedge peat above fluviatile stratified sands and loams, peat layers

profile depth: 50 cm permafrost depth: 17 cm water level depth: --

vegetation: mosses total 98%, height 3...4 cm, Hylocomium splendens 80%; vascular plants total 20% height 25 cm, *Carex aquatilis* 10%, *Salix glauca* 10%, *Dryas octopetala* r, *Pyrola secunda* r, *Polygonum viviparum* r

depth (cm)	horizon[1] (cm)	sample ID LD02-	Properties
0...10	Oi1	7002	organic material, peat, slightly decomposed moss fibers, >30% org. matter, many fine roots, 10YR2/3, inclusions of aeolian sands
10...17	Oi2	7003	organic material, peat, slightly decomposed moss fibers, >30% org. matter, many fine roots, 10YR1.7/1, inclusions of aeolian sands, common *Carex* rhizomes and coarse roots of *Salix*
17...25	Bjjgf1	7004	permafrost, sand, 2...4% org. matter, 10YR3/1, sand layers alternating with slightly decomposed peat layers; at 25cm fossil root horizon; in peat layers high ice content; at 18cm: horizontal crack 0.5...1cm wide, α,α-dipyridyl reaction positive
25...50	Bjjgf2	7005	permafrost, loamy sand, 2...4% org. matter, 10YR2/2, sand layers alternating with very narrow peat layers, along peat layers thin ice layers

remarks: sediments stratified; wavy horizon boundaries: cryoturbation

Soil Taxonomy: Typic Aquiturbel
World Reference Base for Soil Resources: **Turbi-Histic Cryosol (GleyicFluvic)**
Russian Classification (Elovskaya): **Permafrost Peatish Gley**

1) symbols according to Soil Taxonomy 8th edition (USDA 1998)

Table 3-7. Description of soil profile BS-3 (polygon centre).

profile ID: **LD02-BS-3** location: Samoylov, Lena-Delta date: 20.08.02
altitude a.s.l.: 11.5 m UTM: Zone 52, 414853E, 8031988N

relief situation: 1. main delta terrace, depressed centre of polygon
substrate: moss and sedge peat above fluviatile sands

profile depth: 50 cm permafrost depth: 34 cm water level depth: 6 cm

vegetation: mosses total 95%, height 1...5 cm; vascular plants total 40%, height 30 cm, *Carex aquatilis* 40%, *Saxifraga cernua* r, *Caltha palustris* r, *Pedicularis sudetica* r

depth (cm)	horizon[1] (cm)	sample ID LD02-	Properties
0...15	Oi1	7007	organic material, peat, slightly decomposed moss and sedge fibers, >30% org. matter, very many fine roots, 10YR2/3, common *Carex* rhizomes
15...34	Oi2	7008	organic material, peat, slightly decomposed moss and sedge fibers, >30% org. matter, many fine roots, 2.5Y4/4, inclusions of sand layers, more dense than Oi1, α,α-dipyridyl reaction positive
34...50	Bgf	7009	permafrost, sand, 2...4% org. matter, 7.5YR5/1, sand layers alternating with medium-decomposed peat layers (moss + dead roots), α,α-dipyridyl reaction positive

remarks: no cryoturbation

Soil Taxonomy: Typic Historthel
World Reference Base for Soil Resources: **Gleyi-Histic Cryosol (Fluvic Fibric)**
Russian Classification (Elovskaya): **Permafrost Peat Gley**

1) symbols according to Soil Taxonomy 8th edition (USDA 1998)

Temperature and TDR sensors were installed in pairs to measure vertical profiles of soil temperature and soil volumetric water content. In every profile sensors were installed so as to cover the whole depth range of the profile, i.e. from the very top through the active layer and into the permafrost soil. The positions of the sensors were chosen according to the existing soil horizons so that every horizon in the profile was probed at least once. Additionally, a measurement chain of temperature sensors was installed in the ice wedge down to a depth of 220 cm into the ice. Heat flux sensors were installed at small depths below the surface in the rim and centre profiles. Figure 3-13 and Table 3-8 show the configuration of the new measurement station in graphical and Table form respectively.

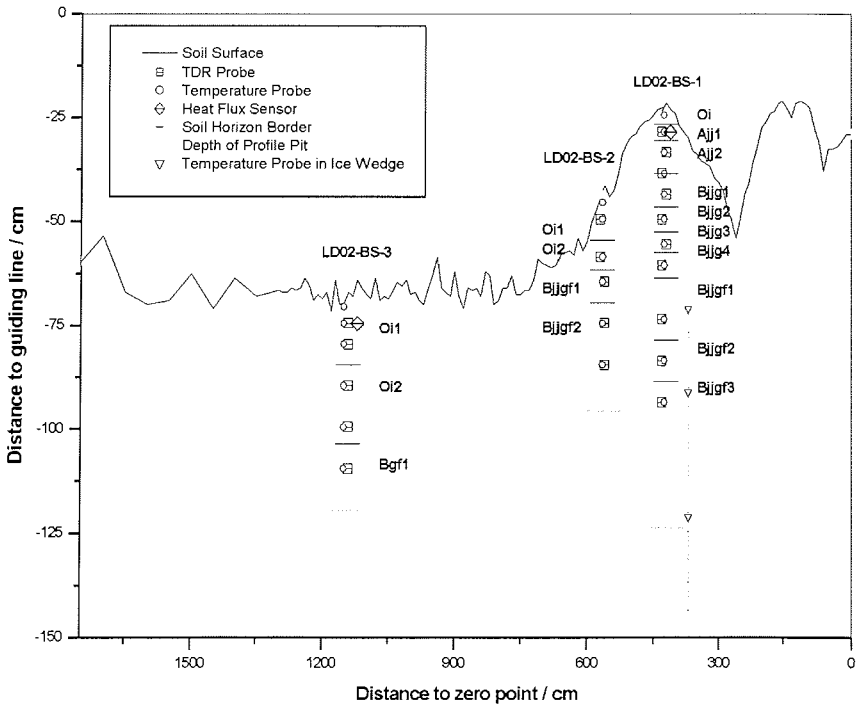

Figure 3-13. Transect of the polygon with the new measurement station. The solid line shows the surface profile of the polygon along the line connecting the measurement profiles. The markers indicate the position of sensors. The chain of temperature probes in the ice wedge continues below the depth range shown.

Table 3-8. Configuration of the measurement profiles. Depth of temperature sensors in ice wedge is given in cm below top surface of ice wedge shoulder.

Profile ID / Description	BS-1 / Polygon Rim										
Depth (cm)	1	5	10	15	20	26	32	37	50	60	70
TDR Sensor ID	--	29	28	27	21	26	25	22	10	12	11
Temp. Sensor ID	22	7	6	11	8	13	12	10	29	28	19
Heat Flux Sensor ID	--	550	--	--	--	--	--	--	--	--	--
Profile ID / Description	Ice Wedge										
Depth (cm)	-10	10	40	70	100	130	160	190	220		
Temp. Sensor ID	9	27	26	25	24	20	16	18	17		
Profile ID / Description	BS-2 / Polygon Slope										
Depth (cm)	1	5	14	20	30	40					
TDR-Sensor ID	--	30	24	23	15	6					
Temp.-Sensor ID	21	5	4	3	2	1					
Profile ID / Description	BS-3 / Polygon Centre										
Depth (cm)	1	5	10	20	30	40					
TDR-Sensor ID	--	8	14	16	9	13					
Temp.-Sensor ID	40	30	23	37	38	39					
Heat Flux Sensor ID	--	551	--	--	--	--					

The tower with meteorological instruments, the sonic ranging sensor for measuring snow depth as well as the power supply equipment were moved from the old measurement station and installed at the new site. A new sensor for the measurement of long wave radiation emitted from the ground was installed on the meteorological tower. Table 3-9 lists the data collected by the new measurement station as well as the sensors used. Meteorological data (Pos. 1-5 in Table 3-9) is sampled every 20 seconds and hourly averages are stored. Soil data (Pos. 6-10 in Table 3-9) is sampled and stored once an hour.

Table 3-9. Data and sensors of new permanent measurement station.

Pos.	Data Measured	Sensor Type
1	Air Temperature and Relative Humidity	Rotronic Meßgeräte GmbH Meteorological Probe for Humidity and Temperature MP340
2	Wind Speed & Direction	R M Young Company Anemometer 05103
3	Net Radiation	Kipp & Zonen B.V. Net Radiometer NR-Lite
4	Long wave Radiation	Kipp & Zonen B.V. Pyrgeometer CG1
5	Precipitation (liquid, i.e. Rain)	R M Young Company Tipping Bucket Rain Gauge 52203
6	Snow Height	Campbell Scientific Ltd. Sonic Ranging Sensor SR 50
7	Soil Temperature	Campbell Scientific Ltd. Thermistor Soil Temperature Probe 107
8	Soil Bulk Electrical Conductivity	Campbell Scientific Ltd. TDR 100, Probe CS605
9	Soil Volumetric Water Content	Campbell Scientific Ltd. TDR 100, Probe CS605
10	Heat Flux out of / into Soil	Hukseflux Thermal Sensors Heat Flux Sensor HFP01

3.2.3 Eddy site soil measurement profile

A second measurement station was installed near the Eddy Covariance measurement site. This station consists of two profiles (BS-4, BS-5) of temperature, TDR and heat flux sensors in a degraded polygon about 35 m northwest of the eddy measurement tower. During future campaigns a preassembled data logging system can be connected to the sensors to deliver additional data for the eddy covariance measurements.

As for the permanent measurement station (see previous chapter), profile pits were dug, soils were described and classified, samples were collected, and sensors were installed. The soil descriptions are given in Table 3-10 and 3-11, a complete sample list is provided in Appendix 3-1.

Table 3-10. Description of soil profile BS-4 (polygon rim).

profile ID: **LD02-BS-4** location: Samoylov, Lena-Delta date: 28.08.02
altitude a.s.l.: 11.5 m UTM: Zone 52, 415383E, 8032420N

relief situation: 1. main delta terrace, summit of elevated polygon rim
substrate: fluviatile loams

profile depth: 50 cm permafrost depth: 32 cm water level depth: --

vegetation: mosses total 98%, height 2...4cm; vascular plants total 20%, height 20cm, *Carex aquatilis*, *Salix reticulata*, *Salix glauca*, *Saxifraga punctata*, *Pyrola secunda*, *Saxifraga hirculus*

depth (cm)	horizon[1] (cm)	sample ID LD02-	Properties
0...6	Oi	7016	organic material, slightly decomposed moss fibers,>30% org. matter, few fine roots, 10YR2/3
6...20	Ajj	7017	sandy loam, sub angular to angular blocky, 2...4% org. matter, many fine roots, 10YR3/2, at the horizon top band of redoximorphic concretions: 10% (2,5YR4/6), no prominent peat layers
20...32	Bjjg	7018	silt loam, subangular blocky to coherent, 2...4% org. matter, many fine roots, 10YR4/1, no prominent peat layers, α,α-dipyridyl reaction negative
32...50	Bjjgf	7019	permafrost,, 1...2% org. matter, 10YR3/1, no stratification noticeable, ice lense in direction crack 3cm thick

remarks: wavy horizon boundaries: slight cryoturbation

Soil Taxonomy: **Typic Aquiturbel**
World Reference Base for Soil Resources: **Gleyi-Turbic Cryosol**
Russian Classification (Elovskaya): **Permafrost Turfness Gley**

1) symbols according to *Soil Taxonomy* 8th edition (USDA 1998)

Table 3-11. Description of soil profile BS-5 (polygon centre).

profile ID: **LD02-BS-5** location: Samoylov, Lena-Delta date: 29.08.02
altitude a.s.l.: 11.0 m UTM: Zone 52, 415379E, 8032418N

relief situation: 1. main delta terrace, depressed centre of polygon
substrate: moss and sedge peat above fluviatile loams

profile depth: 55 cm permafrost depth: 34 cm water level depth: 4 cm

vegetation: mosses total 98%, height 1...5 cm; vascular plants total 30%, height 30 cm, Carex *aquatilis*, *Potentilla palustris*, *Pedicularis sudetica*

depth (cm)	horizon[1] (cm)	sample ID LD02-	Properties
0...10	Oi1	7020	organic material, slightly to medium decomposed moss peat,>30% org. matter, very many fine roots, 10YR1.7/1 + 7.5YR3/4, few aeolian sand
10...26	Oi2	7021	organic material, slightly to medium decomposed moss peat, >30% org. matter, many fine roots, 10YR3/3, few aeolian sand, α,α-dipyridyl reaction positive
26...34	Bg	7022	sandy loam, 15...30% org. matter, 10YR4/2, medium-decomposed sedge and moss peat, α,α-dipyridyl reaction positive
34...55	Bgf	7023	permafrost, sandy loam, 15...30% org. matter, 10YR4/1, loam layers alternating with peat layers (medium-decomposed sedge residues), α,α-dipyridyl reaction positive

remarks: no cryoturbation

Soil Taxonomy: **Typic Historthel**
World Reference Base for Soil Resources: **Gleyi-Histic Cryosol (Fibric)**
Russian Classification (Elovskaya): **Permafrost Peat Gley**

1) symbols according to Soil Taxonomy 8th edition (USDA 1998)

Figure 3-14 and Table 3-12 show the configuration of the measurement profiles in graphical and table form respectively.

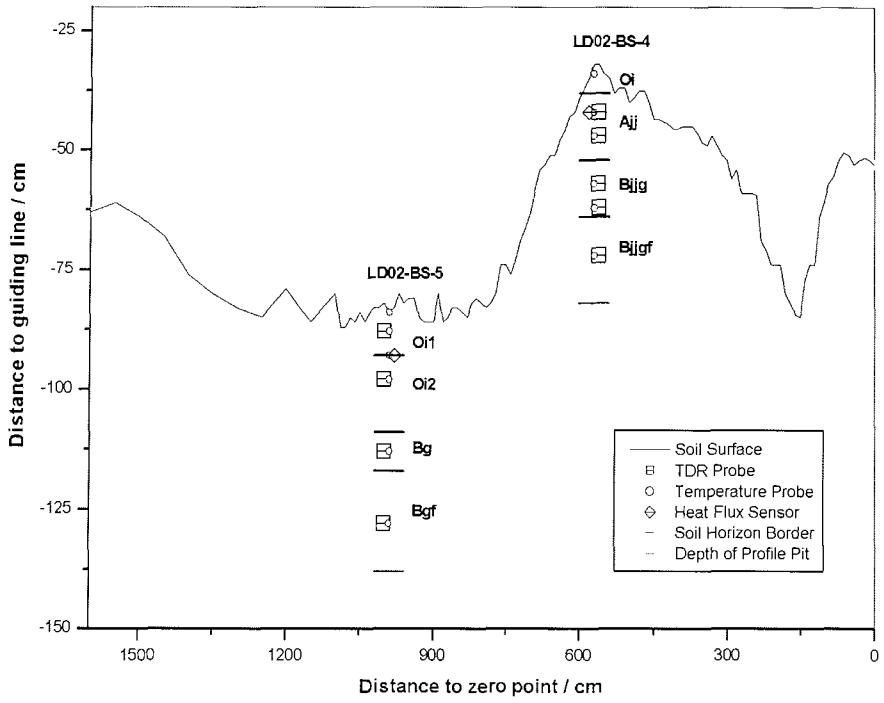

Figure 3-14. Transect of the polygon with the eddy site measurement profiles. The solid line shows the surface profile of the polygon along the line connecting the measurement profiles. The markers indicate the position of sensors. The location of transect is shown in Figure 3-4 (elevation profile-2).

Table 3-12. Configuration of the "Eddy Site" measurement profiles.

Profile ID / Description	BS-4 / Polygon Rim					
Depth (cm)	2	10	15	25	30	40
TDR Sensor ID	--	5	19	2	20	4
Temp. Sensor ID	34	32	33	36	35	31
Heat Flux Sensor ID	--	20	--	--	--	--
Profile ID / Description	BS-5 / Polygon Centre					
Depth (cm)	1	5	10	15	30	45
TDR-Sensor ID	--	3	--	7	17	18
Temp.-Sensor ID	L8	43	L10	44	41	42
Heat Flux Sensor ID	--	--	19	--	--	--

3.3 Studies on recent cryogenesis

Hanno Meyer

3.3.1 Introduction

Samoylov Island is subdivided into four different geomorphologic elements (Akhmadeeva et al. 1999): a lower flood plain, a middle flood plain and a high flood plain in the western part of the island, which are separated by an up to 8 m high cliff from an old river terrace (1st Lena river terrace). The low and middle flood plains are those which are in general annually flooded by Lena river, but for different time spans, whereas the high flood plain is reached by water only during high floods. The 1st Lena river terrace reaches up to 12 m a.s.l. and has been built up since the Middle Holocene. Both, the high flood plain and the 1st Lena river terrace are characterised by polygonal-patterned ground with ice wedge growth. Therefore, studies on recent cryogenesis and on recent ice wedge growth were carried out last summer especially on the high flood plain and the 1st Lena river terrace on Samoylov Island (Figure 3-15).

The main aim of studying recent cryogenesis processes is to establish a stable isotope thermometer for ice wedges. The reconstruction of paleotemperatures with ground ice, especially with ice wedges is possible (Vasil'chuk 1992, Nikolaev & Mikhalev 1995). So far, this is reduced by the missing correlation of the ice veins - of which ice wedges are composed - to the year of their formation as well as by the large distances of field locations to the next weather station. The attribution of recent ice veins to the discrete year of their formation can be carried out with tracer experiments. A tracer (such as coloured spores) applied to a polygon with recent cryogenesis enables us to identify all types of ground ice, which were formed in the considered year. The combination with a nearby climate station would allow to correlate the temperature with the isotope geochemistry of ice wedges. It was also aimed to characterise and to identify the conditions prevailing, when frost cracking and recent ice wedge growth take place. For this purpose, an ice wedge polygon had to be selected in the field for monitoring according to several site-specific characteristics. These were:

1.) the occurrence of recent ice wedge growth,

2.) a clearly visible frost crack,

3.) a well-developed relief between polygon wall and polygon centre, which additionally had to be typical for the site,

4.) a rather young stage of ice wedge polygon formation without signs of degradation such as standing water in the trough above the ice wedge,

5.) for drainage reasons, a low inclination and exposition of the polygon,

6.) a low insolation from above by the soil, the vegetation and the snow cover for best possible cracking conditions (e. g. low temperatures entering the permafrost).

Additionally, it was aimed to select a polygon close to both, the weather and the soil stations on Samoylov in order to use the existing climate and soil data to characterise the site and to better understand the boundary conditions for recent ice wedge growth (see Chapter 3.2).

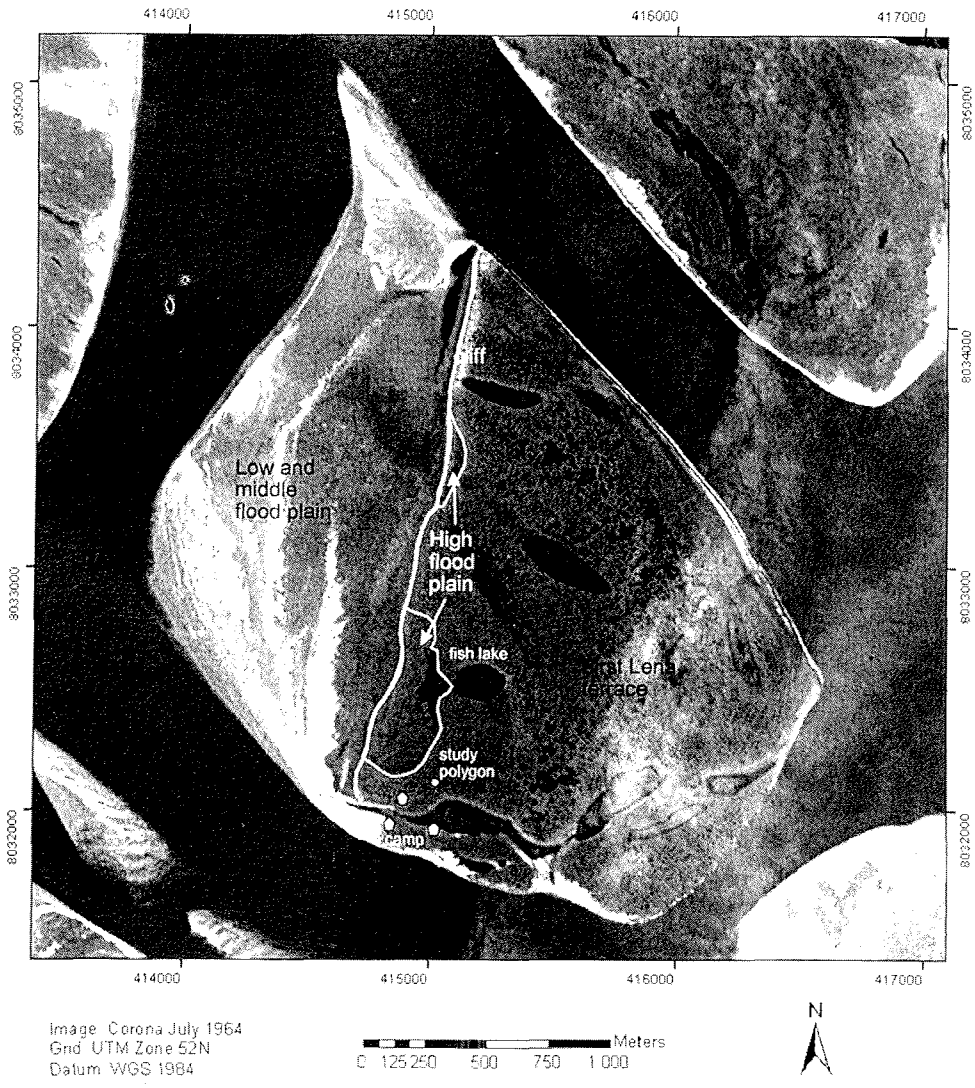

Figure 3-15. Study site on Samoylov Island. Corona satellite image, 1964.

3.3.2 Survey of different polygon types on Samoylov Island

In order to select an ice wedge polygon for studies on recent cryogenesis, the first days were used to recognise the different polygon types occurring on Samoylov Island, which were differentiated by their stage of development and the availability of recent ice veins. For this purpose, the island was subdivided into different specific areas, each of which was briefly visited and mapped for the following characteristics of the polygons.

These characteristics are: polygon size, polygon net type (French 1996), exposition, vegetation cover, soil type, hydrological conditions (drainage and distribution of standing water), thickness of the active layer, relief (height difference between polygon wall and polygon centre) as well as the frost cracking activity (occurrence of recent ice wedge growth). This first survey resulted in seven modern polygon types presently occurring on Samoylov Island.

1. polygon type: juvenile

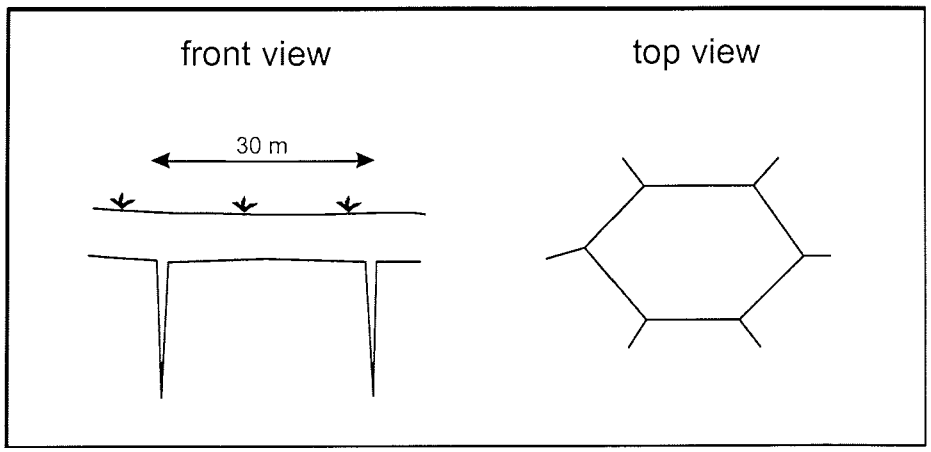

Figure 3-16. Front and top view of the juvenile polygon type.

A juvenile polygon (Figure 3-16) type is found in relatively dry, well-drained sites, such as the uppermost flood plain located between the lower and middle floodplain and the first Lena river terrace (Figure 3-15). It is characterised by a low relief with very small height differences between polygon wall and centre and relatively big (30 m in diameter) hexagonal ice wedge polygons. The active layer is about 0.4 m to 0.5 m thick with a thin vegetation cover without large differences between plant in the polygon wall and the centre. Frost cracks are clearly visible and recent ice veins are regularly found.

2. polygon type: mature

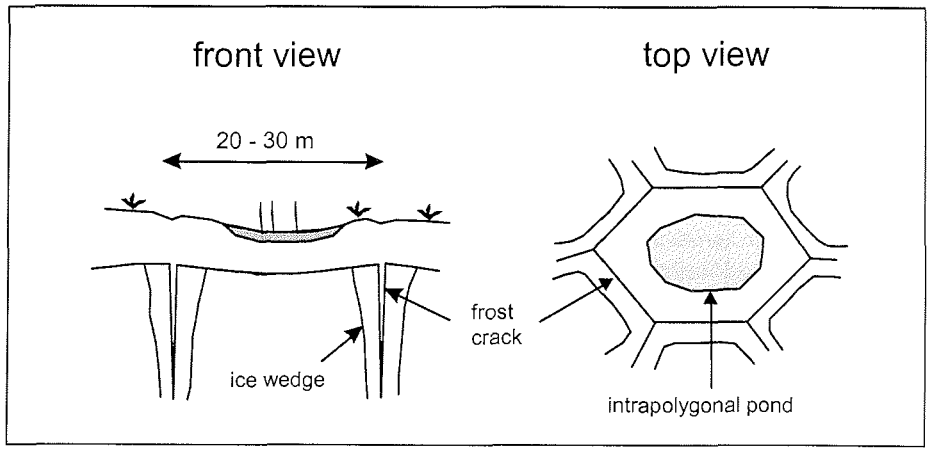

Figure 3-17. Front and top view of the mature polygon type.

The mature polygon type (Figure 3-17) is found all over the first Lena terrace. It is characterised by a relatively high relief with height differences of about 0.5 m between the polygon wall and the centre. An intrapolygonal pond is typical for the polygon centres, but this depends on drainage conditions. A trough above the ice wedge is clearly visible and active frost cracks with recent ice veins are frequent. The moss cover of the polygon wall is often cut into two pieces by the frost cracking process. The polygons are relatively big (20-30 m in diameter) and consist of pentagonal or hexagonal ice wedge nets. In general, the active layer is between 0.2 m to 0.6 m thick, mainly varying around 0.35 m. The vegetation cover differs clearly between polygon wall (mosses dominant) and polygon centre (sedges dominant). Typical mature polygons are located close to the weather station on Samoylov Island.

During the field campaign, different types of ice wedge polygons were found showing signs of degradation (such as water standing in the trough above the ice wedge). Most of them are linked with a change in hydrological conditions of the juvenile or mature polygons. For the selection of a polygon for the experiments on recent cryogenesis, it was differentiated between three main stages: 1.) initial degradation, 2.) degraded and 3.) final degradation (wet and dry). However, numerous substages between these degradation polygons were observed and the transitions between them are smooth.

3. polygon type: initial degradation

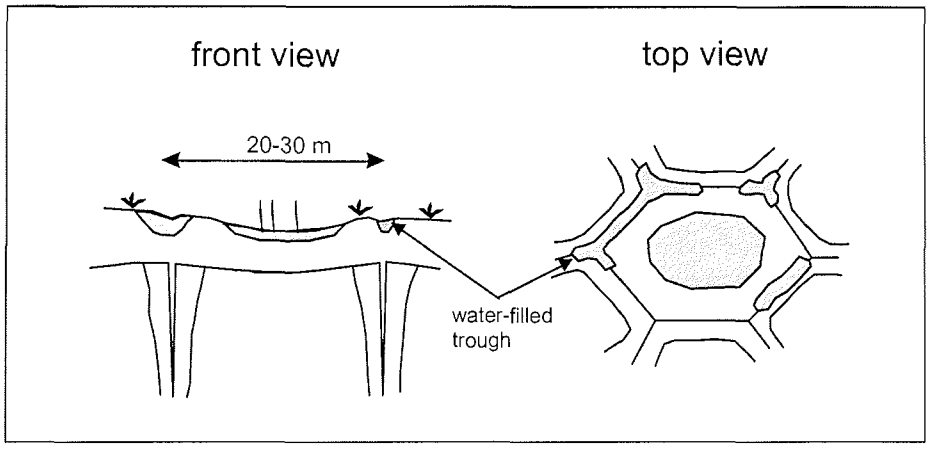

Figure 3-18. Front and top view of the polygon type of initial degradation.

This polygon type develops from the mature type, with the formation of small ponds in the polygon wall, which often form triangular ponds in the triple junctions of frost cracks or elongated ponds along the frost crack. It can actually be considered as intermediate polygon type between the mature and the degraded stages (Figure 3-18). Therefore, the size and the number of edges of the polygon are related to the mature type polygon, which starts degrading. The intrapolygonal pond as well as the clear differentiation of the vegetation between polygon wall and centre are still present. The polygon is characterised by a high relief with height differences of more than half a meter between polygon wall and centre. This polygon type is still active with common frost cracking and recent ice wedges, which are commonly found in the drier parts of the polygon.

4. polygon type: degraded

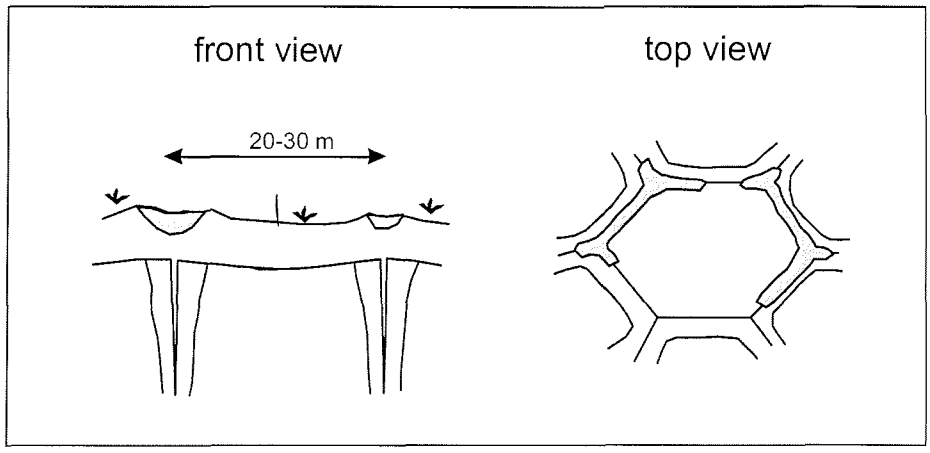

Figure 3-19. Front and top view of the degraded polygon type.

If the degradation of the polygon continues, the intrapolygonal pond falls dry and the vegetation used to standing water disappears (Figure 3-19). In contrast, the ponds in the polygon walls may deepen and sometimes get connected to a pentagonal or hexagonal pond above the frost crack. The relief is still high because of relatively high rims in the polygon walls, but when the pools fall dry, the polygon centres diminish in depth. Frost cracking certainly occurs in these polygons, but the recent ice wedges are hard to sample, because of the water standing in most parts of the trough above the ice wedge. This polygon type is commonly found all over the island, e. g. near the "Fish Lake" and near the northern point of the island.

5. polygon type: final degradation, dry, high centre polygon

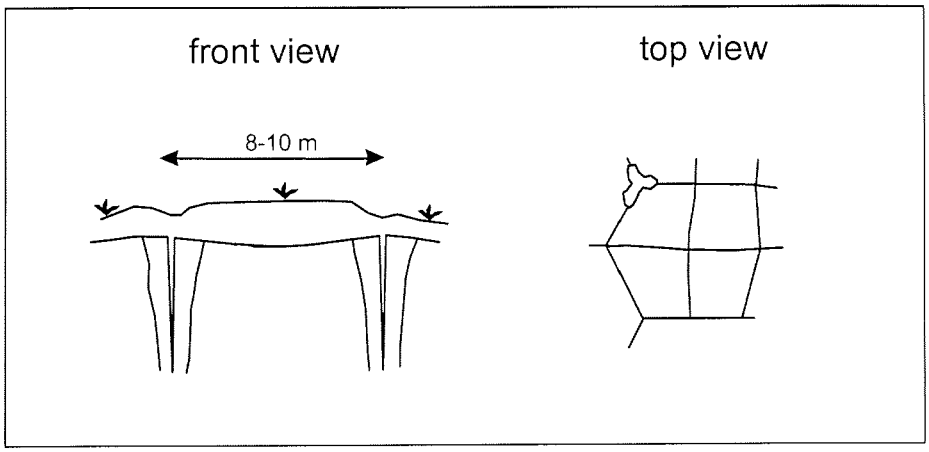

Figure 3-20. Front and top view of the final dry degradation or "high-centre" polygon type.

If degradation occurs in a well-drained and relatively dry environment, the polygon seldom has open water ponds. In general, the trough above the ice wedge is deep and still relatively wet, but the polygon centre is completely dry (Figure 3-20). Secondary polygons subdivide the degraded pentagonal or hexagonal polygons mostly into four smaller polygons which in most cases are tetragonal, sometimes pentagonal in shape. With a size of 8 - 10 m in diameter, the high-centre polygons are much smaller than the preceding low-centre polygons. Recent frost cracking is observed, and especially in the secondary cracks (of the high-centre polygons), recent ice veins are found. This polygon type is found near the northern point of Samoylov Island.

6. polygon type: final degradation, wet

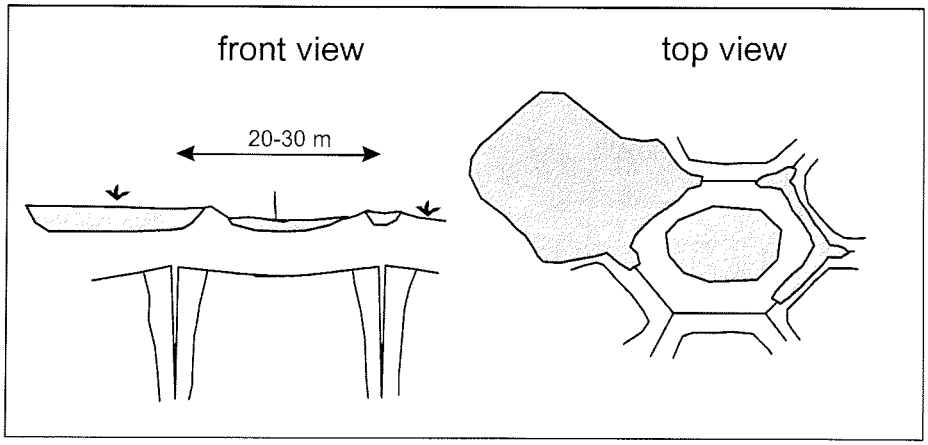

Figure 3-21. Front and top view of the final wet degradation polygon type.

If the degradation propagates in a poorly-drained and wet environment, the polygon is often characterised by standing water and sometimes it is even completely flooded (Figure 3-21). The trough above the ice wedge is deep and wet and the polygon centre has open water ponds, which may extend and then interconnect with ponds in the polygon wall or with intrapolygonal ponds of other polygons. This polygon type is characteristic for depressions on Samoylov, where the flux of surface waters and precipitation often leads to the formation of lakes with variable size and polygonal structure. This polygon type typically occurs e. g. 200 m NW of the eddy covariance tower (here in an old river branch of the paleo-Lena). Recent ice veins were not found in these polygons, because of the water standing in the trough above the ice wedge. Nevertheless, for these lakes, which in general are not deeper than 1.2 m, frost cracking cannot be excluded.

7. polygon type: slope polygon

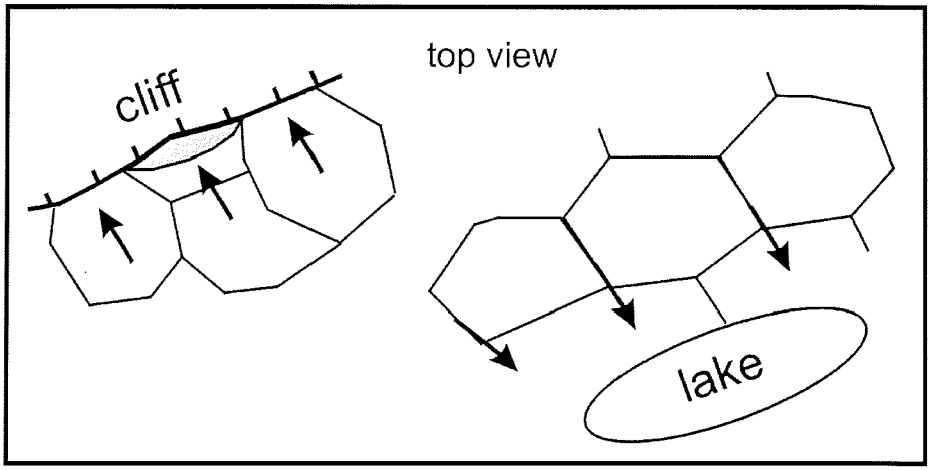

Figure 3-22. Top view of two types of slope polygons (near lakes and cliffs).

Slope polygons (Figure 3-22) develop in all places, where the meso-relief is lowered, i. e. near cliffs and around lakes. The drainage is directed towards the lake or the cliff leading to relatively dry polygons near the slopes. They may develop from all other polygon types and, hence, differ in size, shape and morphology. A low relief similar to that of the juvenile polygon is a common but not necessary observation, even though the trough above the ice wedge is sometimes deepened being used as channel for running water. The main feature is the dryness compared to the surrounding polygons. The slope polygon type is found all along the cliff as well as around every lake. Recent ice wedges have not been found in two dig holes and, therefore, this polygon type has been considered as not appropriate for recent cryogenesis studies.

This classification is certainly a simplification, e. g. not taking into account the soil type as well as the type of sediments, which were found to vary not so much on Samoylov Island. It is mainly based on the drainage conditions and linked phenomena (such as the exposition). The main result of a few days' of field work was the finding, that the presented subdivision of polygons is helpful to track and to characterise polygons, which are suitable for recent ice wedge studies (juvenile, mature type) and which polygons are not useful (degraded types, slope polygons). The subdivision of polygon types may serve as the base for a more detailed mapping of polygon types on Samoylov Island.

3.3.3 Mapping and survey of the selected polygon

According to the subdivision of polygon types on Samoylov Island, juvenile and mature ice wedge polygons seem to be the most promising for studies on recent cryogenesis. Both types commonly show recent frost cracking and no water standing in frost crack, hence, hampering the sampling of the recent ice vein in summer. The mature type is characterised by a well-developed relief between polygon wall and polygon centre and clearly visible frost cracks with troughs above the ice wedge. Therefore, a mature type ice wedge polygon was selected for the studies on recent cryogenesis located near the old weather and soil stations. The same polygon is also used for the new soil and the weather stations, which gives the excellent possibility to combine weather and soil data with the studies on recent cryogenesis.

The selected site is characterised by low inclination towards the north, and is located on the first Lena terrace approximately 250 m NE of the ice cellar of the station. The polygon is hexagonal and 20.6 m in diameter. It is characterised by a relatively high relief with the polygon centre about 0.5 m lower than the polygon walls, which in general are relatively flat. The polygon centre is moist but without open water conditions. The vegetation cover differentiates the polygon walls, which is dominated by mosses from the polygon centre (sedges). This leads to an abrupt transition from the polygon wall to the centre. The moss cover of the polygon wall is often cut by frost cracking activity. The frost cracks are clearly visible and the troughs above the ice wedges may be up to 10 cm wide and 20 cm deep. On two polygon walls, secondary frost cracks were observed. The active layer is usually between 0.2 m to 0.6 m thick, mainly varying around 0.35 m. With a height of approximately 12 m, it is situated relatively high above sea level and, logistically important, relatively close to the camp. A thin snow cover can be expected for the site, since at this height the snow may be easily drifted by wind. Therefore, the heat insolation of the snow cover, which prevents frost cracking (MacKay 1993), can be assumed to be small. This hypothesis will be tested with a snow depth sensor installed near the "study polygon".

For the survey of the polygon carried out in co-operation with Waldemar Schneider, a laser tachymeter (type Trimble 3300) was used. The height of the reflector was 1.4 m; 5 cm were added to every measurement because of the subsidence of the reflector into the vegetation cover. First, a measuring field of 24 x 34 m covering the study polygon and parts of the neighbouring polygons was surveyed with a grid size of 2 x 2 m. This resulted in 204 measuring points. For all of them, the relative x-, y-, z-coordinates of the polygon surface as well as the active layer depth were retrieved relative to a zero angle (Stolb trigonometric point) and a fix point (an elevated point in a neighbouring polygon). In the same way, the polygon walls of the study polygon were mapped with additional 157 points with a special emphasis on the position of frost cracks, highest elevations of the polygon wall as well as the border between polygon wall and centre. Moreover, the position of 22 steel poles was

determined. These poles were inserted into the permafrost as markers for the experiments on recent frost cracking. This results in a total number of 383 measuring points for the study polygon. In Figure 3-23, the results of the survey of the polygon are displayed.

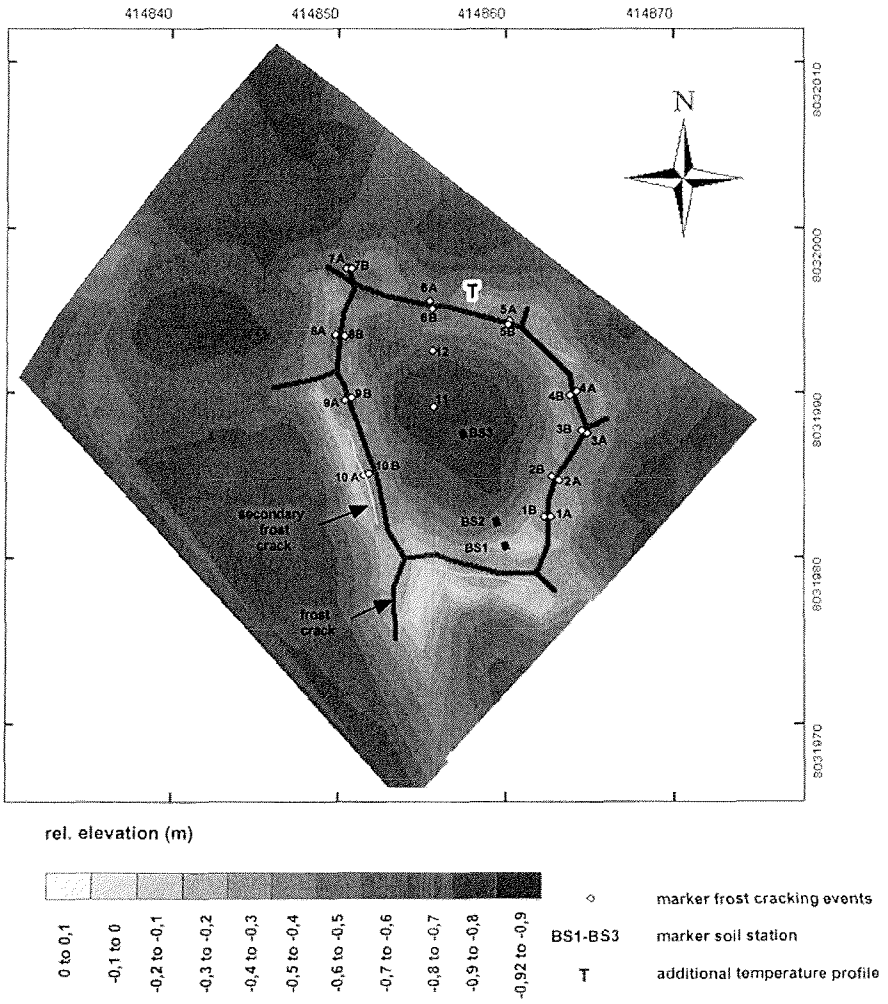

Figure 3-23. Results of the survey of the study polygon with the exact position of the steel poles for frost cracking experiments.

3.3.4 Frost cracking experiments

Studies on recent ice wedge growth were carried out for one selected polygon on the 1st Lena river terrace of Samoylov Island in order to first identify, if in any place recent frost cracking had taken place, and if so, at what time and to what extent. The climatic conditions occurring during frost cracking indicate the boundary conditions (concerning air and soil temperatures, temperature gradients in the sediment, soil moisture, air humidity, wind direction and speed, precipitation and snow cover) necessary for recent ice wedge growth. It must be stressed again that the combination of soil and weather stations with the experiments on recent cryogenesis is optimal for this kind of studies.

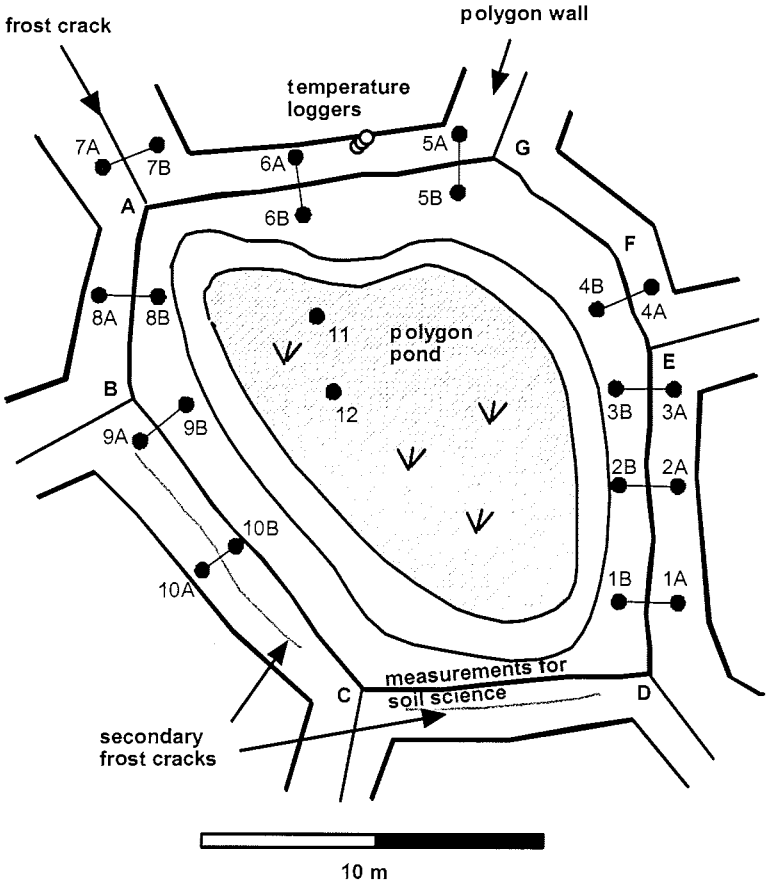

Figure 3-24. "Study polygon" with experimental set-up for the detection of recent frost cracking processes. Black dots represent steel poles, white dots temperature data loggers in the active layer and the uppermost part of permafrost.

For the identification of frost cracking processes, 10 different experiments were carried out. The above mentioned 22 steel poles were used for these recent cracking experiments - only two poles for survey purposes. The general set-up of every single experiment consists of two steel poles (e. g. 1A and 1B) inserted to the permafrost on both sides of a frost crack (see Figures 3-25, 3-26).

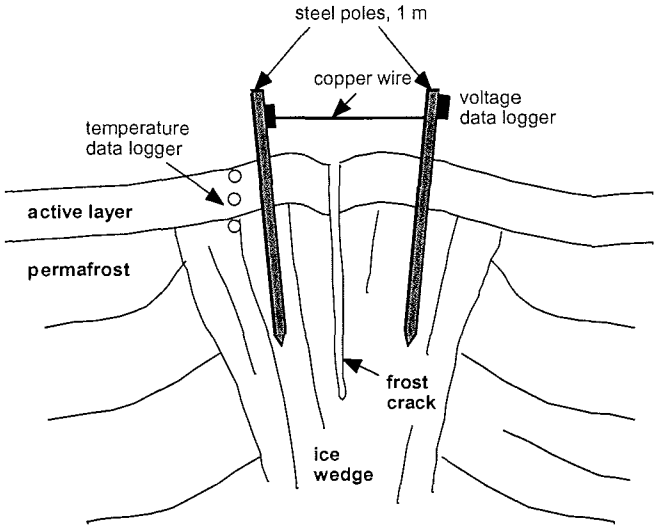

Figure 3-25. Frost cracking experiments on Samoylov Island. A breaking cable connected to a data logger is stretched between two steel poles for the identification of frost cracking and its timing. Temperature loggers are used to derive temperature gradient in the soil.

The two steel poles were 1 m long, and inserted as deep as possible to the permafrost, in general between 30 cm and 45 cm. This depends evidently on the depth of the active layer, which also varies between 30 cm and 45 cm (measured on August 6 and 7, 2002). The length of all 22 steel poles, the height of the poles above surface and the active layer depth as well as the distance to two fix points (poles 11 and 5b) was measured (Table 3-13). Additionally, the respective depth every stick penetrates the permafrost was calculated.

Between two steel poles, a breaking cable was installed. Three different kinds of copper wires were used (Cu wire, 0.5 mm; Cu two-wire braid (HO3VH-H, 2x0.75), Cu single-wire braid (HO3VH-H, 1x0.75). Copper wire was selected, because this metal has a high coefficient of linear extension of about $16.1.10^{-6}$/K. It was assumed that the copper wire may bear intraday temperature variations as well as the cooling in winter without cracking, but breaks when a sudden rupture of about 0.5 cm, e. g. frost cracking, takes place. Tabasco was used to make the cables unattractive for animals.

Table 3-13. Characteristics of 22 steel poles: length, height above surface, distance to fix points (poles 11 and 5b) and depth in permafrost as well as the active layer depth.

Steel pole Nr.	steel pole length (cm)	steel pole above surface (cm)	steel pole in permafrost (cm)	active layer depth (cm)	steel pole distance to M11 (cm)	steel pole distance to 5b (cm)
1a	95	22	39	34	957,4	-
1b	100	22	45	33	930,5	1171,8
2a	100	20	39	41	866,7	-
2b	100	23	42	35	818,8	944,0
3a	92	23	29	40	921,4	-
3b	100	24	37	39	887,2	763,2
4a	100	22	43	35	846,5	-
4b	100	25	39	36	806,7	552,3
5a	93	26	26	41	681,6	-
5b	100	26	42	32	660,2	0,0
6a	92	27	32	33	635,4	-
6b	100	25	38	37	589,3	465,0
7a	100	27	33	40	977,0	-
7b	100	24	40	36	965,0	991,1
8a	92	20	37	35	727,5	-
8b	100	26	34	40	679,3	977,2
9a	98	21	38	39	531,8	-
9b	100	19	42	39	492,0	1030,4
10a	99,5	24	32,5	43	581,1	-
10b	100	25	34	41	555,6	1217,3
11	100	55	16	29	0,0	660,2
12	100	43	22	35	339,3	472,8

Six (out of ten) experiments were equipped with voltage data loggers (type ESIS Minidan Volt) connected to the breaking cables. The loggers started measuring at an amperage of 10 μA and a voltage of 270 mV every 20 minutes from the moment of installation until the moment of frost cracking. If the cable does not break (because no frost cracking took place or for any other reason), the loggers will continue to measure until October 8, 2003. By that, the information if frost cracking takes place should be derived as well as the precise moment of frost cracking.

In Figure 3-26, one of these experimental set-ups is displayed. The breaking cable is connected to the data logger and fixed to the pole. On the other side, the cable is attached to a brass clamping fixture (Figure 3-27). The tension of the wires was increased by counting the revs (or turnarounds) of the nut (type M5) on the thread rods. First, breaking experiments were carried for every cable type. For this purpose, the cables were stretched until rupture and it was found that the number revs are mainly a function of the cable length. Therefore, maximum revs were calculated for every cable type and different initial tensions were then applied to the wires (Table 3-14 and 3-15).

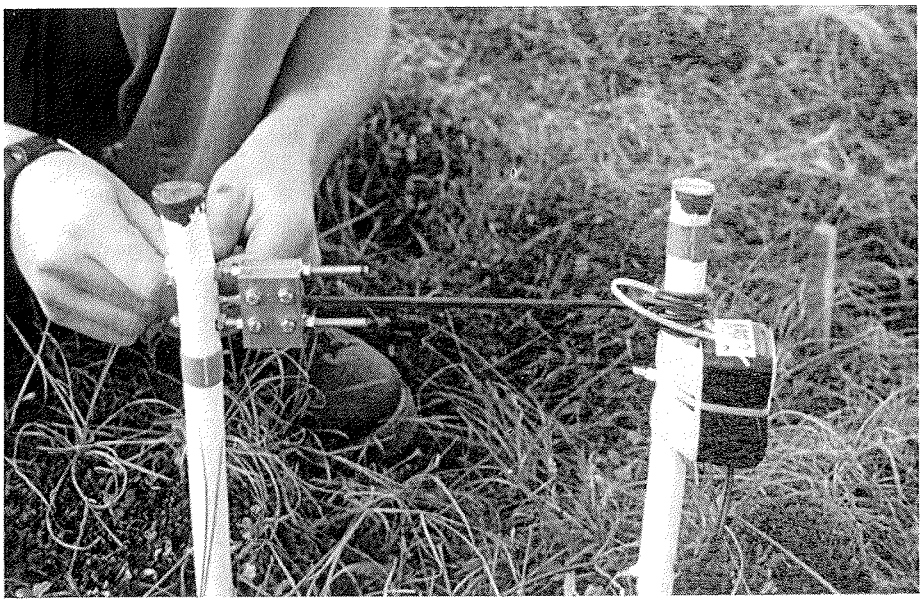

Figure 3-26. Frost cracking experiment 5A-5B with Voltmeter 5. A copper two-wire braid with a length of 181 mm was used. After 32 revs of the nut M5 on the threads, the wire was 184 mm long.

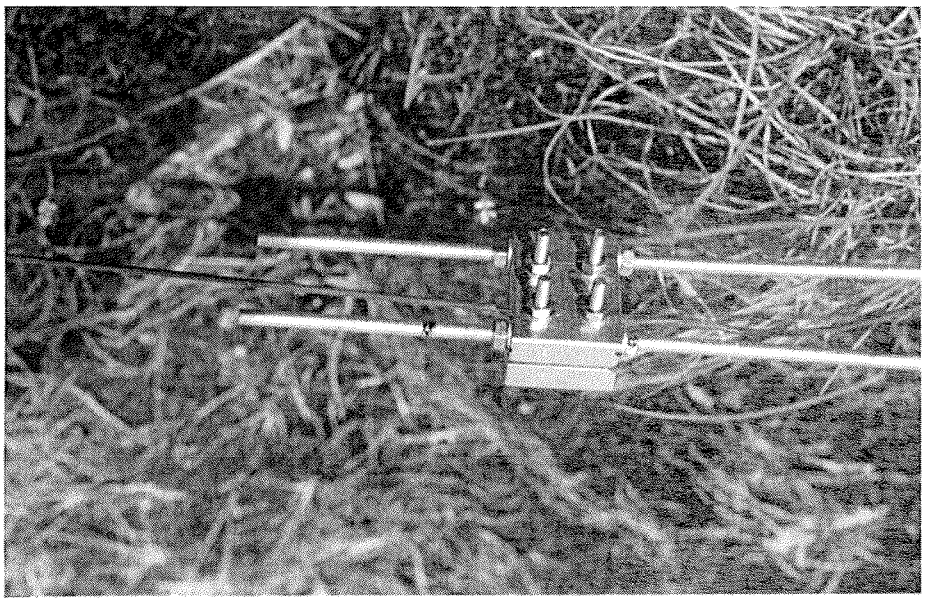

Figure 3-27. A closer view how a copper single-wire braid was fixed to a brass clamping fixture. The tension was regulated by nuts M5 on two thread rods.

Table 3-14. Ten stretching experiments with applied cables and voltmeters, the lengths of the breaking cables between the poles A and B before spanning the cable (1) and after the cables were stretched (2) with a control on September, 4th. The tension of the wires was increased by counting the revs (or turnarounds) of the nut (type M5) on the thread rod. In some cases, the tension was raised on September, 4th. For every cable type, maximum revs were calculated according to its length by means of the breaking experiments.

Marker	Volt-meter	Cable type	Cable length (9.8)		Diffe-rence	Control (4.9)	Turn-arounds	Turn-arounds	Max.
			1	2		2	(9.8)	(4.9)	
1A-1B	None	Cu two-wire braid (HO3VH-H, 2x0.75)	316	321	-5	336 (new)	35	38	75
2A-2B	2	Cu wire, 0.5 mm	263	278	-15	274	24	26	35
3A-3B	None	Cu wire, 0.5 mm	298	301	-3	304 (new)	10	16	40
4A-4B	1	Cu wire, 0.5 mm	359	376	-17	376	30	30	50
5A-5B	5	Cu two-wire braid (HO3VH-H, 2x0.75)	181	184	-3	186	32	32	45
6A-6B	3	Cu single-wire braid (HO3VH-H, 1x0.75)	379	384	-5	386	28	28	38
7A-7B	None	Cu single-wire braid (HO3VH-H, 1x0.75)	296	298	-2	298	10	14	30
8A-8B	4	Cu single-wire braid (HO3VH-H, 1x0.75)	447	453	-6	453	25	25	45
9A-9B	6	Cu two-wire braid (HO3VH-H, 2x0.75)	343	348	-5	350	35	35	85
10A-10B	None	Cu two-wire braid (HO3VH-H, 2x0.75)	216	220	-4	221	38	38	54

In order to understand how the low temperatures in winter penetrate the active layer and the permafrost, temperature loggers were introduced to the permafrost (Figure 3-23 to 3-25) to derive the temperature gradients necessary for frost cracking activity. The loggers were inserted every 15 cm in depths of 0.05 m, 0.2 m, 0.35 m and 0.5 m. In this place the active layer is 0.4 m thick.

Table 3-15. Ten stretching experiments with the respective distances (in mm) between the poles A and B measured from the a.) top to the top, b.) tape mark to the tape mark and c.) bottom to the bottom, before spanning the cable (1) and after the cables were stretched (2).

Marker	Distance Top-Top		Difference	Distance Tape-Tape		Difference	Distance Bottom-Bottom		Difference
	1	2		1	2		1	2	
1A-1B	383	358	25	393	372	21	400	386	14
2A-2B	479	465	14	473	457	16	465	454	11
3A-3B	360	351	9	364	361	3	348	343	5
4A-4B	421	406	15	427	415	12	418	407	11
5A-5B	255	231	24	257	240	17	244	236	8
6A-6B	455	435	20	447	429	18	423	411	12
7A-7B	362	351	11	362	349	13	356	348	8
8A-8B	521	503	18	517	509	8	504	498	6
9A-9B	404	380	24	412	392	20	424	404	20
10A-10B	284	259	25	287	264	23	308	289	19

A second attempt to measure frost cracking processes was undertaken by means of a Sonic Ranging sensor (type SR50). This experiment was installed near experiment 3A-3B (Figure 3-28). The ultrasonic sensor measures the distance from a sensor to a target by transmission of ultrasonic sound pulses and measuring the echoes coming back from the target. The time from transmission to the return of the echo is the basis for the distance measurement (minimum distance 0.5 m). This method is most commonly applied to the measurement of snow depths and water levels. Temperature compensation is necessary for the distance reading, because the speed of sound in air varies with temperature. The accuracy of the absolute distance measurement is ±1cm or 0.4% of the distance to the target (in our case about 0.6 m). However, the resolution is measured with a much higher precision of 0.1 mm. Consequently, a change in the distance between sensor and target (such as a frost cracking event) will be detected with high precision.

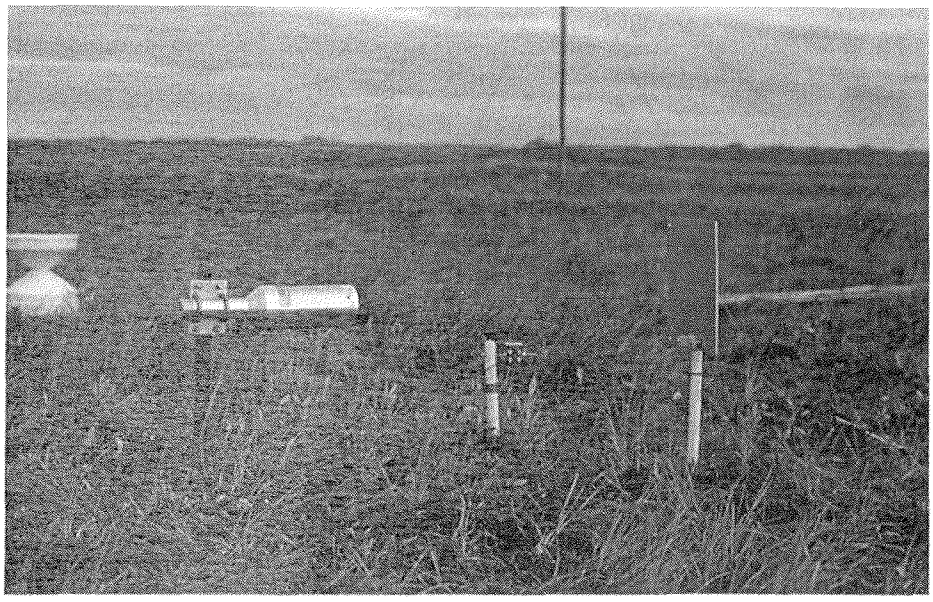

Figure 3-28. The experimental set-up of the detection of frost cracking processes by means of a Sonic Ranging sensor (type SR50).

The knowledge of the existence and timing of recent frost cracking activity is important for the second part of the studies, i. e. to trace recent ice veins (by means of colored spores) in order to attribute an ice vein to the discrete year of its formation. This information derived from ice veins of several years is necessary for a precise calibration of a stable hydrogen and oxygen isotope thermometer for ice wedges. The identification of frost cracking activity provides the information if at one site digging for ice veins has the chance to be successful. For this purpose, recent ice veins of several years will be sampled (after some years), measured for stable isotopes and related to the climatic situation in the year of its formation. In general, it is difficult to know the age of an ice vein. Tritium analyses have shown to be a useful tool (Dereviagin et al. 2002) to decide, whether frost cracking can be considered as active or inactive. However, the discrete year of formation of an ice vein is not derived. The sampling of recent ice veins in early summer at the bottom of the - still frozen - active layer is misleading, since these veins may have been influenced by the surrounding sediment and segregated ice, which is formed in a different way and, thus being chemically and isotopically completely different. Consequently, a tracer experiment is an elegant way to trace the age of an ice vein in order to assign it to the respective climatic situation.

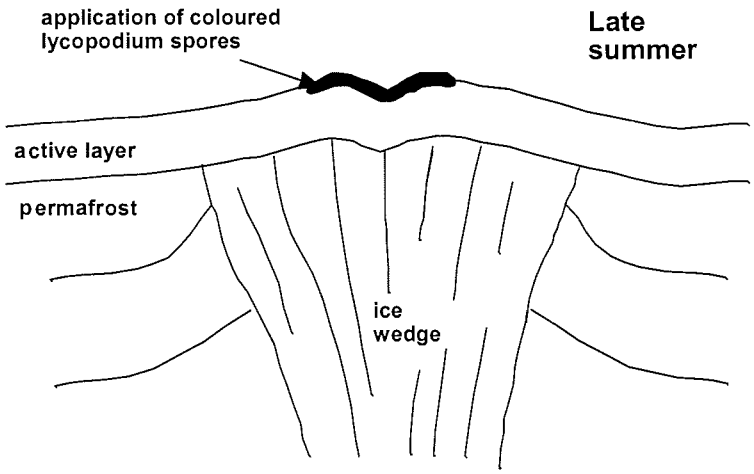

Figure 3-29. Application of *lycopodium* spores to the polygon.

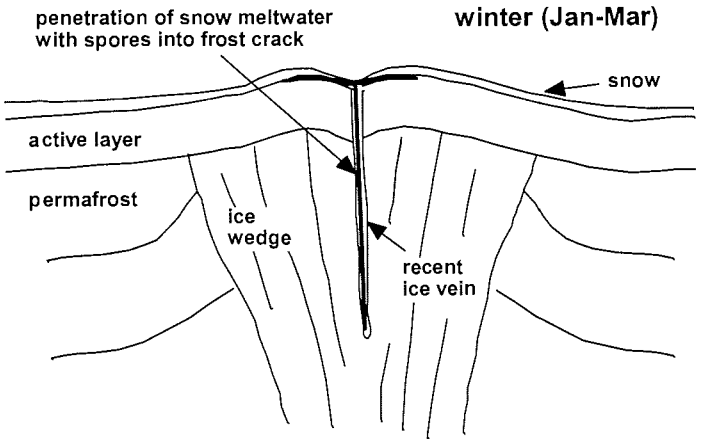

Figure 3-30. Penetration of *lycopodium* spores into the frost crack.

In late summer, 1 kg of red colored *lycopodium* spores was applied to the polygon walls, especially to the troughs in order to avoid drifting of the spores by wind (Figure 3-29). After application, the spores were expected to be covered by the first snow as soon as possible.

In winter, frost cracking takes place and some of the spores may fall into the frost crack. In spring, when the snow cover starts melting, more spores are washed into the crack. Since the water freezes immediately, the spores will be conserved as a thin layer in the newly formed ice vein. This is due to the

movement of particles along the freezing front, e. g. towards the centre of the frost crack (Figure 3-30).

After three to five years, the frost cracking activity of every crack can be evaluated. This will give the chance to find a promising digging location for recent ice veins .

3.4 Seasonal progression of thaw depth dependent on mircrorelief

Lars Kutzbach, Ekatarina N. Abramova and Waldemar Schneider

3.4.1 Background

The topography of the Lena Delta is fairly flat, but well-structured by a prominent microrelief, caused by the development of ice-wedge polygons. Most common are low-centred polygons. The depressed centres of these polygons are surrounded by elevated rims, which are situated above the ice-wedges. The prominent microrelief causes a high spatial heterogeneity of soil properties on the small scale of decimeters to meters. In order to up-scale results of process studies to the landscape scale, it is necessary to describe and quantify the spatial hetorogeneity of soils. A major factor for all physical and biological processes in permafrost soils is the active layer depth (=thaw depth).

3.4.2 Projects

A thaw depth monitoring programm was conducted on Samoylov Island in the period June 10 – August 30. An investigation site of 28 m x 18 m was established close to the new soil survey station (Chapter 3.2, Figure 3.12). A grid of 150 measurement points in intervals of 2 m x 2 m were marked and mapped with a laser tachymeter (type Trimble 3300). At every measurement point, thaw depth was measured every 3 to 7 days by driving a steel rod into the unfrozen soil until the hard frozen sediments were encountered.

3.4.3 First results

Contour maps of the microrelief at the thaw-depth monitoring site and the spatial variability of the mean thaw velocity during the study period are shown in Figures 3-31 and Figure 3-32.

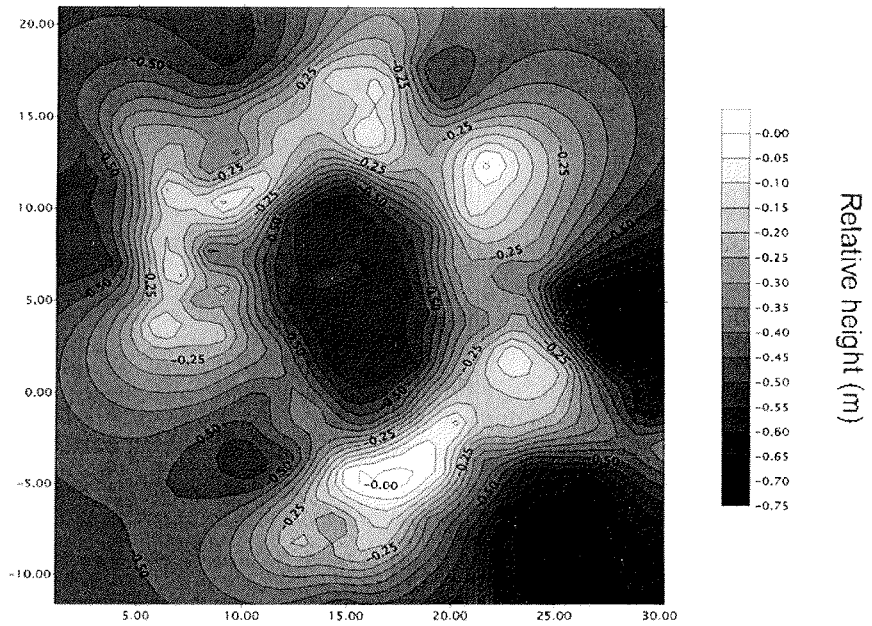

Figure 3-31. Contour map of the microrelief at the thaw-depth monitoring site, Samoylov Island. Units of the coordinate system are meters.

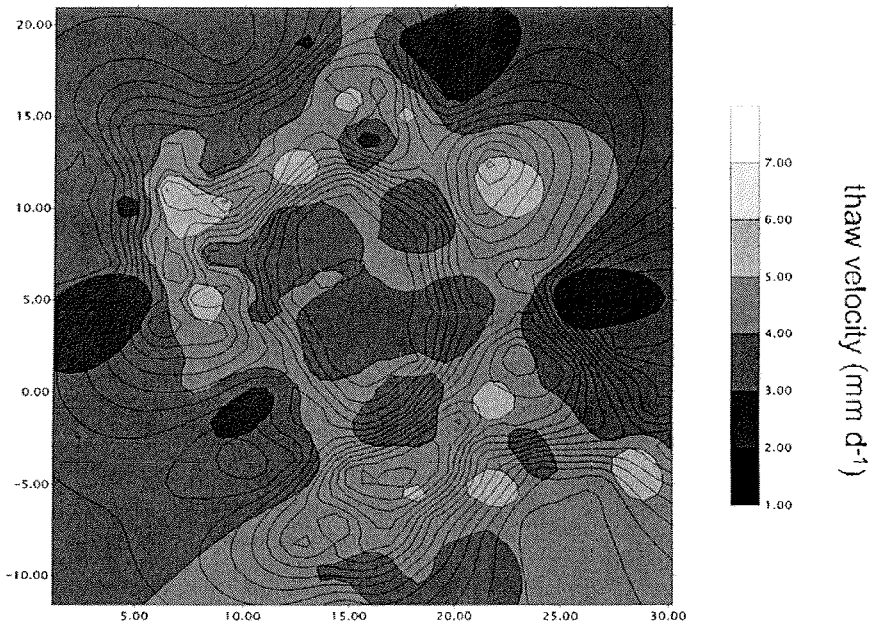

Figure 3-32. Mean thaw velocity during the study period June 10 – August 30 at the thaw depth monitoring site, Samoylov Island. The contour lines of the microrelief (Figure 3-31) are indicated for orientation.

3.5 Patterned ground lakes and their function as sources of atmospheric methane

Oliver Spott, Svenja Kobabe, Lars Kutzbach, Dirk Wagner and Eva-Maria Pfeiffer

3.5.1 Introduction

Lakes are important sources of atmospheric methane (CHANTON et al. 1989; THEBRATH 1991; MICHMERHUIZEN & STRIEGL 1996; SEMILETOV et. al. 1996; PHELPS et al. 1998; DUCHEMIN et al. 1999; MAKHOV et. al. 1999; HUTTUNEN et al. 2001). Permafrost landscapes of the Lena-Delta are often covered by polygonal tundra and patterned ground lakes, respectively. Up to now little is known about the contribution of those small but widespread lakes regarding their function as sources of atmospheric methane. Thus, surveying patterned ground lakes is a necessary part of investigations for estimating both global and local methane fluxes.

3.5.2 Objectives and Methods

In this study, patterned ground lakes were investigated in order to measure their methane fluxes toward the atmosphere. Following questions were set up.

1. How much methane is emitted from the investigated lakes?
2. Which meaning has the path of emission (plant mediation, diffusion, ebullition)?
3. Which habitat parameters (sedimentary, hydrological and atmospheric parameters) are crucial for the emission behavior?

Measurements of methane emissions were carried out by two different types of floating chambers (three of each type) from beginning of July 2002 to beginning of September 2002. Chamber type I was used for measuring methane emissions by plant mediation. The measuring field was stationary and placed within the edge of the lakes where vegetation penetrates the water surface. Plants enclosed by the chamber were *Carex aquatilis* in case of lake IS, *Carex a.*, *Carex chordorhiza* and *Potentilla palustris* concerning PS1 and *Arctophila fulva* within PS2 (Figure 3-33) The enclosure time for plant mediated emission measurements was 30 minutes. Chamber Type II was stationary installed within a non-vegetated lake area (except water mosses at the lake bottom) for measuring both diffusion and ebullition. This type consists of a chamber (diffusion measurements) likewise type I and an additional assembled pyramid below (ebullition measurements) (Figure 3-33). The enclosure time for emission measurements was approx. 48 h. Gas samples from Type I and Type II (concerning only diffusion) were taken by gastight glass receptacles (Gasmaus) (cf. PFEIFFER et al. 1999). Ebullition samples were taken by syringes through a rubber stopper and were immediately conserved in gastight glass tubes filled with saturated NaCl-solution. Emission measurements by the different chamber types were carried out in a time frame of 12.00 to 16.00 o´clock in an alternating

2-day-rhythm. All methane gas analysis were conducted by a gas chromatograph (CP 9003).

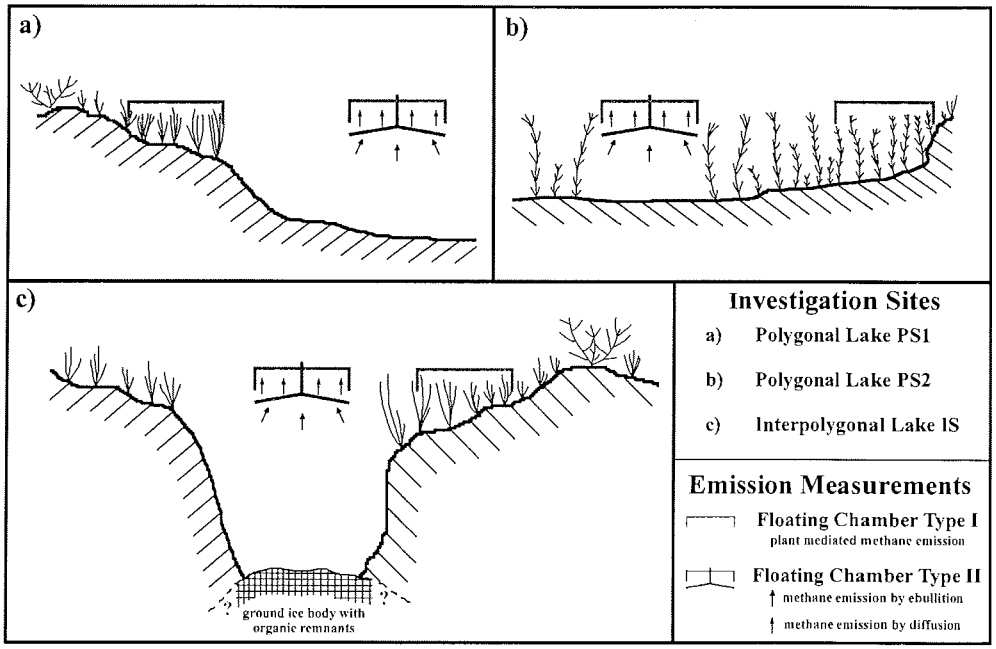

Figure 3-33. Application of floating chambers for methane emission measurements.

Accompanying the methane gas sampling, measurements of permafrost depth, water level, sediment temperature, water temperature, dissolved oxygen (OXI 325 / WTW company) and climatic parameters (temperature, moisture, pressure, wind direction and velocity) where conducted on a daily basis.

Dissolved methane in lake water was analyzed in intervals of 10 to 14 days (Table 3-16). Water samples were collected in gastight glass receptacles (3 parallel samples). Previously an adequate amount of NaCl-salt was weighted into the receptacles to force dissolved methane into headspace. Gas concentrations were analyzed after 1 to 2 days of storage at a room temperature of approx. 18 °C.

For the investigation of lake sediments, 4 drilling cores were captured from PS1 and PS2, respectively (Appendix 3-2). One core in each case were cut up for measuring methane content. Fresh sediment samples (15 to 25 g) were weighted into a 50 ml glass jar (3 parallel samples). 20 ml saturated NaCl-solution was added subsequently to force methane gas into headspace. The glass jar was closed with a septum and a screw cap and gas concentrations were analyzed after one day of storage under cold conditions (0 to 2 °C). The 6 remaining drilling cores were used for analyzing water content, raw density, grain size, pH-value, TOC and DOC as well as for experiments concerning methane production and methane oxidation (Appendix 3-2). For surveying

methane gas enclosed in the ground ice body of lake IS (Figure 3-33), one drilling core of ice was obtained and gas concentrations were analyzed (likewise dissolved methane analysis).

For a general description of investigated sites pH-values of the lakes were analyzed. Vegetation was mapped within an area of 2 to 3 m² spreading from the surrounding lake area to the shallow edge of the lakes. Samples of mosses and lichens were taken for later characterization (Appendix 3-1). Morphology and position of the lakes were surveyed by a tachymeter device.

3.5.3 Investigation Sites

Samoylov Island, as a representative example for Polygonal Tundra, is covered by a large number of small patterned ground lakes. Based on the polygonal network of ice-wedges, superficial depressions enable the formation of patterned ground lakes, that can be distinguished in polygonal and interpolygonal lakes. The first type is formed within a lowered center of an ice-wedge-polygon. Interpolygonal lakes are formed between the polygons within lowered frost-cracks.

During the Expedition "Lena-Delta – New Siberian Islands 2002" two polygonal (PS1 and PS2) and one interpolygonal lake (IS) were investigated. All three lakes are situated close to each other in the middle of Samoylov Island in an area of degenerated ice-wedge-polygons. PS1 is nearly round shaped, approximately 15 m in diameter and 0.9 to 1.0 m in depth. PS2 is of an elliptical shape with an a-axis of approx. 18 m and a b-axis of approx. 9 m. The depth reaches 0.6 to 0.7 m. The lake IS is of an elongated network structure with a maximum extension of approx. 40 m. The depth exceeds 1.2 m in some parts .

The investigated lakes are characterized by some remarkable differences. The lake area of PS2 is densely covered by *Arctophila fulva* grass, whereas this is completely absent within PS1 and IS. Lake IS showed large ground ice bodies (ice wedge?). The upper lake sediments of PS1 and PS2, however, were unfrozen during the field work.

3.5.4 Preliminary results and discussion

Methane emission rates within the vegetated edge of investigated lakes show mean values of 58.6 ± 12.5 mg m^{-2} d^{-1} for PS1, 41.7 ± 13.6 mg m^{-2} d^{-1} for PS2 and 34.2 ± 8.0 mg m^{-2} d^{-1} for IS. The maximum rate of 88.7 ± 0.8 % mg CH_4 m^{-2} d^{-1} was measured on 14th of August for PS1. The minimum rate of 13.7 ± 5.0 % mg CH_4 m^{-2} d^{-1} was measured on 31st of July for PS2 (Figure 3-34).

Relatively high rates are caused by mainly plant mediated methane emissions. The amount of emitted methane depends on composition and density of vegetation cover. Plant mediated methane emissions could be proven for *Arctophila fulva* (Figure 3-34). and *Carex aquatilis* (not depicted) as dominant species within the vegetated edges of the lakes. Additionally, sediment temperature shows a distinct influence of emission strength. In case of PS1 the temperature (5 cm depth) correlates significantly (r = 0.80) with the methane

emission rate. PS2 and IS show less dependency on sediment temperature, but a weak seasonal trend of the emission strength.

The distinct variability of emission rates from vegetated edges of the lakes is assumed to be mainly caused by the continuous change in air temperature and its feedback in microbial activity as well as plant mediation. The higher emission rates of PS1 may be caused by the density and composition of vegetation (see investigation sites) at the measuring field which acts positive on nutrient cycles and methane formation.

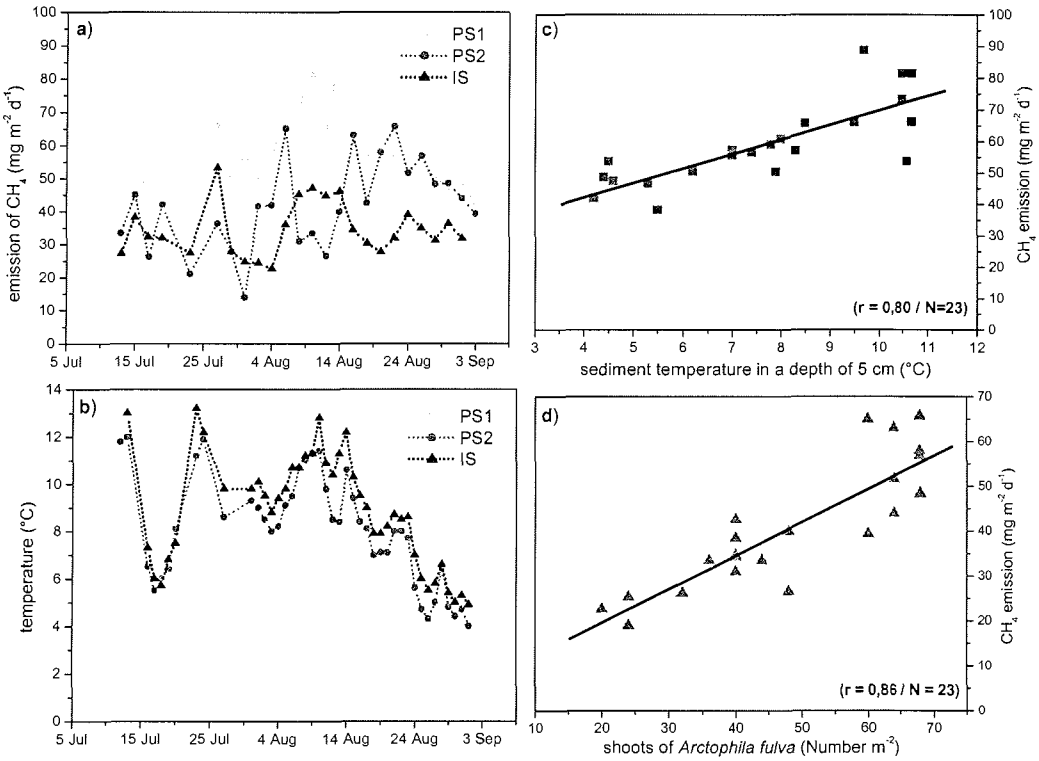

Figure 3-34. Preliminary results of methane flux measurements from vegetated edges of the lakes. (a – methane emission rates; b – sediment temperature in depth of 5 cm; c – temperature dependence of methane emission (PS1); d – plant mediated methane emission by *Arctophila fulva* (PS2))

Methane emission rates from water surface by diffusion show mean values of 1.9 ± 1.1 mg m-2 d-1 for PS1, 3.0 ± 1.6 mg m-2 d-1 for PS2 and 2.2 ± 2.0 mg m-2 d-1 for IS. The maximum and minimum rate were measured for lake IS on 16th of July with 9.9 ± 5.0 % mg m-2 d-1 and on 21st of August with 0.51 ± 1.3 % mg m-2 d-1, respectively. Lake IS shows highest diffusion rates during July whereas PS1 and PS2 increase their diffusion rates at the end of August (Figure 3-35). In case of lake IS the ground ice body is the methane source. Thus, highest emission rates occur in spring time when methane enriched ice

from the freezing period of the previous year is melting. Similar effects were already discussed by Phelps (1998) and Michmerhuizen & Striegl (1996). Diffused methane concerning PS1 and PS2 was currently produced by methanogens within the lake sediment. Thus, highest emission rates occur at the summer and early autumn when microbial activity reaches its maximum.

The diffusion behavior towards the atmosphere shows repeating impulses with emission rates up to 7 times of the mean value (Figure 3-35). Following processes are considered to be causal. Regarding air temperature, higher rates occur after rapid temperature decreases (not depicted). Subsequently the vertical water temperature becomes more homogenous and bottom water enriched with dissolved methane (Table 3-16) can be moved easier to the air-water interface by mass transport. Additionally, diffusion at the air-water interface is intensified during a low gradient between water and air temperature.

Methane emission rates from water surface by ebullition show most distinct differences between the lakes. With mean values of 11.7 ± 8.1 mg m^{-2} d^{-1} only lake PS2 can be considered as important for methane emissions by ebullition. The maximum and minimum rate were measured on 23rd of August with 30.24 ± 0.3 % mg m^{-2} d^{-1} and on 18th of July with 1.27 ± 5.0 % mg m^{-2} d^{-1}, respectively. Emission rates of lake PS1 and IS were continuously lower than 1 mg m^{-2} d^{-1}. In contrast to PS2 diffusion from water surface is the dominant path of emission (Figure 3-35).

Differences of ebullition are caused by the volume and methane content of released bubbles. Mean volume of captured bubbles show 3.8 ± 2.4 ml m^{-2} d^{-1} for PS1, 40.0 ± 20.4 ml m^{-2} d^{-1} for PS2 and 3.1 ± 2.7 ml m^{-2} d^{-1} for lake IS. The methane content, however, seems to be of greater influence. Bubbles released from PS2 show a distinct increase up to 50 % methane towards the end of the season, which remains rather constant. Captured bubbles from PS1 show lower methane contents. Only in mid of July and mid of August some higher values up to 19 % were reached. Different conditions for methane formation and/or oxidation within the sediment are considered to be responsible for measured differences. Bubbles from lake IS show lowest methane contents. The bubble release is considered to work similar to the diffusion where melting ice regulates the emission (Figure 3-35).

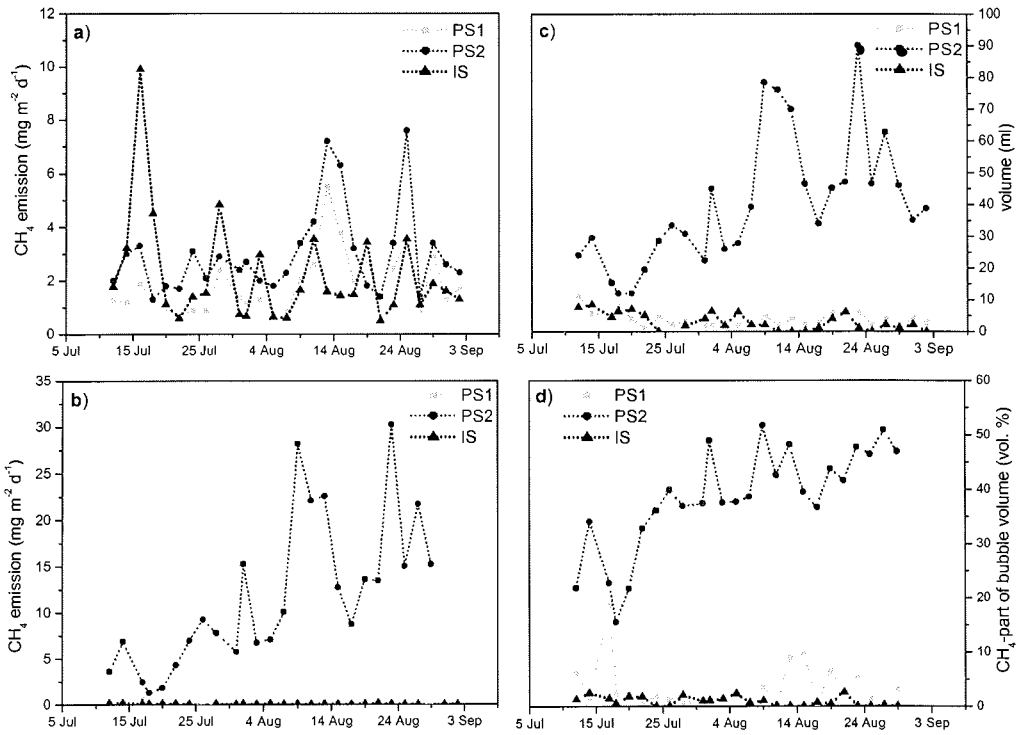

Figure 3-35. Preliminary results of diffusion and ebullition flux measurements from water surface. (a – methane emissions by diffusion; b – methane emissions by ebullition; c – volume of released gas bubbles; d – methane concentration of released gas bubbles).

Table 3-16. Dissolved methane in lake water.

Date of sampling	*surface water (µmol/L)*			*bottom water (µmol/L)*		
	PS1	PS2	IS	PS1	PS2	IS
14. Jul. 2002	0.40	0.98	1.17	0.48	41.09	33.05
24. Jul. 2002	0.34	1.56	1.08	0.38	3.09	32.68
3. Aug. 2002	0.97	1.26	3.97	1.10	0.87	1.48
19. Aug. 2002	1.49	1.50	1.12	1.34	1.99	3.01
31. Aug. 2002	1.45	2.51	2.02	1.83	2.38	2.81

In general, methane emissions from vegetated edges of patterned ground lakes occur similar to methane emissions from wet polygons as described by PFEIFFER et al. (1999; 2000) and WAGNER et al. (2001). Emission by plant mediation acts as the most efficient path for methane gas release into the atmosphere. Thus, vegetated edges of lakes are most important methane sources within investigated lakes. Regarding the efficiency, diffusion as well as

ebullition only serve as ancillary paths of methane release towards the atmosphere. Only in few cases methane emission rates reach values of plant mediated emissions. However, considering the spatial distribution of lake areas unbiased by plant mediation the importance of diffusion and ebullition should be assumed to be higher.

3.6 The flora of Samoylov Island – documentation

Lars Kutzbach, Günther Stoof and Anna Kurchatova

3.6.1 Background

The flora composition in the Lena Delta is comparatively rich (373 vascular plant species, 106 moss species and 74 lichen species). There is a combination of arctic, hyparctic and boreal flora elements. Most of the Lena Delta (and so our study site on Samoylov Island) is situated in the northern belt of the geobotanical subregion of the subarctic tundra. Only the most northern areas of the delta belong to the true-arctic tundra subregion (Aleksandrova 1980).

A variety of multidisciplinary ecological and paleoecological studies are conducted on Samoylov Island and the neighbouring islands in the framework of joint projects of the Alfred Wegener Institute and several Russian partner institutions. For many of these studies, for instance investigations on soil genesis or the carbon budget of tundra landscapes, a profound knowledge of the vegetation composition is of great value. Phytosociological studies of present ecosystems are crucial for the paleoecological interpretation of plant remnants in permafrost or lake sediment cores.

3.6.2 Projects

In summer 2002, we conducted two botanical projects:

(1.) We started to establish a digital image database of plants of the study area with a focus on flowering vascular plants. 94 vascular plants, 8 mosses and 8 lichens were photographed and identified. Vascular plants were determined according to Polunin (1959). Mosses and lichens were determined using a reference herbarium prepared by M. Zhurbenko and I. V. Czernyadeva (Komarov Botanical Institute, St. Petersburg). A list of all plants that were included until now in the photo database is provided in Table 3-17 (n = 110). Two exemplary photographs are shown in Figure 3-36 and Figure 3-37.

This documentation of the flora of the central Lena Delta will be published as internet page. It shall help future students, scientists, and other visitors of the region to recognise the plants of this peculiar landscape.

Table 3-17. List of species included in photo database.

vascular plants 1	vascular plants 2	mosses
Alnus crispa	Pedicularis sudetica	Aulacomnium palustre
Alopecurus alpinus	Pedicularis villosa	Aulacomnium turgidum
Antennaria spec.	Poa alpigena	Cinclidium spec.
Arctagrostis arundinacea	Poa arctica	Dicranum elongatum
Arctagrostis latifolia	Polemonium acutifolium	Dicranum spec
Arctophila fulva	Polygonum bistorta	Limprichtia revolvens
Arctostaphylos alpina	Polygonum Laxmanii	Sphagnum spec.
Arenaria arctica	Polygonum viviparum	Timmia austriaca
Arenaria lateriflora	Potentilla palustris	
Armeria maritima	Pyrola rotundifolia	
Artemisia borealis	Pyrola secunda	
Astragalus alpinus	Ranunculus lapponicus	
Astragalus frigidus	Rhodiola rosea	**lichens**
Betula nana	Rumex arcticus	Cetraria laevigata
Caltha palustris	Rumex graminifolius	Cladonia spec
Campanula rotundiflora	Salix glauca	Dactylina arctica
Cardamine tenuifolia	Salix nummularia	Flavocetraria cucullata
Carex aquatilis	Salix polaris	Peltigera spec.
Carex chordorrhiza	Salix pulchra	Stereocaulon alpinum
Carex ensifolia ssp. arctisibirica	Salix reptans	Stereocaulon rivolorum
Carex maritima	Salix reticulata	Thamnoila vermicularis
Carex rariflora	Sanguisorba officinalis	
Cassiope tetragona	Saussurea alpina	
Castilleja pallida	Saussurea nuda	
Chrysosplenium alterniflorum	Saxifraga bronchialis	
Delphinium cheilanthum	Saxifraga caespitosa	
Deschampsia caespitosa	Saxifraga cernua	
Draba nivalis	Saxifraga hirculus	
Draba oblongata	Saxifraga hieracifolia	
Dryas octopetala	Saxifraga punctata	
Epilobium spec.	Tanacetum bipinnatum	
Equisetum arvensis	Tofielda coccinea	
Equisetum variegatum	Tofielda pusilla	
Eriophorum angustifolium	Trifolium repens	
Eriophorum medium	Trisetum sibiricum	
Eriophorum scheuchzeri	Vaccinium uliginosum	
Eriophorum vaginatum	Vaccinium vitis-idaea	
Habernaria viridis	Valeriana capitata	
Hedysarum hedysaroides		
Hieracium alpinum		
Hippuris vulgaris		
Juncus arcticus		
Koeleria asiatica		
Lagotis glauca		
Ledum paluste		
Luzula confusa		
Luzula nivalis		
Luzula tundricola		
Myosotis alpestris		
Myosotis spec.		
Oxytropis arctica		
Papaver radicatum		
Parnassia palustris		
Parrya nudicaulis		
Pedicularis dasyantha		
Pedicularis oederi		

Table 3-18. Moss communities at different habitats. – Sample ID, habitat, species.

ID	habitat	species		
		dominant	admixed	single
	Samoylov			
I-1	middle floodplain	Tomentypnum nitens		
I-2	- / -	Aulacomnium palustre		
I-3	- / -	Tomentypnum nitens		
I-4	- / -	Tomentypnum nitens		
I-5	- / -	Aulacomnium palustre	Tomentypnum nitens	
II-1-3	high floodplain (microlow)	Limprichtia revolvens	Calliergon giganteum, Meesia uliginosa	Aulacomnium turgidum, Orthothecium chryseum
II-4	(between m/low and m/high)	Ceratodon purpureus	Calliergon giganteum, Limprichtia revolvens	
II-5	(between m/low and m/high)	Tomentypnum nitens	Campylium stellatum, Limprichtia revolvens	
II-6	(microhigh)	Aulacomnium palustre	Tomentypnum nitens, Distichium capillaceum	Campylium stellatum
II-7	(microhigh)	Aulacomnium turgidum	Campylium stellatum	
III-1	first terrace (low-centre polygon)	Meesia longiseta		
III-2	- / -	Calliergon giganteum		
III-3	- / -	Meesia triquetra		
IV-1	first terrace (slope of l/c polygon)	Sphagnum orientale		
IV-5	- / -	Tomentypnum nitens		
IV-6	- / -	Hylocomium splendens var. obtusifolium	Tomentypnum nitens, Aulacomnium palustre, Sphagnum orientale	Aulacomnium turgidum
V-1	first terrace (top of l/c polygon)	Hylocomium splendens var. obtusifolium	Aulacomnium turgidum	
V-2	- / -	Dicranum elongatum		
V-3	- / -	Dicranum congestum		Hylocomium splendens
V-4	- / -	Timmia austriaca var. arctica	Climacium dendroides, Aulacomnium turgidum	
V-5	- / -	Aulacomnium turgidum	Timmia austriaca var. arctica	Abietinella abietina
V-6	- / -	Tetraplodon mnioides	Hylocomium splendens var. obtusifolium	
VI-1-2	first terrace (frost crack)	Limprichtia revolvens	Calliergon giganteum, Campylium stellatum	
VI-4	- / -	Limprichtia revolvens	Tomentypnum nitens	
VI-7	- / -	Campylium stellatum	Limprichtia revolvens	
VII-2	first terrace (low-centre polygon)	Cinclidium arcticum	Calliergon giganteum, Limprichtia revolvens	Aulacomnium turgidum
VII-3	- / -	Meesia uliginosa	Limprichtia revolvens	
VII-4	- / -	Limprichtia revolvens	Calliergon giganteum	
VIII-1	first terrace (wide crack)	Limprichtia cossonii		Calliergon giganteum
VIII-2	- / -	Calliergon giganteum		
VIII-3	- / -	Calliergon giganteum	Limprichtia revolvens	

Table 3-18. continuation.

ID	habitat	species		
		dominant	admixed	single
IX-1	first terrace (high-centre polygon)	Rhytidium rugosum	Hylocomium splendens var. obtusifolium	
X-1	swamp	Tomentypnum nitens	Aulacomnium turgidum	
X-2	polygon	Dircanum congestum		
X-3	polygonal swamp	Limprichtia revolvens	Campylium stellatum,	
1	polygonal lake 1/slope	Timmia austriaca var. arctica	Tomentypnum nitens, **Hylocomium splendens var. obtusifolium,** Rhytidium rugosum	Polytrichum juniperinum, Aulacomnium turgidum
3	polygonal lake 1/surrounding area		Aulacomnium turgidum, Aulacomnium palustre, Climacium dendroides	Sphagnum contortum
4	polygonal lake 1/litoral zone	Hamatocaulis lapponicus		
6+7	polygonal lake 2/ slope	Aulacomnium turgidum	Hylocomium splendens var. obtusifolium, Tomentypnum nitens, Timmia austriaca var. arctica	
8	polygonal lake 2/ slope	Dicranum acutifolium	**Hylocomium splendens var. obtusifolium,** Tomentypnum nitens	
9+10	polygonal lake 2/surrounding area	Tomentypnum nitens, Aulacomnium turgidum	Hylocomium splendens var. obtusifolium	Sphagnum contortum, Sanionia uncinata
11	polygonal lake 2/surrounding area	Dicranum angustum	**Sanionia uncinata,** Aulacomnium palustre Rhizomnium pseudopunctatum	
12	polygonal lake 2/surround. area	Sphagnum contortum	Aulacomnium palustre, Limprichtia cossonii	
1	Kurungnakh	Polytrichum strictum		
2	- / -	Aulacomnium turgidum	Dircanum congestum	
3	- / -	Hylocomium splendens var. obtusifolium		

(2.) A phytosociological study was conducted on mosses and their adaption to different water regimes dependent on the relief situation. 46 samples of moss cushions were collected from typical landscape units of the islands Samoylov and Kurungnakh. Species were determined by Dr. E. I. Ivanovna (Institute for biological problems of cryolithozone SB RAS, Yakutsk). A list of samples, habitat descriptions, and species composition is provided in Table 3-18. A list of all moss species found in the study is given in Table 3-19 (n=31).

Moss remnants are often very well preserved in permafrost sediments. Thus, the analysis of moss remnants in permafrost drilling cores combined with phytosociological studies on recent moss communities may allow conclusions on ecological conditions in ancient times.

Table 3-19. List of all determined moss species.

moss species (n = 31)
Abietinella abietina (Hedw.) Fleisch
Aulacomnium palustre (Hedw.) Schwaegr.
Aulacomnium turgidum (Wahlenb.) Schwaegr.
Calliergon giganteum (Schimp.) Kindb.
Campylium stellatum (Hedw.)
Ceratodon purpureus (Hedw.) Brid.
Cinclidium arcticum Bruch et Schimp.
Climacium dendroides (Hedw.) Web. et Morh
Dicranum acutifolium (Lindb. et H.Arnell) C.Jens ex Weinm.
Dicranum angustum Lindb.
Dicranum congestum Brid.
Dicranum elongatum Schleich. ex Schwaergr.
Distichium capillaceum (Hedw.) Bruch et Schimp.
Hamatocaulis lapponicus (Norrl.) Hedenaes
Hylocomium splendens var. obtusifolium (Geh.) Par.
Limprichtia cossonii (Schimp.) Anderson et al.
Limprichtia revolvens (Sw.) Loeske
Meesia longiseta Hedw.
Meesia uliginosa Hedw.
Meesia triquetra (Richter) Aongstr.
Orthothecium chryseon (Schwaegr. ex Schultes) Schimp.
Polytrichum strictum Brid.
Polytrichum juniperinum Hedw.
Rhytidium rugosum (Hedw.) Kindb.
Sanionia uncinata (Hedw.) Loeske
Sphagnum contortum Schultz
Sphagnum orientale L.Savicz
Tetraplodon mnioides (Hedw.) Bruch et Schimp. in B.S.G.
Timmia austriaca var. arctica (Lindb) Arnell
Tomentypnum nitens (Hedw.)

Determination by Dr. Biol. Ivanova, Elena I.,
Institute for biological problems of cryolithozone SB RAS, Yakutsk

Figure 3-36. *Pedicularis sudetica*, Samoylov – first terrace, July 02.

Figure 3-37. *Eriophorum scheuchzeri*, Samoylov - middle floodplain, August 19.

3.7 Recent freshwater ostracods in the Lena Delta

Sebastian Wetterich

3.7.1 General introduction

Ostracods are small crustacea (in general up to 1 mm in length) occurring most frequently in the plankton and benthos of oceans, but also in rivers, lakes and swamps. They are characterised by a calcite exoskeleton of two valves. Their exoskeleton is often well conserved in sediments and therefore used in paleoenvironmental reconstructions of temperature, calcium content, salinity and water velocity (Meisch, 2000).

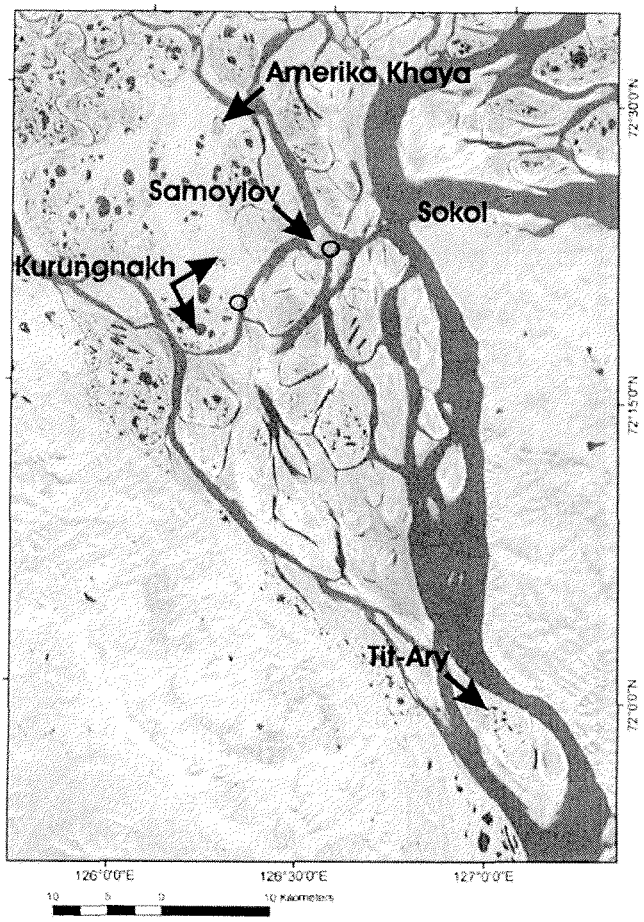

Figure 3-38. Map of the investigation sites (satellite image provided by Statens Kartverk, UNEP/GRID-Arendal and Landsat 2000).

During the Lena Delta Expedition 2002 ostracods were investigated in polygon lakes and alases for description of their species diversity in the delta under recent ecological conditions and for comparison with ostracods of this area dated to the Holocene and the Pleistocene. In total, living ostracods were investigated in 40 lakes in the southern part of the Lena Delta (Figure 3-38) on 4 islands, Samoylov, Kurungnakh (Buor Khaya), Tit-Ary and Amerika Khaya.

3.7.2 Methods

Hydrochemical parameters such as pH, carbonate hardness and total hardness of water [°dH], concentration of oxygen (O_2 [mg/l]), ammonium (NH_4^+ [mg/l]), nitrate (NO_3^- [mg/l]), nitrite (NO_2^- [mg/l]) and phosphate (PO_4^{3-} [mg/l]) were analysed during the fieldwork on means of an analysing set (compact laboratory) by Aquamerck® (Appendix 3-4). The Aquamerck® analysing set works with a scale based on optical gradation, which may be linked with matter concentrations and gives only preliminary results of the investigated parameters. For further investigations in laboratory water samples from each investigated lake were taken (Appendix 3-5). Samples for cation analysis (30 ml) were conserved with 25 µl HNO_3 and samples for anion analysis (15 ml) and residue samples (60 ml) were conserved by freezing. Before conservation samples for cation and anion analysis were filtered on means of a cellulose-acetate filtration set (0.45 µm). Additionally, samples for $\delta^{18}O$-isotope analysis (30ml) were prepared without any conservation and filtration. The conductivity and the surface temperature of the open water bodies were measured with a Conductivity Pocket Meter WTW Cond 330i (Appendix 3-4).

For further analyses samples of the lake sediment about 0.5 kg were taken in each lake. It will be measured the carbon content, ignition loss and granularity. The sediment samples will also be quantitatively analysed for ostracods valves.

Recent ostracods were caught by an exhaustor system (Viehberg, 2000) and conserved in 70 % alcohol. The determination of species will be carried out by characteristics of the soft body in combination with characteristics of the valves.

In addition were described some environmental parameters such as vegetation in and around the lakes, type of sediment and type of lake (Appendix 3-6). For a description of sediments we used the following classification by NÜCHTERLEIN (1969):

- lithogenic (sandy) ground (mineral hard ground)
- loamy ground (mineral soft ground)
- muddy ground (mineral-organic soft ground)
- mouldy ground (organic soft ground, peat)
- plant ground (subaquatic plants).

The most common species of the vegetation in and around the lakes are presented in Appendix 3-6.

The ostracods data in combination with the environmental, ecological and hydrochemical parameters will, for the first time, give a description of the life conditions for ostracods in the Lena Delta.

3.7.3 Types of lakes

In the southern part of the Lena Delta freshwater habitats for ostracods in the periglacial landscape were investigated. The investigated lakes are situated in several geomorphological units (terraces) of the Lena Delta. The most important processes for the evolution of freshwater lakes are the formation and destruction (ice wedge formation and thermokarst) of polygons (Vtyurin, 1956). So the lakes were characterised as erosion-thermokarst lakes (old branches) and thermokarst lakes (polygons and alases). The following types of lakes were differentiated (Appendix 3-6):

- little polygon lakes with distinct polygonal structure (LPL)
- bigger polygon lakes, formed by several little polygon lakes (BPL)
- polygon trench lakes (PTL)
- alas lakes (AL)
- old branches (OB)

3.7.4 Study areas

Investigation site Samoylov

The main study area was Samoylov Island (Figure 3-38). Altogether 35 lakes on the first Lena river terrace and low, middle and high floodplains (Pfeiffer et al., 1999) were investigated. This island is characterised by several types of polygon lakes in different stages of development and old branches of the Lena river. Not all of the these old branches were regularly floated by the Lena up to now.

Investigation site Kurungnakh

In summary, on Kurungnakh island were investigated 4 lakes: two alas lakes, one little polygon lake and one polygon trench lake on southern part of this island (Figure 3-38). These lakes are situated on the third Lena river terrace.

Investigation site Amerika Khaya

On Amerika Khaya island (Figure 3-38) samples were taken in an alas lake on the third Lena river terrace.

Investigation site Tit-Ary

On the island Tit-Ary (Figure 3-38) in distance of about 50 km to the south of the main study area were sampled four lakes on the lowest floodplain, in old branches and in a lake (SAM-06) between the first and the second terrace, probably formed as a result of neotectonic processes (friendly information of M. Grigoriev).

3.7.5 Preliminary results

Because of the very low concentration of nutrients, the lakes were characterised as ultraoligotrophic. The investigated fauna of ostracods is poor, that means only a few number of species is able to exist under the polar conditions. But the here existing species occur with great abundances. The conductivity of the waters depend on their position in geomorphology (terraces). In lakes regularly floated by the Lena river on floodplains or in old branches higher conductivity were measured than in lakes of the higher terraces. The latter get their water only from precipitation. All investigated lakes were characterised by low value for water hardness and depending on temperature relatively high oxygen concentrations.

3.8 Recent insects of the Central Lena Delta

Svetlana Kuzmina

3.8.1 General Introduction

Because the ecology and distribution of some tundra insects are not sufficiently known, a collection of recent insects from the tundra is very interesting for science. Collections of modern insects are of special importance for paleoentomological research, as they are used to identify fossil remains. In 2000, S. Kuzmina collected modern insects (mainly beetles) during the geological research in the western Lena Delta (Nagym) and in the Central Delta (Kurungnakh and Samoylov Islands). In 2002, the collection of recent insects was a special part of the research program. We installed 20 soil traps on Samoylov Island, established in various biotopes: on the stream bank, in wet and dry tundra and on sand patches among scarce vegetation. The traps were checked every three days. However, most insect specimens were collected by hands in different parts of the island. In total, 762 beetle specimens were collected on Samoylov Island (Appendix 3-7, Figure 3-39).

During a short (three days) excursion to the Tit-Ary Island south of the Lena Delta (Figure 3-39) we managed to collect 107 specimens of modern beetles (Appendix 3-7). The insect fauna of the Tit-Ary area is different from that on Samoylov Island, because Tit-Ary still lies within the forest-tundra zone. One of our aims was to visit Belaya Skala (White Rock) on the right bank of the Lena near Tit-Ary. This location is one of the very rare areas in the Arctic, where the recent occurrence of a pill beetle *Morychus viridis* was recorded. This species was very widespread and abundant in the Pleistocene, and is used as one of important indicators of the past environment. Its modern distribution is considered as a relic one. This extant species was described only recently (Kuzmina, Korotyaev, 1987), but the first modern specimens were found in the lower Lena area (near Bulun) as early as in 1908 by E. Pfizenmayer). About 15 years ago A. Tsybulsky collected *Morychus viridis* further north, at Belaya Skala. We intended to visit the site to study the species habitat in more detail, and probably catch more beetles. Unfortunately, our visit to Belaya Skala was only for a few hours, and we failed to find beetles.

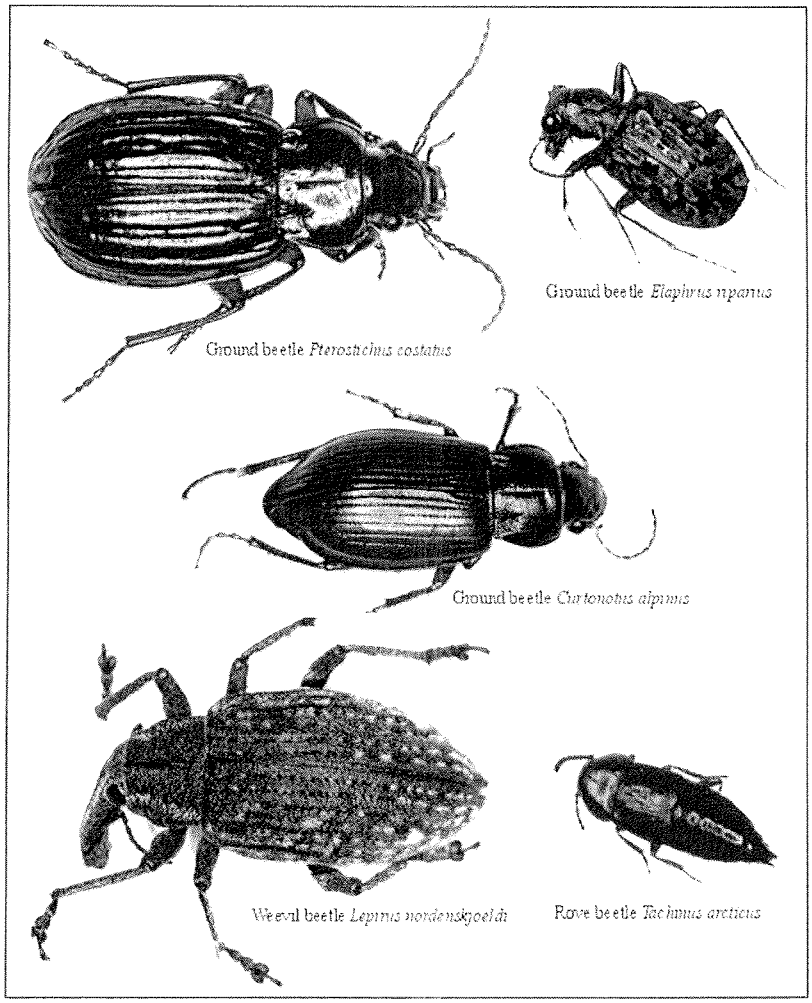

Figure 3-39. Some recent beetles from Samoylov Island.

Some modern beetles were additionally collected by the hydrologists I. Fedorova and M. Tretyakov near the polar station "Sokol", on the right bank of Bykovsky Channel (Figure 3-39). Furthermore, some recent insects were collected near Tiksi. Thus, the collection includes modern beetles from four sites: Samoylov, Tit-Ary, Sokol, and Tiksi (Appendix 3-7).

3.9 Permafrost drilling on Kurungnakh Island

Dirk Wagner, Anna Kurchatova, Waldemar Schneider, Günther Stoof and Mikhail N. Grigoriev

In order to improve our understanding of the carbon dynamic and budget for the Lena Delta region, the methane and carbon content as well as the processes, diversity and physiology of the microbial community have to be addressed not only in the active layer but also in the underlying perennially frozen permafrost deposits. Therefore a permafrost drilling on Kurungnakh Island (N 72°20, E 126°17, Figure 3-38) was carried out in August 2002.

Kurungnakh Island belongs to the oldest terrace of the Lena Delta which was formed in the middle to late Pleistocene and is fragmentarily exposed (30-55 m a.s.l.) in the southern part of the delta. The terrace consists of ice complexes containing fine-grained silty sediments with a high content of segregated ice. The ice complex more over includes enormous layers of organic-rich material and less decomposed peaty material (Chapter 3.10).

The drilling was accomplished with two transportable drilling equipments. The first drilling (KUR-02R) was carried out from the top of the cliff near the exposure (43.4 m a.s.l.), while the second drilling (KUR-02G) was done in an area of thermo erosion, which was about 12 m below the surface (31.2 m a.s.l.) on top of a baydzherakh. With these two drillings it was succeeded to drill through the whole ice complex into the Lena sands. Altogether a 25 m long permafrost core was received by this campaign. A detailed description of the cores is represented in Appendix 3-8. The cores were transported in frozen conditions to Germany for microbiological, molecular ecological and geochemical analysis.

3.10 Paleoecological and sedimentological studies of Permafrost deposits in the Central Lena Delta (Kurungnakh and Samoylov Islands)

Svetlana Kuzmina, Sebastian Wetterich and Hanno Meyer

3.10.1 Introduction

The geological research in the Lena Delta on Kurungnakh (site No. 1: 72° 20' 41" N, 126° 18' 33" E; site No. 2: 72°, 20' 35" N, 126° 18' 20" E) and Samoylov Islands (Figure 3-38) in 2002 was carried out by tree scientists. The main tasks of this small team were:

- cryolithological description of the sections
- sampling of sediments for multi-proxy analysis (e.g. pollen, ostracods, geochemistry, sedimentology) and age determination
- screening sediment for fossil insects
- collection of mammal bones
- determination of the ice content the in the frozen sediments
- taking of ice wedge samples for stable isotope and hydrochemistry analyses by means of an ice screw

The Buor Khaya section on the Kurungnakh Island was the main object of field studies. Besides that we studied two Holocene sections on Samoylov Island. The methods of geological and paleontological investigations were similar as described in the previous expedition reports (Siegert et al., 1999; Sher et al., 2000, 2002). In addition, some other places within the Lena delta were used for recent ecological studies (e.g. Tit-Ary, Sokol).

The Buor Khaya section on the Kurungnakh Island was previously examined by the participants of the Russian-German expeditions "Lena Delta 98, 99, 2000, 2001". (Schwamborn, 1999; Pavlova & Dorozhkina, 2000; Kuznetsova & Kuzmina, 2001; Schirrmeister et al., 2001; Pfeiffer et al., 2002). But for the first time it was possible to study these profiles in more detail. There are a number of age-determinations by radiocarbon and Optic Stimulated Luminescence (OSL) dating and results of sedimentological studies (Schwamborn et al., 2002, Krbetschek et al., 2002). But the sediments have never been screened for fossil insects. During previous research on the Samoylov Island the surface sediments were cored and described (Pfeiffer et al., 2002).

3.10.2 Geological description of the Buor Khaya section (Kurungnakh Island) and two Holocene sections (Samoylov Island)

Chronology

Like in some other Lena Delta sites (Lungersgausen, 1961; Kunitsky, 1989; Grigoryev, 1993), the Quaternary deposits of the Buor-Khaya section are represented by two main units. The lower unit consists sandy deposits corresponding to the stratigraphic locally named Bulukur-Suite. The upper unit

is the ice-rich Kobakh-Suite. In this report we use the more common names "Ice Complex" or "Yedoma" for these ice-rich deposits. The sandy unit was dated from 65 to 88 ka BP by the IR-OSL method and from 57 to 37 ka BP by AMS (Schwamborn, 2002). The contradictions of age determinations by different methods are still under discussion (Grosse et al., 2002). The upper ice-rich unit was dated from 50 to 33 ka BP and 17 ka BP in the uppermost part of the Ice Complex. The top of the Buor Khaya section was dated to 7.7 ka BP (Schirrmeister et al., submitted).

Kurungnakh Island

The sands of the Bulukur-Suite are well exposed along the whole section. In some places, especially in the lower part, the sands contain abundant roots and stems of large grasses, probably of *Arctophila fulva*. The exposed "*Arctophila*"-rich sand usually forms very steep or even vertical walls. We observed a similar situation in the Nagym section in the North of the Olenyok Channel (Schirrmeister et al., 2001). The middle part of the sandy unit usually contains silt layers with plant detritus. The upper part of the Bulukur-Suite is built mostly by clean (washed out) sand with little organic material (Table 3-20). Only in some places we found thin layers of fine plant detritus. Thus, the sandy unit consists of the different facies, changing in vertical and horizontal directions. The Bulukur-Sands were studied at site No.2 (Figure 3-401).

Table 3-20. Description of the lower unit (Bulukur-Suite) at the Kurungnakh section.

Altitude [m, a.r.l]	Description
17.2-17.5	grey fine-grained sand (probably a buried soil layer)
10.5-17.2	yellow medium- and coarse-grained sand without visible stratification
7-10.5	intercalation of yellow clean fine-grained sand and grey silty sand with plant detritus; individual layers are up to 0,1-0,15 m thick
5-7	yellow medium-grained sand without visible stratification
0-5	slope debris: sand from the upper part of Bulukur-Suite, peat blocks and liquid mud from ice-rich Ice Complex

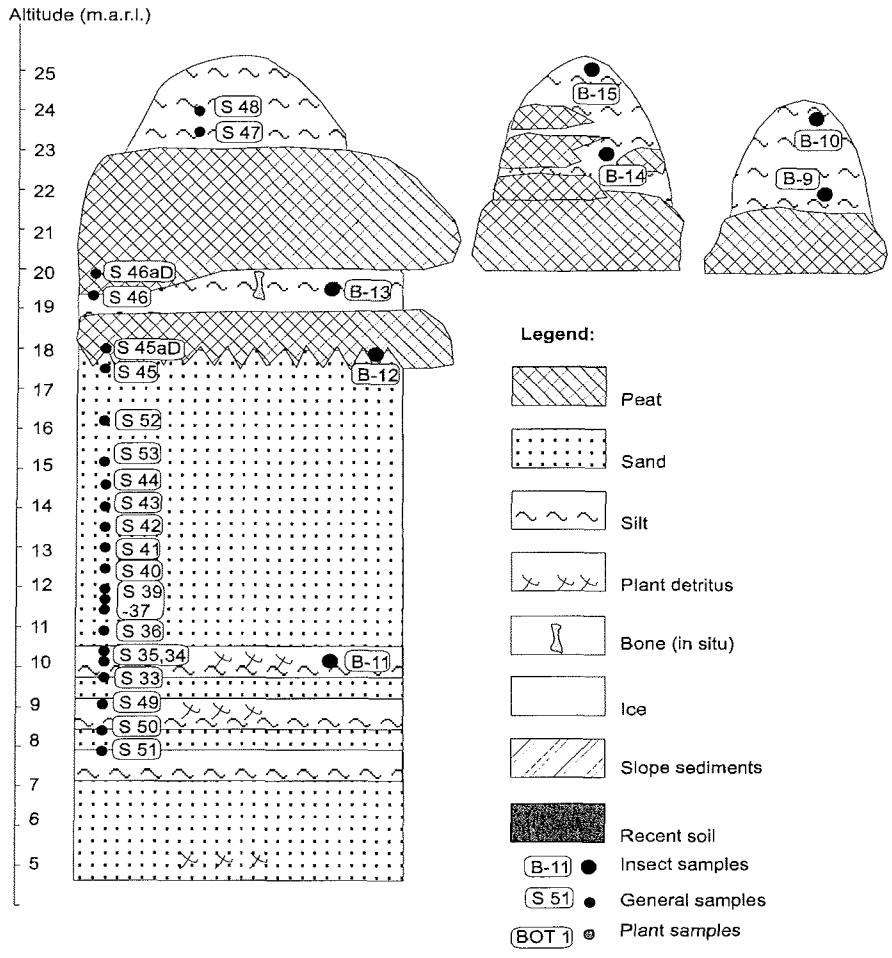

Figure 3-40. Kurungnakh section, site No. 2, Bulukur-Suite and the low part of Yedoma.

The Bulukur-Sands are covered by Ice Complex deposits - ice-rich silt with thick peat horizons, sand lenses and large ice wedges. The boundary between the Bulukur-Suite and Ice Complex is sharp and visible along the whole section (Figure 3-41). The Ice Complex ice wedges sharply narrow near the boundary with the Bulukur-Suite, and their long and narrow tails penetrate 2-3 m into the sand. In 2000, special ice wedges were found and sampled within the Bulukur-Sands (Schirrmeister et al., 2001, p. 95, fig. 5-9, Schirrmeister et al. submitted), but in 2002 we could not observe ice wedges belonging to the Bulukur-Suite. In the Buor Khaya section, the Ice Complex unit is often exposed like an ice wall along the river-bank. This wall, being up to 1 km long, is probably a longitudinal section of the polygonal ice-wedge system. The ice wall is covered by overhanging blocks of peat with frozen silt. These blocks fall down if the underlying ice thaws, and roll down to the Lena bank (Figure 3-41).

Consequently, we could take samples from a block if the place of its original position was evident.

Figure 3-41. Kurungnakh section: Bulukur-Suite and the low part of Yedoma.

The Ice Complex sediments are mostly ice-rich silt with thick peat layers (Table 3-21). The thickest peat layers are observed in the lower part of the Ice Complex. At least three of such layers are clearly observed along the section. In the upper part of the section the peat layers are more rare and less thick. Sandy layers or lenses are often observed near the boundary ice wedge - sediment.

Table 3-21. Description of the Ice Complex sediments at the site No. 1 from the top.

Depth [m]	Description
0-0.2	soil layer
0.2-2.5	grey silt with brown peat hummocks (0.1x 0.15 m) - point 1
2.5-3.2	Ice
3.2-5.7	grey silt with plant detritus – baydzherakhs B and C
5.7-6.5	yellow medium-grained sand near ice wedge – Baydzherakh C
6.0-6.7	grey silt with plant detritus – baydzherakh E
6.7-7.2	reddish-brown peat – baydzherakh E
7.2-9.2	grey silt with plant detritus – baydzherakh E
9.2-11.5	grey sandy silt with grass roots and woody twigs – baydzherakhs F, G, H
11.5-12.2	brown peat – baydzherakh H
12.2-13.2	grey silt – baydzherakh H, G, P
13.2-15.7	brown peat, third (from the bottom) marker horizon in the vertical wall
15.7-19.0	grey silt with plant detritus
19.0-21.5	grey silt with abundant peat lenses and spots
21.5-23.2	brown peat, the second marker horizon in the vertical wall
23.5-24.8	grey silt with plant detritus
24.8-26.5	brown peat, the first marker horizon in the vertical wall

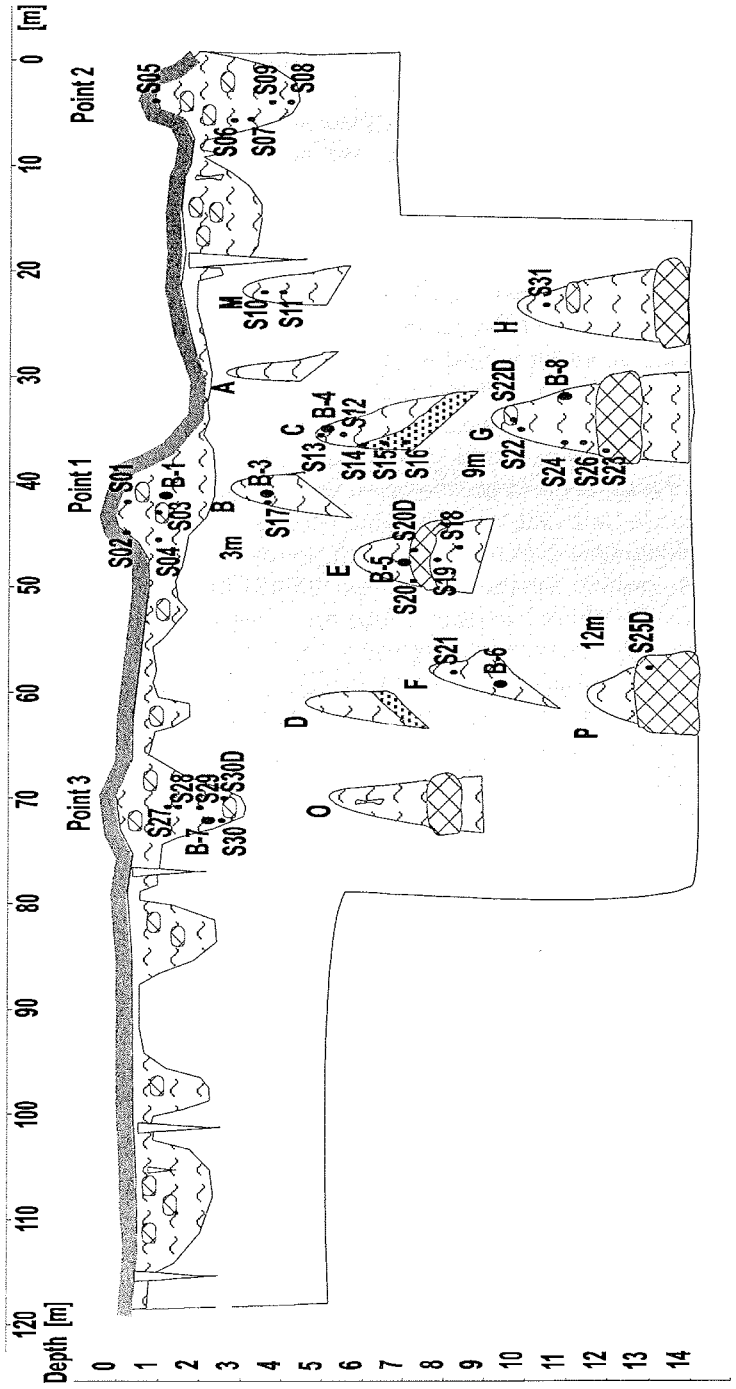

Figure 3-42. Kurungnakh section, site No. 1, Yedoma-Suite.

In the top part of the section, under the active layer, we found a horizon of silt with peat hummocks presumably of the Holocene age. The thickness of this horizon amounts from 0.1 - 0.2 m to 2 m. Small Holocene ice wedges are present here, which often penetrate into the much larger Pleistocene ice wedges (Figure 3-42). A similar situation was observed at the top of the Ice Complex sections on the Bykovsky Peninsula and on Bol'shoy Lyakhovsky Island.

Samoylov Island

In addition, two sections were studied on the Samoylov Island. Section 1 is situated on the bank, 90 m SSE of the camp (the river upstream) on the first terrace above the floodplain, which is built up mostly by peat (Table 3-22) and contains a series of Holocene ice wedges. A site was chosen, where the ice wedges were well- exposed and could be studied best (Figure 3-43). At this site on the South coast of Samoylov Island, a Holocene ice wedge of the first terrace (SAM-IW-1) in the Lena Delta was sampled and described in detail. The ice wedge is 1.4 m wide and 2.2 m high, and because of its preferential thawing, situated approximately 5 m behind the cliff above the Lena river. It is cut perpendicular to its growth direction and characterised by yellowish-white and milky ice with well-developed vertical structures. Single elementary ice veins are 2-3 mm wide, but not easy to differentiate, and contain a lot of small gas bubbles (< 1 mm). At the left side, the ice wedge is limited by clear and transparent ice. At 20 cm from this side, the upper part of a small ice vein continues into the overlying sediment layer. The ice wedge shows a number of cracks, which extend from the upper left to the lower right side of the wedge. These seem to be linked to other processes than frost cracking e.g. tectonic influence, but the reason is still unknown, yet. A number of 17 samples was taken from a 1.4 m long horizontal sampling transsect in a height of 7.0 m a.s.l.. These samples were poured into 30 ml PE bottles, which were closed tightly and sealed with special tape to avoid evaporation of the samples. The samples will be measured for stable oxygen and hydrogen isotope composition at AWI Potsdam.

Table 3-22. Description of the section No. 1 from the Samoylov Island.

Altitude [m, a.r.l]	Description
8.0-7.8	soil layer
7.8-7.3	Horizon I-yellow and greyish-yellow medium grained sand with peat lenses (above the ice wedge) and fine layers (aside of the top of the ice wedge), peat consists of moss and grass stems, the grass is probably Arctophila fulva
7.3-5.7	Horizon II-peat, near the ice wedge turns into peaty silt, brownish-grey silt with woody roots and twigs and relatively large pieces of wood, brown peat, mostly consists of green moss with sedges and "Arctophila" grass, the top of the peat layer has a reddish-brown band of green moss peat.
5.7-5.4	Horizon III-greyish-yellow medium grained sand with grass roots
0-5.4	slope debris

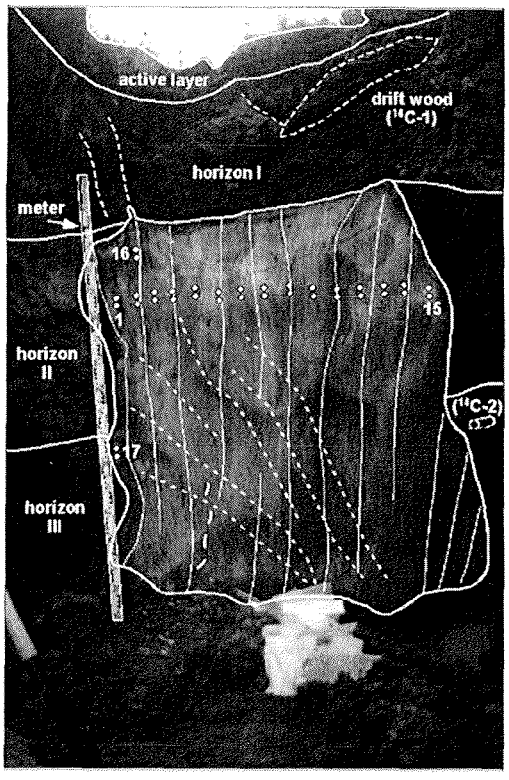

Figure 3-43. Holocene ice wedge in section No. 1on Samoylov Island.

The section No. 2 is the first terrace above the floodplain on Samoylov Island and is composed of silty sand (Table 3-23). The site is situated at the Lena bank, 500 m SSE of the camp. The lower part of the exposure has a wave-cut niche, covered by debris. The upper part is an almost vertical wall, because of abundant plant remains: woody twigs, roots, wood fragments, grass stems, preventing erosion (Figure 3-44).

Table 3-23. Description of the section No. 2 from the Samoylov Island.

Altitude [m, a.r.l]	Description
8.0-7.8	soil layer
7.8-7.2	horizon I-grey fine-grained sand with plant detritus and thin (3-5 cm) layers of yellow clean medium-grained sand
7.2-6.5	horizon II-grey fine-grained sand with lenses of plant detritus, wood fragments, grass roots and stems
6.5-5.5	horizon III-grey silt with woody twigs and roots, plant detritus
0-5.5	slope debris

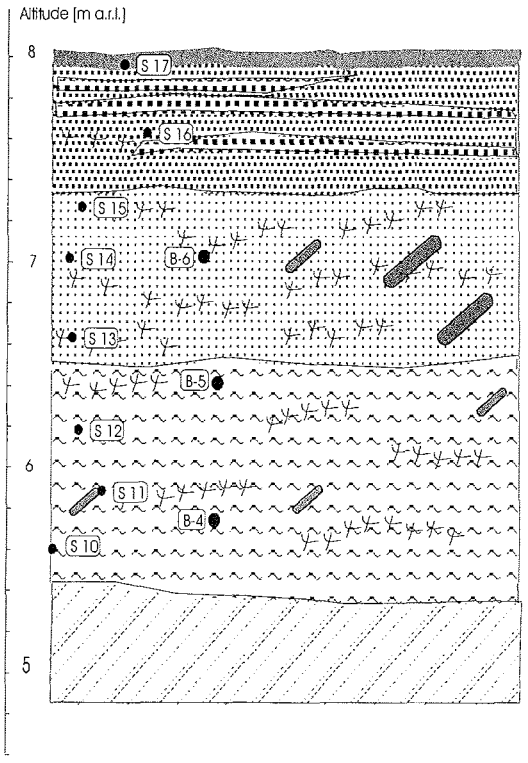

Figure 3-44. section No. 2 on Samoylov Island.

3.10.3 Sampling of permafrost sediment and ice

The samples from the permafrost were taken by knife or axe. In the upper part of the section (Ice Complex unit) we could take samples along a stratigraphic vertical sequence of thermokarst mounds (baydzherakhs) with overlapping tops and bottoms (Figure 3-42). Samples for pollen analyses, ice content determination, sedimentological analysis and ostracod studies were taken separately. Additionally, peat layers were sampled for conventional radiocarbon dating (Appendix 3-9). The ice content was determined gravimetrically on a dry-weight basis, as the ratio of the mass of ice in a sample to the mass of the dry sample, expressed as a percentage (van Everdingen, 1998).

For stable isotope and hydrochemical analysis samples were taken from one Holocene ice wedge penetrating into an older Pleistocene ice wedge in the upper part of the Ice Complex unit (Appendix 3-11, Figure 3-45). We used ice screws to drill a transverse across the ice wedge, in a distance between the drill-holes of about 0.07 m (on three levels) for the this ice wedge. Altogether we get 13 samples for stable isotope analysis and 2 samples for hydrochemical

analysis from the first ice wedge. Ice samples were also taken from an ice wedge in the lower part of the section (Appendix 3-11, Figure 3-46), where ice wedges from the Ice Complex penetrate into the underlying sands of the Bulukur – Suite. Next to the ice wedge we found horizontal layered ground ice. Along a transverse across the ice wedge and the ground ice in a distance between the drill-holes of about 0.1 m (on one level) were taken 12 samples for stable isotope analysis and 2 samples for hydrochemical analysis. After melting the ice samples were poured into 15-ml-HDPE bottles. The samples for anion hydrochemical analyses were conserved by freezing and for cation hydrochemistry analyse were conserved with 25 µl HNO_3.

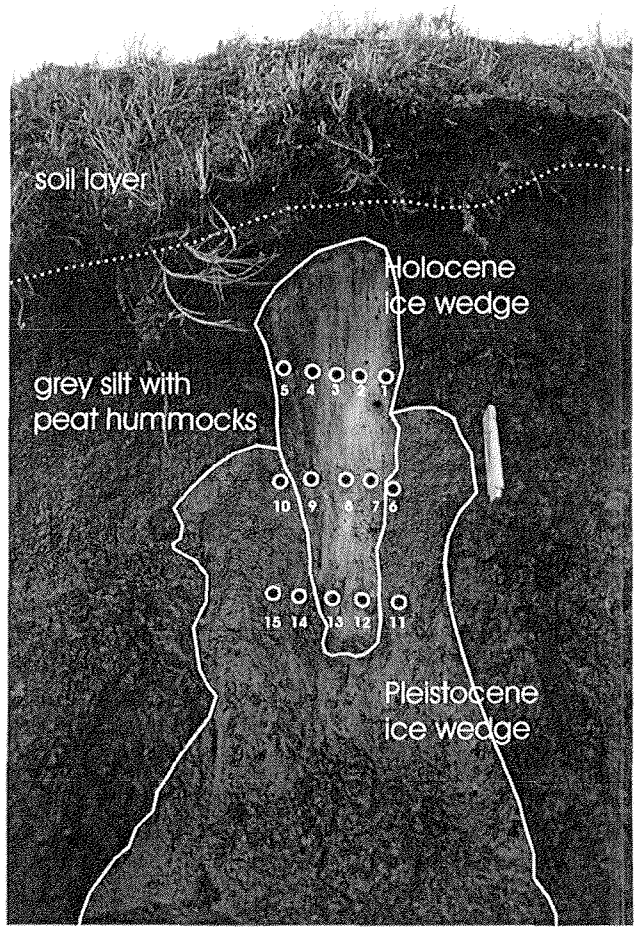

Figure 3-45. Holocene ice wedge in the upper part of the Ice Complex unit on Kurungnakh Island.

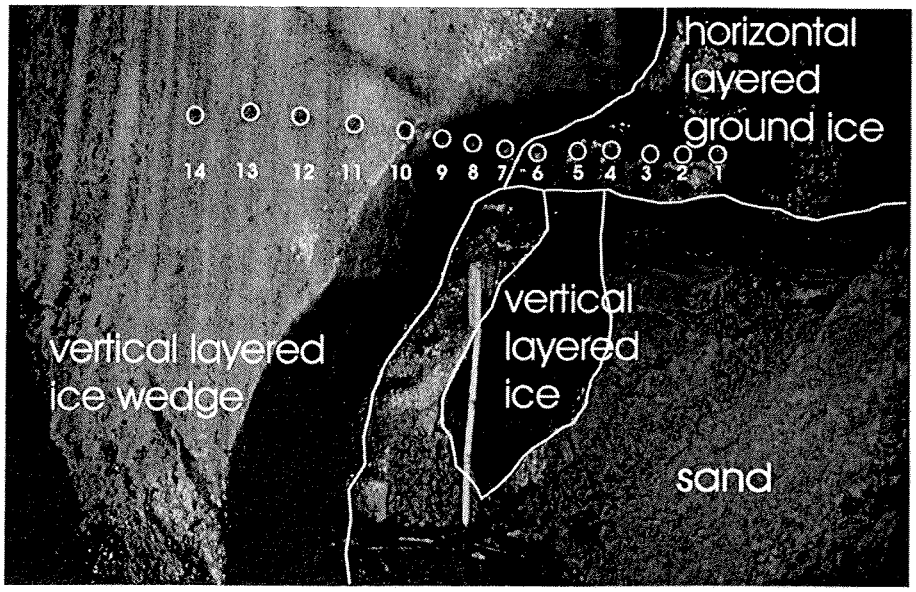

Figure 3-46. Ice wedge in the Bulukur-Suite on Kurungnakh Island.

3.10.4 Screening sediment for insect fossils

In contrast to the previous year, almost all fossil insect samples were taken from thawed sediment in 2002 (Sher et al., 2002). Only one sample (BKh-2002-B7) was chopped by axe from frozen deposits. In this case it was sufficient to take about 30 kg of sediment, instead of 50 kg normally, because insect remains were rather abundant in the screened detritus. Usually, a preliminary screening showed a low content of insect fossils. In these cases, up to 200 kg of sediment were screened.

In the Buor Khaya section, one sample (BKh-02-B1) was screened from the upper, presumably Holocene layer. Nine samples (BKh-02-B2 – B8, B12, B13) were taken from the Ice Complex baydzherakhs (Figure 3-40), four samples (BKh-02-B9, B10, B14, B15) - from two fallen blocks of frozen Ice Complex sediments; one sample (BKh-02-B11) from the Bulukur-Suite (Figure 3-42). From Samoylov Island three samples (Sam-B1 – B3) were taken from the section No.1 (Figure 3-43) and three samples (Sam-B4 – B6) from the section No. 2 (Figure 3-44). In total, we took and screened 15 samples from Buor Khaya site and 6 samples from Samoylov Island (Appendix 3-12).

3.10.5 Collection of mammal bones

Mammal bones were collected during the whole field studies. Following the tradition of 1998-2000 field seasons, we tried to collect all bones found, except evidently indeterminable pieces. In Moscow, Dr. A. Sher helped to identify the bones. However, the total number of collected bones (31) is incomparably less, to those previously found on Bykovsky Peninsula and Bol'shoy Lyakhovsky Island. Only one possibly fossil bone (fragment of reindeer tibia) was found on Samoylov Island. It was picked up on the beach below the section No. 2. During an excursion to Amerika-Khaya Island (Fig. map) a part of deer vertebral column was found, consisting of four connected vertebras. It was buried in peat in the upper part of the first terrace above the floodplain. The terrace is about 6 m high, the vertebral column was found at a depth of 2 m. The main bone collection was found on the Kurungnakh Island. The majority of bones belong to horses. Many bones were found in situ or in liquid mud of the bluff. A few bones (femur, tibia and metatarsale BKh-2002-O9, O17, O20) come from one horse individual. They fell down from the frozen wall related to a location between two peat horizons in progress of permafrost thawing. This place is located about 200 m upstream from section No. 2. A pelvis bone was observed thawing out the permafrost, but it was no chance to collect it. In the same layer near section No. 2 we noticed a big bone, probably femur of horse or bison, that could also not reached. Later, the bone immediately disappeared in liquid mud after melting out and falling down, and our attempts to find it again. In the same layer within several days two branches of one horse mandibula (Bkh-2002-O5, O13) were collected. Thus, the lower horizon of the Ice Complex unit of the Buor Khaya section contains rather abundant bone material. An interesting finding of a muskox metatarsal (BKh-O3), sticking out of frozen silt near an ice wedge was made in the upper part of the Buor Khaya section.

3.11 Hydrological investigations in the Lena River Delta

Dmitry Bolshiyanov, Irina Fedorova and Mikhail Tretiakov

3.11.1 Introduction

The regime of the Lena River as one of the largest rivers of the Arctic has been investigated for more than 70 years (Ivanov and Piskun, 1999). The river delta is most interesting for the study as there is constant reforming of this area related to deposition of a large sediment load.

Exiting to the mouth area, the main river flow divides into numerous arms and transverse channels (Figure 3-47) forming an enormously extensive delta, the third in the world. The total delta area comprises more than 25 thousand km^2 if the Stolb Island is assumed to be the delta apex. If the delta apex is referred to the beginning of bifurcation of its first (Bulkurskaya) channel slightly downstream Tit-Ary Island, the delta area will significantly expand and comprise more than 32 thousand km^2.

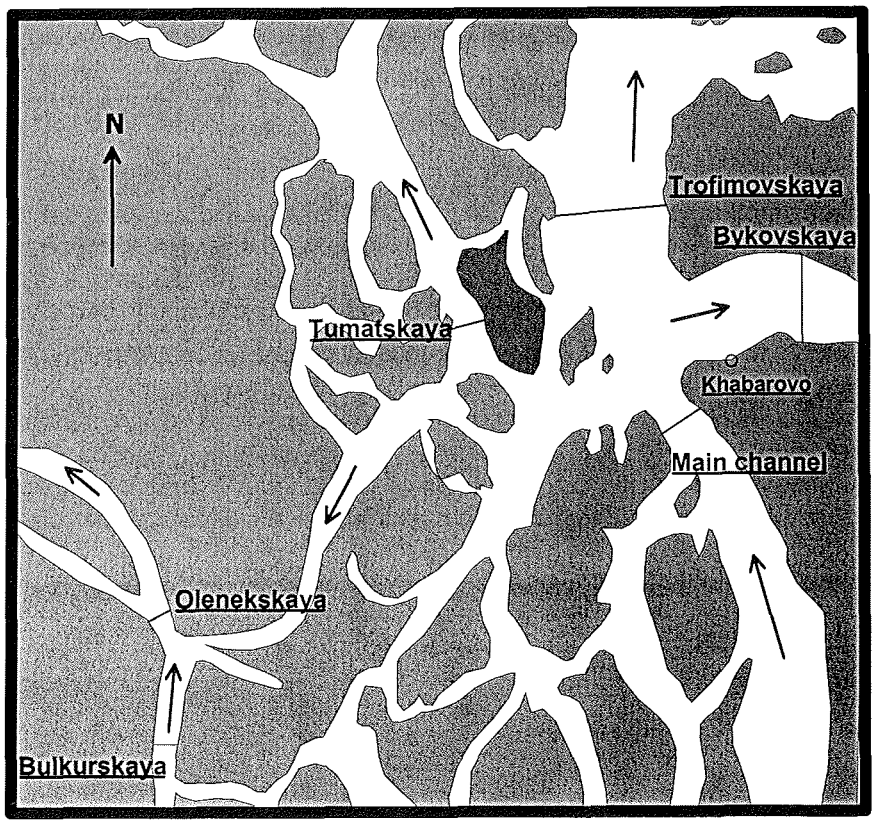

Figure 3-47. Lena River bifurcation by the main delta arms in the vicinity of Stolb Island.

To reveal the typical delta formation features (redeposition of sediments, water discharge changes in the main Lena River channels) for the last decades, a number of hydrometric studies were undertaken in summer of 2002 during the Russian-German Expedition predominantly at the bifurcation point near Stolb Island and at the Sardakh-Trofimovsky bifurcation point. In addition, materials of observations at Khabarov gauging station not published in yearbooks were collected for the period 1982-2002.

3.11.2 Materials and methods

Two main parts of the study can be identified: direct hydrometric measurements and collection of archived data of the Khabarov gauging station. Field observations were conducted twice at the Sardakh-Trofimovsky bifurcation point at the beginning of August and twice at the apex of the Lena delta (Bykovskaya, Trofimovskaya and Main channels in 4.7 km from Stolb Island) – in the middle and end of August.

A complex of hydrometric studies included depth measurements and measurements of the river current speeds and its turbidity (Manual for Hydrological Stations and Posts, 1978).

At the Sardakh-Trofimovsky bifurcation point (STBP), the discharges were measured at four gauge lines made in 2001 (lines 1-4, Bolshiyanov and Tretiakov, 2002) at the time of the "Lena 2001" Expedition and at the additional gauge lines made in 2002 (lines 5-9, Figure 3-48).

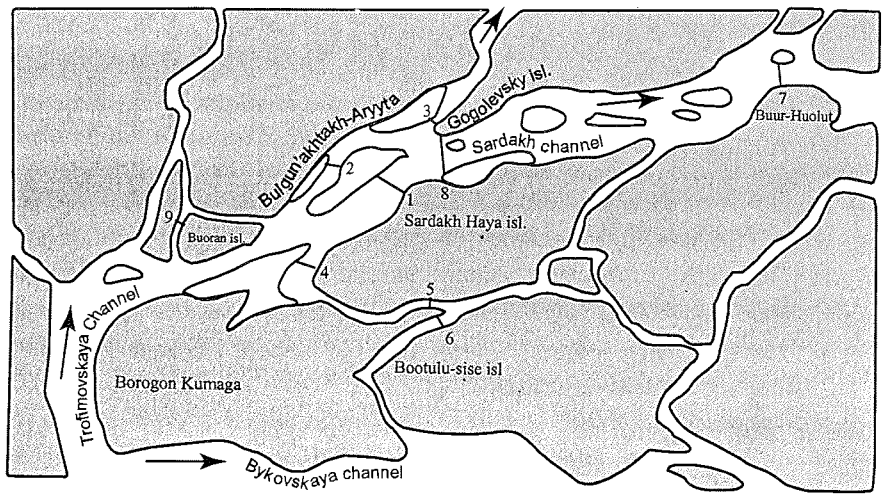

Figure 3-48. Location of the expedition gauge lines in the area of the Sardakh-Trofimovsky bifurcation point in 2002.

At the apex of the Lena River delta, there are 5 gauge lines of standard hydrological observations: the Main Channel of the Lena River in 4.7 km upstream Stolb Island; gauge lines in the Bykovskaya, Trofimovskaya. Tumatskaya and Olenekskaya Channels (Figure 3-47). For the analysis of the river regime at the delta apex and for revealing the main typical features, data on water discharges and turbidity measured in all channels at the main gauge lines (Annual Data on the Regime and Water Quality, 1991-2002) and archived data of multiyear runoff and sediment load fluctuations in the main Lena River channels/Khabarov gauging station were used.

The following scope of work was performed during the expedition:

- Plots of cross-sections of the channels were constructed where in addition to depths, the current speed diagrams are presented allowing us in turn to speak about the distribution of the current speeds in the hydraulic bed section;
- Turbidity in the gauge lines and discharge of the sediment load were calculated;
- Water discharges in the flows of two investigated bifurcation points (first – Sardakh-Trofimovsky and second – near Stolb Island);
- For greater illustration of the runoff redistribution by the channels, the discharges of water and sediment load are plotted in the diagrams.

An analysis of multiyear changes of the water runoff and sediment load discharge in the main channels of the Lena River - Bykovskaya, Trofimovskaya. Tumatskaya and Olenekskaya Channels was performed:

- The percentage ratios of the distribution of water runoff and sediment load discharge by the main channels were obtained;
- The maximum Lena River runoff is estimated;
- The measured and calculated water and sediment load discharges are compared;
- The plots of the water content variations of the main channels over the entire observation period were constructed;
- The difference integral curves of mean annual water discharges of the main channels were plotted.

The cross-profiles of the sections of hydrometric lines in the main Lena channels were constructed on the basis of depth measurements over the period 1980-2000.

3.11.3 Results and discussion

In the course of field work and processing of multiyear observation data, the following facts were revealed:

- The Lena River runoff has a pronounced seasonal character. The greatest runoff portion falls on the first 10 days of June. During this period up to 80 % of the annual water runoff and sediment load discharge passes, that is why the hydrometric measurements during this period are necessary presenting a serious problem due to natural conditions in this period in the Lena delta.
- In the Lena River delta, the water runoff is redistributed as follows: a large portion passes through the Trofimovskaya Channel, 20-25 % falls on the Bykovskaya channel and the fraction of Tumatskaya and Olenekskaya Channels comprises about 10 % (Table 3-24). Thus, the main reformation (deepening) of the river delta bed occurs exactly in the Trofimovskaya Channel.

Table 3-24. Distribution of water discharges for the gauge lines of the main Lena delta channels on August 13 and 26 as compared with a multiyear distribution.

Channel / Date	Main Channel	Bykovskaya	Trofimovskaya	Bykovskaya and Tumatskaya
August 13, 2002	18854	4007	12824	2023
	100%	21,3%	68%	10.7%
August 26, 2002	19247	4778	13394	1075
	100%	24,8%	69,6%	5,6%
Based on multiyear data for the summer low water	100%	25%	65%	10%

During the last twenty years, the runoff fraction through the Trofimovskaya Channel increases. For this, the difference integral curves of the mean annual water runoff in the Main Channel of the Lena River and the main branches of its delta were constructed. As can be seen from Figure 3-49, the water content fluctuations were observed in the Main Channel for the last half a century at the background of the general runoff decrease, however, there is no significant runoff change. Whereas in the Trofimovskaya Channel a clear tendency for the increased water discharge is obvious (Figure 3-50), the same is observed to a lesser extent in the Tumatskaya Channel. For a serious substantiation of these conclusions the currently available data are insufficient and further studies in this direction are required.

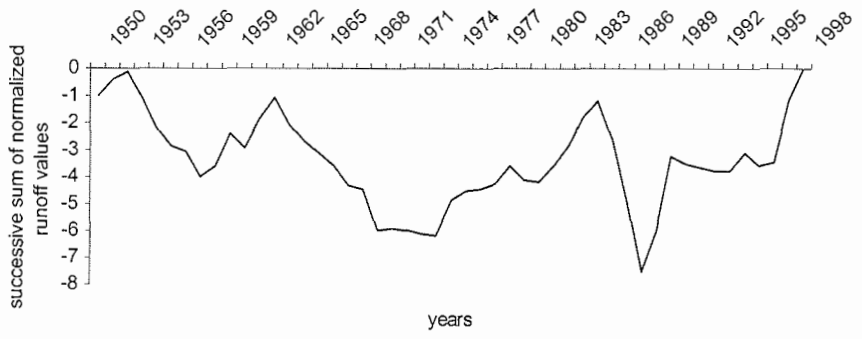

Figure 3-49. Difference intergral curve of the mean annual discharge of the Main Channel.

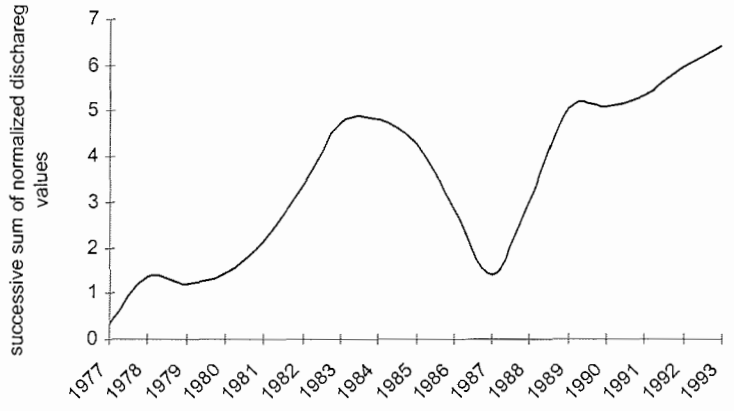

Figure 3-50. Difference integral curve of mean annual discharge of Trofimovskaya Channel.

The distribution of the maximum runoff by the main branches of the Lena River delta presented in Table 3-25 is slightly different: the runoff by the Trofimovskaya Channel decreases to 40-50 % with a simultaneous increase of the fraction of the Olenekskaya and to a greater extent the Tumatskaya Channels.

Table 3-25. Distribution of the maximum water discharge for a multiyear period by the Lena delta branches.

	Period	Main Channel	Bykovskaya	Trofimovskaya	Olenekskaya	Tumatskaya
Greatest discharge (m3/s)	1950-2001	189000 01/06/84	52500 12/06/78			28800 10/06/83
	1977-2001			76300 08/06/74 12/06/83	34300 09/06/85	
		100 %	≅27 %	≅40 %	≅18 %	≅15 %

It is necessary to note that during the measurements and calculations of the maximum runoff (both liquid and solid), large errors are possible. The absence of the observation data on turbidity and sediment load discharge during the flood period does not allow a precise evaluation of the solid discharge volume and its distribution by the main delta channels. For example, the measurements in the Olenekskaya and Tumatskaya Channels are extremely few for their reliable interpretation while measurements of the locality and speeds of current during the flood period are more often absent.

As can be seen from the plots of depth measurements in the Lena River branches, the depth decreases in the major gauge line of the Main Channel of the River and in the Bykovskaya Channel along with its expansion (Figure 3-51). Bed silting is also typical of the Olenekskaya and Tumatskaya Channels. There were no significant bottom changes in the Trofimovskaya Channel for the last 20 years confirming once again the increased water runoff to this delta branch. However, at the Sardakh-Trofimovsky bifurcation point, erosion of Sardakh Island shore occurs (Figure 3-52, Atlas of Sardakh Channel, 1949; Seleznev, 1986), which is accompanied with significant current speeds (Figure 3-53) and a large discharge of sediment load in the Trofimovskaya Channel (between 50 to 80 % of the total solid discharge volume in the delta).

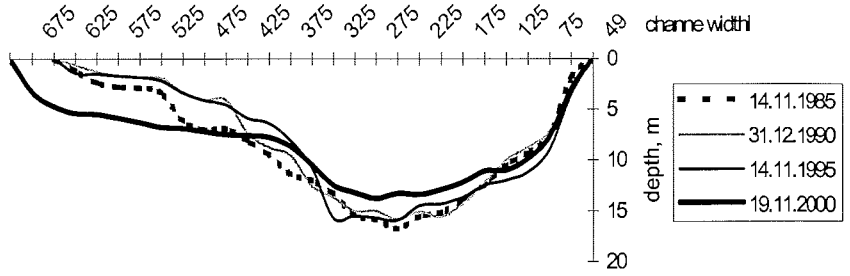

Figure 3-51. Depth change of Bykovskaya Channel for the last 15 years.

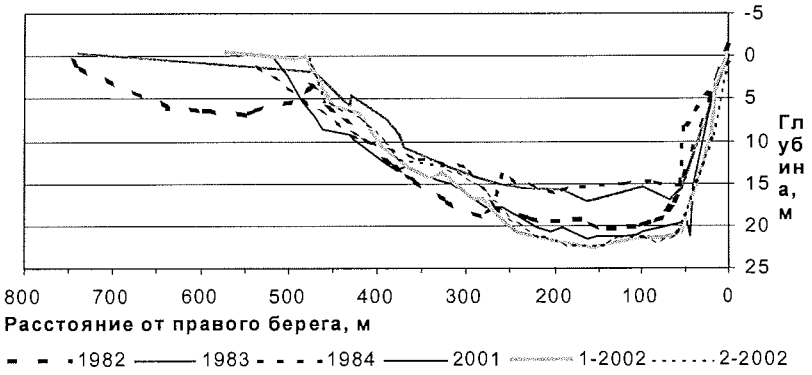

Figure 3-52. Depths in the gauge line No. 3 over the period 1982-2002.

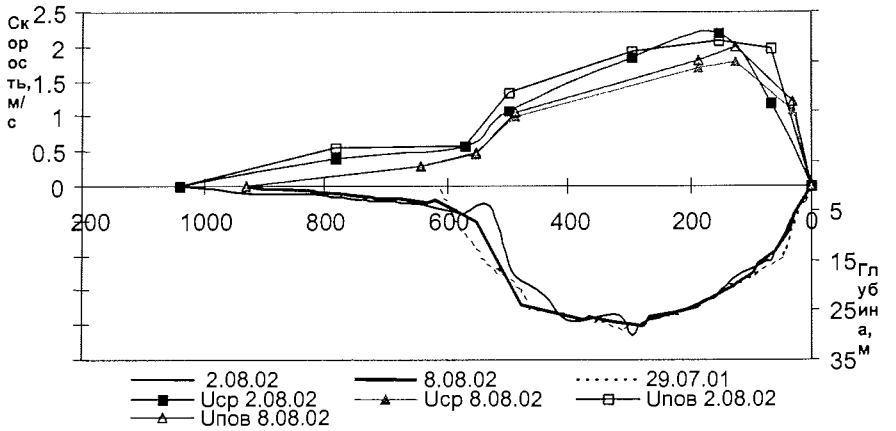

Figure 3-53. Depths and current speeds in the gauge line near Sardakh Island.

- At the Sardakh-Trofimovsky bifurcation point, there is an intense increase of Trofim-Kumaga sand shoal with a simultaneous erosion of the right bank near Sardakh Island (Figure 3-54). At the present time, 95% of the runoff of the Trofimovskaya Channel passes close to this island, which bifurcates then into two parts (Figure 3-55). An evaluation of the bed stability in this region and the construction of the hydrodynamic model can be the next stage of the studies in the Trofimovskaya Channel.

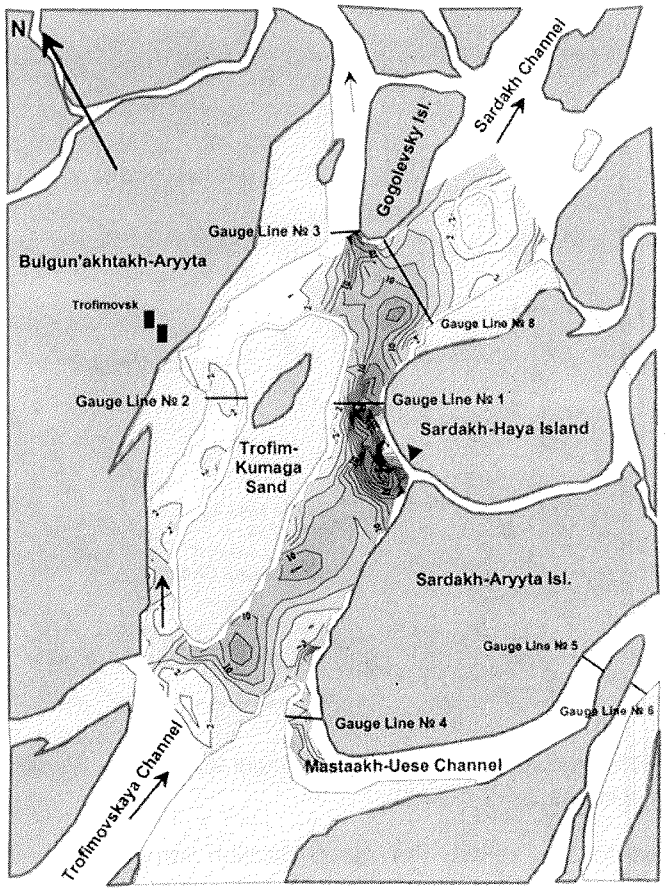

Figure 3-54. Bathymetric map-diagram of depths plotted from data of measurements on August 5-7, 2002.

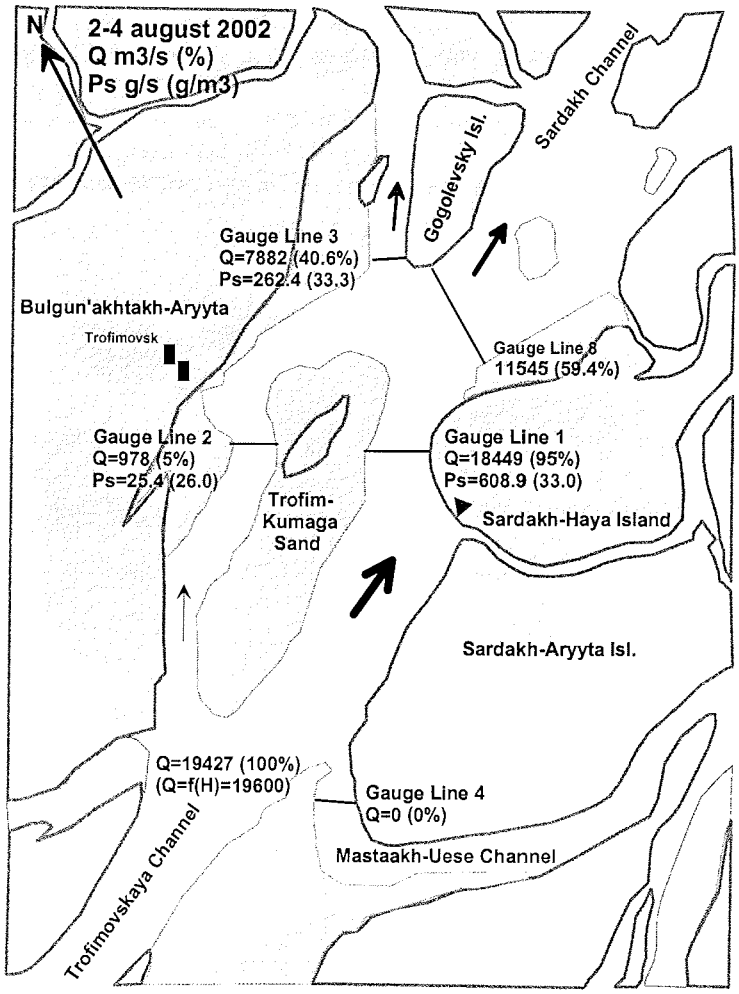

Figure 3-55. Discharges of water and sediment load at the Sardakh-Trofimovsky bifurcation point, August 2-4, 2002.

- Compared to the 1980s, the runoff fraction through the Trofimovskaya Channel has decreased to 40% increasing up to 60% correspondingly for the Sardakh Channel. Water turbidity in this channel downstream the bifurcation point increases. All this indicates that the Sardakh Channel at present is a developing water stream and further changes should be expected here.

3.11.4 Conclusion

The obtained results indicate a constant and sufficiently intense delta formation at two investigated bifurcation points: near Stolb Island and near Sardakh Island. There are obvious tendencies for the change in the direction of bed deformations of the channels in these regions, which provides grounds for further full-scale studies. It is also of interest to investigate the ion and heat sink in the Lena River delta since as compared to large rivers belonging to the Arctic Ocean Basin, the Lena River has a greater concentration of ions. As a qualitative indicator of the heat sink, one can use a constancy of water temperature, which is often twice as high as the air temperature for a long summer period.

The Lena River delta is a unique object of studies especially from the viewpoint of the hydrological and hydrodynamic features of the processes that govern the delta formation factors.

3.12 Shore erosion in the apex of the Lena Delta

Mikhail. N. Grigoriev

3.12.1 Introduction

Accumulation and erosion in the coastal zone and deltas are of major importance for the sediment budget of the Laptev Sea. The sediment balance within the Lena Delta is still an open question. The portion of sediment that is deposited in the Lena Delta and the sediment flux from eroded delta islands is not known. However, the modern sediment output from the Lena Delta exceeds the amount of deposits accumulating in that area.

One of the goals of the coastal team was to conduct reconnoitering studies of shore dynamics in the apex of the Lena Delta. The first part of the studies carried out in July 2002 was to evaluate the dynamics of erosive island shores and to study the resulting sediment flux. In total 34 key sites, which are characterized by active shore erosion, were investigated in order to estimate the range of shore retreat rates and the amount of sediment entering the branches of the Lena Delta due to shore erosion (see Fig. 3-56). Most studied sites belong to the islands composing the first terrace above the floodplain, which is the dominating geomorphological level in the studied area.

3.12.2 Methods

The methods to estimate shore dynamics are simple in principle. Measurements of the distance between the shoreline and some natural land forms (marks), which can be identified on an aerial photograph or a small scale map, have been carried out by a special tape measure. As natural marks mostly small lakes with stable shores were used. Most often we simply measured the distance to the cliff edge ignoring the width of the beach. The comparison of the modern field data with remote sensing information taken in the past decades allows to calculate the average annual retreat rates of selected shores. Aerial photographs (scale 1:40 000-1:70 000, taken 1951, 1962, 1972), topographic maps (scale 1:25 000-1:100 000) and satellite images were used. For the quantification of the sediment flux resulting from shore erosion, average ice content and specific density of the deposits composing the shores in the apex of the Lena Delta were taken into account. In total ca. 60 km of shore cliffs were studied in respect of erosion rate.

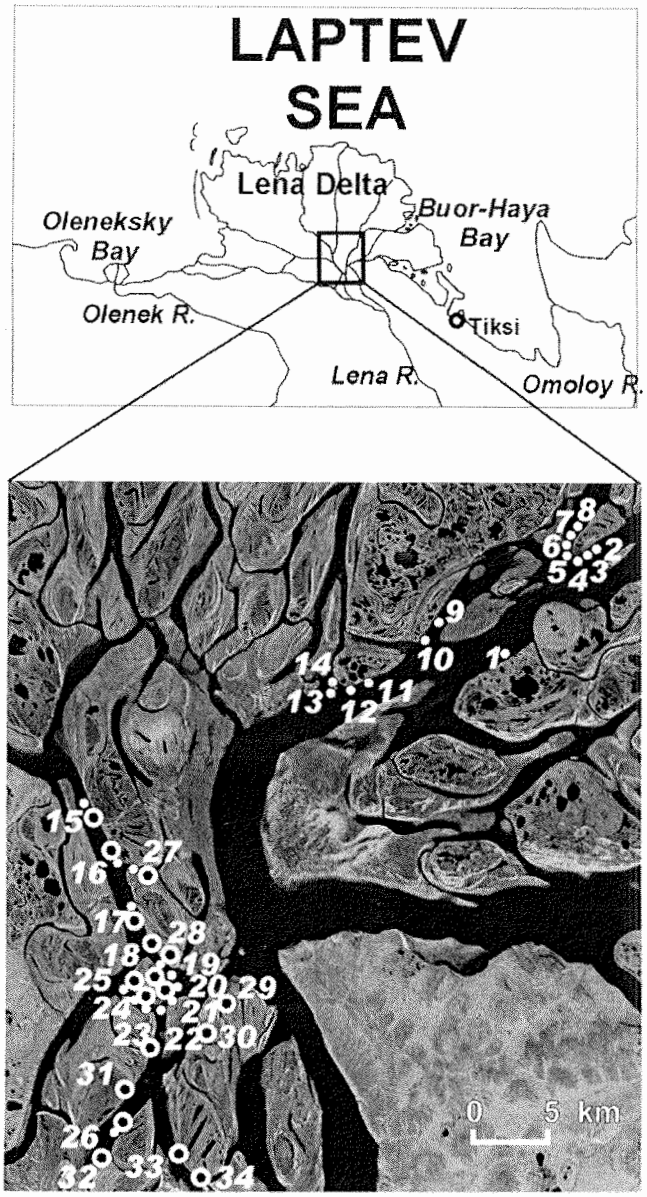

Figure 3-56. Key sites for measurement of shore retreat rates in the Lena Delta Apex (2001-2002). White circles – key sites 2001, Black-and-white circles –key sites 2002.

3.12.3 Results

The main results are shown in Table 3-26. All stations were located along the shores of the first terrace and the floodplain in the delta apex. The average cliff height is about 6 m (3-11 m) and the average retreat rate of actively eroded coast is about 3.9 m/yr. The shores exposed to the current of the main channels

are destroyed much faster - for example stations 4-6 (Gogolevsky Island) and station 20-21 (Samoylovsky Island). The maximum retreat rates were observed at Gogolevsky Island (station 5, south-western cape) which divides the two largest delta channels: Trofimovsky and Sardakhsky (Fig. 3-56).

The comparison of the shoreline position on an aerial photograph of Samoylovsky Island taken in September 1980 with the shoreline taken from a satellite image (Landsat, July 2000) shows that there has been a considerable modification of the margins of the island during the last 20 years. It has to noted that changes of the western and northern shorelines positions are difficult to evaluate because the contours of these low and flooded shores strongly depend on the river-water-level, which is highly variable.

In 2001 the average retreat rate of all studied actively eroded coasts was 4.7 m/yr. In 2002 new data on additional eroded sites were obtained, which indicate lower retreat rates. The average retreat rate of all (2001 and 2002) studied coasts is 3.9 m/yr and the sediment flux calculations were revised accordingly.

At the moment it is not possible to accurately quantify the volume of sediments resulting from eroded shores for the whole delta. But the preliminary results indicates that this sediment flux cannot be ignored. Based on average retreat rates of 3.9 m/yr (R), average cliff height of 6 m (H), average ice content of 20% (Ice coefficient = 0.8) and an average specific density of 1.6 g/cm^3 (SD), the sediment flux from the studied 60 km shores (L) in the Lena Delta can be quantified in the following way:

3.9 (R) • 60000 (L) • 6 (H) • 0.8 (Ice coefficient) • 1,6 (SD) = 1797120 t/yr

3.12.4 Discussion and conclusion

There are a number of unsolved questions concerning the sediment balance of the Lena Delta: (1) it is not known how much sediment is deposited within the delta, e.g. on the surface of floodplains, along the delta margins and within near-delta shallows; (2) it is very difficult to estimate the sediment input from eroded sand banks; (3) there is no information on the volume of the bed-load discharge; (4) almost nothing is know about the sediment dynamics during the spring-flood. Nevertheless, the fact that only local sections (60 km length) of the eroded island shores within the delta can supply about 1.8 m million tons of sediments per year, shows the great importance to erosion processes in the sediment balance of the delta.

We have only studied actively eroded cliffs in the area where the delta channels are characterized by fastest currents and highest water levels. Evidently, it is impossible to transfer the obtained sediment flux parameters to the entire Lena Delta. However, in any case the preliminary results of this study suggest that the sediment flux from eroded shores of the Lena Delta plays an important role in the sediment budget of the Laptev Sea. In 2001-2002 our measurements concentrated on erosive shores only and the next step will be to include accumulative shore sections as well.

Table 3-26. Average retreat rates of actively eroded shores at the key sites in the apex of the Lena Delta (2001-2002).

Key sites	Average retreat rate, m/yr	
	July -August 2001	July 2002
1. Sardakh-Aryta Island	4.8	-
2. Gogolevsky Island	2.1	-
3. Gogolevsky Island	1.9	-
4. Gogolevsky Island	12.2	-
5. Gogolevsky Island	14.2	-
6. Gogolevsky Island	13.4	-
7. Gogolevsky Island	4.5	-
8. Gogolevsky Island	2.3	-
9. Trofimovsky Island	8.4	-
10. Trofimovsky Island	6.7	-
11. Baron Island	9.2	-
12. Baron Island	3.6	-
13. Small Baron Island	5.4	-
14. Small Baron Island	3.7	-
15. Matvey-Aryta Island	4.7	4.5
16. Matvey-Aryta Island	6.1	6.0
17. Yrbylakh-Aryta Island	2.7	2.4
18. Samoylovsky Island	1.4	1.4
19. Samoylovsky Island	1.6	1.5
20. Samoylovsky Island	2.9	3.0
21. Samoylovsky Island	3.4	3.3
22. Samoylovsky Island	1.9	2.0
23. Samoylovsky Island	1.9	1.8
24. Samoylovsky Island	1.5	1.4
25. Samoylovsky Island	2.1	2.0
26. Sordokh-Aryta Island	1.6	1.7
27. Matvey-Aryta Usland	3.3	3.4
28. Yrbylakh-Aryta Ialand	-	1.8
29. Debenek-Aryta Island	-	1.2
30. Sistekh-Aryta Island	-	3.0
31. Sasyl-Ary Island	-	2.4
32. Sordokh-Ary Island	-	2.7
33. Sistekh-Aryta Island	-	4.2
34. Sistekh-Aryta Island	-	5.1
Average retreat rates of actively eroded shores	**3.9**	

3.13 Species composition, ecology, population structure and seasonal dynamic of zooplankton from tundra water basins in the Lena Delta

Ekatarina N. Abramova

3.13.1 Objectives

Information concerning pelagic fauna of the lakes and rivers at extreme latitudes in the Russian Arctic is still limited, and the Lena Delta is no exception. Investigations of zooplankton in the Lena Delta started at the beginning of the XX century, during Russian Polar expedition 1901-1903. However, the knowledge about the structure and functioning of zooplankton community in this big region is insufficient numbering only several papers (Rylov, 1928; Bening, 1942; Urban, 1949; Pirozhnikov & Shulga, 1957; Pirozhnikov, 1958; Botvinnik & Vershinin, 1958; Ammosov, 1961; Kerer, 1968; Serkina, 1969, Sokolova, 1984, Abramova, 1996; Stepanova & Abramova, 1997; Abramova & Sokolova, 1999; Gukov, 2001; Akhmetshina & Abramova, 2002) that offer certain information about species composition and abundance of zooplankton from some parts of the Lena Delta. Generalization of the special investigations is still lacking. This primarily concerns seasonal variations in the structure of zooplankton assemblages.

In the present study, we examined the zooplankton assemblages in channels, terrace lakes, big and small thermokarst lakes from the different regions in the Lena Delta. The data on species composition, distribution, population structure, and seasonal dynamic of zooplankton abundance in relation to water temperature were analyzed.

3.13.2 Materials and Methods

In July – September 2002, 75 quantitative and qualitative zooplankton samples were collected as a part of biological investigations in the Delta-2002 expedition. The samples were obtained in water basins of different type on the Samoilovskii, Tit-Ary, Amerika-Khaya, and Buor-Khaya islands in the Lena Delta (Table 3-27). Regular investigations were carried out on the Samoilovskii Island only.

Table 3-27. Location and number of zooplankton samples.

	Samoilovskii	Tit-Ary	Amerika-Khaya	Buor-Khaya
Olenekskaya channel	9			
Terrace lake	13	5		
Big thermokarst lake	4	3		
Deep polygon without plants	10			
Shallow polygon with plants	9	2		2
Crack between two polygons	9			
Alass			4	5

Sampling was performed by filtering of 100 liters of water through a 100 µm meshsize net with periodicity of 5-10 days and fixation with 70% alcohol. The whole sample or its part was studied in the Bogorov's camera under microscope, and the abundance of organisms was calculated. We determined species, sex and moulting stages. The data were recalculated to 1 m^3 of water. Water temperature was measured simultaneously with plankton sampling.

3.13.3 Preliminary results

Species composition

In the water pools of the Lena Delta, 106 taxa of zooplankton belonging to 2 types (Rotatoria and Arthropoda) were determined: Rotatoria – 61 taxa, Arthropoda, subclass Crustacea – 45 species, among them: Copepoda – 30 species (Cyclopoida – 14, Calanoida – 14, Harpacticoida – 2), Cladocera – 13, Phyllopoda – 2 (Appendix 3-14). There are well-manifested differences in species composition in water basins of different types. The highest species diversity was recognized in the terrace lake on the Samoilivskii Island (54 taxa), and the lowest species diversity was determined in the alass on the Amerika-Khaya Island (11 taxa). Zooplankton species composition was clearly dominated by Rotatoria. The latter reached maximum diversity in the channel, terrace lakes, and alases, where they constituted up to more than 60% of the total species richness (Fig. 3-57). Copepoda (about 45% of the total species number) and two species of Phyllopoda were the main component of zooplankton in the polygon lakes. Cladocera was widely distributed in all types of water pools, especially *Chidorus sphaericus*, but species diversity of this group was comparatively low.

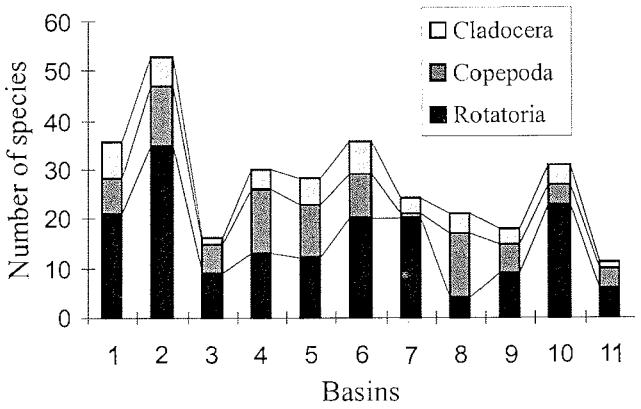

Figure 3-57. Distribution of species numbers in the different water basins in the Lena Delta: Samoilovskii Island: 1 – Olenekskaya channel, 2 - terrace lake, 3 – big thermokarst lake, 4 - polygons , 5 - crack between polygons; Tit-Ary Island: 6 - flood-plain lake, 7 – big thermokarst lake, 8 - polygons; Buor-Khaya Island: 9 - polygons, 10 – alas; America-Khaya Island: 11 - alas.

Variations in the species composition and abundance dynamics

Seasonal variations in the species composition and zooplankton abundance were well manifested in the water basins on the Samoilovskii Island. Rotatoria demonstrated high density in zooplankton communities of the Olenekskaya channel and terrace lake during the whole period of our investigation. Maximum zooplankton abundance in the Olenekskaya channel (16860 ind.m^{-3}) had been observed at the beginning of July at 14°C of water temperature and was related to reproduction of common species of Rotatoria: *Asplanchna priodonta; Keratella cochlearis* and *K. quadrata,* which composed about 60% of the total abundance. Later, a decrease in the total zooplankton abundance and a change in the dominant species were observed (Fig. 3-58).

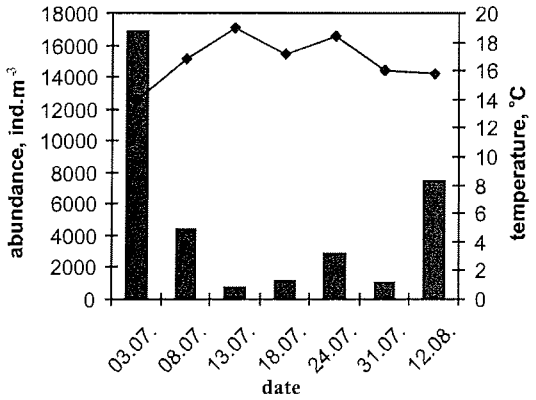

Figure 3-58. Seasonal variations in temperature and total zooplankton abundance in the Olenekskaya channel. (Abundance T° C)

Several species of Euchlanis genus became dominant instead of the above-mentioned. In August the increase in abundance was marked again. *Trichocerca cylindrica* had reproduction period and demonstrated the high density during this period. The average summer zooplankton abundance in the Olenekskaya channel was 4907 ind.m^{-3}.

Strong variations in the total zooplankton abundance were observed in the terrace lake on the Samoilovskii Island (Fig. 3-59). The lower density (less than 700 ind.m^{-3}) was recorded at the beginning of July at 9°C of water temperature. *Synchaeta sp.* was the dominant species. The first peak of the total zooplankton abundance was observed at the end of July (24560 ind.m^{-3}), when four Euchlanis species were numerous. The highest abundance (about 50000 ind.m^{-3}) was marked in middle August, when water temperature was 14°C. This maximum corresponded to the reproduction of several Rotatoria species belonging to Keratella, Polyarthra and Euchlanis genera. The average zooplankton abundance in the terrace lake throughout summer was 12018 ind.m^{-3}.

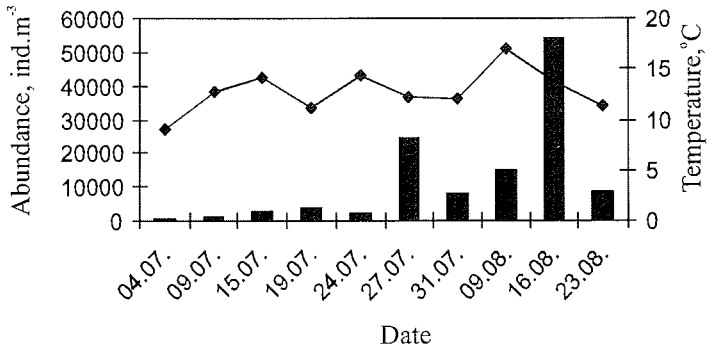

Figure 3-59. Seasonal variations in temperature and total zooplankton abundance in the terrace lake on the Samoilovskii Island. (Abundance T° C)

Copepoda predominated in zooplankton communities of the small polygon lakes of two different types, deep polygon without plants and shallow polygon with plants, and, also, the crack between polygons. Cladocera and Rotatoria occurred in comparatively small amounts. In these types of the water pools seasonal fluctuations in the total zooplankton abundance were insignificant (Fig. 3-60).

Calanoids *Heterocope borealis* and *Mixodiaptomus theeli* were the most numerous copepods during the whole period of investigation. Only in the crack cyclopoids were dominant in mid-August. Variations in zooplankton density were connected with the life cycles of the common Copepoda species. The maximums of the total abundance coincided with appearance of juvenile stages of these species. Three peaks of the total zooplankton abundance were recorded in the deep polygon with maximum (7000 ind. m^{-3}) in the second decade of July at 11.2°C water temperature (Fig. 3-60A). The average summer density was 5018 ind. m^{-3}.

Two peaks of the total zooplankton abundance were observed in the shallow polygon and the crack. In the first case, maximum of the total abundance (14580 ind. m^{-3}) was marked at the beginning of July at 15.2°C water temperature (Fig. 3-60B). The average summer density was comparatively high - 9557 ind. m^{-3}. Opposite, in the crack, maximum zooplankton density (7280 ind. m^{-3}) was recorded in the second decade of August, when water temperature was 13.4°C. The average abundance during the whole period of investigation equaled to 4578 ind.m^{-3}.

It is well known, that zooplankton organisms are susceptible to variations of a wide number of environmental factors including water temperature, light, food, chemistry, etc. According to our results, there was no evident correlation between temperature conditions and dynamics of zooplankton abundance during the period of investigation. Considerable variations in zooplankton density and species composition occurred seasonally due to changes in the life cycles of different populations.

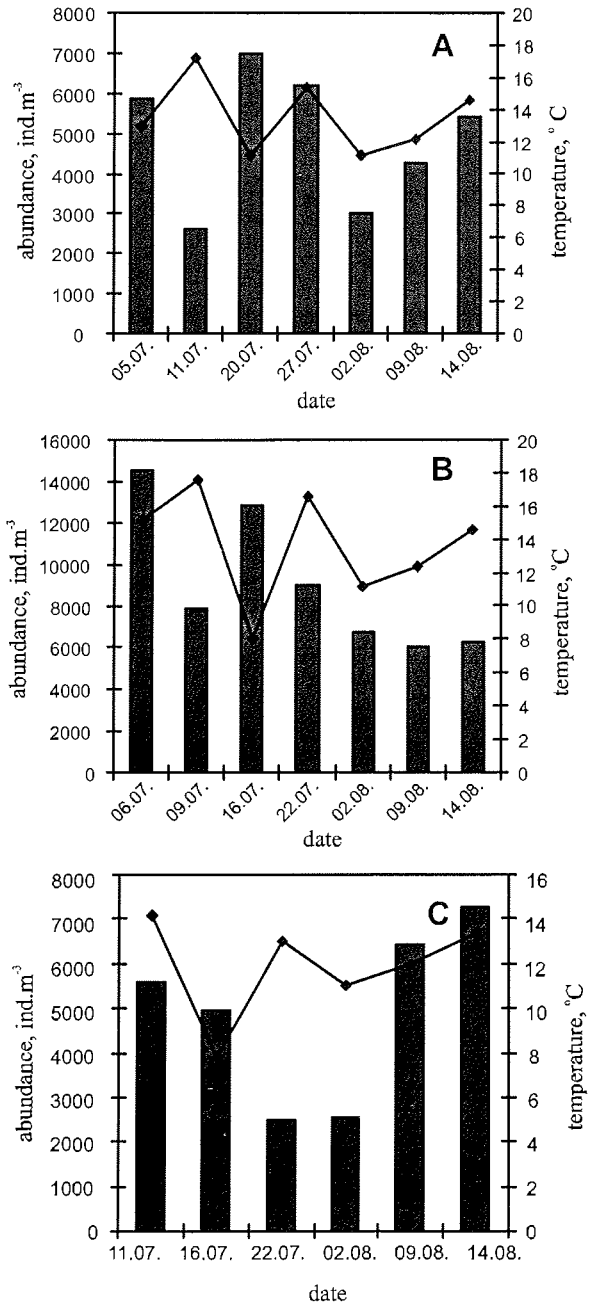

Figure 3-60. Seasonal variations in temperature and total zooplankton abundance in the deep polygon lake (A), shallow polygon lake (B) and in the crack between polygons (C) on the Samoilovskii Island (Abundance T° C)

3.14 Appendix

Appendix 3-1. List of soil and plant samples (total amount = 76), collected at central Lena Delta during the expedition Lena Delta 2002.

no.	sample ID	date	location	description	depth (cm)	planned analyses
1	LD02-6941	22.07.2002	Samoylov 72° 23` 11.9 N 126° 28`54.0 E	soil sample, profile 2002-1	0-5	geo chemical,microbiological, molecularbiological
2	LD02-6942	22.07.2002	Samoylov 72° 23` 11.9 N 126° 28`54.0 E	soil sample, profile 2002-1	5-9	geo chemical,microbiological, molecularbiological
3	LD02-6943	22.07.2002	Samoylov 72° 23` 11.9 N 126° 28`54.0 E	soil sample, profile 2002-1	9-18	geo chemical,microbiological, molecularbiological
4	LD02-6944	22.07.2002	Samoylov 72° 23` 11.9 N 126° 28`54.0 E	soil sample, profile 2002-1	20-35	geo chemical,microbiological, molecularbiological
5	LD02-6945	22.07.2002	Samoylov 72° 23` 11.9 N 126° 28`54.0 E	soil sample, profile 2002-1	35-40	geo chemical,microbiological, molecularbiological
6	LD02-6946	22.07.2002	Samoylov 72° 23` 11.9 N 126° 28`54.0 E	soil sample, profile 2002-1	40-52	geo chemical,microbiological, molecularbiological
7	LD02-6947	22.07.2002	Samoylov 72° 23` 11.9 N 126° 28`54.0 E	soil sample, profile 2002-1	>52	geo chemical,microbiological, molecularbiological
8	LD02-6948	24.07.2002	Kurungnakh 72° 20' 00.6 N 126° 17`09.2	soil sample, active layer on top of permafrost drill hole	+7-0	geo chemical,microbiological, molecularbiological
9	LD02-6949	24.07.2002	Kurungnakh 72° 20' 00.6 N 126° 17`09.2	soil sample, active layer on top of permafrost drill hole	0-10	geo chemical,microbiological, molecularbiological
10	LD02-6950	24.07.2002	Kurungnakh 72° 20' 00.6 N 126° 17`09.2	soil sample, active layer on top of permafrost drill hole	10-20	geo chemical,microbiological, molecularbiological
11	LD02-6951	24.07.2002	Kurungnakh 72° 20' 00.6 N 126° 17`09.2	soil sample, active layer on top of permafrost drill hole	20-35	geo chemical,microbiological, molecularbiological
12	LD02-6952	24.07.2002	Kurungnakh 72° 20' 00.6 N 126° 17`09.2	soil sample, active layer on top of permafrost drill hole	35-60	geo chemical,microbiological, molecularbiological
13	LD02-6953	24.07.2002	Kurungnakh 72° 20' 00.6 N 126° 17`09.2	soil sample, active layer on top of permafrost drill hole	60-80	geo chemical,microbiological, molecularbiological
14	LD02-6954	24.07.2002	Kurungnakh 72° 20' 00.6 N 126° 17`09.2	soil sample, active layer on top of permafrost drill hole	80-110	geo chemical,microbiological, molecularbiological
15	LD02-6968	07.08.2002	Samoylov 72° 22.2' N 129° 28.5' E	soil sample, polygoncentre	0-5	microbiological
16	LD02-6969	07.08.2002	Samoylov 72° 22.2' N 129° 28.5' E	soil sample, polygoncentre	5-10	microbiological
17	LD02-6970	07.08.2002	Samoylov 72° 22.2' N 129° 28.5' E	soil sample, polygoncentre	10-15	microbiological
18	LD02-6971	07.08.2002	Samoylov 72° 22.2' N 129° 28.5' E	soil sample, polygoncentre	15-20	microbiological
19	LD02-6972	07.08.2002	Samoylov 72° 22.2' N 129° 28.5' E	soil sample, polygoncentre	20-23	microbiological
20	LD02-6973	07.08.2002	Samoylov 72° 22.2' N 129° 28.5' E	soil sample, polygoncentre	23-30	microbiological
21	LD02-6974	07.08.2002	Samoylov 72° 22.2' N 129° 28.5' E	soil sample, polygoncentre	30-35	microbiological
22	LD02-6975	07.08.2002	Samoylov 72° 22.2' N 129° 28.5' E	soil sample, polygoncentre	35-40	microbiological
23	LD02-6976	07.08.2002	Samoylov 72° 22.2' N 129° 28.5' E	soil sample, polygoncentre	40-45	microbiological
24	LD02-6983	16.08.2002	Samoylov 414.860m 8.031.980m	soil sample, top of polygonborder, BS 1	0-3	geo chemical,microbiological, molecularbiological
25	LD02-6984	16.08.2002	Samoylov 414.860m 8.031.980m	soil sample, top of polygonborder, BS 1	3-7	geo chemical,microbiological, molecularbiological
26	LD02-6985	16.08.2002	Samoylov 414.860m 8.031.980m	soil sample, top of polygonborder, BS 1	7-15	geo chemical,microbiological, molecularbiological
27	LD02-6986	16.08.2002	Samoylov 414.860m 8.031.980m	soil sample, top of polygonborder, BS 1	15-23	geo chemical,microbiological, molecularbiological
28	LD02-6987	16.08.2002	Samoylov 414.860m 8.031.980m	soil sample, top of polygonborder, BS 1	23-29	geo chemical,microbiological, molecularbiological
29	LD02-6988	16.08.2002	Samoylov 414.860m 8.031.980m	soil sample, top of polygonborder, BS 1	29-34	geo chemical,microbiological, molecularbiological
30	LD02-6989	16.08.2002	Samoylov 414.860m 8.031.980m	soil sample, top of polygonborder, BS 1	34-40	geo chemical,microbiological, molecularbiological
31	LD02-6990	16.08.2002	Samoylov 414.860m 8.031.980m	soil sample, top of polygonborder, BS 1	40-55	geo chemical,microbiological, molecularbiological
32	LD02-6991	16.08.2002	Samoylov 414.860m 8.031.980m	soil sample, top of polygonborder, BS 1	55-65	geo chemical,microbiological, molecularbiological
33	LD02-6992	16.08.2002	Samoylov 414.860m 8.031.980m	soil sample, top of polygonborder, BS 1	>65	geo chemical,microbiological, molecularbiological
34	LD02-6993	19.08.2002	Samoylov 72° 23` 11.9 N 126° 28`54.0 E	soil sample, profile 2002-1	0-5	molecularbiological
35	LD02-6994	19.08.2002	Samoylov 72° 23` 11.9 N 126° 28`54.0 E	soil sample, profile 2002-1	5-9	molecularbiological
36	LD02-6995	19.08.2002	Samoylov 72° 23` 11.9 N 126° 28`54.0 E	soil sample, profile 2002-1	9-20	molecularbiological
37	LD02-6996	19.08.2002	Samoylov 72° 23` 11.9 N 126° 28`54.0 E	soil sample, profile 2002-1	20-35	molecularbiological
38	LD02-6997	19.08.2002	Samoylov 72° 23` 11.9 N 126° 28`54.0 E	soil sample, profile 2002-1	35-40	molecularbiological
39	LD02-6998	19.08.2002	Samoylov 72° 23` 11.9 N 126° 28`54.0 E	soil sample, profile 2002-1	40-52	molecularbiological
40	LD02-6999	19.08.2002	Samoylov 72° 23` 11.9 N 126° 28`54.0 E	soil sample, profile 2002-1	52-60	molecularbiological
41	LD02-7000	19.08.2002	Samoylov 72° 23` 11.9 N 126° 28`54.0 E	soil sample, profile 2002-1	60-65	molecularbiological
42	LD02-7001	20.08.2002	Samoylov 414.860m 8.031.981m	plant sample, polygonborder, BS 2	+4	
43	LD02-7002	20.08.2002	Samoylov 414.860m 8.031.981m	soil sample, polygonborder, BS 2	0-10	geo chemical,microbiological, molecularbiological
44	LD02-7003	20.08.2002	Samoylov 414.860m 8.031.981m	soil sample, polygonborder, BS 2	10-17	geo chemical,microbiological, molecularbiological
45	LD02-7004	20.08.2002	Samoylov 414.860m 8.031.981m	soil sample, polygonborder, BS 2	17-25	geo chemical,microbiological, molecularbiological
46	LD02-7005	20.08.2002	Samoylov 414.860m 8.031.981m	soil sample, polygonborder, BS 2	>25	geo chemical,microbiological, molecularbiological

Appendix 3-1. cont.

no.	sample ID	date	location	description	depth (cm)	planned analyses
47	LD02-7006	20.08.2002	Samoylov 414.858m 8031.987m	plant sample, polygoncentre, BS 3	+1	
48	LD02-7007	20.08.2002	Samoylov 414.858m 8031.987m	soil sample, polygoncentre, BS 3	0-15	geo chemical,microbiological, molecularbiological
49	LD02-7008	20.08.2002	Samoylov 414.858m 8031.987m	soil sample, polygoncentre, BS 3	15-34	geo chemical,microbiological, molecularbiological
50	LD02-7009	20.08.2002	Samoylov 414.858m 8031.987m	soil sample, polygoncentre, BS 3	>34	geo chemical,microbiological, molecularbiological
51	LD02-7016	28.08.2002	Samoylov 415.386m 8.032.421m	soil sample, top of polygonborder, BS 4	0-6	geo chemical,microbiological, molecularbiological
52	LD02-7017	28.08.2002	Samoylov 415.386m 8.032.421m	soil sample, top of polygonborder, BS 4	6-20	geo chemical,microbiological, molecularbiological
53	LD02-7018	28.08.2002	Samoylov 415.386m 8.032.421m	soil sample, top of polygonborder, BS 4	20-32	geo chemical,microbiological, molecularbiological
54	LD02-7019	28.08.2002	Samoylov 415.386m 8.032.421m	soil sample, top of polygonborder, BS 4	>32	geo chemical,microbiological, molecularbiological
55	LD02-7020	29.08.2002	Samoylov 415.382m 8.032.419m	soil sample, polygoncentre, BS 5	0-10	geo chemical,microbiological, molecularbiological
56	LD02-7021	29.08.2002	Samoylov 415.382m 8.032.419m	soil sample, polygoncentre, BS 5	10-26	geo chemical,microbiological, molecularbiological
57	LD02-7022	29.08.2002	Samoylov 415.382m 8.032.419m	soil sample, polygoncentre, BS 5	26-34	geo chemical,microbiological, molecularbiological
58	LD02-7023	29.08.2002	Samoylov 415.382m 8.032.419m	soil sample, polygoncentre, BS 5	>34	geo chemical,microbiological, molecularbiological
59	LD02-7024	26.07.2002	Kurungnakh 72° 20' 00.6 N 126° 17`09.2	plant sample	surface	C/N-content, 13C-content
60	LD02-7025	26.07.2002	Kurungnakh 72° 20' 00.6 N 126° 17`09.3	plant sample	surface	C/N-content, 13C-content
61	LD02-7026	26.07.2002	Kurungnakh 72° 20' 00.6 N 126° 17`09.4	plant sample	surface	C/N-content, 13C-content
62	LD02-7027	26.07.2002	Kurungnakh 72° 20' 00.6 N 126° 17`09.5	plant sample	surface	C/N-content, 13C-content
63	LD02-7028	26.07.2002	Kurungnakh 72° 20' 00.6 N 126° 17`09.6	plant sample	surface	C/N-content, 13C-content
64	LD02-7029	26.07.2002	Kurungnakh 72° 20' 00.6 N 126° 17`09.7	plant sample	surface	C/N-content, 13C-content
65	LD02-7030	26.07.2002	Kurungnakh 72° 20' 00.6 N 126° 17`09.8	plant sample	surface	C/N-content, 13C-content
66	LD02-7031	25.07.2002	Kurungnakh 72° 20' 00.6 N 126° 17`09.9	plant sample	surface	C/N-content, 13C-content
67	LD02-7032	25.07.2002	Kurungnakh 72° 20' 00.6 N 126° 17`09.10	plant sample	surface	C/N-content, 13C-content
68	LD02-7033	25.07.2002	Kurungnakh 72° 20' 00.6 N 126° 17`09.11	plant sample	surface	C/N-content, 13C-content
69	LD02-7040	02.09.2002	Samoylov 72° 23` 11.9 N 126° 28`54.0 E	soil sample, profile 2002-1	0-5	molecularbiological
70	LD02-7041	02.09.2002	Samoylov 72° 23` 11.9 N 126° 28`54.0 E	soil sample, profile 2002-1	5-9	molecularbiological
71	LD02-7042	02.09.2002	Samoylov 72° 23` 11.9 N 126° 28`54.0 E	soil sample, profile 2002-1	9-18	molecularbiological
72	LD02-7043	02.09.2002	Samoylov 72° 23` 11.9 N 126° 28`54.0 E	soil sample, profile 2002-1	20-35	molecularbiological
73	LD02-7044	02.09.2002	Samoylov 72° 23` 11.9 N 126° 28`54.0 E	soil sample, profile 2002-1	35-40	molecularbiological
74	LD02-7045	02.09.2002	Samoylov 72° 23` 11.9 N 126° 28`54.0 E	soil sample, profile 2002-1	40-52	molecularbiological
75	LD02-7046	02.09.2002	Samoylov 72° 23` 11.9 N 126° 28`54.0 E	soil sample, profile 2002-1	52-60	molecularbiological
76	LD02-7047	02.09.2002	Samoylov	soil sample	4-9	geo chemical,microbiological, molecularbiological

Appendix 3-2. List of sediment samples (total amount = 76), collected at central Lena Delta during the expedition Lena Delta 2002.

no.	sample ID	date	location	description	depth (cm)	planned analyses
1	LD02-6977	08.08.2002	Samoylov 415.290m 8.032.337m	sediment sample	0-2	geo chemical,microbiological, molecularbiological
2	LD02-6978	08.08.2002	Samoylov 415.290m 8.032.337m	sediment sample	2-4	geo chemical,microbiological, molecularbiological
3	LD02-6979 A	08.08.2002	Samoylov 415.290m 8.032.337m	sediment sample	4-7	geo chemical,microbiological, molecularbiological
4	LD02-6979 B	08.08.2002	Samoylov 415.290m 8.032.337m	sediment sample	7-10	geo chemical,microbiological, molecularbiological
5	LD02-6980A	08.08.2002	Samoylov 415.290m 8.032.337m	sediment sample	10-13	geo chemical,microbiological, molecularbiological
6	LD02-6980B	08.08.2002	Samoylov 415.290m 8.032.337m	sediment sample	13-16	geo chemical,microbiological, molecularbiological
7	LD02-6981A	08.08.2002	Samoylov 415.290m 8.032.337m	sediment sample	16-17	geo chemical,microbiological, molecularbiological
8	LD02-7010	23.08.2002	Samoylov 415.305m 8.032.350m	plant sample	~+15	microbiological, molecularbiological
9	LD02-7011	23.08.2002	Samoylov 415.305m 8.032.350m	sediment sample	0-2	geo chemical,microbiological, molecularbiological
10	LD02-7012	23.08.2002	Samoylov 415.305m 8.032.350m	sediment sample	2-4	geo chemical,microbiological, molecularbiological
11	LD02-7013A	23.08.2002	Samoylov 415.305m 8.032.350m	sediment sample	4-7	geo chemical,microbiological, molecularbiological
12	LD02-7013B	23.08.2002	Samoylov 415.305m 8.032.350m	sediment sample	7-10	geo chemical,microbiological, molecularbiological
13	LD02-7014A	23.08.2002	Samoylov 415.305m 8.032.350m	sediment sample	10-13	geo chemical,microbiological, molecularbiological
14	LD02-7014B	23.08.2002	Samoylov 415.305m 8.032.350m	sediment sample	13-16	geo chemical,microbiological, molecularbiological
15	LD02-7015	23.08.2002	Samoylov 415.305m 8.032.350m	sediment sample	16-19	geo chemical,microbiological, molecularbiological

Appendix 3-3. List of water samples (total amount = 19), collected at central Lena Delta during the expedition Lena Delta 2002.

no.	sample ID	date	location	description	depth (cm)	planned analyses
1	LD02-6955	14.07.2002	Samoylov 415.290m 8.032.337m, polygonal lake 1	filter (water sample)	surface	molecularbiological
2	LD02-6956	14.07.2002	Samoylov 415.290m 8.032.337m, polygonal lake 1	filter (water sample)	bottom	molecularbiological
3	LD02-6957	14.07.2002	Samoylov 415.305m 8.032.350m, polygonal lake 2	filter (water sample)	surface	molecularbiological
4	LD02-6958	14.07.2002	Samoylov 415.305m 8.032.350m, polygonal lake 2	filter (water sample)	bottom	molecularbiological
5	LD02-6959	14.07.2002	Samoylov 415.370m 8.032.350m, ice wedge lake	filter (water sample)	surface	molecularbiological
6	LD02-6960	14.07.2002	Samoylov 415.370m 8.032.350m, ice wedge lake	filter (water sample)	bottom	molecularbiological
7	LD02-6961	03.08.2002	Samoylov 415.370m 8.032.350m, ice wedge lake	filter (ice sample)	bottom	molecularbiological
8	LD02-6962	03.08.2002	Samoylov 415.290m 8.032.337m, polygonal lake 1	filter (water sample)	surface	molecularbiological
9	LD02-6963	03.08.2002	Samoylov 415.290m 8.032.337m, polygonal lake 1	filter (water sample)	bottom	molecularbiological
10	LD02-6964	03.08.2002	Samoylov 415.305m 8.032.350m, polygonal lake 2	filter (water sample)	surface	molecularbiological
11	LD02-6965	03.08.2002	Samoylov 415.305m 8.032.350m, polygonal lake 2	filter (water sample)	bottom	molecularbiological
12	LD02-6966	03.08.2002	Samoylov 415.370m 8.032.350m, ice wedge lake	filter (water sample)	surface	molecularbiological
13	LD02-6967	03.08.2002	Samoylov 415.370m 8.032.350m, ice wedge lake	filter (water sample)	bottom	molecularbiological
14	LD02-7034	31.08.2002	Samoylov 415.290m 8.032.337m, polygonal lake 1	filter (water sample)	surface	molecularbiological
15	LD02-7035	31.08.2002	Samoylov 415.290m 8.032.337m, polygonal lake 1	filter (water sample)	bottom	molecularbiological
16	LD02-7036	31.08.2002	Samoylov 415.305m 8.032.350m, polygonal lake 2	filter (water sample)	surface	molecularbiological
17	LD02-7037	31.08.2002	Samoylov 415.305m 8.032.350m, polygonal lake 2	filter (water sample)	bottom	molecularbiological
18	LD02-7038	31.08.2002	Samoylov 415.370m 8.032.350m, ice wedge lake	filter (water sample)	surface	molecularbiological
19	LD02-7039	31.08.2002	Samoylov 415.370m 8.032.350m, ice wedge lake	filter (water sample)	bottom	molecularbiological

Appendix 3-4: List of sediment and water samples.

No	Sample No.	Date	Site	Sedi-ment	Ostra-cods	Cat-ion	An-ion	Iso-topes	Resi-due
01	SAM-01	02.08.02	Samoylov	X	X	X	X	X	X
02	SAM-02	03.08.02	Samoylov	X	X	X	X	X	X
03	SAM-03	03.08.02	Samoylov	X	X	X	X	X	X
04	SAM-04	04.08.02	Amerika Khaya	X	X	X	X	X	X
05	SAM-05	06.08.02	Tit-Ary	X	X	X	X	X	X
06	SAM-06	06.08.02	Tit-Ary	X	X	X	X	X	X
07	SAM-07	07.08.02	Tit-Ary	X	X	X	X	X	X
08	SAM-08	07.08.02	Tit-Ary	X	X	X	X	X	X
09	SAM-09	14.08.02	Samoylov	X	X	X	X	X	X
10	SAM-10	14.08.02	Samoylov	X	X	X	X	X	X
11	SAM-11	14.08.02	Samoylov	X	X	X	X	X	X
12	SAM-12	15.08.02	Kurungnakh	X	X	X	X	X	X
13	SAM-13	15.08.02	Kurungnakh	X	X	X	X	X	X
14	SAM-14	18.08.02	Samoylov	X	X	X	X	X	X
15	SAM-15	19.08.02	Samoylov	X	X	X	X	X	X
16	SAM-16	19.08.02	Samoylov	X	X	X	X	X	X
17	SAM-17	19.08.02	Samoylov	X	X	X	X	X	X
18	SAM-18	20.08.02	Samoylov	X	X	X	X	X	X
19	SAM-19	20.08.02	Samoylov	X	X	X	X	X	X
20	SAM-20	20.08.02	Samoylov	X	X	X	X	X	X
21	SAM-21	21.08.02	Samoylov	X	X	X	X	X	X
22	SAM-22	21.08.02	Samoylov	X	X	X	X	X	X
23	SAM-23	21.08.02	Samoylov	X	X	X	X	X	X
24	SAM-24	21.08.02	Samoylov	X	X	X	X	X	X
25	SAM-25	25.08.02	Samoylov	X	X	X	X	X	X
26	SAM-26	25.08.02	Samoylov	X	X	X	X	X	X
27	SAM-27	25.08.02	Samoylov	X	X	X	X	X	X
28	SAM-28	26.08.02	Samoylov	X	X	X	X	X	X
29	SAM-29	26.08.02	Samoylov	X	X	X	X	X	X
30	SAM-30	27.08.02	Samoylov	X	X	X	X	X	X
31	SAM-31	27.08.02	Samoylov	X	X	X	X	X	X
32	SAM-32	27.08.02	Samoylov	X	X	X	X	X	X
33	SAM-33	29.08.02	Samoylov	X	X	X	X	X	X
34	SAM-34	29.08.02	Samoylov	X	X	X	X	X	X
35	SAM-35	30.08.02	Samoylov	X	X	X	X	X	X
36	SAM-36	30.08.02	Samoylov	X	X	X	X	X	X
37	SAM-37	30.08.02	Samoylov	X	X	X	X	X	X
38	SAM-38	31.08.02	Kurungnakh	X	X	X	X	X	X
39	SAM-39	31.08.02	Kurungnakh	X	X	X	X	X	X
40	SAM-40	01.09.02	Samoylov	X	X	X	X	X	X
41	SAM-41	01.09.02	Samoylov	X	X	X	X	X	X
42	SAM-42	02.09.02	Samoylov	X	X	X	X	X	X
43	SAM-43	02.09.02	Samoylov	X	X	X	X	X	X
44	SAM-44	03.09.02	Samoylov	X	X	X	X	X	X

Appendix 3-5: List of results of water investigations.

No	Sample No.	pH	Conductivity [µS/cm]	Temperature [°C]	O_2 [mg/l]	Total hardness [°dH]	Carb. hardness [°dH]	NH_4^+ [mg/l]	NO_3^- [mg/l]	NO_2^- [mg/l]	PO_4^{3-} [mg/l]
01	SAM-01	7.0	90.4	11.4	9.8	5.1	2.3	0	0	<0.025	<0.25
02	SAM-02	7.5	68.5	11.6	8.7	4.4	2.6	0	0	0	0.25
03	SAM-03	7.5	84.6	13.6	9.3	6.0	2.5	0	0	0	0
04	SAM-04	7.0	24.3	14.1	9.4	3.8	2.0	0	0	0	0
05	SAM-05	7.0	70.9	15.7	8.3	3.4	3.2	<0.2	0	0.025	0.25
06	SAM-06	7.0	66.8	16.9	8.6	4.6	2.4	0	0	0	0
07	SAM-07	7.5	117.9	19.4	7.2	4.8	3.6	0	0	0	0
08	SAM-08	7.5	136.0	18.9	8.4	4.0	3.8	<0.4	0	0	<0.25
09	SAM-09	7.0	44.5	15.5	7.2	5.0	2.4	0	0	0	0
10	SAM-10	7.5	45.3	14.2	6.8	3.2	1.6	0	0	0	0
11	SAM-11	7.0	92.7	12.4	7.3	5.0	3.2	<0.4	0	0	0
12	SAM-12	7.0	28.0	13.4	7.7	2.4	1.0	0	0	0	0
13	SAM-13	6.5	27.0	13.6	5.9	3.8	1.0	0	0	0	0
14	SAM-14	7.5	86.6	12.6	8.8	3.6	2.4	0	0	0	0
15	SAM-15	7.5	72.8	11.2	8.9	3.2	2.2	0	0	0	0
16	SAM-16	7.5	64.7	11.3	9.3	2.8	2.4	0	0	0	0
17	SAM-17	7.5	64.9	12.0	8.4	3.4	2.4	0.4	0	0	0
18	SAM-18	7.5	115.8	11.2	7.6	4.5	4.0	0	0	0	0
19	SAM-19	7.5	53.1	12.5	8.8	3.3	2.0	0	0	0	0
20	SAM-20	7.5	76.8	12.6	8.9	4.0	3.0	0	0	0	0
21	SAM-21	7.5	105.6	11.4	9.0	4.8	4.4	0	0	0	0
22	SAM-22	7.5	94.2	12.3	8.1	5.2	4.2	0	0	0	0
23	SAM-23	7.5	98.8	13.9	8.3	4.8	3.4	0.2	0	0	0
24	SAM-24	7.0	254.0	15.3	5.3	9.4	9.4	0	0	0	0
25	SAM-25	7.5	94.3	6.2	9.4	7.4	4.6	0	0	0	0
26	SAM-26	7.5	78.5	7.7	10.6	7.8	3.0	0	0	0	0
27	SAM-27	7.5	109.4	8.3	10.0	7.2	4.4	0	0	0	0
28	SAM-28	7.6	122.6	7.8	8.8	7.0	5.0	0	0	0	0
29	SAM-29	7.5	110.8	10.3	11.0	5.6	4.4	0	0	0	0
30	SAM-30	7.5	106.6	8.0	10.6	7.2	4.4	0	0	0	0
31	SAM-31	7.5	97.6	10.3	10.0	5.2	4.0	0.2	0	0	0
32	SAM-32	7.5	113.2	9.8	10.8	7.0	4.6	0	0	0	0
33	SAM-33	7.5	96.9	6.7	9.7	5.6	3.4	0	<10	0	0
34	SAM-34	7.5	107.7	6.1	9.5	6.3	4.4	0	0	0	0
35	SAM-35	7.0	44.8	7.8	9.8	5.2	2.2	0	0	0	0
36	SAM-36	7.0	48.7	10.2	11.4	4.8	2.4	0	0	0	0
37	SAM-37	7.0	93.3	9.3	11.3	6.0	3.8	0	0	0	0
38	SAM-38	7.5	109.2	7.8	9.8	7.0	4.2	0	<10	0	0
39	SAM-39	6.5	54.5	6.3	7.8	6.4	2.0	0	<10	0	0
40	SAM-40	7.5	77.8	5.9	11.2	5.0	2.6	0	<10	0	0
41	SAM-41	7.5	79.6	6.3	9.4	4.2	2.8	0	0	0	0
42	SAM-42	7.5	100.3	5.6	10.7	4.4	3.8	0	0	0	0
43	SAM-43	7.5	86.7	7.0	10.7	4.2	3.6	0	0	0	0
44	SAM-44	7.5	70.8	7.0	9.0	3.4	2.8	0	0	0	0

Appendix 3-6: List of environmental parameters.

No.	Sample No.	Vegetation	Ground	Type of lake	Remarks
01	SAM-01	Carex sp.	mouldy over sand	BPL	
02	SAM-02	Carex sp.	mouldy over sand	LPL	
03	SAM-03	Carex sp.	mouldy	BPL	
04	SAM-04	-	loamy	AL	
05	SAM-05	Hippuris vulgaris	mouldy	OB	
06	SAM-06	Arctophila sp., Hippuris vulgaris	mouldy over sand	?	
07	SAM-07	Arctophila sp.	mouldy over sand	OB	
08	SAM-08	Carex sp.	mouldy	BPL	
09	SAM-09	Carex sp.	mouldy	LPL	= SAM-35
10	SAM-10	Arctophila sp.	mouldy	LPL	= SAM-36
11	SAM-11	Carex sp., Potentilla palustris	mouldy	PTL	= SAM-37
12	SAM-12	Carex sp., Potentilla palustris	mouldy	AL	
13	SAM-13	Carex sp.	muddy	LPL	
14	SAM-14	Arctophila sp., Hippuris vulgaris	mouldy over sand	OB	
15	SAM-15	Arctophila sp., Hippuris vulgaris, Potentilla palustris	mouldy over sand	OB	
16	SAM-16	Carex sp.	mouldy over sand	OB	
17	SAM-17	Carex sp., Arctophila sp., Hippuris vulgaris	mouldy over sand	OB	
18	SAM-18	Carex sp., Potentilla palustris, Hippuris vulgaris	muddy	OB	
19	SAM-19	Arctophila sp.	mouldy over sand	OB	
20	SAM-20	Carex sp.	mouldy	BPL	
21	SAM-21	Hippuris vulgaris, Potentilla palustris, Caltha palustris	muddy over sand	LPL	= SAM-30
22	SAM-22	Hippuris vulgaris, Potentilla palustris, Caltha palustris	muddy over sand	BPL	
23	SAM-23	Carex sp., Potentilla palustris	mouldy	PTL	
24	SAM-24	Arctophila sp., Hippuris vulgaris	mouldy	OB	
25	SAM-25	Carex sp., Potentilla palustris, Arctophila sp.	plants	PTL	
26	SAM-26	Carex. sp., Potentilla palustris, Arctophila sp.	mouldy	BPL	
27	SAM-27	Carex. sp., Potentilla palustris, Arctophila sp.,	mouldy	BPL	
28	SAM-28	Potentilla palustris, Caltha palustris, Politricum alpinum	mouldy	BPL	
29	SAM-29	Potentilla palustris,	mouldy	BPL	

No.	Sample No.	Vegetation	Ground	Type of lake	Remarks
		Caltha palustris, Politricum alpinum			
30	SAM-30	Hippuris vulgaris, Potentilla palustris, Caltha palustris	muddy	LPL	= SAM-21
31	SAM-31	Hippuris vulgaris, Potentilla palustris, Caltha palustris	muddy	LPL	
32	SAM-32	Potentilla palustris, Arctophila sp., Carex sp.	muddy	BPL	
33	SAM-33	Potentilla palustris, Arctophila sp., Carex sp.	muddy	BPL	
34	SAM-34	Potentilla palustris, Arctophila sp., Carex sp.	muddy	BPL	
35	SAM-35	Carex sp.	mouldy	LPL	= SAM-09
36	SAM-36	Arctophila sp.	mouldy	LPL	= SAM-10
37	SAM-37	Carex sp., Potentilla palustris	mouldy	PTL	= SAM-11
38	SAM-38	Arctophila sp., Hippuris vulgaris	mouldy over sand	AL	
39	SAM-39	Arctophila sp.	mouldy	PTL	
40	SAM-40	Arctophila sp., Hippuris vulgaris	mouldy over sand	BPL	
41	SAM-41	Carex sp., Hippuris vulgaris, Politricum alpinum	mouldy	BPL	
42	SAM-42	Carex sp., Potentilla palustris, Caltha palustris, Politricum alpinum, Hippuris vulgaris	mouldy	BPL	
43	SAM-43	Carex sp., Potentilla palustris, Caltha palustris, Politricum alpinum, Hippuris vulgaris	mouldy	BPL	
44	SAM-44	Carex sp., Potentilla palustris, Politricum alpinum	mouldy	LPL	

Appendix 3-7. List of recent beetles collected in the Lena Delta in 2002.

No.	Species	Locality	Habitat	Date	Num-ber
Ord. Coleoptera **Fam. Carabidae**					
1	Carabus odoratus Motsch.	Tit-Ary	forest-tundra, south-facing slope, motley grass	06.08.02	4
				Total	**4**
2	Nebria nivalis Payk.	Samoylov	shrub tundra, river bank, sedge	18.08.02	2
				Total	**2**
3	Pelophila borealis Payk.	Samoylov	shrub tundra, river bank, sedge	01.09.02	4
		Tit-Ary	forest-tundra, near pool	06.08.02	1
				Total	**5**
4	Notiophilus aquaticus L.	Samoylov	shrub tundra, on sand	01.09.02	2
		Samoylov	shrub tundra, on sand	14.08.02	1
				Total	**3**
5	Elaphrus riparius L.	Samoylov	shrub tundra, stream bank	14.08.02	1
		Samoylov	shrub tundra, stream bank	01.09.02	4
		Sokol	rocky tundra, near water	23.08.02	1
				Total	**6**
6	Bembidion (Plataphus) sp.	Samoylov	shrub tundra, near stream, sandy soil	01.09.02	7
		Samoylov	shrub tundra, near stream, sandy soil	02.09.02	5
				Total	**14**
7	Pterostichus (Cryobius) brevicornis (Kirby)	Samoylov	shrub tundra, middle flood-plain, under driftwood	18.08.02	6
		Samoylov	shrub tundra, middle flood-plain, under driftwood	01.09.02	10
		Samoylov	shrub tundra, middle flood-plain, under driftwood	02.09.02	4
		Samoylov	shrub tundra, middle flood-plain, under driftwood	10.08.02	7
		Tit-Ary	forest-tundra, high flood-plain with small willow and alder	07.08.02	10
		Tiksi	wet tundra	06.09.02	7
				Total	**37**
8	Pterostichus (Cryobius) spp.	Samoylov	shrub tundra, middle flood-plain, under driftwood	18.08.02	36

		Samoylov	shrub tundra, middle flood-plain, under driftwood	25.08.02	9
		Samoylov	shrub tundra, middle flood-plain, under driftwood	01.09.02	27
		Samoylov	shrub tundra, middle flood-plain, under driftwood	02.09.02	10
		Samoylov	shrub tundra, middle flood-plain, under driftwood	10.08.02	10
		Samoylov	shrub tundra, middle flood-plain, under driftwood	01.08.02	62
		Samoylov	shrub tundra, middle flood-plain, under driftwood	02.08.02	16
		Sokol	rocky tundra	23.08.02	2
		Tit-Ary	forest-tundra, high flood-plain with small willow and alder	07.08.02	14
		Tiksi	wet tundra	06.08.02	13
				Total	**199**
9	P. (Stereocerus) haematopus Dej.	Samoylov	shrub tundra, middle flood-plain, under driftwood	25.08.02	20
		Samoylov	shrub tundra, middle flood-plain, under driftwood	01.09.02	9
		Samoylov	shrub tundra, middle flood-plain, under driftwood	03.08.02	13
		Samoylov	shrub tundra, middle flood-plain, under driftwood	18.08.02	29
		Samoylov	shrub tundra, middle flood-plain, under driftwood	01.09.02	19
		Samoylov	shrub tundra, middle flood-plain, under driftwood	03.08.02	13
		Samoylov	shrub tundra, middle flood-plain, under driftwood	01.08.02	17
		Tit-Ary	forest-tundra, high flood-plain with small willow and alder	07.08.02	20
				Total	**140**
10	P. (Steroperis) vermiculosus Men.	Tit-Ary	forest-tundra, high flood-plain with small willow and alder	06.08.02	10
				Total	**10**

11	P. (Steroperis) costatus Men.	Samoylov	shrub tundra, middle flood-plain, under driftwood	18.08.02	91
		Samoylov	shrub tundra, middle flood-plain, under driftwood	01.08.02	19
		Samoylov	shrub tundra, middle flood-plain, under driftwood	10.08.02	2
		Samoylov	shrub tundra, middle flood-plain, under driftwood	14.08.02	2
		Samoylov	shrub tundra, middle flood-plain, under driftwood	02.09.02	8
		Samoylov	shrub tundra, middle flood-plain, under driftwood	25.08.02	4
		Samoylov	shrub tundra, middle flood-plain, under driftwood	01.08.02	15
		Tit-Ary	forest-tundra, high flood-plain with small willow and alder	07.08.02	4
				Total	**145**
12	P. (Petrophilus) abnormis Sahlb.	Tit-Ary	forest-tundra, high flood-plain with small willow and alder	07.08.02	1
				Total	**1**
13	*Curtonotus alpinus* Payk.	Samoylov	shrub tundra, middle flood-plain, under driftwood	18.08.02	4
		Samoylov	shrub tundra, middle flood-plain, under driftwood	25.08.02	3
		Samoylov	shrub tundra, middle flood-plain, under driftwood	01.09.02	9
		Tiksi	rocky tundra	07.09.02	8
		Tit-Ary	forest-tundra, high flood-plain with small willow and alder	07.08.02	17
				Total	**41**
14	Amara glacialis Mnnh.	Samoylov	shrub tundra, middle flood-plain, under driftwood	01.08.02	2
		Samoylov	shrub tundra, middle flood-plain, under driftwood	18.08.02	1
		Samoylov	shrub tundra, middle flood-plain, under driftwood	25.08.02	2
		Samoylov	shrub tundra, middle flood-plain, under	14.08.02	1

			driftwood		
		Tit-Ary	forest-tundra, high flood-plain with small willow and alder	06.08.02	20
				Total	**26**
15	A. interstitialis Dej.	Samoylov	shrub tundra, middle flood-plain, under driftwood	18.08.02	1
		Samoylov	shrub tundra, middle flood-plain, under driftwood	10.08.02	1
				Total	**2**
Fam. Dytiscidae					
16	Hydroporus sp.	Tit-Ary	forest-tundra, small pool inside sphagnum bog	06.08.02	2
17	Agabus moestus (Curt.)	Tit-Ary	forest-tundra, in lake near bank	06.08.02	2
		Samoylov	shrub tundra, high flood-plain, in lake	18.08.02	1
				Total	**3**
18	Colymbetes dolobratus (Payk.)	Samoylov	shrub tundra, first flood-plain terrace, in lake	18.08.02	2
				Total	**2**
Fam. Silphidae					
19	Thanatophilus lapponicus Hbst.	Samoylov	shrub tundra, near camp	18.08.02	1
		Samoylov	shrub tundra, near camp	18.08.02	1
		Sokol	near house	23.08.02	1
		Tit-Ary	forest-tundra, in settlement	06.08.02	1
				Total	**4**
Fam. Staphylinidae					
20	Stenus sp.	Tiksi	rocky tundra, under driftwood	08.09.02	3
				Total	**3**
21	Lathrobium sp.	Samoylov	shrub tundra, sandy soil, under wood	18.08.02	1
		Samoylov	shrub tundra, sandy soil, under driftwood	01.08.02	4
				Total	**5**
22	Micralymma sp.	Samoylov	shrub tundra, sandy soil, under wood	01.08.02	1
		Tiksi	rocky tundra, under driftwood	07.08.02	9
		Tiksi	rocky tundra, under driftwood	08.08.02	1
				Total	**11**
23	Tachinus arcticus Motsch	Samoylov	shrub tundra, middle flood-plain, under driftwood	01.09.02	12
		Samoylov	shrub tundra, middle flood-plain, under driftwood	14.08.02	3

		Samoylov	shrub tundra, middle flood-plain, under driftwood	10.08.02	4
		Samoylov	shrub tundra, middle flood-plain, under driftwood	01.08.02	19
		Tiksi	rocky tundra, under a wood	08.09.02	1
		Tiksi	rocky tundra, under driftwood	07.09.02	2
				Total	**41**
24	Staphylininae gen.indet.	Samoylov	shrub tundra, sandy soil, under driftwood	14.08.02	2
		Samoylov	shrub tundra, sandy soil, under driftwood	10.08.02	2
		Samoylov	shrub tundra, sandy soil, under driftwood	01.08.02	2
		Tiksi	rocky tundra, under a wood	08.09.02	1
		Tiksi	rocky tundra, under a wood	08.09.02	1
				Total	**8**
Fam. Buprestidae					
25	Melanophila acuminata Deg.	Samoylov	shrub tundra, on a wood	25.08.02	2
				Total	**2**
FAM. COCCINELIDAE					
26	Hyppodamia arctica Schneid.	Samoylov	shrub tundra, on wood boards near camp	18.08.02	2
		Samoylov	shrub tundra, on a wood	01.09.02	1
		Sokol	rocky tundra, near a house	23.08.02	2
				Total	**5**
27	Coccinella spp.	Samoylov	shrub tundra, on wood boards near camp	18.08.02	10
		Samoylov	shrub tundra, on wood boards near camp	10.08.02	13
		Samoylov	shrub tundra, on wood boards near camp	01.08.02	11
		Samoylov	shrub tundra, on a wood	14.08.02	5
		Tiksi	rocky tundra, on a wood	07.08.02	1
				Total	**40**
Fam. Cerambycidae					
28	Monochamus sutor L.	Samoylov	shrub tundra, on a wood	14.08.02	2
		Samoylov	shrub tundra, on a wood	18.08.02	3
		Samoylov	shrub tundra, on a wood	02.08.02	1
		Sokol	bank of Lena, on a wood	23.08.02	1
				Total	**7**
29	Asemum striatum L.	Samoylov	on beach (dead)	10.08.02	1
				Total	**1**

Fam. Chrysomelidae					
30	Chrysolina septentrionalis Men.	Samoylov	shrub tundra, middle flood-plain, under driftwood	18.08.02	5
		Samoylov	shrub tundra, flood-plain, under driftwood	02.09.02	4
		Samoylov	shrub tundra, near camp	10.08.02	1
		Samoylov	shrub tundra, middle flood-plain, under driftwood	01.09.02	4
		Samoylov	shrub tundra, middle flood-plain, under driftwood	14.08.02	2
		Sokol	rocky tundra	23.08.02	1
		Tiksi	rocky tundra under driftwood	07.09.02	3
		Tiksi	rocky tundra under a wood	08.09.02	1
				Total	**21**
Fam. Curculionidae					
31	Lepyrus norden-skjoeldi Faust	Samoylov	shrub tundra, middle flood-plain, under driftwood	01.08.02	13
		Samoylov	shrub tundra, middle flood-plain, under driftwood	18.08.02	10
		Samoylov	shrub tundra, high flood-plain, under driftwood	01.09.02	3
		Samoylov	shrub tundra, high flood-plain, under driftwood	14.08.02	10
		Samoylov	shrub tundra, high flood-plain, under driftwood	02.09.02	1
		Tit-Ary	forest-tundra, high flood-plain with small willow and alder	06.08.02	1
				Total	**38**
				All	**828**

Appendix 3-8. Field description of the permafrost cores drilled on Kurungnakh Island, August 2002.

sample ID	sample No	depth [cm]	description	date
Island Kurungnakh-Sise, KUR-02R/3a N 72°20` / E 126°17` H=43 m, active layer 32 cm, 3 m off exposure				
LD-02	5007	28-48 (48 b.h.d.)	28-40 cm thawing peat, decomposed, dense, reddish-brown with silt and living roots 40-48 cm frozen, the same, lense-shaped structure, ice lenses ≈ 0,3 cm	13.07.02
LD-02	5008	48-66 (66 b.h.d.)	48-66 cm cryoturbate: silt, grey, ice-rich, transparent with chains of air babbles, and decomposed peat, reddish-brown, irregular reticulated: ice lenses > 1 cm	13.07.02
LD-02	5009	68-136 (136 b.h.d.)	3 parts 66-78 cm silt, ice-rich, grey, irregular reticulated, ice lenses up to 0.8 cm 78-86 cm ice-rich silt with peat, irregular reticulated, lenses ≈ 0.8 cm 86-110 cm peat, reddish-brown, with twigs (Salix?), lense-shaped structure, lenses: 0.4-0.5 cm 110-136 cm cryoturbate: silt with peat, like subvertical sublayer, reticulated, ice lenses ≈ 0.3 cm	13.07.02
			On the depth about 2 m equipment was lost	
KUR-02R/3b – the same polygon: 30 cm from KUR-02/3a				
LD-02	5010	106-162 (163 b.h.d.)	4 parts 106-129 cm cryoturbate: peat, reddish-brown, with silt sublayer, grey, ice-rich, reticulated (lenses 0.4-0.5 cm) 129-143 cm peat, reddish-brown, with twigs, thin-reticulated: 0,2-0,3 cm 143-162 cm silt with small amount of peat inclusions, grey, ice-rich, reticulated, ice lenses ≈ 0,4-0,5 cm	13.07.02
LD-02	5011	163-249 (249 b.h.d.)	6 parts 163-182 cm peat, reddish-brown, with shrub (?) roots-twigs, thin-reticulated 182-201 cm icing silt, grey, irregular reticulated, ice lenses ≈ 0.7-1.0 cm 201-249 cm cryoturbate: peat, decomposed, reddish-brown, thin-reticulated, with silt, grey, ice-rich, lenses up to 0.8 cm	13.07.02
LD-02	5012	249-320 (320 b.h.d.)	3 parts 249-266 cm peat, reddish-brown decomposed, with twigs (∅≈0.4 cm) of horizontal position, thin-reticulated 266-294 cm silt, ice-rich, irregular reticulated, lenses up to 1 cm 294-305 cm peaty silt, grayish-brown, thin-reticulated 305-320 cm silt, grey, ice-rich, lenses 1 cm	13.07.02
LD-02	5013	320-385 (385 b.h.d.)	320-342 cm silt, grey, ice-rich, irregular reticulated, lenses up to 1 cm 342-358 cm silt with m/sand, ice lenses ≈ 0.5 cm 358-369 cm silty peat, grayish-brown, lenses 0.3 up to 0.6 cm	13.07.02

			369-385 cm silty peat, thin-reticulated: 0.2 cm	
			Equipment was frozen on the depth about 4 m	
KUR-02R/3c – the same polygon				
LD-02	5014	344-384 (384 b.h.d.)	2 parts 344-372 cm f/sandy silt with peat, plant remnants (twigs), reticulated, ice lenses ≈ 0.3-0.4 cm 372-384 cm f/sandy silt with peat, thin-reticulated	19.07.02
LD-02	5015	384-425 (425 b.h.d.)	384-391 cm f/sandy silt with peat, reticulated, ice lenses ≈ 0.30 cm 391-425 cm silty peat, grayish-brown, thin-reticulated, ice lenses ≈ 0.2 cm with twigs of horizontal and subhorizontal position	19.07.02
LD-02	5016	425-485 (485 b.h.d.)	5 parts 425-460 cm silt, grey, ice-rich, alternation of reticulated texture, lenses ≈ 0.3 cm, and ice sublayer up to 1.0-1.2 cm 460-485 cm sandy silt, with peat and small amount of twigs, lenses 0.3-0.4 cm	19.07.02
LD-02	5017	485-544 (544 b.h.d.)	4 parts 485-495 cm the same 495-517 cm sandy silt, thin-reticulated, 500-503 cm – ice layer 517-544 cm sandy silt with peat, reticulated, with twigs of subhorizontal position	19.07.02
LD-02	5018	544-613 (613 b.h.d.)	3 parts 544-574 cm silt+f/sand, ice-rich, lenses 0.3-0.4 cm 574-607 cm silt+f/sand+twigs of vertical position 607-613 cm silt+f/sand, reticulated	19.07.02
LD-02	5019	616-647 (647 b.h.d.)	616-647 cm silt+f-m/sand, ice-rich, lenses 0.3 up to 0.6 cm; 640-645 cm with twigs	20.07.02
LD-02	5020	647-728 (728 b.h.d.)	3 parts 647-669 cm f/sandy silt, thin-reticulated, 0.1-0.2 cm 669-695 cm silt, grey, ice-rich with twigs of subvertical position, lenses 0.3-0.8 cm 695-728 cm f/sandy silt with twigs of subvertical position, thin-reticulated, 0.1-0.2 cm	20.07.02
LD-02	5021	728-798 (798 b.h.d.)	5 parts 728-744 cm f/sandy silt, grey, reticulated, lenses 0.2 cm 744-746 cm ice sublayer 746-763 cm f/sandy silt, greyish, thin-reticulated, 0.1 cm 763-798 cm silt with f/sand, grey, reticulated, 0.2 cm with more ice sublayer in the middle	20.07.02
LD-02	5022	798-847 (847 b.h.d.)	3 parts 798-832 cm sandy silt with sparse twigs (subvertical position), lense-like reticulated, lenses ≈ 0.2 cm 832-847 cm cm sandy silt with sparse twigs (subvertical position), reticulated, lenses ≈ 0.3 cm	20.07.02
LD-02	5023	847-900 (900 b.h.d.)	847-861 cm f/sandy silt, reticulated, lenses 0.2-0.3 cm with thin white roots (?) – 0.1-0.15 cm of vertical position 861-900 cm m/sandy silt, thin reticulated: lenses 0.1 cm	20.07.02

			882-887 cm – more ice sublayer	
LD-02	5024	902-934 (934 b.h.d.)	2 parts 902-934 cm m-f/sandy silt with thin white roots and twigs of horizontal position, reticulated: lenses 0.1 cm	20.07.02
LD-02	5025	934-990 (990 b.h.d.)	6 parts 934-956 cm m-f/sandy silt with plant remnants (twigs and white roots), lenses < 0.1 cm 956-990 cm f/sandy silt with thin white roots, reticulated, lenses 0.3-0.4 cm	20.07.02
LD-02	5026	990-1048 (1048 b.h.d.)	4 parts 990-1005 cm f/sandy silt, grey, reticulated; 996-998 cm 2 ice lenses ≈ 1.0 cm 1005-1024 cm silty f-m/sand and thin white roots, massive 1024-1048 cm f/sandy silt, reticulated, lenses 0.3-0.4 cm	22.07.02
LD-02	5027	1048-1091 (1091 b.h.d.)	5 parts f-m/sandy silt, ice-rich, ice layers 1.5-2.0 cm	22.07.02
LD-02	5028	1091-1153 (1153 b.h.d.)	7 parts f-m/sand with silt, ice-rich: irregular layers > 1 cm, with thin subvertical roots	22.07.02
LD-02	5029	1153-1204 (1204 b.h.d.)	1153-1169 cm the same lake 1091-1153 cm 1169-1199 cm silty f-m/sand with sparse plant remnants (moss?) 1195-1196 cm ice layer, transparent ` 1199-1201 cm sandy silt with peaty spot (on side) 1201-1204 cm peat, brown, slightly decomposed	22.07.02
Island Kurungnakh-Sise, KUR-02G/4 N 72°19` / E 126°17` The top of baydzherakh, H=31 m, active layer 62 cm				
LD-02	5505	62-107 (107 b.h.d.)	∅ = 76 mm 62-66 cm silt, grey, with m/sand, ice-rich: lenses ≈ 0.7 cm 66-67 cm ice layer 1.2 cm 67-107 cm silty sand, yellow-grey, with turbate of decomposed organic and plant remnants of chaotic position, inclined lenticular	15.07.02
LD-02	5506	107-169 (169 b.h.d.)	4 parts – all layers have angle ≈ 45° - NB! 107-111 (up to 113) cm ice layer with silt and f/sand 111(113)-147(150) cm – sandy silt with plant remnants, reticulated, 0.7-0.8 cm 147(150)-169 cm silty sand + plant remnants of subhorizontal position, yellow-greyish, cryogenic texture: subhorizontal lenticular with subvertical layered	15.07.02
LD-02	5507	169-200 (202 b.h.d.)	2 parts 169-**186** cm silty sand, yellow-brown, with plant remnants, lense-shaped **186**-200 cm silty-sandy-peat with plant remnants, reticulated	15.07.02
LD-02	5508	202-231 (231 b.h.d.)	3 parts (202-210; 210-223; 223-231 cm) 202-231 cm turbate(?): silty sand and peat with plant remnants, yellow-grey, reticulated	15.07.02
LD-02	5509	231-253 (253 b.h.d.)	3 parts: 231-238, 238-243, 243-253 231-247cm f/sandy silt, greyish, reticulated, with sand inclusions, yellow, with oxidized points, massive and plant remnants	15.07.02

			247-253 cm cm silty f-m/sand with silty organic matter, thin-reticulated	
LD-02	5510	257-296 (299 b.h.d.)	3 parts 257-296 cm f-m/sand, yellow, with gleyish vertically elongated inclusions of decomposed organic matter, thin-reticulated (<0.1 cm), in sand - massive	15.07.02
LD-02	5511	299-314 (314 b.h.d.)	2 parts 299-304 cm f/sandy silt with decomposed organic, brown-grey, loose frozen 304-310 cm m/sand, yellow, with grey silt spots 310-314 cm peat with sandy silt, dark grey, and twigs of chaotic position, massive	17.07.02
LD-02	5512	314-335 (335 b.h.d.)	2 parts 314-335 cm subvertical border between m/sandy, yellow-gray, massive and decomposed silty organic matter, brown, thin-reticulated with twigs of vertical position	17.07.02
LD-02	5513	335-355 (355 b.h.d.)	4 parts 335-343; 343-**347** (350)cm turbate: peat with twigs of chaotic position and silty sand, thin-reticulated, ≈0.2 cm **347**(350)-355 cm ice (ice wedge?), transparent with air babbles and m/sand, yellow	17.07.02
LD-02	5514	355-374 (374 b.h.d.)	4 parts – *looks like contact zone with ice wedge* 355-374 cm diagonal border between ice, milky-white, and silty-f-m/sand + twigs	17.07.02
LD-02	5515	374-404 (404 b.h.d.)	3 parts 374-**378** cm silty sand with lateral contact of ice **378-391** cm silt with sand, grayish-yellowish, plant remnants of chaotic position **391**-404 cm silt + sand, oxidized points, horizontal thin-reticulated, 0.1-0.2	17.07.02
LD-02	5516	404-424 (424 b.h.d.)	3 parts (404-415; 415-420; 420-424 cm) f-m/sandy silt, grey, thin-reticulated (0.1-0.15 cm) with twigs of horizontal position	17.07.02
LD-02	5517	425-440 (440 b.h.d.)	3 parts (425-433; 433-438; 438-440 cm) the same as above layer f-m/sand silt, dark grey with oxidized spots and plant remnants	17.07.02
LD-02	5518	440-476 (476 b.h.d.)	2 parts **440**-444 cm lost sediment 444-453(460) cm silty sand, greyish, with twigs, thin-reticulated (<0.1), close to massive 453(460)-**469** cm sandy silt, with twigs (0.15-0.2 cm), reticulated, 0.3-0.4 cm **469**-476 cm m/sand, yellow, with turbated layeres of decomposed organic matter, close to massive	18.07.02
		476-505	Lost material: probably it was m/sand, loose, massive, yellow, with oxidized points	
LD-02	5519	505-549 (549 b.h.d.)	505-549 cm silty f-m/sand, yellow-grey, twigs (0.2 cm), ice lenses ≈ 0.3 cm	18.07.02
LD-02	5520	549-571 (571 b.h.d.)	3 parts 549-556, 556-561, 561-571 cm silty-f/sand, grey, thin-reticulated, 0.3 cm, with twigs (0.15 cm)	18.07.02
LD-02	5521	571-579 (579 b.h.d.)	f-m/sand with twigs (0.2 cm) and brown spots of decomposed organic, loose frozen, thin-reticulated, grey-brown	18.07.02
LD-02	5522	579-601 (601 b.h.d.)	**579**-580 cm the same like above 580-595 cm f-m/sand with vertically elongated silt	18.07.02

			spots and twigs of vertical position, thin lense-shaped 595-601 cm more silty sand, grey, thin-reticulated (0.1-0.2 cm)	
LD-02	5523	601-610 (610 b.h.d.)	601-**605** cm the same like above **605**-610 cm turbate: m/sand with peat and plant remnants, massive	18.07.02
LD-02	5524	610-628 (628 b.h.d.)	3 parts - all layers have angle ≈ 40° ! 610-615(**617**) cm peaty sand with a lot of twigs and other plant remnants 615(**617**)-625; 625-628 cm silt with sand, lenses ≈ 0.2-0.3 cm up to ice sublayer of 0.8 cm	18.07.02
LD-02	5525	628-634 (634 b.h.d.)	silty sand, grey, with plant remnants, thin-reticulated 634 cm ice lens 0.5 cm	18.07.02
LD-02	5526	634-650 (650 b.h.d.)	2 parts 634-646 cm silt with f/sand, grey, thin-reticulated (0.2 cm) 646-**650**(652) cm the same + ice lenses ≈ 0.4 cm – angle = 40°	19.07.02
LD-02	5527	650-663 (663 b.h.d.)	f-m/sand with twigs of subvertical position, reticulated 0.3-0.4 cm	19.07.02
LD-02	5528	663-**669** (669 b.h.d.)	f-m/sand and silt, yellow-brown, with twigs of subvertical position, lenses ≈ 0.3 cm	19.07.02
LD-02	5529	669-701 (701 b.h.d.)	669-**690** cm silty sand, yellow-grey, thin-reticulated **690**-701 cm f-m/sand, yellow with small amount of twigs	19.07.02
LD-02	5530	701-716 (716 b.h.d.)	701-710 cm f-m/sand, yellow, with twigs 710-716 cm silty sand, grey, with twigs, thin-reticulated	19.07.02
LD-02	5531	716-734 (734 b.h.d.)	2 parts: 716-730, 730-734 cm f-m/sand, yellow, with grey strips and twigs (0.15-0.2 cm) of subvertical position, massive	19.07.02
LD-02	5532	734-745 (745 b.h.d.)	2 parts f-m/sand, grayish-yellow, thin-reticulated	19.07.02
LD-02	5533	745-**792** (792 b.h.d.)	2 parts – changed spoon! 745-**758** cm the same like above 758-**792** cm silt and f-m/sand, yellowish-grey, with twigs of chaotic position, reticulated	19.07.02
LD-02	5534	792-813 (813 b.h.d.)	**792**-811 cm the same 811-813 cm ice, transparent, with silt, angle ≈ 40°	19.07.02
LD-02	5535	813-827 (827 b.h.d.)	2 parts 813-817 cm broken ice layer 817-820 cm ice with f/sandy silt, grey 820-827 cm sandy silt, grey, with ice layer on the bottom 1.2 cm	19.07.02
LD-02	5536	827-847 (847 b.h.d.)	3 parts 827-830 cm f-m/sand with twigs of subhorizontal position 830-847 cm f/sand, grayish-yellow, with twigs of subhorizontal position, reticulated + ice lens ≈ 1 cm	20.07.02
LD-02	5537	847-867 (867 b.h.d.)	3 parts silty sand, ice-rich, lenses up to 0.8 cm, with big plant remnants and decomposed organic	20.07.02
LD-02	5538	867-**898** (898 b.h.d.)	2 parts f/sand and silt, grey, reticulated (0.1-0.2), with twigs of subhorizontal position and ice sublayer up to 1-1.2 cm	20.07.02
LD-02	5539	**898**-914	f/sand with silt, grayish-yellow, twigs of	20.07.02

		(914 b.h.d.)	subhorizontal position, reticulated ≈ 0.1-0.3 cm	
LD-02	5540	914-934 (934 b.h.d.)	f/sand with twigs and plant remnants, ice lenses 0.2 up to 1.4 cm	20.07.02
LD-02	5541	934-954 (954 b.h.d.)	934-943 cm f/sand, grayish-yellow, ice-rich, lenses ≈ 0.3 cm up to 1.4 cm 943-954 cm f-m/sand, yellow, with plant remnants of chaotic position, thin-reticulated	20.07.02
LD-02	5542	954-985 (985 b.h.d.)	4 parts 954-**958** cm f/sand, grey, ice-rich, thin-reticulated: 0.1-0.2 cm **958**-965 cm organic layer: decomposed peat 965-**985** cm m/sand, layered, yellow, near organic layer – slightly grey, massive from 979 with plant remnants	20.07.02
LD-02	5543	985-999 (999 b.h.d.)	2 parts **985**-990 cm f/sand and silt, grayish, reticulated: lenses 0.2-0.3 cm up to 1.5 cm 990-999 cm the same, but more yellow sand	20.07.02
LD-02	5544	999-**1012** (1012 b.h.d.)	3 parts f-m/sand and silt, yellowish-grey, thin-reticulated: ≈ 0.15 cm, nearly the bottom – ice lens 0.7 cm	20.07.02
LD-02	5545	1023-1050 (1050 b.h.d.)	2 parts 1023-1034, 1034-1039 cm peat consisting of twigs (horizontal and subhorizontal position) with silt and m/sand, brown-grey, thin-reticulated 1039-**1046** silt and m/sand, grey, thin-reticulated **1046**-1050 cm m/sand, grayish-yellow, massive	24.07.02
LD-02	5546	1050-1088 (1088 b.h.d.)	2 parts 1050-1080 cm m/sand, orange-oxidized, loose-frozen, massive – NB! The middle part of this layer was lost 1080-1088 cm m/sand, grayish-yellow, dense, massive	24.07.02
LD-02	5547	1088-**1108** (1108 b.h.d.)	4 parts m/sand, slightly layered, grayish-yellow, loose-frozen, massive	24.07.02

Appendix 3-9. List of general samples from the Buor-Khaya section, Kurungnakh Island.

No.	Sample No.	Date	Altitude [m,a.r.l.]	Depth [m]	Sediment	Bayd-zherakh (Point)	Ice con-tent [%]	Pol-len
01	Bkh2002 S01	10.08.02	42.75	0.25	grey silt with peat lenses	point 1	-	x
02	Bkh2002 S02	10.08.02	42.75	0.25	grey silt	point 1	100.0	x
03	Bkh2002 S03	10.08.02	42.0	1.0	peat	point 1	94.4	x
04	Bkh2002 S04	10.08.02	42.0	1.0	grey silt	point 1	56.8	x
05	Bkh2002 S05	10.08.02	42.2	0.8	grey silt with peat lenses	point 2	100.0	-
06	Bkh2002 S06	10.08.02	40.2	2.8	grey silt	point 2	73.1	x
07	Bkh2002 S07	10.08.02	39.8	3.2	grey silt	point 2	150.0	x
08	Bkh2002 S08	10.08.02	38.7	4.3	grey sandy silt	point 2	121.7	x
09	Bkh2002 S09	10.08.02	39.2	3.8	grey sandy silt	point 2	78.3	x
10	Bkh2002 S10	11.08.02	38.5	4.5	sandy silt, roots	M	58.1	x
11	Bkh2002 S11	11.08.02	38.0	5.0	sandy silt	M	59.3	x
12	Bkh2002 S12	11.08.02	37.5	5.5	sand	C	64.0	x
13	Bkh2002 S13	11.08.02	38.0	5.0	sandy silt	C	-	x
14	Bkh2002 S14	12.08.02	37.0	6.0	sand	C	55.2	x
15	Bkh2002 S15	12.08.02	36.5	6.5	sand, roots	C	60.0	x
16	Bkh2002 S16	12.08.02	36.0	7.0	sand with peat	C	133.3	x
17	Bkh2002 S17	12.08.02	39.5	3.5	grey silt	B	23.8	x
18	Bkh2002 S18	12.08.02	34.7	8.3	brown silt, roots	E	70.8	x
19	Bkh2002 S19	12.08.02	35.3	7.7	brown silt, roots	E	61.3	x
20	Bkh2002 S20	12.08.02	36.2	6.8	silt	E	63.4	x

No.	Sample No.	Date	Altitude [m,a.r.l.]	Depth [m]	Sediment	Bayd-zherakh (Point)	Ice con-tent [%]	Pol-len
21	Bkh2002 S20D	12.08.02	36.2	6.8	peat	E	-	-
22	Bkh2002 S21	13.08.02	34.8	8.2	silt, plants	F	106.3	x
23	Bkh2002 S22	13.08.02	33.1	9.9	peat	G	77.8	x
24	Bkh2002 S22D	13.08.02	33.3	9.7	peat	G	-	-
25	Bkh2002 S23	13.08.02	31.0	12.0	peat	G	108.7	x
26	Bkh2002 S24	13.08.02	32.0	11.0	grey silt, plants	G	86.4	x
27	Bkh2002 S25D	13.08.02	30.0	13.0	peat	P	-	-
28	Bkh2002 S26	13.08.02	31.5	11.5	silt, roots	G	104.3	x
29	Bkh2002 S27	16.08.02	41.7	1.3	grey silt with peat lenses	point 3	117.6	x
30	Bkh2002 S28	16.08.02	41.5	1.5	grey silt with peat lenses	point 3	48.4	x
31	Bkh2002 S29	16.08.02	41.0	2.0	grey silt with peat lenses	point 3	51.5	x
32	Bkh2002 S30	16.08.02	40.5	2.5	grey silt with peat lenses	point 3	58.8	x
33	Bkh2002 S30D	16.08.02	40.4	2.5	peat lenses in silt	point 3	-	-
34	Bkh2002 S31	16.08.02	32.5	10.5	brown silt, plants	H	100.0	x
35	Bkh2002 S32	22.08.02	20-24	-	peat		67.9	x
36	Bkh2002 S32D	22.08.02	20-24	-	peat		-	-
37	Bkh2002 S33	22.08.02	9.6	-	yellow sand with fine layers of silt		-	x
38	Bkh2002 S34	22.08.02	10.0	-	yellow sand, roots		-	x
39	Bkh2002 S35	22.08.02	10.5	-	alternation of yellow sand and dark silt layers, roots		-	x
40	Bkh2002 S36	22.08.02	11.0	-	yellow sand		-	x

No.	Sample No.	Date	Altitude [m,a.r.l.]	Depth [m]	Sediment	Bayd-zherakh (Point)	Ice con-tent [%]	Pol-len
41	Bkh2002 S37	22.08.02	11.5	-	yellow sand		-	x
42	Bkh2002 S38	22.08.02	11.7	-	peat		52.6	x
43	Bkh2002 S39	22.08.02	12.0	-	sand with fine dark layers		28.6	x
44	Bkh2002 S40	22.08.02	12.5	-	sand (fine layers)		26.1	x
45	Bkh2002 S41	22.08.02	13.0	-	sand		24.5	x
46	Bkh2002 S42	22.08.02	13.5	-	sand		23.9	x
47	Bkh2002 S43	22.08.02	14.0	-	sand (fine layers)		-	x
48	Bkh2002 S44	22.08.02	14.5	-	sand (fine layers)		23.1	x
49	Bkh2002 S45	22.08.02	17.5	-	brown silt with peat		74.1	x
50	Bkh2002 S45aD	22.08.02	17.9	-	peat		-	x
51	Bkh2002 S46	22.08.02	19.4	-	sandy silt with peat		78.3	x
52	Bkh2002 S46aD	22.08.02	19.8	-	peat		-	x
53	Bkh2002 S47	23.08.02	23.5	-	peat		38.3	x
54	Bkh2002 S48	23.08.02	24.0	-	grey silt, plants		56.8	x
55	Bkh2002 S49	23.08.02	9.0	-	sand		18.3	x
56	Bkh2002 S50	23.08.02	8.5	-	sand (fine layers)		-	x
57	Bkh2002 S51	23.08.02	8.0	-	sand (fine dark layers)		-	x
58	Bkh2002 S52	24.08.02	16.1	-	grey sand (fine layers)		-	x
59	Bkh2002 S53	24.08.02	15.3	-	sand (fine dark layers)		-	x

Appendix 3-10. List of permafrost samples from Samoylov Island.

No.	Sample No.	Date	Altitude [m, a.r.l.]	Section	Sample description	Remarks
1	Sam-1-S-1	02.08.02	7.55	1	greyish-yellow medium grained sand (upper ice wedge)	
2	Sam-1-S-1a	03.08.02	7.5	1	peat (to right from ice wedge top)	
3	Sam-1-S-2	02.08.02	7.35	1	yellow medium grained sand with reddish spots (upper ice wedge)	
4	Sam-1-S-2a	03.08.02	7.35	1	peat (to right from ice wedge top)	
5	Sam-1-S-3	02.08.02	7.2	1	peaty silt with plant detritus	
6	Sam-1-S-4	02.08.02	7.0	1	silt with plant detritus	
7	Sam-1-S-5	02.08.02	6.7	1	silt with plant detritus	
8	Sam-1-S-6	02.08.02	6.4	1	silt with peat spots	
9	Sam-1-S-7	02.08.02	6.1	1	silt with peat spots	
10	Sam-1-S-8	02.08.02	5.8	1	peat and peaty silt	
11	Sam-1-S-9	02.08.02	5.6	1	greyish-yellow sand with grass roots	
12	Sam-1-BOT-1	03.08.02	7.2	1	moss peat	for plant determination
13	Sam-1-BOT-2	03.08.02	6.0	1	grass roots	for plant determination
14	Sam-1-BOT-3	03.08.02	6.4	1	moss, grass, shrub roots	for plant determination
15	Sam-2-S-10	20.08.02	5.5	2	silt with woody twigs	
16	Sam-2-S-11	20.08.02	5.9	2	silt with woody twigs and roots	
17	Sam-2-S-12	20.08.02	6.2	2	silt and sand from sand lens	
18	Sam-2-S-13	20.08.02	6.6	2	sand with grass stems and roots	
19	Sam-2-S-14	20.08.02	7.0	2	sand with plant detritus	
20	Sam-2-S-15	20.08.02	7.3	2	sand with plant detritus	

No.	Sample No.	Date	Altitude [m, a.r.l.]	Sec-tion	Sample description	Remarks
					detritus	
21	Sam-2-S-16	20.08.02	7.6	2	sand	
20	Sam-2-S-17	20.08.02	7.9	2	modern soil	

Appendix 3-11. List of ice samples from Buor Khaya section on Kurungnakh Island.

No.	Sample No.	Date	Isotopes	Hydro-chemistry	Altitude [m, a.r.l,]	Depth [m]
01	Bkh IW I/01	17.08.02	X	-	-	0.7
02	Bkh IW I/02	17.08.02	X	-	-	0.7
03	Bkh IW I/03	17.08.02	-	X	-	0.7
04	Bkh IW I/04	17.08.02	X	-	-	0.7
05	Bkh IW I/05	17.08.02	X	-	-	0.7
06	Bkh IW I/06	17.08.02	X	-	-	1.0
07	Bkh IW I/07	17.08.02	X	-	-	1.0
08	Bkh IW I/08	17.08.02	X	-	-	1.0
09	Bkh IW I/09	17.08.02	-	X	-	1.0
10	Bkh IW I/10	17.08.02	X	-	-	1.0
11	Bkh IW I/11	17.08.02	X	-	-	1.3
12	Bkh IW I/12	17.08.02	X	-	-	1.3
13	Bkh IW I/13	17.08.02	X	-	-	1.3
14	Bkh IW I/14	17.08.02	X	-	-	1.3
15	Bkh IW I/15	17.08.02	X	-	-	1.3
16	Bkh IW II/01	28.08.02	X	-	16.1	-
17	Bkh IW II/02	28.08.02	X	-	16.1	-
18	Bkh IW II/03	28.08.02	X	-	16.1	-
19	Bkh IW II/04	28.08.02	-	X	16.1	-
20	Bkh IW II/05	28.08.02	X	-	16.1	-
21	Bkh IW II/06	28.08.02	X	-	16.1	-
22	Bkh IW II/07	28.08.02	X	-	16.1	-
23	Bkh IW II/08	28.08.02	X	-	16.1	-
24	Bkh IW II/09	28.08.02	X	-	16.1	-
25	Bkh IW II/10	28.08.02	X	-	16.1	-
26	Bkh IW II/11	28.08.02	-	X	16.1	-
27	Bkh IW II/12	28.08.02	X	-	16.1	-
28	Bkh IW II/13	28.08.02	X	-	16.1	-
29	Bkh IW II/14	28.08.02	X	-	16.1	-

Appendix 3-12: List of the samples for insect fossils from Kurungnakh and Samoylov Islands.

No.	Samples No.	Date	Altitude [m,a.r.l.]	Depth [m]	Site, Section	Bayd-zherakh (Point)	Sedi-ment
1	Bkh-02-B-1	10.08.02		1.0-1.3	Buor Khaya, 1	point 1	silt and peat
2	Bkh-02-B-2	11.08.02		6.0-6.3	Buor Khaya, 1	C	sand
3	Bkh-02-B-3	12.08.02		3.5-3.7	Buor Khaya, 1	B	silt
4	Bkh-02-B-4	13.08.02		5.0-5.3	Buor Khaya, 1	C	silt
5	Bkh-02-B-5	15.08.02		6.7-7.0	Buor Khaya, 1	E	silt
6	Bkh-02-B-6	15.08.02		9.2-9.5	Buor Khaya, 1	F	silt
7	Bkh-02-B-7	16.08.02		2.0-2.3	Buor Khaya, 1	point 3	silt
8	Bkh-02-B-8	17.08.02		10,7-11,0	Buor Khaya, 1	G	silt
9	Bkh-02-B-9	19.08.02	21.5-21.8		Buor Khaya, 2	block 1	silt
10	Bkh-02-B-10	19.08.02	23.5-23.8		Buor Khaya, 2	block 1	silt
11	Bkh-02-B-11	19.08.02	10.0-10.3		Buor Khaya, 2		silt and sand
12	Bkh-02-B-12	22.08.02	17.5-17.7		Buor Khaya, 2		silt and peat
13	Bkh-02-B-13	22.08.02	19.2-19.4		Buor Khaya, 2		silt
14	Bkh-02-B-14	25.08.02	22.7-23.0		Buor Khaya, 2	block 2	silt
15	Bkh-02-B-15	25.08.02	24.7-25.0		Buor Khaya, 2	block 2	silt
16	Sam-1-B-1	3.08.02	6.6-6.9		Samoylov, 1		silt and peat
17	Sam-1-B-2	3.08.02	7.0-7.3		Samoylov, 1		silt and peat
18	Sam-1-B-3	3.08.02	5.9-6.2		Samoylov, 1		silt
19	Sam-2-B-4	20.08.02	5.5-5.9		Samoylov, 2		silt
20	Sam-2-B-5	20.08.02	6.4-6.6		Samoylov, 2		sand
21	Sam-2-B-6	20.08.02	7.0-7.2		Samoylov, 2		sand

Appendix 3-13. List of mammal bones collected on Lena Delta in 2002.

No.	Sample No.	Taxon	Skeleton element	Notes	Preser-vation	Location	Locality
1	BKh2002 O-1	Rangifer (?)	Vertebra		Compl.	depth 8,5 m in mud flow	Buor Khaya
2	BKh2002 O-2	Rangifer tarandus (L.)	Horn	n/s	Frag.	depth 2 m in froz-en silt near contact with ice wedge	Buor Khaya
3	BKh2002 O-3	Ovibos sp.	Metatarsal		Comp.	depth 5,5 m in dry mud	Buor Khaya
4	BKh2002 O-4	Mammuthus primigenius (Blum.)	Femur (caput)	tra-shed	Frag.	Lena bank	Buor Khaya
5	BKh2002 O-5	Equus (Equus) sp.	Mandibula ramus dex		Frag.	height 19,5 m on the slope between two peat layers	Buor Khaya
6	BKh2002 O-6	Equus caballus L.	Atlas		Comp.	height 4,5 m. in dry mud	Buor Khaya
7	BKh2002 O-7	Equus caballus L.	Pelvis		Frag.	Lena bank	Buor Khaya
8	BKh2002 O-8	Equus caballus L.	Carpale III		Comp.	Lena bank	Buor Khaya
9	BKh2002 O-9	Equus caballus L.	Metatarsale		Comp.	height 19-20 m from the frozen silt between two peat layers	Buor Khaya
10	BKh2002 O-10	Mammuthus primigenius (Blum.)	Vertebra		Comp.	Lena bank	Buor Khaya
11	BKh2002 O-11	Equus caballus L.	Vertebris cervicale		Comp.	Lena bank	Buor Khaya
12	BKh2002 O-12	?	?	define	Frag.	Lena bank	Buor Khaya
13	BKh2002 O-13	Equus caballus L.	Mandibula	Same as Bkh 2002-O-5	Frag.	height 19,5 m on the slope between two peat layers	Buor Khaya
14	BKh2002 O-14	Mammuthus	Rib		Frag.	height 26,5 m in mud flow	Buor Khaya
15	BKh2002 O-15	Mammuthus primigenium (Blum.)	tooth lower		Frag.	height 26,5 m in mud flow	Buor Khaya
16	BKh2002 O-16	Equus caballus L.	Tibia		Comp.	Lena bank	Buor Khaya
17	BKh2002 O-17	Equus caballus L.	Tibia		Comp.	height 19-20 m from the frozen silt between two peat layers	Buor Khaya
18	BKh2002 O-18	Bison priscus	Mandibula	juv.	Frag.	Lena bank	Buor Khaya

No.	Sample No.	Taxon	Skeleton element	Notes	Preser-vation	Location	Locality
19	BKh2002 O-19	?	?	define	Frag.	height near 24 m from frozen peat	Buor-Khaya
20	BKh2002 O-20	Equus caballus L.	Femur		Comp.	height 19-20 m from the frozen silt between two peat layers	Buor Khaya
21	BKh2002 O-21	Mammuthus	Femur	tra-shed	Frag.		Buor Khaya
22	BKh2002 O-22	Equus caballus L.	Radius		Comp.		Buor Khaya
23	BKh2002 O-23	Rangifer tarandus (L.)	Tibia		Comp.		Buor Khaya
24	BKh2002 O-24	Ovibos sp.	vert. Thor.		Da-maged		Buor Khaya
30	BKh2002 O-30	Equus caballus L.	Ante-brachium		Comp.	Lena bank	Buor Khaya
31	AKh2002 O-1	Rangifer tarandus (L.)	Vertebrae cervic. (epi-stroph.+3)		Comp.	from Holocene terrace, in dry peat, height 6m, depth 1,5	Amerika Khaya
32	Sam2002 O-1	Rangifer tarandus (L.)	tibia		Frag.	Lena bank	Samoy-lov

Appendix 3-14. Species composition and distribution of zooplankton in the Lena Delta in summer 2002.

I - Samoilovskii Island: 1 – Olenekskaya channel, 2 - flood-plain lake, 3 – big thermokarst lake, 4 – polygons , 5 - crack between polygons.

II - Tit-Ary Island: 6 - terrace lake, 7 – big thermokarst lake, 8 - polygons

III - Buor-Khaya Island: 9 - polygons, 10 - alas

IV - America-Khaya Island: 11 - alas

Taxa	I					II			III		IV
	1	2	3	4	5	6	7	8	9	10	11
Rotatoria:											
Anuraeopsis fissa				+						+	
Asplanchna girodi?										+	
Asplanchna priodonta	+	+	+			+	+		+	+	
Bipalpus hudzoni	+	+				+	+			+	
Brachionus calyciflorus	+										
Brachionus diversicornis	+										
Brachionus quadridentatus	+					+					
Cephalodella gibba		+									
Collotheca sp.							+	+			
Colurella obtusa		+									
Colurella colurus		+									
Colurella uncinata										+	
Conochilus unicornis	+	+	+							+	+
Dicranophorus forcipatus		+					+				
Dicranophorus lutkeni										+	
Eosphora najas					+						
Euchlanis dapidula	+	+		+			+		+	+	
Euchlanis deflexa		+									
Euchlanis dilatata	+				+						
Euchlanis incisa										+	
Euchlanis lyra		+		+							
Euchlanis lucksiana	+	+		+	+	+	+		+		
Euchlanis myersi		+									
Euchlanis sp.							+				+
Filinia terminalis		+									
Filinia longiseta			+					+		+	
Keratella cochlearis	+	+	+	+		+	+		+	+	+
Keratella irregularis										+	
Keratella quadrata	+	+									
Keratella serrulata										+	
Keratella testudo		+									
Keratella sp.		+									
Kellicottia longispina	+	+	+			+	+		+	+	+
Lecane bulla							+			+	
Lecane brachydactyla										+	
Lecane cornuta										+	
Lecane luna						+	+				
Lecane lunaris		+			+	+	+				
Lecane sp.		+									
Lepadella ovalis		+					+				
Macrotrachella quadricornifera					+						

Appendix 3-14. continuation.

Taxa	I					II			III		IV
	1	2	3	4	5	6	7	8	9	10	11
Mytilina mucronata					+		+			+	
Mytilina ventralis		+						+			
Notholca acuminata	+	+	+	+	+		+	+	+		+
Notholca caudata	+	+			+	+	+			+	
Notholca squamula		+		+	+						
Polyarthra dolychoptera	+	+	+								
Polyarthra major	+	+							+		+
Polyarthra minor	+	+									
Testudinella patina		+									
Tretocephala ambiqua		+									
Trichocerca cylindrica	+			+							
Trichocerca brachyura	+										
Trichocerca elongata				+			+			+	
Trichocerca longiseta	+				+						
Trichotria pocillum		+		+		+				+	
Trichotria tetractis		+									
Trichotria truncata		+		+	+		+		+		
Synchaeta pectinata		+									
Synchaeta sp.	+	+	+				+			+	
Bdelloida	+	+	+	+	+		+		+	+	
Copepoda											
Cyclopoida:											
Acanthocyclops vernalis	+	+		+	+	+		+		+	
Acanthocyclops americanus		+			+	+					
Acanthocyclops capillatus						+					
Cyclops abyssorum		+		+				+			+
Cyclops kolensis	+		+								
Cyclops strenuus			+	+	+			+			
Cyclops vicinus			+								+
Diacyclops bicuspidatus	+		+	+	+			+			
Diacyclops bisetosus		+				+					
Diacyclops languidus				+				+			
Eucyclops serrulatus				+	+	+	+	+	+		
Megacyclops gigas								+			
Megacyclops viridis	+	+		+	+	+		+	+		
Mesocyclops leuckartii	+		+								
Calanoida:											
Arctodiaptomus acutilobatus				+							
Arctodiaptomus bacillifer	+										
Diaptomus glacialis				+							
Heterocope appendiculata	+	+				+					
Heterocope borealis				+	+			+	+		+
Eudiaptomus graciloides		+	+								
Eudiaptomus gracilis				+					+	+	
Eurytemora arctica					+						
Eurytemora bilobata		+				+				+	
Eurytemora gracilis		+				+					
Eurytemora sp.		+									

Appendix 3-14. continuation.

Taxa	I					II			III		IV
	1	2	3	4	5	6	7	8	9	10	11
Leptodiaptomus angustilobus				+	+			+	+		+
Limnocalanus johanseni		+									
Mixodiaptomus theeli				+	+			+	+		
Harpacticoida:											
Canthocamptus glacialis		+		+	+			+		+	
Mesochra sp.								+			
Cladocera:											
Alonopsis elongata	+	+		+	+			+	+		
Alonella sp.	+	+		+	+		+	+			
Bosmina longirostris	+	+				+				+	
Bosmina obtusirostris						+					
Bosminopsis deitersi	+	+									
Chydorus sphaericus	+	+	+	+	+	+	+	+	+	+	+
Daphnia cucullata	+					+				+	
Daphnia longiremis	+										
Daphnia pulex	+	+		+	+			+	+		
Eurycercus glacialis						+	+			+	
Polyphemus pediculus						+					
Pseudochydorus globosus					+						
Simocephalus serrulatus						+					
Phyllopoda											
Polyarthemia forcipata				+	+						
Artemiopsis bungei								+			

3.15 References

Abramova, E.N. (1996). Copepoda (Crustacea, Copepoda) of the Lena Delta Reserve. Hydrobiological investigations in natural reserves. Moscow, 8, 5-16. (in Russian).

Abramova, E.N., Sokolova, V.A. (1999). About findings and life cycle of Limnocalanus johanseni (Copepoda, Calanoida) in the Lena Delta. Zoologicheskii Zhurnal, 78, 11, 1360-1363. (in Russian).

AG Boden (1994): Bodenkundliche Kartieranleitung. 4th edition. Stuttgart. E. Schweizerbartsche Verlagsbuchhandlung. 392 p.

Akhmadeeva, I., Becker, H., Friedrich, K., Wagner, Pfeiffer, E.-M., D., Quass, W., Zhurbenko, M., Zöllner, E., Bojke, J., (1999). Modern processes in Permafrost Affected Soils. In: Rachold, V. and Grigoriev, M. (ed.) : Expeditions in Siberia 1998. Reports on Polar Research, 315: pp.19-21.

Akhmetshina, I., Abramova, E. (2002). Zooplankton abundance, biomass and production in the Lena Delta polygon lakes: preliminary results. Climate Driver of the North, Kiel, May 8-11, 20.

Aleksandrova, V. D. (1980): The Arctic and Antarctic: their division into geobotanical areas. Cambridge. University Press. 247 p.

Ammosov, Yu.N. (1961). Plankton of the tundra lake Raspadochnoe and its feeding importance for fishes and fry. Uchenye zapiski Yakutskogo universiteta, 2, 47-54. (in Russian).

Annual data on the regime and water quality of the seas and marine mouths of rivers, 1990-2001, part 2, Marine mouths of rivers, volume 5, Tiksi, 1991-2002.

Atlas of the Sardakh channel of 1949 // Sailing Directions. Tiksi Hydrographic Base.

Bening, A.L. (1942). About the Lena River plankton. Izvestiya Biol.-Geogr. NII pri Vostochno-Sib. Gos. Universitete, IX, 3-4, 217-230. (in Russian).

Bolshiyanov D.Yu., Tretiakov M.V. Investigation of Run off in the Sardakh-Trofimovsky Bifurcation Point of the Lena River Delta. Russian-German Cooperation SYSTEM LAPTEV SEA 2000: The Expedition LENA 2001, Reports on Polar and Marine Research, 426, 2002, pp.57-62

Botvinnik, E.F., N.V. Vershinin (1958). Some results of the Lower Lena River fishering expedition of 1957. Uchenye zapiski Yakutskogo universiteta, 4, 137-146. (in Russian).

Dereviagin A. Yu., Meyer H., Chizhov A. B., Hubberten H.-W., & Simonov E. F. (2000 (published 2002)). New data on the isotopic composition and evolution of modern ice wedges in the Laptev Sea Region. Polarforschung, 70, 27-35.

Elovskaya L.G. (1987): Classification and diagnostics of Yakutian permafrost soils. Yakutsk, 172 p. (in Russian).

FAO (Food and Agriculture Organization of the United nations) (1998): World Reference base for Soil Recourses. World Soil Recources Reports 84. Rom: FAO. 88 p.

French H. M. (1996). The Periglacial Environment, Longman Singapore Publishers, Singapore.

Grigoriev, M.N. (1993): Cryomorphogenesis of the Lena River mouth. Permafrost Institute Press Yakutsk 176 pp. (in Russian).

Grosse, G., Schirrmeister L., Krbetschek, M., Schwamborn, G, Oezen, D., Kunitsky, V., Kuznetsova, T., Kuzmina, S. (2002) New data on Late Quaternary terrestrial permafrost deposits of the Laptev Sea region by IR-OSL, radiocarbon and U/Th age determination. - In Terra Nostra (Climate drivers of the North, Program and Abstracts) pp. 47-47.

Gukov, A.Yu. (2001). Hydrobiology of the Lena River mouth region. M., Nauchnyi mir. 285 pp. (in Russian).

Ivanov, V.V., A.A. Piskun. Distribution of the River Water and Suspended Sediment Loads in the Deltas of Rivers in the Basin of the Laptev and East-Siberian Seas. In: H. Kassens, H.A. Bauch, I.A. Dmittrenko, H. Eicken, H.-W. Hubberten, M. Mellis, J. Thiede, L. A. Timokhov (eds.) Land-Ocean Systems in the Siberian Arctic: Dynamics and History. Springer-Verlag Berlin, 1999, p.239-250.

Kerer, E.F. (1968). Zooplankton of the flood plain lakes in the lower reaches of the Lena River. Uchenye zapiski Leningradskogo Gos. Ped. Instituta, 311, 1, 37-60. (in Russian).

Krbetschek, M.R., Gonser, G., Schwamborn, G., 2002. Luminescence dating results on sediment sequences of the Lena Delta. Polarforschung 70: pp. 83-88.

Kunitsky, V.V. (1989): Cryolithology of the lower Lena region. - Permafrost Institute Press, Yakutsk, 162 p. (In Russian).

Kuzmina, S., Korotyaev, B. (1987): New species of the pill beetle genus Morychus Er. (Coleoptera, Byrrhidae) from the North-West of USSR. Entomol. review, v. 66, N 2, pp. 342-344 (in Russian).

Kuznetsova, T., Kuzmina, S. (2001): Study area of the Eastern Olenyok-Channel – Kurungnakh Island (Buor Khaya), Paleontological study - In Rachold, V. and Grigoryev, M. N. (eds.): Russian-German Cooperation SYSTEM LAPTEV SEA 2000: The Expedition LENA 2000. Reports on Polar Research, 388: pp. 96-98.

Lungersgausen, G. F. (1961): Stratigraphy of Cenozoic deposits of the middle and lower Lena and Lena Delta. (In Russian).

Mackay J. R. (1993). Air temperature, snow cover, creep of frozen ground, and the time of ice-wedge cracking, western Arctic coast. Canadian Journal of Earth Sciences, 30, 1720-1729.

Manual for Hydrometeorological stations and posts. Issue 6, Part 1. Gidrometeoizdat. L., 1978.-384 p.

Meisch, C. (2000): Freshwater Ostracoda of Western and Central Europe. Springer Akademischer Verlag, Heidelberg Berlin, pp. 1-515.

Mostakhov, C.E. (1973). Lakes in the cryolithozone of the USSR. Ground waters of the cryolithozone. 2nd International Conference on Permafrost Studies. Yakutsk, vol. 5, 118-120. (in Russian).

Nikolaev V. I. & Mikhalev D. V. (1995). An oxygen-isotope paleothermometer from ice in Siberian permafrost. Quaternary Research, 43 (1), 14-21.

Nüchterlein, H. (1969): Süßwasserostracoden aus Franken. Ein Beitrag zur Systematik und Ökologie der Ostracoden. In: Int. Revue ges. Hydrobiol. 54/1: pp. 223-287.

Pavlova, E., Dorozhkina, M. (2000): Geological-geomorphological studies in the western and central part of the Lena Delta - In Rachold, V. and Grigoriev, M. N. (eds.): Russian-German Cupertino SYSTEM LAPTEV SEA 2000: The Expedition LENA 1999. Reports on Polar Research, 354: pp. 75-90.

Pfeiffer, E.-M., Akhmadeeva, I., Becker, H., Friedrich, K., Wagner, D., Quass, W., Zhurbenko, M., Zöllner, E., Boike, J. (1999): Modern Processes in Permafrost Affected Soils. In: Rachold V. and M.N. Grigoriev (ed.) Expeditions in Siberia 1998. Reports on Polar Research 315. pp 19-80

Pfeiffer, E.-M., Wagner D., Kobabe, S., Kutzbach L., Kurchatova A., Stof, G., Wille, C. (2002): Modern processes in permafrost affected soils.- In Pfeiffer, E.-M., and Grigoryev, M. N. (eds.): Russian-German Cooperation SYSTEM LAPTEV SEA 2000: The Expedition LENA 2001. Reports on Polar Research, 426: pp. 21-41.

Pirozhnikov, P.L. (1958). About the area of distribution and ecology of copepoda Senecella calanoides Juday. Zoologicheskii Zhurnal, 37, 4, 625-629. (in Russian).

Pirozhnikov, P.L., Shulga, E.L. (1957). The main characterishes of zooplankton from the Lower Lena River. Trudy Vsesoyuznogo gidrobiologicheskogo obshestva, 8, 219-230. (in Russian).

Polunin, N. (1959): Circumpolar Arctic Flora.Oxford. University Press. 514 p.

Post, W.M., Emanuel, W.R., Zinke, P.J., Stangenberger, A.G. (1982): Soil carbon pools and world life zones. Nature 298, 156-159.

Report on the hydrological studies in the Lena delta. 1985 // Report. TTUGMiKPS, Hydrographic party, Head – P.V. Seleznev. Tiksi, 1986, 88 p.

Rylov, V.M. (1928). Materials on the fauna of freshwater copepods (Copepoda, Calanoida) of the Northern Siberia. Trudy komissii po izucheniyu Yakutskoi ASSR, 11, 1-32. (in Russian).

Schirrmeister, L., Kunitsky, V., Grosse, G., Kuznetsova, T. (2001): Kurungnakh Island (Buor Khaya), Geological-cryological survey - In Rachold, V. and Grigoryev, M. N. (eds.): Russian-German Cooperation SYSTEM LAPTEV SEA 2000: The Expedition LENA 2000. Reports on Polar Research, 388: pp. 94-96.

Schirrmeister, L. , Kunitsky, V. , Grosse, G. , Schwamborn, G. , Andreev, A.A., Meyer, H., Kuznetsova T., Bobrov, A., Oezen, D. (submitted): Late Quaternary history of the accumulation plain north of the Chekanovsky Ridge (North East Yakutia).- Polar Geography.-

Schlesinger ME, Mitchell JFB (1987): Climate model simulations of the equilibrium climatic response to increased carbon dioxide. Rev Geophys 25: 760-798.

Schwamborn, G, Schneider, W., Grigoryev, M., Rachold, V., Antonow, M. (1999): Sedimentation and environmental history of the Lena Delta. - In Rachold, V. and Grigoryev, M. N. (eds.): Russian-German Cooperation SYSTEM LAPTEV SEA 2000: The Lena Delta 1998 Expedition. Reports on Polar Research, 315: pp. 94-111.

Schwamborn, G., Andreev, A.A., Rachold, V., Hubberten, H.-W., Grigoriev, M.N., Tumskoy, V., Pavlova, E.Yu., Dorozhkina, M. V., 2002. Late Quaternary sedimentation history of the Lena Delta. Quaternary International, 89: 119-134.

Serkina, R.A. (1969). Plankton and benthos of the Lena Delta and adjacent coastal waters. Trudy Yakutskogo otdeleniya Sibirskogo NII rybnogo khozyaistva, Yakutsk, 3: 188-196. (in Russian).

Siegert, C., Schirrmeister, L, Kunitsky, V, Tumskoy, V., Derevyagin, A., Meyer, H., Kuznetsova, T., Kuzmina, S., Sher, A, Syromyatnikov I, (1999): Paleoclimate Signals of ice-rich permafrost. - In Rachold, V. and Grigoryev, M. N. (eds.): Russian-German Cooperation SYSTEM LAPTEV SEA 2000: The Lena Delta 1998 Expedition. Reports on Polar Research, 315: pp. 145-259.

Sher, A, Kuzmina, S., Lisitsyna, O., Parmuzin, I., Demmyankov, S. (2002): Paleoecological and permafrost studies of Ice Complex in the Laptev Sea area (Bykovsky Peninsula) - In Pfeiffer, E.-M., and Grigoryev, M. N. (eds.): Russian-German Cooperation SYSTEM LAPTEV SEA 2000: The Expedition LENA 2001. Reports on Polar Research, 426: pp. 94-107.

Sher, A, Parmuzin, I., Bortsov, A. (2000): Ice Complex on Bykovsky Peninsula. - In Rachold, V. and Grigoryev, M. N. (eds.): Russian-German Cooperation SYSTEM LAPTEV SEA 2000: The Expedition LENA 1999. Reports on Polar Research, 354: pp. 169-182.

Soil Survey Staff (1998): Keys to Soil Taxonomy. 8th edition. Lincoln, Nebraska: USDA-The National Recources Conservation Sevice. 599 p.

Sokolova, V.A. (1984). Composition of zooplankton in the Lower Lena River. Byulleten' nauchno-tekhnicheskoi informatsii, Yakutsk, 16-19. (in Russian).

Stepanova, L.A., Abramova, E.N. (1997). Historical-faunistic analysis of copepoda from the Lena Delta Reserve. Abstracts of the Conference "Facvtors of taxonomic and biochorological diversity". St.Petersburg, 77. (in Russian).

Urban, V.V. (1949). Hydrobiologycal investigations in the Lena Delta. Izvestiya VNIORKH. Leningrad, Volum 29. 75-95. (in Russian).

Van Everdingen, R.O. (ed.)(1998): Multi-Language Glossary of Permafrost and Related Ground-Ice Terms. International Permafrost Association, p. 31 (definitions).

Vasil'chuk Yu. K. (1992). Oxygen isotope composition of ground ice. - Application to paleogeocryological reconstructions, Moscow, Russia. pp. 420.

Viehberg, F. (2000): Faunistische und ökologische Untersuchungen zur Ostracodenfauna ausgewählter Kleingewässer der Stadt Greifswald (diploma thesis). University of Greifswald. pp. 1-141.

Vtyurin, B. I. (1956): About some geomorphological terms in geogeokryology (O nekotorykh geomorfologicheskikh terminakh v geokriologii). In: Meyster, L.A. (ed.) Materials of basic knowledge about permafrost zones of the Earth crust (Materialy k osnovam ucheniya o merzlykh zonakh zemnoy kory), Academy of Science USSR, Moscow, pp 126-134 (In Russian).

Wagner, D., Kutzbach, L., Becker, H., Vlasenko, A. and Pfeiffer, E.-M. (2000): Seasonal variability of trace gas emission (CH4, CO2) and in situ process studies In: Rachold V. and M.N. Grigoriev (ed.) The Expeditions Lena 1999. Reports on Polar Research 354. pp 28-36.

Zhang T, Barry RG, Knowles K, Heginbotton JA, Brown J (1999): Statistics and characteristics of permafrost and ground-ice distribution in the northern hemisphere. Polar Geography 23, 2:132-154.

4 Periglacial features around Tiksi

Guido Grosse, Lutz Schirrmeister, Viktor Kunitsky and Alexander Dereviagyn

4.1 Aims and study area

The study of the recent periglacial environment in combination with former periglacial processes helps to reconstruct the Quaternary landscape history of the Arctic coastal region. Of special interest are relationships between the areas of coastal lowlands and the adjoining coastal ranges. Consequently, the area around Tiksi is quite suitable for studying periglacial processes in both landscape types. The investigation area extends from the Khorogor Valley in the north to the Sevastyan Lake in the south and includes the Bykovsky Peninsula in the east (Figure 4-1). Our studies focused on five topics:

1. The observation, characterisation, geodetic survey and sampling of various periglacial surface phenomenons like ice wedge polygons, cryoplanation terraces, thermokarst structures, nival niches, snowfields, pingos and lagoons. The results serve as field verification of typical periglacial structures for the interpretation of remote sensing data. For that purpose the study objects were characterized qualitatively by collecting surface samples, measuring soil temperature and –moisture on a mobile soil probe and photographical documentation. Shape, extension and position were determined by laser tachymeter (Zeiss ELTA 3) or by measuring tape.

2. To determine the influence of modern nival processes on the Arctic landscape genesis recent snowfields and their surroundings were studied concerning size, structure and composition of snow and sediments. As is known, there is the assumption that a close connection exists between the Ice Complex genesis in the Laptev Sea coastal lowlands and the occurrence of perennial snowfields or embryonic glaciers within close mountain ranges during the Pleistocene (Galabala 1997, Kunitsky 1987). The new studies are connected with former work in the Chekanovsky Ridge and on Bol'shoy Lyakhovsky Island (Kunitsky et al. 2002).

3. Around Tiksi traces of glacial conditions were re-investigated (drumlin-, glacial boulder-and moraine-like features), which serve as evidence for an arctic shelf glacier according to Grosswald & Spektor (1993).

4. Investigation of exposed permafrost deposits (thermokarst mounds, coastal outcrops) as supplement to previous studies carried out on the Bykovsky Peninsula (Schirrmeister et al. 2002).

5. Investigation of recent processes of ground ice formation using stable isotope and tritium methods. The isotopic composition (^{3}H, $\delta^{18}O$, δD) of both types of ground ice (texture ice and ice wedges) and of various forms of water and (rain, snow, suprapermafrost groundwater, surface water) was studied.

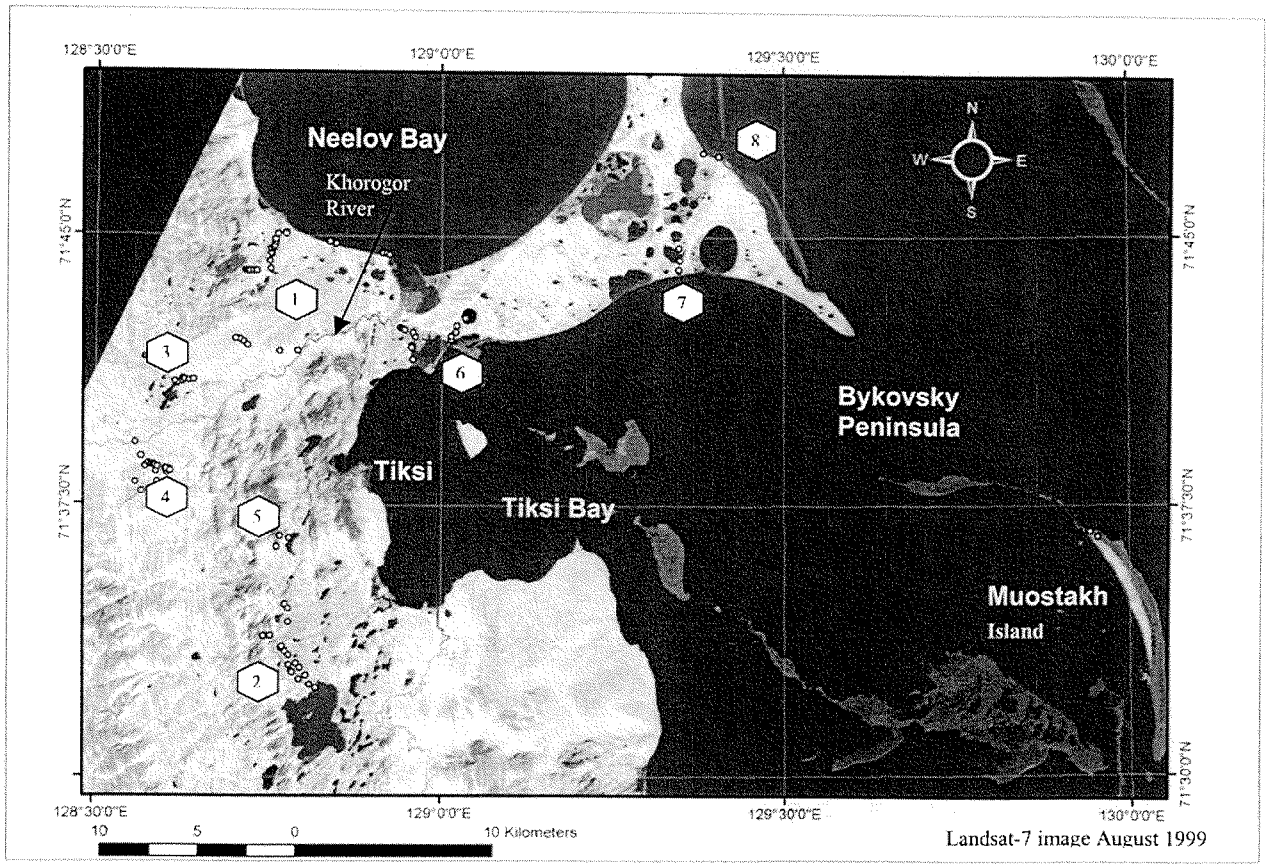

Figure 4-1: Overview map of the region around Tiksi: 1 – Khorogor Valley; 2 – Sevastyan Lake; 3 – Figurnoye Lake; 4 – upper Khorogor Valley with terraces; 5 – nival monitoring site; 6 – old Khorogor Delta; 7 – Polar Fox Lake; 8 – Mamontovy Khayata & Mamontovy Bulgunnyaga; small circles represent investigation sites

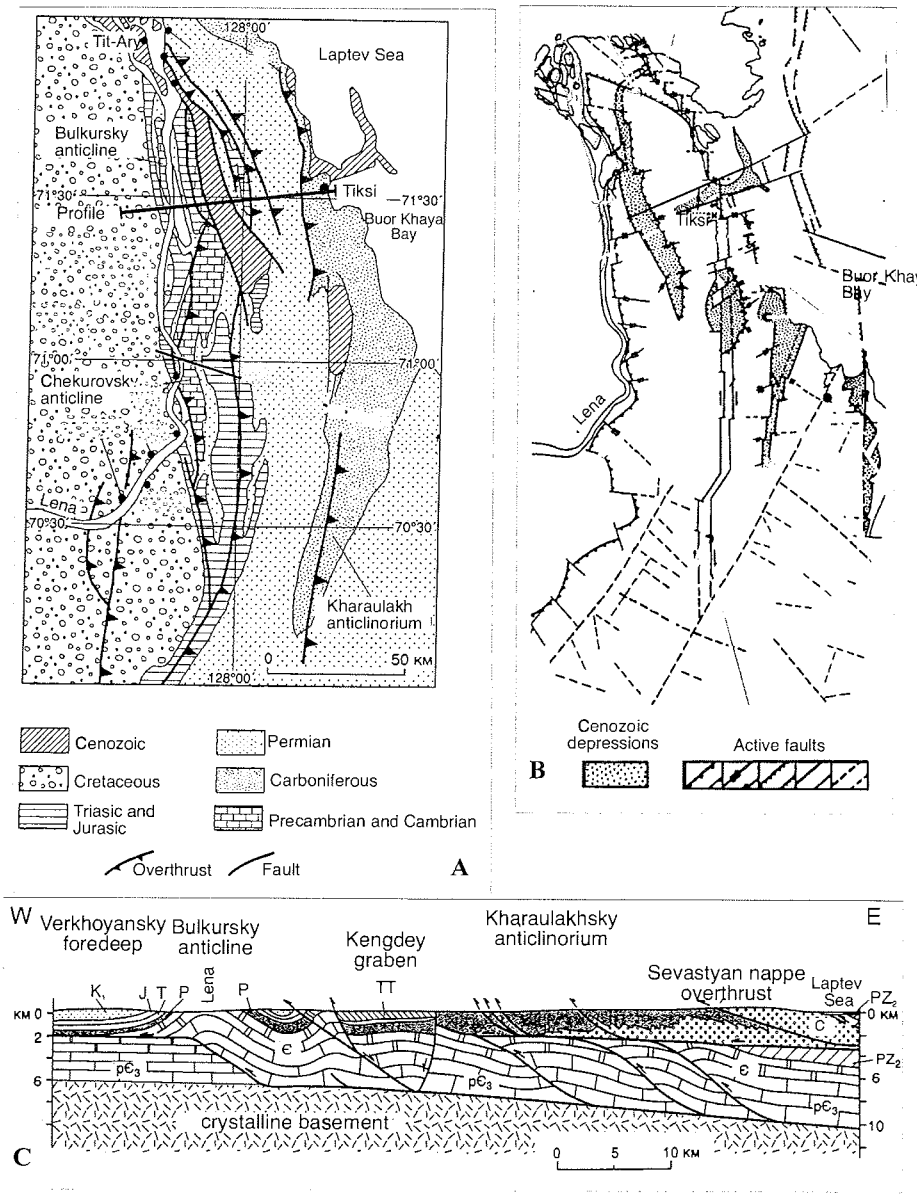

Figure 4-2: Schematic geological map (A) of the Kharaulakh region, tectonical map of modern active faults (B) and the E-W-profile across the Kharaulakh Ridge near Tiksi (C); according to Imaev et al. (2000) and Parfenov (2001).

The area in the region of Tiksi is subdivided into two main parts - the coastal mountain range of the Kharaulakh Ridge in the west and the remains of a former accumulation plain including the Bykovsky Peninsula in the east. The mountains close to Tiksi between the Khorogor Valley and Sevastyan Lake

belong to the Kharaulakhsky anticlinorium (Parfenov 2001). This area is situated within the central zone of the Kharaulakh seismotectonical zone (Imaev et al. 2000). The entire region of the Kharaulakh Ridge between the Lena River and the Laptev Sea is shaped by Cretaceous overthrust tectonics and Cenozoic block tectonics (Figure 4-2). The geological and tectonical evolution of the concerned area is controlled by position at the boundary between the Eurasian and the North American plates. The intensely folded and imbricated rocks consist of Permo-Carboniferous sequences of sandstone-slate-beddings, which were assigned to a shallow shelf facies (Imaev et al. 2000).

During the pre-Cretaceous period the Siberian Plate had a passive margin in this region, where several kilometres of sediments of a Precambrian Mesozoic mega-complex had been accumulated. The lower Cretaceous main folding of the Verkhoyansky collision orogen resulted in typical compression tectonics. The Kharaulakhsky anticlinorium has to be interpreted as a blind autochthonous roof duplex structure with a subjacent overthrust plain to the crystalline basement and a roof overthrust plain, covered by upper Palaeozoic and early Mesozoic series (Figure 4-2). Overthrusts were generally orientated to the west, which is evident in asymmetrical to overturned folds. They are up to some hundred metres large with a western vergency. A special area is the Sevastyan nappe overthrust. The rocks there consist only of Carboniferous to lower Permian distal turbidites and contourites. They were overthrusted at the Kharaulakhsky seismo-tectonical zone. The associated foliation is inclined N to NNW.

The later geological and tectonical evolution is connected with the rift-genesis of the Gakkel Ridge and its extension on the continental plate (Ust Lena rift, Moma 'rift') (Drachev et al. 1998, Franke et al. 2000). Deposits of the Cenozoic mega-complex are mainly connected with the Tertiary graben system and cover the Precambrian-Mesozoic mega-complex with a strong discordance. The lignite deposits within the Sogo graben south of Tiksi belong to this complex, too. In addition, local compression during the Cenozoic period is evident by folding and overthrusting of Tertiary deposits. Tectonical uplift connected with peneplain formation in different heights within the Kharaulakh Ridge as well as block tectonics in the Lena delta and eastern Laptev Sea region were typical processes during Cenozoic times (Imaev et al. 2000). This is proved by dislocations of the Neogene weathering crust along the Buor Khaya Gulf coasts as well as by different base levels of the late Pleistocene to Holocene deposits within the Lena delta (Galabala 1980, Grigoriev 1993).

The relief in the central part of Kharaulakh Ridge is characterized by strong dissection. According to Imaev et al. (2000) deep-cutting, steep river valleys, ridge-like watersheds with peaks above, kars, small glaciers and numerous snowfields form an alpine character in this area. Flat upland areas of erosive-tectonical denudation origin were formed at the western and eastern slopes. The steps of these old peneplains are directly related to Cenozoic uplift. In addition, traces of mountain glacier activities like moraine deposits, trough shoulders and down-washed bottoms of old glacier valleys were reported by

Imaev et al. (2000) in various river valleys. There seem to be connections between the length of valleys and their orientations within the uplifting areas. Long valleys of some ten kilometres length are orientated to NE within dislocation zones. However, the N-S orientated valleys are clearly shorter (some km) and were formed by erosion of rocks like slate. The large u-shaped valleys connected with fracture zones have a broad, flat valley bottom, which is covered by patchwork-like tundra. Accumulation and pediment terraces of 2 to 15 m height above the valley bottom are typical at the slope base. The Kharaulakh Ridge are restricted to the east by an accumulation plain with a small inclination to the sea. Ice Complex hills, thermokarst depressions and valleys, thermokarst mounds and pingos are very common in this area.

According to Imaev et al. (2000) the Cenozoic landscape history of the Kharaulakh Ridge include an initial stage with uplift in the south during Eocene to early Oligocene and a major stage (late Oligocene to early Pleistocene), when the relief forming linear uplifts occurred. Only in the north an erosional denudation plain had already existed. During the final stage (middle Pleistocene to Holocene) a new uplift occurred which formed the present-day ridges and depressions and the related hydrological situation. Nowadays, tectonical movements still keep on, as is proven by seismic studies and levelling measurements. The oldest documented earthquake with a magnitude of 6.8 occurred near the Lena delta in 1909. Numerous earthquakes were recorded during the following years too, sometimes with magnitudes between 4 and 5.8. Therefore, the Quaternary landscape history of our study area is closely connected with neotectonic processes.

4.2. Periglacial phenomena of the eastern Khorogor valley

4.2.1. Between the rivers Vassily and Khorogor

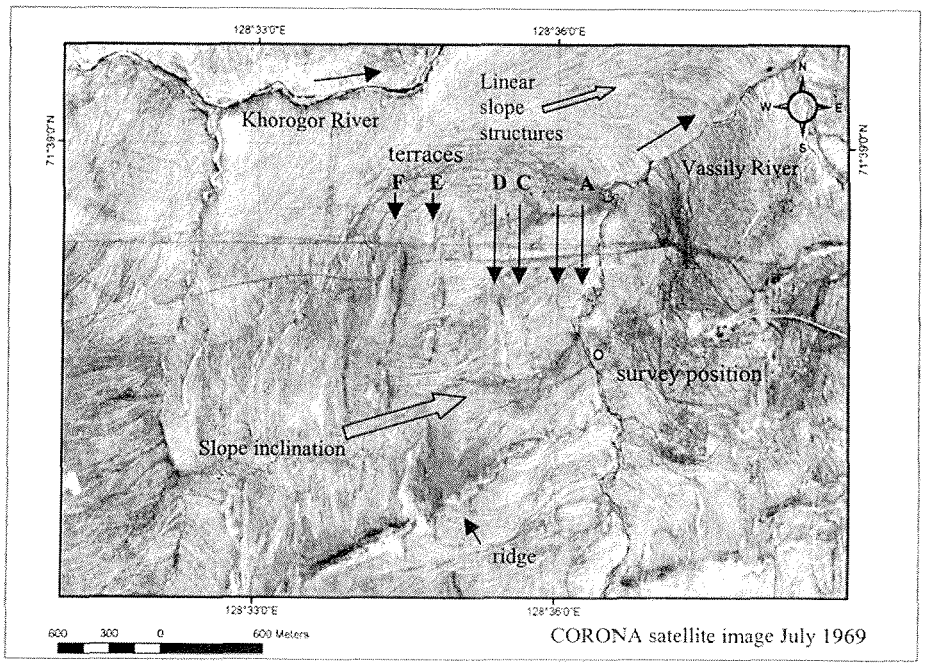

Figure 4-3: Overview map of the investigation area between the Vassily River and Khorogor river

In the area between the Vassily River and the Khorogor River a geodetic survey of cryoplanation terraces at valley slopes had been carried out within two days (Figure 4-3). On the first day the terrain was examined. A favourable location for the laser tachymeter was found and the boundaries of 6 terraces were marked with wooden sticks. On the second day we surveyed the terraces, named A to F, using some 157 measuring points which were situated on the upper and the lower edge of each terrace (Figure 4-4). For time reasons no points were measured between the terraces. Therefore, the density of points allows only a simple modelling of the terraces themselves, but not of the interspaces (Figure 4-4). A schematic slope profile shows that the terraces have their origin in the changing lithology and resistance of the sandstone-slate alternation in the basement (Figure 4-5). The terraces are more or less strictly N-S oriented whereas the slope is inclining to the east. The relief got its character with gently slopes by periglacial weathering and transport processes where the basement consists of soft slates and of flat terraces where the harder, more resistant sandstone layers occur. Only in a few places the bedrocks crop out. Mostly they are covered by weathering detritus and silty to sandy nivation deposits.

Table 4-1: Properties of the studied cryoplanation terraces area north of the Vassily River

Area	Height	Description	Sample
Terrace F	116 m	Several steep basset edges, coarse-grained debris, vegetation-debris-strips (2-3 m wide)	Khg-19-1
Area F-E	108 m	Vegetation cover 100 %, *Betula nana*, moss, slope inclination <5°, active layer depth 40-50 cm, loamy sand with small gravels, frost boils 30-80 cm, polygons 7-10 m	Khg-19-2
Terrace E		Vegetation cover 80%, mostly moss, coarse-grained debris	
Area E-D	90 m	Dense grass-moss-vegetation, meandering grass brooks (1.5 to 6 m wide), subsurface ice layer, moss peat patches (Ø 10 m) with frost cracks and ice wedge polygons, silty fine sand	Khg-95-12 Khg-19-3
Terrace D	84 m	Coarse-grained rock debris (Ø 10 to 20 cm), partly covers of mixtures of plant detritus and fine sand (Chionoconite)	Khg-19-6 Khg-19-5
Area D-C	82 m	Grass cover 100%, silty fine sand, only few gravels, frost boils, polygons, grass brook (2 m wide) with flat thermokarst mounds	Khg-19-7

The terraces are covered with stones (up to 15 cm in ∅) in a fine-grained matrix (Table 4-1). The processes occurring at these slopes are frost scattering of the basement at outcrops, solifluction and cryoturbation on the slopes and in the active layer, melt water runoff in spring, aeolian transport on the slope surfaces and at last accumulation of sediment material by the Vassily and Khorogor rivers. On the grass and moss covered plain between terraces E and D a transparent, 2-3cm thick ice layer with vertical ice needles was observed and sampled (Khg-95-12).

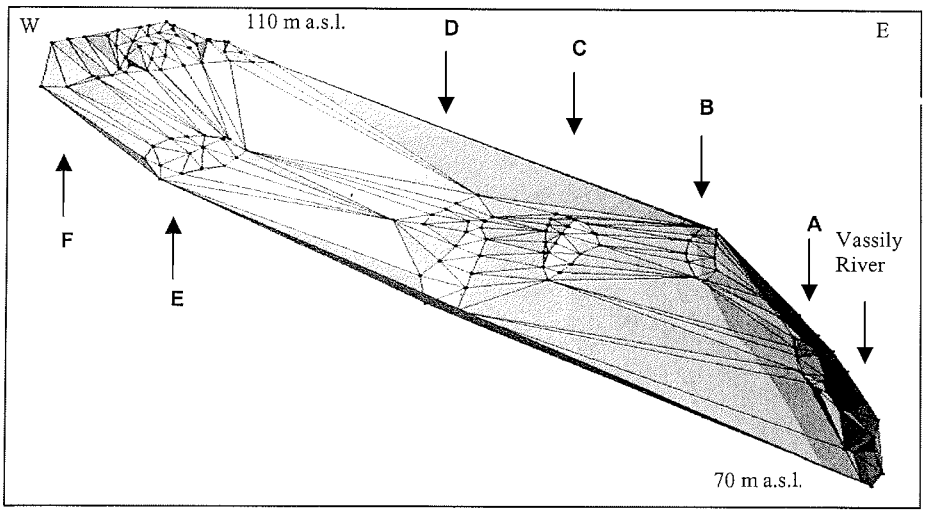

Figure 4-4: The height exaggerated 3-D model of the cryoplanation terrace survey

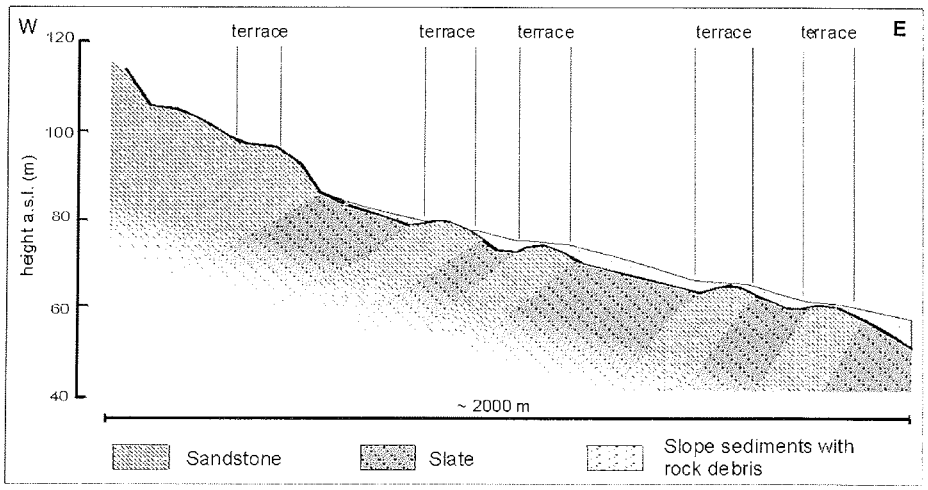

Figure 4-5: Schematic view for the lithological situation below the cryoplanation terraces

South of the cryoplanation terraces the basement crops out partially. In remote sensing images a ridge is clearly visible (Figure 4-3) cross-cutting the terraces from NE to SW. Its highest point is about 190 m a.s.l., so that the whole ridge overlooks the surrounding surface with relatively steep slopes. Beds of Permian sandstones and slates dominate the geology of the basement of this area with the same north-south striking direction like the terraces. Further, there are some dolerite dykes, which intruded into the sedimentary rocks (Figure 4-6). The differing hardness of these rocks is visible again by the shape of the geomorphological relief. The sandstones with calcareous cement and quartz filled fissures and the dolerites formed elevations and single rocks while the strongly weathered slates formed the depressions in the ridge. The ridge itself is covered only by coarse-grained weathering material but not by fine-grained sediments (Figure 4-7). Hence it is considered as one source area for sediment material on the terraces. The ridge could be an example for similar basement characteristics below the cryoplanation terraces. Several samples had been taken from outcropping rocks (Khg-2, Khg-3, Khg-4-1 & -2).

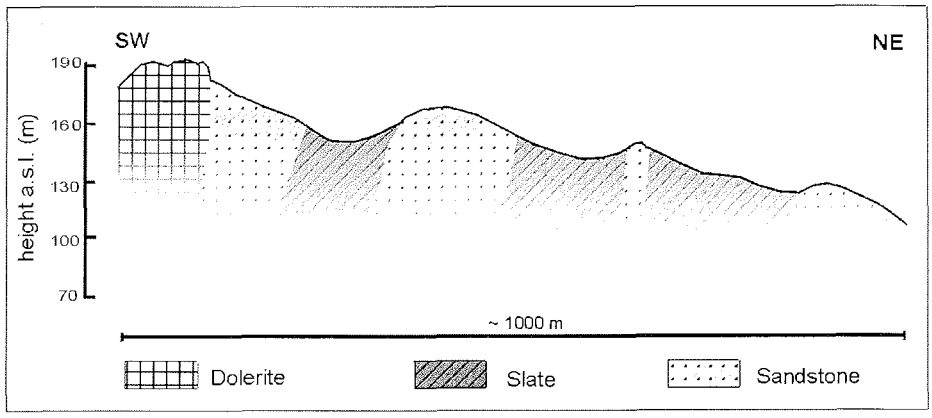

Figure 4-6: Geological situation of the ridge south of the cryoplanation terraces

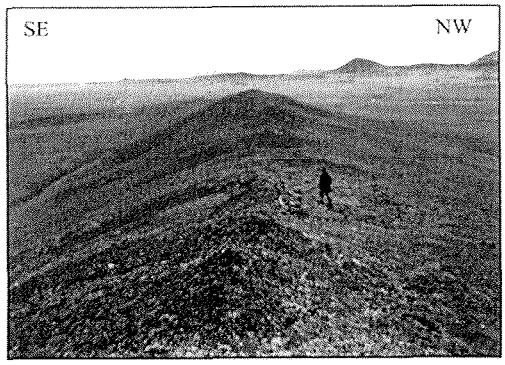

Figure 4-7: The bedrock ridge is covered only by coarse-grained frost weathering material

North of the cryoplanation terraces the Khorogor river is situated. Between terraces and the Khorogor River a gently inclined accumulation plain of about 1 km width has been formed. In this area silty to sandy sediments occur. Frost boils in that area contain only a few (near the river, sample Khg-5-1) or no pebbles at all (more south from the river, sample Khg-6).

The southern riverbank of the Khorogor River is a steep cliff of the same outcropping basement rocks as described above. The interbedding of sandstone and slates has a very steep inclination and seems to be folded in a large scale (Figure 4-8). The cliff is 6-8 m high and the discordant sedimentary layer on top is approximately 1 m thick. The river water was sampled there (Khg-96-1) as well as the black coarse-grained river sand.

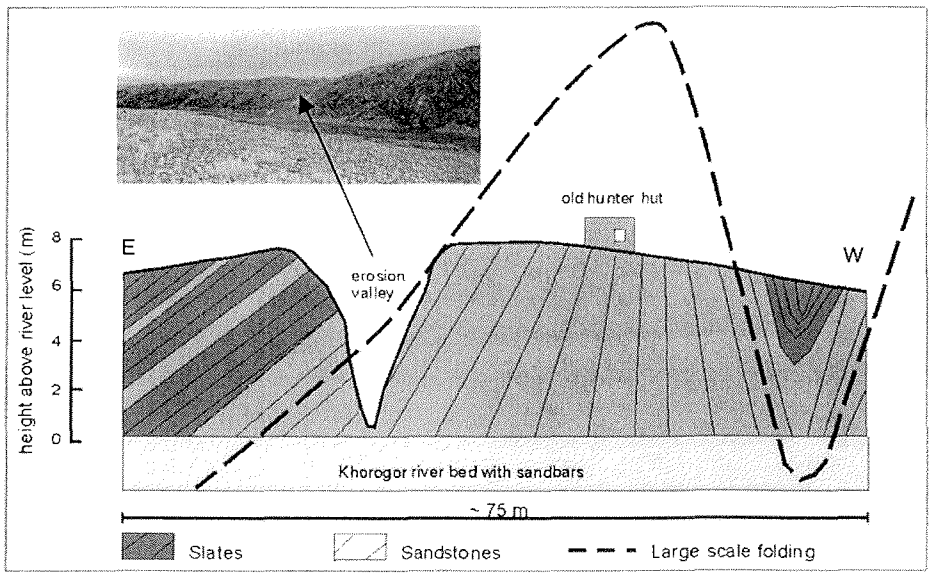

Figure 4-8: Bank of the Khorogor River with steep inclined sandstone-slate interbedding and large scale folding.

On the lowermost river terrace of the Vassily River several frost boils were found. The terrace was gently inclined towards the river and the vegetation on the terrace was dominated by moss, grass and species of Salix and Betula. The diameters of the frost boils varied between 40 and 100 cm. One frost boil was excavated and described in detail (Figure 4-9). A cross section of active layer depths (Figure 4-10) around the frost boil showed, that the largest depth with 43 cm was found at the centre of the frost boil. With greater distance from the frost boil the active layer depth decreased to 20-25 cm.

Figure 4-9: Frost boil at the Vassily River terrace

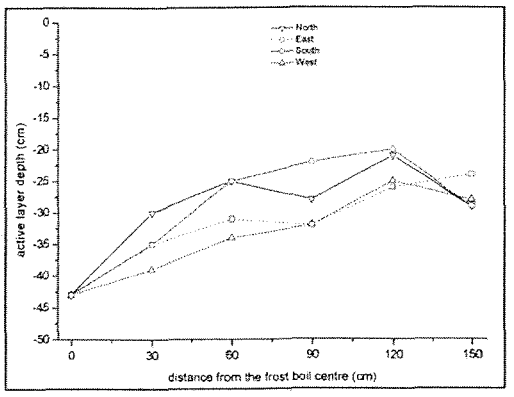

Figure 4-10: Active layer depth on 1st of August around the investigated frost boil

The surface of the frost boil consisted of dry, silty to fine grained sandy material (Figure. 4-11). Some small gravels (1 cm in ∅) were found in the centre of the surface. The upper horizon of loamy silty fine sand is about 30 cm deep and has a very low water content. Only a few grass roots were found, showing that the frost boil is still active. This upper part is irregularly interstratified by oxidative (brown) and reductive (grey-black) spots. The material is not laminated in a certain way. Below this horizon a thin water-saturated layer with a higher clay content and a reduced milieu is situated. Within the clayish matrix many pebbles were found (2-8 cm in ∅). At about 45 cm depth the ice containing permafrost starts with fine- to medium grained sand rich in pebbles. From the frost boil two samples were taken, one from the upper dry horizon (Khg-20-2) and one from the lower wet and reduced horizon (Khg-20-1).

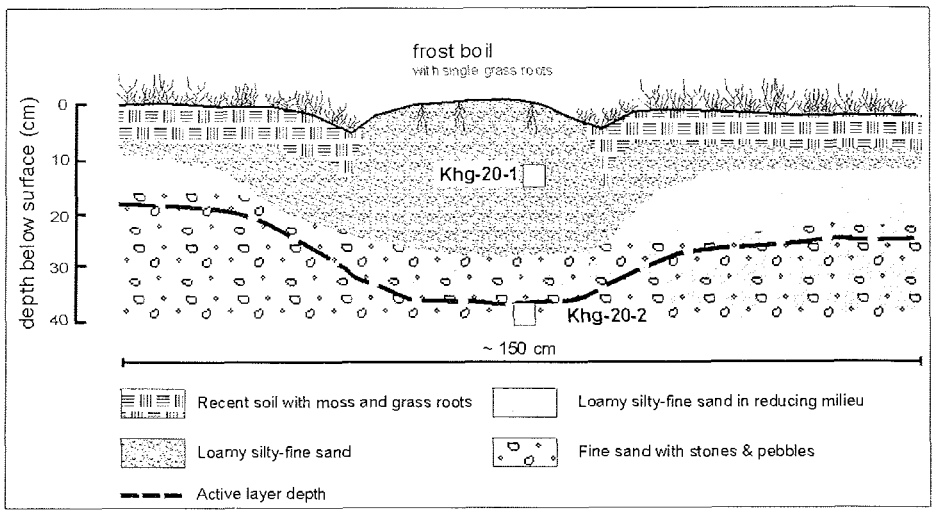

Figure 4-11: Schematic section across a frost boil at the Vassily River terrace

Approximately 1 km N of our terrace survey position we investigated a landscape on a gently inclined slope within a wet grass tundra setting. In the CORONA satellite image runoff structures, so-called "delly", were observed in that area (Figure 4-3, upper right corner). These structures were visible in the image as elongated parallel stripes oriented into the direction of the slope inclination, producing a fan-like widening with decreasing relief energy. These structures usually end at larger discharges like the Vassily River. Although we believed to find easily its expression in vegetation or relief differences on the ground, in the field we could not observe these structures. One assumption is, that they are more or less discharging in the active layer (subsurface), another assumption is, that episodic precipitation events cause these strips (surface). On explanation for dellies as initial thermokarst features on hill slopes is given by Katasonova (1963).

On the same slope, in a position equal to the lowest cryoplanation terrace, some polygons were found. A profile for active layer depths was measured (Figure 4-12) and a sediment sample (Khg-7) and an ice sample (Khg-95-1) was taken from a young ice wedge of about 15 cm wide below a frost crack. Here, too, frost boils occurred with diameter of 60-90 cm and active layer depths down to 40 cm.

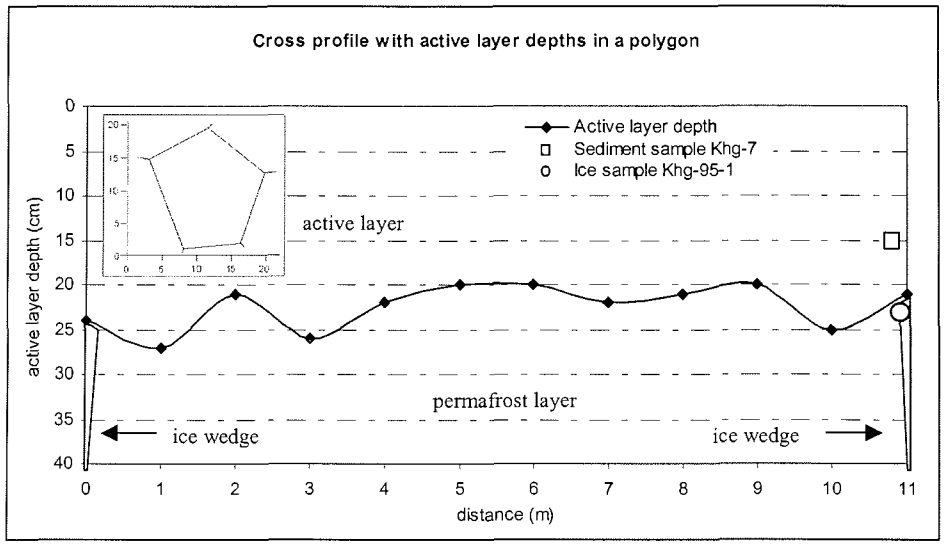

Figure 4-12: Active layer profile (1st August), size of the polygon and sample position for Khg-7 and Khg-95-1

On the northern upper slope of the Vassily River groundwater and an ice wedge were sampled near some buildings in a small pit (Khg-98-3, Khg-95-9). More ice, ground and surface water were sampled about 200 m lower at the slope within an ice wedge polygon (Khg-95-10 & 11, Khg-98-4, Khg-96-9 & 10).

4. 2. 2. Between Khorogor River and Lake Figurnoe

The area between the Khorogor River and Lake Figurnoe east of the settlement Tiksi 3 represents the plane, 2 to 3 km wide central part of the lower Khorogor Valley. Large ice wedge polygons and thermokarst mounds at the less inclined southern valley slopes possibly reflect the existence of a thin horizon of Ice Complex-like deposits there. The valley bottom has heights between 40 and 50 m a.s.l., and it is covered by a wet grass-tundra. Numerous peat patches (up to 40 m x 20 m) and peat circles (15 to 20 m in Ø) occur in distances between 30 to 50 m. These may represent former peat filled small ponds. Polygonal nets of different generations were observed within such peat patches. Large polygons (about 9 m in Ø) are subdivided into smaller polygons with diameters between 1 and 2 m.

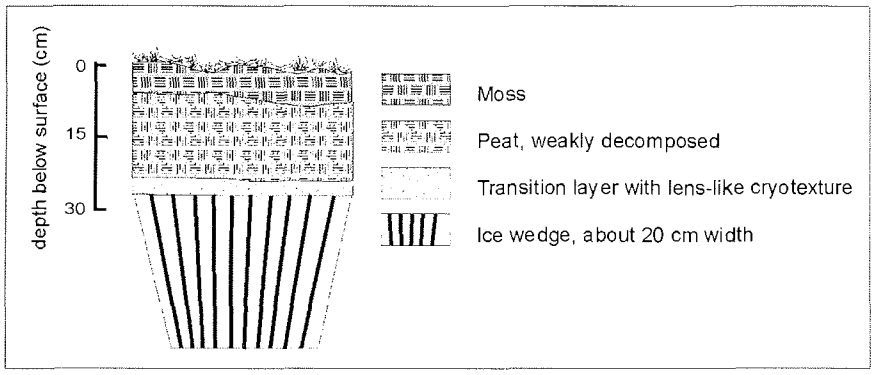

Figure 4-13: Pit Khg-8 with peat layers above an ice wedge

Additionally, frost boils are irregularly distributed in the whole area. In parts gravels and weakly subrounded stones (size 7-15 cm) of sandstone are concentrated in the centres of the frost boils. Therefore, the debris layer of the Khorogor valley should not be very deep below the surface. Other frost boils contain only silty fine sand. The active layer thickness varied between 40-60 cm in frost boils, 20 cm above frost cracks and between about 30-40 cm in polygonal sites. The material from the frost boils is transported by cryoturbation from greater depths up to 40-60 cm and might be useful as indicator for the basement below. Therefore the differences in the gravel content are most likely caused by the changing relief structure of the basement, which is composed by tilted alternations of more resistant sandstone and less resistant slate layers (Figure 4-14).

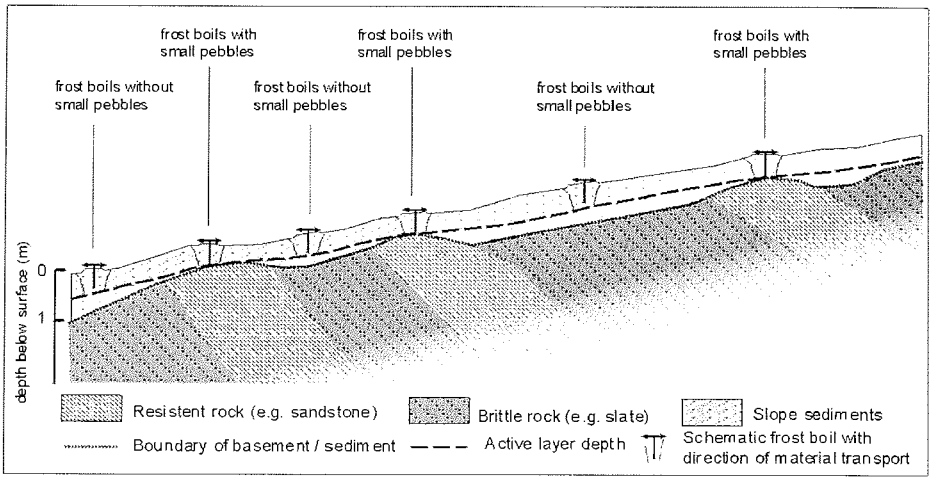

Figure 4-14: Schematic view of the occurrence of frost boils with material content of different grain sizes

All frost boils, which were investigated in more detail in the region around Tiksi are listed in table 4-2.

Table 4-2: Investigated frost boils in the region around Tiksi with their most characteristic properties (1st week of August)

Frost boil	Location and geomorphological position	Size (∅)	Lithology	Active layer depth	
				Frost boil	Surrounding
Khg-1	Flat plain at the base of the cryoplanation terraces; grass tundra	60 cm	Silty fine sand with pebbles (8 cm)	40 cm	35-40 cm
	Upper terraces, flat plain; sparse vegetation	200 cm	Fine sand with pebbles	45-50 cm	30-35 cm
Khg-5-1	Gently inclined plain towards the Khorogor River; grass tundra	35 cm	Silty fine sand with pebbles (6 cm)	45 cm	35-40 cm
Khg-6	Base of a moderate inclined slope towards the Khorogor River; dense, wet grass tundra	70 cm	Silty fine sand	52 cm	35 cm
	Former winter airport landing site; wet grass-moss tundra		Silty fine sand	50-57 cm	30-40 cm
Khg-9	Former winter airport landing site, within a large moss patch (15 x 30 m); wet grass-moss tundra	150 cm	Silty sand with quartz gravels	55 cm	
Khg-15	Flat plain in the northern part of the central Khorogor Valley, covered densely by frost boils; moss-lichen tundra	60 cm	Silty fine sand with gravels	50 cm	25 cm
Khg-19-2	Gently inclined slope between the cryoplanation terraces; dry grass tundra with mosses and Betula		Silty sand with unrounded pebbles	40-50 cm	
Khg-19-3	Gently inclined slope between the cryoplanation terraces; dry grass tundra	60-70 cm	Clayey fine sand with a few little rounded pebbles	40-50 cm	
Khg-19-7	Gently inclined slope between the cryoplanation terraces; dry grass tundra	60 cm	Silty fine sand		
Khg-20	Bank of the Vassily River, gently inclined slope; grass-moss tundra	50 cm	Loamy-silty fine sand	43 cm	20-35 cm
	Shore of the Neelov Bay near the recent Khorogor Delta, flat plain; wet grass tundra	180-200 cm	Silty sand with gravels	58 cm	25-43 cm
	Western Bykovsky Peninsula, evolving thermo-erosion valley; moss-lichen tundra		Silty fine sand		17-30 cm

The active layer close to a modern ice wedge was studied in detail and sampled in a small pit (Figure 4-13). It consisted of a 2 cm thick transition layer with lens-like cryostructure, a 20 cm thick layer of brownish weakly decomposed unfrozen peat and a 5 cm thick moss cover (Khg-8-1 to 8-3). Crossing the valley several samples were taken from a modern ice wedge (Khg-95-2), from ground water within our working pits (Khg-98-1, 2) and from surface water of the Khorogor River (Khg-96-3) and a small pond (Khg-96-4).

The surface of the valley bottom rises up to 80 m a.s.l. in the west and there the flat grass plain is delimited by Lake Figurnoe. In contrast to the circular shallow thermokarst ponds often observed this large lake has an irregular shape and seems to be much deeper. Weathered rocks of interbedding slates and fine-grained quartzitic sandstone surround the lake (Figure 4-15). Therefore it is assumed that Lake Figurnoe is of tectonic origin. The gently inclined slope towards the lake of about 200 to 300 m width is covered by weakly subrounded alluvial debris with sandstone pebbles of up to 10 cm and slate gravels of 1 to 2 cm size (Khg-10-4 and 5). Similar debris was observed within frost boils as described above. However, angular sandstone and slate debris were observed on the lake bottom near the shore. Again the lake water (Khg-96-5) and the lake bottom deposits (Khg-10-3) were sampled.

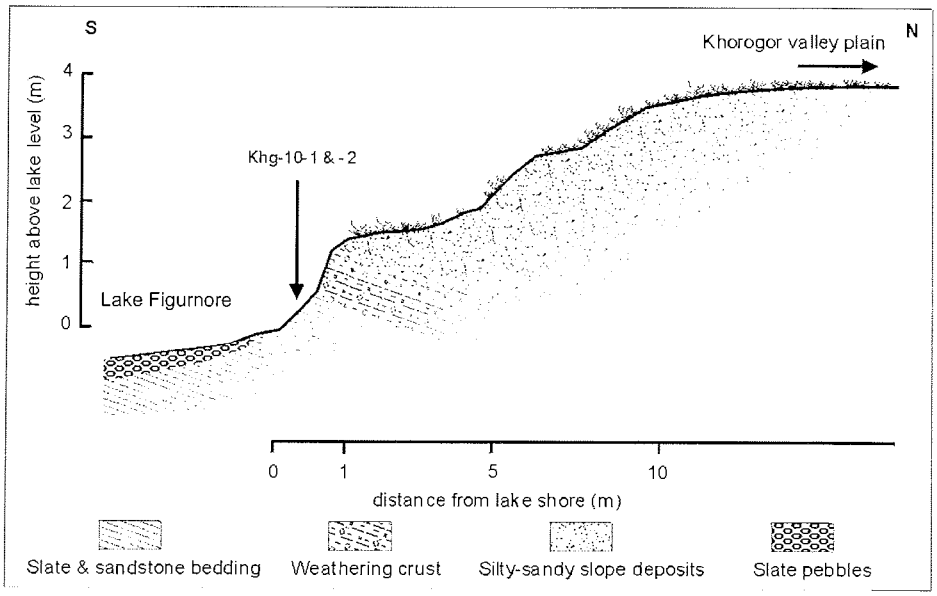

Figure 4-15: Cross profile of Lake Figurnoe northern slope

The area covered by dense grass tundra is bounded in the south by debris slopes with small inclination towards the Khorogor River (Figure 4-16A). On these slopes some larger boulders (50 – 70 cm in Ø) with weakly rounded edges and a bent and angular shaped surface structures were found (Figure 4-16B). This might be the area of a so-called boulder fan of a washed-out glacial moraine deposit (Grosswald & Spektor 1993). According to our interpretation the coarse grained debris is of fluvial or alluvial origin.

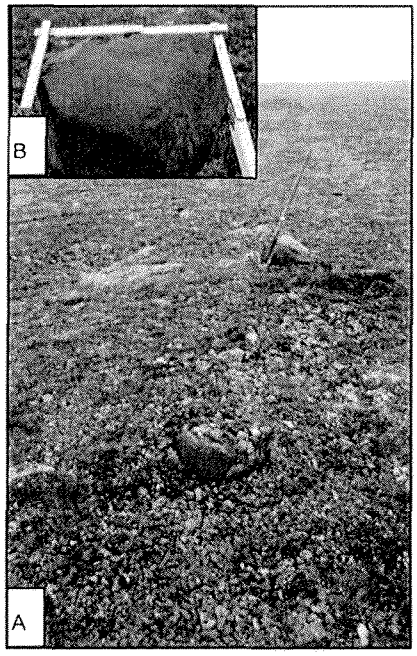

Figure 4-16: Debris slopes with large partially rounded boulders near Lake Figurnoe

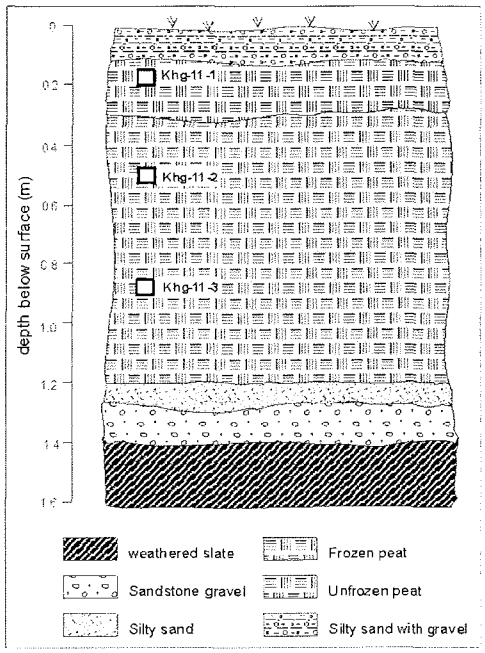

Figure 4-17: Profile Khg-11 of a thermokarst mound on the way near the Khorogor River

Thermokarst mounds were studied in the area further east of Lake Figurnoe on the way to the Khorogor River. They indicate thicker permafrost deposits and the occurrence of thermokarst processes. Our profile covers the permafrost horizon down to the weathering crust of the basement (Figure 4-17). The profile is composed of slate debris, a thin layer of pebbles, a thin layer of organic-rich, an about 1 m thick horizon of weakly decomposed moss peat (Khg-11-1 to 3) and a cover of a 0.5 m thick mixture of fine grained silty sand and gravels. This sequence reflects a development starting with fluvial processes, followed by accumulation within stagnant water of an old river branch, which was silted-up with moss peat and buried by a solifluction cover or by alluvial deposits.

4.2.3. Between the rivers Khorogor and Khatys-Yuryakh – the mouth of the Khorogor valley

The Khorogor Valley opens to the Neelov Bay in the area northwest of Tiksi airport. The valley here is bounded by the rivers Khorogor in the southeast and the Khatys-Yuryakh in the northwest and it has a width of about 7 km (Figure 4-18). The area is like a plain with a very gentle inclination towards the Neelov Bay and both rivers. In high-resolution satellite images a wide net of surface water dischargers is visible which are best explained with a delly-like development (Katasonova 1963). Many lakes occur there in the shore area of the Neelov Bay. A sharp boundary between the area of the lakes and the valley hinterland without lakes can be observed 1.5-2.0 km from the recent shoreline. Some of the lakes are supposed to be thermokarst lakes already, some are initial thermokarst lakes fed by surface runoff from the valley hinterland. Others contain coarse-grained fluvial material pointing to their origin in former fluvial beds. Meandering chains of small lakes indicate old river branches. In the north of the plain several initial flat thermo-erosional channels with depths of about one meter were observed. Their flow direction was towards the Khatys-Yuryakh River and the Neelov Bay. Anyway, the presence of thermokarst features in that region points to thicker ice-rich deposits in the ground than in the main part of the valley.

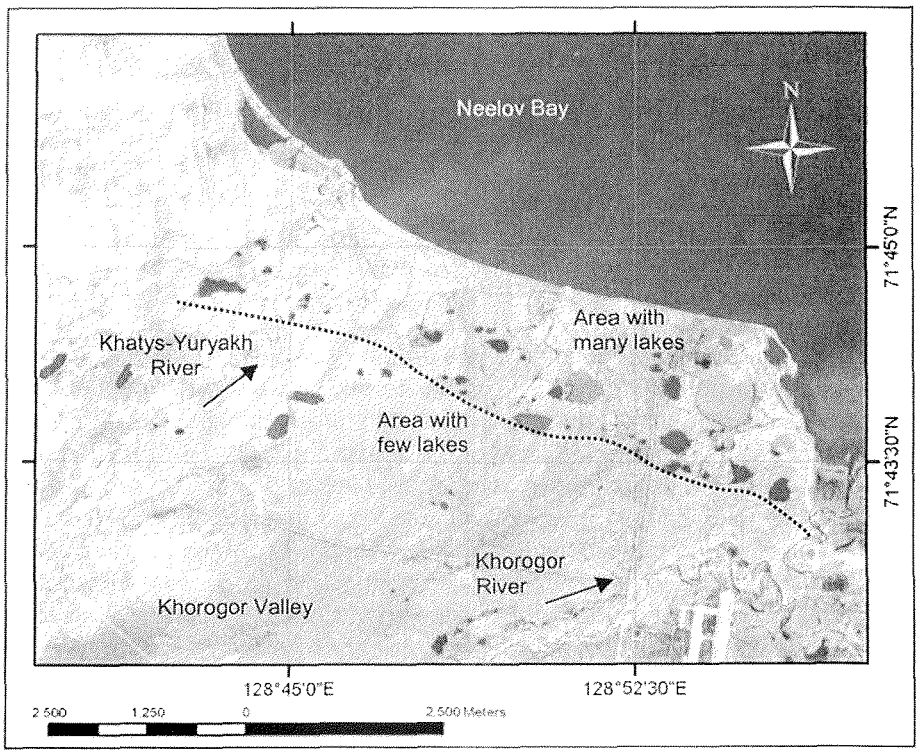

Figure 4-18: CORONA-Satellite image from July 1969 with the northeastern Khorogor Valley and the Neelov Bay shore

The central valley is dominated by typical moss-lichen (and few grass) tundra with polygonal patterns. The polygons had diameters from 8-20 m, and sometimes larger ones were split by younger frost crack generations. In several places dense moss patches with up to 25 m in diameter were found, possibly representing dried out shallow lakes. In other places standing water of 5-10 cm depth was found with grass vegetation. In places the polygons are still active as we found recent ice veins in polygonal frost cracks intruding older ice wedges. The recent ice vein had a width of only 1-3 cm while the older one had a width of about 18 cm. We sampled a recent ice vein (Khg-95-4), older ice wedges (Khg-95-3 and 5) and the surrounding sediment and soil (Khg-13-1 to 13-3) in two pits (Figure 4-19). The active layer depth in these polygons was between 15-35 cm.

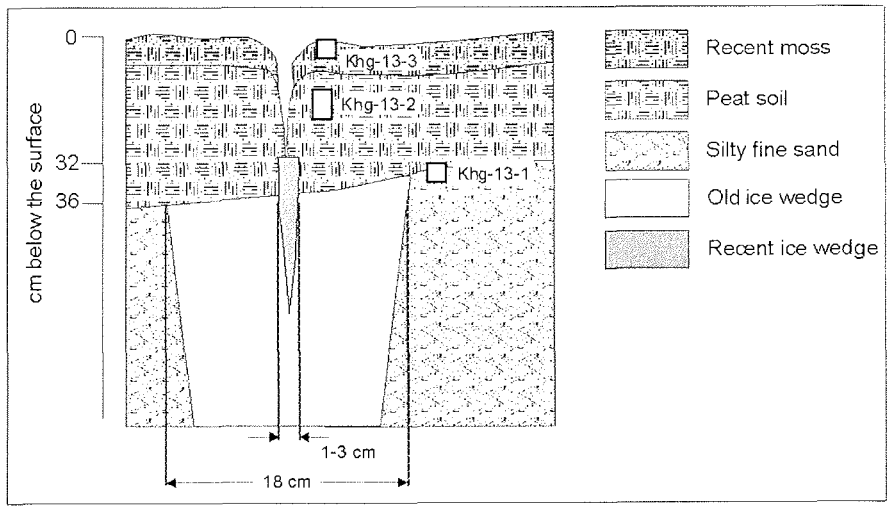

Figure 4-19: Pit Khg-13 with a recent ice vein intruding an older ice wedge

Other interesting features found in that area are frost mounds of which several were found in the central valley. Their conic shape is similar to known pingos but their size is much smaller with maximum one meter in height. The development is exemplarily interpreted for one investigated frost mound in Figure 4-20. They contain an ice lens, that is growing by subsurface water transport. Because the sediment layer on the basement is not very thick, as coarse-grained pebbles of the basement in the sediment indicate, the frost mound growth seems to be restricted to a certain height. The water comes from nearby water-filled polygonal troughs and has favourable transport conditions in the mixed grained sediment. The active layer thickness is decreased above the frost mound due to surface bulging. The thickness of the ice-lens could not be determined.

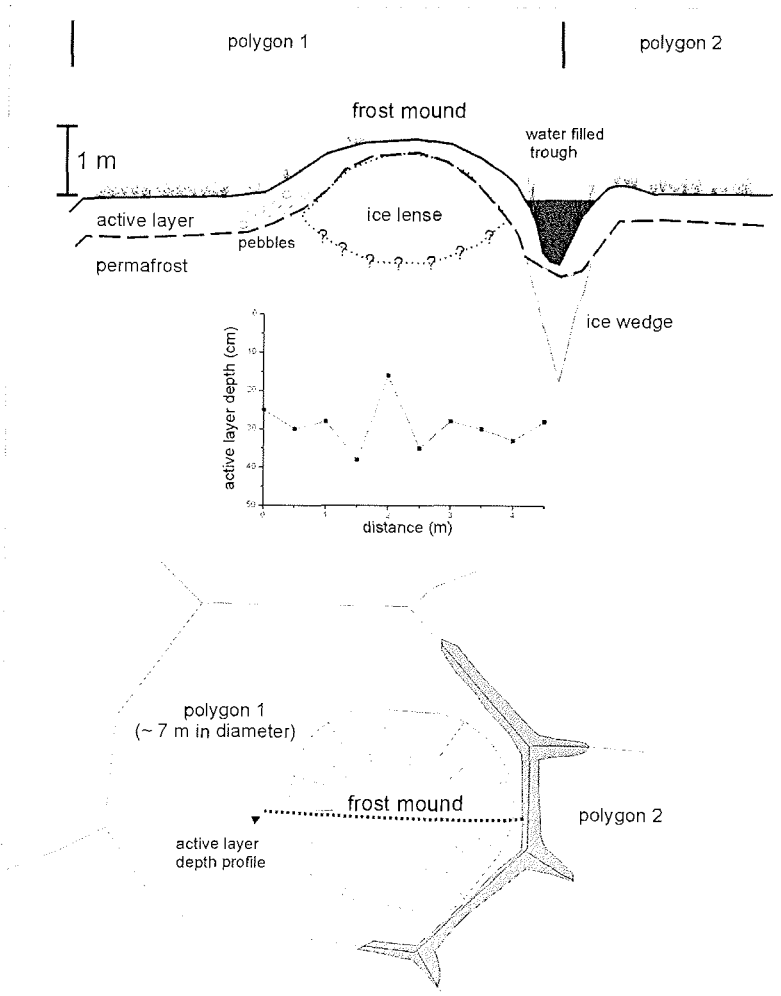

Figure 4-20: Frost mound in the central Khorogor Valley

Near the Khorogor River one of the lakes mentioned above was investigated in detail (Figure 4-21). It was more or less circular and had a diameter of about 40 m. The water and active layer depth was measured. The maximum water depth was 70 cm and the maximum active layer depth beneath the lake bottom was 45 cm. The rims of the lake were relatively steep. No talik was found below this shallow lake. This seems to be an initial stage of thermokarst. In another larger lake the coarse-grained bottom sediment was sampled (Khg-14-2). This lake might be a remnant of an old river branch.

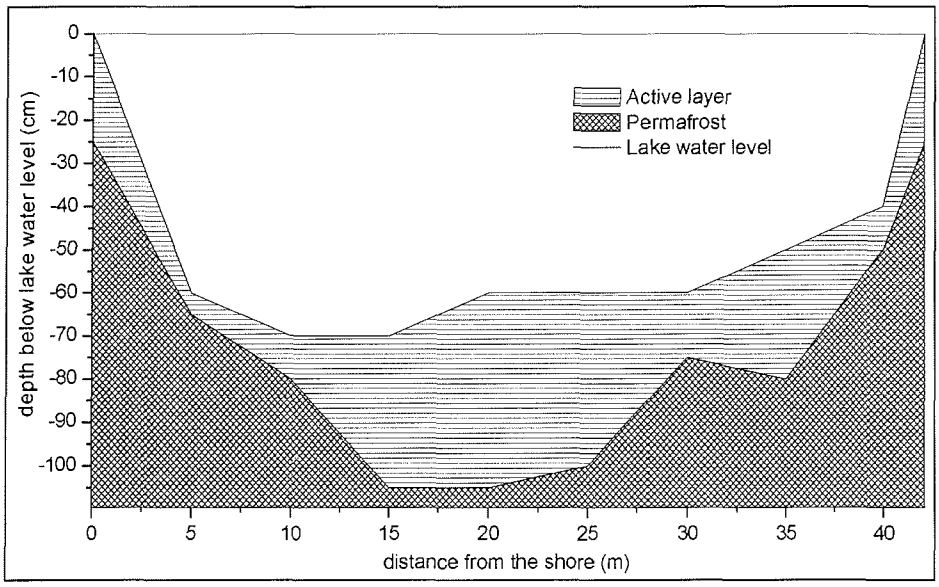

Figure 4-21: Lake profile with water depths and active layer depths (3rd August)

At the banks of the mouth of the Khorogor River several thermokarst mounds had formed, which point to ice-rich deposits, too. They were covered by a thick layer of unfrozen moss-peat and consisted mainly of frozen silty to sandy organic rich sediments. No regular ice texture was visible but ice intruded into root channels forming subvertical ice veins. One thermokarst mound was investigated in detail (Figure 4-22). The height of the riverbank in this locality was about 3 m. The riverbed itself was filled with medium- to coarse-grained sand and gravel. Several sediment samples were taken (Khg-17-1 to 12 from the thermokarst hill, Khg-16-1 and 2 from the river sediment).

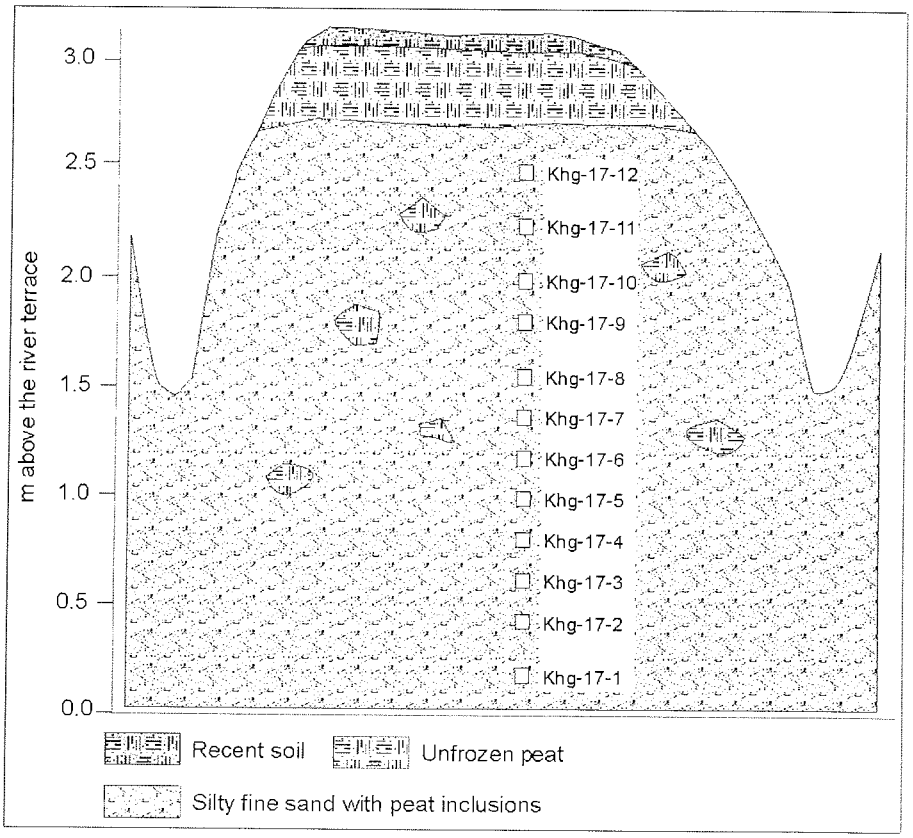

Figure 4-22: Thermokarst mound near the Khorogor river mouth with sediment sample positions

4.2.4. The old Khorogor River delta

The Khorogor River, running from the Kharaulakh Mountains towards the Bykovsky Peninsula is actually discharging into the Neelov Bay to the NE. An almost inactive old Khorogor delta has its mouth reaching to the SE into the Tiksi Bay (Figure 4-23). In this old delta only a few channels have a connection to the sea whereas many channels were separated and have become an elongated chain of lakes. Moss peat patches (Ø 15 m) occur with polygons of 0.3 m height and 1.5 m wide walls. The absolute height of the whole area is not more than 1-2 m a.s.l.. Thus, parts of the terraces are flooded through tidal or wind forced sea level high-stands, which is marked by driftwood trunks in the hinterland of the old delta. The area of the old delta is situated about 5 to 10 m deeper than the surroundings.

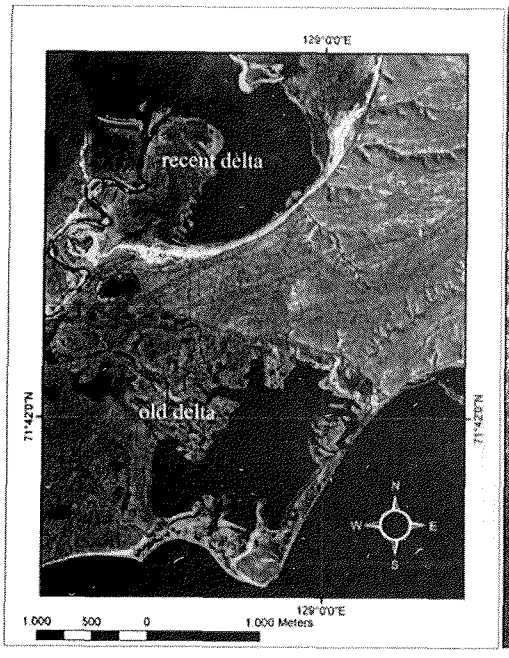

Figure 4-23: CORONA satellite map of the western Bykovsky Peninsula with the old and the recent Khorogor delta

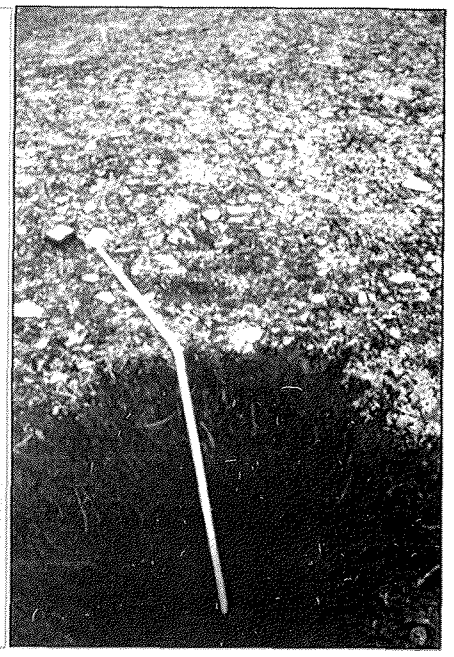

Figure 4-24: Sample pit for Khg-18-1 and Khg-18-2; note the pebble covered sediment surface

In general, the sediments have a matrix of middle-coarse grained light to dark grey sands with a high content of weakly rounded pebbles and stones. Within this river setting, which is thought to be similar to the early development stages of the basal layers of the Bykovsky Peninsula (Slagoda 1993), we observed the general sedimentological and geomorphological features. Further we investigated in detail some polygonal frost cracks of huge diameters on a gently inclined channel shore. In this place several generations of frost cracks were recognisable. We only surveyed the generation with the widest cracks, which also seemed to be the oldest, as other generations sometimes were only poorly

developed and had dead end cracks branching off with different angles from the wide cracks. The polygons have a more or less plain morphology while the crack itself is slightly lowered (5-10 cm) compared to the polygon centre. The polygonal structures are only poorly covered with vegetation, just the lowered cracks are covered more densely with grass and moss. In addition we took sediment samples (Khg-18-1 and Khg-18-2) from a pit in different depths down to 70 cm from a polygon centre (Figure 4-24). Active layer depths in the area varied from 30 to 100 cm.

For surveying we marked the junction points of the frost cracks with wooden sticks. The survey of 10 of the very irregular polygons on a very smooth slope (less than 5 degrees) close to an active delta channel proved diameters of up to 50 m (Figure 4-25). The main cracks seem to be perpendicular to the orientation of the water channel. It is assumed, that in general the cracks are relatively young because of their location in a Holocene river delta and their irregular, not well-formed shape. Further we can assume a surface, which is stable only during short timescales because of a changing delta setting and the repeated flooding with sediment accumulation or erosion events. The large size of polygons may depend on the large active layer depth of this coarse-grained and therefore well-drained material.

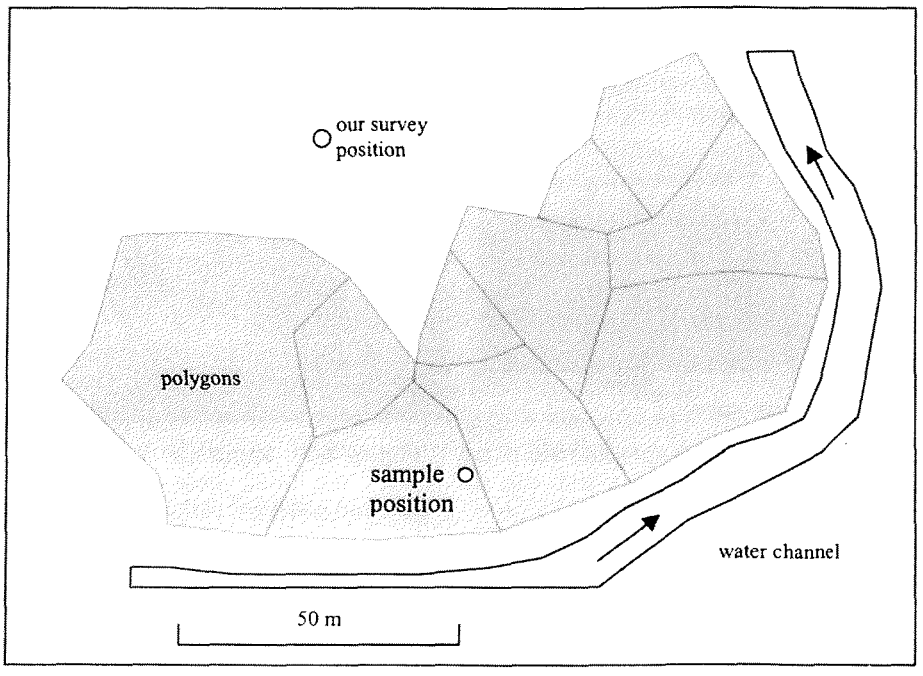

Figure 4-25: Survey of giant polygons in the old Khorogor delta

4.3. Ice Complex deposits at Neelov Bay

A cliff of about 2 to 5 m height forms the western coast of the Neelov Bay between the river mouth of Khatys Yuryakh and Khorogor. A profile of 3 m thick permafrost deposits with three ice wedge generations was studied here (Figure 4-26). The lower part of the profile down to the beach was buried by mud. A huge syngenetic ice wedge represents the first ice wedge generation. The head of this ice wedge is located about 1 m below the surface and has a width of 2.5 m. The root of the ice wedge seems to reach depths below sea level. A lot of pebbles and gravels were observed in the lateral contact zones of the ice wedge and the sediment. The ice is turbid and dirty with numerous mineral particles and air bubbles. The vertical striation is not clear. Seventeen samples of this ice wedge were taken from the left to the right with a distance of 12-15 cm (Khg-95-6). A thin vertical ice wedge with a width of 5-8 cm and a vertical size of 1.5 m represents a second generation. Its ice is clean and transparent and contains vertically oriented pebbles inside. The upper part of the ice wedge does not show any modern growth or frost cracks above and thus the ice wedge is not active. Three samples were taken from this ice wedge Khg-95-8. The third generation is represented by a thin hade ice wedge (Khg-95-6), which has intruded into the ice wedge of the first generation with an inclination of 30-40 degrees and a width of about 8 to 12 cm. Its milky-white ice intruded into the old ice wedge down to 1 m depth. It is an active ice wedge, since a modern frost crack was observed above. The sampling number of the ice wedge is Khg-95-8, and 3 samples of ice were taken.

The exposed permafrost deposits consist of a yellowish sandy loamy material with weakly subrounded pebbles (Ø 1 to 4 cm) and a lens-like cryostructure in the lowermost unburied part above beach-level. The following horizon is about 2 m thick and is composed of a mixture of gray silty fine-sand, weakly rounded pebbles and numerous smaller (Ø 1-5 cm) and larger (Ø 30 cm) peat inclusions. The upper horizon covers the large old ice wedge and consists of a frozen lower part with large peat lenses and a 0.5 m thick unfrozen part – the seasonal active layer. Altogether the conditions of this outcrop are pretty similar to the Late Pleistocene Ice Complex deposits studied in detail on the Bykovsky Peninsula further east (Mamontovy Khayata section, see chapter 4.5). Probably because of the nearby Kharaulakh Mountains the deposits are more coarse-grained at the Neelov Bay coast than at the eastern shore of Bykovsky Peninsula.

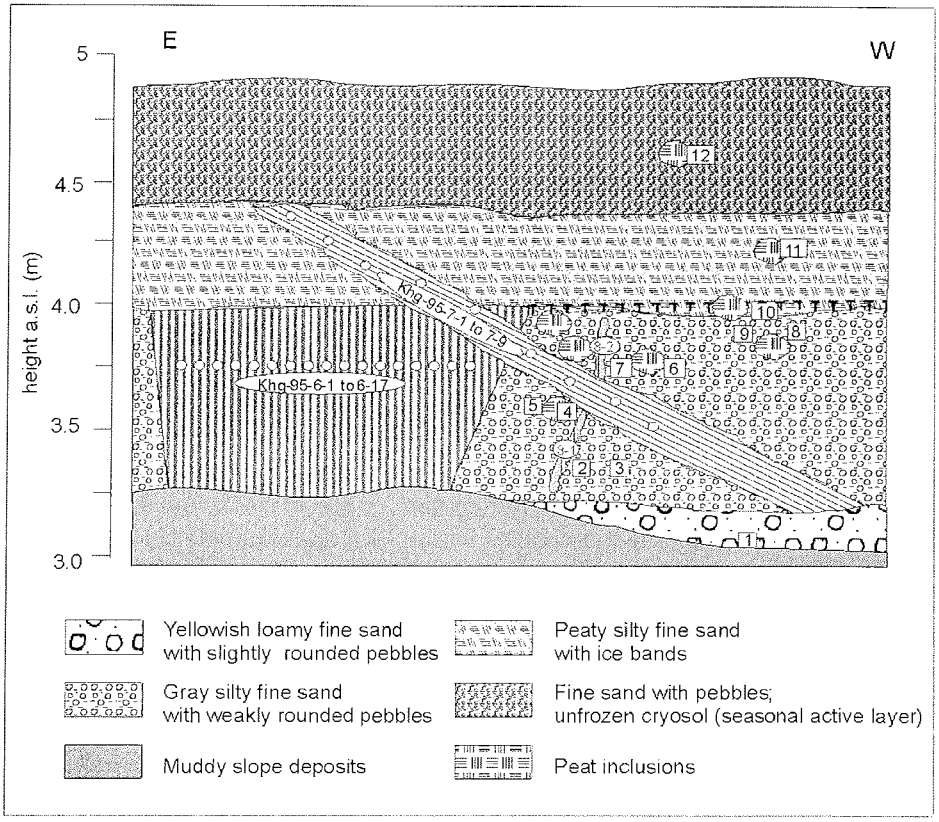

Figure 4-26: Profile Neb-1, Ice Complex outcrop at the Neelov Bay with ice wedges of various generations (Khg-95-6, Khg-95-7, Khg-95-8)

4.4. Nival processes and the periglacial / glacial (?) landscape in the region of Sevastyan Lake

The background for studying the area between Suononakh River, Sevastyan River and Sevastyan Lake were papers of Grosswald & Spektor (1993) and Grosswald (1998) describing traces of glacio-dislocations around Sevastyan Lake, drumlins and boulders scratched by glacial processes. We tried to re-investigate these very controversially discussed features. In addition, a perennial snowfield in the Sevastyan River valley and the periglacial landscape around the Sevastyan Lake were also part of our studies. The Sevastyan Lake is surrounded by a cuesta landscape (heights from 100-200 m a.s.l.) in the east, south and west. On the mountain slopes kar-like shapes with several 100 meters or some kilometres in diameter are visible, which might have been formed by perennial or seasonal snowfields or embryonic glaciers. The northern continuation of the Sevastyan Lake depression represents a large plain with several asymmetrical rocky hills of slate covered by weathered slate debris and large patches of rock debris which are almost free of vegetation (apart from a few lichens and mosses). The hard rock seems to be situated not very deep below these patches. The surface is dissected by sorted ground polygonal structures (large ones with 25 m and small ones with 3-5 m in Ø). The hills of slate ridges are common shapes in that plain. They are up to 10 to 15 m high but mostly they are much flatter (Figure 4-27). The general striking orientation is ENE-WSW like the valleys and ridges of the surrounding mountains. The permo-carboniferous basement cropping out here with slates and sandstones again is subject to subsidence within a tectonical graben structure (see Figure 4-2B).

Figure 4-27: Slate ridge in the Sevastyan plain (height ~15 m)

The orientation of the layer bedding, cleavage and shistosity of the slate ridges was measured at various sites in the region (Figure 4-28). These properties can be distinguished quite well and the way the are arranged to each othercould be a reason for the formation of the ridge-like shapes.

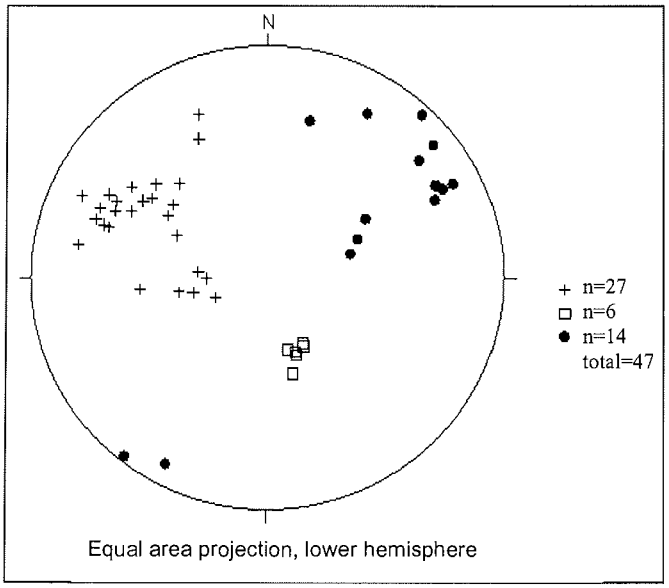

Figure 4-28: Schmidt's net of rock properties from the slate ridges in the Sevastyan area (plusses: shistosity, filled circles: cleavage, rectangles: sedimentary bedding)

The plain area north of the Sevastyan Lake is scarcely covered by vegetation (20-50 %). The surface is covered by weakly rounded debris of weathered sandstones and slates. Near the lake a zone of dense moss tundra is situated. The soil substrate mainly consists of silty sand with moderate debris content. Ice wedge polygons (Ø 15 to 20 m) and frost boils occur in that area. Chains of small ponds (Ø 10-15 m, 0.5-1 m deep) with interspaces of 20-25 m probably represent former small brooks flowing towards the lake. The lake water was sampled (Svy-96-2) as well as lake bottom sediment (Svy-2) and sediment from a frost boil (Svy-3).

A snowfield at the bank of the Sevastyan River was studied in detail. It was located at the southern inner bank of a river meander loop several 100 m before discharging into the Sevastyan plain (Figure 4-29 and 4-30). The site was well protected from direct sun insolation by steep rocks (~50 m above the river level) in the SE. More snowfields were noted in similar locations upstream. Polygons and thermokarst mounds were visible at the moderately inclined slope in the W above the snowfield reflecting relatively thick permafrost deposits. In higher positions above the moderate slopes only terraces covered by debris were formed. The snowfield had an extension of 350 m length, 10-100 m width and 2-2.5 m thickness. A mixture of plant detritus and silty sand densely covers the snow representing thaw residues of snow and wind transported material. These residues, named "chionoconite" according to Kunitsky et al. (2002) were also found in 1-2 cm thick covers on the pebble dominated valley bottom downstream and they reflect the largest extension of the snowfield.

The studied profile consists of about 0.1-0.5 m river ice in the lower part followed by 2 m well laminated firn-ice alternations with cross-bedding. Individual firn layers are up to 10 cm thick and ice layers about 1-2 cm. Densities between 0.76 and 0.84 g/cm^3 were measured from 3 different cubes of firn (Svy-1-4 to 1-6). A vertical profile in the snowfield was sampled for hydrochemical and isotope analysis (Svy-97-1 to 14). In order to study evaporation processes by stable isotope analysis about 1.5 mm snow was scraped off from one m^2 of the snow surface seven times and one reference sample in a depth of 5 cm (Svy-E1 to E-8). Additionally, Sevastyan River water (Svy-96-1) was sampled. More samples were taken from thaw residues of chionoconite (Svy-1-1, 1-2) and slope material above the snowfield (Svy 1/3).

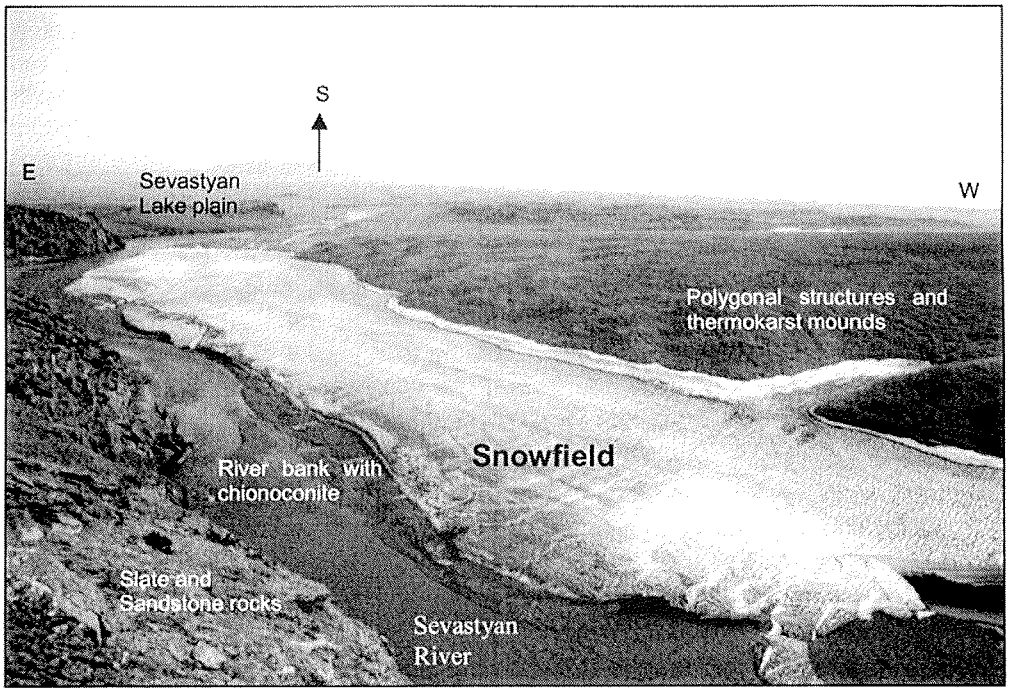

Figure 4-29: Snowfield in the Sevastyan River valley, view from N to S

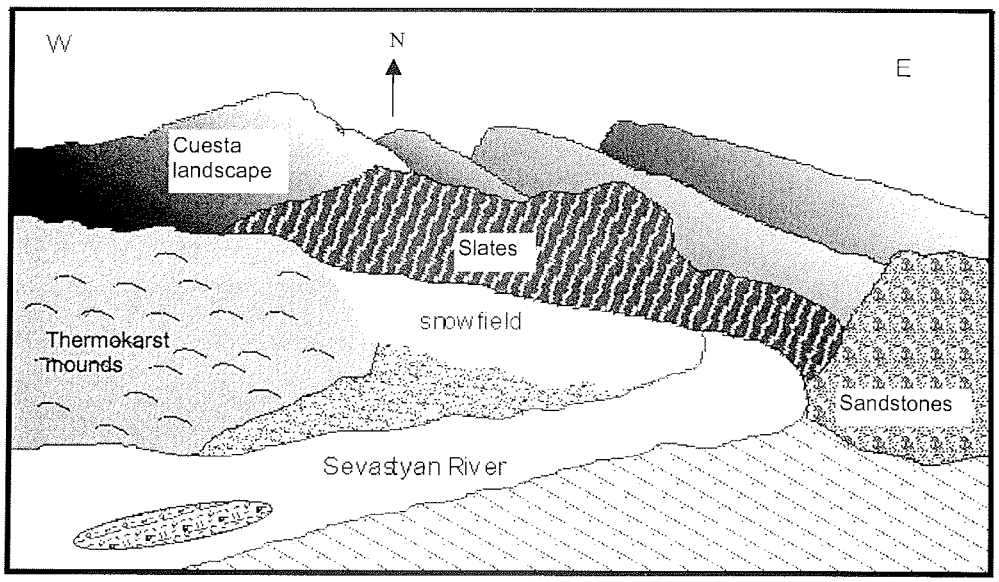

Figure 4-30: Scheme of the snowfield location and the surrounding geomorphological situation in the Sevastyan River valley, view from S to N

4.5 Periglacial processes and landscapes on Bykovsky Peninsula

4.5.1. Surface phenomenons on the southwestern Bykovsky Peninsula

In the southwest of the Bykovsky Peninsula a one day field trip was carried out to investigate the geomorphology and sedimentology of this possibly genetical link of the Khorogor Valley and the Ice Complex deposits of the peninsula. The field trip started at the most western point of the Safroneeva Lagoon at the southern shore of the peninsula. The east shore of the Safroneeva Lagoon as well as the north and south shores of the peninsula consist of cliffs of about 10-15 m height. The cliffs show formations of large thermokarst mounds, which are an indication for the former existence of large ice wedge polygons, hence ice-rich deposits. In general, the area consists of a gently rising plain towards the east from 15 to 40 m a.s.l.. Proceeding from an initial thermokarst depression in the central higher part of the region, the plain is separated by radial oriented thermo-erosional valleys (Figure 4-31).

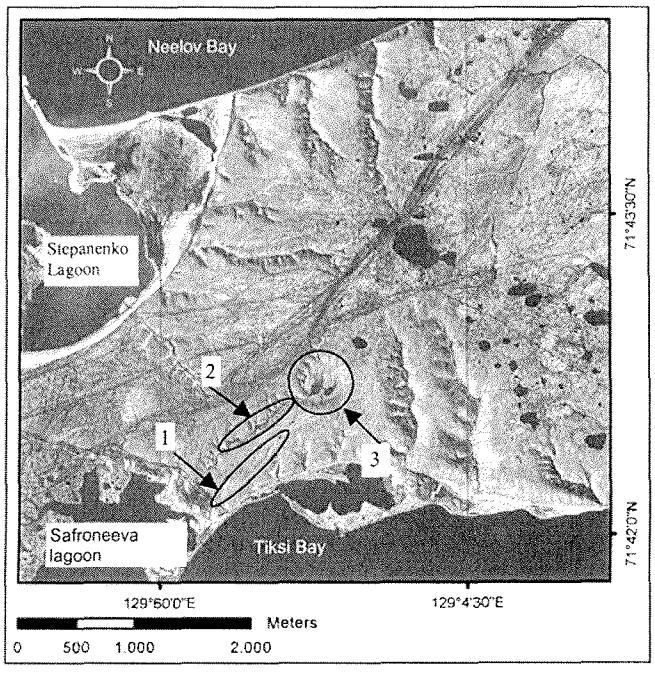

Figure 4-31: Study area on the SW Bykovsky Peninsula (CORONA image, July 1969)
1 Initial thermoerosional valley, 2 Large thermoerosional valley, 3 Small thermokarst

First an initial thermo-erosional valley was investigated. In the flat bottom of a gentle depression close to the coastal cliff a small erosional channel of about 1 m depth with running water has developed right above the ice wedge net (Figure 4-31). Large ice wedge polygons with 10-20 m in diameter were

observed there and several polygons were measured by tape. The generally wet depression was lowered by about 1 m compared to the surrounding surface and vegetated by mosses, few grasses and lichens. The running water from the channel flowed on the permafrost table (supra-permafrost water) down the slopes and represents mainly meteoric water. Sediment and ice samples were taken from an outcrop in the erosional channel (Kol-1, Kol-2-1 to 4, Kol-95-2-1 to 3)(Figure 4-32). Approximately 400 m north of this initial valley a large thermo-erosional valley was observed. The valley was lowered down 8-10 m below the surface forming a U-shaped valley with steep rims and a flat bottom. The wet bottom was densely covered by grass, in some places standing water of up to 10 cm depth was found. At the rims large thermokarst mounds had developed. The sizes and distances of some of them were measured by tape. The thermokarst mounds had diameters of about 7 m and heights of 4-6 m and they consist of silty sand with gravels (samples Kol-4-2, 4-3). The size of the former polygons was estimated with about 10-15 m in diameter.

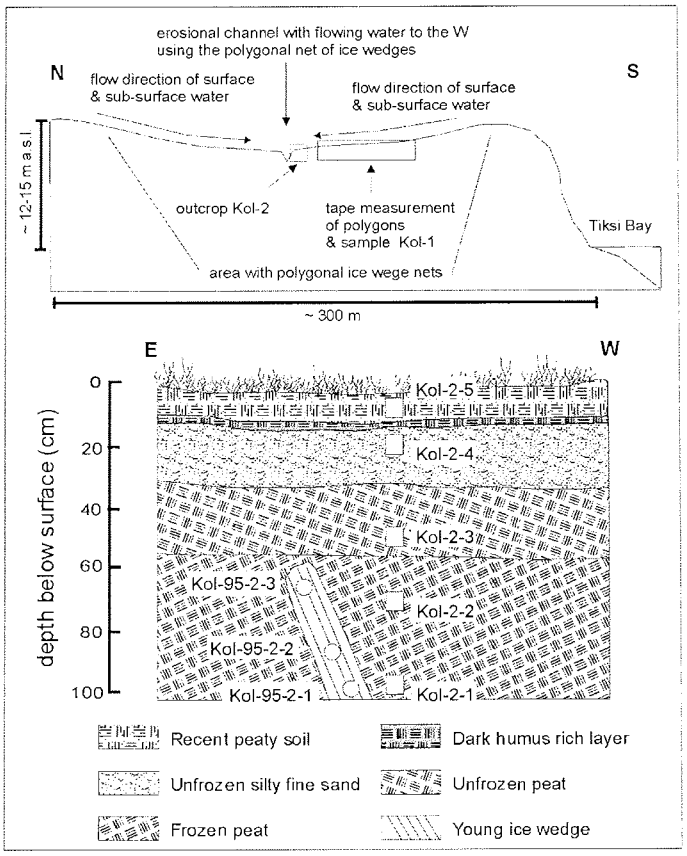

Figure 4-32: Cross-profile of the south shore of the western Bykovsky

This valley had its origin in a small circular thermokarst depression. The bottom of the depression was lowered approximately 10 m and 2 elongated lakes (110 x 55 m and 100 x 75 m) had developed therein (Figure 4-33). In the north a flat valley is discharging into the depression forming a gentle wet slope of silty fine sand covered with grass. On this slope flat terraces form steps of 10-30 cm, which may represent individual sedimentation and accumulation events produced by running water during the snow melt. Around the lakes very wet moss-grass tundra with rectangular, water-filled low-centre polygons was found. Compared to the western part the eastern part of the depression is raised several decimetres. The step is marked by silty sand rich in sandstone pebbles, which only occur in the eastern part (sample Kol 4-1). Several erosion channels separate the rim of the depression and thermokarst mounds have formed in the upper parts.

Outgoing from our landing point towards the small thermokarst depression we also examined several frost boils. In most of them we found more or small less rounded gravels (1 cm in ∅, sample Kol-3)). This indicates that layers with coarser grained material can be found right below the fine-grained, silty-sandy surface deposits.

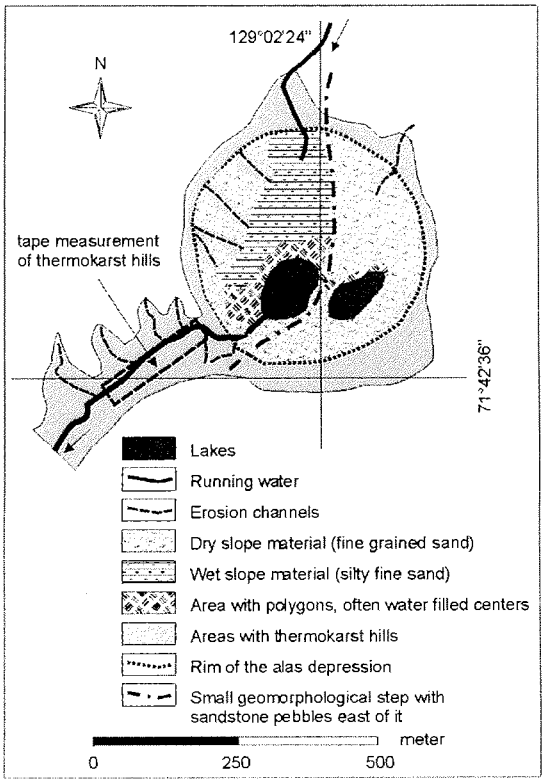

Figure 4-33: Scheme of the investigated thermokarst depression on the western Bykovsky Peninsula

4.5.2. Mamontovy Khayata section and the Mamontovy Bulgunyakh pingo

A most detailed profile of ice wedges was sampled for stable isotope analyses at Mamontovy Khayata outcrop on Bykovsky Peninsula (Figure 4-34). Sampling at this site started in 1998 (Meyer et al. 1999, ROPR 315), when an overview stable isotope record was gained between sea level and the top of the outcrop (Meyer, 2001, Meyer et al. 2002). In 2001, a group of Russian scientists refined the ice wedge sampling in the upper part of the outcrop at Mamontovy Khayata section (Sher et al. 2002). The main aim was to complete the stable isotope profile of ice wedges especially in that part of the section, which is assumed to be as old as or postdating the Late Glacial Maximum (LGM). It could not be sampled before for reasons of difficult outcrop conditions. Two horizontal ice wedge transects could be sampled in respective heights of 32 m and 29.5 m. Both heights correspond to a period predating the LGM, according to the age-height relationship published in Meyer et al. (2002) and Schirrmeister et al. (2001). Therefore, on September 4th 2002, a new attempt was undertaken to sample the LGM part of the profile in order to answer the question whether the winter temperatures were colder or warmer during the LGM than in the Kargin interstadial.

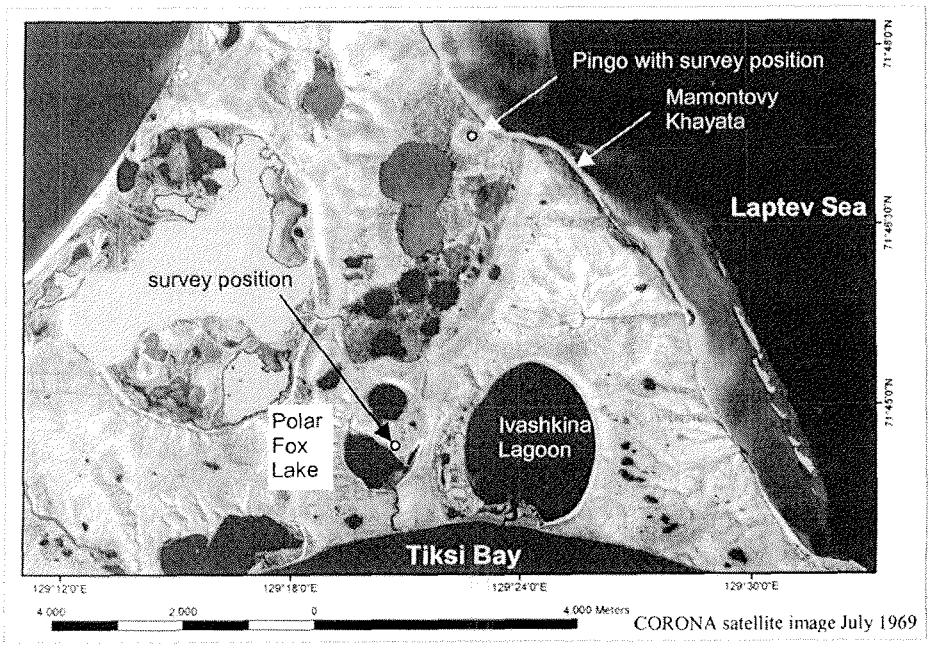

Figure 4-34: CORONA Satellite image of the SE region of the Bykovsky Peninsula

In 2002, the outcrop conditions allowed the sampling of the uppermost section assumed to be of LGM age. Ice wedge sampling was carried out (as described in more detail in chapter 3.9) for one horizontal sampling transect in a depth of 4.85 m below the surface and a depth of 4.5 m below the permafrost table (Figure 4-35). This means a height of about 34.5 m above sea level for the sampled profile, corresponding to about 14 ka BP ^{14}C age.

The selected ice wedge MKh-02 is characterised by clear, transparent and sometimes yellowish ice, with well-developed vertical structures such as 1 - 5 mm wide elementary ice veins and elongated gas bubbles (up to 8 mm long), especially on the left part of the wedge. Elementary ice veins might cross each other. The vertical structures are less well developed on the right part of the ice wedge, which also contains a relatively high amount of organic matter (e.g. lemming coprolites and plant fragments). In general, the content of mineral particles is low in the ice wedge, although some mineral veins of about 1 mm in width occur. A peculiarity was the finding of a fluid inclusion of ca. 6 mm in diameter in the ice.

The sediment column is covered by an active layer about 35 cm thick, and it is subdivided into two main units: in the upper 2 m of the profile (between 36.8 m and 38.8 m a.s.l.), the sediment surrounding the ice wedge is composed of ice-rich silty sand of greyish colour and a fine (above) to coarse (below) lens-like reticulate cryostructure interrupted by ice belts (Appendix 4-1). A horizon of peaty soil pockets of up to 40 cm separates the subunits of different cryostructure, and is inserted into the lower subunit.

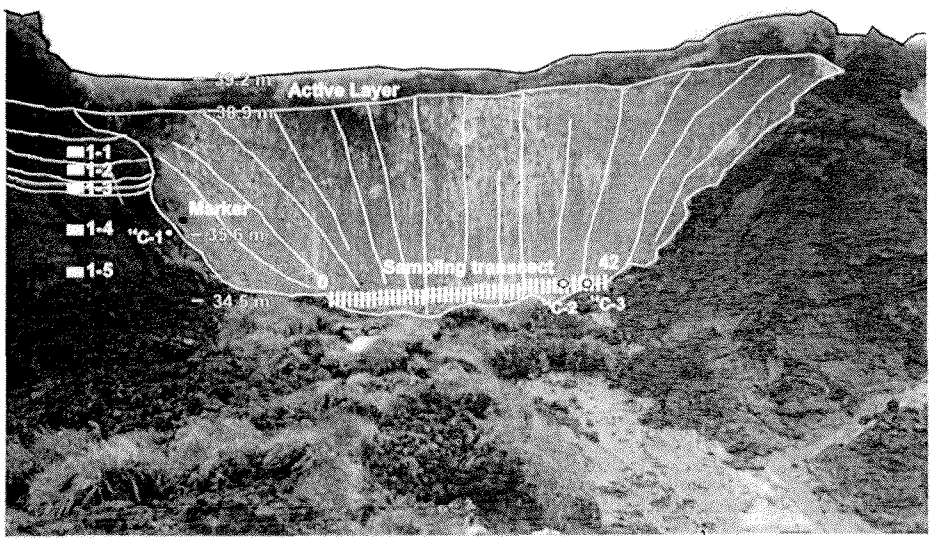

Figure 4-35: Ice wedge and sediment sequences below the top of Mamontovy Khayata section, Bykovsky Peninsula, profile Mkh-02 .

Below 36.8 m, the sediment consists of greenish-grey "loess-like" silty sand with massive cryostructure, cut by a few thin ice belts with a much lower ice content compared to the upper unit. From above, organic-rich cryoturbation pockets penetrate into this lower unit.

A small bone was found *in situ* at a height of 35.6 m in the sediment 5 cm beneath the left rim of the ice wedge, which may be used for an age estimate of the sediment. Two additional samples of datable organic matter could be found in the ice wedge at 3.55 m and 4.05 m of the left edge of the transect. Ice wedge samples were taken in 10 cm intervals by means of a chain saw with an approximate width of each ice sample varying between 1.5 and 2 cm. A total number of 43 samples were retrieved from the 4.35 m long horizontal sampling transect. The samples were sealed in plastic pockets and transported in frozen state to the AWI, where they will be measured for stable oxygen and hydrogen isotopic composition, using a Finnigan MAT Delta-*S* mass spectrometer.

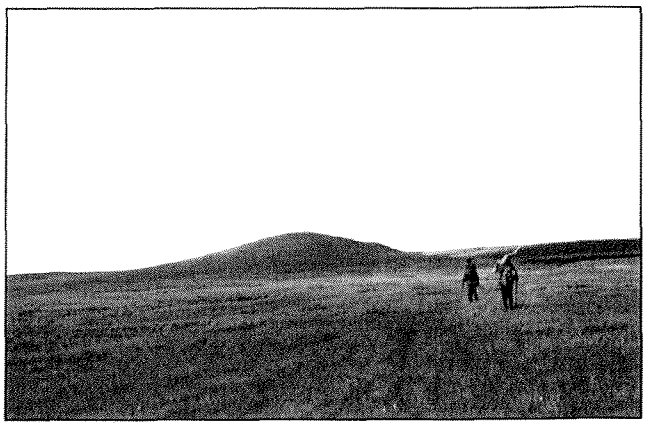

Figure 4-36: The pingo Mamontovy Bulgunnyakh within the thermokarst depression Mamontovy Bysagasa.

Pingos are very common in the NE Siberian lowlands as well as in Alaska, Canada, Sweden and Spitsbergen. In NE Siberia these structures are connected with thermokarst depressions and certain sedimentary and hydrological conditions. On the Bykovsky peninsula 4 pingos are known, of which Mamontovy Bulgunyakh is the second biggest with about 25 m a.s.l. and coverage of about 90.000 m^2. This pingo is situated within the thermokarst depression of Mamontovy Bysagasa close to the western shoreline of the peninsula and the Mamontovy Khayata outcrop in the SE (Figure 4-34 and Figure 4-36). It was subject to a drilling campaign in 1998 by the German-Russian expedition "Lena-Delta 1998" (Siegert et al., 1999).

The core drilling was stopped at a depth of about 6.5 m from top of the pingo when reaching the massive ice lens. The sediments consist mainly of silty sand with a low gravimetric ice content of 25-50 wt-% and an alternating cryostructure of horizontal, subvertical and diagonal lenses, massive structures and broken horizontal ice veins.

The pingo surface is covered by dry hummocky grass vegetation and is disturbed by solifluction. Several sediment fans occur at the pingo base and at a step at the eastern slope. This is caused by a nival niche, which obviously appears as a snowfield on some satellite pictures. The pingo outline was determined by the boundary to the wet tundra plain, which is characterized by brownish moss and peat vegetation as well as polygonal patterns.

The pingo is visible on high-resolution CORONA satellite images but its extent could not be determined, as there is no exact boundary to the surrounding areas. During this expedition the pingo was surveyed in detail by laser tachymetry. The survey was made from 2 survey positions on top of the pingo by measuring points along downslope transects. Altogether 27 transects with 213 data points were measured (Figure 4-37). Along 12 transects distributed over the pingo surface additionally 89 active layer depths were measured (Fig 4-38).

The absolute height of the pingo was determined with 25.57 ± 0.25 m a.s.l. according to the present sea level that day. This measurement has still to be corrected by water-depth gauge values obtained from the Tiksi Hydrometeorological Station.

Figure 4-37: Isoheights of the pingo Mamontovy Bulgunnyakh.

Figure 4-38: Active layer depths of the pingo Mamontovy Bulgunnyakh.

4.5.3. The Polar Fox Lake

The Polar Fox Lake is situated within a thermokarst depression at the south coast of the Bykovsky Peninsula (Figure 4-34). Some hundred meters to the east the large Ivashkina Lagoon is located in another thermokarst depression. The Polar Fox depression contains two large water bodies (> 200.000 m^2) and two small ones (< 30.000 m^2). The southern water body, which is the Polar Fox Lake in *sensu strictu*, is connected with the Tiksi Bay by an up to 8 m wide channel, which is a former thermo-erosional or dry valley (Figure 4-39). Therefore, the "lake" is actually a lagoon in a kind of a "pre-Ivashkina phase". On remote sensing images of different years (1951-1999) we could observe a change in the water level and the shoreline of the lake. On the shore some terraces with tree-trunks were deposited, originally transported into the depression by seawater or sea ice (Figure 4-40). The wood is partially strongly weathered and looks very old and sometimes it is deeply buried under peat and slope sediments. Thus we assume, that the sea influence has been active in the lagoon for at least several hundred years. Samples were taken from lake deposits (Ope 4 & 6), from surface material (Ope 5) as well as from lake water (Ope 1 to 3).

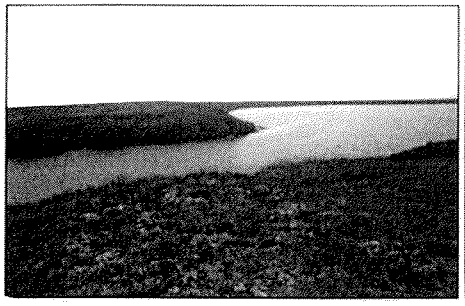

Figure 4-39: Mouth of the about 8 m wide channel from the Tiksi Bay into Polar Fox lake

Figure 4-40: Terraces of old tree-trunks at the eastern shore of Polar Fox Lake, sometimes already covered by slope deposits

The geodetic survey of the southern part of the depression was done from a single position on a flat central land bridge dividing the two large water bodies. We surveyed the shore of the Polar Fox lagoon and the upper rim of the depression. The shore survey represents the water level situation of that day. We have to verify these results by data of water-depth gauges for the Tiksi bay collected by the Tiksi Hydrometeorological Station. Even during our survey campaign the water level oscillated several dm forced by tidal and wind effects in the Tiksi bay. We registered changes in the water level of up to 60 cm relative to our survey position.

To illustrate the amount of sea level changes in that region and hence the influence on lake level changes, Figure 4-41 shows water level data from the gauge in Tiksi during July/August in 2000.

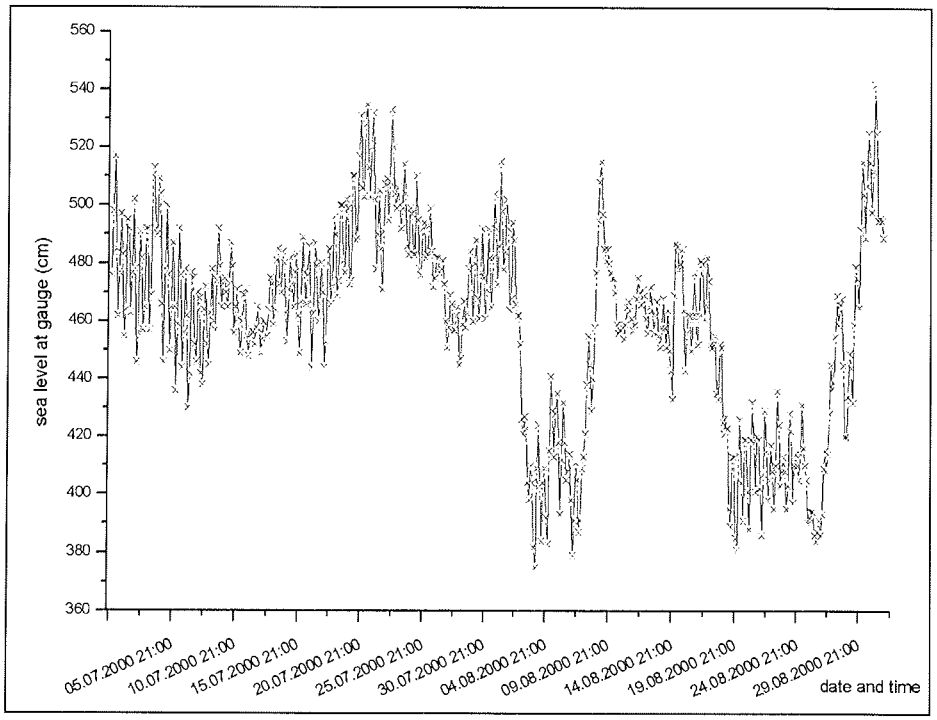

Figure 4-41: Data from the sea level gauge of the Hydrometeorological Station in Tiksi from July and August in 2000 (with friendly permission of A. Gukov).

As the graph shows, sea level changes during one day are moderate with 40-50 cm while sometimes changes of up to 150 cm within 24 hours are also possible. The sea level gauge of Tiksi is about 19 km far away from the investigation site.

The absolute height a.s.l. could not be determined in the field, because no trigonometric points were visible from the survey position within the depression, but after we had applied the tidal data to our measurements, we could interpolate a height above the sea level. Altogether we measured 120 points.

4.6. The snowfield at the "Stolovaya Gora" – a potential nival monitoring area

Nival processes connected with snowfields shape the modern as well as the past Arctic landscape at larger scales. Therefore, to understand the landscape development here, detailed monitoring and measurement of various parameters influencing nival processes or resulting from them are necessary. One task of our studies was the selection of a future nival monitoring area near Tiksi, which has to be easily reached and observed. Such a site was obviously found at the southeast slope of the southern flank of Stolovaya Gora hill below the Diring-Kyuel Lake near Tiksi. The Stolovaya Gora hill ("Table Mountain") is characterized by a large nival kar at its eastern slope, which is well visible from Tiksi. Perennial snowfields occur in some hundred meter long narrow ravines down-cutting the slope as well as on nival steps and kars parallel to the contour lines at ca. 200 m a.s.l. (Figure 4-42).

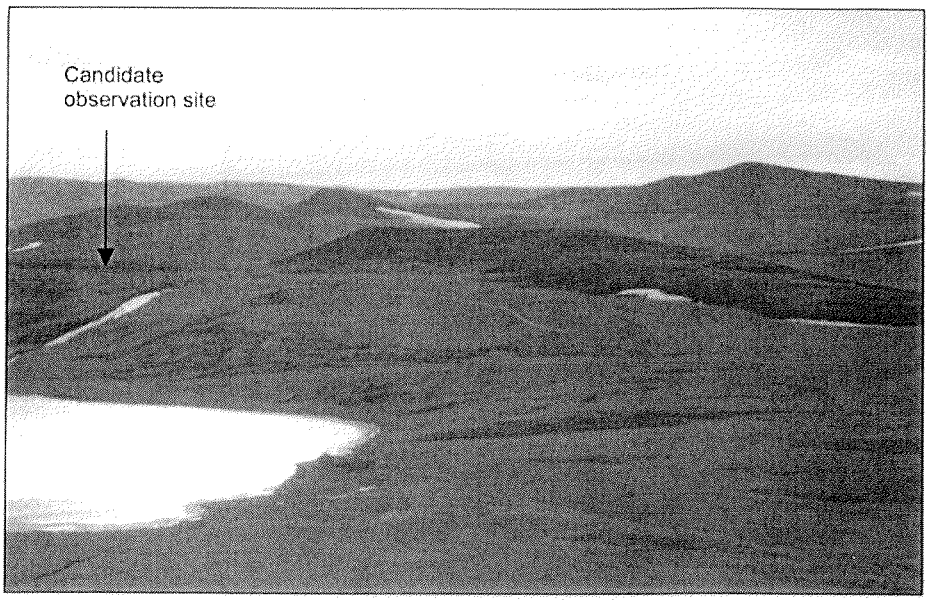

Figure 4-42: Snow fields at the south-eastern slope of the Stolovaya Gora hill south-flank above the Diring-Kyuel Lake (photo from summer 1998)

Below the top of the slope a steep and long edge of about 3 m in height was found consisting of dry rock-debris covered by lichens (Figure 4-43). Below this edge a gently inclined slope area spreads with one-meter broad streaks of rock debris with vegetation alternating each other (striped sorted ground). These stripes disperse into several frost boils and puddles (water sample Svy-96-11) in a wet nival meadow by a very small slope inclination. Below this terrace the slope is subdivided into three sections. The upper slope shows a grass surface torn up by solifluction, whereas at the lower slope the grass cover is compressed to solifluction terraces of about one meter height. Ice wedge polygons were formed at the lowermost flat part of the slope.

This year a snowfield was preserved within an up to 7 meters deep and ca. 400 m long erosional trench. Most likely this trench was filled with snow up to the top during winter. Actually the snow thickness on August 9th was less than one meter and only an area of about 150 x 5-10 m was covered by snow.

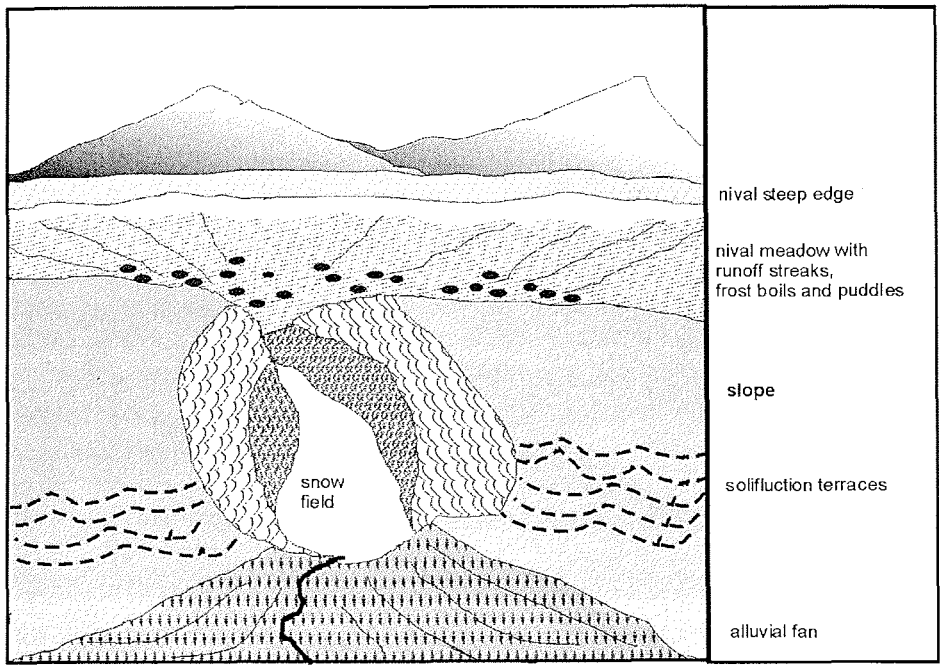

Figure 4-43: Schematic view on the candidate monitoring site for the snow field at the Stolovaya Gora hill.

The snow was sampled in a vertical profile with interspaces of 10 cm (Svy-97-15 to 23 (Figure 4-44). Chionoconite (mixture of organic and fine-grained sediment material) covers the snow (samples Stg-1-1, 1-3) as well as the surrounding rock debris and the trench slopes up to heights of 5 m. The stones at the bottom are obviously slightly rounded by running water (sample Stg-1-4). Individual boulders have diameters up to one meter. Linear surface patterns on

such boulders are stratification structures of sandstones cleared out by weathering. There were no traces of glacier movement at all. The slope material exposed at the steep wall of the trench contains slate debris and fine-grained material (sample Stg-1-2). The nival trench ends up with an alluvial cone and a small melt-water runoff brook (sample Svy-96-13) into lake Diring-Kyuel (sample Svy-96-14).

The idea for future studies of nival processes is the installation of measurement equipment within the central part of the snowfield for measuring snow thickness, temperatures in various depths, as well as above and below the snow cover, and other meteorological data (direction and force of wind, insolation, precipitation). Additional measurement equipment could be installed in the surrounding area in order to record more data like soil temperature and moisture. A regular monitoring of melt-water runoff rates and sediment discharge and the changes in snowfield extension and the slope morphology should be made as well as a regular sampling of snow, meltwater and sediments. For such investigations a detailed digital topographic model is necessary. If we manage to establish such a nival monitoring field it would enable us to determine more exactly the dependency of nival landscape morphology from climate parameters as well as balancing various influencing factors like snow volume, melt-water rates and sediment transport.

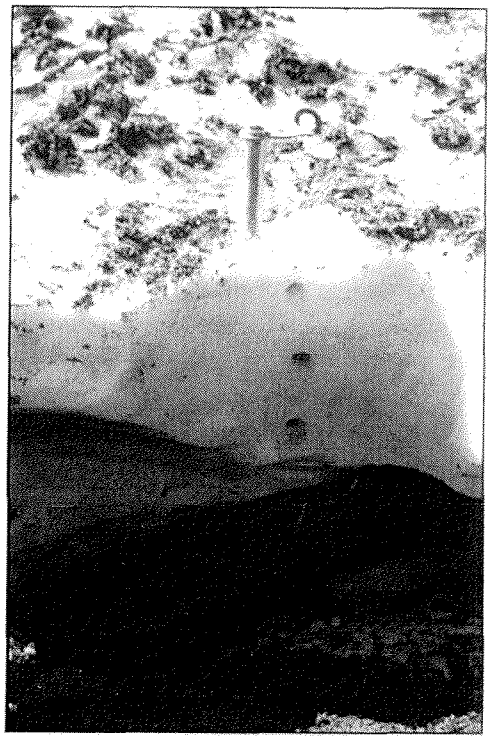

Figure 4-44: Photo of snowfield cross-section and the uppermost sample points

4.7 Appendices

Appendix 4-1. List of sediment samples collected around Tiksi.

	Sample description			Position						
No.	**Sample**	**Sedimentology**	**Cryolithology, ice content abs./grav. [wt %]**	**N 71°**	**E 128°**	**H NN (m)**	**Depth (m)**	**Remarks**	**Date**	**Ice/water samples**
1	Khg-1	Silty fine sand, single stones (weakly subrounded 2-7 cm)	Active layer	38.35	36.18		0	Frost boil Ø 0.6 m, station of transportable surface probe (TSP)	01.08.	
2	Khg-2	Sandstone		38.10	35.37		0			
3	Khg-3	Slate					0	Rocky ridge	01.08.	
4	Khg-4-1	Dolerit				ca. 190	0			
5	Khg-4-2	Dolerit				ca. 190	0			
6	Khg-5-1	Silty fine sand, single stones (2-7 cm)	Active layer (centre: 0.45 m, edge: 0.3-0.4 m)	39.9	33.00		0	Frost boil Ø 35 cm, v	01.08.	
7	Khg-5-2	Dark coarse-grained river sand		39.19	33.45			Khorogor River	01.08.	KHG-96-1
8	Khg-6	Silty fine sand	Active layer (centre: 0.52 m, edge: 0.35 m)	38.80	33.97		0	Frost boil Ø 70 cm, station of TSP	01.08.	
9	Khg-7	Brownish-gray, organic-rich, fine sand	Active layer (0.4 m)	38.39	35.27		15	Ice wedge (0.10-0.15 m) polygon (Ø 15 m) with recent frost fissures and frost boils (Ø 0.6-0.9 m)	01.08.	KHG-95-1
10	Khg-8-1	Silty sand	Transition layer, lens like structures	42.12	42.44		25	Emergency airstrip of an old airport	02.08.	KHG-96-3
11	Khg-8-2	Peat, brownish, weakly decomposed					0.15-0.20	Station of TSP		KHG-98-2
12	Khg-8-3	Moss				50	0-0.05	Large moss pad (40 x 17 m with polygons Ø 9 m)		KHG-96-4

Appendix 4-1. continuation.

Sample description				Position						
No.	**Sample**	**Sedimentology**	**Cryolithology, ice content abs./grav. [wt %]**	**N 71°**	**E 128°**	**H NN (m)**	**Depth (m)**	**Remarks**	**Date**	**Ice/water samples**
13	Khg-9-1	Silty sand	Active layer (0.55 m)	42.13	42.11		0	Moss pad (15 x 30 m) with frost boil (Ø 1.5 cm)	02.08.	
14	Khg-9-2	Gravel, weakly subrounded					0	Frost boil		
15	Khg-10-1	Slate		40.92	36.87	68.5	0		02.08.	
16	Khg-10-2	Fine-grained quartzitic sandstone		40.92	36.87		0			
17	Khg-10-3	Lake deposit		40.92	36.87			Figurnoe Lake, 0.5 m water depth, 3 m from the bank		KHG-96-5
18	Khg-10-4	Gravel, slates and sandstones, subrounded		40.92	37.47		0	Alluvial deposits		
19	Khg-10-5	Soil and gravels		40.92	37.47	75	0	Alluvial deposits		
20	Khg-10-6	Fine-grained quarzitic sandstone		40.97	37.74		0	Gravel plain		
21	Khg-11-1	Peat	Unfrozen, active layer 0.37-0.40 m	41.79	45.96		0.10-0.15	Station of TSP	02.08.	
22	Khg-11-2	Peat	Frozen				0.50-0.60	Thermokarst mound		
23	Khg-11-3	Peat	Frozen				0.75-0.85	(baydzherakh)		
24	Khg-12-1	Fluvial gravel		41.80	47.57			Khorogor River	02.08.	KHG-95-2
25	Khg-12-2	River sand								
26	Khg-13-1	Silty sand	Coarse lens-like structures, lower-most part of the seasonal active layer	44.01	43.17		0.27-0.33	Pit on the surface of an ice wedge polygon	03.08.	KHG-95-3
27	Khg-13-2	Moss peat					0.12-0.19			KHG-95-4
28	Khg-13-3	Moos					0-0.03			KHG-95-5

Appendix 4-1. continuation.

	Sample description			Position						
No.	**Sample**	**Sedimentology**	**Cryolithology, ice content abs./grav. [wt %]**	**N 71°**	**E 128°**	**H NN (m)**	**Depth (m)**	**Remarks**	**Date**	**Ice/water samples**
29	Khg-14-1	Water moss (Drepanocladus)		44.08	45.14	18.5		Flat (0.2-0.5 m depth) lake	03.08.	
30	Khg-14-2	Lake deposit					0.5	10 m from the bank		KHG-96-6
31	Khg-15-1	Silty fine sand, single stones	Active layer (centre: 0.50 m, edge: 0.25 m)	44.51	45.16		0	Frost boil (Ø 0.60 m)	03.08.	
32	Khg-15-2	Gravels, partly subrounded					0	Fluvial alluvium		
33	Khg-16-1	River sand		44.897	45.534			Khatis-Yuryakh River	03.08.	KHG-96-7
34	Khg-16-2	Fluvial gravel								
35	Khg-17-1	Silty fine sand		45.042	45.782		2.80	Thermokarst mound	03.08.	
36	Khg-17-2	with peat	small ice lines				2.60	(baydzherakh)		
37	Khg-17-3	inclusions					2.40			
38	Khg-17-4						2.20			
39	Khg-17-5						2.00			
40	Khg-17-6						1.80			
41	Khg-17-7						1.60			
42	Khg-17-8						1.40			
43	Khg-17-9						1.20			
44	Khg-17-10						1.00			
45	Khg-17-11						0.80			
46	Khg-17-12						0.60	Station of TSP on the surface		

Appendix 4-1. continuation.

Sample description				Position						
No.	**Sample**	**Sedimentology**	**Cryolithology, ice content abs./grav. [wt %]**	**N 71°**	**E 128°**	**H NN (m)**	**Depth (m)**	**Remarks**	**Date**	**Ice/water samples**
47	Svy-1-1	Plant remains, silty sand		33.917	44.848		0	Chionoconit, fresh from the snow field surface	04.08.	river water Svy-96-1
48	Svy-1-2	Plant remains, silty sand					0	Chionoconit layer, dry, 1 cm thick		surface SVY-97-E1 to 97-E-8
49	Svy-1-3	Silty fine sand						Below the snow field		
50	Svy-1-4		Ice cube				0.60-0.70	Above the Sevastyan river		SVY-97-1 to 97-14
51	Svy-1-5		Ice cube				0.80-1.00			
52	Svy-1-6		Ice cube				1.40-1.50			
53	Svy-2	Lake deposit		32.497	49.275		1 m water depth	Sevastyan lake	04.08.	SVY-96-2
54	Svy-3	Silty fine sand, grus					0	Frost boil	04.08.	
55	Neb-1-1	Loamy fine sand, gravels	Ice rich (46.9 / 88.3 %)	44.789	50.855	2.10	2.90	Coastal section at the Neelov Bay	05.08.	KHG-95-6
56	Neb-1-2	Dark brown peat, weakly decomposed	Frozen			2.60	2.40	Peat inclusion (Ø 0.05 m), for dating		to KHG-95-8
57	Neb-1-3	Greyish silty fine sand, gravels	Ice rich (47.4 / 90.0 %)			2.60	2.40			
58	Neb-1-4	Brown peat, weakly decomposed	Ice rich			3.20	1.80	Peat inclusion (Ø 0.30 m), for dating		
59	Neb-1-5	Greyish silty fine sand, gravels	Very ice rich (64.9 / 182.2 %)			3.20	1.80			
60	Neb-1-6	Brown peat, weakly decomposed	Very ice rich			3.45-3.55	1.45-1.55	Peat inclusion (Ø 0.20 - 0.30 m), for dating		
61	Neb-1-7	Greyish silty fine sand, gravels	Very ice rich (55.5 / 124.6 %)			3.35-3.45	1.55-1.65			

Appendix 4-1, continuation.

	Sample description			Position						
No.	**Sample**	**Sedimentology**	**Cryolithology, ice content abs./grav. [wt %]**	**N 71°**	**E 128°**	**H NN (m)**	**Depth (m)**	**Remarks**	**Date**	**Ice/water samples**
62	Neb-1-8	Brown peat, weakly decomposed	Very ice rich			4.00-4.10	0.90-0.100	Peat inclusion (Ø 0.05m), for dating		
63	Neb-1-9	Greyish silty fine sand, gravels	Very ice rich (60.1 / 150.9 %)			3.90-4.00	1.00-1.10			
64	Neb-1-10	Peaty silty fine sand, gravels	Very ice rich (70.1 / 234.0 %)			4.20	0.80	Thermokarst mound		
65	Neb-1-11	Peat, brown, fresh	Unfrozen			4.50	0.50	For dating		
66	Neb-1-12	Sandy soil	Uppermost part of the active layer			4.90	0.10			
67	Neb-1-13	Gravels				2.10-4.90	0.10-2.90	Mixture by the whole profile		
68	Khg-18-1	Coarse sand, gravels		42.196	57.794		0.5-0.6	Pit in the old Khorogor river delta	06.08.	
69	Khg-18-2	Fluvial gravel					0.1-0.2			
70	Khg-19-1	Gravel		38.524	34.324	ca. 116	0	Terrace F, Top	07.08.	
71	Khg-19-2	Loamy fine sand		38.617	34.581	ca. 108	0	Terrace F		KHG-95-9 to 11
72	Khg-19-3	Silty fine sand, gravels		38,580	34.832	ca. 98		Between terraces F-D		KHG-98-4
73	Khg-19-4	Silty fine sand		38.573	35.048	ca. 90	0.15	Between terraces E-D		
74	Khg-19-5	Plant detritus, fine sand		38.515	35.386	ca. 84	0	Chionoconit, Terrace D		KHG-96-9 to 10
75	Khg-19-6	Gravels, subrounded (0.1-0.2 m)		38.515	35.386	ca. 84	0	Terrace D		
76	Khg-19-7	Silty fine sand, single gravels		38.480	36.065	ca. 82	0.10	Frost boil (Ø 0.60 m) between terraces C-B		
77	Khg-20-1	Silty fine sand, gravels	Frozen	38.412	36.500	ca. 80	0.40	Frost boil (Ø 0.50 m)	09.08.	
78	Khg-20-2	Dark gray silty fine sand, loamy	Unfrozen				0.10	Active layer 0.21 to 0.35 m thick		ground-water

Appendix 4-1. continuation.

No.	Sample	Sample description: Sedimentology	Cryolithology, ice content abs./grav. [wt %]	Position: N 71°	E 128°	H NN (m)	Depth (m)	Remarks	Date	Ice/water samples
79	Stg-1-1	Plant remains, fine sand		36.645	46.106		0	Chionoconit from snowfield surface near the Stolovaya Gora hill	10.08.	SVY-96-11 to 14
80	Stg-1-2	Silty fine sand, gravels					0	Slop material		SVY-97-15 to 23
81	Stg-1-3	Plant remains, fine sand					0.10	Chionoconit from snowfield surface		
82	Stg-1-4	Subrounded gravels, sandstone, quartz					0			
83	Kol-1-1	Peaty soil		42.326	01.236		0-0.05	Ice wedge polygon	11.08.	KOL-95-1
84	Kol-1-2	Silty fine sand					0.15	Western Bykovsky Peninsula		
85	Kol-2-1	Peat	Frozen	42.338	01.299		1.00	Western Bykovsky Peninsula	11.08.	KOL-95-2
86	Kol-2-2	Peat	Frozen				0.70			
87	Kol-2-3	Peat	Unfrozen, active layer 0.45 m				0.50			
88	Kol-2-4	Silty fine sand	Unfrozen				0.20			
89	Kol-2-5	Peaty soil					0.10	Surface		
90	Kol-3	Subrounded gravels		42.514				Sampled on the surface of various frost boils	11.08.	
91	Kol-4-1	Subrounded gravels, sandstone								
92	Kol-4-2	Subrounded gravels		42.710	02.215					
93	Kol-4-3			42.710	02.215					

Appendix 4-1. continuation.

	Sample description			Position						
No.	**Sample**	**Sedimentology**	**Cryolithology, ice content abs./grav. [wt %]**	**N 71°**	**E 128°**	**H NN (m)**	**Depth (m)**	**Remarks Mamontovy Khayata**	**Date**	**Ice/water samples**
94	MKh-02-1-1	Silty fine sand	Ice rich, fine lens like reticulated, ice bands				1.65	Thermokarst mound	05.09.	MKH-02-1. 1 to 42
95	MKh-02-1-2	Cryoturbated peaty soil, peat pockets	Ice rich, coarse lens like reticulated				2.15		05.09.	
96	MKh-02-1-3	Silty fine sand, green-brownish, cryoturbated, peat pockets,	Ice poor, ice bands				2.75		05.09.	
97	MKh-02-1-4	Silty fine sand, grey, wood remains, small grass roots	Ice poor				3.05		05.09.	
98	MKh-02-1-5	Silty fine sand, grey, wood remains, small grass roots					5.25		05.09.	

No.	**Sample**	**Sedimentology**	**Cryolithology, ice content abs./grav. [wt %]**	**N 71°**	**E 129°**	**H NN (m)**	**Depth (m)**	**Polar fox lake (Ozera Petsa)**	**Date**	**Ice/water samples**
99	Ope-4	Middle-grained sand		44.696	20.784			Beach sand	06.09.	OPE-1 to 3
100	Ope-5	Silty sand + gravel		44.696	20.784			Surface sample, frost boil	06.09.	
101	Ope-6	Middle-grained sand		44.696	20.784			Beach sand	06.09.	

Appendix 4-2. List of ice, water and snow samples collected around Tiksi.

No.	Date	Sample	Type	Isotopes ^{18}O	Isotopes ^{2}H	^{3}H	Anion/ cation	Remarks
1	31.07.	TIK 99-1	RW	X	X	X	-	
2	01.08.	KHG 96-1	SW	X	X	X	-	Khorogor River
3	01.08.	KHG 95-1	RIW	X	X	X	X	Recent ice wedge
4	01.08.	KHG 96-2	SW	X	X	X	-	Vassily River
5	02.08.	KHG 96-3	SW	X	X	-	-	Pond Khorogor Valley
6	02.08.	KHG 98-1	GW	X	X	-	-	
7	02.08.	KHG 96-4	SW	X	X	X	-	Pond Khorogor Valley
8	02.08.	KHG 98-2	GW	X	X	-	-	
9	02.08.	KHG 99-2	RW	X	X	X	-	
10	02.08.	KHG 96-5	SW	X	X	X	-	Figurnoe lake
11	02.08.	KHG 95-2	RIW	X	X	X	X	Khorogor River, point 8
12	03.08.	KHG 96-6	SW	X	X	X	-	unnamed lake
13	03.08.	KHG 96-7	SW	X	X	X	-	Khatys Yuryakh River
14	03.08.	KHG 96-8	SW	X	X	X	-	Neelov Bay
15	03.08.	KHG 95-3	RIW	X	X	X	X	Head
16	03.08.	KHG 95-4	RIW	X	X	X	X	Head
17	03.08.	KHG 95-5	RIW	X	X	X	-	Head
18	04.08.	SVY 96-1	SW	X	X	X	-	Sevasyan Yurege River
19	04.08.	SVY 97-1	SP	X	X	X	-	Bottom of snowfield
20	04.08.	SVY 97-2	SP	X	X	X	-	
21	04.08.	SVY 97-3	SP	X	X	X	-	
22	04.08.	SVY 97-4	SP	X	X	X	-	
23	04.08.	SVY 97-5	SP	X	X	X	-	
24	04.08.	SVY 97-6	SP	X	X	X	-	
25	04.08.	SVY 97-7	SP	X	X	X	-	
26	04.08.	SVY 97-8	SP	X	X	X	-	
27	04.08.	SVY 97-9	SP	X	X	X	-	
28	04.08.	SVY 97-10	SP	X	X	X	-	
29	04.08.	SVY 97-11	SP	X	X	X	-	
30	04.08.	SVY 97-12	SP	X	X	X	-	
31	04.08.	SVY 97-13	SP	X	X	X	-	
32	04.08.	SVY 97-14	SP	X	X	X	-	Top of snow field
33	04.08.	SVY 97-E1	SP	X	X	X	-	Evaporation experiment
34	04.08.	SVY 97-E2	SP	X	X	X	-	
35	04.08.	SVY 97-E3	SP	X	X	X	-	
36	04.08.	SVY 97-E4	SP	X	X	X	-	
37	04.08.	SVY 97-E5	SP	X	X	X	-	
38	04.08.	SVY 97-E6	SP	X	X	X	-	
39	04.08.	SVY 97-E7	SP	X	X	X	-	
40	04.08.	SVY 97-E8	SP	X	X	-	-	
41	04.08.	SVY 96-2	SW	X	X	X	-	Sevastyan Lake

Appendix 4-2. continuation.

No.	Date	Sample	Type	^{18}O	^{2}H	^{3}H	Anion/ cation	Remarks
42	05.08.	KHG 95-6-1	IW	X	X	X	-	Ice Complex
43	05.08.	KHG 95-6-2	IW	X	X	X	-	Neelov Bay
44	05.08.	KHG 95-6-3	IW	X	X	-	-	
45	05.08.	KHG 95-6-4	IW	X	X	-	-	
46	05.08.	KHG 95-6-5	IW	X	X	-	-	
47	05.08.	KHG 95-6-6	IW	X	X	-	-	
48	05.08.	KHG 95-6-7	IW	X	X	X	-	
49	05.08.	KHG 95-6-8	IW	X	X	-	-	
50	05.08.	KHG 95-6-9	IW	X	X	-	-	
51	05.08.	KHG 95-6-10	IW	X	X	X	-	
52	05.08.	KHG 95-6-11	IW	X	X	-	-	
53	05.08.	KHG 95-6-12	IW	X	X	-	-	
54	05.08.	KHG 95-6-13	IW	X	X	-	-	
55	05.08.	KHG 95-6-14	IW	X	X	-	-	
56	05.08.	KHG 95-6-15	IW	X	X	-	-	
57	05.08.	KHG 95-6-16	IW	X	X	-	-	
58	05.08.	KHG 95-6-17	IW	X	X	-	-	
59	05.08.	KHG 95-7-1	IW	X	X	X	-	Holocene
60	05.08.	KHG 95-7-2	IW	X	X	X	-	Holocene
61	05.08.	KHG 95-7-3	IW	X	X	X	-	Holocene
62	05.08.	KHG 95-7-4	IW	X	X	X	-	Holocene
63	05.08.	KHG 95-7-5	IW	X	X	X	-	Holocene
64	05.08.	KHG 95-7-6	IW	X	X	X	-	Holocene
65	05.08.	KHG 95-7-7	IW	X	X	X	-	Holocene
66	05.08.	KHG 95-7-8	IW	X	X	X	-	Holocene
67	05.08.	KHG 95-7-9	IW	X	X	X	-	Holocene
68	05.08.	KHG 95-8-1	IW	X	X	X	-	Holocene/modern ice wedge
69	05.08.	KHG 95-8-2	IW	X	X	X	-	Holocene/modern ice wedge
70	06.08.	TIK 99-3	RW	X	X	X	-	
71	07.08.	KHG 95-9	RIW	X	X	X	-	
72	07.08.	KHG 95-10	RIW	X	X	X	-	
73	07.08.	KHG 95-11	RIW	X	X	X	-	
74	07.08.	KHG 95-12	TI	X	X	X	-	Segregated ice/ice lens
75	07.08.	KHG 98-3	GW	X	X	X	-	
76	07.08.	KHG 98-4	GW	X	X	X	-	
77	07.08.	KHG 96-9	SW	X	X	X	-	
78	07.08.	KHG 96-10	SW	X	X	X	-	
79	09.08.	KHG 98-5	GW	X	X	X	-	Vasili valley (point 2)
80	10.08.	TIK 99-4	RW	X	X	X	-	
81	10.08.	SVY 96-11	SW	X	X	X	-	Stolovoya Gora hill Terrace near snow field
82	10.08.	SVY 96-12	SW	X	X	X	-	Upper part of snow field (stream)
83	10.08.	SVY 96-13	SW	X	X	X	-	Bottom part of snow field (stream)
84	10.08.	SVY 97-15	SP	X	X	X	-	Snow field
85	10.08.	SVY 97-16	SP	X	X	X	-	Snow field
86	10.08.	SVY 97-17	SP	X	X	X	-	Snow field
87	10.08.	SVY 97-18	SP	X	X	X	-	Snow field
88	10.08.	SVY 97-19	SP	X	X	X	-	Snow field

Appendix 4-2. continuation.

No.	Date	Sample	Type	^{18}O	^{2}H	^{3}H	Anion/ cation	Remarks
89	10.08.	SVY 97-20	SP	X	X	X	-	Snowfield
90	10.08.	SVY 97-21	SP	X	X	X	-	Snowfield
91	10.08.	SVY 97-22	SP	X	X	X	-	Snowfield
92	10.08.	SVY 97-23	SP	X	X	X	-	Snowfield
93	10.08.	SVY 96-14	SW	X	X	X	-	Lake Dering Kuyel'
94	11.08.	KOL 95-1	RIW	X	X	X	-	Kolychev (SW-Bykovsky Peninsula)
95	11.08.	KOL 95-2-1	RIW	X	X	X	-	1,0 m,
96	11.08.	KOL 95-2-2	RIW	X	X	X	-	0,8 m,
97	11.08.	KOL 95-2-3	RIW	X	X	X	-	0,6 m,
98	14.08.	TIK 99-5	RW	X	X	X	-	
99	10.08.	SVY-1-4	SP		X	X	-	Snowfield, Sevastyan River, CAF
100	10.08.	SVY-1-5	SP		X	X	-	CAF
101	10.08.	SVY-1-6	SP		X	X	-	CAF
368	04.09.	MKH-02-1.0	IW	X	X	-	X	FROZEN
369	04.09.	MKH-02-1.1	IW	X	X	-	X	FROZEN
370	04.09.	MKH-02-1.2	IW	X	X	-	X	FROZEN
371	04.09.	MKH-02-1.3	IW	X	X	-	X	FROZEN
372	04.09.	MKH-02-1.4	IW	X	X	-	X	FROZEN
373	04.09.	MKH-02-1.5	IW	X	X	-	X	FROZEN
374	04.09.	MKH-02-1.6	IW	X	X	-	X	FROZEN
375	04.09.	MKH-02-1.7	IW	X	X	-	X	FROZEN
376	04.09.	MKH-02-1.8	IW	X	X	-	X	FROZEN
377	04.09.	MKH-02-1.9	IW	X	X	-	X	FROZEN
378	04.09.	MKH-02-1.10	IW	X	X	-	X	FROZEN
379	04.09.	MKH-02-1.11	IW	X	X	-	X	FROZEN
380	04.09.	MKH-02-1.12	IW	X	X	-	X	FROZEN
381	04.09.	MKH-02-1.13	IW	X	X	-	X	FROZEN
382	04.09.	MKH-02-1.14	IW	X	X	-	X	FROZEN
383	04.09.	MKH-02-1.15	IW	X	X	-	X	FROZEN
384	04.09.	MKH-02-1.16	IW	X	X	-	X	FROZEN
385	04.09.	MKH-02-1.17	IW	X	X	-	X	FROZEN
386	04.09.	MKH-02-1.18	IW	X	X	-	X	FROZEN
387	04.09.	MKH-02-1.19	IW	X	X	-	X	FROZEN
388	04.09.	MKH-02-1.20	IW	X	X	-	X	FROZEN
389	04.09.	MKH-02-1.21	IW	X	X	-	X	FROZEN
390	04.09.	MKH-02-1.22	IW	X	X	-	X	FROZEN
391	04.09.	MKH-02-1.23	IW	X	X	-	X	FROZEN
392	04.09.	MKH-02-1.24	IW	X	X	-	X	FROZEN
393	04.09.	MKH-02-1.25	IW	X	X	-	X	FROZEN
394	04.09.	MKH-02-1.26	IW	X	X	-	X	FROZEN
395	04.09.	MKH-02-1.27	IW	X	X	-	X	FROZEN
396	04.09.	MKH-02-1.28	IW	X	X	-	X	FROZEN
397	04.09.	MKH-02-1.29	IW	X	X	-	X	FROZEN
398	04.09.	MKH-02-1.30	IW	X	X	-	X	FROZEN
399	04.09.	MKH-02-1.31	IW	X	X	-	X	FROZEN
400	04.09.	MKH-02-1.32	IW	X	X	-	X	FROZEN
401	04.09.	MKH-02-1.33	IW	X	X	-	X	FROZEN
402	04.09.	MKH-02-1.34	IW	X	X	-	X	FROZEN
403	04.09.	MKH-02-1.35	IW	X	X	-	X	FROZEN
404	04.09.	MKH-02-1.36	IW	X	X	-	X	FROZEN
405	04.09.	MKH-02-1.37	IW	X	X	-	X	FROZEN
406	04.09.	MKH-02-1.38	IW	X	X	-	X	FROZEN
407	04.09.	MKH-02-1.39	IW	X	X	-	X	FROZEN
408	04.09.	MKH-02-1.40	IW	X	X	-	X	FROZEN

Appendix 4-2. continuation.

No.	Date	Sample	Type	^{18}O	^{2}H	^{3}H	Anion/ cation	Remarks
409	04.09.	MKH-02-1.41	IW	X	X	-	X	FROZEN
410	04.09.	MKH-02-1.42	IW	X	X	-	X	FROZEN
411	05.09.	OPE-1	SW	X	X	-	X	FROZEN
412	05.09.	OPE-2	SW	X	X	-	X	FROZEN
413	05.09.	OPE-3	SW	X	X	-	X	FROZEN
414	07.09.	TIK-SP-1	SP	X	X	X	-	

Abbreviations : SP = Snow patch; RW = rain water; IW = ice wedge ice; RIW = recent ice wedge ice ; SW = surface water; GW = ground water; TI = texture ice; CAF = cellulose acetat filter

4.8 References

Drachev, S.S., Savostin, L.A., Groshev, V.G., Bruni I.E. (1998): Structure and geology of the continental shelf of the Laptev Sea, Eastern Russian Arctic,. Tectonophysics 298: 357-393.

Franke, D., Krüger, F. & Klinge, K. (2000): Tectonics of the Laptev Sea – Moma 'rift' region: investigation with seismologic broadband data.- J. of Seismology, 4: 99-116.

Galabala (1980): New data on the structure of Lena Delta.- In: Chetvertichny period Severo-Vostoka Asii (Quaternary period of Northeast Asia).- Magadan:SVKNII DVO AN SSS%: 152-171 (In Russian).

Galabala, R.O. (1997): Pereletki and the initiation of glaciation in Siberia.- Quat. Int. 41/42: 27-32.

Grigoriev, M (1993): Cryomorphogenesis in the Lena Delta.- Permafrost Institute Press, Yakutsk, pp. 176 (In Russian).

Grosswald, M.G., Spektor, V.B. (1993): The glacial relief of the Tiksi region (west shore of Buor-Khaya inlet, Northern Yakutia.- Polar Geography and Geology, 17/2: 154-166.

Imaev, V.S., Imaeva, L.P. & Koz'min, B.M. (2000): Seismotektonika Yakutii,- GEOS, Moscow, pp. 226.

Katasonova, E.G. (1963): The role of thermokarst for the development of delly; In: Uslowya i osowennosti raswitya merslykh toltsch w Sibiri i na Sewero-Wostokye; Moscow; 91-100; (In Russian).

Kunitsky, V., Schirrmeister, L., Grosse, G., Kienast, F. (2002): Snow patches in nival landscapes and their role for the Ice Complex formation in the Laptev Sea coastal lowlands, Polarforschung, 70: 53-67.

Kunitsky, V.V. (1987): Role of glaciers and snow patches for cryolithogenic formations in the lower Lena area.- Theses of dissertation, cand. geograph science, Yakutsk, 21 pp. (In Russian).

Kunitsky, V.V. (1989): Cryolithology of the lower Lena.- Permafrost Institute Yakutsk, 164 pp. (In Russian).

Parfenov, L.M. (ed.) (2001): Tektonika, Geoidynamika i Metallogeniya territorii Respublik Sakha (Yakutiya) (Tectonik, Geodynamics and metallogeny of Sakha Republic, Yakutia).- Russian Academy of Science "Nauk/Interperiotika",pp 571 (In Russian).

Schirrmeister, L., Siegert, C., Kuznetsova, T., Kuzmina, S., Andreev, A.A., Kienast, F., Meyer, H., Bobrov, A.A. (2002): Paleoenvironmental and paleoclimatic records from permafrost deposits in the Arctic region of Northern Siberia, Quaternary International 89: 97-118.

Siegert, C., Schirrmeister, L., Kunitsky, V.V., Sher, A.,Tumskoy, V., Meyer, H. (1999): Paleoclimate signals of ice-rich permafrost; In: Russian-German Cooperation System Lapev Sea 2000: The Lena Delta 1998 Expedition (ed: Rachold, V. & Grigoryev, M.N.); Reports on Polar Research, 315: 145-190.

Slagoda, E.A. (1993): Genesis and microstructure of cryolithogenic deposits at the Bykovsky Peninsula and the Muostakh Island. Thesis, RAS Siberian section, Permafrost Institute, Yakutsk, pp 218 (In Russian).

5 Cruise to the New Siberian Islands onboard RV Pavel Bashmakov

5.1 Introduction

Volker Rachold and Mikhail N. Grigoriev

The third stage of the expedition Lena 2002 focused on coastal and permafrost studies along the coastlines of the New Siberian Islands. From 14 August to 2 September 2002 twelve pre-selected key sites have been investigated (Fig. 5.1-1). The work program and the results of the two groups participating in this stage of the expedition are presented in detail in the next sub-chapters:

- permafrost, periglacial and paleo-environmental studies on the New Siberian Islands (chapter 5.2)
- coastal studies on the New Siberian Islands (chapter 5.3)

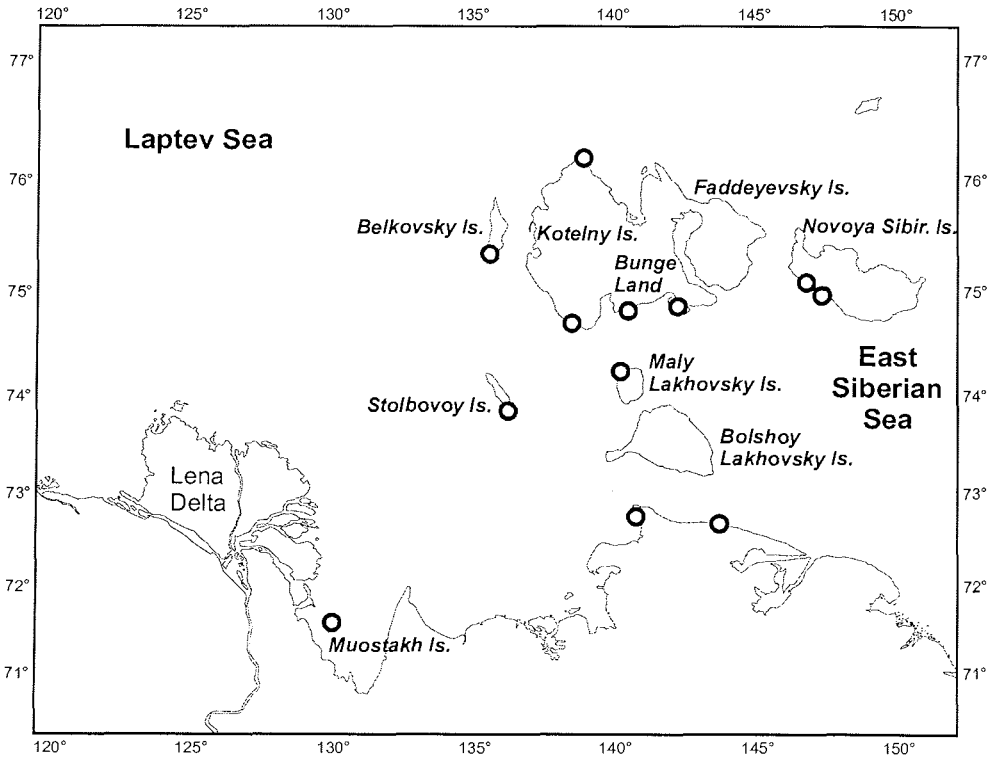

Figure 5.1-1: Study area during the cruise to the New Siberian Islands onboard RV Pavel Bashmakov, landing locations are marked by circles.

The participants of both teams were based on RV Pavel Bashmakov, which is an ice-going research vessel (Fig. 5.1-2, Table 5.1-1). The ship was used for transport and accommodation of the 14 participants (Fig. 5.1-3). A special landing craft (Fig. 5.1-4) was applied to bring the participants to the working areas, i.e. the coastal sections. The field work was performed during day trips and during the nights Pavel Bashmakov sailed to the next station and obtained samples were processed in the laboratory installed onboard the ship.

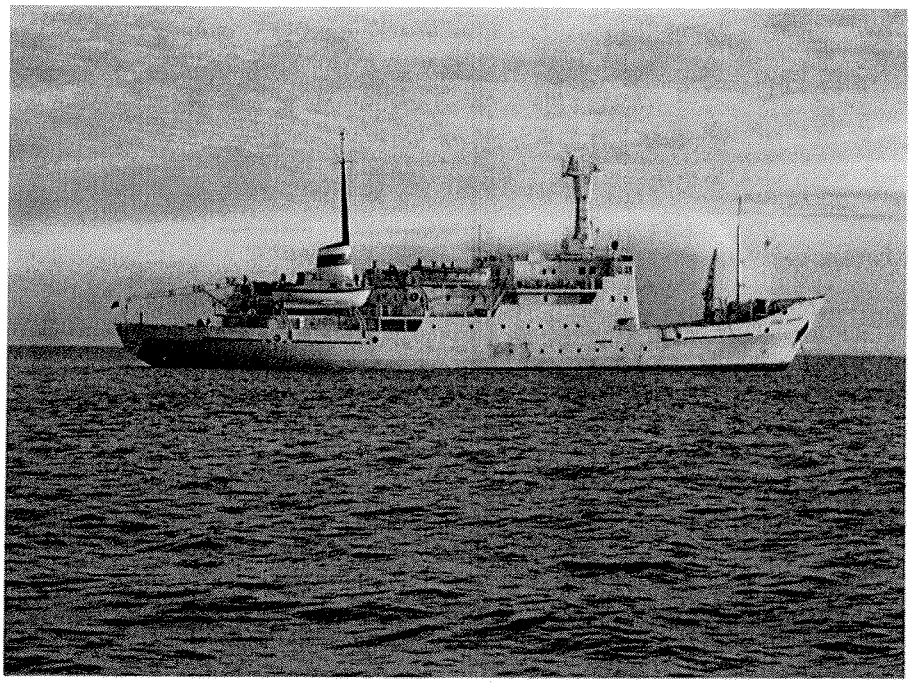

Figure 5.1-2: RV Pavel Bashmakov.

Table 5.1-1. Technical data of RV Pavel Bashmakov.

Lengths	68.87 m
Width	12.42 m
Draught	5.2 m
Water displacement	1267 BRT
Engine	1472 kW
Technical Crew	20
Scientific Crew	up to 28

Figure 5.1-3. Participants of the cruise to the New Siberian Islands.

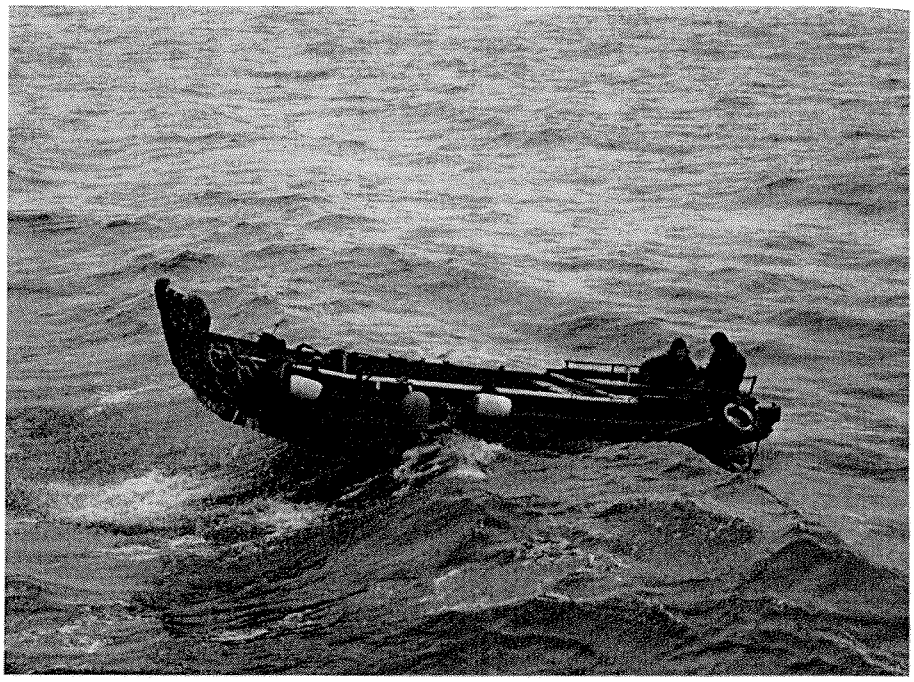

Figure 5.1-4: Landing craft used to disembark.

5.2. Permafrost, periglacial and paleo-environmental studies on New Siberian Islands

Lutz Schirrmeister, Guido Grosse, Viktor Kunitsky, Hanno Meyer, Alexander Derivyagin and Tatyana Kuznetsova

5.2.1 Introduction

5.2.1.1 General topics

The study of permafrost sequences in coastal sections of the New Siberian Archipelago and of the Yana-Indigirka-Interfluve deliver information on Quaternary environmental changes of this poorly studied Arctic area. The combined studies of frozen sediments and ground ice in selected sections were carried out in close co-operation with the "coastal erosion" team (see chapter 5.3). The main objectives of our investigations were the overview of the geomorphologic, geological, and geocryological situation in various locations of islands and mainland's coasts and the reconnaissance of scientific as well as logistically favourable sites for future detailed surveys.

Special topics of the "permafrost" team were

- The extension of the studying area for the investigations of permafrost paleo-environmental archives, concerning geocryology, ground ice isotopic composition and hydrochemistry, paleontology and geochronology;
- Studies of frozen middle to late Quaternary marine deposits in coastal sections;
- Continuation of field studies of periglacial surface phenomenons (s. chapter 4.2) using field observation and remote sensing data;
- Sedimentological and geochronological studies regarding the origin of Bunge Land.

In contrast to former expeditions we daily changed the study sites by the hydrographical research vessel "Pavel Bashmakov" and therefore the studies were mostly exemplary. Our "permafrost"-team consisted of three Russian and three German scientists and was supported for the first time by a field laboratory and a technician, in order to realize first hydrochemical and geocryological analyses and to preserve all samples for the transport.

Twelve locations were studied between Muostakh Island near Tiksi in the south and Cape Anisy at the north coast of Kotel'ny Island; between Derevyannye Gory (Novaya Sibir Island) and Oyogos Yar (Laptev Strait south coast) in the East and Bel'kovsky Island and Stolbovoy Island in the West (Fig. 5.2.1-1).

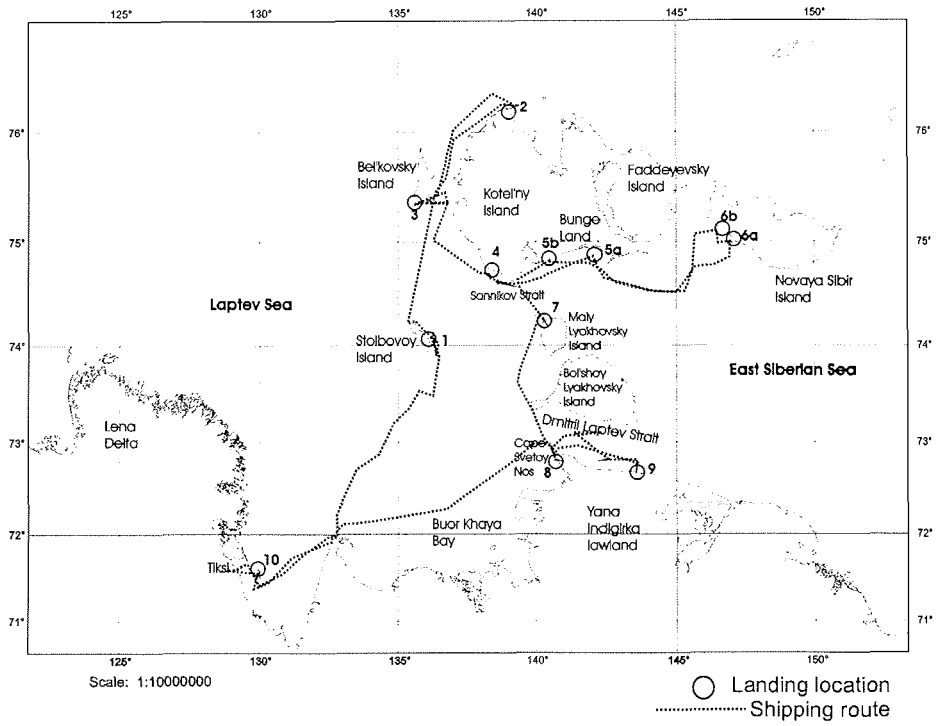

Figure 5.2.1-1: Schematic map of the study area in the eastern Laptev Sea and western East Siberian Sea with ship route and the study locations: 1 - Stolbovoy Island; 2 - Bel'kovsky Island; 3 - Kotel'ny Island (Cape Anisy); 4 - Kotel'ny Island (Khomurgannakh River mouth); 5a - Bunge Land (High terrace); 5b - Bunge Land (Low terrace); 6a - Novaya Sibir Island (Derevyannye Gory); 6b - Novaya Sibir Island (Location Hedenstrom); 7 - Maly Lyakhovsky Island; 8 - Cape Svyatoy Nos; 9 - Oyogos Yar; 10 - Muostakh Island.

5.2.1.2 General geological background

The area of the eastern Laptev Sea and the western part of East Siberian Sea belongs to the Verkhoyansk-Kolymsk Fault Region and consists of a syncline-anticline system formed on the western margin of the North American Plate. The position at the inactive plate margin has determined the accumulation of thick Palaeozoic and Mesozoic carbonate and clastic complexes, which were folded and thrusted during the Early Cretaceous (Drachev et al. 1998). Two main structures of the study area were formed during this period. The first is the northern part of the New Siberian-Chukchi Fold Belt, exposed on Kotel'ny and Bel'kovsky Islands. It consists of a 6 to 10 km thick sequence of Ordovician to Lower Cretaceous deposits (Kos'ko et al. 1990). In general, the anticlines there contain Paleozoic weakly metamorphic marine and terrigene limestones, sandstones and slates with tuffite, gypsum and anhydrite interlayers (Krasny 1981, Spektor 1981). In synclines, Mesozoic and Cenozoic deposits cover such sequences. The second is the South Anyuy-Lyakhov Ophiolitic Suture, exposed

on Cape Svyatoy Nos and Bol'shoy Lyakhovsky Island, which separates this fold belt from the Verkhoyansky fold belt (Parfenov 2000). Typical rocks are Late Paleozoic ophiolites, Late Jurassic to Early Cretaceous islands arc volcanic rocks and Cretaceous granodiorites and granites (Drachev 1998). Deformation stages occurred during Neocomian and Late Aptian.

The geological and tectonical situation of the Cenozoic is characterized by rifting processes at the plate margin. Therefore, the Laptev Sea Rift system consists of several rifts and uplifts (Ust-Lena-rift, East Laptev horst, Stolbovoy horst, Anisy rift, Kotel'ny uplift, Bel'kovsky-Svyatonosski rift, New Siberian or Faddeevsky rift and Tastakhsky rift). This is the reason for the existence of some graben and horst structures in the eastern Laptev Sea (Fig. 5.2.1-2).

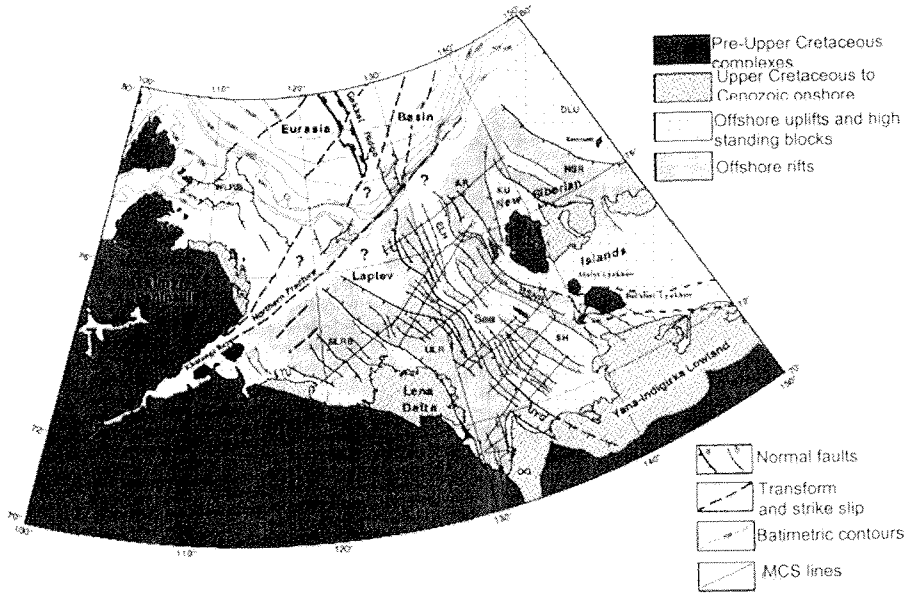

Figure 5.2.1-2: The main structural elements of the Laptev Shelf (Drachev et al. 1998): WLRB - West Laptev rift basin; LTU - Lena-Taimyr uplift; SLRB - South Laptev basin; ULR - Ust' Lena rift; UYG - Ust' Yana graben; OG - Omoloy graben; ELH - East Lena horst; AR - Anisy rift; BSNR - Bel'kov-Svyatoy Nos rift; SH - Stolbovoy horst; KU - Kotel'ny uplift; NSR - New Siberian rift; DLU - De Long uplift.

While seismic studies from Drachev et al. (1998) and Franke et al. (2000) show generally NNW-SSE oriented tectonic and geologic structures (Fig. 5.2.1-2), the map of Spektor (1981) shows a NE-SW orientation of tectonical elements. These are the Svyatoy Nos segment, the Lyakhovsky segment, the Kotel'ny segment and the Henrietta segment (Fig. 5.2.1-3). Fracture zones parallel to the general orientation of the coasts and marine straits are the boundaries of each segment. According to Spektor (1981), a fracture zone forms the northern rim of the Svyatoy Nos segment parallel to the mainland's coast along the Dmitrii Laptev Strait.

Folded terrigene Jurassic sediment (sandstones, aleurolite and tuffs) are discordantly covered by volcanites (andesite, basalts) and intruded by granodiorites. According to K-Ar-dating the basalts are formed before 148 to 159 Ma and the granodiorite before 95 to 115 Ma (Prokhorova & Ivanov, 1973, Parfenov, 2001).

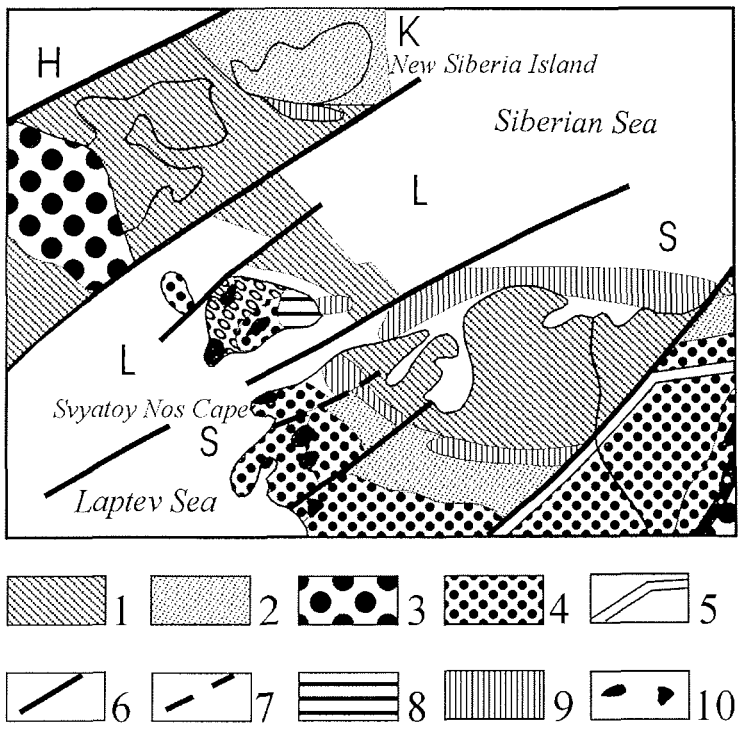

Figure 5.2.1-3: Part of schematic map of the tectonic order of the western New Sibirian-Chukchi-Fold System (according to Spektor et al. 1981): 1 - Inner zone; 2 - Transition step; 3 - Mesozoic outer depressions; 4 - Palaeozoic central depressions; 5 - Faults bounding the New Sibirian-Chukchi-Fold System; 6 - Faults between segments; 7 - Faults within segments; 8 - Gabbro, resp. ultramafic rocks, exposed at the surface; 9 - Gabbro, resp. ultramafic rock, suspected according to geophysical data; 10- Granitoids; S - Svyatoy Nos segment; L - Lyakhovsky segment; K - Kotel'ny segment; H - Henrietta segment

The northern boundary of the Lyakhovsky segment is a fault zone parallel to the Sannikov Strait between both the Lyakhovsky Islands and Kotel'ny Island. Within this segment there occur fragments of the central uplift zone of the New Siberian-Chukchi fold system with Proterozoic crystalline slates and amphibolites as well as fragments of the outer zone with granite massifs. Higher in the profile the complex of terrigene Permian deposits contain diabase and ultramafic rocks. The outer zone of the fold system here is characterized by weakly disturbed Cretaceous deposits and stronger disturbed Jurasic deposits

both folded and in places intruded by granitoids, which had been formed before 92 to 114 Ma. According to Spector (1981) the northern boundary of the Kotel'ny segment is a fault zone parallel to 76° latitude and the north coast of Kotel'ny Island. Palaeozoic carbonate sediments of the central uplift zone are folded and outcropped together with concordantly disturbed Triassic argillites on Kotel'ny Island. In the Kotel'ny segment the inner zone (Bunge Land, Faddeyevsky Island) and the transition step of the fold system are filled with Cenozoic terrigene and effusive-terrigene layers and the Cenozoic sediments of the transition step (Novaya Sibir Island) are folded as well.

The Cenozoic unit is subdivided in the Neogene and Quaternary deposits at the Svyatoy Nos segment, in Paleogene, Neogene to Quaternary and Quaternary deposits at the Lyakhovsky segment and in Paleogene, Paleogene to Neogene, Neogene, Pliocene to Quaternary and Quaternary deposits. Quaternary deposits are dated to a lesser amount and have mostly local stratigraphical orders. Therefore, a generalized Quaternary stratigraphy of the New Siberian Islands and the adjoining Yana-Indigirka Lowland is not available yet. The current knowledge of the Quaternary will be represented describing each study location.

5.2.1.3 Methodical approach

The main topics mentioned in chapter 5.2.1.1 were realized in close co-operation with the other study disciplines. Numerous sediment sub-profiles were studied at coastal cliffs and thermokarst mounds in close connection with ground ice investigations. Cryostructures and sediment structures were observed as well as sediment colour, grain size and the content of fossil plant material was described. Permafrost deposits were mostly sampled in frozen stage using small axes and hammers. Samples of 0.5 to 1 kg were taken and then packed into plastic bags. Separate samples were taken for gravimetric ice content determination in aluminum boxes. The field laboratory and the support by the lab technician on the research vessel "Pavel Bashmakov" was very helpful for sample preparation and the first measurements. We want to express especially thanks to our colleague Antje Eulenburg for her excellent work in the lab almost around the clock.

For ice content determination, the sediment samples were first weighed in frozen state and then again after drying. The gravimetric ice content was calculated as the ratio of mass of the ice in a sample to the mass of dry sample, what the common method in geocryology studies (v. Everdingen 1998). The weight determination by electronic balance was only possible on land because of strong ship movements. Besides of frozen/thawed sediment samples, some pebbles and boulders were sampled in order to determine the rocks and to examine their origin. In addition, single samples of wood remains were taken for radiocarbon age determination. A special sampling was carried out for sandy sediments on Bunge-Land, which will be dated by Infrared Optical Stimulated Luminescence (IR-OSL). These samples were taken with a hand-drilling

machine (HILTI) and a special drilling head with opaque plastic cylinders. The samples, which had to be protected from sunlight, were stored and transported in the cylinders and additional black plastic bags. Finally, each sediment sample was well-wrapped in the laboratory for the transport to Germany.

Ice wedges were studied in close connection with sediment profiles. The study conception for ice wedges (stable isotopes and hydrochemistry) is briefly described in chapter 3.11 and presented in more detail in former field reports (Rachold et al. 1999; 2000). A special emphasis was put on the sampling of recent ice veins and precipitation on New Siberian Islands. The precipitation was continuously sampled by a rain-water sampling device (type Hellmann) onboard the ship. Additionally, samples were taken from snow patches, to study in detail the connection between recent ice wedges and precipitation. During the sampling of ice-rich sediment, the segregated ice is melting. This supernatant water was extracted with a plastic syringe for the determination of the stable isotope composition and hydrochemistry of segregated ice. In addition, samples were taken from surface waters (lakes, rivers brooks, polygonal ponds), seawater and sea ice in order to get an overview of the hydrological situation of the whole region.

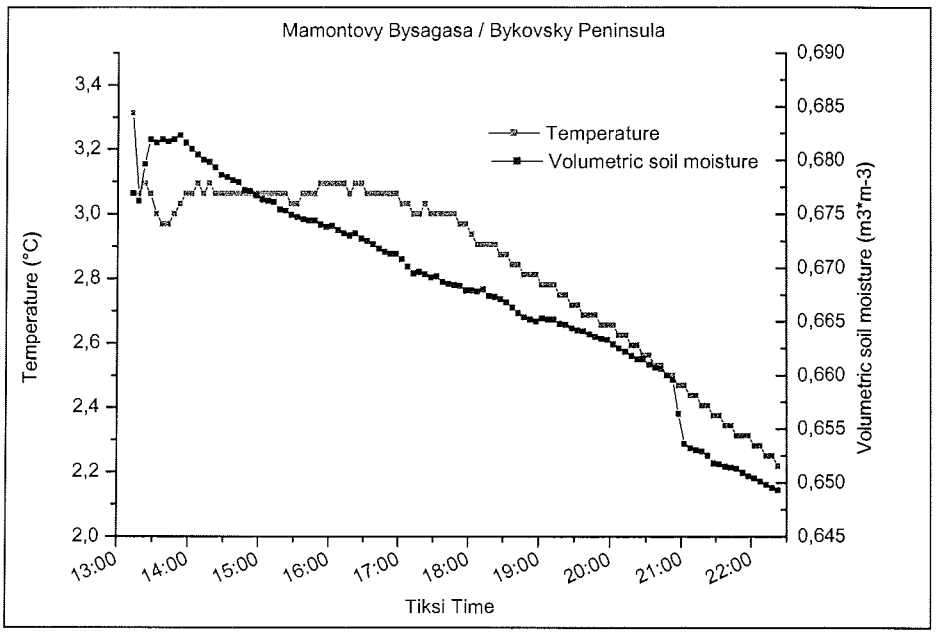

Figure 5.2.1-4: Exemplary surface data of soil temperature and soil moisture, measured with a transportable soil probe on Bykovsky Peninsula and on New Siberian Islands (alas depression Mamontovy Bysagasa, 04.09.2003)

In order to characterize the surface conditions for the interpretation of remote sensing date a transportable soil probe (TSP) was placed at each landing site for the whole time of the stay. The soil probe measured the soil temperature and soil tension voltage, which can be transfer into volumetric soil moisture

(Figure 5.3.1-4). The measurement was done for the entire stay at a typical tundra site near the landing location. Every site was chosen by its characteristic surface properties: relief, surface sediment, vegetation, and homogeneity. Altogether 10 sites were described, all of them different in their characteristics. Depending on the stay, soil temperature and soil moisture were permanently (5 min interval) measured for 2-8 hours. In Appendix 5.2-4 the sites are listed with their coordinates and their average, minimum and maximum value for temperature and volumetric soil moisture for the measurement interval.

The sizes of typical relief forms, like thermokarst mounds and ice wedge polygons were studied by measuring tape. By comparing the morphometry of recent polygonal nets from different relief positions with remains of former polygonal nets (thermokarst mounds) we want to draw conclusions on the characteristics for the Ice Complex paleo-landscape. Further, thermokarst mounds mark sites, where ice-rich deposits had existed earlier. The size and shape, hence the stage of development, of thermokarstic and erosional structures (especially valleys) were also measured. A comparison of lateral distribution over the New Siberian Islands and the adjacent coasts may detect latitudinal or longitudinal gradients in thermokarst or thermo-erosion effects. Therefore they can give hints on the effectiveness of environmental changes in the area.

5.2.2 Stolbovoy Island (15.08.)

Stolbovoy Island is the highest part of the Stolbovoy tectonical Horst (Drachev et al. 1998) and the westernmost part of Verkhoyansk-Kolymsk Fold Region within the study area. Its basement consists of Jurassic and Cretaceous sedimentary rocks, often exposed at the island's coast as well as in higher hill positions. Two ridges of about 140-220 m a.s.l. in the southern part and of 100-140 m in the northern part form the "spine" of this island. The lower relief down to the beach is dominated by a step-like morphology of cryoplanation terraces on various levels (140 m, 120 m, 60-80 m, 50 m, 25-30 m, Figure 5.2.2-1). The lowest terrace is covered by Ice Complex deposits, which were studied there on August 15.

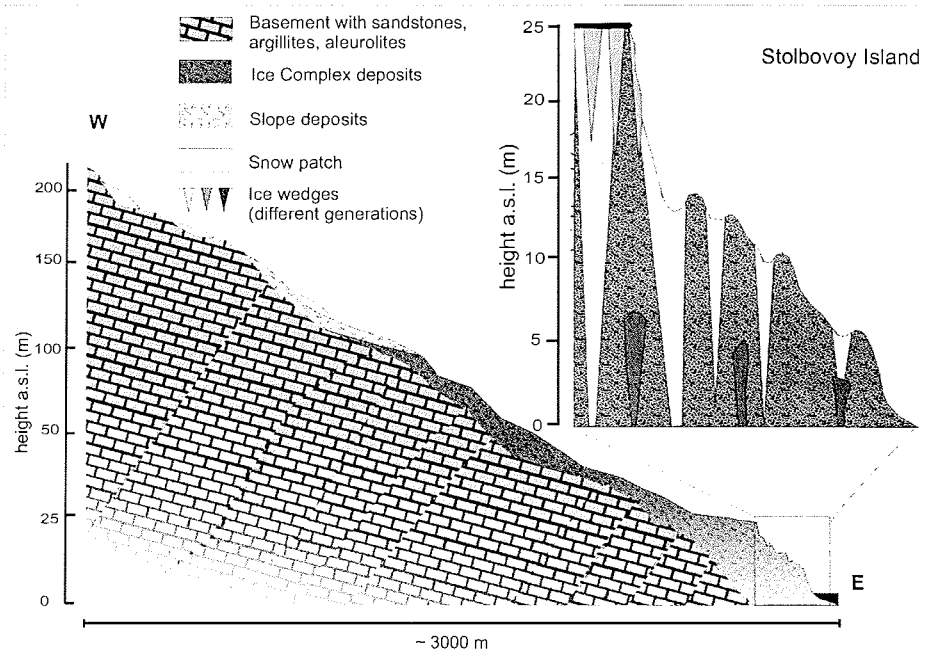

Figure 5.2.2-1: Scheme of the frequently observed geomorphological situation at the Stolbovoy Island coast with steps of cryoplanation terraces

Our study site was situated at the east coast of Stolbovoy Island 3.5 km north of the Stolbovaya River mouth (Figure 5.2.2.-2). Ice Complex deposits cover the surface of the lowest (30 m) terrace and thermo-erosional valleys occur. Four sub-profiles were sampled in various levels of the coast (Figure 5.2.2.-3 and -4).

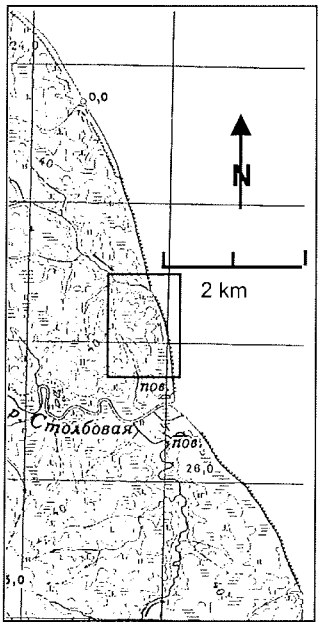

Figure 5.2.2-2: Study site at the east coast of Stolbovoy Island in August 15

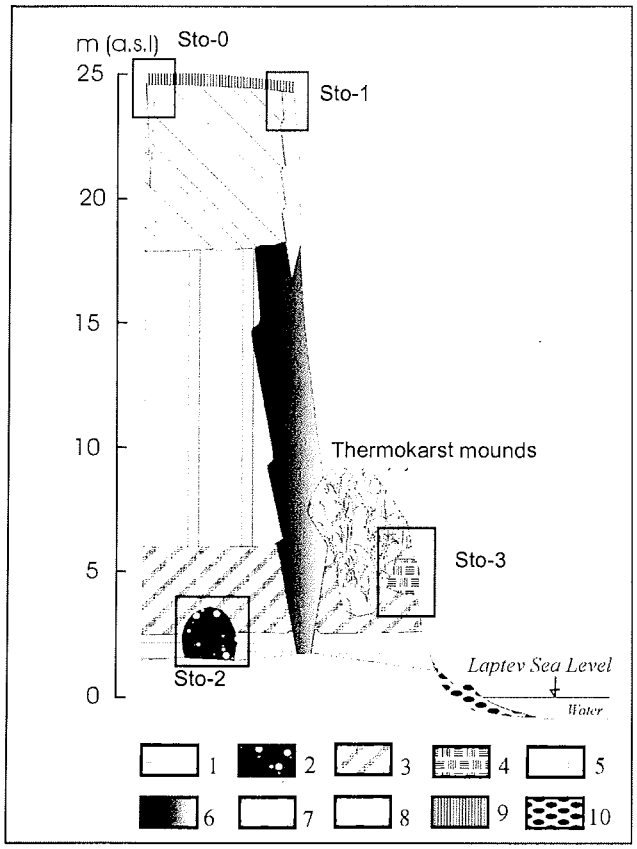

Figure 5.2.2-3:
General scheme of the studied Ice Complex section
1 - Silty sand brownish, layered, frozen, including shrub twigs and grass roots, massive;
2 - Buried, Ice wedge (Polosatic);
3 - Silty sand dark-grey, layered, with peat nests and grass roots, ice belts, massive;
4 - Moss-peat, brownish, with lenses of clear injection ice
5 - Silty sand, dark grey, layered, grass roots, ice belts
6 - Ice wedge, light-grey, 4 to 5 m wide, compact;
7 - Silty sand, grey, layered, frequent small peat lenses, grass roots, ice belts;
8 - Ice wedge, white, small (1.5 m), less compact;
9 - Active layer;
10 - Beach pebbles.

At the study site the coast is very steep and Ice Complex deposits about 25 m thick with large and small ice wedges are exposed there. In the lower part a special phenomenon was visible - a buried ice wedge with rounded head, which had deformed the covering layers above (Figure 5.2.2-4A STO 2). The sediment consists of grey silty sand (aleurit), containing some vertical grass roots *in situ.* A massive cryostructure and a gravimetric ice content of 51-60 wt-% was observed.

The ice wedge (Stb-IW-2) with round (thawing) head was striped in the baydzherakh at the height about 3 m a.s.l.. The width of ice wedge is about 1-1,2 m, and the visible thickness is about 2 m. The ice wedge ice is very dirty and has numerous mineral particles and looks like "polosatic" ice wedge, founded and described at Bol'shoy Lyakhovsky Island 1999. The thickness of vertical oriented mineral stripes is about 0.7-1 cm, the thickness of vertical oriented ice stripes is about 0,5-0,7 cm. The cryogenic construction of the ice wedge as well as of the enclosed sediments (with ice belts, ice shoulders and peat nests and pockets) may be an evidence for syngenetic evolution of this ice wedge. The general construction of the section suggests that the head of the ice wedge was thaw-treated and then buried under the sediments. 5 samples of ice wedge ice (25 cm distance) were collected.

A big peat lens of about 1-2 m thickness and 150 m length was exposed in several thermokarst mounds at the height of 5-7 m a.s.l. (Figure 5.2.2-4B STO3). This moss peat was imbedded by greyish-brown silty fine sand with grass roots, small peat nests containing ice belts and a fine lens-like cryostructure (gravimetric ice content about 56 wt-%). Large lenses of transparent injection ice were observed and sampled within this peat lens. The gravimetric ice content of the peat changes between 70 to 270 wt-%. Ice wedges of this level are 4-5 m wide, grey and compact, showing vertical striation and edgewise shoulders.

An additional ice wedge (Figure 5.2.2-4D, Sto-IW-5) was sampled at the height about of 15 m a.s.l. in the instable middle part of the outcrop. The thawed "head" of ice wedge had a width of about 3 m and the visible was about 1.5 m. The ice was turbid, and dirty and contains numerous vertical oriented mineral particles ("Polosatic") and air bubbles. Ice shoulders at the contact between ice wedge and sediment are typical feature of syngenetic ice wedges. In total 9 samples of ice wedge ice were collected in a distance of 30-35 cm.

Sediment and an ice wedge of the upper part of the outcrop were studied below the terrace surface at about 22 m a.s.l. (Figure 5.2.2-4E, STO 1). The ice wedge there consisted of yellowish-grey to milky-white transparent ice containing a lot of small gas bubbles (< 1mm) and sediment streaks. Gas bubbles were randomly distributed and not orientated. A dark-light striation was visible but single ice veins are badly recognisable. Such ice veins are 2-6 mm wide. In total, 16 samples were taken from this 1.6 m wide ice wedge (STO-IW-1). The ice wedge belongs to a series of narrow and 5-6 m high ice wedges at the top of the Ice Complex. These ice wedges are connected with the underlying wider "normal" Ice Complex ice wedges. Therefore, the question has

be solved, whether the small ice wedges still belong to the Ice Complex or whether they were formed after the deposition of the Ice Complex and what may have limited the growth of the narrow ice wedges. Grey silty fine sand with small grass roots and low ice content (gravimetric ice content 38-59 wt-%) and a massive cryostructure composed the Ice Complex deposits beneath this ice wedge near the top. The polygons at the surface point to the inactive character of ice wedge growth. They are 8-10 m in diameter and characterised by an apex, being 0.5 m lower than the elevated polygon centre. The vegetation cover is sparse and the active layer depth about 40-50 cm.

About 250 m further to the NW, a younger generation of ice wedges, possibly of Holocene age, was sampled (Figure 5.2.2-4F, STO 4). The ice wedge STO-IW-4 is composed of white and milky ice with a lot of small gas bubbles. 2-4 mm wide elementary ice veins were easily recognised. From this 0.8 m wide ice wedge, five samples were taken. Additionally, a 4 cm wide complex of three single recent ice veins, which were found at the bottom of the (still frozen) active layer, was sampled for isotope and tritium analyses. The cryogenic structure was irregular-reticulate with a low content of ice in the silty-sandy "loess-like" sediment. The polygons are again 8-10 m in diameter, with little vegetation and characterised by an apex 0.5 m lower than the centre.

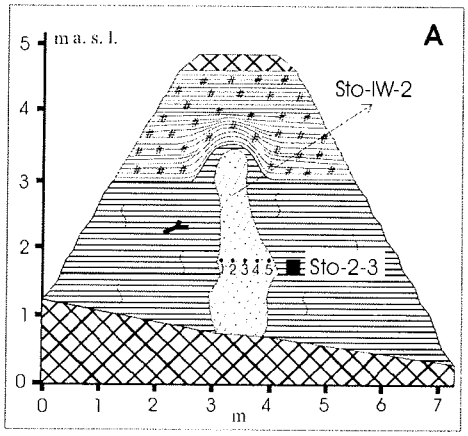

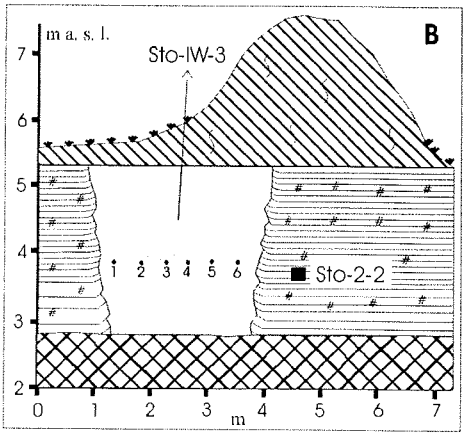

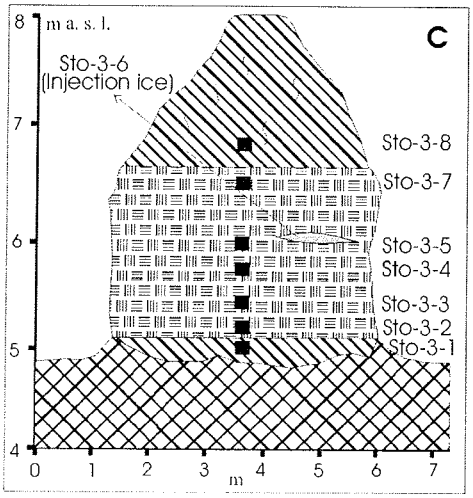

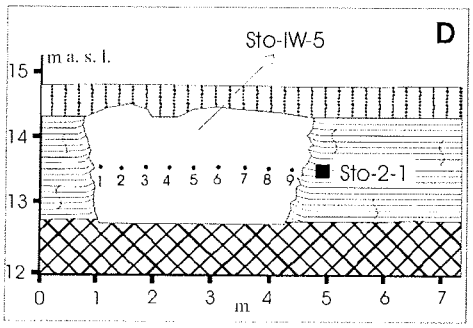

Legend:

- dark-grey silt;
- peat;
- grey silt;
- blue-grey silt with peat lenses and pockets;
- slump;
- ice wedge with numerous silt inclusions (polosatic);
- ice wedge
- lens of injection ice;
- grass roots;
- wood remains;
- bones;
- tundra plant cover;
- sample points and number of ice samples;
- sample points and number of samples of sediments;

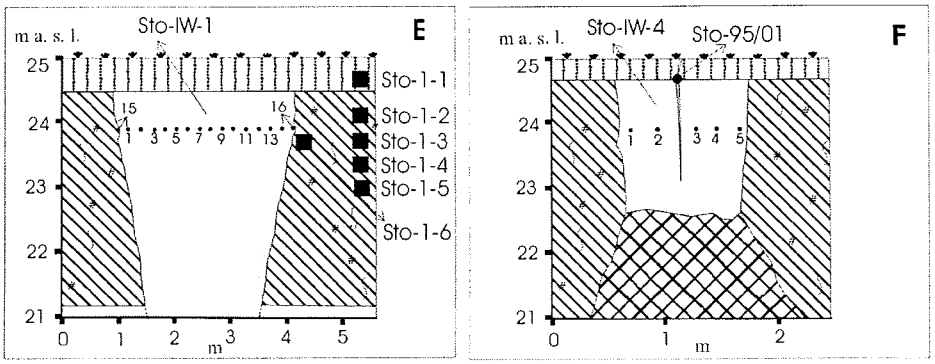

Figure 5.2.2-4: Schematic sketches of the studied sub-profiles of Stolbovoy Island.
A: Sub-profile Sto-2 – Buried ice wedge IW-2 ("Polozatic") near the beach;
B: Sampled larger ice wedge IW-3 at the beach, extending below sea level;
C: Sub-profile Sto-2 – A thermokarst mound exposes a large peat lens within Ice Complex deposits;
D: Samples of ice wedge IW-5 in the middle part of the coastal section;
E: Sub-profile Sto-1 – Ice wedge and Ice Complex deposits below the top of the coastal cliff;
F: Sub-profile Sto-0 – A recent ice wedge penetrates through an older one below the top of the coastal cliff.

Wide thermokarst valleys with flat floors are formed within a thermokarst depression north of the studied section. Very impressive polygonal nets, forming flat thermokarst mounds occurred at the slopes of these valleys (Figure 5.2.2-5). A Holocene peat cover, grown within such valley, was sampled at a small pit of a flat thermokarst mound at about 10 m a.s.l. (samples Sto 4-1 to 4-4). The distance of thermokarst mound centres were measured from one top to the other top in two locations in order to reconstruct size and shape of former polygonal nets. The distances at the top of the Ice Complex elevation (Yedoma) varied between 8 m and 20.5 m. Therefore, a more irregular shape of the ice wedge polygons is suspected. In a slope position near the beach, the distances between thermokarst mounds were smaller between 5 m and 12.5 m. A scarce vegetation of grass and moss covered the dry and sandy surface of the Ice Complex elevation as well as the slopes of thermokarst valleys. Only on the more wet valley floors a denser grass vegetation was growing.

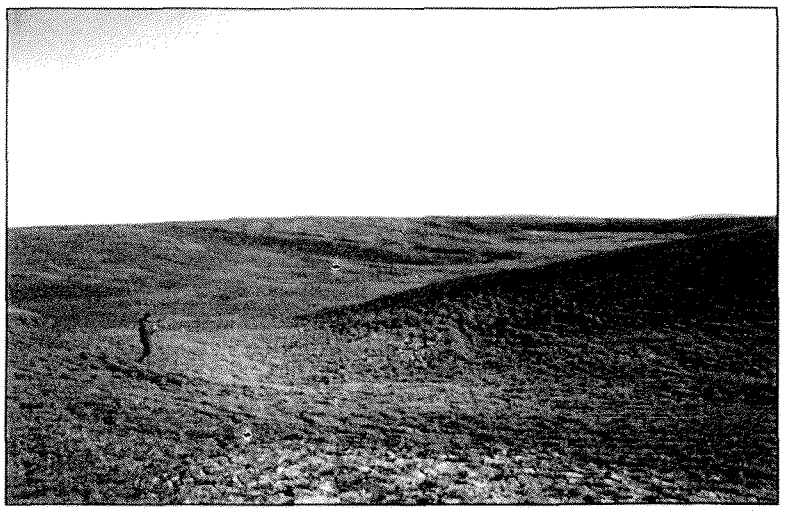

Figure 5.2.2-5: Themokarst valley with thermokarst mounds at the slope of Ice Complex elevations (Yedoma), east coast of Stolbovoy Island

At the east coast of the Stolbovoy Island at 2–4 km north from the Stolbovaya River mouth we found only 13 bones but the main part of these bones was collected at the exposure. Probably two of them (NS-Stl-O1, NS-Stl-O2) belong to an individual of musk-ox and other three bones (NS-Stl-O3, NS-Stl-O4, NS-Stl-O5) belong to an individual of horse. On the shore M. Grigor'ev found a good fragment of skull of Bison priscus with horn.

5.2.3 Kotel'ny Island – Cape Anisy (16.08.)

The northernmost station of our expedition was the coast of Kotel'ny Island near Cape Anisy (Figure 5.2.3-1). The Palaeozoic basement with Ordovician limestone (Lopatin 1998) is exposed at the beach. The relief near the NE coast of Kote'ny Island is formed by cryoplanation terraces, which extend from the hills (about 100 m a.s.l.) to the sea. Numerous snowfields were observed from a remote location at the steep edges of such cryoplanation terraces. The lowest terrace is a 5 km wide plain between 7-13 m a.s.l. covered by Ice Complex deposits.

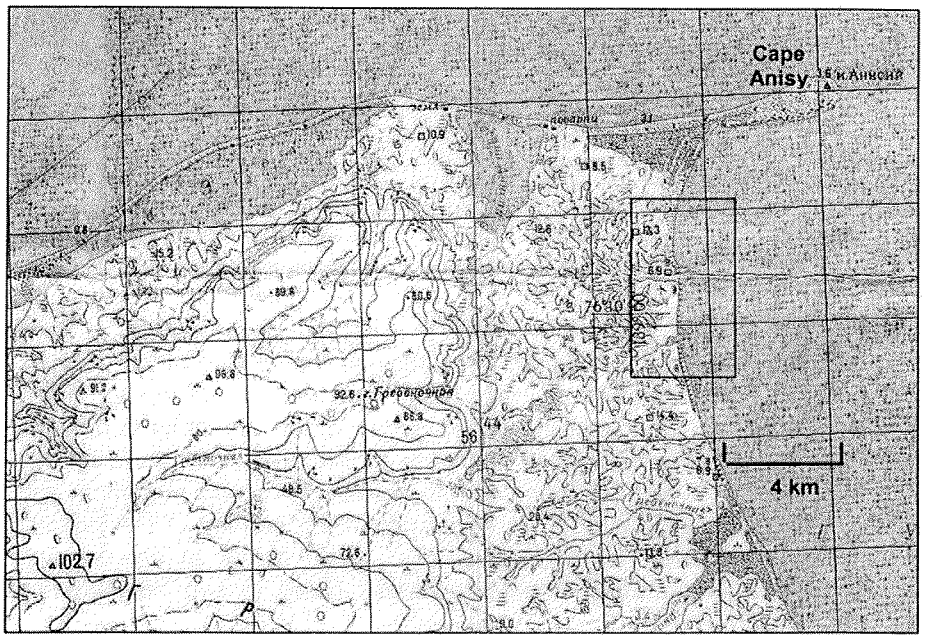

Figure 5.2.3-1: Study area near Cape Anisy with typical relief of cryoplanation terraces

Thermokarst mounds at the surface indicate the occurrence of this ice-rich permafrost deposit. The thermokarst mounds are about 1.5 m high and up to 6 m in diameter. The distances between thermokarst mounds amount to 8.5-18 m and on average are 13 m (Figure 5.2.3-2). Shallow thermokarst valleys (3–5 m deep) with wide (20-30 m) and plain floors cut the surface of the lowest terrace. Shallow brooks flow through the valley floors, where dense grass vegetation grows. The Ice Complex surface is scarcely covered by moss, grass and lichens. Numerous frost boils occur there containing fragments of basement rocks. The maximum thickness of the Ice Complex deposits seems to be 5-10 meters, as concluded from the visible basement outcrop on the beach, the shallow thermokarst valleys and the occurrence of basement rock fragments in frost boils and at valley floors.

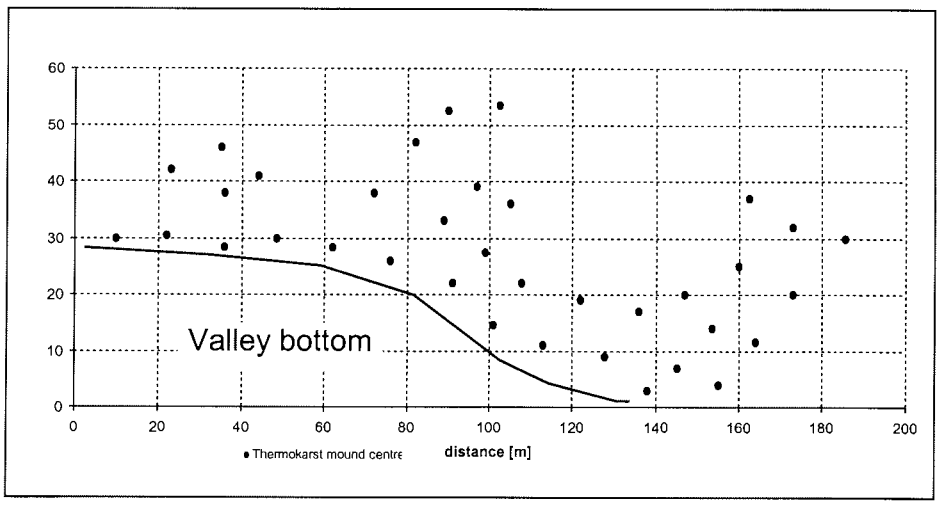

Figure 5.2.3-2: Example of mapping thermokarst mounds on Cape Anisy, N-Kotel'ny. The distances are measured by tape from the centres of thermokarst mounds to neighbouring mounds using a triangulation method. These mounds were situated along the slope of a thermokarst valley within ice-rich permafrost deposits.

Paleontological collection from Cape Anisy does not contain so much samples (49 bones and their fragments) but the most bones were found *in situ*. These bones (31) were collected from the frozen sediments of thermokarst mounds (baydzherakhs) at about 10 m a.s.l., because in this area does not exist any outcrops. We suppose that we found partial skeletons of woolly mammoth and horse. Not only *in situ* bones but also bones from the surface of thermokarst mounds probably belong to these skeletons. Large bones of anterior and posterior legs of *Mammuthus primigenius* were found in two neighbouring thermokarst mounds.

6 bones (NS-KAn-O13 a-f) were found *in situ*, two of them in natural conjunction. Probably two additional bones were moved by frost heaving to the surface of these thermokarst mounds and they belong also to this woolly mammoth' skeleton (Appendix 5.2-3). Vertebras (thorax and cervical), ribs and their fragments mainly belong to a partial horse skeleton(NS-KAn-O30 a-z). All these bones were found *in situ* in one thermokarst mound, which was named "Horse Baydzherakh" (Figure 5.2.3-3). The preservation of bones is very good. We also found two cartilage parts of a rib. Because of the plain area the transport of bones on the tundra surface is insignificant. Some bones, which were found on tundra surface probably belong to an other skeleton - for example, horse's bones (samples NS-Kan-O16 to O20) (Appendix 5.2-3).

As no large profile of Ice Complex deposits was exposed in this area, a pit was dug on the side of a thermokarst mound for geocryological studies (Figure 5.2.3-3). In the same thermokarst mound many horse bones were found. The small profile of 1.5 m thickness consists of greyish-brown cryoturbated silty to

sandy soil with fine lens-like cryostructure and contains a lot of twig fragments. The sediment was relatively poor in ice. An ice wedge (MYA-IW-1) was excavated beneath the frost mound. Three samples were taken from this ice wedge. The ice was grey and milky with numerous small gas bubbles, and it consists of 2-4 mm thick elementary ice veins.

Two additional samples were taken from a peat horizon, which covered a thermokarst mound about 1 km west of the location mentioned above (Mya-peat-1, -2).

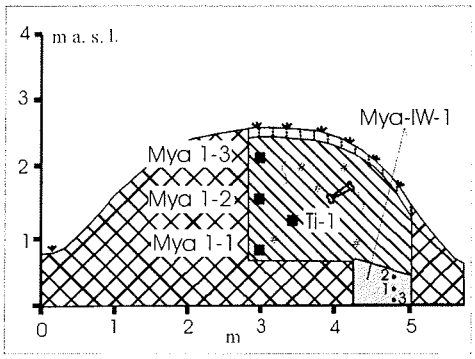

Figure 5.2.3-3: Thermokarst mound ("Horse Baydzherakh") with the sediment profile Mya-1 and the sampled ice wedge MYA-IW-1.

5.2.4 Bel'kovsky Island, Cape Skalisty (Cape Rocks) (17.08.)

A similar relief situation like that on Stolbovoy and Cape Anisy was noted at the south coast of Bel'kovsky Island, which is the westernmost island of New Siberian Archipelago (Figure 5.2.4-2). At least three steps of cryoplanation terraces were observed at about 80 m, 60-40 m and 25 m a.s.l.. According to the geological map, the basement consists of Devonian sedimentary rocks, with faults in NW-SE orientation (Lopatin 1998). The coast consists of alternations of rocky cliffs, Ice Complex fragments and thermokarst as well as thermo-erosion forms. The surface relief of the study area is shaped like a depression, which is bordered by cliffs of the exposed basement in the E and the W. The occurrence of thermokarst mounds directly above the exposed basement rocks indicates, that ice-rich permafrost deposits cover the basement (Figure 5.2.4-1).

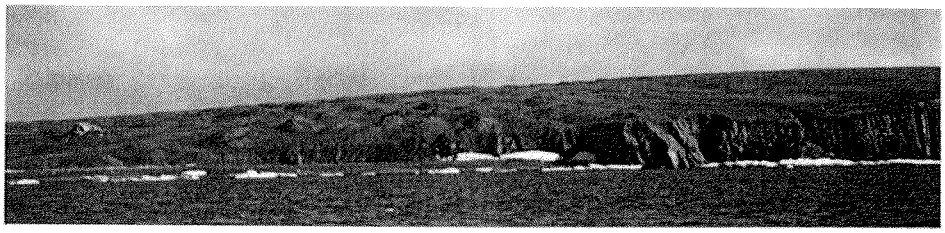

Figure 5.2.4-1: South coast of Bel'kovsky Island, Ice Complex deposits with thermokarst mounds cover basement rocks at the eastern slope of a depression, Cape Skalisty.

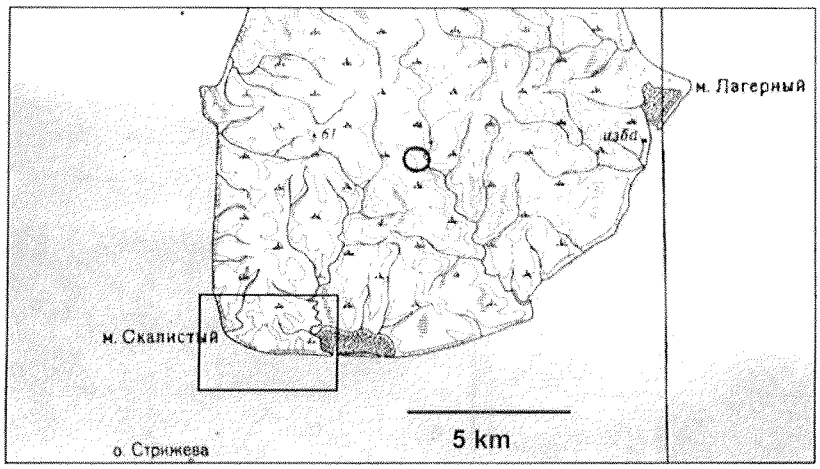

Figure 5.2.4-2 Study area near Cape Skalisty, south coast of Bel'kovsky Island

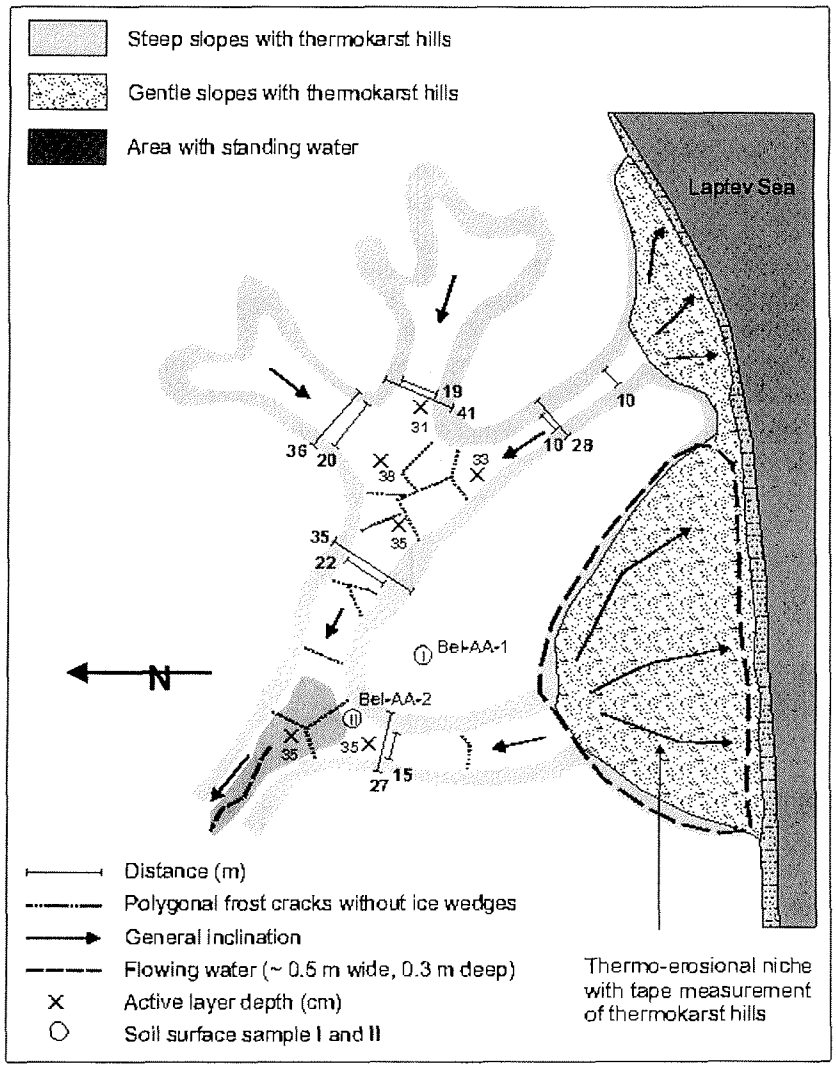

Figure 5.2.4-3: Studied thermokarst valley system at the south coast of Bel'kovsky Island.

Today this depression looks like a thermokarst depression (alas), but it may also be a result of tectonical activities. Several thermokarst valleys cross the alas floor. The valleys are 30 to 40 m wide at the top and 15 to 22 m at the bottom (Figure 5.2.4-3). The valleys are wet and boggy and densely covered by grass. Recent ice wedges could not be sampled, because of the wetness of the active layer. Nevertheless, in these depressions a lot of recent frost cracks were observed forming ideal hexagonal polygons with angles of 120° between the cracks. The active layer there is 31 to 38 cm thick. The general inclination and orientation of one studied valley system is to the northwest, towards the depression centre in the hinterland, instead of towards the sea. Hence, the

valleys were formed during thermokarst formation and their drainage is not influenced by coastal erosion. At the slope of a thermo-erosional niche near the beach (Figure 5.2.4-3) distances between thermokarst mounds were measured by measurement tape. The distances are between 3.5 and 18.5 m with an average value of 11.5 m.

In general, two different types of formations were studied. First, the exposed Ice Complex deposits with 3 to 4 m broad ice wedges. Ice wedges were exposed in a lower beach cliff (0-10 m a.s.l.) and in an upper cliff (15-25 m a.s.l.). Thermokarst mounds covered the central part of the section. The base of the Ice Complex is possibly situated below sea level because of large ice wedges near the sea level (Figure 5.2.4-4). This horizon consists of greyish silty sand containing thin grass roots and shows a banded cryostructure. Further, profiles of alas deposits with fine-laminated lacustrine sediments were studied (Figure 5.2.4-5). They contain shells, small ice wedges in the upper part and ice wedge casts at the base.

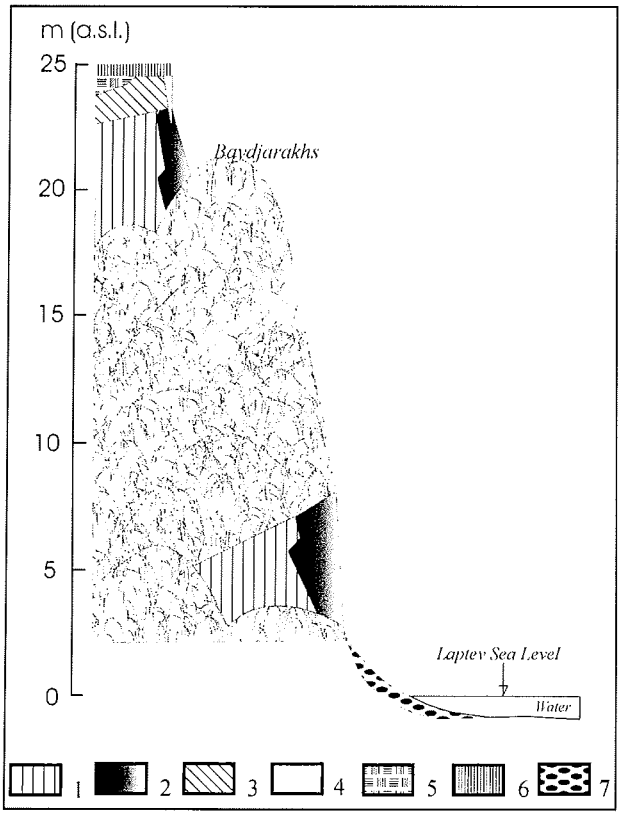

Figure 5.2.4-4:
Schematic profile of a Ice Complex fragment of the 25 m cryoplanation terrace, south coast of Bel'kovsky Island

1 – Silty sand (aleurite), light-grey, layered, with grass roots and ice belts;
2 - Ice wedge, grey, 3-4 m wide, dense, rarely with small sediment veins;
3 – Silty sand with small peat nests and shrub roots and twigs, lens-like cryostructure;
4 – Ice wedge, white, less dense,
1 m wide;
5 – Moss peat, brown, with lenses of silty sand and with shrub roots, ice-rich, supersaturated
6 – Active layer;
7 – Strand pebbles

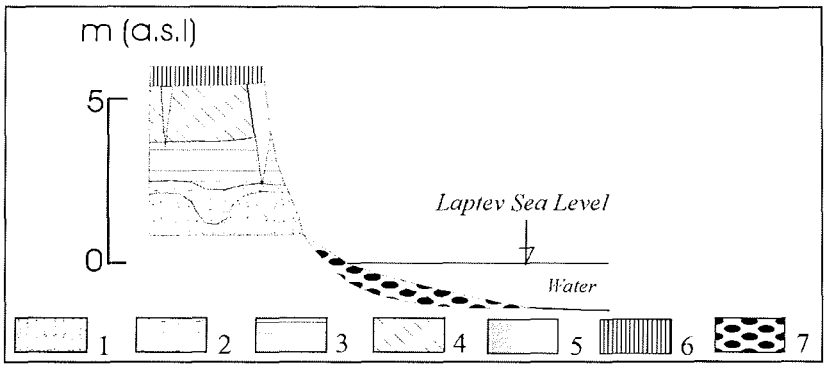

Figure 5.2.4-5: Schematic profile of an alas sequence.
1 – Silty sand, bluish-grey, deformed, loamy, skew lattice-like or lens-like cryostructure; 2 – Silty sand grey to bluish-grey, alternating with laminas of plant detritus, within ice wedge casts, lens-like cryostructure; 3 – Silty sand, grey, fine- laminated, skew or horizontal lens-like bedded cryostructure; 4 – Silty sand, dark-grey, with peat nests and grass roots, lens-like reticulated cryostructure; 5 – Ice wedge, white, small (1.2 m wide), less dense; 6 – Active layer; 7 – Strand pebbles.

All together a coastal section of about 1 km extension was studied in seven sub-profiles representing different stages of the landscape history (Figure 5.2.4-6A to J).

The easternmost section was the sub-profile Bel-3, where the Ice Complex horizon was exposed at about 3.5 to 5 m a.s.l. (Figure 5.2.4-6B). An ice wedge (BEL-IW-1) exposed about 2.5 m in width and 1.5 m in height was sampled here. In total, 21 samples were taken in 10 cm intervals with an ice screw from the right to the left. The height of the horizontal sampling transect was estimated to be at 4 m a.s.l. The ice wedge consists of grey, transparent, most likely Pleistocene ice and was estimated to be part of the Ice Complex. Many gas bubbles, which were small (<1 mm) and spherical, and not elongated were noticed in the ice. Additionally, numerous subvertical structures were observed such as 2-4 mm wide elementary ice veins and few elongated sediment veins of several decimetres in length. Hence, the ice wedge was relatively rich in sediment. The subvertical structures were cut by cracks without filling extending from the upper left to the lower right side of the ice wedge. These cracks did not seem to be related to regular frost cracking activity rather to other mechanical tensions in the permafrost. The ice wedge seemed to be subject to sublimation, which leads to a weathered appearance of the crust of the ice wedge. Therefore, this outer crust was discarded from sampling. In addition, three samples of Ice Complex deposits were exemplarily taken there. It was the typical grey silty sand with grass roots and fine lens-like reticulated cryostructure (gravimetric ice content 41 wt %)

In a distance of about 105 m to the West a 0.2 m wide and 0.7 m high ice wedge was exposed in the small sub-profile Bel-4 at about 2.5 m a.s.l. (Figure 5.2.4-6F). This ice wedge is composed of very clear, transparent ice with a lot of gas bubbles interrupted by yellowish sediment veins. This clear vertically-

striped alternation of ice and sediment veins (tiger-striped ice), so-called "Polosatic ice" (Kunitsky 1998), points to relatively dry winter conditions and high sediment supply. This may lead to the competition of the frost crack filling either by snow melt-water or by sediment. The single ice veins are 2-8 mm wide and very easily recognisable. Narrower veins are observed in the middle part and wider veins near the edge of the ice wedge. The sediment streaks are 1-3 mm wide. The sediment beneath the ice wedge is the same material as described above.

The sub-profile Bel-2 was situated 180 m west of the first profile. This was a thermokarst mound with Ice Complex deposits covered by a 0.5 to 0.8 m thick peaty soil (Figure 5.2.4-6A), which was observed in flanking mounds, too. In the lower part the silty sand is brownish coloured cryoturbated and has a lens-like cryostructure. No ice bands occurred. This cryosol is overlain by grey silty sand with fine lens-like reticulated cryostructure with ice bands. The gravimetric ice content of this frozen material is between 70 and 90-wt %. This part does not contain any large plant remains. Finally a peaty cryosol with large peat nests and shrub roots closed this profile.

About 560 m West of the first point Bel-3 the upper part of alas deposits were exposed in the sub-profile Bel-5 (Figure 5.2.4-6C). In a 20 m wide and 1.6 m high outcrop, the top being 5 m height a.s.l., Six sediment samples were taken in different positions of the outcrop. One sample was recovered from the brownish peaty soil of a 25 cm thick active layer. Second one origins from a transition horizon, which was characterised by brownish-grey, peat- and ice-rich silty sand with some clay and regular-reticulate cryostructure. The other samples were retrieved from deposits with brownish-grey ice-rich silty sand and a coarse irregular-reticulate cryostructure. Four different Holocene ice wedge generations were sampled in alas deposits. The ice wedge BEL-IW-3 is 2.3 m wide and consists of white, milky and very clean ice with big ice crystals and contains a few organic remains (mainly moss fragments). The right part of the ice wèdge belongs to a second small ice wedge connected with the main ice wedge. A number of 12 samples were retrieved from this double ice wedge by means of an ice screw in a horizontal sampling transect at ca. 4.1 m a.s.l. Elementary ice veins are relatively difficult to differentiate, in general between 2-5 mm wide and rich in small bubbles of about 1 mm in diameter.

A recent ice wedge (BEL-IW-6) penetrating into a Holocene ice wedge (BEL-IW-4) was sampled together with the Holocene ice wedge in alas deposits near the ice wedge BEL-IW-3 (Figure 5.2.4-6C). The ice of the Holocene ice wedge was clean, milky-white and characterized by large ice crystals (up to 0.5-1.0 cm in diameter). A frost crack and a recent ice wedge were located above the Holocene ice wedge. The thickness of the active layer is about 35 cm. The width of the upper part of recent ice wedge (ice vein) amounts not more than 0.5-0.8 cm (sample BEL-IW-6-1). This Ice was transparent and yellowish. The width of ice vein is increased with the depth up to 4-5 cm (sample BEL-IW-6-2) because of the penetration into older ice veins. The width increased up to 15 cm when the recent ice wedge penetrated into the Holocene ice wedge (sample

BEL-IW-6-3). Transparent and clean ice of the recent ice wedge are visible in the milky-white Holocene ice down to the depth of 30-40 cm (sample BEL-IW-6-4). Four samples of the Holocene ice wedge were also collected.

Ice wedge casts containing lacustrine deposits and allochtonous peat lenses were observed at the sub-profiles Bel-7 and Bel-8 directly above the beach level. The sub-profile Bel-7 is situated 80 m west of Bel-5. A 2 m long and 2.5 m broad ice wedge cast is exposed there (Figure 5.2.4-6D). The layer below the ice wedge cast consists of bluish-grey clay. The cast structure is filled by fine-laminated silt-organic-sand alternations, which are bent parallel to the cast structure. This indicates a post-sedimentary thawing within a thermokarst depression forming ice wedge casts. The cast structure is overlain by greyish-brown silty sand with fine-laminated cryostructure. More disturbed was the ice wedge cast of the sub-profile Bel-8 (Figure 5.2.4-6E), which is situated at about 100 m west Bel-7. Fine-laminated black-white silt-organic alternations occur as well as peaty sands with shrub twigs, allochtonous moss peat with shrub remains, and yellowish fine sand. The ice wedge cast is covered by homogenous grey sediment with mussel-shells.

Finally, large ice wedges of about two meters width were observed in a distance of about 850 m from first sub-profile Bel-3. The ice wedges were overlain by a lacustrine horizon of silt-organic alternation. Further up a smaller milky ice wedge was found, that appeared like a Holocene ice wedge. Numerous sand fans, formed during thawing and flowing out of permafrost deposits, cover the beach there. Various shapes of such sediment fans were measured. A single fan was about 5 m long and 4 m wide. The sand cover was only 3-4 cm thick near the outflow and 40-42 cm thick in front of the sand fan. Numerous fans of various shapes overlay each other. The fan material is eroded periodically by normal wave erosion, hence it is a factor of coastal erosion without strong wind and waves.

Paleontological material from the south coast of Bel'kovsky Island was meagre - only 18 bones were found. The most interesting bones are six bison bones, which were collected on the exposure. According to conservation and position these bones probably belong to one individual.

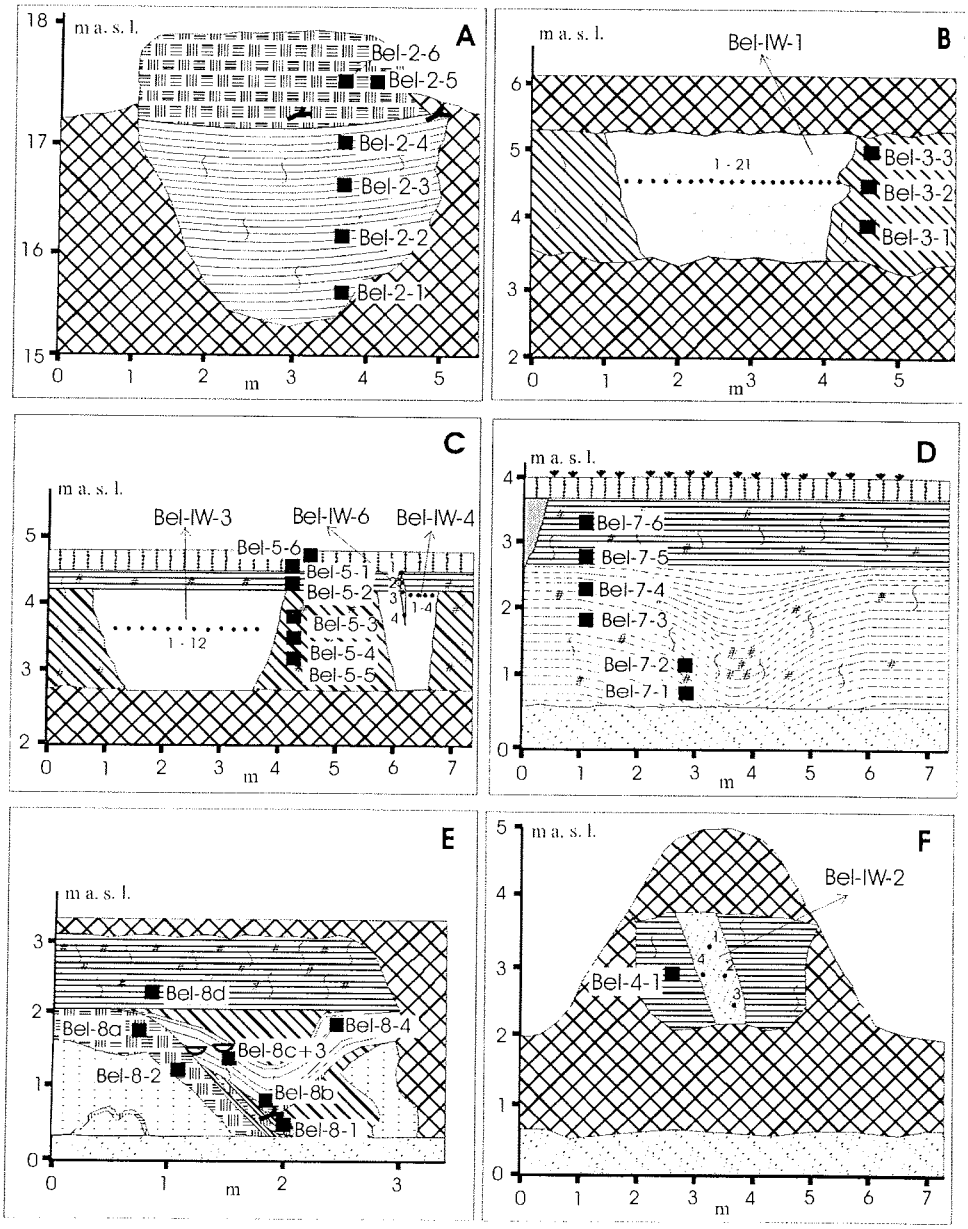
A
m a. s. l.
Bel-2-6
Bel-2-5
Bel-2-4
Bel-2-3
Bel-2-2
Bel-2-1
B
m a. s. l.
Bel-IW-1
1 - 21
Bel-3-3
Bel-3-2
Bel-3-1
C
m a. s. l.
Bel-IW-3
Bel-IW-6
Bel-IW-4
Bel-5-6
Bel-5-1
Bel-5-2
Bel-5-3
Bel-5-4
Bel-5-5
1 - 12
1 - 4
D
m a. s. l.
Bel-7-6
Bel-7-5
Bel-7-4
Bel-7-3
Bel-7-2
Bel-7-1
E
m a. s. l.
Bel-8d
Bel-8a
Bel-8-4
Bel-8c+3
Bel-8-2
Bel-8b
Bel-8-1
F
m a. s. l.
Bel-IW-2
Bel-4-1
m

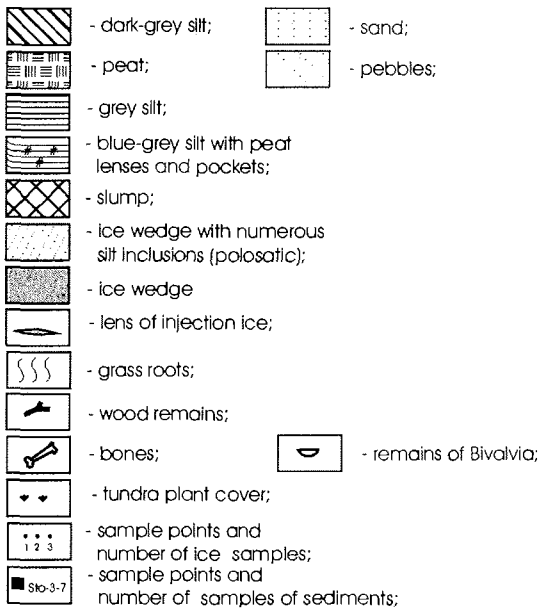

Figure 5.2.4-6: Schematic sketch of the studied sub-profiles of Bel'kovsky Island A – Sub-profile Bel-2, B – Sub-profile Bel 3 with the ice wedge Bel-IW-1, C – Sub-profile Bel 5 with the ice wedges Bel-IW-2, IW-4 and IW-6; D – Sub-profile Bel 7; E Sub-profile Bel 8; F – Sub-profile Bel 4 with the ice wedge Bel-IW-2

5.2.5 Kotel'ny Island, south coast – Khomurgannakh River mouth (18.08)

The general relief at the south coast of Kotel'ny Island again is dominated by cryoplanation terraces reaching from the Sogurum Tas hill (172 m a.s.l.) down to the sea (Figure 5.2.5-1). On the step edges of terraces some snowfields were observed. The lowest terrace at about 20 m a.s.l. is covered by Ice Complex deposits. Thermo-erosional valleys with steep slopes, plain bottoms and shallow brooks, cut the surface there. In these valleys ice wedge polygons of 30 to 40 m diameter were formed. They are 3 to 3.5 times larger than those of the Ice Complex indicated by distances of thermokarst mounds.

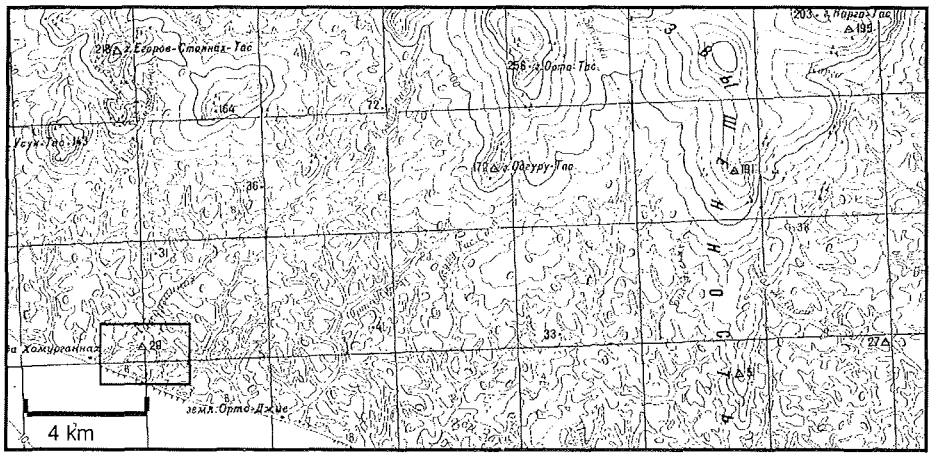

Figure 5.2.5-1: Map of the studied coastal section near the Khomurgannakh River mouth

The TSP was placed on the bottom of a wide and flat depression of the coastal cliff. The surface was covered by scarce vegetation of grass and lichens. Hummocks, frost boils and small polygons formed the patterned ground on the depression floor. Here, the active layer is 45 to 50 cm thick. In addition, several erosion forms were observed during the walk along the coast, e.g. steep ravines with brooks and U-shaped, 25 to 30 m broad thermo-erosional valleys. Brook deposits contain debris and pebbles up to 30 cm in diameter.

At the coast only one section with two sub-profiles in a distance of 1.5 km from the Khomurgannakh River mouth was studied in detail. The general situation is shown in Figure 5.2.5-2. Of the two observed units the lower unit consists of coarse-grained yellowish weathered material (cryogenic eluvium) and contains an about 1.5 m wide ice wedge, which was totally embedded in the coarse-grained deposit.

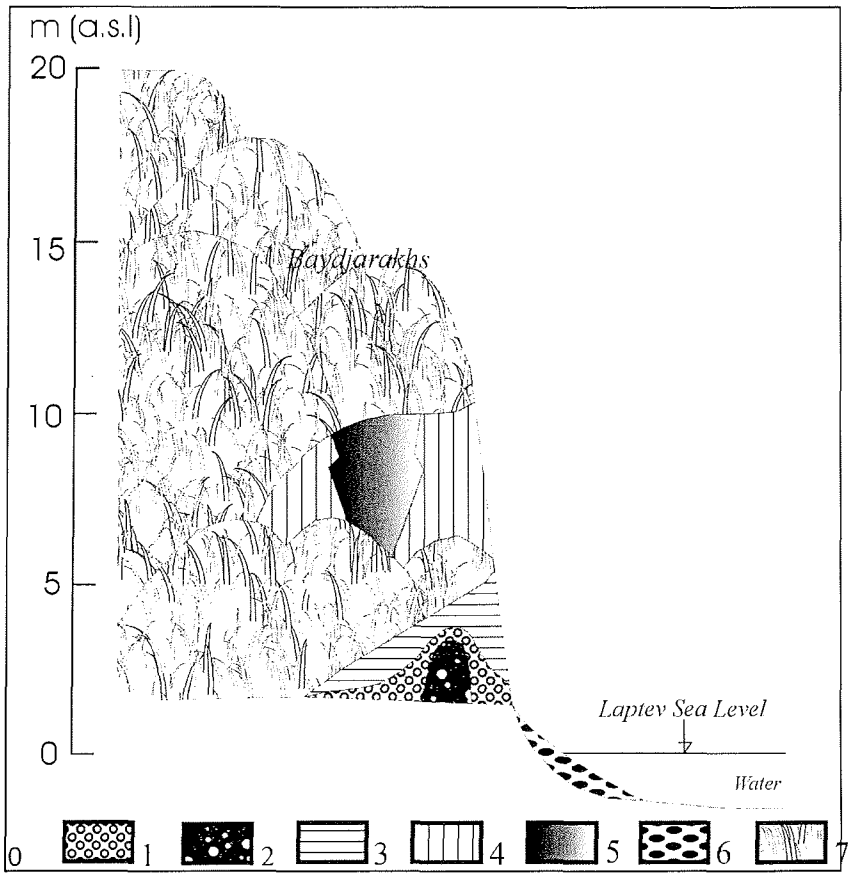

Figure 5.2.5-2: Scheme of the profile Kys 2 of the Ice Complex fragment of the 20 m cryoplanation terrace near the Khomurgannakh River mouth
1 – Gravel layer, yellowish-brown, small, with sandy loamy matrix, crusts and nests of segregation ice, 2 – Ice wedge, yellowish-brown, with a lot of sediment veins and inclusions of gravels, "Polosatic"; 3 – Silty sand, grey-blue to grey, in parts black, small peat nests (5-10 cm Ø), thin ice bands; 4 – Silty sand, dark-grey, with thin grass roots, 3 to 5 cm thick ice belts; 5 – Ice wedge, grey, any grey silt veins, 4 m thick, small rim of brownish silty sand; 6 – Beach pebbles; 7 – Active layer surface with thermokarst mounds

At about 2.5 m a.s.l. an ice wedge (KYS-IW-2), 1.5 m high and 1 m wide, was excavated. It shows a characteristically rounded head with upward bound ice bands above the ice wedge (Figure 5.2.5-3). A similar ice wedge was observed near the beach on Stolbovoy Island (see chap. 5.2.2, Figure 5.2.2-4A). The ice wedge is enclosed in sediment containing at lot of sub-rounded yellowish gravel, and also the ice itself contains some pebbles. A similar feature is found on Bol'shoy Lyakhovsky Island near Zimov'e River (Rachold et al. 2000). Additionally, large gas bubbles (1-2 mm in diameter) were observed in the ice. The ice wedge ice is of white colour interrupted by dark grey to black parts, probably because of a varying content of organic matter in the ice. The vertical structures, such as elementary ice veins, are evident especially in the upper

part of the ice wedge. Six samples were taken in 15 cm intervals in a height of about 3 m a.s.l., additionally one sample of organic matter for radiocarbon dating at about 2.7 m.

The ice wedge was surrounded by yellowish ice-rich sandy gravels and debris (gravimetric ice content about 40-wt %), consisting of sub-rounded pebbles. This material was pressed up by the ice wedge. The deposits were undisturbed and layered horizontally only at a distance of 1 m besides the ice wedge. Ice-rich grayish silty sand (aleurite) with single non-rounded stones, a coarse lens-like cryostructure and ice bands occur. The next layer consists of ice-poor silty sand followed by an alternation of sandy gravels and ice bands. An about 0.5 m thick ice-rich gravel layer was bent by the head of the ice wedge. The next layer was an alternation of peat laminas and ice-rich gray silty sand with lens-like reticulated cryostructure. In general, the coarse-grained layers seem to be of fluvial origin. This unit is covered by a cryoturbated paleosol consisting of sandy and organic-rich layers and have a lens-like reticulated and ice-bent cryostructure. Above the paleosol, a 2 m thick horizon follows, which consists of ice-rich silty sand and contains numerous peat nests (Ø 10 cm) and single stones and ice bands.

The middle part of the section was covered by thermokarst mounds and debris and was not studied therefore. However, below the top of the cliff Ice Complex deposits of about 1.2 m were exposed. Two broad ice wedges framing a sequence of greyish to brownish ice-rich silty sand with small ice bands, broken lens-like cryostructure and small grass roots (gravimetric ice content 52 to 82 wt-%) was found there. A small ice wedge penetrated into the sediment beside the large ice wedge (Figure 5.2.5-3B). A small zone was coloured by brownish iron oxide at the contact between the ice wedges and the sediment packet. In this section at about 8 m a.s.l., two ice wedges were examined. A broad ice wedge at the left side (KYS-IW-1) was sampled in 20 cm intervals from right to left. In total, 18 samples were taken from this 3.5 m wide ice wedge. This ice wedge contained a lot of organic matter, especially lemming coprolithes as well as plant remains. Two of these coprolithes could be sampled in frozen state for radiocarbon analyses. According to former datings, lemming coprolithes have been proven to give highly reliable ^{14}C ages. The ice wedge is characterised by greyish milky ice, which is not typical for the Ice Complex because of its turbidity. This is due to the large quantity of gas bubbles, which mostly are smaller than 0.5 mm. Single ice veins are moderately to recognise and in general between 1.5 and 3 mm thick. From a smaller ice wedge of a younger generation (KYS-IW-3), 2 samples were retrieved. This ice wedge is 8-10 cm wide, and penetrates KYS-IW-1, and crosses the ice belts besides the other sampled ice wedge. The ice veins are easily to recognise and between 2 and 5 mm thick.

30 bones and their fragments were found at the south coast of Kotel'niy Island near the Khomurgannakh River mouth. It is unusual, that there is no one bone from the shore. This can only be explained little coastal erosion. The same processes are on the Belkovsky Island. All bones were collected on the

exposure, on thermokarst mounds in coastal outcrops as well as in the tundra. For parts of them the initial stratigraphical position could be reconstructed (Appendix 5.2-3).

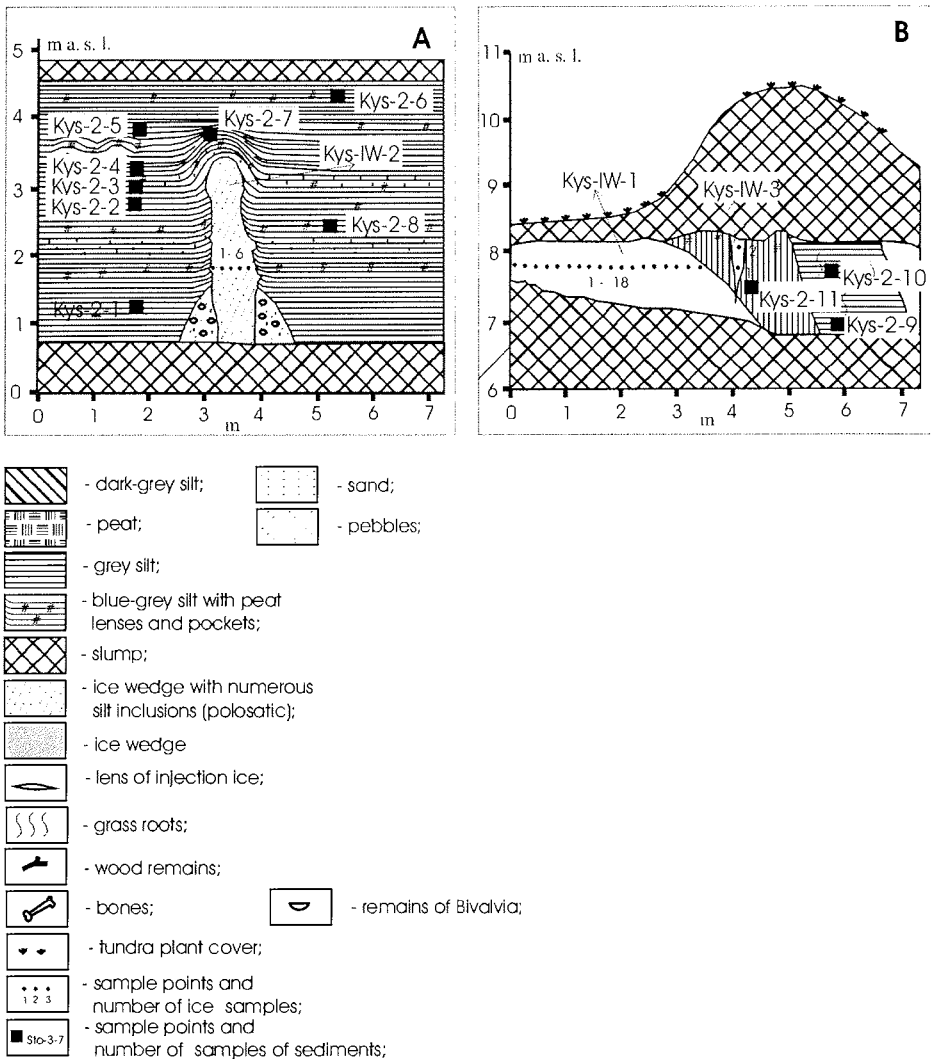

Figure 5.2.5-3: Schematic sketch of the studied sub-profiles of Kotel'ny Island south coast, site Khomurgannakh;
A – Lower part with an old buried ice wedge;
B – Upper part with Ice Complex deposits.

5.2.6 Bunge-Land (19./25.08)

Bunge-Land is one of the least studied regions of the New Siberian Archipelago. The largest part of Bunge-Land is a flat, sandy plain with heights between 2-12 m (low terrace) and a very gentle inclination towards the sea. Only in the southeast a small area of about 25 x 15 km extension has a higher surface (11 to 21 m a.s.l.) with a stronger relief (high terrace). According to the modern map of Quaternary deposits (Ivanenko 1998), the low terrace is a Holocene marine terrace and the higher level a Pleistocene marine terrace.

Large areas of the low terrace are episodically flooded during storm surges mainly up to the level of about 2 m a.s.l. (Figure 5.2.6-1). The surface is not covered by vegetation and can be classified as Arctic desert. Driftwood is found in some kilometres distance from the coast. The surface of this area is covered by water saturated thixotropic sand and the active layer is maximum 0.6 m thick.

The TSP was placed within the wet, homogenous sand surface about 100 m from the shoreline.

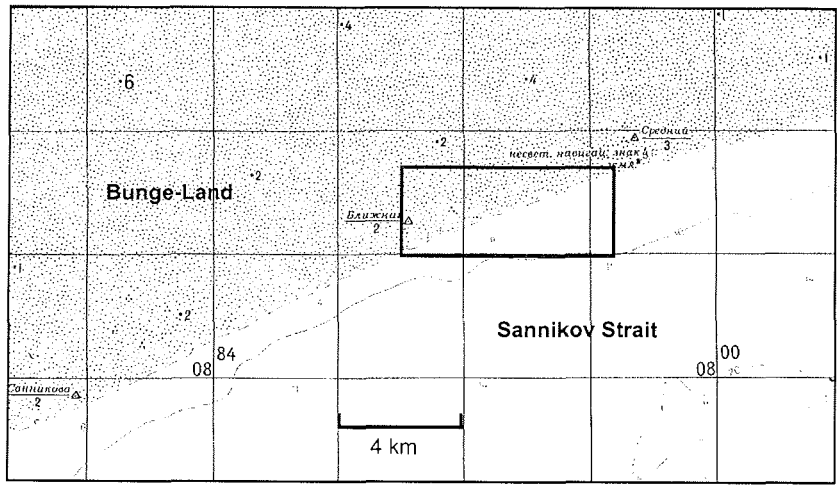

Figure 5.2.6-1: Study area on the low terrace of Bunge Land

A small, elevated (3 m a.s.l.) area close to the coast was scarcely covered by grass tussocks. The size of this area was about 400 x 600 m. Separate grass hummocks occurred in a distance of 1.5-2 m. The active layer there was about 95 cm below grass hummocks and 20-40 cm in the inter-spaces. The small depressions between grass hummocks are comparable with small deflation hollows.

A pit down to the permafrost table was dug on this elevated area (Figure 5.2.6-2). The small profile consisted of frozen silty fine-grained sand (gravimetric ice content 34 wt %), followed by unfrozen dark gray fine sand with clay inclusions or nests. The upper horizon of about 50 cm thickness was formed by a wet, brownish-grey fine to medium sand with grass roots. Three samples were taken there for sedimentological analysis (Bun-7-1 to 7-3) and two samples for OSL-dating (Bunge 4 & 5). Unfortunately, recent ice wedges were not found in this place.

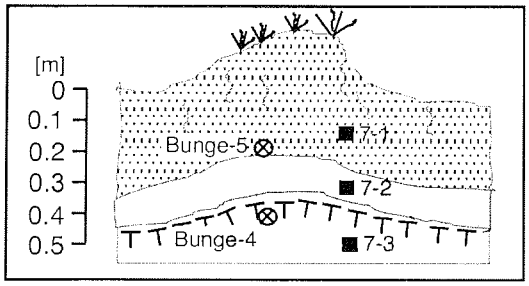

Figure 5.2.6-2:
Sub-profile Bun-7 on the low terrace of Bunge-Land

The relief character of the high terrace of Bunge-Land is totally different. The study area was located southeast of the polar station "Zemlya Bunge". The TSP was placed near the polar station for about 8 hours. The scarce vegetation consists of dry grass tussocks and moss and is covered by yellowish fine sand with pebbles. The surface (20-10 m a.s.l.) is a landscape, weakly inclined towards the sea and crossed by wide valleys with flat bottom and periodical streams. The vegetation of this area is more dense than on the low terrace of Bunge-Land, but also scarce. Only on the valley bottom more grass is growing. Several initial thermokarst lakes occur in the areas between the valleys. The diameter of one small lake amounts to 60 x 80 m. Its water-depth was 0.4 m and the active layer thickness about 0.6 m. Lake deposits (Bun-1) and lake water were sampled there. A depth profile was measured from the shore of a large lake (800 x 600 m) near the polar station. This lake is very shallow – 0.5 m deep at a distance of 100 m from the shore. The active layer thickness is almost constant at about 0.1 m. Lake sediment (Bun-2) and lake water were sampled at a distance of 7 m from the lake shore.

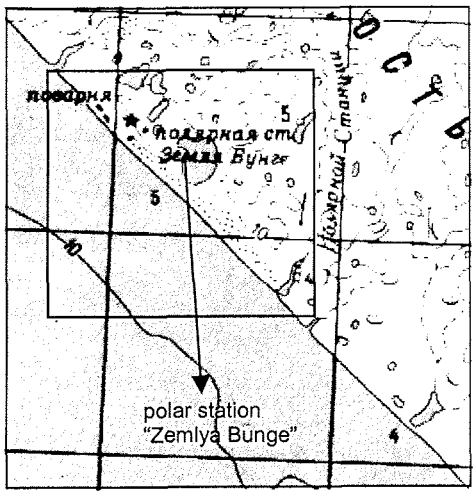

Figure 5.2.6-3:
Study area of Bunge-Land high terrace near the polar station „ Zemlya Bunge".

The detailed studied sections were located about 2 km Southeast of the polar station (Figure 5.2.6-3). Thermokarst mounds were visible at the terrace slopes as well as on valley margins, indicating the existence of ice wedge polygonal nets. Although frost cracks were visible there, we were unable to find recent ice wedges on the beach. The schematic profile of the Bunge-Land high terrace is presented in Figure 5.2.6-4. Ice wedge polygons were found especially in higher areas between the valleys. They have diameters of 18-20 m. Small, 0.3 m deep trenches often outline the polygons. One small frost crack was dug during our studies (Figure 5.2.6-5). A thin ice vein shades away into a composite ice-sand wedge or so-called "Polosatic" – a vertically striped alternation of ice and sediment veins. The ice veins as well as the "Polosatic" structure were sampled for stable isotope and tritium analyses.

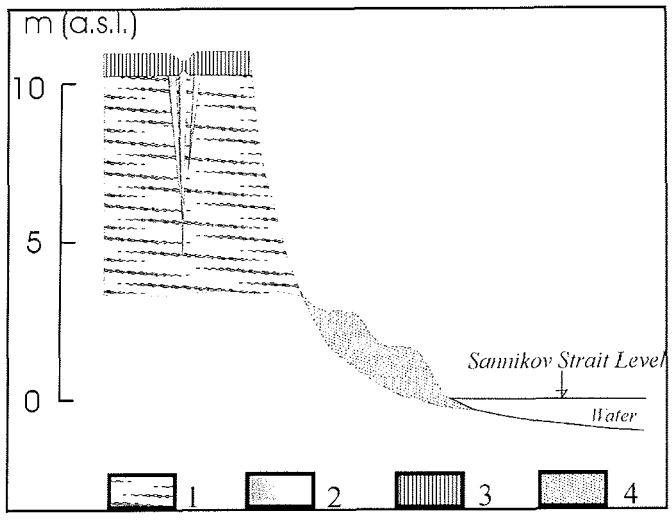

Figure 5.2.6-4:
Schematic profile of Bunge-Land high terrace.
1 – Greyish-blue sand, horizontal and cross-bedded, deformed by ground wedges and microfaulting, frozen;
2 – Ice wedge, white, „Polosatic", ice-sediment stripes; 3 – Active layer;
4 – Beach sand, yellowish-grey, cross-bedded, with gravels and pebbles, permanently frozen.

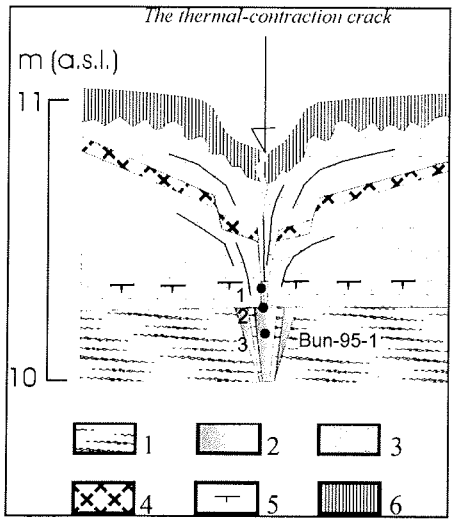

Figure 5.2.6-5: Schematic Profile of the active layer with the upper part of a so-called „Polosatic" on Bunge-Land, high terrace.

1 – Fine and greyish-blue;
2 – Ice wedge, „Polosatic";
3 – Fine sand, lightgrey with humic laminaes;
4 – Fine sand reddish-brown, riddled with iron and manganese;
5 – Permafrost table
6 – Fine sand, dark grey, with roots.

In addition, a 4 m thick section with two sub-profiles was studied in more detail at the steep slope of an erosional valley 2 km southeast of the polar station (Fig. 5.2.6-6). The lower part (1 m) of the sub-profile (Bun-4) consisted of grey frozen, fine sand layers alternating with black organic-rich layers. This interbedding was disturbed syn-sedimentary by small faults. The next part contains thicker sand and organic-rich layers. In general, these two horizons look like lacustrine or stillwater deposits of an old river channel. Their gravimetric ice content was between 18-22 wt-%. The horizon below the permafrost table was brownish coloured spotty, non-bedded, fine sand that was influenced by soil formation. Some 0.4-0.6 m long and about 1 cm wide ground wedges were observed. The gravimetric ice content amounts to about 18 wt-%. The upper horizon of this subprofile consisted of unfrozen, interbedded fine sand, whereas its lower part is strongly cryoturbated.

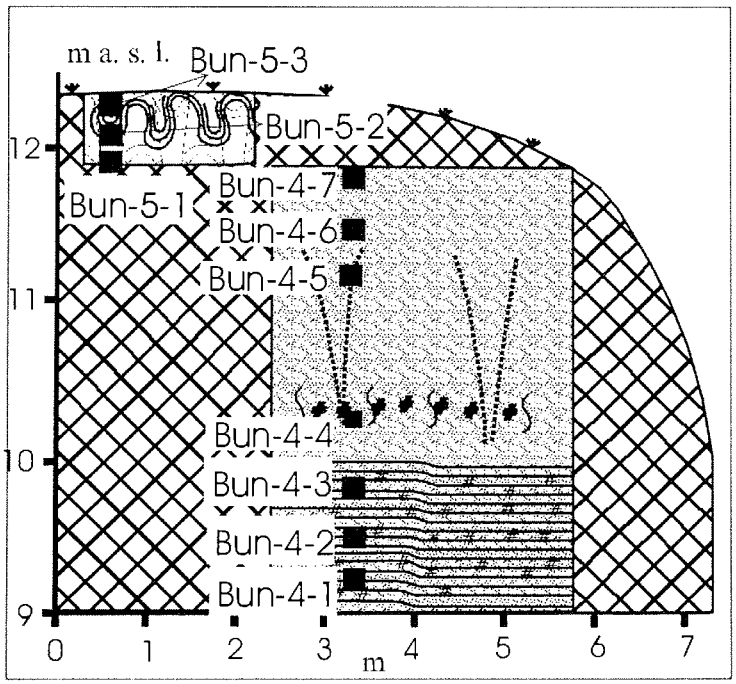

Figure 5.2.6-6: Sub-profiles Bun-4 and Bun-5; Laminated organic-rich sand, cryoturbated soils, ground wedges

The second sub-profile Bun-5 represents the uppermost part of the whole section up to the surface at about 12 m a.s.l.. It is a strongly cryoturbated unfrozen soil, containing dark brown and light brown fine sand layers (Figure 5.2.6-6). In addition to the regular sampled profile 3 samples were taken for IRSL dating there.

Age determination, analysis of grain size, grain shape and heavy minerals as well as pollen analysis could help to understand the genesis of the large desert-like sand plain of Bunge-Land.

5.2.7 Novaya Sibir Island (20./21. 08.)

The southwest coast of the Island Novaya Sibir was the easternmost study region. On August 20th, the very impressive coast section of Derevyannye Gory (Wood hills) and parts of a coastal region named "Urochishche Gedenshtroma" (Location Hedenstrom) were studied (Figure 5.2.7-1).

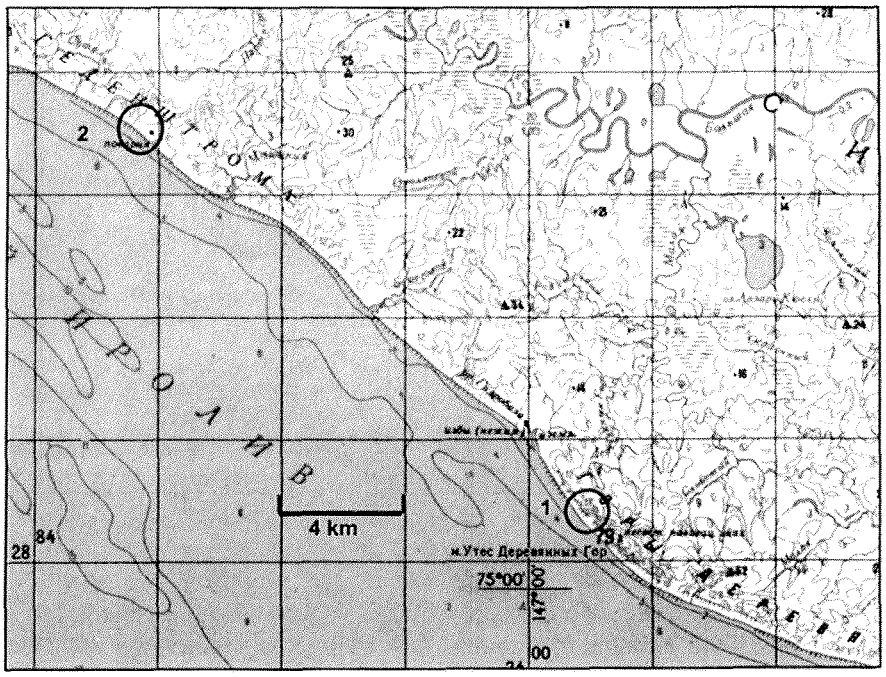

Figure 5.2.7-1: Study areas at the southwest coast of the Novaya Sibir Island
1 – Derevyannye Gory; 2 – Location Hedenstrom

5.2.7.1 Derevyannye Gory

The coast of Derevyannye Gory exposes Upper Cretaceous and Cenozoic loose rocks. By approaching the coast the markant light-dark alternation of sand and coal layers below lighthouse catches the eyes (Figure 5.2.7-3A). This unit is overlain by Paleogene to Neogene silty sands (aleurite) and gravels. The Tertiary deposits were mostly covered by clays, silty sands and sands of the early Quaternary Kanarchasky Suite. According to Parfenov et al. (2001), Jurassic, Upper Cretaceous and Upper Miocene deposits were upfaulted during Late Miocene and early Pliocene (Figure 5.2.7-2).

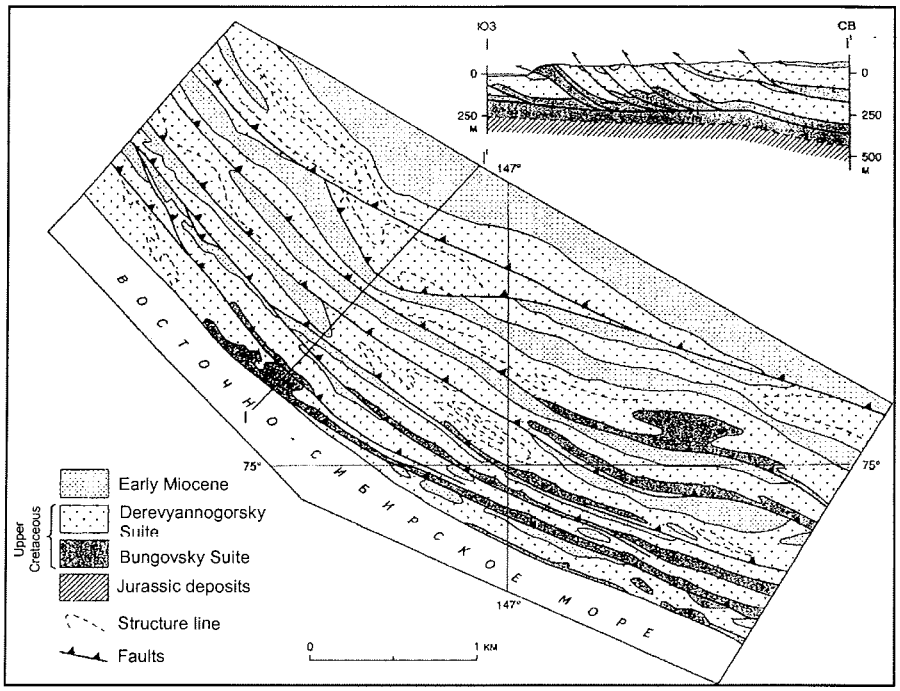

Figure 5.2.7-2: Geological situation of the study site Derevyannye Gory; late Miocene to early Pliocene faults (according to Parfenov et al. 2001)

The upper Cretaceous frozen sand-coal interbedding contained numerous thin coal layers and trunk remains of *Sequoia.* Different types of ice were sampled on Novaya Sibir Island. First, 20 cm long and 5-8 cm wide lenses of injection ice were observed at the contact of old coal deposits with silty gray sediments. Voids in these highly tectonised deposits seem to be filled with very clear and transparent injection ice with a lot of gas bubbles especially in the central part. In addition, remains of snow patches as well as sea ice were observed and sampled near the coast. In a cavity formed by wave erosion, a snow patch was sampled in direct contact with an overlying coal layer. This snow patch consisted of white and brown ice pointing to the percolation of water from above (Figure 5.2.7-3C). A second, 1.5 m thick snow patch was sampled 5 m a.s.l., consisting of clear ice almost without any gas bubbles. These two snow patches are surely influenced by seawater (e. g. by spray), whereas a third one of 1 m (sub)-recent snow was sampled further landwards (without marine influence).

Intensive erosion cuts the island's surface near the coast and the zebra-like stripes of the upper Cretaceous deposits were visible all over (Figure 5.2.7-3B). The erosion seems to be dominated by periodical meltwater runoff from the hills. No vegetation is covering the surfaces, hence the soil is easily transported downhill by running water. These slopes are covered by rock debris with different degrees of rounding. The slopes of Derevyannye Gory hill are also shaped by nivation niches in form of wide kars. The kar bottoms are about 20-

30 m a.s.l.. Single snow fields were observed at the steep walls of such kars. One of these snow patches was about 2 m thick and the thawing-remains, so-called "Chionochonite", did not contain larger amount of plant remains because of the polar desert conditions in the surroundings. Two terraces are formed in about 50 m and 80 m height, respectively. Valley bottoms as well as the terrace surfaces are covered by large pebbles (10-20 cm Ø) and boulders up to 1 m in diameter (Figure 5.2.7-3D). Many of them show traces of striation. They contain a wide spectrum of rocks, like porphyry vulcanite's, gabbroids, granate gneisses, quartzitic sandstones, slates, limestones and others. All these rocks do not occur on Novaya Sibir Island. The origin of this material and the formation of these terraces are still under discussion. The most realistic hypothesis will be the glacio-marine transport of this coarse grained material, perhaps during Early Quaternary periods. Patterned ground with circles, stripes and frost boils were observed in places (Figure 5.2.7-3E).

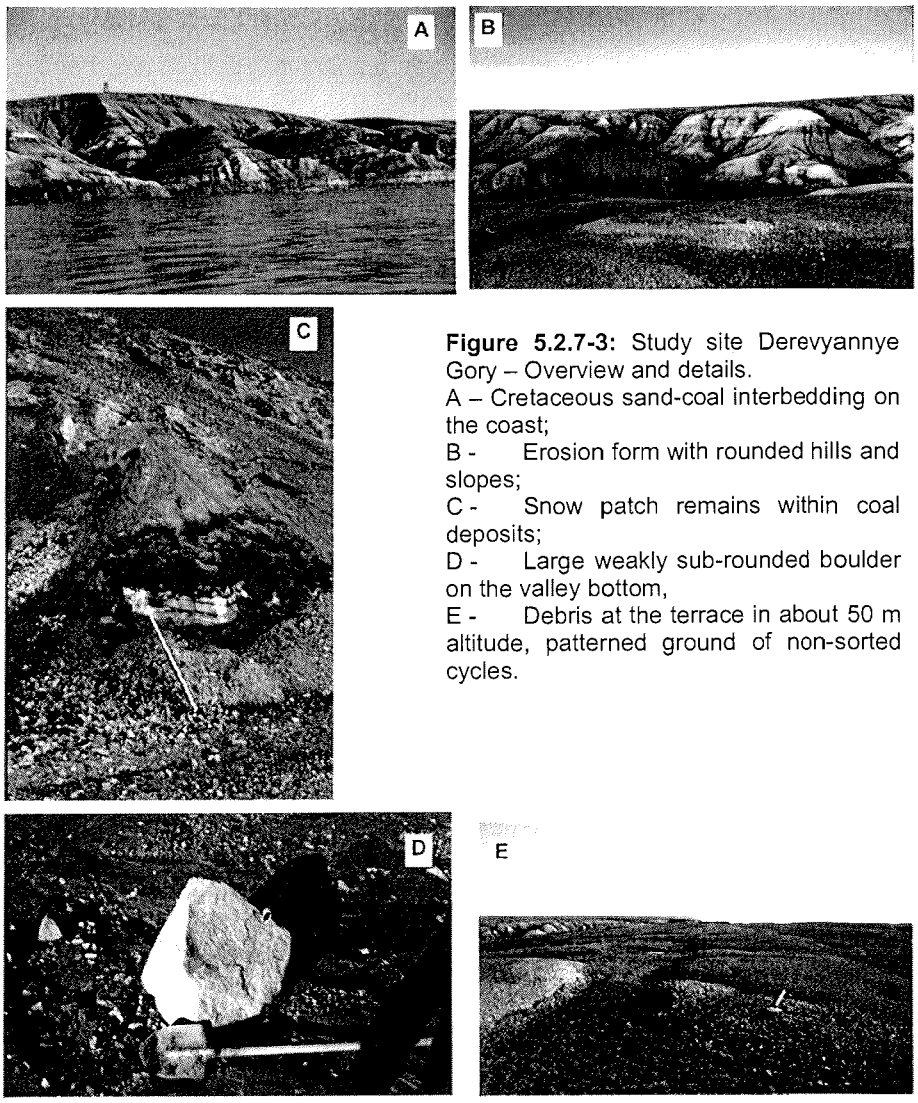

Figure 5.2.7-3: Study site Derevyannye Gory – Overview and details.
A – Cretaceous sand-coal interbedding on the coast;
B - Erosion form with rounded hills and slopes;
C - Snow patch remains within coal deposits;
D - Large weakly sub-rounded boulder on the valley bottom,
E - Debris at the terrace in about 50 m altitude, patterned ground of non-sorted cycles.

5.2.7.2 Island Novaya Sibir - Location Hedenstrom

Frozen marine deposits with terrestrial permafrost deposits were studied for the first time during our expedition at about 40 km NW of Derevyannye Gora along a 2 km long coastal section. The general profile is presented in Figure 5.2.7-4 and shows marine deposits containing ice bodies of unknown origin, Ice Complex deposits as well as alas deposits.

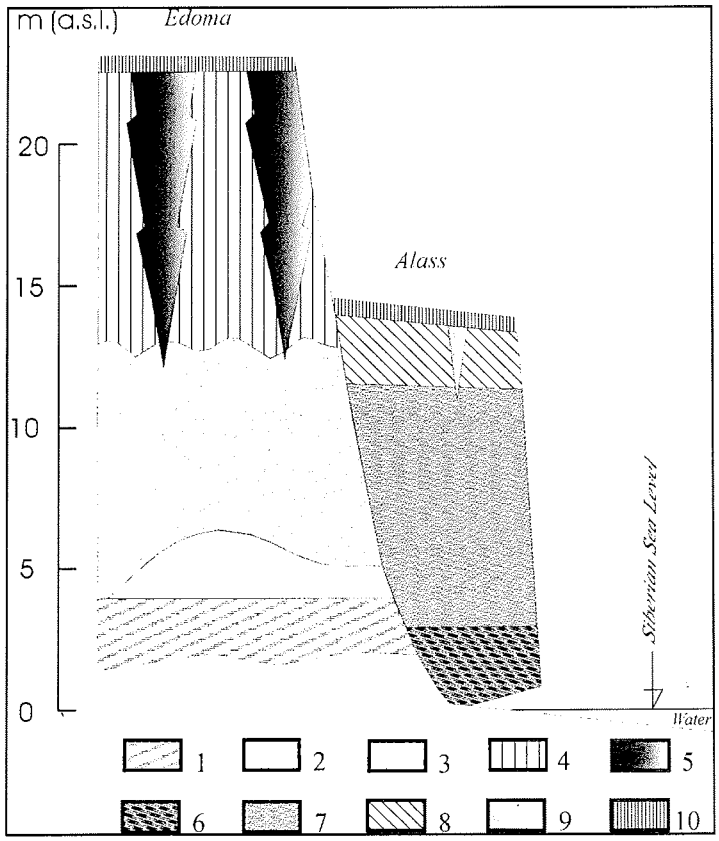

Figure 5.2.7-4: Schematic profile of clayish marine or lacustrine deposits with an ice body framed by alas deposits and covered by Ice complex deposits
1 – Dark-grey, dense silty fine sand (aleurite), bedded, with inclusions of debris, gravels and single pebbles, frozen, blocky cryostructure; 2 – Blue-grey clay, unclearly bedded, with shells of marine molluscs, frozen, blocky or lattice cryostructure; 3 – Transparent ice of unknown origin, dense; 4 – Brownish-grey silty to clayish fine sand (aleurite) with sand lenses with thin grass roots, frozen, ice bands; 5 – Ice wedge, grey, dense, 3 m wide; 6 - Yellow-brown sand of various grain size, with inclusions of gravels, debris and fine sand interlayers, massive cryostructure; 7 – Grey-blue loam, diagonal lattice cryostructure in the lower part, brownish patches and diagonal lens-like cryostructure in the upper part; 8 – Grey loam with thin grass roots, lens-like reticulate or bedded cryostructure, 9 – Small, white ice wedge, 1m wide, 10 – Active layer.

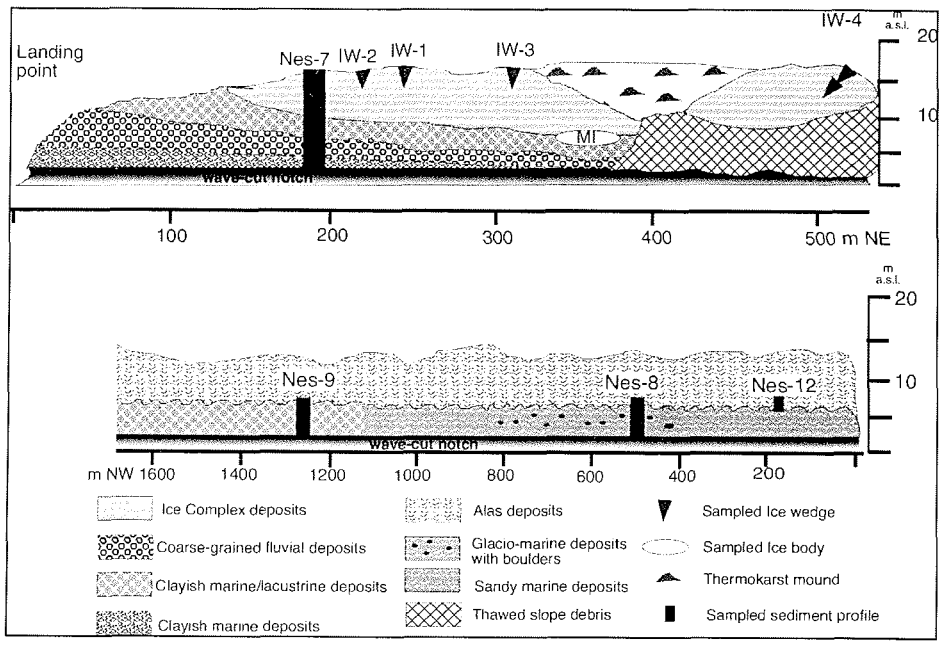

Figure 5.2.7-5: Scheme of sampling positions and general stratification of the study area location Hedenstrom

Several sub-profiles were studied during a stay of 8 hours there (Figure 5.2.7-5). The TSP was placed in a distance of 80 m from the coast line at about 16 m a.s.l.. The surface of this place was characterized by scarce, dry tundra (grass and moss) and frost boils.

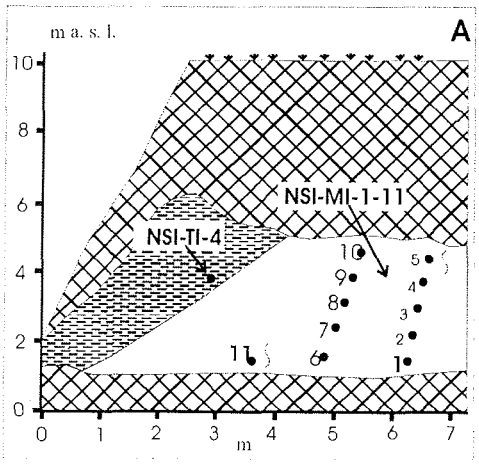

Figure 5.2.7-6: Buried massive ice body NSI-MI with sample positions

In the southern part of the coast section a massive ice body of more than 6 m width and 3 m height was exposed between 3 m and 6 m a.s.l. (Fig.5.2.7-6). Ice-rich deposits overlie the seaward part of the ice body with reticulated cryostructure dipping about 20-30° towards the sea. The inclination of the ice body is similar below the segregated ice. The landward part of the ice body is covered by about 4-5 m of Ice Complex baydzerakhs. This part of the ice body does not show the same inclination, since the structures are rather vertically oriented. This impression is supported by the alternation of different types of ice in this section. A 1.2 m wide zone of milky, white ice with a high amount of very small gas bubbles occurs between two zones of clear transparent ice with some bigger sized gas bubbles (> 1 mm). From this ice body, 11 samples were taken by means of an axe. Five samples were retrieved in different heights from the white and milky ice, six from the clear and transparent ice. Some of these samples contain organic material such as black coal particles (presumably derived from the Dereviannye Gora section) as well as small red organic particles, possibly moss fragments. The genesis of this massive ice body is still unknown yet and its age can be assumed to be older than the Ice Complex. Stable isotope and hydrochemical analyses will help to clarify these questions.

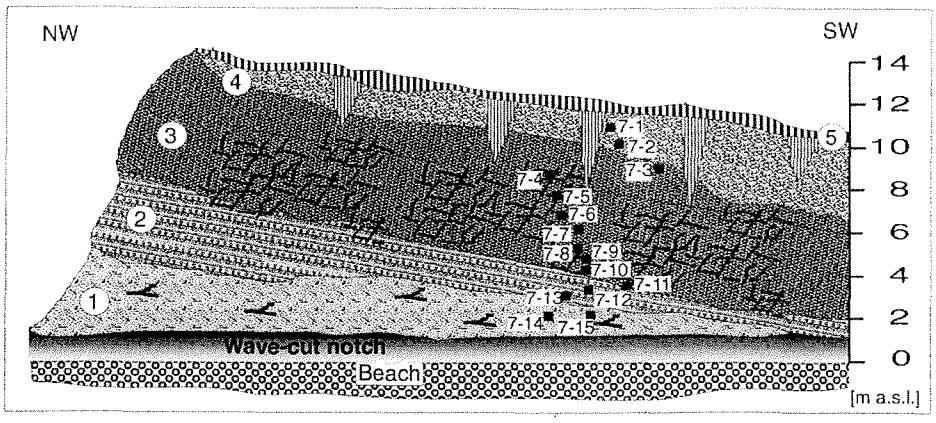

Figure 5.2.7-7: Sub-profile Nes-7, a sequence terrestrial and aquatic deposits at the SW-coast of Novaya Sibir Island; 1 – Silty sand (aleurite), ice banded, shrub fragments; 2 – Interbedding of silty fine sand, coarse-grained sand and gravel; 3 – Bluish-grey clay. diagonal lattice ice veins; 4 – Ice Complex deposits; 5 – Active layer

About 300 m to the north the 10 m thick sub-profile Nes 7 was studied and sampled in detail (Figure 5.2.7-7). Above the wave-cut notch a 0.5-0.8 m thick frozen horizon (gravimetric ice content 47 wt-%) of ice-banded silty fine sand with shrub fragments occurs, which is overlain by 1m thick interbedding of silty fine sand layers and coarse-grained sand with gravels (gravimetric ice content 21-38 wt-%) and thick ice schlieren. Both horizons represent terrestrial deposits and the coarse-grained part was probably of fluvial origin. The following horizon consisted of frozen bluish-grey clayish silt (gravimetric ice content 40-73 wt-%) with a net of diagonal lattice ice veins. Such ice veins are 1-2 cm thick and 10-20 cm long. Ice Complex deposits overlie these aquatic perhaps marine or

lacustrine deposits and show the typical lens-like reticulated cryostructure. The gravimetric ice content amounts to 132 wt-%. Ice wedges at this place penetrated 1 m into the horizon situated below. The transition zone between both horizons is of brown colour because of iron oxide patches. A 0.3-0.4 m thick active layer borders the described profile.

Ice wedges of different generations were studied near this location. In a height of 7 m a.s.l., a 2.2 m wide ice wedge was sampled (Figure 5.2.7-8A). This ice wedge (NSI-IW-1) is of milky, white colour with a lot of very small (0.1-1 mm), slightly elongated gas bubbles. The ice wedge contains a very small amount of sediment and organic particles and vertical structures are poorly recognisable. It is embedded in very ice-rich sediment (Ice Complex ?) with ice belts bound upward near the ice wedge. These features as well as some ice shoulders in the ice wedge point to the synsedimentary growth of this ice wedge. Nevertheless, the appearance of the ice wedge is not typical for Ice Complex but rather for Holocene ice wedges. From this ice wedge, 16 samples were taken (in 15 cm intervals from the left to the right) by means of an ice screw to answer the question, whether this ice wedge is of Holocene age or older, and to understand if these ice wedges are formed without simultaneous sedimentation. Secondly, four samples of ice wedge and four samples of texture ice (ice belts in the contact of the ice wedge) were gained from a narrow ice wedge (NSI-IW-2) approximately in the same level of the (Ice Complex ?) deposits as NSI-IW-1. It shows nice ice belts in the sediment and ice wedge shoulders, the contact of which was sampled in detail (Figure 5.2.7-8B).

80 m further to the SE, a third ice wedge was studied (NSI-IW-3). This 0.4 m wide and 2.2 m high ice wedge is surrounded by ice-rich Ice Complex deposits (Figure 5.2.7-8C), but in contrast to NSI-IW-1, the ice belts are not bound upward near this ice wedge. Therefore, this classical epigenetic ice wedge is assumed to be younger than the Ice Complex, possibly of Holocene age, which is sustained by its white, milky colour. The milky appearance is, again, caused by a lot of small gas bubbles (< 1mm) and some bigger ones, which are slightly elongated. Elementary ice veins are smaller than 3 mm but they are not so easy to differentiate.

The Ice Complex thermokarst mounds on top of the outcrop near the massive ice body have small diameters between 8 and 10 m and contain a lot of debris from different rock types (e.g. quartzite, basalt, sandstone, granite, metamorphic rocks). About 100 m further to the SE, a 20 m high outcrop was studied, the upper 12 m of which consist of Ice Complex deposits. Two generations of Ice Complex ice wedges are observed in this section. Smaller 1.5 m wide and 4-5 m high ice wedges penetrate into an older generation of 3 m wide ice wedges. An ice wedge of 1.2 m in horizontal extension (NSI-IW-4) of the younger generation of Ice Complex ice wedges was sampled (Figure 5.2.8-8C). Because of lack in time, a more detailed study and description of this section was unfortunately not possible.

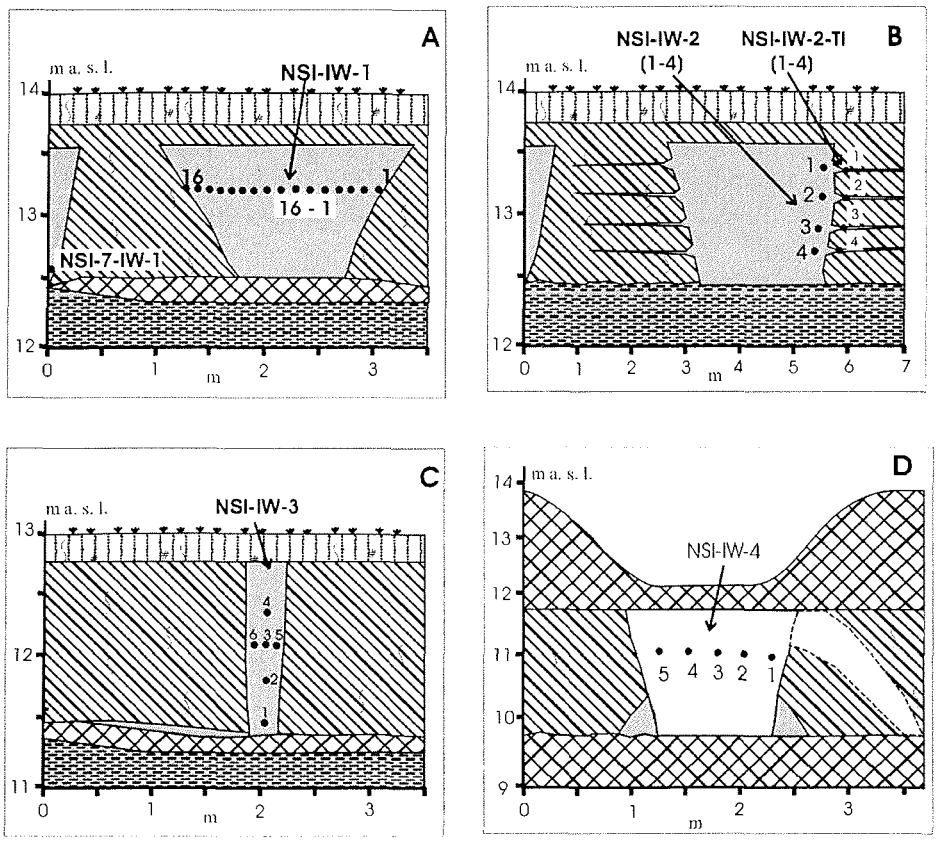

Figure 5.2.7-8: Various studied ice wedges of SW-coast of Novaya Sibir Island

A lateral succession of various marine deposits overlain by thermokarst (alas) deposits was exposed at the coast some 1.4 km further northwest. In the lowermost part, frozen bluish-grey, compact and bedded clay with shells occurs (sub-profile Nes 9, Figure 5.2.7-9A).

This clay contains horizontal 1 cm thick ice bands in a distance of 20 cm. They are 1 cm thick, vertical ice veins forming lattice-like cryostructure (gravimetric ice content 36-40 wt-%). The horizon was regularly wave-like deformed with amplitude of 10 m width (Figure 5.2.7-11A). The marine deposits are covered by 3-4 m thick yellowish-brown alas deposits in a height of 8-9 m a.s.l., which were deformed accordingly. They consist of bedded silty sands and contain layers of plant remains or thin peat layers. After some hundred meters to the SE the lower marine horizon changes to coarse-grained, well-bedded deposits. Cross-bedded, wave-like deformed sands occur, (Figure 5.2.7-11D) overlain by similar alas deposits as described before. Next to the SE (sub-profile Nes 8, Figure 5.2.7-8B) the bedded and also wave-like deformed marine horizon looks like a till because of numerous rounded pebbles (Figure 5.2.7-11E) within a grey-blue fine-grained matrix. In addition, dropstones up to 0.5 m in diameter are embedded within this matrix (Figure 5.2.7-11C). Therefore, a glacio-marine

formation is assumed. The cryostructure is also lattice like with diagonal ice veins. Brownish, bedded and wave-like deformed alas deposits with organic rich interlayers overlay this material in about 3.5 m a.s.l.. In general, a lateral transition from marine clayish deposits to marine sandy deposits and glacio-marine deposits was studied. This marine sequence was totally covered by deposits of thermokarst depression.

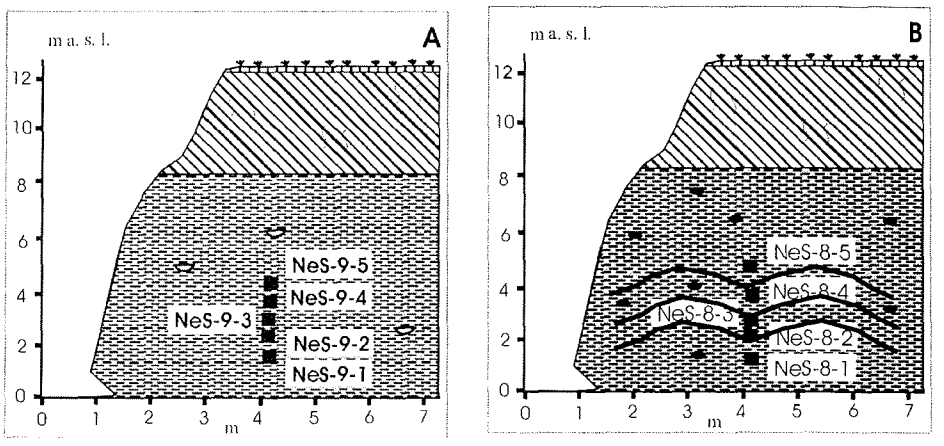

Figure 5.2.7-9: Studied sub-profiles Nes-9 and Nes-8 with marine deposits and thermokarst deposits

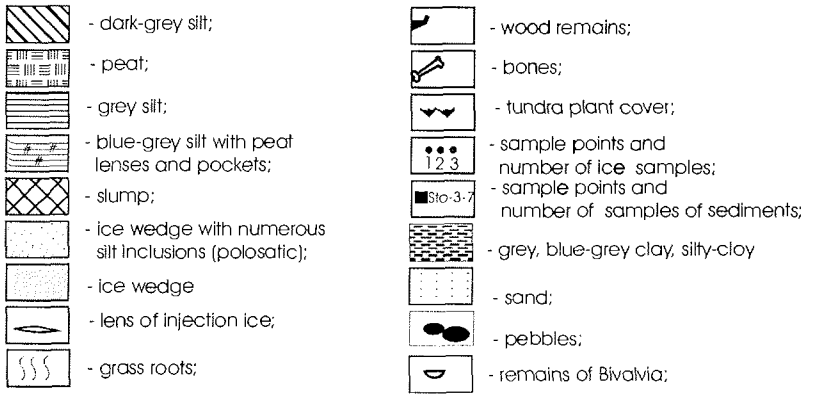

Figure 5.2.8-10: Legend to figures 5.2.7-6, -8, -9

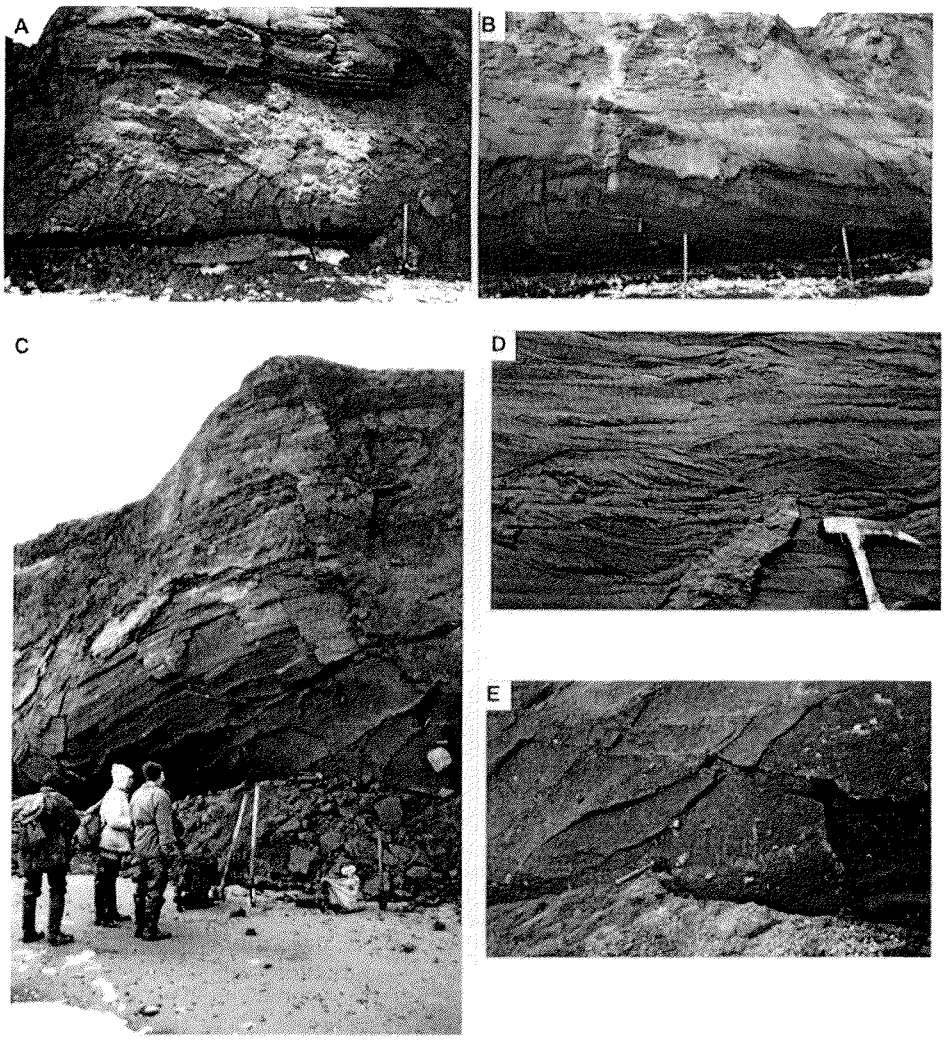

Figure 5.2.7-11: Deposits of a marine to glacio-marine succession on the southeast coast of Novaya Sibir island, location Gedenstrom.
A – Bluish-grey marine clay with shells and lattice-like cryostructure (sub-profile Nes 9) covered by sandy alas deposits with organic-rich interlayers;
B – Bedded marine sands overlain by yellowish-brown alas deposits;
C – Cross-bedded marine sand horizon;
D – Glacio-marine deposits with a large boulder of dropstones, overlain by alas deposits;
E – Detailed section of glacio-marine deposits with numerous well-rounded pebbles.

5.2.8 Maly Lyakhovsky Island (27.08.)

The basement of Maly Lyakhovsky Island consists of upper Jurassic and lower Cretaceous sediments (Lopatin 1998). The highest elevation of the island is about 32 m a.s.l and the islands surface has step-like character with some terraces. Thermokarst lakes occur in the centre of the island at the highest terrace of 30-32 m a.s.l.. The second terrace at about 25 m a.s.l. is characterized by thermokarst valleys with flat bottoms. The third terrace at about 20 m a.s.l. is cut by a net of deeper thermokarst valleys. At the lowest level on the beach numerous pebbles and boulders up to 1-1.5 m occur. The study area was located southeast of Cape Vaygach (Figure 5.2.8-1). The frequent distribution of thermokarst mounds and thermokarst valleys indicate the existence of an Ice Complex cover on these terraces (Figure 5.2.8-2).

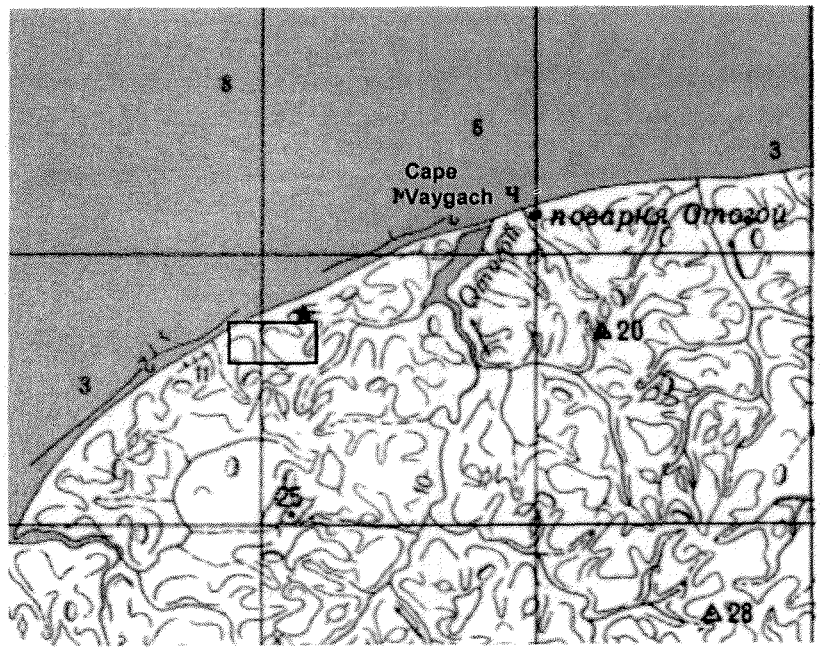

Figure 5.2.8-1: North coast of Maly Lyakhovsky Island with the study area west of Cape Vaygach

The TSP was placed on top of the coastal cliff near a thermokarst valley about 7 m a.s.l.. Dry cryoturbated soil, dried grass, and lichens covered the surface. The vegetation was generally denser than the Arctic tundra and than Arctic desert of Kotel'ny Island and Novaya Sibir Island. The valley bottom was wet and a dense grass cover was growing, whereas the higher located surface between the valleys was quite dry.

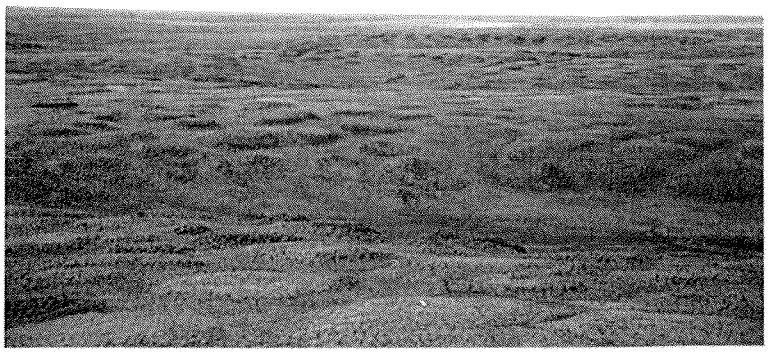

Figure 5.2.8-2: The step-like surface of Maly Lyakhovsky Island; terraces with thermokarst mounds and thermokarst valleys.

Thermokarst mounds were measured at a valley slope. They are between 1-2.5 m high and have mostly a flat top. The distance of thermokarst mounds reflecting the size of a former ice wedge polygon net is between 8-18.5 m (in average 12 m). The surface of the mounds is also covered by cryoturbated ground and dry grass.

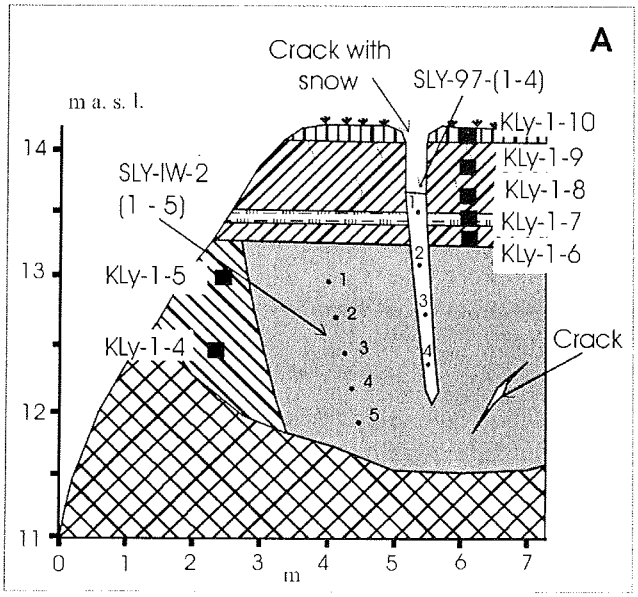

Figure 5.2.8-3: Ice Complex deposits covered by laminated deposits of a thermokarst valley (profile Kly 1)

Only one permafrost sequence of about 8 m in length could be dug on two sub-profiles at a thermokarst mound situated at the steep slope of a deep thermokarst valley near the sea (Figure 5.2.8-3). The first sub-profile on the foot of the mound consists of grey ice-rich silty fine sand (aleurite) with broken reticulated cryostructure and 2 cm thick ice belts (samples Kly 1-1 to 1-3, gravimetric ice content 74-132 wt-%). The second sub-profile in a higher position continued these Ice Complex deposits (samples Kly 1-4, 1-5). In addition, the contact of an ice wedge was exposed there. Both, ice wedge and Ice Complex deposits were firstly covered by a horizon of buried cryosol containing small peat nests followed by fine-laminated light-brown and dark-brown interbedding of silty fine sand and organic-rich layers (samples Kly 1-6 to 1-10). A frost crack penetrating from the surface 3 m down into the ice wedge was filled by snow of the preceding year, which also was sampled. In general, the described profile presents presumably a late Pleistocene Ice Complex sequence, covered by Holocene deposits of a thermokarst valley.

The largest paleontological collection of New Siberian Islands is from the north coast of Maly Lyakhovsky Island (59 samples). In comparison with other islands we found there a lot of bones at the shore and at the slopes of small brooks in tundra. That indicates an active erosion of Pleistocene deposits in this part of Maly Lyakhovsky Island. The taxonomic composition is typical for the "Mammoth" fauna. All finds were separately found. Only four bones of rein deer were found together and they probably belong to one individual (Appendix 5.2-3).

5.2.9 Cape Svyatoy Nos (22.08.)

A chain of Cretaceous granite domes up to 433 m a.s.l. dominates the landscape of Cape Svyatoy Nos (Lopatin 1998) (Figure 5.2.9-1). Cryoplanation terraces are formed around these elevations at various levels. The lowest terrace was studied about 8 km south of this cape near the former polar station "Mys Svyatoy Nos". Former studies by Russian colleagues point to the occurrence of early Pleistocene deposits there (Figure 5.2.9-2). According to them, the upper part of the basement of the 30 m terrace consists of greenish-grey sands of various grain sizes below a peat horizon with up to 15 cm thick wood remains. This wood was radiocarbon dated of > 30 ka BP (PI-2014). The described sand horizon is comparable with similar deposits west of Cape Svyatoy Nos, which were assigned to the Ebelyakhsky Suite (Nikolsky et al. 1999). The Ebelyakhsky Suite was dated paleomagnetically with more than 700 ka (Nikolaev et al. 2000). The main part of the early Pleistocene sands was probably eroded during cryoplanation processes.

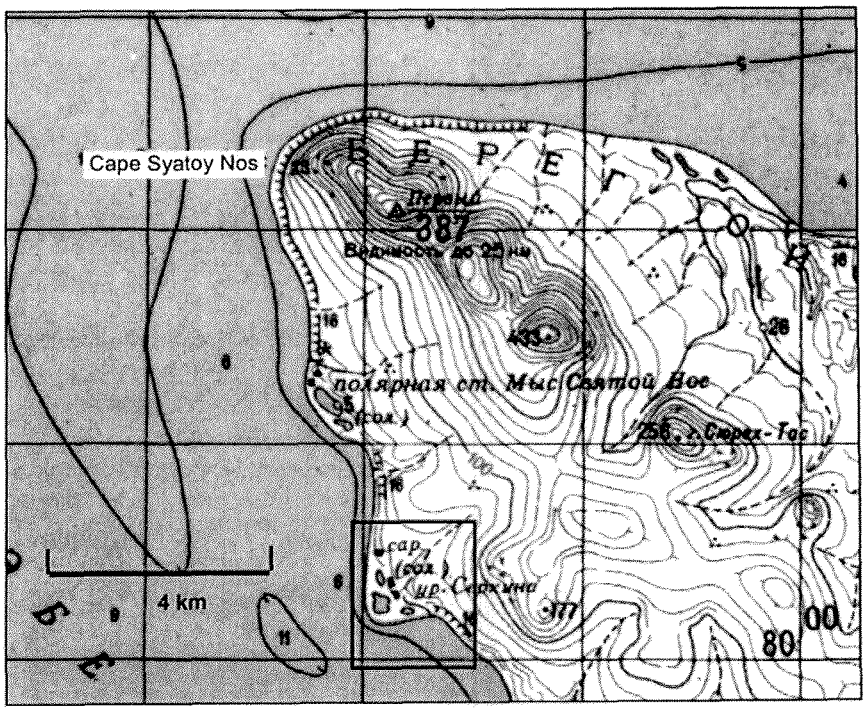

Figure 5.2.9-1: Study area south of Cape Svyatoy Nos

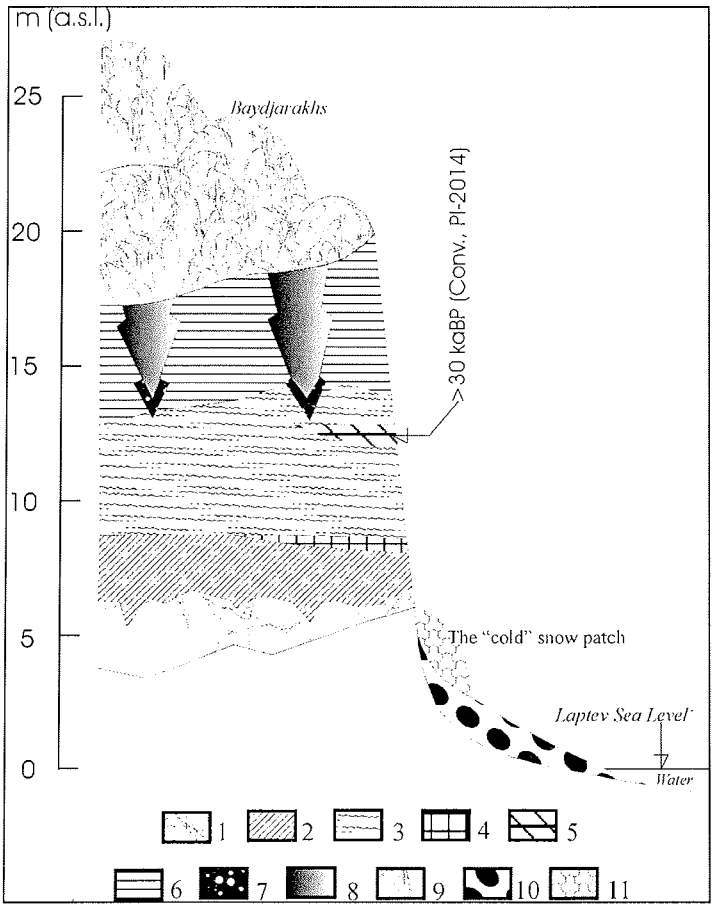

Figure 5.2.9-2: Schematic profile of the Ice Complex fragment as part of the 30 m cryoplanation terrace near Cape Svyatoy Nos, Compilation of former Russian expeditions by V.V. Kunitsky.

1- Strongly weathered light grey granite, frozen, with ice filled cracks;
2 – Dark-grey loam;
3 – Dark-brown peat, grass, moss shrub remains (up to 15 cm Ø);
4 – Greenish-grey sand, cross-bedded, with gravel interlayers;
5 – Brown alluvial peat, small plant detritus with shrub fragments;
6 – Ice Complex deposits, brown silty sand with gravel inclusions and ice belts;
7 – Ice wedge with sediment veins ("Polosatic")
8 – Ice wedge, grey
9 – Surface with thermokarst mounds;
10 - Large pebbles on the beach (up to 3 m Ø)
11 - Snow patch

Table 5.2.9-1: Radiocarbon age determination of *Mammuthus primigenius* found east of the Svyatoy Nos Cape

Lab.No.	Age (a BP)	Bone	Reference
GIN-9555	>16000	bone	Nikolaev et al., 2000
GIN-9556	17100±300	bone	Nikolaev et al., 2000
GIN-9045	25200±300	bone,	Nikolsky et al., 1999
GIN-9563	26100±600	bone	Nikolaev et al., 2000
GIN-9559	>36900	bone	Nikolaev et al., 2000
GIN-9566	40900±1200	bone	Nikolaev et al., 2000
GIN-9552	42900±900	bone	Nikolaev et al., 2000
GIN-9568	43100±1000	bone	Nikolaev et al., 2000
GIN-9557	47400±1200	tusk ?	Nikolaev et al., 2000
GIN-9044	48800±1400	tooth?	Nikolsky et al., 1999

Unfortunately, only a stop of two hours was possible in the evening of August, 22 because of bad weather conditions. Therefore, no detailed coastal section but only some landscape observations and sampling of small reconnaissance profiles were made.

The TSP was placed at the stony slope of the coastal cliff 8 m a.s.l.. The cliff was about 10 m high, and cut by V-shaped thermo-erosional valleys. A snow patch was preserved at the bottom of the southern slope of one of the valleys. Three samples were taken from this snow patch for stable isotope analyses. The surface on top of the cliff was covered by cryoturbated soil with frost boils containing a lot of rock debris. Boulders of sub-rounded weathered granite and dolerite (up to 1 m in diameter) occur at this surface as well as in the valley bottom and on the beach (samples Svy 4-1 to 4-4). Similar boulders also occur further north near the abandoned polar station. They were shaped by sea ice and seawater but not by glacial processes (Kunitsky & Grigoriev 2000). The visible material of the coastal cliff mostly consists of reworked material from higher levels. About 350 m south of the landing point bedded sediments were found containing large remains of shrubs. They were interpreted as stillwater deposits. The lowest horizon of the studied profile was a 5 m thick laminated silty fine-sand (aleurite) at 2.5 m a.s.l.. Laminas were 0.1-4 cm thick and consisted of light-grey silty sand with orange coloured clay lenses alternating with plant detritus (sample Svy 1-1). This horizon was spotted with iron oxide. The next horizon was a 5 m thick, bedded alluvial peat (sample Svy 1-2), containing a shrub root horizon in the lower part (sample Svy 1-3) covered by a 0.5 m thick layer of grey silty fine sand. An additional wood horizon with shrub remains was found 200 m to the north in 15 m a.s.l. (sample Svy 1-4). The wood remains of both horizons showed bluish-grey thin Vivianite crusts on the surface. We collected only tree bones on the shore during the two hours stop.

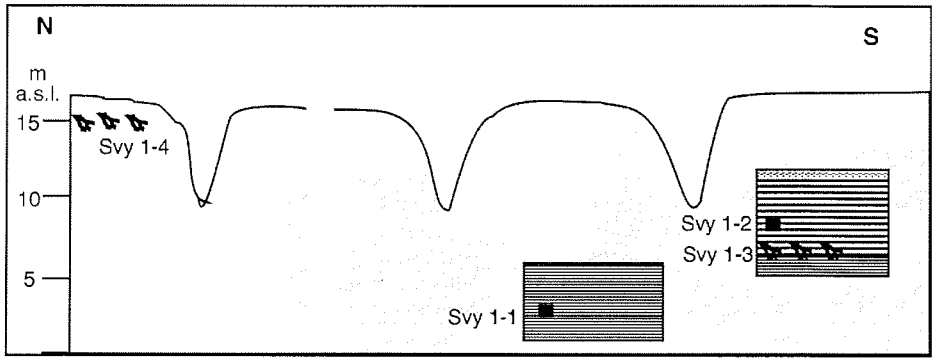

Figure 5.2.9-3: Scheme of the only studied profile at the coastal section 5 km south of Svyatoy Nos polar station; laminated deposits with shrub remains.

5.2.10 Oyogos Yar coast (30.08.)

The coast of Oyogos Yar was already the study object of some Russian scientist during the last decades. Two main units characterize the coastal section. They are separated by a thermo-terrace (Figures 5.2.10-1 and 10-3). The stratigraphical classification of the lower unit is still under discussion. Opinions vary between middle to upper Pleistocene (Kayalaynen & Kulakov 1966, Ivanov 1972, Vereshagin 1982). This dark bluish-grey, bedded deposit with shells is clearly a subaquatic formation and was named Khomsky-Suite (Vereshagin1982). The Khomsky-Suite is exposed in the Yana-Indigirka Lowland up to 100 m a.s.l. and above (Kayalaynen & Kulakov 1966) and contains freshwater diatoms as well as saline forms.

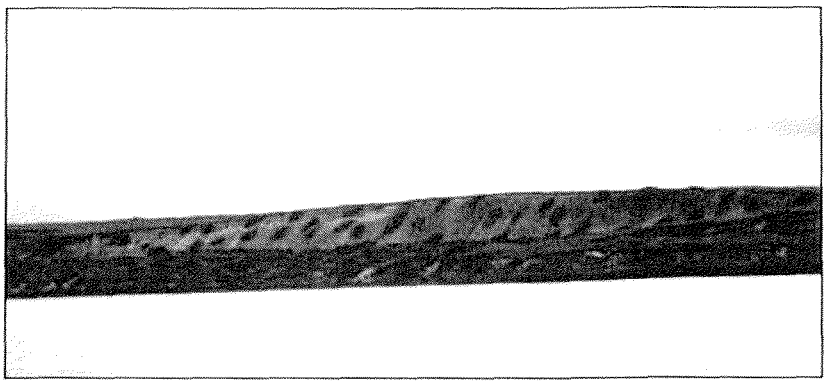

Figure 5.2.10-1: The studied coastal cliff of Oyogos Yar; a thermo-terrace devides the Ice Complex horizon from the underlaying subaquatic deposits

The upper unit with large ice wedges is named Oyogossky-Suite and presents the Ice Complex in this region. Ice Complex deposits cover the less inclined step-like surface of the Yana-Indigirka Lowland and were formerly interpreted as sequences of interlocked lake terraces (Kayalaynen & Kulakov 1966). The step-like distribution of this horizon is supposed to be connected with steps of cryoplanation terraces (Kunitsky 1996). The outcrops of Oyogos Yar were also studied by Gravis (1978). He found shrub remains below the Ice Complex, which were dated > 42 ka BP, as well as shrub remains and peat of Holocene age (about 3-8 ka BP) at the top of the Ice Complex. Gravis (1978) and also Konishev and Kolesnikov (1981) supposed that the Oyogossky-Suite was formed within a thermokarst depression (alas). But Tomirdiaro (1970, 1980) assumed an eolian origin of these deposits. Some age determinations from Oyogos Yar sections dated by other authors are summarized in table 5.2.10-1. In general, the situation is comparable with that of the Laptev Strait coast on Bol'shoy Lyakhovsky Island.

Table 5.2.10-1: Radiocarbon age determinations of the Oyogos Yar Section

sample Index	Location	Depth [m]	Material	Radiocarbon age [y BP]	Reference
IM-235				> 42 000	Gravis 1978
IM-233	Cliff	6	Peat	33720±1500	Gravis, 1978
IM 230			Peat	5750±230	Gravis 1978
IM 229			Peat	3890±250	Gravis 1978
NUTA3521	Cliff	5		22 940±390	Nagaoka et al 1995
OG 34	Ice Complex top	1	Methane	3539±87	Moriizumi et al 1995
MAG-544	Mouth of Rebrov River	5	Peat	34200±2300	Kaplina & Lozhkin, 1985
MAG-543	- " -	8.5	Peat	37700±2200	Kaplina & Lozhkin, 1985
MAG-545	- " -	17	Peat	> 41 000	Kaplina & Lozhkin, 1985

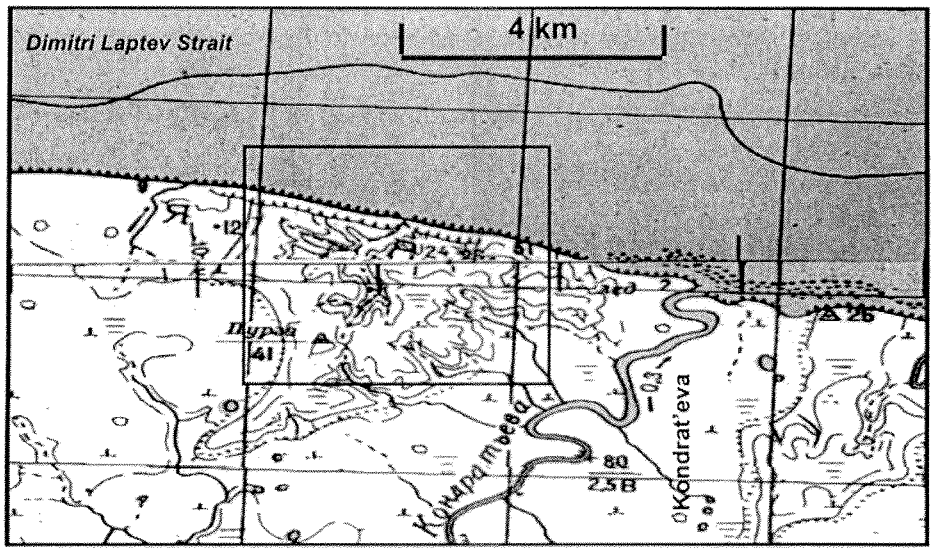

Figure 5.2.10-2: Study area of Oyogos Yar coast west of the Kondrate'eva River mouth

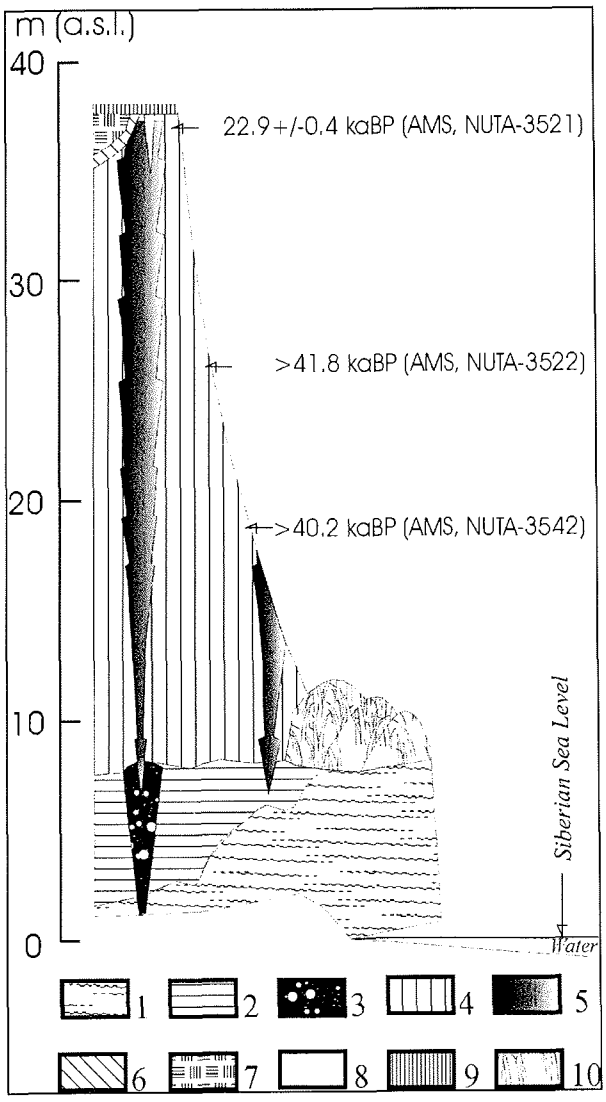

Figure 5.2.10-3:
Schematic profile of the Oyogos Yar coast west of the Kondrateva River:

1 – Dark-blue silt, bedded with shells, slanting ice lenses;

2 – Brownish-grey silty fine sand, bedded, dense, with shrub fragments and grass roots, diagonal cryostructures;

3 – Ice wedge with sediment veins

4 – Dark-grey loess-like silty fine sand (aleurite) with peat nests and ice belts, Ice Complex deposit;

5 – Ice wedge of the Ice Complex horizon;

6 - Dark-grey aleurite, involution layer, with peat, shrub remains, bedded and reticulated cryostructure;

7 – Brown moss peat;

8 – Ice wedge, white, less

In order to get an overview of the stratigraphical, cryolithological and geomorphological situation, profiles were studied 2 km along the cliff of Oyogos Yar (Figure 5.2.10-4) as well as some outcrops in the hinterland. The coast is dominated by Ice Complex elevations (20-30 m a.s.l.) interrupted by thermokarst valleys and thermokarst depressions.

The TSP station was placed at the slope of the Ice Complex elevation (Yedoma) in 8 to 9 m a.s.l.. The surface was completely covered by alternating dry and wet grass vegetation. In addition, a lot of *Salix* and mosses occurred there.

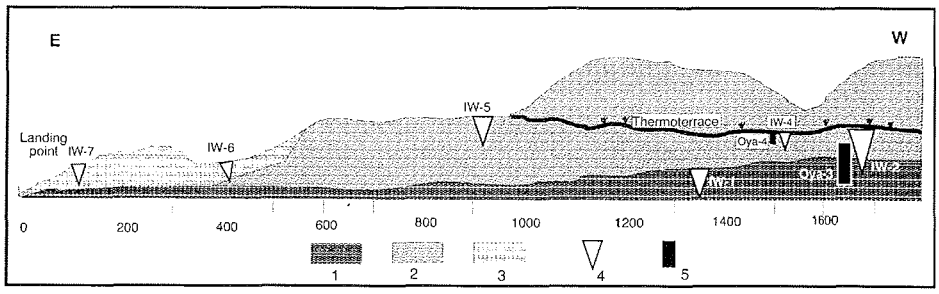

Figure 5.2.10-4: Schematic overview and study locations at the coast of Oyogos Yar; 1 – Subaquatic deposits, 2 – Ice Complex deposits; 3 – Alas deposits; **4** – Studied ice wedges; 5 – Studied sediment profiles.

In the lower part of the section near the beach, three profiles were studied. They involved possible lacustrine deposits, a buried sediment-rich ice wedge ("Polosatic) with rounded head, horizons with large ice wedge casts and shrub remains and the lower part of the Ice Complex with roots of large ice wedges. Such special buried ice wedges were also found in the lower level of the coastal section on Stolbovoy Island (chapter 5.2.2) and on Kotel'ny Island, south coast (chapter 5.2.5). The ice wedge (0.75 m wide) is incorporated in a well-bedded silty fine-sand (aleurite) with banded cryostructure (Figure 5.2.10-5).

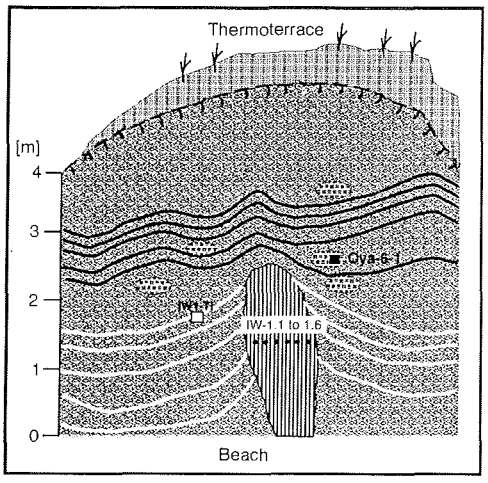

Figure 5.2.10-5: Buried ice wedge in the lowest horizon of Oyogos Yar covered by laminated peaty sand.

Six samples were taken from this ice wedge (OYA-IW-1) and one from the ice belt near the ice wedge in a height of about 1.5 m a.s.l. The width of the ice wedge is about 0,7-0,8 m. The visible height is about 2,5-3 m. The head of this ice wedge was thawed and buried under the yellow-grey aleurite with numerous peat nests and lenses. The ice wedge showed belts, shoulders and tracks of up-ward-squeeze of ice wedge, which are typically for syngenetic formation. The Ice is dirty, turbid with vertical oriented striation. The ice crystals are very big and reach about 0.5-0.7 cm in diameter.

A second study site of the lower level was located some hundred metres further to the north (Figure 5.2.10-3) exposing deposits and ice wedges below the

thermo-terrace (Figure 5.2.10-6). Bluish-grey, clayish laminated lacustrine deposits with a net-like, broken cryostructure (gravimetric ice content 38-99 wt-%) contained a horizon of ice wedge casts. These ice wedge pseudomorphs are 1-2 m long and consist of grey, laminated clayish sand with peat nests and wood remains. They occur in distances of 10-20 m to each other. These probably lacustrine deposits are covered by a greyish-brown transition horizon of iron oxide colour (gravimetric ice content 48-57 wt-%). The overlying grey silty fine sand (aleurite) of the Ice Complex had a lens-like cryostructure (gravimetric ice content 37-50 wt-%) with ice bands. The lower part of an ice wedge of the Ice Complex penetrated downward into the lacustrine deposits. The ice wedge was about 1.2 m wide and consisted of yellowish ice, possibly due to a high amount of organic matter in the ice.

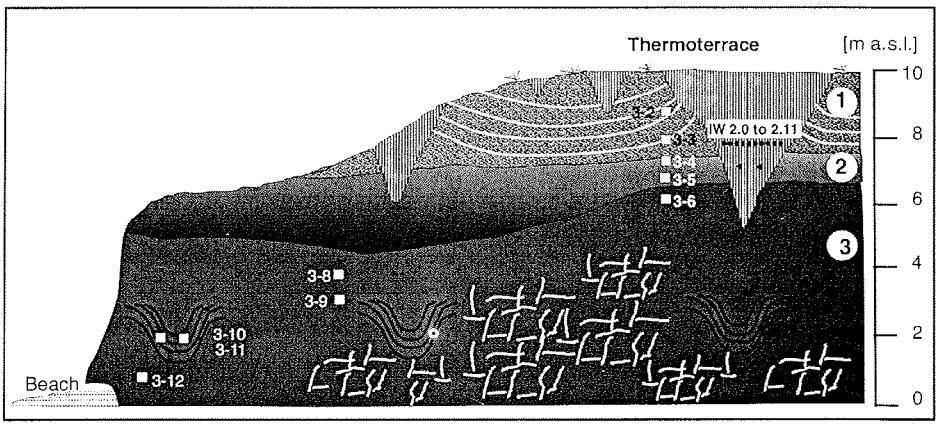

Figure 5.2.10-6: Studied profile Oya-3 and ice wedge OYA-IW-2 below the thermo terrace; 3 – Lacustrine deposits with ice wedge casts, 2 – Oxidic transition zone, Ice wedge of the Ice Complex penetrating lacustrine sediments.

The sampling for OYA-IW-2 was carried out in a height of about 7 m a.s.l. and in total, 12 samples were taken. The ice wedge is characterised by narrow ice veins of 0.5-2.5 mm, which may penetrate into each other, and also by low sediment content and very small gas bubbles < 1 mm leading to a milky appearance of this ice wedge. Small vertical ice veins, up to 4 cm wide and 0.8 m long occur on the left side of the ice wedge.

A high amount of shrub fragments was found in the upper part of the lacustrine horizon (sample Oya 3-13). Two additional samples were taken from the lower unit further to the west – at first from subaquatic deposits with shells (sample Oya-5-1) and secondly from alder shrub fragments (sample Oya-5-2).

Further ice wedges, belonging to the Ice Complex horizon were studied at the level below the edge of the thermoterrace (IW-4, IW-5). Ice wedge OYA-IW-4 was sampled (6 samples, in a distance of about 30 cm) in a height of about 35 m a.s.l. and a depth of 4 m below the cliff top edge. Ice wedge ice was dirty, turbid, and contained numerous air bubbles. Elementary ice veins were not

observed. The ice wedge OYA-IW-5 was about 5 m high and 3 m wide and was surrounded by very ice-rich brownish-grey silty sand with ice belts bound upward (in an angle of up to 80°) and peat inclusions. 15 samples were taken in a horizontal sampling transect (20 cm intervals) in a height of about 16 m a.s.l. (Figure 5.2.10-7A). This typical Ice Complex ice wedge is composed of yellowish slightly milky ice. Elementary ice veins are between 1-3 mm thick.

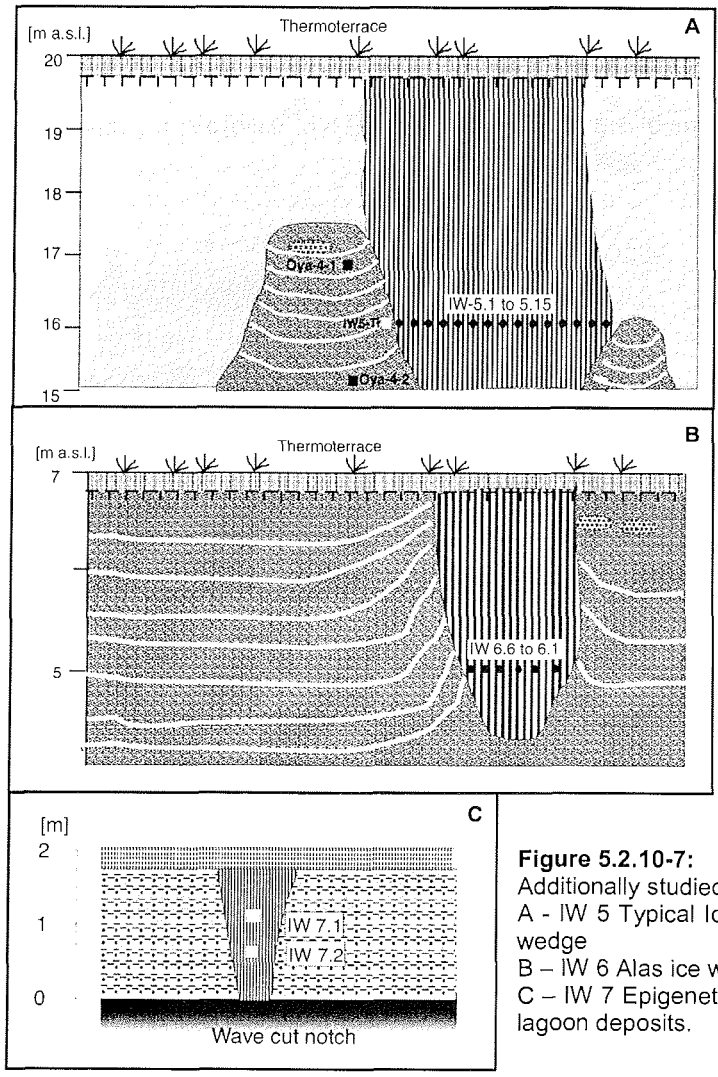

Figure 5.2.10-7:
Additionally studied Ice wedges
A - IW 5 Typical Ice Complex ice wedge
B – IW 6 Alas ice wedge
C – IW 7 Epigenetic ice wedge in lagoon deposits.

Two generations of ice wedges younger than the Ice Complex were observed at the Oyogos Yar coast. Six samples were taken in a height of 5 m a.s.l. of an ice wedge which was about 1.5 m wide, probably belonging to alas deposits (OYA-IW-6) (Figure 5.2.10-7B). These deposits consist of ice-rich brownish silty sand with peat inclusions and ice belts bound upward. The ice wedge consists of

yellowish to white, milky ice. A second ice wedge was sampled just above the wave-cut notch near the landing point in grey sediments (oxygen reducing conditions) with oxidised fissures of yellowish-brown colour and lens-like reticulate to laminated cryostructure. These sediments were possibly associated with lagoon deposits. The ice wedge OYA-IW-7 is 0.3 m wide and 1.2 m high and it is composed of grey to white milky ice. It is assumed to be epigenetic and of Holocene age (Figure 5.2.10-7C).

The landscape was studied about 1.5 km to the south as supplement to the general investigations on coastal sections. The surface rises up to 40-50 m a.s.l.. Larger and smaller thermokarst depressions occur in various levels. The various bottom levels of these depressions might reflect the altitude of former cryoplanation terraces. Additionally, U-shaped thermokarst valleys with flat, wet, and grass-covered bottom characterised the coastal hinterland. Such valleys are 50-60 m wide on the top and 10 m at the bottom. Brooks flowing at the valley bottom formed small cascades of about 2-3 m height in distances of 400 to 500 m. These cascades were possibly formed at the edges of a step-like bottom surface. Such barriers may also reflect the relief of former cryoplanation terraces, which is now covered by Ice Complex deposits.

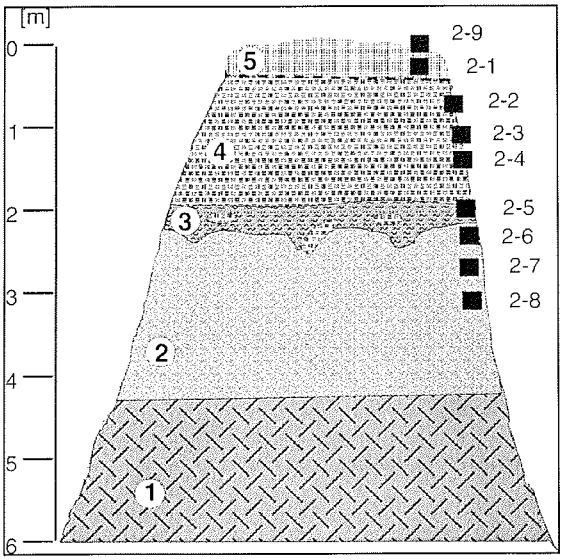

Figure 5.2.10-8:
Profile Oya-2; Thermokarst mound at the slope of a thermokarst valley about 1.5 km south of the coastal section;
1 – Talus
2 – Ice complex deposit, ice-rich silty fine sand (aleurite);
3 – Cryoturbated peaty paleosol;
4 – Moss peat, fresh, with twigs;
5 – Active layer:

A thermokarst mound at the steep slope of a thermokarst valley was exemplarily studied, as it was thought to be the highest Ice Complex level (Figure 5.2.10-8). This profile consists of frozen silty fine sand with twig fragments and coarse lens-like reticulated cryostructure (gravimetric ice content 54-118 wt-%). The Ice Complex horizon is covered by a cryoturbated peaty paleosol and an about 2 m thick, non-decomposed peat horizon with a lot of twigs. All thermokarst mounds at the valley slopes also had a peat cover.

An ice wedge of the highest Ice Complex level was studied 200 m to the north at the top of a small thermo-cirque (Figure 5.2.10-9). This ice wedge was

vertically striped, dense and contains small gas bubbles and only a few clastic inclusions. The wall of the thermo-cirque cuts the ice wedge at an angle of 10-20 ° and, therefore the ice wedge looks very broad. The ice wedge was covered by frozen slope material with banded and reticulated cryostructure. This horizon

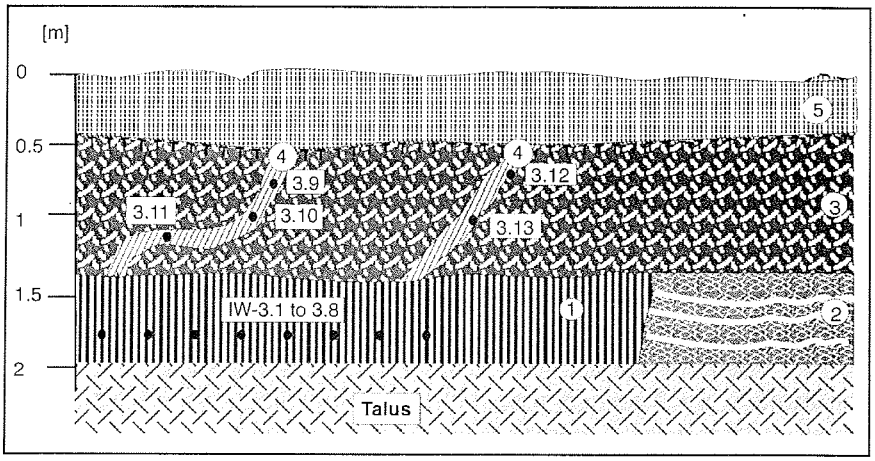

Figure 5.2.10-9: Ice wedge of the upper Ice Complex level exposed at a small thermo-erosional cirque about 1.3 km south of the coastal section;
1 – Old Ice wedge; 2 – Ice Complex deposits, buried by talus, 3 – Frozen slope deposits; 4 – Young disturbed ice wedges, 5 – Active layer.

contains additional small ice wedges, which were disturbed during solifluction processes. Both types of ice wedges were sampled but unfortunately the Ice Complex deposits were buried by talus material and sampling therefore was impossible.

Figure 5.2.10-10:
Small part of the collection of woolly mammoth found at the Oyogos Yar section

Apart from geomorphological, geocryological and sedimentological studies, which had been carried out the stop at Oyogos Yar was very useful for paleontological studies (Figure 5.2.10-10, Table 5.2.10-1). The paleontological collection from Oyogos Yar site is the most comprehensive. We collected 369 bones and their fragments. Unfortunately we worked on this outcrop one day only. Bones were collected from the 5 different types of location groups. 48 bones were found at the exposure itself. Among them one bone (group "a") – rib of woolly mammoth - was collected strictly *in situ*, from the coastal outcrop on

the altitude 1m from the water level. Nearby we also saw small pieces of several limb bones, which stuck still within frozen sediments. Probably they are part of one skeleton of *Mammuthus primigenius*. Two half of pelvis, left femur and left humerus already fell out from the cliff sediments and we had found they nearby. Concerning preservation and position of these bones, they probably belong to an individual. Large amount of bones (47) was found on the termoterrace of the exposure (location group "c"). The possible altitude range of their initial stratigraphical position could be estimated between the height of their occurrence (height of termoterrace) and the height of the upper cliff. On tundra surface were found 4 bones only (group "d" and "f"). One of them (NS-OgK-O430 - mammoth ulnare) is submitted to determination of radiocarbon age.

The largest group of bones – 317 samples was collected from the shore (group "e"), which is typical for permafrost regions in Arctic Siberia. All these bones divided into three subgroups. Two subgroups contain bones from the open shore (west and east part). The third subgroup (68 bones) was collected on the small part of shore near the small stream mouth. All large limb bones of *Mammuthus primigenius* were usually measured, photographed and finally cut off in pieces of 2 – 3 kg. These are samples of mammoth for the radiocarbon dating. We are planning to determine the radiocarbon age near 20 bones of different species on mammals from the Oyogos Yar at the Radiocarbon Laboratory of the Geological Institute, Russian Academy of Sciences. Taxonomic composition of the Oyogos Yar collection is the same to our collection from the New Siberian Islands and differs in the found of *Panthera spelaea* bone only (Tab. 5.2.10-2). The main dominants of both collections are woolly mammoth, horse, bison and reindeer. It is typical for all known Late Quaternary collections from the Arctic Siberia. But the percentage correlation is different for our two collections. In collection from the Oyogos Yar bones of *Mammuthus primigenius* dominate (39,8%), than *Bison priscus* (22,0%), *Equus caballus* (15,7%) *and Rangifer tarandus* (11,7%) follow (Figure 5.2.10-11).

Table 5.2.10-2: Preliminary list of mammal taxa of the Oyogos Yar collection.

Class MAMMALIA – mammals
- Order Proboscidea
  - *Mammuthus primigenius (Blum).* (woolly mammoth)
- Order Artiodactyla
  - Family Cervidae
    - *Rangifer tarandus (L.)* (reindeer)
  - Family Bovidae
    - *Ovibos moschatus Zimm.* (muskox)
    - *Bison priscus (Boj.)* (Pleistocene bison)
- Order Perissodactyla
  - Family Equidae
    - *Equus caballus L.* (horse)
- Order Carnivora
  - Family Felidae
    - *Panthera spelaea (Gold.)* (Pleistocene "lion")
- Order Lagomorpha
  - *Lepus sp.* (hare)

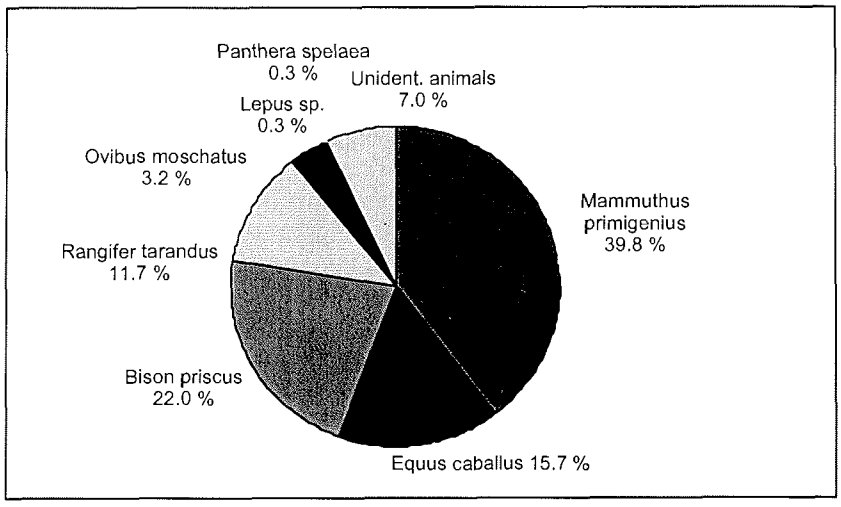

Figure 5.2.10-11: Composition of mammal bones collection from Oyogos Yar, 369 specimens.

5.2.11 Muostakh Island (02.09.)

The last stop was made on Muostakh Island during the return to Tiksi. This slender island of about 10 km length and less than 750 m width, is located 25 km north-east of the mainland and 15 km south-east of Bykovsky Peninsula. It presents the southeastern continuation of the Bykovsky Peninsula coast (Figure 5.2.11-1, 11-2). The island mainly consists of Ice Complex deposits, which are exposed at the east coast from sea level up to the island's surface at about 23 m a.s.l.

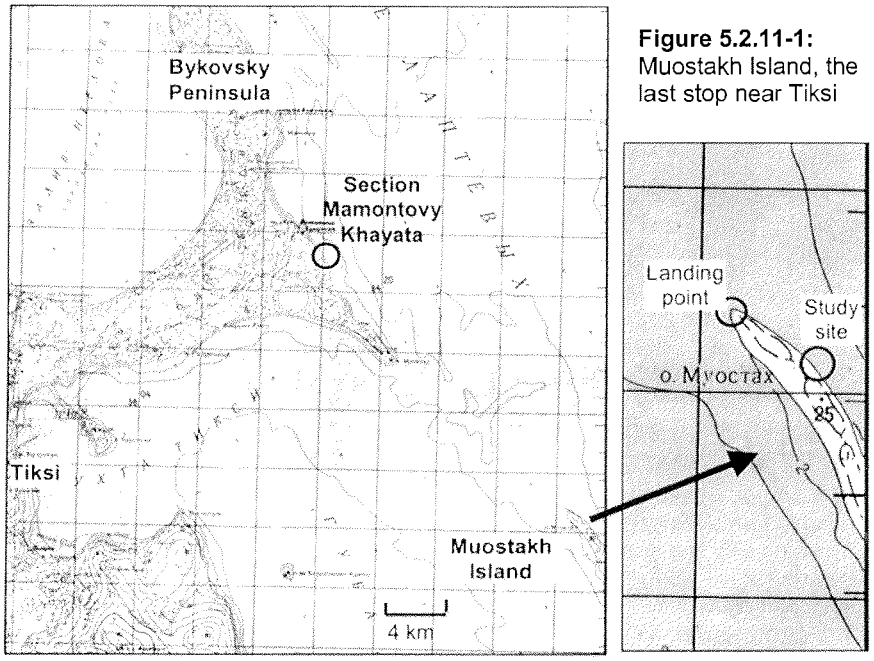

Figure 5.2.11-1: Muostakh Island, the last stop near Tiksi

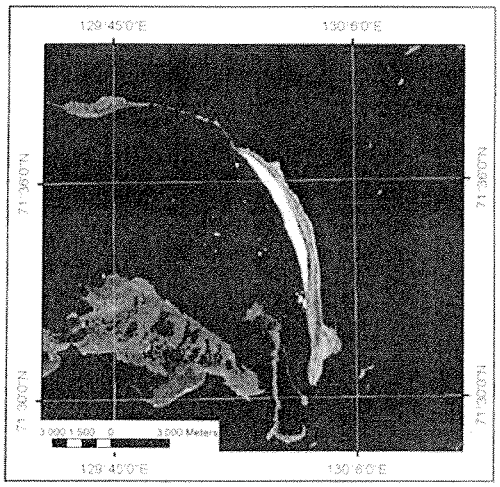

Figure 5.2.11-2: Cloudy Landsat-7 picture of Muostakh Island (August 1999)

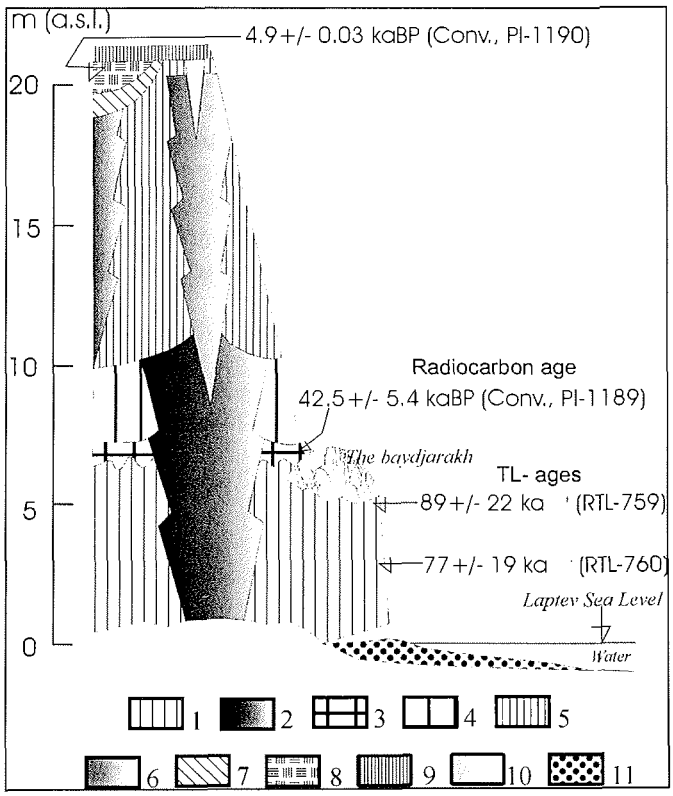

Figure 5.2.11-3: Columnar section of Muostakh Island, compiled by V.V. Kunitsky according to former Russian studies;
1 – Grey-blue silty fine sand laminated, ice banded;
2 – Grey dense ice wedge, single sediment veins, 3-4 m wide;
3 – Black peat, autochtonous
4 – Dark-grey, bedded silty fine sand with sandy interlayers and lenses,
5 – Black sand, gravels and debris, bedded cryostructure;
6 – Small (1-2 m), grey ice wedge;
7 – Dark-grey sandy loam, with sand lenses and shrub remains;
8 – Dark-brown, frozen moss peat;
9 - Dark-brown, thawed moss peat;
10 - White, small (0.5 m wide) ice wedge,
11 - Grey beach sand.

The columnar section of Muostakh Island is shown in Figure 5.2.11-3, as compilation of former Russian studies and datings. The aim of the study was to obtain samples of a large ice wedge sequence and permafrost sediment for comparison with the section Mamontovy Khayata at the Bykovsky Peninsula studied in detail before (Meyer et al. 2002, Schirrmeister et al. 2002, Siegert et al. 2002).

The TSP was placed at the black sandy beach near the landing point about 1 m a.s.l.. The active layer there was 1 m thick. There did not occur any vegetation at the beach. However the plain surface of the island (20-25 m a.s.l.) was dense

covered by moss, grass, lichen and single small shrubs. Ice wedge polygons were observed, indicating recent ice wedge formation. A study site was chosen on the east coast 160 m southeast of the landing point (Figure 5.2.11-1).

A large ice wedge was sampled by chain saw in order to gather ice samples, which were transported to Germany in the frozen state. Consequently, the ice crystallography, all gaseous, liquid and solid inclusions and their distribution in the ice as well as internal structures can be studied in detail in the ice laboratory at AWI Bremerhaven. Additionally, samples can be taken in very high resolution for all kinds of analyses, such as for stable isotopes, hydrochemistry, gas content etc.

The 4.5 m wide ice wedge was sampled in a height of 1 m a.s.l. above the wave-cut notch (Figure 5.2.11-4). 18 blocks of ice (up to 30 cm long and between 10 and 15 cm high) were cut. Altogether only 3 m (out of 4.5 m) were retrieved in a horizontal transect starting from the right side. Because of lack in time and due to technical problems with the chain saw 1.8 m from the left side could not be sampled.

The left side (samples Muo-01 to -04) was characterised by relatively white ice without clear internal structures, except a few vertical sediment stripes. The right side (samples Muo-05 to -11) was composed of rather typical Ice Complex ice with yellowish-grey tiger-striped ice with clear, transparent ice veins, which were relatively easy to recognise. Muo-12 and -13 were taken from the grey ice-rich silty sand in the left continuation of the sampling transect. These samples were taken for a detailed study on exchange processes (hydrochemical and stable isotopes) between the ice wedge and adjacent segregated ice, which were identified for ice wedges on the Bykovsky Peninsula (Meyer et al. 2002).

The Ice Complex deposits next to the studied ice wedge consist of ice-rich grey silty fine sand (gravimetric ice content 97-136 wt%) with small peat nests and thin grass roots. The lens-like reticulated cryostructure and ice belts are typical for most of the studied Ice Complex deposits. In addition, Ice Complex deposits were sampled in higher levels about 100 m to the south. Here above a thermoterrace peat horizons and sand-silty interbeddings occurred (Figure 5.2.11-3 and 11-4).

We collected only six bones from the shore of Muostakh Island (Appendix 5.2-3) and one bone (NS-Mst-O535) from the exposure about 3 - 6 m a.s.l..

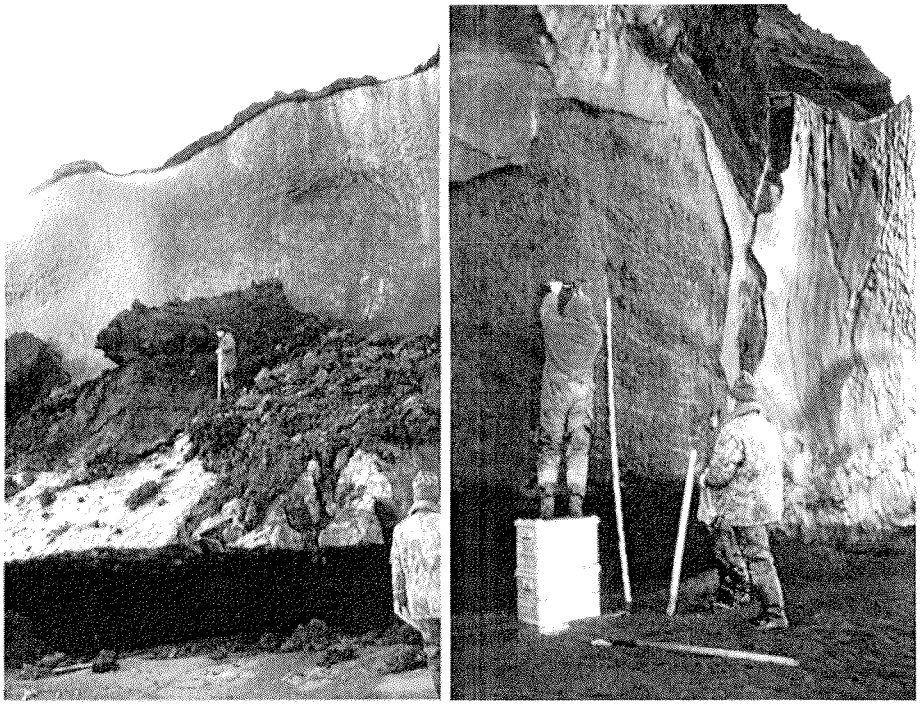

Figure 5.2.11-4: Sampling of Ice Complex profiles on Muostakh Island

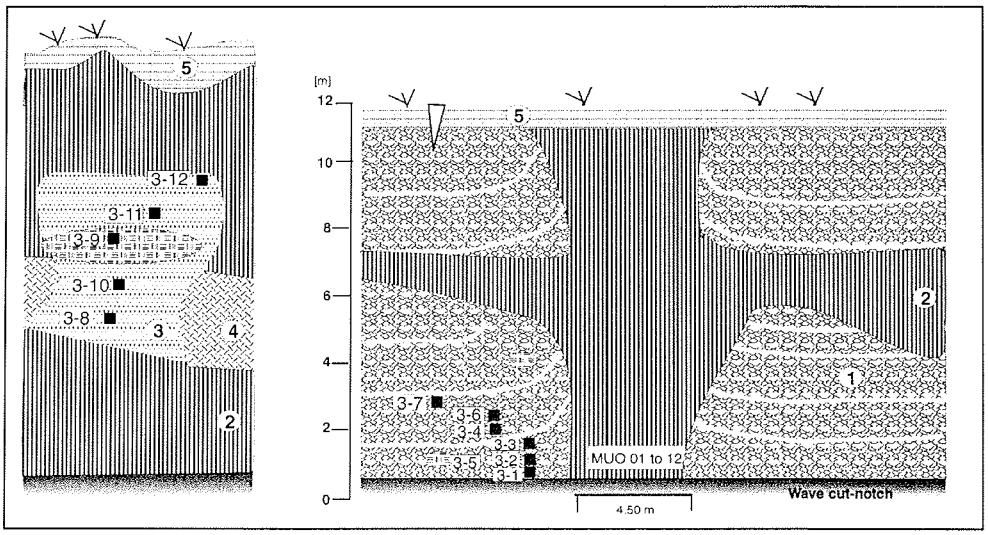

Figure 5.2.11-5: Schemes of sampled permafrost profiles on Muostakh Island
1 – Ice Complex deposits; 2 – Large Ice wedges; 3 – Sandy bedded horizon; 4 – Debris; 5 – Active layer; 6 – Peat lens

5.2.12 Paleontological study on New Siberian Islands

Paleontological studies of Pleistocene and Holocene deposits on the New Siberian Islands included the collection and research of large fossil mammal bones. All participants of the expedition helped to collect and work on bone material. During our stay on the New Siberian Islands we collected 176 bones. As in previous expeditions (1998, 1999, 2000) all of the bones and fragments found were registered in order to obtain fairy most complete statistics of the species composition.

The bones were collected from 7 different places and 5 islands (Stolbovoy, Kotel'ny, Bel'kovsky, New Siberia, Maly Lyakhovsky). Unfortunately, we had only a very short time, not more than one day for each locality. The largest collection on New Siberian Islands is from Maly Lyakhovsky Island (near Cape Vaygach) – 54 samples, and followed by that Kotel'ny Island (Cape Anisy and Khomurgunakh River mouth).

Bones were collected from 6 different types of localities. An unexpected amount of material - 31 bones and fragments - were found *in situ* (group "a"). All these bones are from Kotel'ny Island (Cape Anisy). They belong to mammoth's and horse's skeletons. On Cape Anisy 6 bones from one single mammoth skeleton (bones from forelegs and hind legs) were found *in situ* (samples from NS-Kan-O13-a to O13-f). At the same place several vertebrae and some bones from legs were also found *in situ*.

The second group "b" includes only 5 bones found within the exposures and the altitude of their occurrence was instrumentally determined as well as the level of minimum height of the original position of these bones. Group "c" – 15 samples – includes also bones found at the exposure, but in talus debris. For these bones it is not possible to reconstruct their original position in the exposure.

The most comprehensive material was collected within thawed sediments in different outcrops and valleys. It is group "d" which contains 86 bones. 26 bones (group "e") were collected on the shore and 13 bones were collected in various areas of islands, mainly in tundra.

Table 5.2.12-1: Preliminary list of mammal taxa identified in the New Siberians collection.

Class MAMMALIA – mammals
- Order Perissodactyla
  - Family Equidae
    - *Equus caballus L.* (horse)
- Order Proboscidea
  - *Mammuthus primigenius (Blum).* (woolly mammoth)
- Order Artiodactyla
  - Family Cervidae
    - *Rangifer tarandus (L.)* (reindeer)
  - Family Bovidae
    - *Ovibos moschatus Zimm.* (muskox)
    - *Bison priscus (Boj.)* (Pleistocene bison)
- Order Lagomorpha
  - *Lepus sp.* (hare)

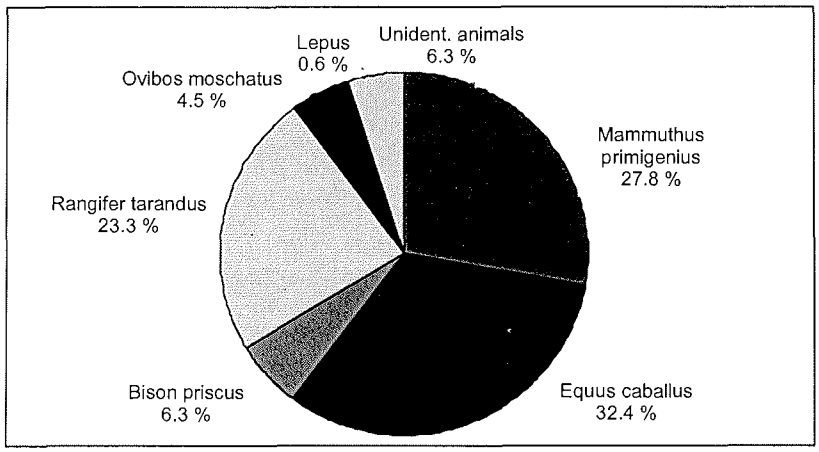

Figure 5.2.12-1: Composition of mammal bones collection from New Siberian Islands, 176 specimens.

Figure 5.2.12-2: Mammoth humerus *(in situ)* in the high Arctic tundra near Cape Anisy (Kotel'ny Island)

5.2.13 Results and Conclusions

The studies made during our three week's expedition have shown the large potential for further geocryological, paleo-ecological and geomorphological research on the New Siberian Islands and the neighbouring coasts of the mainland. Some general remarks and results of our fieldwork should be concluded in short:

Landscapes concerning to three different vegetation zones were observed: Subarctic tundra (Muostakh Island, Stolbovoy Island, Oyogos Yar coast), Arctic tundra (Bel'kovsky Island, Kotel'ny Island, Maly Lyakhovsky Island), Arctic desert (Bunge-Land, Novaya Sibir Island).

Repeatedly step-like cryoplanation terraces were observed, especially close to basement elevations. Snow patches were often situated at the terrace edges. Their occurrence supports the important role may play nival processes during relief formation, already discussed by Kunitzky et al. (2002). The lowest terraces in general consist of Ice Complex deposits. This ice-rich permafrost formation is widely distributed in the coastal regions of the New Siberian Islands and the neighbouring coasts. U-shaped thermo-erosional valleys with flat, grass-covered bottoms always cut the terrace surface. In addition, thermokarst depressions occur if the surface inclination is very low.

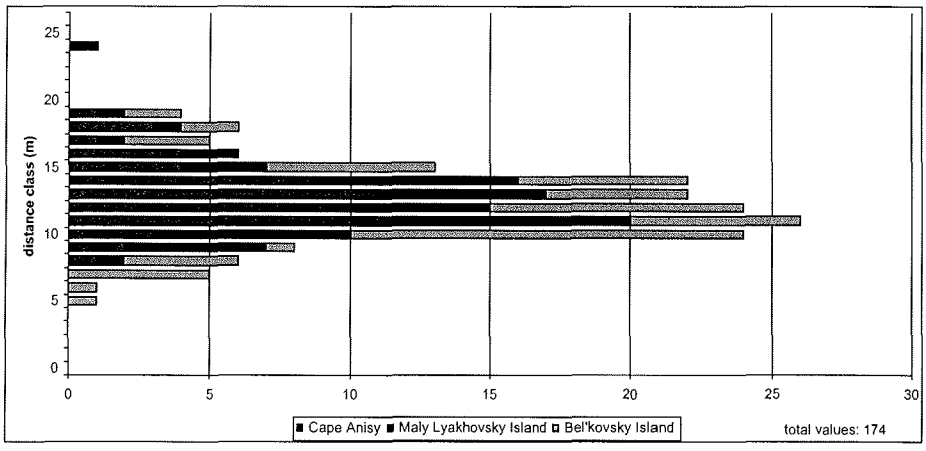

Figure 5.2.13-1: Frequency of distance classes (classes = 1, 2, 3, 4 ... 24, 25 m) for central tops of thermokarst mounds: the values originate from three denudated Ice Complex localities on New Siberian Islands; Most distances from top to top are between 10-15 m, the mean is situated at 12.2 m

Thermokarst mounds at the slopes of thermokarst depressions and valleys reflect the former ice wedge polygon systems. They had various shapes (flat, broad, peaky). Distances of the thermokarst mounds, representing the distances of former polygonal centres, were measured from their centre top to the neighbouring mounds. They mostly vary in a narrow range of 10-15 m, which seems to be typical for former ice-rich, silty to sandy deposits like the Ice Complex in NE Siberia (Figure 5.2.13-1).

Ground-truth activities are an integral part of the analysis of remote sensing data. Until now we collected ground data for calibration from geomorphological, geological, sedimentological and cryological fieldwork. Further, vegetation investigations were done and soil moisture as well soil temperature data were collected for this purpose. For future remote sensing studies it would be most desirable, to employ a field spectrometer. Such a field spectrometer should have a spectral range from 300-2500 nm wavelength, comparable to the Landsat-7 spectral range. This will help to characterise individual surface covers. Such spectra can be compared directly with multi-spectral satellite data in a much more accurate way. Especially for the classification of Landsat-7 multi-spectral images it is favourable to collect on-site reflectance spectra for individual vegetation components, bare surfaces or periglacial structures, hence such data for typical periglacial landscapes are very rare in spectral libraries. A field spectrometer is not equally replaceable with a laboratory spectrometer for serious reasons:

- In-situ atmospheric conditions and natural illumination are different from lab conditions
- A lot of material changes from being sampled until reaching the lab (e.g. thawing of ground ice, drying out of soils, wilting of vegetation, etc.).

Besides late Pleistocene Ice Complex deposits and Holocene thermokarst formation, subaquatic (marine and/or lacustrine) and glacio-marine deposits were found at the coast of Novaya Sibir Island and Oyogos Yar. These horizons perhaps point to the early and middle Pleistocene history of this region. Old buried ice wedges of a special conus-like shape with rounded heads were studied in three different sites. They are traces of an older stage of permafrost formation and are possibly linked with melting processes after ice wedge growth. Together with such ice wedges, a so-called cryogenic eluvium occurs. It consists of coarse-grained debris and yellowish loam and seems to be material of a reworked weathering crust.

Bunge-Land is a completely different formed landscape. Its origin is not associated with periglacial permafrost conditions. The area of the high terrace of Bunge-Land does in fact seem to be of terrigeneous and not of marine origin. Thermokarst phenomena indicate the existence of ice-rich permafrost in this location. For future studies on Bunge-Land, tracked vehicles and / or helicopters and drilling equipment are necessary because of the broad flat shore, the remoteness of interesting investigation sites from the coast and the absence of relief exposures.

The best study conditions were found at the coasts of Stolbovoy Island, Bel'kovsky Island, at the south coast of Kotel'ny Island (Khomurgannakh River mouth), at the southwest coast of Novaya Sibir Island (location Hedenshtrom) and at the Oyogos Yar coast. This concerns the excellent outcrop conditions as well as the occurrence of driftwood (heating material), freshwater and protected places for field camps. For future expeditions at least 2-3 weeks are necessary for detailed stratigraphical studies.

In total, 395 samples of ice, surface water and precipitation were taken during the expedition to the New Siberian Islands (Appendix 5.2-2), among them 30 ice wedges of different generations were sampled (see Table 5.2.13-1).

Table 5.2.13-1: Total number of samples and ice wedges of every location visited during the expedition as well as the occurrence of snow patches and recent ice wedges. A rough estimate of the ice wedge stratigraphy is given in the right column of the table (R= recent ice wedges, H= Holocene ice wedges, I= Ice Complex ice wedges, O= ice wedges older than the Ice Complex).

Location	No. (ice wedges)	No. (samples)	Recent ice wedges	Snow	Ice wedge stratigraphy
Stolbovoy Island	5	48	X	X	O, I, H, R
Bel'kovsky Island	6	63	X	-	O, I, H, R
Kotel'ny Island - Cape Anisy	1	10	-	X	?
Kotelny Island - Khomurgannakh R.	3	36	-	-	O, I
Bunge-Land. Low terrace	-	3	-	-	?
Bunge-Land, High terrace	-	12	X	-	?, R
Novaya Sibir Island - Derevyannye Gory	-	14	-	X	?
Novaya Sibir Island Location Hedenstrom	4	52	-	-	I, H
Maly Lyakhovsky Island	2	18	-	X	I?
Oyogos Yar coast	7	72	X?	-	O, I, H, R?
Cape Svyatoy Nos	-	14	-	X	?
Muostakh Island	1	11	-	-	I, H
Bykovsky Peninsula	1	42	-	-	I
Total	30	395			

Additionally, 210 sediment samples (Appendix 5.2-1) and 556 mammal fossil remains were collected (Appendix 5.2-3).

New study ideas are:

- Obtaining regional climate information by studying ice wedges in a great number of places as well as in extended areas,

- Study of connections the between geological basement construction, surface relief and the distribution of Ice Complex deposit and thermokarst formation;

- Comparison of coastal profiles along the Dimitri Laptev Strait (Bol'shoy Lyakhovsky Island, Oyogossky Yar, Svyatoy Nos area) in order to reconstruct Eemian and Pre-Eemian conditions,

- Study of marine deposits on Novaya Sibir Island and Faddeyevsky Island to estimate Quaternary sea level variations in the region;

- Facies analysis of Bunge-Land area (marine, glacigene, periglacial ?).

5.2.14 Appendices

Appendix 5.2-1. List of sediment samples collected on the New Siberian Islands.

No.	Sample	Sample description		Position			Depth below surface [m]	Ice content, abs./grav. [wt %]	Remarks	Date	Ice/water samples
		Sedimentology	Cryolithology	N	E	Height. a.s.l. [m]					
	East coast of Stolbovoy Island			**74°**	**136°**						
1	Sto-0-1	Silty fine sand	Ice rich, broken cryotexture				0.3	37.4/59.6	Below an Holocene ice wedge	15.08.	STO-IW-4 STO-95/01
2	Sto-1-1	Silty fine sand, small roots	Active layer, unfrozen	03.598	04.798	27	0.25		Recent cryosoil	15.08.	Sto-IW-1
3	Sto-1-2	Silty fine sand	Active layer trasition zone			27	0.5		Reducing horizon		
4	Sto-1-3	Silty fine sand	Few ice, massive texture			27	0.8	38.0/61.4	With small grass roots		
5	Sto-1-4	Silty fine sand	Few ice, massive texture			27	1.3	28.8/38.6	With small grass roots		
6	Sto-1-5	Silty fine sand	Few ice, massive texture			27	1.8	34.0/51.6	With small grass roots		
7	Sto-1-6	Grass roots				27	1	-	AMS-dating		
8	Sto-2-1	Silty fine sand	Few ice, massive texture	03.598	04.798	10		34.3/52.2		15.08.	STO-IW-5
9	Sto-2-2	Silty fine sand	Few ice, massive texture	03.598	04.798	1		33.3/50.0		15.08.	STO-IW-3
10	Sto-2-3	Silty fine sand	Few ice, massive texture	03.598	04.798	3		37.4/59.7		15.08.	STO-IW-2
11	Sto-3-1	Silty fine sand, gray, with small peat inclusions	Small ice lenses	03.598	04.798	5		36.1/56.4	Thermokarst mound with large peat lense (145 m long, 1.5-2 m thick)	15.08.	
12	Sto-3-2	Silty peat				5.25		38.8/63,4			

Appendix 5.2-1. continuation.

No.	Sample	Sample description: Sedimentology	Sample description: Cryolithology	Position: N	Position: E	Position: Height. a.s.l. [m]	Depth below surface [m]	Ice content, abs/grav. [wt %]	Remarks	Date	Ice/water samples
13	Sto-3-3	Peat, brown, fresh				5.5		50.1/100.4			
14	Sto-3-4	Peat, brown, fresh	Transparent injection ice			5.75		49.6/98.3			
15	Sto-3-5	Peat, brown, fresh				6		63.0/170.1			
16	Sto-3-6	Peat, brown, fresh	Transparent injection ice			6.25		72.7/266,2			STO-3-6
17	Sto-3-7	Peat, brown, fresh				6.5		49.6/ 98,4			
18	Sto-3-8	Silty fine sand, grayish-brown, grass roots				6.75		36.1/56.5			
19	Sto-4-0	Peat		03.915	04.544	ca. 10	0.9		Top of a thermokarst mound	15.08.	
20	Sto-4-1	Peat		03.915	04.544	ca. 10	0.7				
21	Sto-4-2	Peat		03.915	04.544	ca. 10	0.5				
22	Sto-4-3	Peat		03.915	04.544	ca. 10	0.3				
23	Sto-5	Beach pebbles		03.915	04.544	0				15.08.	
	Kotel'nylsland, Kap Anisii			**76°**	**139°**						
24	Mya-1-1	Silty fine sand, cryoturbated soil, twigs	Fine lense like cryotextur	10.220	00.816		1.5	--	Thermokarst mound	16.08.	MYA-IW-1.1 to 1.3
25	Mya-1-2	Silty fine sand, twigs					1	--	With many bones		
26	Mya-1-3	Silty fine sand					0.5				
27	Mya-peat-1	Peat		Ca. 1km to North			0.2				ANS-96-1 to 2
28	Mya-peat-2	Peat					0.6				

Appendix 5.2-1. continuation.

No.	Sample	Sample description		Position			Depth below surface [m]	Ice content, abs/grav. [wt %]	Remarks	Date	Ice/water samples
		Sedimentology	Cryolithology	N	E	Height. a.s.l. [m]					
	South cape of Bel'kovsky Island			**75°**	**135°**						
29	Bel-1	Beach pebbles		21.949	35.337		0		Up to 0.2 cm in diameter	17.08.	
30	Bel-2-1	Silty fine sand, cryoturbated	Lens like, vertical streaks (1-3 cm)	21.961	35.247	12.3	2.7	40.6/68.4	Thermokarst mound	17.08.	
31	Bel-2-2	Silty fine sand	Fine lens like cryostructure			12.8	2.2	46.2/86.5			
32	Bel-2-3	Silty fine sand	Fine lens like reticulated, ice bands			13.2	1.8	46.7/87.6			
33	Bel-2-4	Silty fine sand, single grass roots	Lens like reticulated, ice bands			13.4	1.6	45.2/82.4			
34	Bel-2-5	Peat inclusion				13.7	1.3				
35	Bel-2-6	Silty fine sand, with peat inclusions				13.75	1.25				
36	Bel-2-7	Twigs inthe peat horizon				14.6	0.6		AMS-dating, peat horizon of the next thermokarst mound		
37	Bel-3-1	Silty fine sand, plant roots	Fine lenslike reticulated	21.953	35.620	3.7		29.3/41.4		17.08.	BEL-IW-
38	Bel-3-2	Silty fine sand, plant roots				4.2				17.08.	1.1 to
39	Bel-3-3	Silty fine sand, plant roots				4.6				17.08.	1.21

Appendix 5.2-1. continuation.

No.	Sample	Sample description		Position			Depth below surface [m]	Ice content, abs/grav. [wt %]	Remarks	Date	Ice/water samples
		Sedimentology	Cryolithology	N	E	Height. a.s.l. [m]					
40	Bel-4-1	Silty fine sand, small grass roots	Fine lenslike reticulated	21.950	35.391	2.5				17.08.	BEL-W-2.1 to 2.4
41	Bel-AA-1	Recent surface		22.012	35.275		0-0.10		Thermokarst mound, pollen analyses	17.08.	
42	Bel-AA-2	Recent surface					0-0.10		Thermo-erosional valley		
43	Bel-5-1	Silty fine sand	Active layer, unfrozen	21.985	34.432		0.2			17.08.	BEL-IW-3.1 to 3.12
44	Bel-5-2	Silty fine sand	Transition zone frozen				0.6				
45	Bel-5-3	Silty fine sand					0.9				
46	Bel-5-4	Silty fine sand					1.3				
47	Bel-5-5	Silty fine sand					1.6				
48	Bel-5-6	Recent surface					0-0.05				
49	Bel-6	Gravels		22.005	34.160		0		Brock bed of a thermo-erosional valley	17.08.	
50	Bel-7-1	Silty clay, gray-blue	Fine laminated cryostructure	21.995	34.275	1			Lake deposit, ice wedge cast	17.08.	
51	Bel-7-2	Interbedding				1.8					
52	Bel-7-3	Of silt, sand				2.5					
53	Bel-7-4	And organic				3					
54	Bel-7-5	Detritus lamines				3.5					
55	Bel-7-6					3.8					

Appendix 5.2-1. continuation.

No.	Sample	Sample description: Sedimentology	Sample description: Cryolithology	Position: N	Position: E	Position: Height. a.s.l. [m]	Depth below surface [m]	Ice content, abs/grav. [wt %]	Remarks	Date	Ice/water samples
56	Bel-8-1	Shrub fragments, peat, sand		50 m		1.2			Ice wedge cast	17.08.	
57	Bel-8-2 Bel-8a	Allochton moss peat with twigs, weakly decomposed		West of		2			Ice wedge cast		
58	Bel-8b	Interbedding of organic and fine sand lamines		Bel-6		2.1					
59	Bel-8-3 Bel-8c	Silty fine sand with shells				2.2-2.3			Lake deposits		
60	Bel-8-4	Silty fine sand with shells				2.7-2.8			Lake deposits		
61	Bel-8d	Fine laminated fine sand				3			Lake deposits		
		Kotel'ny Island Southwest coast		**74°**	**138°**						
62	Kys-1	Beach boulder		43.991	27.229	1	0			18.08.	
63	Kys-2-1	Sandy silt, gray, single non subrounded gravels	Ice band, coarse lens like reticulated cryostructure	44.003	27.071	1.6		48.4/93.8	Thermokarst mound at the beach	18.08.	KYS-IW-2.1 to 2.6
64	Kys-2-2	Coarse-grained sandy gravels	Ice bands			2.1		33.7/50.8			
65	Kys-2-3	Coarse-grained sandy gravels	Ice bands, fine lens-like cryostructure			2.35		39.2/64.6			
66	Kys-2-4	Silty sand, small roots	Fine lenslike cryostructure			2.7		46.5/87.0			

Appendix 5.2-1. continuation.

No.	Sample	Sample description		Position			Depth below surface [m]	Ice content, abs/grav. [wt %]	Remarks	Date	Ice/water samples
		Sedimentology	Cryolithology	N	E	Height. a.s.l. [m]					
67	Kys-2-5	Silty fine sand, cryoturebated paleosol	Few ice			3		49.5/97.8			
68	Kys-2-6	Silty fine sandwith peat inclusions (3-7 cm)	Coarse lenslike reticulated			4		60.8/155			
69	Kys-2-7	Selcted gravels				1.75-2.4					
70	Kys-2-8	Yelloish sandy gravel, subrounded	Ice lenses			1.5		28.4/39.7	"cryogenic alluvium", weathered material		
71	Kys-2-9	Silty fine sand	Ice bands (0.5 mm), broken lenslike cryostructure	44.003	27.071	ca. 7.3		33.6/50.5	Themokarst mound about 8 m above the beach	18.08.	KYS-IW-1.1 to 1.18
72	Kys-2-10	Silty fine sand, small grass roots	Ice bands, broken lenslike cryostructure			ca. 8.4		45.0/81.8			
73	Kys-2-11	Silty fine sand, brownish	Near the ice wedge			ca. 8.1		38.0/61.2			
74	Kys-3	Beach material				ca. 1	0		Shells, sponges	18.08.	
75	Kys-AA	Surface material		44.321	24.200	ca. 3.5	0-0.05		Thermokarst depression, pollen analyses	18.08.	

Appendix 5.2-1. continuation.

No.	Sample	Sample description		Position			Depth below surface [m]	Ice content, abs/grav. [wt %]	Remarks	Date	Ice/water samples
		Sedimentology	Cryolithology	N	E	Height. a.s.l. [m]					
	Bunge Land upper terrace			74°	142°						
76	Bun-1	Recent lake deposit		52.050	09.703		0-0.05		Small thermokarst lake, 10 m from the bank, 0.4 m water depth	19.08.	Surface water ?
77	Bun-2	Recent lake deposit		52.357	09.470		0-0.05		Large thermokarst lake, 7m from the bank, 0.2 m water depth	19.08.	
78	Bun-3-1 AA	Fine sand		52.163	09.651		0		Surface of the valley bottom, pollen analyses	19.08.	
79	Bun-3-2 AA	Fine sand					0		Surface of the valley rim, pollen analyses		
80	Bun-4-1	Interbedding of fine sand and black organic-rich laminae		52.163	09.651		3	18.3/22.3	Section in the step valley rim	19.08.	
81	Bun-4-2	See above					2.70-2.80	-	Sand layers 2-30 mm thick		
82	Bun-4-3	See above					2.40-2.30	25.3/33.9	Organic-rich layers 2-6 mm thick		
83	Bun-4-4	Sand, organic rich					1.80-1.90	15.9/18.9			
84	Bun-4-5	Fine sand, oxiding, cryoturbated					1.50-1.60	15.1/17.8	Paleosol		
85	Bun-4-6	Fine sand					0.80-0.90				
86	Bun-4-7	Fine sand					0.30-0.40				

Appendix 5.2-1. continuation.

No.	Sample	Sample description		Position			Depth below surface [m]	Ice content, abs/grav. [wt %]	Remarks	Date	Ice/water samples
		Sedimentology	Cryolithology	N	E	Height. a..s.l. [m]					
87	Bun-5-1	Fine sand		52.163	09.651		0.50-0.60		Valley rim	19.08.	
88	Bun-5-2	Cryoturbated soil		52.163	09.651		0.20-0.30				
89	Bun-5-3	Fine sand		52.163	09.651		0.10-0.20				
90	Bun-5-AA	Surface sample		52.163	09.651		0-0.05		Pollen analyses		
91	Bun-6	Fine sand, middle sand, gravels		52.458	07.920		0		Collected from the surface		
92	Bunge-1	Interbedding of fine sand and black organic-rich laminae	Frozen	52.163	09.651		3		Drilled, like Bun-4-1	19.08.	
93	Bunge-1-y						3		γ-spectrometry		
94	Bunge-2	Fine sand	Unfrozen				0.7	0	Hammered, like Bun-4-7		
95	Bunge-2-y						0.7	0	γ-spectrometry		
96	Bunge-3	Fine sand	Unfrozen				0.7	0	Hammered, like Bun-5-1		
97	Bunge-3-y						0.7	0	γ-spectrometry		
98	Bun-95-I	Fine sand		50m E of Bun-4				--	Near of a recent ice wedge		BUN-95

Appendix 5.2-1. continuation.

No.	Sample	Sample description		Position			Depth below surface [m]	Ice content, abs/grav. [wt %]	Remarks	Date	Ice/water samples
		Sedimentology	Cryolithology	N	E	Height. a.s.l. [m]					
	Bunge Land lower terrace			**74°**	**140°**						
99	Bun-7-1	Silty fine sand	Frozen	50.352	23.206	ca.1-1.5	0.6	25.7/34.5	Small pit	25.08.	
100	Bun-7-3-Eis		Texture ice				0.6				
101	Bun-7-2	Clayish fine sand	Unfrozen				0.5				
102	Bun-7-3	Fine sand, recent roots	Unfrozen, dry				0.25				
103	Bun-7-4	Carex-species					0		Vegetation, pollen analyses		
104	Bun-7-5	Fine sand					0.3		Pit		
105	Bun-8	Fine sand				ca. 0.3	0		Beach sand		
106	Bun-9	Beach material							Shells, sponges	19./25, 08.	
107	Bunge-4	Silty fine sand	Frozen				0.6		Drilled like Bun-7-1	25.08.	
108	Bunge-4-y	Silty fine sand					0.6		γ-spectrometry		
109	Bunge-5	Sand	Unfrozen				0.4		Hammered		
110	Bunge-5-y	Sand					0.4		γ-spectrometry		
	New Siberian Island, Derevyaniy Gora			**75°**	**147°**						
111	Nes-AA-1	Surface material					0-0.05		Pollen analyses	20.08.	
112	Nes-4	Boulders		01.096	05.136	ca. 50	0				
113	Nes-5	Boulders					0				
114	Nes-6	Boulders		01.096	05.136	ca. 50	0				
115	Nes-1-1	Coal							Cretaceous wood coal stems		
116	Nes-1-2	Coal									
117	Nes-2	Coal									

Appendix 5.2-1. continuation.

No.	Sample	Sample description		Position			Depth below surface [m]	Ice content, abs/grav. [wt %]	Remarks	Date	Ice/water samples
		Sedimentology	Cryolithology	N	E	Height. a.s.l. [m]					
	New Siberian Island, Urositse Hedenstrom			**75°**	**146°**						
118	Nes-7-1	Clayish silt	Horizontal to subhorizontal ice lenses, reticulated	07.156	38.857	ca. 12.3	1.2	56.9/ 132.3	Coastal outcrop	21.08.	
119	Nes-7-2	Clayish silt	Thin ice streaks			ca. 11.7	1.8	42.1/72.6	Marine or alas deposit		
120	Nes-7-3	Bluish-gray fine sandy silt	Diagonal ice streaks			ca. 11.4	2.1	30.8/44.6	With brownish oxydations patches		
121	Nes-7-4	Bluish-gray fine sandy silt	Diagonal ice streaks			ca. 11	2.5	29.6/42.0	Marine or alas deposit		NSI-IW-
122	Nes-7-5	Bluish-gray fine sandy silt	Diagonal ice streaks			ca. 10.5	3	34.5/52.6			1.1 to 1.16
123	Nes-7-6	Bluish-gray fine sandy silt	Diagonal ice streaks			ca 10.1	3.4	39.5/65.2			
124	Nes-7-7	Bluish-gray fine sandy silt	Thick ice streaks			ca 9	4.5	32.8/48.7			NSI-TI-1
125	Nes-7-8	Bluish-gray fine sandy silt	Diagonal ice streaks			ca. 7.7	5.8	42.4/75.5			
126	Nes-7-9	Bluish-gray fine sandy silt	Diagonal ice streaks			ca. 6.5	7	36.7/58.0			
127	Nes-7-10	Bluish-gray fine sandy silt	Diagonal ice streaks			caa. 5	8.5	27.6/38.1			
128	Nes-7-11	Bluish-gray fine sandy silt, small subrounded gravels	Diagonal ice streaks			ca. 4	9.5	27.7/38.4			
129	Nes-7-12	Sand-silt-interbedding, ripple marks				ca. 3.8	9.7	17.1/20.7			
130	Nes-7-13	Gravels, subrounded,1cm				ca. 3.7	9.8	19.7/24.6			
131	Nes-7-14	Silty fine sand, twig fragments	Ice bands			ca. 2.7	10.8	31.8/46.7			NSI-TI-3
132	Nes-7-15	Twig fragments				ca. 2.7	10.8		AMS-dating		

Appendix 5.2-1. continuation.

No.	Sample	Sample description		Position			Depth below surface [m]	Ice content, abs/grav. [wt %]	Remarks	Date	Ice/water samples
		Sedimentology	Cryolithology	N	E	Height. a.s.l. [m]					
133	Nes-8-1	Clayish silt to silty clay, bluish-gray, with dropstones	Diagonal ice streaks	07.331	37.559	1.3			Marine deposit	21.08.	
134	Nes-8-2	Clayish silt to silty clay, bluish-gray, with dropstones	Diagonal ice streaks			2.2			Marine deposit		
135	Nes-8-3	Clayish silt to silty clay, bluish-gray, with dropstones	Diagonal ice streaks			3			Marine deposit		
136	Nes-8-4	Clayish silt to silty clay, bluish-gray, with dropstones	Diagonal ice streaks			4			Marine deposit		
137	Nes-8-5	Silty fine sand				5			Alas deposit (?)		
138	Nes-8-6	Pebbles							Dropstones (IRD), selected		
139	Nes-9-1	Silty clay		07.594	36.340	1.4		26.7/39.6	Marine deposit	21.08.	
140	Nes-9-2	Silty clay		07.594	36.340	2		28.4734.5	Marine deposit		
141	Nes-9-3	Silty clay		07.594	36.340	2.6		25.6/36.3	Marine deposit		
142	Nes-9-4	Silty clay		07.594	36.340	3.5		--	Marine deposit		
143	Nes-9-5	Clayish silt, laminated with organic layers		07.594	36.340	4		--	Lacustrine deposits		
144	Nes-AA-3	Surface material		07.196	38.535	ca. 3	0-0.05		Pollen analyses		
145	Nes-10	Pebbles				2-3.5			Dropstones (IRD), selected		
146	Nes-11	Pebbles					0		Pebbles from various *thermokarst* mounds		

Appendix 5.2-1. continuation.

No.	Sample	Sample description		Position			Depth below surface [m]	Ice content, abs/grav. [wt %]	Remarks	Date	Ice/water samples
		Sedimentology	Cryolithology	N	E	Height. a.s.l. [m]					
	Maly Lyakhov Island			**74°**	**140°**						
147	Kly-1-1	Fine sandy silt	Ice banded	14.763	21.052		5	42.4/73.5	Thermokarst mound	27.08.	
148	Kly-1-2	Fine sandy silt	Ice banded				4.5	37.4/59.6			
149	Kly-1-3	Fine sandy silt	Ice banded				4	57/132.5			
150	Kly-1-4	Fine sandy silt	Ice banded				3.3	48.1/92.8			
151	Kly-1-5	Fine sandy silt	Ice banded				2.8	45/81.8			
152	Kly-1-6	Fine sandy silt, soil horizon with peat inclusions	Transition zone of the active layer				2.1	43.7/77.6			
153	Kly-1-7	Allochtonous peat layer					2				
154	Kly-1-8	Silty fine sand, laminated					1.8				
155	Kly-1-9	Silty fine sand, laminated					1.5				
156	Kly-1-10	Recent soil, rooted					0-0.05		Pollen analyses		
157	Kly-AA-1	Surface material				25-28	0-0.05		Pollen analyses		
158	Kly-2	Beach material		14.591	19.181				Sponges		

Appendix 5.2-1. continuation.

No.	Sample	Sample description		Position			Depth below surface [m]	Ice content, abs/grav. [wt %]	Remarks	Date	Ice/water samples
		Sedimentology	Cryolithology	N	E	Height. a.s.l. [m]					
S of Cape Svyatoy Nos				72°	140°						
159	Svn-1-1	Silty fine sand light gray, laminated		47.095	50.542	2.5			Cliff	28.08.	
160	Svn-1-2	Allochtonous peat		47.095	50.542	6				28.08.	
161	Svn-1-3	Shrub fragments		47.095	50.542	3				28.08.	
162	Svn-1-4	Shrub fragments		47.095	50.542	ca. 15			Thermokarst mound	28.08.	
163	Svn-1-5	Shrub fragments				ca. 15			Thermokarst mound	28.08.	
164	Svn-2	Twigs, vivianite				3			Cliff, 350 m SE of the landing point	28.08.	
165	Svn-3	Beach sand							Beach, 300 m NW of the landing point	28.08.	
166	Svn-4-1	Pebble.surface lineation		47.415	49.186				Valley with snow patch	28.08.	
167	Svn-4-2	Beach pebbles									
168	Svn-4-3	Beach pebbles									
169	Svn-4-4	Stones							Valley with snow patch, comparison granite dolerit	28.08.	

Appendix 5.2-1. continuation.

No.	Sample	Sample description		Position			Depth below surface [m]	Ice content, abs/grav. [wt %]	Remarks	Date	Ice/water samples
		Sedimentology	Cryolithology	N	E	Height. a.s.l. [m]					
	Oyogosky Ya			**72°**	**143°**						
170	Oya-1	Surface material		40.519	35.922	ca. 8-9	0-0.05		Pollenanalyses	30.08.	
171	Oya-2-1	Peat, non-decomposed with wood fragments	Ice rich	39.166	33.500	40	0.4-0.5		Co-ordinates according to the map	30.08.	
172	Oya-2-2	Peat, non-decomposed with wood fragments					0.7-0.8				
173	Oya-2-3	Peat, non-decomposed with wood fragments					1.2-1.3		Thermokarst mound,		
174	Oya-2-4	Peat, non-decomposed with wood fragments					1.6-1.7				
175	Oya-2-5	Peat with vertically twigs, cryoturbated soil					1.9-2.0				
176	Oya-2-6	Silty fine sand, cryoturbated paleosol					2.2-2.3	35.3/54.4	Ice Complex deposit		
177	Oya-2-7	Silty fine sand, twigs	Coarse lens like reticulated				2.3-2.4	54.1/118			
178	Oya-2-8	Silty fine sand, twigs	Coarse lens like reticulated				3.0-31.0	51/ 104.1			
179	Oya-2-9	Surface material					0-0.05		Pollen analyses		

Appendix 5.2-1. continuation.

No.	Sample	Sample description		Position			Depth below surface [m]	Ice content, abs/grav. [wt %]	Remarks	Date	Ice/water samples
		Sedimentology	Cryolithology	N	E	Height. a.s.l. [m]					
180	Oya-3-2	Silty fine sand	Lens like reticulated	40.759	33.085		1.4		Coastal cliff, lowest part, Ice Complex	30.08.	
181	Oya-3-3	Silty fine sand, fine-laminated, with thin organic layers	Injection ice				2.4	49.7/99.0	Ice Complex deposit		OYA-IW-2.0 to 2.11
182	Oya-3-4	Silty fine sand	Few ice				3	36.7/58.0	Oxidic transition zone		
183	Oya-3-5	Silty fine sand	Few ice				3.6	35.9/55.9	Oxidic transition zone		
184	Oya-3-6	Grayish-blue silt	Few ice				4.1	32.2/47.6	Reductic part, lacustrine deposit		
185	Oya-3-8	Dark-gray clayish silt	Few ice				5.8	27.6/38.0	Lacustrine deposit		
186	Oya-3-9	Dark-gray clayish silt	Ice rich				6.4	49.1/96.6	Lacustrine deposit		
187	Oya-3-10	Gray, clayish silt, laminated	Few ice				7.4		Ice wedge cast with lacustrine deposit		
188	Oya-3-11	Peat, wood	Frozen				7.4		Pseudomorphose, like Oya-3-10		
189	Oya-3-12	Gray, clayish silt, laminated	Frozen				8.2		Lacustrine deposit		
190	Oya-3-13	Shrub wood							Selected, near ice wedge casts		
191	Oya-4-1	Silty fine sand		40.669	33.857			60.5/ 153.2	Ice Complex, middle part	30.08.	Oya- iW-5.1
192	Oya-4-2	Silty fine sand		40.669	33.857					30.08.	to 5.15
193	Oya-5-1	Silt, gray				3.5			With shells	30.08.	
194	Oya-5-2	Wood				13			Alass at the end of the thermocirque	30.08.	
195	Oya-6-1	Peat inclusion		40.524	36.024	3.25			Near of an old ice wedge	30.08.	OYA-IW-1.1 to 1.6

Appendix 5.2-1. continuation.

No.	Sample	Sample description: Sedimentology	Sample description: Cryolithology	Position: N	Position: E	Position: Height. a.s.l. [m]	Depth below surface [m]	Ice content, abs/grav. [wt %]	Remarks	Date	Ice/water samples
Muostakh Island					**71 129**						
196	Muo-1	Surface material		36.820	56.179	ca. 23			Vegetation cover, pollen analyses Frost boil, pollen analyses	02.09.	
197	Muo-2	Surface material		36.623	56.179	23					
198	Muo-3-1	Silty fine sand	Fine lenslike	36.804	56.446	0.5		49.3/97.4	Section 1	02.09.	
199	Muo-3-2	Silty fine sand	Rediculated			1		53.4/ 114.5			MUO-IW
200	Muo-3-3	Silty fine sand	Cryostructure,			1.5		57.6/ 135.8			01 to 12
201	Muo-3-4	Silty fine sand	Ice bands			2		54.5/ 119.6			
202	Muo-3-5	Peat inclusion				1					
203	Muo-3-6	Silty fine sand				2.5		55/122.2			
204	Muo-3-7	Silty fine sand				3					
205	Muo-3-8	Fine sand	Massive cryostructure	36.773	56.615	5		37/ 58.7	Section 2	02.09.	
206	Muo-3-9	Peat, roots				7.5					
207	Muo-3-10	Middle sand				6.5		52.5/ 110.5			
208	Muo-3-11	Sand-silt-interbedding	Unfrozen			9.7					
209	Muo-3-12	Sand	Frozen			8.5					
210	Muo-4	Beach sand		36.820	56.179	1				02.09.	

Ice content, abs./grav. [wt %]
abs. = absolut; ratio of ice mass to wet sample mass
grav. = gravimetric; ratio of ice mass to dry sample mass (> 100 % indicates an ice oversaturation)

Appendix 5.2-2. List of ice and water samples collected on the New Siberian Islands.

				Isotopes			Chemistry				
Nr.	date	sample	type	^{18}O	^{2}H	^{3}H	anion/ cation	LF [µS/cm]	pH	filter	Remarks
1	15.08.	STO-97/01	SP	x	x	x	x	30.5	6.89	-	
2	15.08.	STO-IW-1.1	IW	x	x	-	x	131.6	8.15	-	
3	15.08.	STO-IW-1.2	IW	x	x	-	-	-	-	CAF	
4	15.08.	STO-IW-1.3	IW	x	x	-	x	161.0	8.03	-	
3	15.08.	STO-IW-1.4	IW	x	x	-	-	-	-	CAF	
6	15.08.	STO-IW-1.5	IW	x	x	-	x	180.8	7.91	-	
7	15.08.	STO-IW-1.6	IW	x	x	-	-	-	-	-	
8	15.08.	STO-IW-1.7	IW	x	x	-	x	145.5	7.87	-	
9	15.08.	STO-IW-1.8	IW	x	x	-	-	-	-	CAF	
10	15.08.	STO-IW-1.9	IW	x	x	-	x	159.2	7.82	-	
11	15.08.	STO-IW-1.10	IW	x	x	-	-	-	-	-	
12	15.08.	STO-IW-1.11	IW	x	x	-	x	177.6	7.89	-	
13	15.08.	STO-IW-1.12	IW	x	x	-	-	-	-	-	
14	15.08.	STO-IW-1.13	IW	x	x	-	x	204	7.96	-	
15	15.08.	STO-IW-1.14	IW	x	x	-	-	-	-	-	
16	15.08.	STO-IW-1.15	IW	x	x	-	x	104.2	8.34	-	
17	15.08.	STO-IW-1.16	IW	x	x	x	x	157.9	7.91	-	
18	15.08.	STO-IW-4.1	IW	x	x	-	x	97.7	7.67	-	
19	15.08.	STO-IW-4.2	IW	x	x	-	-	-	-	CAF	
20	15.08.	STO-IW-4.3	IW	x	x	x	x	83.5	7.73	-	
21	15.08.	STO-IW-4.4	IW	x	x	-	-	-	-	CAF	
22	15.08.	STO-IW-4.5	IW	x	x	-	x	82.9	7.67	-	
23	15.08.	STO-94/01	RIW	x	x	x	x	273	7.56	-	
24	15.08.	STO-3-6	II	x	x	x	-	-	-	-	
25	15.08.	STO-IW-3.1	IW	x	x	-	x	158	7.92	-	
26	15.08.	STO-IW-3.2	IW	x	x	x	-	-	-	-	
27	15.08.	STO-IW-3.3	IW	x	x	x	-	-	-	-	
28	15.08.	STO-IW-3.4	IW	x	x	-	x	122	7.83	-	
29	15.08.	STO-IW-3.5	IW	x	x	-	-	-	-	-	
30	15.08.	STO-IW-3.6	IW	x	x	-	-	-	-	CAF	
31	15.08.	STO-TI-1	IW	x	x	-	-	550	7.76	-	
32	15.08.	STO-IW-2.1	IW	x	x	-	x	120	7.94	-	
33	15.08.	STO-IW-2.2	IW	x	x	x	-	-	-	CAF	
34	15.08.	STO-IW-2.3	IW	x	x	-	x	95.1	8.04	-	
35	15.08.	STO-IW-2.4	IW	x	x	x	-	-	-	CAF	
36	15.08.	STO-IW-2.5	IW	x	x	-	x	-	-	-	
37	15.08.	STO-IW-5.1	IW	x	x	-	-	136	7.75	CAF	
38	15.08.	STO-IW-5.2	IW	x	x	-	x	129	7.98	-	
39	15.08.	STO-IW-5.3	IW	x	x	-	-	116	7.82	CAF	
40	15.08.	STO-IW-5.4	IW	x	x	-	x	117.2	8.00	-	
41	15.08.	STO-IW-5.5	IW	x	x	-	-	-	-	-	
42	15.08.	STO-IW-5.6	IW	x	x	x	x	104.1	7.73	-	
43	15.08.	STO-IW-5.7	IW	x	x	-	-	407	8.01	CAF	
44	15.08.	STO-IW-5.8	IW	x	x	-	x	395	7.88	-	
45	15.08.	STO-IW-5.9	IW	x	x	-	-	200	8.02	-	
46	16.08.	ANS-96-1	SW	x	x	x	-	-	-	-	
47	16.08.	ANS-96-2	SW	x	x	x	-	-	-	-	
48	16.08.	MYA-96/01	SW	x	x	x	-	284	7.96	-	
49	16.08.	ANS-97-1	SP	x	x	x	-	-	-	CAF	
50	16.08.	ANS-97-2	SP	x	x	x	-	-	-	CAF	
51	16.08.	MYA-IW-1.1	IW	x	x	x	-	-	-	-	
52	16.08.	MYA-IW-1.2	IW	x	x	-	x	111.1	8.37	CAF	
53	16.08.	MYA-IW-1.3	IW	x	x	-	x	114.2	7.94	-	
54	16.08.	MYA-TI-1	TI	x	x	-	-	-	-	-	
55	17.08.	BEL-IW-1.1	IW	x	x	-	x	265	7.57	-	

				Isotopes				Chemistry				
Nr.	date	sample	type	^{18}O	^{2}H	^{3}H	anion/ cation	LF [µS/cm]	pH	filter	Remarks
56	17.08.	BEL-IW-1.2	IW	x	x	-	x	128	7.76	-	
57	17.08.	BEL-IW-1.3	IW	x	x	-	x	114	7.8	-	
58	17.08.	BEL-IW-1.4	IW	x	x	x	-	-	-	-	
59	17.08.	BEL-IW-1.5	IW	x	x	-	x	213	7.85	-	
60	17.08.	BEL-IW-1.6	IW	x	x	-	-	-	-	CAF	
61	17.08.	BEL-IW-1.7	IW	x	x	-	x	170	7.81	-	
62	17.08.	BEL-IW-1.8	IW	x	x	-	-	-	-	-	
63	17.08.	BEL-IW-1.9	IW	x	x	-	x	152	7.75	-	
64	17.08.	BEL-IW-1.10	IW	x	x	-	-	-	-	CAF	
65	17.08.	BEL-IW-1.11	IW	x	x	-	x	163	7.71	-	
66	17.08.	BEL-IW-1.12	IW	x	x	-	-	-	-	-	
67	17.08.	BEL-IW-1.13	IW	x	x	-	x	152	7.63	-	
68	17.08.	BEL-IW-1.14	IW	x	x	-	-		-	CAF	
69	17.08.	BEL-IW-1.15	IW	x	x	-	x	147	7.69	-	
70	17.08.	BEL-IW-1.16	IW	x	x	x	-	-	-	-	
71	17.08.	BEL-IW-1.17	IW	x	x	-	x	125	7.75	-	
72	17.08.	BEL-IW-1.18	IW	x	x	-	-	-	-	CAF	
73	17.08.	BEL-IW-1.19	IW	x	x	-	x	117	7.75	-	
74	17.08.	BEL-IW-1.20	IW	x	x	-	-	-	-	CAF	
75	17.08.	BEL-IW-1.21	IW	x	x	-	x	160	7.88	-	
76	17.08.	BEL-IW-2.1	IW	x	x	-	-	-	-	CAF	
77	17.08.	BEL-IW-2.2	IW	x	x	-	x	284	7.79	-	
78	17.08.	BEL-IW-2.3	IW	x	x	-	-	-	-	CAF	
79	17.08.	BEL-IW-2.4	IW	x	x	x	x	180	7.56	-	
80	17.08.	BEL-IW-3.1	IW	x	x	-	x	97.4	6.64	GFF	
81	17.08.	BEL-IW-3.2	IW	x	x	x	-	-	-	-	
82	17.08.	BEL-IW-3.3	IW	x	x	-	x	65.4	6.37	GFF	
83	17.08.	BEL-IW-3.4	IW	x	x	-	-	-	-	-	
84	17.08.	BEL-IW-3.5	IW	x	x	-	x	73.3	6.48	-	
85	17.08.	BEL-IW-3.6	IW	x	x	-	-	-	-	CAF	
86	17.08.	BEL-IW-3.7	IW	x	x	-	x	50.5	6.24	-	
87	17.08.	BEL-IW-3.8	IW	x	x	-	x	75.4	6.12	-	
88	17.08.	BEL-IW-3.9	IW	x	x	-	-	-	-	CAF	
89	17.08.	BEL-IW-3.10	IW	x	x	-	x	68.7	6.51	-	
90	17.08.	BEL-IW-3.11	IW	x	x	-	x	38.3	6.38	-	
91	17.08.	BEL-IW-3.12	TI	x	x	-	-	-	-	-	
92	17.08.	BEL-IW-4.1	IW	x	x	x	-	-	-	CAF	
93	17.08.	BEL-IW-4.2	IW	x	x	-	x	166	6.23	-	
94	17.08.	BEL-IW-4.3	IW	x	x	x	-	-	-	CAF	
95	17.08.	BEL-IW-4.4	IW	x	x	-	x	68.5	6.08	-	
96	17.08.	BEL-IW-5.1	IW	x	x	x	-	-	-	CAF	
97	17.08.	BEL-IW-5.2	IW	x	x	-	x	155	6.77	-	
98	17.08.	BEL-IW-5.3	TI	x	x	-	x	370	5.53	-	
99	17.08.	BEL-IW-6.1	IW	x	x	x	-	-	-	-	
100	17.08.	BEL-IW-6.2	IW	x	x	x	x	79.3	5.84	CAF	
101	17.08.	BEL-IW-6.3	IW	x	x	x	-	-	-	CAF	
102	17.08.	BEL-IW-6.4	IW	x	x	x	x	131	5.86	-	
103	17.08.	BEL-96/01	SW	x	x	-	x	423	7.19	-	
104	17.08.	BEL-96/02	SW	x	x	x	x	27700	7.72	-	SAL=18.9‰
105	17.08.	BEL-95/01	SI	x	x	x	x	287	6.43	-	
106	18.08.	KYS-IW-1.1	IW	x	x	-	x	73.6	-	-	
107	18.08.	KYS-IW-1.2	IW	x	x	-	x	64.5	-	-	
108	18.08.	KYS-IW-1.3	IW	x	x	-	x	63.5	7.3	-	
109	18.08.	KYS-IW-1.4	IW	x	x	x	-	-	-	CAF	
110	18.08.	KYS-IW-1.5	IW	x	x	-	x	71.3	6.99	-	
111	18.08.	KYS-IW-1.6	IW	x	x	-	-	-	-	CAF	
112	18.08.	KYS-IW-1.7	IW	x	x	-	x	120	7.38	-	

				Isotopes			Chemistry				
Nr.	date	sample	type	^{18}O	^{2}H	^{3}H	anion/ cation	LF [µS/cm]	pH	filter	Remarks
113	18.08.	KYS-IW-1.8	IW	x	x	-	-	-	-	CAF	
114	18.08.	KYS-IW-1.9	IW	x	x	-	x	70.8	7.38	-	
115	18.08.	KYS-IW-1.10	IW	x	x	-	-	-	-	-	
116	18.08.	KYS-IW-1.11	IW	x	x	-	x	87.6	7.44	-	
117	18.08.	KYS-IW-1.12	IW	x	x	-	-	-	-	CAF	
118	18.08.	KYS-IW-1.13	IW	x	x	-	x	111	7.67	-	
119	18.08.	KYS-IW-1.14	IW	x	x	-	-	-	-	-	
120	18.08.	KYS-IW-1.15	IW	x	x	-	x	70.5	7.43	-	
121	18.08.	KYS-IW-1.16	IW	x	x	x	-	-	-	CAF	
122	18.08.	KYS-IW-1.17	IW	x	x	-	x	149	7.48	-	
123	18.08.	KYS-IW-1.18	IW	x	x	-	-	-	-	-	
124	18.08.	KYS-IW-2.1	IW	x	x	-	x	125	7.37	-	
125	18.08.	KYS-IW-2.2	IW	x	x	x	-	-	-	CAF	
126	18.08.	KYS-IW-2.3	IW	x	x	-	x	93.5	7.7	-	
127	18.08.	KYS-IW-2.4	IW	x	x	x	-	-	-	CAF	
128	18.08.	KYS-IW-2.5	IW	x	x	-	x	89.3	7.85	-	
129	18.08.	KYS-IW-2.6	IW	x	x	-	-	-	-	CAF	
130	18.08.	KYS-IW-3.1	IW	x	x	x	x	378	6.68	-	
131	18.08.	KYS-IW-3.2	IW	x	x	-	x	149	6.72	-	
132	18.08.	KYS-96-1	SW	x	x	x	-	-	-	-	
133	18.08.	KYS-96/02	SW	x	x	x	x	25300	7.77	-	SAL=17.2‰
134	18.08.	KYS-95/01	SI	x	x	x	x	1352	6.78	-	
135	17.08.	BEL-5-2.TI	TI	x	x	-	x	1263	5.84	-	SAL=0.5‰
136	17.08.	BEL-5-3.TI	TI	x	x	-	x	137	6.74	-	
137	17.08.	BEL-5-4.TI	TI	x	x	-	x	218	6.55	-	
138	17.08.	BEL-5-5.TI	TI	x	x	-	x	211	6.43	-	
139	19.08.	BUN-96/01	SW	x	x	x	x	64.1	6.99	-	
140	19.08.	BUN-96/02	SW	x	x	x	x	37.2	6.56	-	
141	19.08.	BUN-96/03	SW	x	x	x	x	24200	7.58	-	SAL=16.4‰
142	19.08.	BUN-95/01	RIW	x	x	x	x	60.0	6.65	-	
143	19.08.	BUN-95/02	RIW	x	x	x	-	-	-	-	
144	19.08.	BUN-95/03	RIW	x	x	-	-	-	-	-	
145	19.08.	BUN-95/04	SI	x	x	x	x	13.4	6.13	-	
146	19.08.	BUN-96/04	SW	x	x	x	-	-	-	-	
147	17.08.	BEL-2-1.TI	TI	x	x	-	x	546	7.35	-	
148	17.08.	BEL-2-2.TI	TI	x	x	-	x	556	6.57	-	
149	17.08.	BEL-2-4.TI	TI	x	x	-	x	-	-	-	
150	17.08.	BEL-2-6.TI	TI	x	x	-	-	63.2	6.1	-	
151	17.08.	BEL-3-2.TI	TI	x	x	-	x	-	-	-	
152	17.08.	BEL-3-3.TI	TI	x	x	-	x	-	-	-	
153	17.08.	BEL-4-1.TI	TI	x	x	-	-	5320	7.39	-	SAL=3.2‰
154	17.08.	BEL-7-1.TI	TI	x	x	-	x	-	-	-	
155	15.08.	STO-0-1.TI	TI	x	x	-	x	1595	7.19	-	
156	15.08.	STO-1-3.TI	TI	x	x	-	x	-	-	-	
157	15.08.	STO-2-3.TI	TI	x	x	-	x	4160	7.21	-	SAL=2.4‰
158	16.08.	MYA-1-1.TI	TI	x	x	-	-	-	-	-	
159	18.08.	KYS-2-1.TI	TI	x	x	-	x	450	7.55	-	
160	18.08.	KYS-2-2.TI	TI	x	x	-	-	-	-	-	
161	18.08.	KYS-2-3.TI	TI	x	x	-	x	471	6.89	-	
162	18.08.	KYS-2-4.TI	TI	x	x	-	-	376	5.86	-	
163	18.08.	KYS-2-8.TI	TI	x	x	-	x	-	-	-	
164	18.08.	KYS-2-9.TI	TI	x	x	-	x	1219	7.16	-	
165	18.08.	KYS-2-10.TI	TI	x	x	-	-	930	7.3	-	
166	20.08.	NSI-95/01	II	x	x	x	x	903	4.93	-	
167	20.08.	NSI-95/02	II	x	x	x	-	-	-	-	
168	20.08.	NSI-97/01	SP	x	x	x	x	800	5.93	-	
169	20.08.	NSI-97/02	SP	x	x	x	-	-	-	CAF	

			Isotopes			Chemistry				
Nr.	date	sample	type	^{18}O	^{2}H	^{3}H	anion/ cation	LF [μS/cm]	pH	filter	Remarks
170	20.08.	NSI-97/03	SP	x	x	x	x	608	6.15	-	
171	20.08.	NSI-97/04	SP	x	x	x	-	921	6.21	-	
172	20.08.	NSI-97/05	SP	x	x	x	x	392	5.56	CAF	
173	20.08.	NSI-97/06	SP	x	x	x	x	317	6.14	-	
174	20.08.	NSI-97/07	SP	x	x	x	-	-	-	CAF	
175	20.08.	DER-97/01	SP	x	x	x	-	-	-	CAF	
176	20.08.	DER-97/02	SP	x	x	x	x	23.6	6.06	CAF	
177	20.08.	DER-97/03	SP	x	x	x	-	-	-	CAF	
178	20.08.	DER-97/04	SP	x	x	x	x	31.5	6.36	-	
179	20.08.	DER-97/05	SP	x	x	x	-	-	-	-	
180	20.08.	DER-96/01	SW	x	x	x	-	-	-	-	
181	20.08.	DER-96/02	SW	x	x	x	-	-	-	-	
182	21.08.	NSI-IW-1.1	IW	x	x	-	x	496	7.61	-	
183	21.08.	NSI-IW-1.2	IW	x	x	-	x	218	7.91	-	
184	21.08.	NSI-IW-1.3	IW	x	x	-	x	145	7.71	-	
185	21.08.	NSI-IW-1.4	IW	x	x	-	-	-	-	CAF	
186	21.08.	NSI-IW-1.5	IW	x	x	-	x	118	7.62	-	
187	21.08.	NSI-IW-1.6	IW	x	x	-	-	-	-	-	
188	21.08.	NSI-IW-1.7	IW	x	x	-	x	276	7.72	-	
189	21.08.	NSI-IW-1.8	IW	x	x	-	-	-	-	CAF	
190	21.08.	NSI-IW-1.9	IW	x	x	-	x	196	7.7	-	
191	21.08.	NSI-IW-1.10	IW	x	x	-	-	-	-	CAF	
192	21.08.	NSI-IW-1.11	IW	x	x	-	x	231	7.92	-	
193	21.08.	NSI-IW-1.12	IW	x	x	x	-	-	-	CAF	
194	21.08.	NSI-IW-1.13	IW	x	x	-	-	-	-	-	
195	21.08.	NSI-IW-1.14	IW	x	x	-	x	112	7.78	-	
196	21.08.	NSI-IW-1.15	IW	x	x	-	x	246	7.76	-	
197	21.08.	NSI-IW-1.16	IW	x	x	x	x	580	7.86	-	
198	21.08.	NSI-IW-2.1	IW	x	x	-	x	85.3	7.72	-	
199	21.08.	NSI-IW-2.2	IW	x	x	x	-	-	-	CAF	
200	21.08.	NSI-IW-2.3	IW	x	x	-	x	194.8	7.88	-	
201	21.08.	NSI-IW-2.4	IW	x	x	x	-	-	-	CAF	
202	21.08.	NSI-IW-3.1	IW	x	x	-	x	194.5	7.4	-	
203	21.08.	NSI-IW-3.2	IW	x	x	-	-	-	-	CAF	
204	21.08.	NSI-IW-3.3	IW	x	x	-	x	169.5	7.43	-	
205	21.08.	NSI-IW-3.4	IW	x	x	x	-	-	-	-	
206	21.08.	NSI-IW-3.5	IW	x	x	-	x	246	7.53	-	
207	21.08.	NSI-IW-3.6	IW	x	x	-	-	-	-	CAF	
208	21.08.	NSI-IW-4.1	IW	x	x	-	x	169.5	7.91	-	
209	21.08.	NSI-IW-4.2	IW	x	x	x	-	-	-	CAF	
210	21.08.	NSI-IW-4.3	IW	x	x	-	x	192	7.91	-	
211	21.08.	NSI-IW-4.4	IW	x	x	-	-	-	-	CAF	
212	21.08.	NSI-IW-4.5	IW	x	x	-	x	210	7.59	-	
213	21.08.	NSI-MI-1	MI	x	x	x	-	391	7.34	-	
214	21.08.	NSI-MI-2	MI	x	x	x	-	-	-	-	
215	21.08.	NSI-MI-3	MI	x	x	x	x	440	7.37	-	
216	21.08.	NSI-MI-4	MI	x	x	x	-	-	-	GFF	
217	21.08.	NSI-MI-5	MI	x	x	x	x	1441	7.36	GFF	
218	21.08.	NSI-MI-6	MI	x	x	x	-	-	-	-	
219	21.08.	NSI-MI-7	MI	x	x	x	-	-	-	-	
220	21.08.	NSI-MI-8	MI	x	x	x	x	247	7.41	GFF	
221	21.08.	NSI-MI-9	MI	x	x	x	-	-	-	-	
222	21.08.	NSI-MI-10	MI	x	x	x	x	231	7.3	-	
223	21.08.	NSI-MI-11	MI	x	x	x	x	321	6.89	GFF	
224	21.08.	NSI-TI-1	TI	x	x	x	x	1666	7.34	-	
225	21.08.	NSI-TI-4	TI	x	x	x	-	3880	7.36	-	
226	21.08.	NSI-TI-2	TI	x	x	-	x	1876	7.37	-	

Nr.	date	sample	type	Isotopes ^{18}O	^{2}H	^{3}H	Chemistry anion/ cation	LF [µS/cm]	pH	filter	Remarks
227	21.08.	NSI-TI-3	TI	x	x	-	x	224	7.52	-	
228	21.08.	NSI-IW2-TI1	TI	x	x	-	x	515	7.75	-	
229	21.08.	NSI-IW2-TI2	TI	x	x	x	-	-	-	-	
230	21.08.	NSI-IW2-TI3	TI	x	x	-	x	337	7.93	-	
231	21.08.	NSI-IW2-TI4	TI	x	x	x	-	-	-	-	
232	21.08.	NES-7-IW-1	IW	x	x	-	-	-	-	CAF	
233	20.08.	NSI-St.6-6m	SW	x	x	-	-	26600	7.71	-	SAL=18.2‰
234	20.08.	NSI-St.6-6.7m	SW	x	x	-	-	27300	7.73	-	SAL=18.5‰
235	21.08.	NES-7-1.TI	TI	x	x	-	x	-	-	-	
236	21.08.	NES-7-2.TI	TI	x	x	-	-	-	-	-	
237	21.08.	NES-7-10.TI	TI	x	x	-	-	-	-	-	
238	21.08.	NES-7-14.TI	TI	x	x	-	x	-	-	-	
239	23.08.	BUN-99/01	RW	x	x	x	x	29.1	6.63	-	
240	23.08.	BUN-99/02	RW	x	x	x	x	-	-	-	
241	24.08.	BUN-99/03	RW	x	x	-	-	-	-	-	
242	25.08.	BUN2-96/01	SW	x	x	x	-	-	-	-	
243	25.08.	BUN2-96/02	SW	x	x	x	x	-	-	-	
244	25.08.	BUN2-98/01	GW	x	x	x	-	-	-	-	
245	25.08.	BUN-7-1.TI	TI	x	x	-	x	1736	6.23	-	
246	27.08.	SLY-96/01	SW	x	x	x	x	27000	7.72	CAF	SAL=18.0‰
247	27.08.	SLY-IW-1.1	IW	x	x	x	x	117.2	7.09	CAF	
248	27.08.	SLY-IW-2.1	IW	x	x	-	x	116.3	7.74	-	
249	27.08.	SLY-IW-2.2	IW	x	x	x	-	-	-	CAF	
250	27.08.	SLY-IW-2.3	IW	x	x	-	x	100.2	7.47	-	
251	27.08.	SLY-IW-2.4	IW	x	x	x	-	-	-	CAF	
252	27.08.	SLY-IW-2.5	IW	x	x	-	x	101.6	7.49	-	
253	27.08.	SLY-97/01	SP	x	x	x	-	-	-	CAF	
254	27.08.	SLY-97/02	SP	x	x	x	x	50.8	7.7	-	
255	27.08.	SLY-97/03	SP	x	x	x	-	-	-	CAF	
256	27.08.	SLY-97/04	SP	x	x	x	x	70	7.59	-	
257	27.08.	SLY-96/02	SW	x	x	x	x	390	-	-	
258	27.08.	KLY-1-1.TI	TI	x	x	-	x	695	7.17	-	
259	27.08.	KLY-1-2.TI	TI	x	x	-	x	1295	7.05	-	
260	27.08.	KLY-1-3.TI	TI	x	x	x	x	373	7.38	-	
261	27.08.	KLY-1-4.TI	TI	x	x	-	x	655	7.12	-	
262	27.08.	KLY-1-5.TI	TI	x	x	-	x	499	7.13	-	
263	27.08.	KLY-1-6.TI	TI	x	x	-	-	-	-	-	
264	28.08.	SVN-99/01	RW	x	x	-	-	-	-	-	
265	28.08.	SVN-96/01	SW	x	x	x	x	47	7.23	-	
266	28.08.	SVN-96/02	SW	x	x	x	x	23800	7.58	-	SAL=16.4‰
267	28.08.	SVN-96/03	SW	x	x	x	x	23200	7.7	CAF	SAL=15.8‰
268	28.08.	SVN-97/01	SP	x	x	x	-	-	-	CAF	
269	28.08.	SVN-97/02	SP	x	x	x	x	23.4	6.63	-	
270	28.08.	SVN-97/03	SP	x	x	x	-	-	-	CAF	
271	29.08.	SVN-99/02	RW	x	x	-	x	440	6.6	-	
272	30.08.	OYA-96/01	SW	x	x	x	x	23700	7.63	CAF	SAL=15.9‰
273	30.08.	OYA-IW-1.1	IW	x	x	-	x	94	8.05	CAF	
274	30.08.	OYA-IW-1.2	IW	x	x	-	-	-	-	-	
275	30.08.	OYA-IW-1.3	IW	x	x	-	x	97	7.89	-	
276	30.08.	OYA-IW-1.4	IW	x	x	x	-	-	-	CAF	
277	30.08.	OYA-IW-1.5	IW	x	x	-	x	125	7.94	-	
278	30.08.	OYA-IW-1.6	IW	x	x	-	-	-	-	-	
279	30.08.	OYA-IW-2.1	IW	x	x	-	x	200	7.53	-	
280	30.08.	OYA-IW-2.2	IW	x	x	-	-	75.3	6.86	CAF	
281	30.08.	OYA-IW-2.3	IW	x	x	-	-	79.1	6.26	-	
282	30.08.	OYA-IW-2.4	IW	x	x	-	x	58.6	6.28	-	

Nr.	date	sample	type	Isotopes ^{18}O	Isotopes ^{2}H	Isotopes ^{3}H	Chemistry anion/ cation	Chemistry LF [µS/cm]	Chemistry pH	Chemistry filter	Remarks
283	30.08.	OYA-IW-2.5	IW	x	x	-	-	-	-	CAF	
284	30.08.	OYA-IW-2.6	IW	x	x	x	-	-	-	-	
285	30.08.	OYA-IW-2.7	IW	x	x	-	x	57.1	6.23	-	
286	30.08.	OYA-IW-2.8	IW	x	x	-	-	-	-	CAF	
287	30.08.	OYA-IW-2.9	IW	x	x	-	x	135	7.37	-	
288	30.08.	OYA-IW-2.10	IW	x	x	-	-	-	-	-	
289	30.08.	OYA-IW-2.11	IW	x	x	-	x	63.9	6.88	CAF	
290	30.08.	OYA-IW-2.0	IW	x	x	-	-	79.4	7.42	-	
291	30.08.	OYA-IW-4.1	IW	x	x	-	x	90.2	7.51	-	
292	30.08.	OYA-IW-4.2	IW	x	x	-	-	-	-	CAF	
293	30.08.	OYA-IW-4.3	IW	x	x	-	x	81.6	7.31	-	
294	30.08.	OYA-IW-4.4	IW	x	x	x	-	-	-	CAF	
295	30.08.	OYA-IW-4.5	IW	x	x	-	-	-	-	-	
296	30.08.	OYA-IW-4.6	IW	x	x	-	x	62.6	7.25	CAF	
297	30.08.	OYA-IW-5.1	IW	x	x	-	x	54.9	6.99	-	
298	30.08.	OYA-IW-5.2	IW	x	x	-	-	-	-	CAF	
299	30.08.	OYA-IW-5.3	IW	x	x	-	x	102	7.57	-	
300	30.08.	OYA-IW-5.4	IW	x	x	-	-	-	-	-	
301	30.08.	OYA-IW-5.5	IW	x	x	-	x	83.4	7.38	-	
302	30.08.	OYA-IW-5.6	IW	x	x	-	-	-	-	CAF	
303	30.08.	OYA-IW-5.7	IW	x	x	-	-	114	7.47	-	
304	30.08.	OYA-IW-5.8	IW	x	x	x	-	-	-	-	
305	30.08.	OYA-IW-5.9	IW	x	x	-	x	123	7.65	-	
306	30.08.	OYA-IW-5.10	IW	x	x	-	-	-	-	CAF	
307	30.08.	OYA-IW-5.11	IW	x	x	-	-	-	-	-	
308	30.08.	OYA-IW-5.12	IW	x	x	-	x	77.3	7.45	-	
309	30.08.	OYA-IW-5.13	IW	x	x	-	-	-	-	-	
310	30.08.	OYA-IW-5.14	IW	x	x	-	-	-	-	CAF	
311	30.08.	OYA-IW-5.15	IW	x	x	-	x	73.9	7.41	-	
312	30.08.	OYA-IW-6.1	IW	x	x	-	x	56.3	6.56	CAF	
313	30.08.	OYA-IW-6.2	IW	x	x	x	-	-	-	-	
314	30.08.	OYA-IW-6.3	IW	x	x	-	x	51.3	6.09	CAF	
315	30.08.	OYA-IW-6.4	IW	x	x	-	-	-	-	-	
316	30.08.	OYA-IW-6.5	IW	x	x	-	x	60.0	6.07	CAF	
317	30.08.	OYA-IW-6.6	IW	x	x	-	-	-	-	-	
318	30.08.	OYA-IW-7.1	IW	x	x	x	-	-	-	CAF	
319	30.08.	OYA-IW-7.2	IW	x	x	-	x	114	6.52	-	
320	30.08.	OYA-IW-3.1	IW	x	x	-	x	60.3	6.67	CAF	
321	30.08.	OYA-IW-3.2	IW	x	x	-	-	-	-	-	
322	30.08.	OYA-IW-3.3	IW	x	x	-	x	62.0	7.04	-	
323	30.08.	OYA-IW-3.4	IW	x	x	x	-	-	-	CAF	
324	30.08.	OYA-IW-3.5	IW	x	x	-	x	68.9	7.12	-	
325	30.08.	OYA-IW-3.6	IW	x	x	-	-	-	-	CAF	
326	30.08.	OYA-IW-3.7	IW	x	x	-	-	-	-	-	
327	30.08.	OYA-IW-3.8	IW	x	x	-	-	-	-	-	
328	30.08.	OYA-IW-3.9	RIW	x	x	x	x	69.7	6.30	-	
329	30.08.	OYA-IW-3.10	RIW	x	x	x	-	-	-	-	
330	30.08.	OYA-IW-3.11	RIW	x	x	x	x	71.4	6.42	-	
331	30.08.	OYA-IW-3.12	RIW	x	x	x	-	-	-	-	
332	30.08.	OYA-IW-3.13	RIW	x	x	x	x	29.7	6.57	-	
333	30.08.	OYA-3-2.TI	TI	x	x	-	x	2400	7.61	-	SAL=1.3‰
334	30.08.	OYA-3-4.TI	TI	x	x	-	-	-	-	-	
335	30.08.	OYA-3-9.TI	TI	x	x	-	x	747	7.38	-	
336	30.08.	OYA-4-1.TI	TI	x	x	-	x	486	5.66	-	
337	30.08.	OYA-4-2.TI	TI	x	x	x	-	-	-	-	
338	30.08.	OYA-IW1.TI	TI	x	x	-	x	182	7.70	-	
339	30.08.	OYA-IW-5.TI	TI	x	x	-	x	67.8	5.80	-	

			Isotopes			Chemistry				
Nr.	date	sample	type	^{18}O	^{2}H	^{3}H	anion/ cation	LF [µS/cm]	pH	filter	Remarks
340	30.08.	OYA-2-1.TI	TI	x	x	-	-	-	-	-	
341	30.08.	OYA-2-2.TI	TI	x	x	x	-	-	-	-	
342	30.08.	OYA-2-6.TI	TI	x	x	-	x	323	6.24	-	
343	30.08.	OYA-2-8.TI	TI	x	x	-	x	563	5.76	-	
344	30.08.	STAT-11-5 (2 m)	SW	x	x	-	-	-	-	-	
345	30.08.	STAT-11-1 (6 m)	SW	x	x	-	-	-	-	-	
346	27.08.	BW SERGEY	SW	-	-	-	-	26400	6.43	-	SAL=17.9‰
347	01.09.	aqua dest. Blank	-	-	-	-	x	-	-	-	
348	01.09.	tap water ship	-	-	-	-	x	-	-	-	
349	02.09.	MUO-3-1.TI	TI	-	-	-	-	-	-	-	
350	02.09.	MUO-3-2.TI	TI	-	-	-	-	-	-	-	
351	02.09.	MUO-3-3.TI	TI	-	-	-	x	-	-	-	Unfiltered. Frozen
352	02.09.	MUO-3-6.TI	TI	-	-	-	x	-	-	-	Unfiltered. Frozen
353	02.09.	MUO-3-7.TI	TI	-	-	-	x	-	-	-	Unfiltered. Frozen
354	02.09.	MUO-3-8.TI	TI	-	-	-	x	-	-	-	Unfiltered. Frozen
355	02.09.	MUO-3-10.TI	TI	-	-	-	x	-	-	-	Unfiltered. Frozen
356	02.09.	MUO-01	IW	x	x	-	x	-	-	-	Frozen
357	02.09.	MUO-02	IW	x	x	-	x	-	-	-	Frozen
358	02.09.	MUO-03	IW	x	x	-	x	-	-	-	Frozen
359	02.09.	MUO-04	IW	x	x	-	x	-	-	-	Frozen
360	02.09.	MUO-05	IW	x	x	-	x	-	-	-	Frozen
361	02.09.	MUO-06	IW	x	x	-	x	-	-	-	Frozen
362	02.09.	MUO-07	IW	x	x	-	x	-	-	-	Frozen
363	02.09.	MUO-08	IW	x	x	-	x	-	-	-	Frozen
364	02.09.	MUO-09	IW	x	x	-	x	-	-	-	Frozen
365	02.09.	MUO-10	IW	x	x	-	x	-	-	-	Frozen
366	02.09.	MUO-11	IW	x	x	-	x	-	-	-	Frozen
367	02.09.	MUO-12	IW	x	x	-	x	-	-	-	Frozen

Appendix 5.2-3. List of bone samples of the New Siberian Islands.

No.	samples	Taxon	Skeleton element	Preservation	Type Loc.	Locality	Remarks
		Stolbovoy Island (2 – 4 km from Stolbovaya River mouth)					
1	NS-Stl-O1	Ovibos sp.	Cranium with horn cores, female	Fragment	C	Exposure	Probably, samples 1 and 2 from one individual
2	NS-Stl-O2	Ovibos sp.	Cervical vertebra	Damaged	C	Exposure	
3	NS-Stl-O3	Equus caballus	Mandibula (right stem) with P2 - M3	Fragment	C	Exposure	Probably, samples 3, 4, 5 (C14) from one individual
4	NS-Stl-O4	Equus caballus	Thorax vertebra	Damaged, sore	C	Exposure	
5	NS-Stl-O5	Equus caballus	Tibia, left (with marrow)		C	Exposure	
6	NS-Stl-O6	Rangifer tarandus	Shed antler		B	Exposure, altitude 10-11 m	
7	NS-Stl-O7	Rangifer tarandus	Shed antler		B		Vivianit
8	NS-Stl-O8	Rangifer tarandus	Calcaneus, right		B		
9	NS-Stl-O9	Rangifer tarandus	Pelvis	Fragment	B		Trashed
10	NS-Stl-O10	Lepus sp.	Cranium	Fragment	E	Shore	
11	NS-Stl-O11	Rangifer tarandus	Sacrum	Fragment	E	Shore	Trashed
12	NS-Stl-O12	Bison priscus	Cranium with right horn	Fragment	E	Shore	
13	NS-Stl-O91	Large herbivorus mammal	Limb bone	Fragment	C	Exposure	

Appendix 5.2-3, continuation.

No.	samples	Taxon	Skeleton element	Preservation	Type Loc.	Locality	Remarks
		Kotel'ny Island (Cape Anisy area)					
14	NS-KAn-O13-a	Mammuthus primigenius	Humerus, right	Damaged	A	In situ, Baydzherakh in the tundra, altitude 10 m	Juv., trashed
15	NS-KAn-O13-b		Humerus, left	Damaged,	A		Juv., C14
16	NS-KAn-O13-c		Ulna	3 pieces, cut off	A		Juv., C14, samples 13c and 13e in natural conjunction
17	NS-KAn-O13-d		Femur, left		A		Juv., trashed
18	NS-KAn-O13-e		Radius	2 pieces, cut off	A		Juv., C14
19	NS-KAn-O13-f		Femur, right	Cut off	A		Juv., C14
20	NS-KAn-O14		Thorax vertebra	Damaged	D		Probably, samples 13, 14, 15 from one individual
21	NS-KAn-O15	Mammuthus primigenius	Cervical vertebra	Damaged	D	Baydzherakh in the tundra	
22	NS-KAn-O16	Equus caballus	Mandibula with P2-M3		D		Probably, samples 16, 17, 18, 19, 20 from one individual
23	NS-KAn-O17	Equus caballus	Pelvis	3 pieces	D		
24	NS-KAn-O18	Equus caballus	Mt III, left		D		
25	NS-KAn-O19	Equus caballus	Atlas		D		
26	NS-KAn-O20	Equus caballus	Ph I, left		D		
27	NS-KAn-O21	Ovibos sp.	Tibia, left	Distal fragment	D		
28	NS-KAn-O22	Rangifer tarandus	Shed antler	Fragment	D		
29	NS-KAn-O23	Rangifer tarandus	Mt III + IV, left		D		
30	NS-KAn-O24	Mammuthus primigenius	Tusk	Fragment	D		C14
31	NS-KAn-O25	Mammuthus primigenius	Tusk	Fragment	D		C14
32	NS-KAn-O26	? Rangifer tarandus	Thorax vertebra	2 pieces	D		

Appendix 5.2-3. continuation.

No.	samples	Taxon	Skeleton element	Preservation	Type Loc.	Locality	Remarks
33	NS-KAn-O27	Mammuthus primigenius	Tusk	Fragment	D	Baydzherakh in the tundra	C 14
34	NS-KAn-O28	Equus caballus	Humerus, left	Damaged	D		
35	NS-KAn-O29	Equus caballus	Ph I, left		D		
36	NS-KAn-O30-a	Equus caballus	Pelvis	Fragment, left part	D		Probably, samples 30b and 30c from one individual
37	NS-KAn-O30-b	Equus caballus	Humerus, left		A	In situ, baydzherakh in the tundra, altitude 10 m	Probably, samples from 30-i to 30-z from one individual, juv.
38	NS-KAn-O30-c	Equus caballus	Antebrachium, left	2 pieces	A		
39	NS-KAn-O30-d	Equus caballus	Tibia, left		A		
40	NS-KAn-O30-e	Equus caballus	Astragalus, right		A		
41	NS-KAn-O30-f	Equus caballus	Patella		A		
42	NS-KAn-O30-g	Equus caballus	Sacrum	Damaged, 2 pieces	A		
43	NS-KAn-O30-h	Equus caballus	Vertebra (8 bones)	Fragments	A		
44	NS-KAn-O30-i	Equus caballus	Epistropheus		A		
62	NS-KAn-O30-j	Equus caballus	3-rd cervical vertebra	Damaged	A		
62	NS-KAn-O30-k	Equus caballus	4-th cervical vertebra	2 pieces, damaged	A		
62	NS-KAn-O30-l	Equus caballus	5-th cervical vertebra	2 pieces, damaged	A		
62	NS-KAn-O30-m	Equus caballus	6-th cervical vertebra	2 pieces, damaged	A		
62	NS-KAn-O30-n	Equus caballus	7-th cervical vertebra	2 pieces, damaged	A		
62	NS-KAn-O30-o	Equus caballus	1-st thorax vertebra	2 pieces, damaged	A	In situ, baydzherakh in the tundra, altitude 10 m	Probably, samples 30-i to 30-z from one individual, juv.
62	NS-KAn-O30-p	Equus caballus	Thorax vertebra	2 pieces, damaged	A		
62	NS-KAn-O30-q	Equus caballus	Thorax vertebra	2 pieces, damaged	A		
62	NS-KAn-O30-r	Equus caballus	Thorax vertebra	2 pieces, damaged	A		
62	NS-KAn-O30-s	Equus caballus	Thorax vertebra	4 pieces, damaged	A		
62	NS-KAn-O30-t	Equus caballus	Thorax vertebra	Fragment	A		

Appendix 5.2-3. continuation.

No.	samples	Taxon	Skeleton element	Preservation	Type Loc.	Locality	Remarks
62	NS-KAn-O30-u	Equus caballus	Lumbar vertebra	2 fragments, damaged	A	In situ, baydzherakh in the tundra, altitude 10 m	
62	NS-KAn-O30-v	Equus caballus	Thorax vertebra	Fragment	A		
62	NS-KAn-O30-w	Equus caballus	Costa (5 bones)		A		
62	NS-KAn-O30-x	Equus caballus	Costa (35 bones)	Fragments	A		
62	NS-KAn-O30-y	Equus caballus	Vertebra, spinous process (8 bones)	Fragments	A		
62	NS-KAn-O30-z	Equus caballus	Costa (2 pieces)	Fragments, cartilage part	A		
62	NS-KAn-O31	Rangifer tarandus	Femur, left	Distal fragment	D	Baydzherakh in the tundra	Recent?
		Bel'kovsky Island (Cape Skalisty)					
63	NS-Bel-O32	Bison priscus	Radius, left	Damaged	C	Exposure	Probably, samples 32, 33, 34 (C14), 35, 36, 37 from one individual.
64	NS-Bel-O33	Bison priscus	Thorax vertebra	Damaged	C		
65	NS-Bel-O34	Bison priscus	Lumbar vertebra	Damaged	C		
66	NS-Bel-O35	Bison priscus	Humerus, right	Distal fragment	C		
67	NS-Bel-O36	Bison priscus	Pelvis (right part)	Damaged, 2 pieces	C		
68	NS-Bel-O37	Bison priscus	Thorax vertebra	Fragment, 2 pieces	C		
69	NS-Bel-O38	Mammuthus primigenius	Humerus	Fragment, cut off	D	Baydzherakh in the tundra	C 14
70	NS-Bel-O39	Equus caballus	Pelvis (left part)	Fragment	D	Baydzherakh in coastal outcrop	
71	NS-Bel-O40	Rangifer tarandus	Antler	Fragment	D		Trashed
72	NS-Bel-O41	Equus caballus	Humerus, right	Distal fragment	D	Baydzherakh in the tundra	
73	NS-Bel-O42	Equus caballus	Radius, left	Fragment	D		Trashed
74	NS-Bel-O43	Equus caballus	Mt III, right	Distal fragment	D		
75	NS-Bel-O44	Rangifer tarandus	Tibia, right	Fragment	D		Recent?
76	NS-Bel-O45	Mammuthus primigenius	Tusk	Fragment	E	Shore	C14, rounded

Appendix 5.2-3. continuation.

No.	samples	Taxon	Skeleton element	Preservation	Type Loc.	Locality	Remarks
77	NS-Bel-O46	? Rangifer tarandus	Tibia, left	Damaged	E		
78	NS-Bel-O47	Bison priscus	Horn sheet	Fragment, 2 pieces	E		
79	NS-Bel-O48	Equus caballus	Upper tooth	Fragment (6 pieces)	D	Baydzherakh in coastal outcrop	
80	NS-Bel-O92	Rangifer tarandus	Intermedium		D	Baydzherakh in the tundra	
		Kotel'ny Island (south-west coast, Khomurgannakh River mouth)					
81	NS-khom-O49	Mammuthus primigenius	Tusk	Fragment	D	Baydzherakh in the valley	C 14
82	NS-Khom-O50		Mc V, left	Damaged	D		
83	NS-Khom-O51		Tusk	Fragment	D		Probably, samples 51, 52 from one individual; trashed
84	NS-Khom-O52		Tusk	Fragment	D		
85	NS-Khom-O53	Rangifer tarandus	Shed antler	Fragment	D	Baydzherakh in the tundra	Recent?
86	NS-Khom-O54	Rangifer tarandus	Shed antler	Fragment, 2 pieces	D		Recent?
87	NS-Khom-O55	Rangifer tarandus	Antler	Fragment	D		Recent?
88	NS-Khom-O56	Rangifer tarandus	Mc III+IV, right	Damaged	D		Juv., recent?
89	NS-Khom-O57	Rangifer tarandus	Mc III+IV	Distal fragment	D		
90	NS-Khom-O58	Rangifer tarandus	Femur, right	Fragment, 2 pieces	D		Juv., sore, recent?
91	NS-Khom-O59	Mammuthus primigenius	Tusk	Fragment	C	Exposure	C 14
92	NS-Khom-O60		Upper tooth (M2 or M3)	Damaged	C		
93	NS-Khom-O61	Equus caballus	Scapula, right	Damaged	B	Exposure, altitude 15 m	Probably, samples 61, 62 from one individual
94	NS-Khom-O62		Radius, left		C		
95	NS-Khom-O63	Ovibos sp.	Humerus, left	Distal fragment	D	Baydzherakh in coastal outcrop	
96	NS-Khom-O64	Equus caballus	Mc III, right		D		Probably, samples 64, 65,

Appendix 5.2-3. continuation.

No.	samples	Taxon	Skeleton element	Preservation	Type Loc.	Locality	Remarks
97	NS-Khom-O65	Equus caballus	Ph I, right		D		66 from one individual
98	NS-Khom-O66	Equus caballus	Ph II		D	Baydzherakh in coastal outcrop	
99	NS-Khom-O67	Ovibos sp.	Mc III+IV, right	Damaged	D		
100	NS-Khom-O68	Large herbivorous mammal	Limb bone	Fragment	D	Baydzherakh in the tundra	Trashed
101	NS-Khom-O69		Limb bone	Fragment	D		Trashed
102	NS-Khom-O70		Limb bone	Fragment	D		Trashed
103	NS-Khom-O71	Rangifer tarandus	Ph I	Distal fragment	D		
104	NS-Khom-O72		Vertebra	Damaged	D		Recent?
105	NS-Khom-O73		Shed antler	Fragment	D		Trashed
106	NS-Khom-O74		Upper molar tooth		D		
107	NS-Khom-O75		Tibia, right	Distal fragment	D		
108	NS-Khom-O76		Scapula, right	Fragment	D		
109	NS-Khom-O77	Mammuthus primigenius	Vertebra	Fragment	D		C 14
110	NS-Khom-O78		Tusk	Fragment (3 pieces), cut off	D		C 14
		Novaya Sibir Island ("Derevyannye Gory)					
111	NS-Ndg-O79	Mammuthus primigenius	Tusk	Fragment	F	Near zimov'e	C 14
112	NS-Ndg-O80		Tusk	Fragment	F	Near zimov'e	C 14
113	NS-Ndg-O81	Mammuthus primigenius	Costa	Fragment	E	Shore	Trashed
114	NS-Ndg-O82	Rangifer tarandus	Scapula, left	Fragment	E	Shore	
115	NS-Ndg-O83	Equus caballus	Cervical vertebra		F	Tundra	C 14
116	NS-Ndg-O84	Large herbivorous mammal	Limb bone	Fragment	E	Shore	Heavily rounded, trashed

Appendix 5.2-3. continuation.

No.	samples	Taxon	Skeleton element	Preservation	Type Loc.	Locality	Remarks
		Novaya Sibir Island (south-east part of the location Hedenshtrom					
117	NS-Ndg-O85	Mammuthus primigenius	Limb bone	Fragment (2 pieces)	F	Tundra	C 14
118	NS-Ndg-O86		Tusk	Fragment	F	Tundra	C 14
119	NS-Ndg-O87		Tooth	Fragment	F	Tundra	
120	NS-Ndg-O88	Rangifer tarandus	Calcaneus, right		F	Tundra	
121	NS-Ndg-O89	Rangifer tarandus	Humerus, right	Distal fragment	E	Shore	
122	NS-Ndg-O90	Large herbivorous mammal	Limb bone	Fragment	E	Shore	Trashed
		Maly Lyakhovsky Island (2 - 3 km to the west of Cape Vaygach)					
123	NS-ML-O93	Mammuthus primigenius	Metacarpale		E	Shore	Heavily rounded
124	NS-ML-O94	Equus caballus	Tibia, left	Distal fragment	E	Shore	Rounded
125	NS-ML-O95	Large herbivorous mammal	Limb bone	Fragment	E	Shore	Rounded, trashed
126	NS-ML-O96	Bison priscus	Thorax vertebra	Fragment, 2 pieces	E	Shore	
127	NS-ML-O97	Bison priscus	Ulna	Fragment	E	Shore	
128	NS-ML-O98	? Ovibos sp.	Metapodium	Distal fragment	E	Shore	Rounded
129	NS-ML-O99	Ovibos sp.	Scapula, right	Fragment	E	Shore	
130	NS-ML-O100	Mammuthus primigenius	Tusk	Fragment	E	Shore	Rounded, C 14
131	NS-ML-O101		Tusk	Fragment	E	Shore	Rounded, C 14
132	NS-ML-O102		Tusk	Fragment	E	Shore	Trashed
133	NS-ML-O103	Rangifer tarandus	Tibia, left	Distal fragment	E	Shore	
134	NS-ML-O104	Bison priscus	Ph 1, left		E	Shore	
135	NS-ML-O105	Phoca sp.	Humerus	Damaged	E	Shore	Recent
136	NS-ML-O106	Rangifer tarandus	Ph 1		E	Shore	Recent

Appendix 5.2-3. continuation.

No.	samples	Taxon	Skeleton element	Preservation	Type Loc.	Locality	Remarks
137	NS-ML-O107	?Alopex sp.	Epistropheus		E	Shore	Recent
138	NS-ML-O108	Equus caballus	Cranium	Damaged	F	Tundra	
139	NS-ML-O109	Mammuthus primigenius	Tusk	Fragment	F	Tundra	
140	NS-ML-O110		Tibia	Fragment	F	Tundra	Trashed
141	NS-ML-O111		Humerus	Fragment	F	Tundra	Trashed
142	NS-ML-O112	Equus caballus	Mandibula with teeth (except I3)	Damaged (2 pieces)	F	Tundra	Very old
143	NS-ML-O113	Mammuthus primigenius	Pelvis (left part)	Fragment	D	Baydzherakh in tundra, 500 m E of the lighthouse	C 14
144	NS-ML-O114	Equus caballus	Tibia, left	Distal fragment	D	Baydzherakh near lighthouse	
145	NS-ML-O115	Equus caballus	Radius, left		D	Baydzherakh near lighthouse	
146	NS-ML-O116	Mammuthus primigenius	Scapula, left	Fragment	D	Baydzherakh in tundra, 500 m E of the lighthouse	Small, C 14
147	NS-ML-O117	Mammuthus primigenius	Vertebra	Fragment, spinous processum	D	Baydzherakh near the lighthouse	C 14
148	NS-ML-O118	Equus caballus	Mt III, left		D		
149	NS-ML-O119	Rangifer tarandus	Antler	Fragment	D		
150	NS-ML-O120	Rangifer tarandus	Femur, left	Distal fragment	D		
151	NS-ML-O121	? Rangifer tarandus	Radius, right		D		Probably, samples 121, 122, 123, 124 (trashed) from one individual, recent?
152	NS-ML-O122	Rangifer tarandus	Humerus, right	Distal fragment	D		
153	NS-ML-O123	Rangifer tarandus	Carpale II+III		D		
154	NS-ML-O124	Rangifer tarandus	Pelvis	Fragment	D	Baydzherakh near the lighthouse	
155	NS-ML-O125	Equus caballus	Mt III, right	Damaged	D		
156	NS-ML-O126	Mammuthus primigenius	Vertebra	Fragment, spinous processum	D		C 14
157	NS-ML-O127	Equus caballus	Humerus, right	Fragment	D		Trashed

Appendix 5.2-3. continuation.

No.	samples	Taxon	Skeleton element	Preservation	Type Loc.	Locality	Remarks
158	NS-ML-O128	Equus caballus	Humerus, right	Distal fragment	D		
159	NS-ML-O129	Mammuthus primigenius	Costa	Fragment	D		C 14
160	NS-ML-O130	Ovibos sp.	Mt III+IV, right		D		
161	NS-ML-O131	Rangifer tarandus	Mt III+IV, left	Proximal fragment	D		Recent ?
162	NS-ML-O132	Rangifer tarandus	Mt III+IV, right		D		Recent ?
163	NS-ML-O133	Rangifer tarandus	Ph I, left		D		Recent ?
164	NS-ML-O134	Rangifer tarandus	Radius	Fragment	D		Juv., recent?
165	NS-ML-O135	Rangifer tarandus	Shed antler	Fragment	D	Baydzherakh in tundra, 500 m from the lighthouse to the east	
166	NS-ML-O136	Mammuthus primigenius	Humerus	Fragment	D		C 14
167	NS-ML-O137		Tibia	Fragment, cut off	D		Juv., C 14
168	NS-ML-O138		Tusk	Fragment, cut off	D		C 14
169	NS-ML-O139		Femur, right	Fragment (2 pieces), cut off	D		C 14
170	NS-ML-O140		Femur, left	Fragment, cut off	D		C 14
171	NS-ML-O141		Humerus	Fragment, cut off	D		C 14
172	NS-ML-O142	Equus caballus	Mandibula (left stem) with teeth P2 - M1	Fragment	D		Trashed
173	NS-ML-O143	Mammuthus primigenius	Ulna, right	Distal fragment	F	Tundra	Juv.
174	NS-ML-O147	Mammuthus primigenius	Tooth	Fragment	D	Baydzherakh in tundra, 500 m E of the lighthouse	
175	NS-ML-O291		Pelvis	Fragment, cut off	D		C 14
176	NS-ML-O292		Limb bone	Fragment, cut off	D		C 14

Appendix 5.2-3. continuation.

No.	samples	Taxon	Skeleton element	Preservation	Type Loc.	Locality	Remarks
		Svyatoy Nos Cape (2 - 3 km from Serkin Urochichshe)					
177	NS-SN-O144	Equus caballus	Pelvis (right part)	Fragment	E	Shore	C 14
178	NS-SN-O145	Mammuthus primigenius	Tusk	Fragment	E		Trashed
179	NS-SN-O146		Tooth	Fragment	E		
		Oyogos Yar (4 km from Kondrat'eva River mouth to the west)					
180	NS-Ogk-O148	Mammuthus primigenius	Radius, right	Proximal fragment	F	Tundra	
181	NS-Ogk-O149		Tusk	Fragment	F		Trashed
182	NS-Ogk-O150	Bison priscus	Tibia, left	Fragment	C	Thermoterrace	
183	NS-Ogk-O151	Equus caballus	Femur, right	Damaged	C		
184	NS-Ogk-O152	Equus caballus	Mt III, left		C		
185	NS-Ogk-O153	Equus caballus	Mc III, right		C		
186	NS-Ogk-O154	Bison priscus	Humerus, left	Fragment	C		
187	NS-Ogk-O155	Bison priscus	Mt III+IV, left	Damaged	C		
188	NS-Ogk-O156	Equus caballus	Femur, right	Distal fragment	C	Thermoterrace	
189	NS-Ogk-O157	? Bison priscus	Mandibula (right stem) without teeth	Fragment	C		
190	NS-Ogk-O158	Bison priscus	Femur, right	Damaged	C		
191	NS-Ogk-O159	Bison priscus	Femur, left	Fragment	C		
192	NS-Ogk-O160	Equus caballus	Tibia, right		C		
193	NS-Ogk-O161	Bison priscus	Pelvis (right part)	Fragment	C		
194	NS-Ogk-O162	? Panthera spelaea	Femur	Fragment	C	Thermoterrace	
195	NS-Ogk-O163	Rangifer tarandus	Antler	Fragment	C		Trashed
196	NS-Ogk-O164	Rangifer tarandus	Scapula, right	Fragment	C		
197	NS-Ogk-O165	Rangifer tarandus	Tibia, right	Proximal fragment	C		

Appendix 5.2-3. continuation.

No.	samples	Taxon	Skeleton element	Preservation	Type Loc.	Locality	Remarks
198	NS-Ogk-O166	Bison priscus	Tibia, left	Fragment	C	Thermoterrace	Juv.
199	NS-Ogk-O167	Rangifer tarandus	Humerus, left		C		
200	NS-Ogk-O168	Rangifer tarandus	Astragalus		C		
201	NS-Ogk-O169	Rangifer tarandus	Radius, left	Proximal fragment	C		
202	NS-Ogk-O170	Rangifer tarandus	Mc III+IV	Proximal fragment, 2pieces	C		
203	NS-Ogk-O171	Mammuthus primigenius	? Ulna	Fragment	C		C 14
204	NS-Ogk-O172	Large herbivorous mammal	Limb bone	Fragment	C		Trashed
205	NS-Ogk-O173		Limb bone	Fragment	C		Trashed
206	NS-Ogk-O174		Costa	Fragment	C		
207	NS-Ogk-O175	Mammuthus primigenius	Tibia, right	Fragment	C		Juv.
208	NS-Ogk-O176		Femur, right	Fragment	C		Probably, samples 176 and 177 from one individual, juv
209	NS-Ogk-O177		Femur, left	Fragment	C		
210	NS-Ogk-O178	Equus caballus	Femur, left	Distal articulation	C		Juv.
211	NS-Ogk-O179	Bison priscus	Humerus, right	Distal fragment	C	Thermoterrace	
212	NS-Ogk-O180	Bison priscus	Femur, right	Proximal fragment	C		
213	NS-Ogk-O181	Bison priscus	Femur, left	Proximal fragment	C		
214	NS-Ogk-O182	Equus caballus	Mandibula (left stem) with teeth P2-M3 and I1 - I3	Fragment	C		
215	NS-Ogk-O183	Ovibos sp.	Horn sheet	Fragment	C		
216	NS-Ogk-O184	Rangifer tarandus	Tibia, left	Fragment	C		Juv.
217	NS-Ogk-O185	Rangifer tarandus	Tibia, left	Proximal fragment	C		
218	NS-Ogk-O186	Equus caballus	Thorax vertebra	Damaged	C		
219	NS-Ogk-O187	Rangifer tarandus	Shed antler	Fragment	C		
220	NS-Ogk-O188	Mammuthus primigenius	Femur	Fragment	C		Juv., C 14
221	NS-Ogk-O189	Mammuthus primigenius	Vertebra	Fragment, spinous processum	C	Thermoterrace	Trashed

Appendix 5.2-3. continuation.

No.	samples	Taxon	Skeleton element	Preservation	Type Loc.	Locality	Remarks
222	NS-Ogk-O190	Bison priscus	Radius, left		C		
223	NS-Ogk-O191	Bison priscus	Pelvis	Fragment	C		Juv.
224	NS-Ogk-O192	Mammuthus primigenius	Limb bone	Fragment	C		C 14
225	NS-Ogk-O193	Large herbivorous mammal	Costa	Fragment	E	Shore, near stream mouth	Trashed
226	NS-Ogk-O194	Mammuthus primigenius	Tusk	Fragment	E	Shore, near stream mouth	Trashed
227	NS-Ogk-O195		Tusk	Fragment	E		Trashed
228	NS-Ogk-O196		Tusk	Fragment	E		Trashed
229	NS-Ogk-O197		Tusk	Fragment	E		Trashed
230	NS-Ogk-O198		Tusk	Fragment	E		Trashed
231	NS-Ogk-O199		Tusk	Fragment	E	Shore, near stream mouth	Trashed
232	NS-Ogk-O200		Tusk	Fragment	E		Trashed
233	NS-Ogk-O201		Tusk	Fragment	E		Trashed
234	NS-Ogk-O202	Rangifer tarandus	Antler	Fragment	E		Trashed
235	NS-Ogk-O203	Rangifer tarandus	Antler	Fragment	E		Trashed
236	NS-Ogk-O204	Rangifer tarandus	Antler	Fragment	E		Trashed
237	NS-Ogk-O205	Large herbivorous mammal	Mandibula	Fragment	E		Trashed
238	NS-Ogk-O206	Large herbivorous mammal	Limb bone	Fragment	E		Trashed
239	NS-Ogk-O207	Equus caballus	Tooth (M)	Fragment	E		Trashed
240	NS-Ogk-O208	Equus caballus	Scapula, right	Fragment	E		
241	NS-Ogk-O209	Equus caballus	Ph I, right		E		Rounded
242	NS-Ogk-O210	Equus caballus	Antebrachium, right	With marrou	E		
243	NS-Ogk-O211	Bison priscus	Horn sheet	Fragment	E		
244	NS-Ogk-O212	Bison priscus	Horn sheet	Damaged	E		
245	NS-Ogk-O213	Equus caballus	Cranium	Occipital fragment	E		
246	NS-Ogk-O214	Mammuthus primigenius	Tusk	Fragment	E	Shore	
247	NS-Ogk-O215		Cranium	Fragment	E	Shore, near	C 14

Appendix 5.2-3. continuation.

No.	samples	Taxon	Skeleton element	Preservation	Type Loc.	Locality	Remarks
248	NS-Ogk-O216		Upper tooth (? M3)	Fragment	E	stream mouth	
249	NS-Ogk-O217		Upper tooth (M3)	Fragment	E	West shore	
250	NS-Ogk-O218		Upper tooth (M2 or M3)	Fragment	E	Shore, near stream mouth	
251	NS-Ogk-O219		Tooth	Fragment	E		
252	NS-Ogk-O220		Tusk	Fragment	E		C 14
253	NS-Ogk-O221		Costa	Fragment	E		C 14
254	NS-Ogk-O222	Bison priscus	Mc III+IV, left		E		
255	NS-Ogk-O223	Rangifer tarandus	Mandibula (left stern) with teeth dp2-dp4, M1-M2	Fragment	E		
256	NS-Ogk-O224	Bison priscus	Centrotarsale	Fragment	E		Trashed
257	NS-Ogk-O225	Mammuthus primigenius	Humerus, left	Fragment	E		C 14
258	NS-Ogk-O226	Bison priscus	Ph I, right		E		
259	NS-Ogk-O227	Mammuthus primigenius	Tooth	Fragment	E		
260	NS-Ogk-O228		Tooth	Fragment	E		
261	NS-Ogk-O229	Bison priscus	Ph II, left	Fragment	E		
262	NS-Ogk-O230	? Bison priscus	Small limb bone	Fragment	E		
263	NS-Ogk-O231	? Bison priscus	Small limb bone	Fragment	E		
264	NS-Ogk-O232	Equus caballus	Astragalus, right	Fragment	E		Rounded, trashed
265	NS-Ogk-O233	? Bison priscus	Small limb bone	Fragment	E		
266	NS-Ogk-O234	Rangifer tarandus	Calcaneus	Fragment	E		Trashed
267	NS-Ogk-O235	? Mammuthus primigenius	Costa		E		Rounded, trashed
268	NS-Ogk-O236	Mammuthus primigenius	Ph I, font 4-th, left		E	Shore, near stream mouth	
269	NS-Ogk-O237	Bison priscus	Ph I, right		E		
270	NS-Ogk-O238	Bison priscus	Mc III+IV	Fragment	E		Trashed
271	NS-Ogk-O239	Bison priscus	Astragalus, left	Damaged	E		
272	NS-Ogk-O240	Bison priscus	Tarsale II+III, right		E		
273	NS-Ogk-O241	Rangifer tarandus	Astragalus	Fragment	E		Rounded, trashed

Appendix 5.2-3. continuation.

No.	samples	Taxon	Skeleton element	Preservation	Type Loc.	Locality	Remarks
274	NS-Ogk-O242	Rangifer tarandus	Antler	Fragment	E		Trashed
275	NS-Ogk-O243	Equus caballus	Pelvis	Fragment	E		Trashed
276	NS-Ogk-O244	Rangifer tarandus	Upper tooth		E		
277	NS-Ogk-O245	Rangifer tarandus	Lower tooth (M3)	Damaged	E		
278	NS-Ogk-O246	Mammuthus primigenius	Epistropheus	Damaged	E		
279	NS-Ogk-O247	Large herbivorous mammal	Limb bone	Fragment	E		Trashed
280	NS-Ogk-O248	? Mammuthus primigenius	Costa	Fragment	E		C 14
281	NS-Ogk-O249	Mammuthus primigenius	Thorax vertebra	Fragment, spinous processum	E	West shore	C 14
282	NS-Ogk-O250	Bison priscus	Femur, right	Fragment	E		C 14
283	NS-Ogk-O251	Bison priscus	Mc III+IV, left	Fragment	E		
284	NS-Ogk-O252	Bison priscus	Radius, right	Distal fragment, with marrow	E		
285	NS-Ogk-O253	Bison priscus	Calcaneus, right	Fragment	E		
286	NS-Ogk-O254	Equus caballus	Scapula, right	Fragment	E		
287	NS-Ogk-O255	Mammuthus primigenius	Limb bone	Fragment	E		Trashed
288	NS-Ogk-O256	Equus caballus	Mt III, right	Proximal fragment	E		
289	NS-Ogk-O257	Equus caballus	Mc III, right	Distal fragment	E		Rounded
290	NS-Ogk-O258	Large herbivorous mammal	Pelvis	Fragment	E		Trashed
291	NS-Ogk-O259	? Bison priscus	Humerus	Fragment	E	West shore	Trashed
292	NS-Ogk-O260	Mammuthus primigenius	Tusk	Fragment	E		
293	NS-Ogk-O261		Tusk	Fragment	E		
294	NS-Ogk-O262	Bison priscus	Antebrachium, right	Damaged	E		
295	NS-Ogk-O263	Bison priscus	Ph I, right		E		
296	NS-Ogk-O264	Mammuthus primigenius	Tooth	Fragment	E		

Appendix 5.2-3. continuation.

No.	samples	Taxon	Skeleton element	Preservation	Type Loc.	Locality	Remarks
297	NS-Ogk-O265	Large herbivorous mammal	? Humerus	Fragment	E		Trashed
298	NS-Ogk-O266	Rangifer tarandus	Pelvis (left part)	Fragment	E		
299	NS-Ogk-o267a	Mammuthus primigenius	Pelvis (left part)	Cut off	E	East shore	Samples 267-a (C 14) and 267-b (trashed) from one individual
300	NS-Ogk-o267b		Pelvis (right part)		E		
301	NS-Ogk-O268		Femur, left	Fragment, with marrow, cut off	E		Juv., C 14
302	NS-Ogk-O269		Humerus, left	Fragment, with marrow, cut off	E		C 14
303	NS-Ogk-O270		Ulnae, left	Fragment, cut off	C	Thermoterrace	C 14
304	NS-Ogk-O271		Ulnae, left	Fragment, with marrow, cut off	E	West shore	C 14
305	NS-Ogk-O272		Femur, right	Fragment, cut off	E		C 14
306	NS-Ogk-O273		Femur	Fragment, cut off	E		C 14
307	NS-Ogk-O274		Femur, right	Fragment, cut off	E		C 14
308	NS-Ogk-O275		Tusk	Fragment, cut off	E		C 14
309	NS-Ogk-O276		Tusk	Fragment	E		Trashed
310	NS-Ogk-O277		Tusk	Fragment, cut off	E		C 14
311	NS-Ogk-O278		Antebrachium, right	Fragment, cut off	E	West shore	C 14
312	NS-Ogk-O279		Humerus	Fragment, cut off	E	West shore	C 14
313	NS-Ogk-O280		Antebrachium, right	Fragment, cut off	E	West shore	C 14
314	NS-Ogk-O281		Tusk	Fragment, cut off	E	West shore	C 14
315	NS-Ogk-O282	Mammuthus primigenius Mammuthus primigenius	Humerus, left	Fragment, cut off	E	West shore	C 14
316	NS-Ogk-O283		Tusk	Fragment, cut off	E	West shore	C 14
317	NS-Ogk-O284		Tibia, left	Fragment, cut off	E	West shore	C 14
318	NS-Ogk-O285		Humerus, left	Fragment, cut off	E	West shore	C 14

Appendix 5.2-3. continuation.

No.	samples	Taxon	Skeleton element	Preservation	Type Loc.	Locality	Remarks
319	NS-Ogk-O286		Costa	Fragment	A	In situ, costal outcrop, 100 m east of the stream mouth, altitude 1 m	Probably, samples 267-a, 267-b, 268, 269, 286 (C 14) from one individual
320	NS-Ogk-O287		Humerus, left	Fragment	E	West shore	C 14
321	NS-Ogk-O288		Scapula, right	Fragment, cut off	E	West shore	C 14
322	NS-Ogk-O289		Tusk	Fragment, cut off	F	Tundra	C 14
323	NS-Ogk-O290		Tusk	Fragment, cut off	E	West shore	C 14
324	NS-Ogk-O293		Tusk	Fragment	E	West shore	Trashed
325	NS-Ogk-O294		Tusk	Fragment	E	West shore	Trashed
326	NS-Ogk-O295		Tusk	Fragment	E	West shore	Trashed
327	NS-Ogk-O296		Tusk	Fragment	E	West shore	Trashed
328	NS-Ogk-O297		Tusk	Fragment	E	West shore	Trashed
329	NS-Ogk-O298		Tusk	Fragment	E	West shore	Trashed
330	NS-Ogk-O299		Tusk	Fragment	E	West shore	Trashed
331	NS-Ogk-O300		Tusk	Fragment	E	West shore	Trashed
332	NS-Ogk-O301		Tusk	Fragment	E	West shore	C 14
333	NS-Ogk-O302		Tusk	Fragment	E	West shore	C 14
334	NS-Ogk-O303		Tusk	Fragment	E	West shore	C 14
335	NS-Ogk-O304		Tusk	Fragment	E	West shore	C 14
336	NS-Ogk-O305		Tusk	Fragment	E	West shore	Trashed
337	NS-Ogk-O306		Tusk	Fragment	E	West shore	C 14
338	NS-Ogk-O307		Tusk	Fragment	E	West shore	Trashed
339	NS-Ogk-O308		Tusk	Fragment	E	West shore	Trashed
340	NS-Ogk-O309		Tusk	Fragment	E	West shore	Trashed
341	NS-Ogk-O310	Mammuthus primigenius	Tusk	Fragment	E	West shore	Trashed
342	NS-Ogk-O311		Tusk	Fragment	E	West shore	Trashed
343	NS-Ogk-O312		Tusk	Fragment	E	West shore	Trashed
344	NS-Ogk-O313		Tusk	Fragment	E	West shore	Trashed

Appendix 5.2-3. continuation.

No.	samples	Taxon	Skeleton element	Preservation	Type Loc.	Locality	Remarks
345	NS-Ogk-O314		Tusk	Fragment	E	West shore	Trashed
346	NS-Ogk-O315		Tusk	Fragment	E	West shore	Trashed
347	NS-Ogk-O316		Tusk	Fragment	E	West shore	C 14
348	NS-Ogk-O317		Tusk	Fragment	E	West shore	C 14
349	NS-Ogk-O318		Tusk	Fragment	E	West shore	C 14
350	NS-Ogk-O319		Tusk	Fragment	E	West shore	Trashed
351	NS-Ogk-O320		Tusk	Fragment	E	West shore	C 14
352	NS-Ogk-O321		Tooth	Fragment	E	West shore	Trashed
353	NS-Ogk-O322		Tooth	Fragment	E	West shore	Trashed
354	NS-Ogk-O323	Rangifer tarandus	Shed antler	Fragment	E	West shore	
355	NS-Ogk-O324	Mammuthus primigenius	Limb bone	Fragment	E	West shore	Trashed
356	NS-Ogk-O325	Bison priscus	Radius, right		E	West shore	
357	NS-Ogk-O326	Bison priscus	Radius, right	Distal fragment	E	West shore	
358	NS-Ogk-O327	Equus caballus	Mt III, right	Fragment	E	West shore	Rounded
359	NS-Ogk-O328	Mammuthus primigenius	Tusk	Fragment	E	West shore	C 14
360	NS-Ogk-O329		Costa	Fragment	E	West shore	C 14
361	NS-Ogk-O330	Bison priscus	Humerus, right	Distal fragment	E	West shore	
362	NS-Ogk-O331	Bison priscus	Femur, left	Fragment	E	West shore	C 14
363	NS-Ogk-O332	Mammuthus primigenius	Limb bone	Fragment	E	West shore	Trashed
364	NS-Ogk-O333		Femur, left	Distal fragment	E	West shore	C 14
365	NS-Ogk-O334	Equus caballus	Ph I, left		E	West shore	
366	NS-Ogk-O335	Equus caballus	Ph I, right		E	West shore	
367	NS-Ogk-O336	Mammuthus primigenius	Scapula	Fragment	E	West shore	C 14
368	NS-Ogk-O337		Humerus, left	Fragment	E	West shore	C 14
369	NS-Ogk-O338	Equus caballus	Mandibula (right stem) with teeth dp2-dp4	Fragment	E	West shore	
370	NS-Ogk-O339	Equus caballus	Pelvis (right part)	Fragment	E	West shore	
371	NS-Ogk-O340	Mammuthus primigenius	Femur, left	Fragment	A	West shore	C 14

Appendix 5.2-3. continuation.

No.	samples	Taxon	Skeleton element	Preservation	Type Loc.	Locality	Remarks
372	NS-Ogk-O341	Bison priscus	Scapula, left	Fragment	E	Shore, near stream mouth	
373	NS-Ogk-O342	Bison priscus	Astrogalus, left		E		
374	NS-Ogk-O343	Ovibos sp.	Cervical vertebra	Damaged	E		
375	NS-Ogk-O344	Bison priscus	Astrogalus, left	Fragment	E		
376	NS-Ogk-O345	Ovibos sp.	Thorax vertebra	Damaged	E		Trashed
377	NS-Ogk-O346	Mammuthus primigenius	Vertebra	Fragment, spinous processum	E		Trashed
378	NS-Ogk-O347	Large herbivorous mammal	Limb bone	Fragment	E		Trashed
379	NS-Ogk-O348		Limb bone	Fragment	E		Trashed
380	NS-Ogk-O349	Ovibos sp.	Astrogalus, left		E		
381	NS-Ogk-O350	Mammuthus primigenius	Mc IV	Fragment	E		Juv.
382	NS-Ogk-O351		Tusk	Fragment	E	West shore	C 14
383	NS-Ogk-O352		Tusk	Fragment	E	West shore	C 14
384	NS-Ogk-O353		Tusk	Fragment	E	West shore	C 14
385	NS-Ogk-O354		Lower tooth (?M2)	Damaged	E	West shore	
386	NS-Ogk-O355		Scapula, left	Fragment	E	West shore	C 14
387	NS-Ogk-O356	Bison priscus	Humerus, left	Distal fragment	E	West shore	
388	NS-Ogk-O357	Bison priscus	Mc III+IV, left		E	West shore	
389	NS-Ogk-O358	Bison priscus	Carpal intermedium, left		E	West shore	
390	NS-Ogk-O359	Mammuthus primigenius	Limb bone	Fragment	E	West shore	Trashed
391	NS-Ogk-O360	Equus caballus	Tibia, right	Distal fragment	E	West shore	
392	NS-Ogk-O361	Equus caballus	Astrogalus, left		E	West shore	
393	NS-Ogk-O362	? Bison priscus	Ulnae, right	Fragment	E	West shore	
394	NS-Ogk-O363	Equus caballus	Ph III	Fragment	E	West shore	
395	NS-Ogk-O364	Ovibos sp.	Astrogalus, right		E	West shore	
396	NS-Ogk-O365	Ovibos sp.	Astrogalus, left	Damaged	E	West shore	
397	NS-Ogk-O366	Ovibos sp.	Astrogalus, right		E	West shore	
398	NS-Ogk-O367	Bison priscus	Ph I		E	West shore	
399	NS-Ogk-O368	Equus caballus	?Cuneiforme III	Fragment	E	West shore	Trashed

Appendix 5.2-3. continuation.

No.	samples	Taxon	Skeleton element	Preservation	Type Loc.	Locality	Remarks
400	NS-Ogk-O369	Equus caballus	Scapula, right	Fragment	E	West shore	
401	NS-Ogk-O370	Mammuthus primigenius	Femur, left	Fragment	E	West shore	Juv.
402	NS-Ogk-O371	Rangifer tarandus	Costa	Fragment	E	West shore	
403	NS-Ogk-O372	Mammuthus primigenius	Lower tooth (M2 or M3)	Fragment	E	West shore	
404	NS-Ogk-O373		Mandibula (right stem) without teeth	Fragment (3 pieces)	E	West shore	Juv., C 14
405	NS-Ogk-O374	Equus caballus	Ulnae, right	Damaged	E	West shore	
406	NS-Ogk-O375	Bison priscus	Upper tooth	Damaged	E	West shore	
407	NS-Ogk-O376	Bison priscus	Femur, right	Fragment	E	West shore	
408	NS-Ogk-O377	Bison priscus	Lumbar vertebra	Damaged	E	West shore	
409	NS-Ogk-O378	Rangifer tarandus	Mandibula (right stem) with tooth M3	Fragment	E	West shore	
410	NS-Ogk-O379	Mammuthus primigenius	Tooth, heavily worn	Fragment	E	West shore	
411	NS-Ogk-O380		Tooth, heavily worn	Fragment	E	West shore	
412	NS-Ogk-O381	Equus caballus	Pelvis	Fragment	E	West shore	Trashed
413	NS-Ogk-O382	Bison priscus	Tibia, right	Distal fragment	E	West shore	
414	NS-Ogk-O383	Mammuthus primigenius	Limb bone	Fragment	E	West shore	Rounded, trashed
415	NS-Ogk-O384	Large herbivorous mammal	Cervical vertebra	Fragment	E	West shore	Trashed
416	NS-Ogk-O385	Bison priscus	Horn sheet	Fragment	E	West shore	
417	NS-Ogk-O386	Equus caballus	Tibia, right	Distal fragment	E	West shore	
418	NS-Ogk-O387	Bison priscus	Cranium	Fragment	E	West shore	Trashed
419	NS-Ogk-O388	Mammuthus primigenius	Tibia, left	Fragment	E	West shore	C 14
420	NS-Ogk-O389	? Mammuthus primigenius	Limb bone	Fragment	E	West shore	Trashed
421	NS-Ogk-O390	Mammuthus primigenius	Humerus, right	Fragment	E	West shore	C 14

Appendix 5.2-3. continuation.

No.	samples	Taxon	Skeleton element	Preservation	Type Loc.	Locality	Remarks
422	NS-Ogk-O391	Rangifer tarandus	Scapula, right	Fragment	E	West shore	
423	NS-Ogk-O392	Rangifer tarandus	Mt III+IV	Distal fragment	E	West shore	
424	NS-Ogk-O393	Rangifer tarandus	Calcaneus	Damaged	E	West shore	
425	NS-Ogk-O394	Large herbivorous mammal	Limb bone	Fragment	E	West shore	Trashed
426	NS-Ogk-O395	Mammuthus primigenius	Vertebra	Fragment, spinous processum	E	West shore	Trashed
427	NS-Ogk-O396	? Bison priscus	Humerus, left	Fragment	E	West shore	Trashed
428	NS-Ogk-O397	Rangifer tarandus	Shed antler	Fragment	E	West shore	Trashed
429	NS-Ogk-O398	Bison priscus	Ulnae	Fragment	E	West shore	Trashed
430	NS-Ogk-O399	Large herbivorous mammal	? Humerus	Fragment	E	West shore	Trashed
431	NS-Ogk-O400	Equus caballus	Ph I, right	Fragment	E	West shore	
432	NS-Ogk-O401	Equus caballus	Ulnae, left	Fragment	E	West shore	Trashed
433	NS-Ogk-O402	? Bison priscus	Pelvis	Fragment	E	West shore	Trashed
434	NS-Ogk-O403	Bison priscus	Ulnae	Fragment	E	West shore	Trashed
435	NS-Ogk-O404	Bison priscus	Small limb bone	Fragment	E	West shore	
436	NS-Ogk-O405	Rangifer tarandus	Metapodia	Fragment	E	West shore	Juv.
437	NS-Ogk-O406	? Equus caballus	Thorax vertebra	Fragment	E	West shore	Trashed
438	NS-Ogk-O407	Bison priscus	Ph I, left	Fragment	E	West shore	
439	NS-Ogk-O408	Large herbivorous mammal	Limb bone	Fragment	E	West shore	Trashed
440	NS-Ogk-O409		Limb bone	Fragment	E	West shore	Trashed
441	NS-Ogk-O410		Limb bone	Fragment	E	West shore	Trashed
442	NS-Ogk-O411		Limb bone	Fragment	E	West shore	Trashed
443	NS-Ogk-O412		Limb bone	Fragment	E	West shore	Trashed
444	NS-Ogk-O413	Mammuthus primigenius	Tusk	Fragment	E	West shore	C 14
445	NS-Ogk-O414	Equus caballus	Ph I	Fragment	E	West shore	Trashed
446	NS-Ogk-O415	Equus caballus	Mc III	Fragment	E	West shore	Trashed
447	NS-Ogk-O416	Equus caballus	Lower tooth	Fragment	E	West shore	Trashed

Appendix 5.2-3. continuation.

No.	samples	Taxon	Skeleton element	Preservation	Type Loc.	Locality	Remarks
448	NS-Ogk-O417	? Equus caballus	Cervical vertebra	Fragment	E	West shore	
449	NS-Ogk-O418	Equus caballus	Ph I	Fragment	E	West shore	Trashed
450	NS-Ogk-O419	Rangifer tarandus	Shed antler	Fragment	E	West shore	Trashed
451	NS-Ogk-O420	Rangifer tarandus	Shed antler	Fragment	E	West shore	Trashed
452	NS-Ogk-O421	Rangifer tarandus	Sacrum	Fragment	E	West shore	Trashed
453	NS-Ogk-O422	Large herbivorous mammal	Costa	Fragment	E	West shore	Trashed
454	NS-Ogk-O423	? Bison priscus	Tooth	Fragment	E	West shore	Trashed
455	NS-Ogk-O424	Equus caballus	Naviculare	Fragment	E	West shore	Trashed
456	NS-Ogk-O425	Mammuthus primigenius	Lower tooth (P4 or M1)		C	Thermoterrace	
457	NS-Ogk-O426	Bison priscus	Tibia, left	Distal fragment	E	West shore	
458	NS-Ogk-O427	Bison priscus	Ph I, right		E	West shore	
459	NS-Ogk-O428	Mammuthus primigenius	Femur	Fragment	E	West shore	C 14
460	NS-Ogk-O429		Limb bone	Fragment	E	West shore	C 14
461	NS-Ogk-O430		Ulnare		D	Baydzherakh in tundra, near to the theodolite	C 14
462	NS-Ogk-O431	Rangifer tarandus	Shed antler	Fragment	E	West shore	Vivianit
463	NS-Ogk-O432	Mammuthus primigenius	Atlas	Damaged	E	Shore, near stream mouth	C 14
464	NS-Ogk-O433		Mc IV, right		E		
465	NS-Ogk-O434	Bison priscus	Lumbar vertebra	Damaged	E	Shore, near stream mouth	
466	NS-Ogk-O435	Mammuthus primigenius	Humerus	Distal fragment	E	Shore, near stream mouth	Juv.
467	NS-Ogk-O436		Mandibula (right stem) without teeth	Fragment	E	West shore	C 14
468	NS-Ogk-O437		Ulnae	Fragment	E	West shore	C 14
469	NS-Ogk-O438	Bison priscus	Cervical vertebra	Damaged	E	West shore	
470	NS-Ogk-O439	Ovibos sp.	Humerus, left	Distal fragment	E	West shore	
471	NS-Ogk-O440	Large herbivorous	Cranium	Fragment	E	West shore	Trashed

Appendix 5.2-3. continuation.

No.	samples	Taxon	Skeleton element	Preservation	Type Loc.	Locality	Remarks
		mammal					
472	NS-Ogk-O441	Mammuthus primigenius	Cervical vertebra	Fragment	E	West shore	Trashed
473	NS-Ogk-O442		Radius, right	Fragment	E	West shore	C 14
474	NS-Ogk-O443	Equus caballus	Ph I, left		E	West shore	
475	NS-Ogk-O444	Mammuthus primigenius	Limb bone	Fragment (2 pieces)	E	West shore	
476	NS-Ogk-O445	Bison priscus	Pelvis (left part)	Fragment	E	West shore	C 14
477	NS-Ogk-O446	Mammuthus primigenius	Pelvis	Fragment	E	West shore	Trashed
478	NS-Ogk-O447		Tusk	Fragment	E	West shore	C 14
479	NS-Ogk-O448	Bison priscus	Epistropheus	Damaged	E	West shore	
480	NS-Ogk-O449	Rangifer tarandus	Mt III+IV	Fragment	E	West shore	
481	NS-Ogk-O450	Bison priscus	Ph II, left		E	West shore	
482	NS-Ogk-O451	Rangifer tarandus	Mandibula (left stem) with teeth P2-P3	Fragment	E	West shore	
483	NS-Ogk-O452	Mammuthus primigenius	Vertebra	Fragment, spinous processum	E	West shore	Trashed
484	NS-Ogk-O453	Large herbivorous mammal	Costa	Fragment	E	West shore	Trashed
485	NS-Ogk-O454	Bison priscus	Ph II, right	Fragment	E	West shore	Trashed
486	NS-Ogk-O455	Mammuthus primigenius	Vertebra	Fragment	E	West shore	Trashed
487	NS-Ogk-O456	Bison priscus	Pelvis, left	Fragment	E	West shore	
488	NS-Ogk-O457	Equus caballus	Astrogalus, right		E	West shore	
489	NS-Ogk-O458	Equus caballus	Ph II	Damaged	E	West shore	
490	NS-Ogk-O459	Equus caballus	Ph III		E	West shore	
491	NS-Ogk-O460	Equus caballus	Astrogalus, right	Fragment	E	West shore	Trashed
492	NS-Ogk-O461	Ovibos sp.	Vertebra	Fragment	E	West shore	
493	NS-Ogk-O462	Bison priscus	Cervical vertebra		E	West shore	
494	NS-Ogk-O463	Bison priscus	Ph III, right		E	West shore	
495	NS-Ogk-O464	Bison priscus	Ph II, left		E	West shore	

Appendix 5.2-3. continuation.

No.	samples	Taxon	Skeleton element	Preservation	Type Loc.	Locality	Remarks
496	NS-Ogk-O465	? Rangifer tarandus	Sacrum	Fragment	E	West shore	
497	NS-Ogk-O466	? Ovibos sp.	Ph II, left		E	West shore	
498	NS-Ogk-O467	Equus caballus	Ph II	Damaged	E	West shore	Juv.
499	NS-Ogk-O468	Bison priscus	Ulnare	Fragment	E	West shore	
500	NS-Ogk-O469	Bison priscus	Calcaneus, left	Fragment	E	West shore	Trashed
501	NS-Ogk-O470	Ovibos sp.	Astrogalus, right	Damaged	E	West shore	
502	NS-Ogk-O471	Bison priscus	Cervical vertebra	Fragment	E	West shore	
503	NS-Ogk-O472	Bison priscus	Sacrum	Damaged	E	West shore	
504	NS-Ogk-O473	Bison priscus	? Thorax vertebra	Fragment	E	West shore	
505	NS-Ogk-O474	Mammuthus primigenius	Mt V, left	Fragment	E	West shore	Trashed
506	NS-Ogk-O475	? Bison priscus	? Cervical vertebra	Fragment	E	West shore	
507	NS-Ogk-O476	Mammuthus primigenius	Mc III, left	Damaged	E	West shore	
508	NS-Ogk-O477		Centrale		E	West shore	
509	NS-Ogk-O478		Epistropheus	Damaged	E	West shore	
510	NS-Ogk-O479		Tibia, right	Proximal fragment	E	West shore	Juv., C 14
511	NS-Ogk-O480	Equus caballus	Ph I	Distal fragment	E	West shore	
512	NS-Ogk-O481	Mammuthus primigenius	Tooth	Fragment	E	West shore	Trashed
513	NS-Ogk-O482		Tooth, heavily worn	Fragment	E	West shore	Trashed
514	NS-Ogk-O483		Tooth, heavily worn	Fragment	E	West shore	Trashed
515	NS-Ogk-O484	Equus caballus	Ph II	Fragment	E	West shore	
516	NS-Ogk-O485	Equus caballus	Magnum, right		E	West shore	
517	NS-Ogk-O486	? Ovibos sp.	Ph I, right	Fragment	E	West shore	
518	NS-Ogk-O487	Equus caballus	Ph I	Fragment	E	West shore	Trashed
519	NS-Ogk-O488	Equus caballus	Upper tooth	Fragment	E	West shore	
520	NS-Ogk-O489	Mammuthus primigenius	Tooth	Fragment	E	West shore	Trashed
521	NS-Ogk-O490	Rangifer tarandus	Ph II, right	Fragment	E	West shore	
522	NS-Ogk-O491	Mammuthus primigenius	Tusk	Fragment	E	West shore	

Appendix 5.2-3. continuation.

No.	samples	Taxon	Skeleton element	Preservation	Type Loc.	Locality	Remarks
523	NS-Ogk-O492	Lepus sp.	Tibia	Fragment	E	West shore	
524	NS-Ogk-O493	Mammuthus primigenius	Tooth	Fragment	C	Thermoterrace	
525	NS-Ogk-O494		Tooth		C	Thermoterrace	Trashed
526	NS-Ogk-O495	Mammal	? Lumbar vertebra	Fragment	E	West shore	Trashed
527	NS-Ogk-O496	Large herbivorus mammal	Palanx	Fragment	E	West shore	Trashed
528	NS-Ogk-O497	Equus caballus	Ph I	Distal fragment	E	West shore	Rounded, trashed
529	NS-Ogk-O498	Equus caballus	Tibia, left	Distal fragment	E	West shore	Trashed
530	NS-Ogk-O499	Rangifer tarandus	Metapodium	Fragment	E	West shore	Trashed
531	NS-Ogk-O500	Rangifer tarandus	Mt III+IV	Fragment	E	West shore	Trashed
532	NS-Ogk-O501	Equus caballus	Humerus	Fragment	E	West shore	Trashed
533	NS-Ogk-O502	Bison priscus	?	Fragment	E	West shore	
534	NS-Ogk-O503	Equus caballus or Bison priscus	Intermedium	Fragment	E	West shore	
535	NS-Ogk-O504	? Equus caballus	Incisor, heavily worn		E	West shore	
536	NS-Ogk-O505	Bison priscus	Lower tooth	Damaged	E	West shore	
537	NS-Ogk-O506	Bison priscus	Upper premolare tooth	Damaged	E	West shore	
538	NS-Ogk-O507	Bison priscus	Lower tooth	Fragment	E	West shore	Trashed
539	NS-Ogk-O508	Bison priscus	Upper tooth	Fragment	E	West shore	Trashed
540	NS-Ogk-O509	Rangifer tarandus	Ph I, left	Distal fragment	E	West shore	Rounded
541	NS-Ogk-O510	Rangifer tarandus	Carpale II+III		E	West shore	
542	NS-Ogk-O511	Rangifer tarandus	Ph II, left	Proximal fragment	E	West shore	
543	NS-Ogk-O512	Equus caballus	Cuneiforme III	Fragment	E	West shore	Trashed
544	NS-Ogk-O513	Rangifer tarandus or Ovibos sp.	Astragalus	Fragment	E	West shore	Rounded, trashed
545	NS-Ogk-O514	? Rangifer tarandus	Pelvis	Fragment	E	West shore	Rounded, trashed
546	NS-Ogk-O515	Large herbivorus mammal	Metapodium	Distal fragment	E	West shore	Rounded, trashed
547	NS-Ogk-O516	Large herbivorus mammal	Costa	Fragment	E	West shore	Rounded, trashed

Appendix 5.2-3. continuation.

No.	samples	Taxon	Skeleton element	Preservation	Type Loc.	Locality	Remarks
548	NS-Ogk-O517	Equus caballus	Radius	Proximal fragment	E	West shore	Trashed
		Muostakh Island (north part)					
549	NS-Mst-O532	Mammuthus primigenius	Scapula	Fragment	E	Shore	C 14
550	NS-Mst-O533		Costa	Fragment	E	Shore	C 14
551	NS-Mst-O534	Bison priscus	Astrogalus		E	Shore	
552	NS-Mst-O535	Large herbivorus mammal	Pelvis	Fragment	B	Exposure, altitude 3 - 6 m	Juv., from Lutz, AMS
553	NS-Mst-O536	Mammuthus primigenius	Mt III, left		E	Shore	Rounded
554	NS-Mst-O537	Equus caballus	Ph III	Damaged	E	Shore	Small
555	NS-Mst-O538	Large herbivorus mammal	Vertebra	Fragment	E	Shore	Trashed
		Bykovsky Peninsula, Mamontovy Khayata					
556	Mkh-02-O539	Rangifer tarandus	Shed antler	Fragment	A	In situ, exposure, altitude 35.6m	From Hanno, AMS

Appendix 5.2-4. Measuring sites for soil temperature and soil moisture; Measurement interval as well as average, minimum and maximum values are given.

Location	Descriptive text in Chapter	Lat	Long	Measuring time (5 min interval)		Temperature (°C)			Volumetric moisture for organic soils ($m^3 \times m^{-3}$)		
				start - end	data points	Average	Min	Max	Average	Min	Max
Kotel'ny south coast, Komurganakh R.- mouth	5.2.5	74°44.317'	138°24.219'	10:59 – 16:39	69	5.3	4.5	5.8	0.519	0.518	0.521
Bunge-Land, high terrace	5.2.6	74°52.849'	142°06.277'	10:37 – 18:17	93	6.5	5.4	7.0	0.210	0.208	0.213
Island Novaya Sibir	5.2.7	75°07.183'	146°38.843'	13:12 – 18:17	62	1.9	1.5	2.4	0.420	0.416	0.421
Bunge-Land, low terace	5.2.6	74°50.662'	140°29.007'	15:33 – 18:26	37	-	-	-	0.301	0.298	0.310
Maly Lyakhovsky Island	5.2.8	74°14.576'	140°19.167'	17:17 – 21:27	52	4.3	3.4	5.6	0.384	0.383	0.384
Cape Svyatoy Nos	5.2.9	72°53.188'	140°48.237'	19:10 – 21:30	29	5.2	4.9	5.9	0.255	0.252	0.257
Oyogos Yar coast	5.2.10	72°40.525'	143°35.925'	13:03 – 21:03	97	3.8	2.5	5.3	0.380	0.366	0.381
Muostakh Island	5.2.11	71°36.801'	129°56.175'	09:56 – 12:51	36	6.2	4.3	7.6	0.169	0.166	0.170
Mamontovy Bysagassa	4.5.2	71°47.236'	129°24.260'	13:13 – 22:23	111	2.8	2.2	3.3	0.583	0.563	0.600
Polar Fox Lake	4.5.3	71°44.099'	129°20.775'	10:29 – 17:09	81		-	-	0.543	0.540	0.546

5.3 Coastal Studies on the New Siberian Islands

5.3.1 Introduction

Volker Rachold and Mikhail N. Grigoriev

The main goal of the investigations carried out by the coastal team within the framework of the expedition "Lena-New Siberian Islands 2002" was a quantitative evaluation of the main parameters of coastal dynamics. From August 12 to September 4 twelve key sites along the coast of the Laptev and East-Siberian Seas were studied in detail in respect of both onshore and offshore coastal relief and dynamics (Figure 5.3.1-1).

The following sub-chapters summarize the work program and the preliminary results of the coastal team. Sub-chapter 5.3.2 concentrates on the offshore and sub-chapter 5.3.3 on the onshore coastal studies. The results of water temperature measurements and the study of thermoterraces are presented in separate sub-chapters (5.3.4 and 5.3.5, respectively).

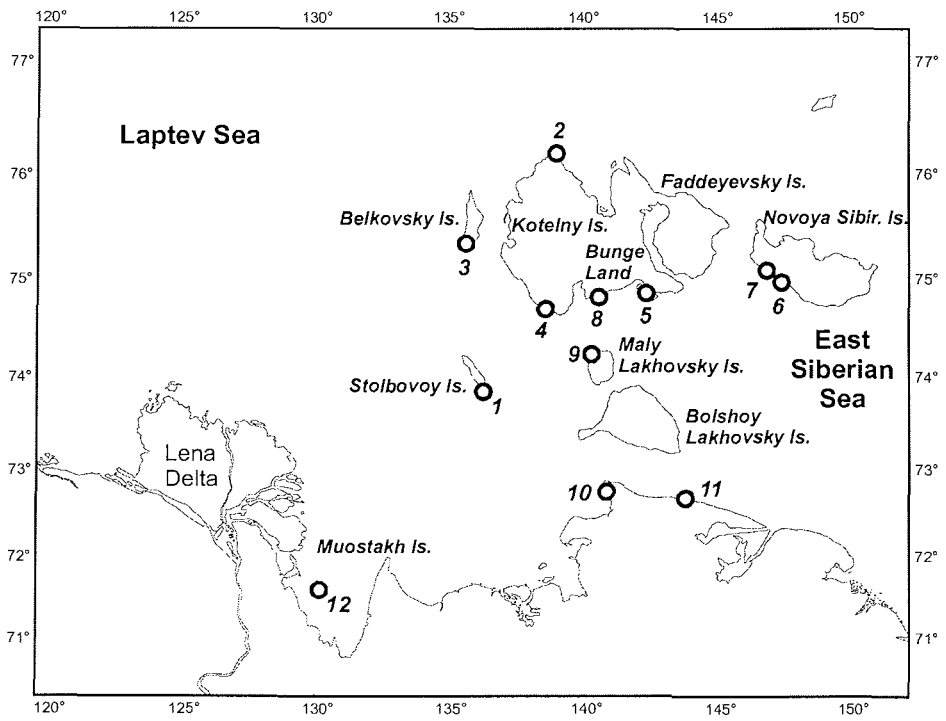

Figure 5.3.1-1. Coastal sections studied during the expedition LENA 2002.

5.3.2 Offshore coastal studies - shoreface profile measurements

Feliks E. Are, Mikhail N. Grigoriev, Olga A. Gruzdeva, Hans-W. Hubberten, Volker Rachold, Sergey O. Razumov and Waldemar Schneider

5.3.2.1 Introduction

The coastal team of the expedition had continued bathymetric measurements of the shoreface profiles started in 1999. The measurement goal is investigation of the morphology and dynamics of the shoreface in the Arctic seas. In 2002 these measurements were carried out for the first time on the islands of New Siberian Archipelago. The team surveyed 10 coastal sections in the Laptev and East-Siberian seas on the islands Stolbovoy, Belkovsky, Kotelny, Novaya Sibir, Maly Lakhovsky and 1 section on the south coast of Dmitry Laptev Strait (Fig. 5.3.1-1).

The ice complex sediments are wide spread on these islands just as on the continental coast but on the islands the ice complex is based on the bedrock. The bedrock is usually situated near the sea level or above it. On the continental coast the bedrock under the ice complex is absent. Therefore the geological and geocryological conditions of the shoreface evolution on the islands and on the continent differ strongly.

One section composed of ice complex was surveyed on the south coast of the Dmitry Laptev Strait (11 in Fig. 5.3.1-1). The ice complex is underlayed there by a thickness of clayey silts with low ice content and small ice wedges. The top of this thickness in coastal outcrops rises as high as 8.5 m above the sea level. The bedrock was not observed on this coast.

Beside the coasts composed of ice complex, a section composed of weekly lithified low Quaternary and upper Neogenic (Pleocene) sediments with low ice content was surveyed on Novaya Sibir Island (6 in Fig. 5.3.1-1). These sediments do not contain ice wedges and easily undergo erosion by waves and water streams.

Two sections composed of sands with low ice content were surveyed on the south coast of Bunge Land (5 and 8 in Fig. 5.3.1-1). Their composition is identical with the coasts of Arga Island in the Lena River delta, which were surveyed in 1999 and 2001. But there are significant morphological differences. For example, unlike Arga Island, the shore on Bunge Land is aligned, lagoons and barrier islands are absent, wind surges are low.

The lease of the ship «Pavel Bashmakov» from August 14 until September 2 limited the working time of the coastal team. During this time 14 shoreface profiles on 9 sections of the coast were measured (1,3,4,5,6,8,9,10,11 in Fig. 5.3.1-1). Twenty one profiles, including profiles along the tracks of bathymetric measurements, was taken from bathymetric charts to study shoreface dynamics. The scales of charts used are in the range of 1:200 000 - 1:25 000. The charts are based on the measurements carried out 16-43 years ago.

As a whole the data obtained will give a possibility to improve our understanding of the shoreface shape in different geological, geocryological and hydrological conditions and to supplement considerably the data base on the formation of the Arctic shoreface morphology.

5.3.2.2 Methods

The tracks of shoreface profile measurements were chosen using the State Map of Quaternary Formations in the New Siberian Islands Area at the 1:100 000 scale published in 1998, navigation charts at different scale and results of visual survey of the coasts.

The water depth measurements were carried out the same way as in 2001 using a portable echo-sounder from a motor boat. All data were measured every second and stored on a computer. The accuracy of measurements was 1 cm for the water depth. The linear increment of measurements along the track was 2 m at a speed of 5 km/hour. Surface sediments for sedimentological analyses were sampled every 1 m water depth.

Tracks were run along courses chosen beforehand and monitored on a computer display. The standard deviation of the actual azimuth from its mean value during the boat movement was in the range of 4-6 degrees. The maximum short-term deviations reached 20 degrees. A diagram of recorded azimuth fluctuations along the track of the shoreface profile of Bunge Land lower part is presented in Fig. 5.3.2-1 for example. During the recording of this profile the mean value of the azimuth was 155.5° with a standard deviation 4.2°. An inclination of the trend line in Fig. 5.3.2-1 shows a small deviation of the measured track from a strait line.

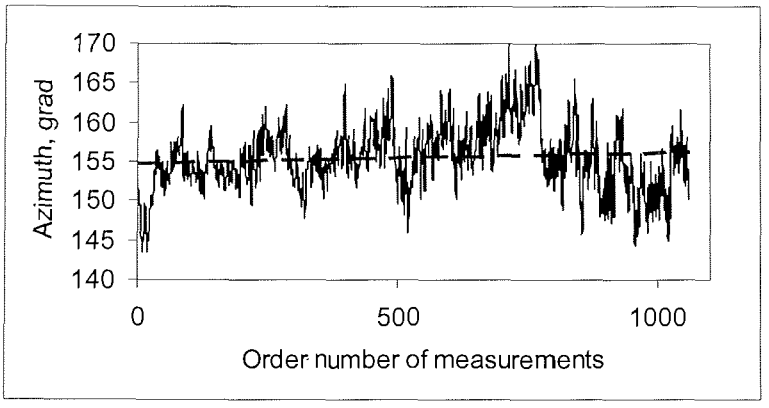

Figure 5.3.2-1: A diagram of measured azimuth fluctuations during the survey of the shoreface profile on the Bunge Land low part.

The horizontal distances between all points of depth measurement and the first point nearest to the shore were calculated for the purpose of drawing complete shoreface profiles. The calculations were made using software kindly provided

by Dr. D. Drozdov (Cryosphere Institute, RAS). Another software was used to verify results of calculations with the help of exact geodetic formulas. The divergences of calculations by the use of two kinds of software were negligible.

As it was marked in the previous cruise reports; one of the main tasks of the shoreface morphology investigations is to study the shoreface shape by means of mathematical description. The AISN Corporation software TableCurve 2D v5 will be used for this purpose. The TableCurve presents the widest possibilities for automated processing of the shoreface measurement results, extensive selection of mathematical functions for description of the shoreface shape, and gives a comprehensive statistical evaluation of the function fitness with the actual shoreface shape. But we used a simpler software Grapher v3.01, Golden Software Corporation, with limited possibilities of statistical evaluations for a preliminary presentation of the field work results in this report.

Availability of the shoreface profiles measured in 2002 and bathymetric charts based on the measurement data obtained 16-43 years ago give opportunity to evaluate the shoreface dynamics during these years. Unfortunately the scale of charts and accuracy of field measurements usually are insufficient for assessment of the shore line displacements. However a comparison of the measured shoreface profiles with the same profiles taken from the bathymetric charts permits sometimes to reveal the changes of shoreface shape and corresponding erosion or accretion volumes in the coastal zone.

5.3.2.3 Preliminary results

The shoreface profiles measured in different geological and geocryological conditions in sections 6,8 and 9 (Fig. 5.3.1-1) are considered below for preliminary illustration of field investigations carried out.

Section 6 is situated on the southwest coast of Novaya Sibir Island in the area of "Utyos Derewyannukh Gor" (Wood Mountain Cliff) Cape (75° 0.8′ N., 147° 6.1′ E.). As it was marked above, the coast in this section is composed of weakly lithified sediments of all kinds from clays till rock debris with low ice content. The slopes of seaboard hills as high as 85 m have no vegetation. Their base is cut with steep crumbling cliffs (Fig. 5.3.2-2). In some places the cliffs are plumb, with last year's wave cut niches filled with snow at their base. No large accumulations of thermodenudation products were observed on the beach but recent talus were present everywhere and single destruction blocks of frozen sediments were met. Water streams extensively erode the seaboard slopes above the cliffs. The mouths of some ravines are uplifted for 1-2 m above the beach. These morphological features testify that the sediments composing the coast undergo intensive erosion.

The narrow beach is build by sand with two stripes of gravel with pebbles along the shore. The seawater in the surf zone is very turbid.

One shoreface profile about 3 km long was measured in section 6 (Fig. 5.3.2-3). The doubtless signs of coastal erosion mentioned above caused to anticipate that the shoreface in this section is moulded by waves and has a concave

shape. But a flat slope in Fig. 5.3.2-3 stretches up to 6-m depth at 1-km distance from the shore. A strait line fits this part of the shoreface profile with a high coefficient of determination R^2 = 0.9915.

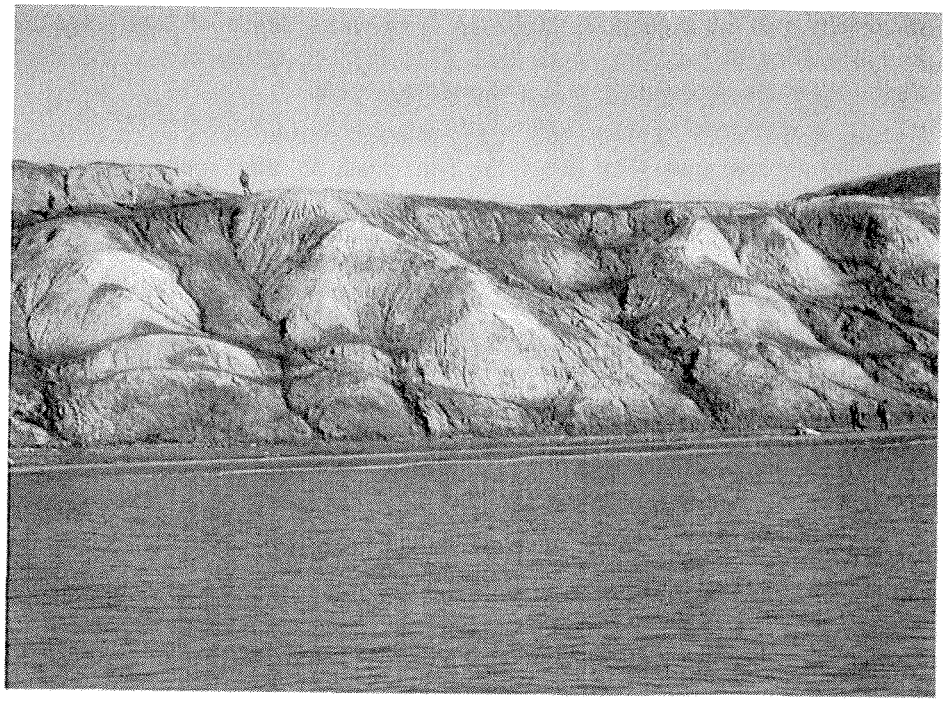

Figure 5.3.2-2. Erosion coast of Novaya Sibir Island in the area of Cape Utyes Derewannykh Gor, section 6.

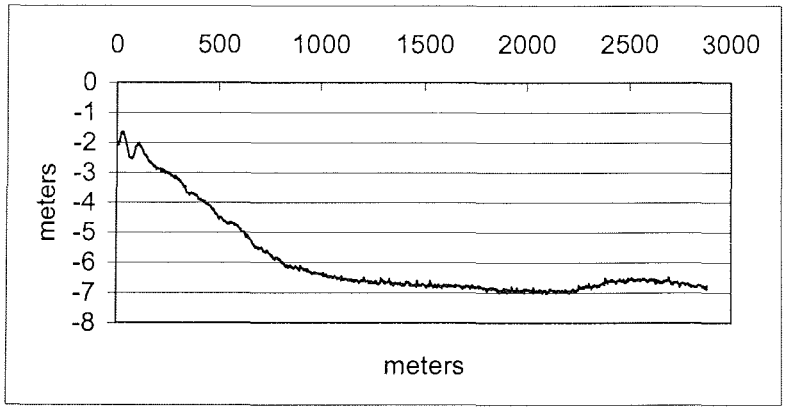

Figure 5.3.2-3. Shoreface profile near the Cape Utyes Derewannykh Gor, Novaya Sibir Island, section 6.

Unfortunately the shoreline location and the coastal shallow profile until 2-m depth were not measured. Extrapolation of the shoreface profile strait trend line in the depth range 2-6 m gives position of the first measurement point (2-m isobath) 340 m from the shoreline. Actually the first point was situated no more than several tens of meters from the shore. It means that the slope of the shoreface part not measured increases in on-shore direction. This peculiarity and existence of two long-shore bars (Fig. 5.3.2-2) testify that in the depth range 0-3 m the shoreface profile is formed by waves.

Section 8 (74° 50,5′ N, 140° 29,2′ E) is situated on the south coast of Bunge Land in its low part (Fig. 5.3.1-1). The coast in this section represents remarkably flat plain, which almost does not rise above the sea level and regularly undergoes flooding for several kilometers up the land. Therefore the shoreline position is very variable and reasonably is shown on the maps with a dotted line.

A long-shore sand bar on the coast about 100 m wide and at most 1 m high was observed on August 25. The surface sand behind the bar to the distance over 2 km from the shore was saturated and semi-liquefied (Fig. 5.3.2-4). Evidently the seaboard area underwent flooding during the storm the previous day.

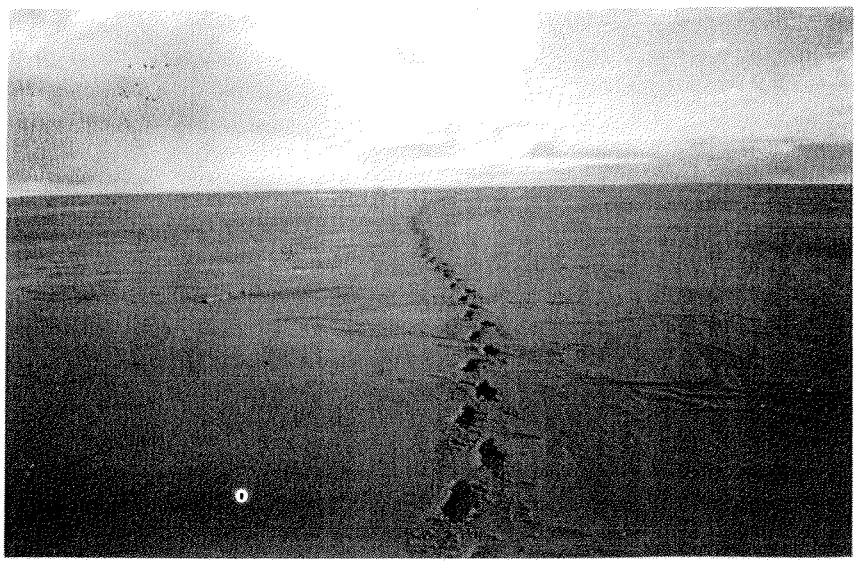

Figure 5.3.2-4. Seaboard surface of the Bunge Land low coast, August 25, 2002, section 8.

One shoreface profile was measured in section 8 (Fig. 5.3.2-5). It was the first time during 4 years of measurements in the Laptev Sea that we met a combined shoreface profile (Inman et al., 1993) consisting of two parts. According to Inmann et al., the lower part called shorerise is formed by shallow waves. The upper part called bar-berm is formed by breaking waves. The both parts follow the formula $y = -A \cdot x^k$ with equal coefficients A and k.

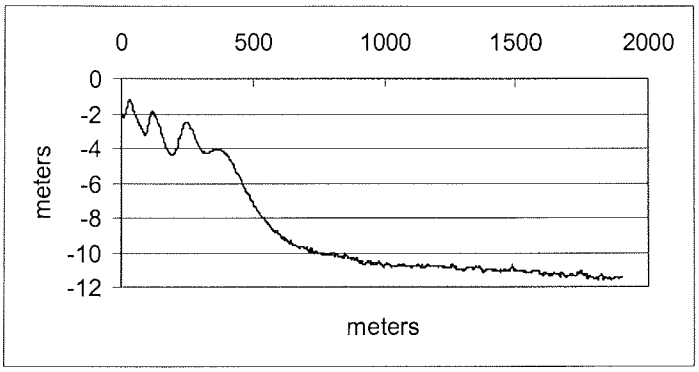

Figure 5.3.2-5. Shoreface profile near Bunge Land low coast, section 8.

The shoreline position on the shoreface profile presented in Fig. 5.3.2-5 was not measured. The water depth measurements were started at a considerable distance from the shore because of very shallow water. Father offshore three underwater long-shore bars as high as 2 m were measured (Fig. 5.3.2-5). A linear extrapolation of the in shore shoreface part gave a position of shoreline at the distance of 73 m from the first point of measurements (x = 0; y =1.97 m in Fig. 5.3.2-5). The upper part of the shoreface profile with the origin of coordinates at the point x = -73 m follow equation

$$y = -0.21 \cdot x^{0.49} \quad (1)$$

with a very low coefficient of determination R^2 = 0.60 (Fig. 5.3.2-6). A low R^2 is no surprise because of the presence of bars about 2 m high. The values of coefficients in equation (1) are in the range usual for Laptev Sea (Are et al., 2002).

A mathematical description of the shoreface lower part in the depth range of 6-10 m is obtained in the form of equation

$$y = -2.93(x-509)^{0.22} \quad (2)$$

with a rather high R^2 = 0.9924. Equation (2) corresponds to a simple power function

$$y = -2.93 \cdot x^{0.22} \quad (3)$$

with the origin of coordinates in the point x = 509 m. The A values in equations (3) and (1) differ in order of magnitude. It is in disagreement with the above-mentioned statement of Inmann et al. about the equal shape of upper and lower parts of the combined shoreface profile. Furthermore the value A = 2.93 oversteps substantially the usual limits 0.002-1.38 for the Laptev Sea and 0.19-0.89 for the Beaufort Sea (Are et al, 2002). These discrepancies suggest that the lower part of the shoreface in Fig. 5.3.2-5 is not created by modern hydrodynamics but reflects the geological structure of the sea floor.

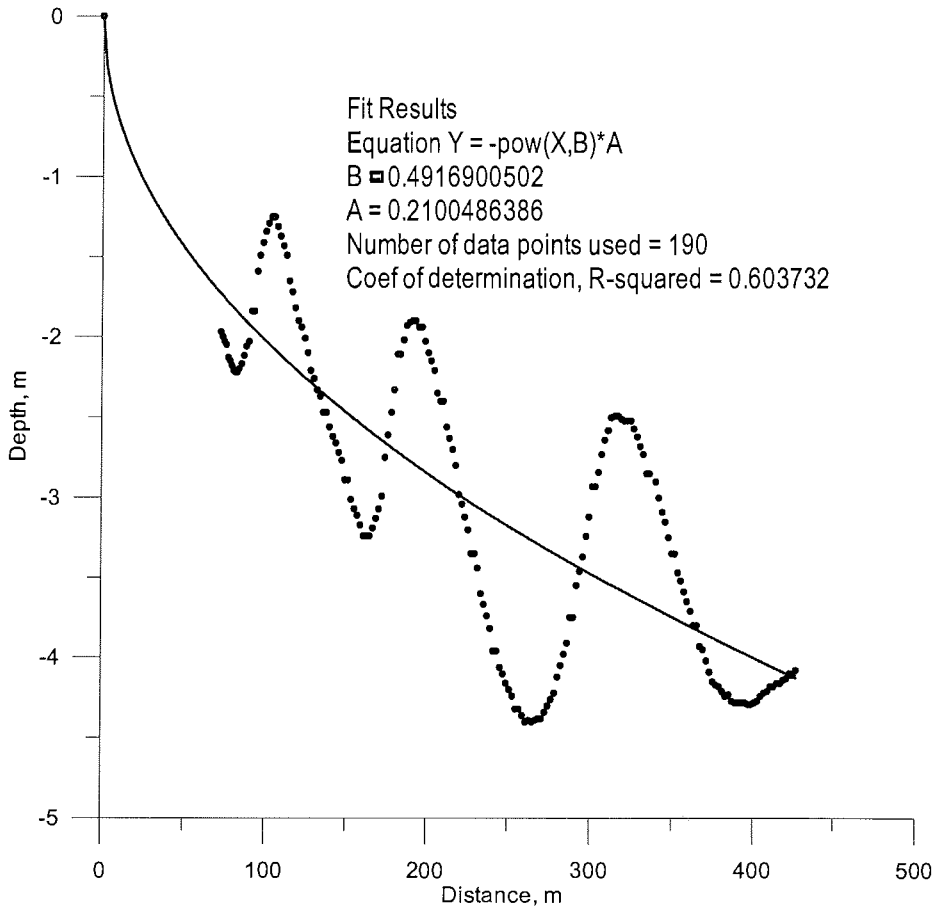

Figure 5.3.2-6. Approximation of the near shore shoreface profile with a simple power function, section 8.

Section 9 (74° 14.6′ N, 140° 19.1′ E) is situated on the north coast of the Maly Lyakhovsky Island. The coast here is composed of ice complex. The coastal bluffs as high as 15 m are sloping. Their vegetated surface is complicated by buydjarakhs. Any signs of coastal erosion are absent (Fig. 5.3.2-7).

Schistose bedrock is exposed on the bottom of water stream mouths. Evidently the bedrock underlies the ice complex on the sea level.

The beach in surf zone is sandy. The seawater is clear. A stripe of poorly rounded gravel is spread along the upper limit of the swash zone. Farther on-shore the beach is covered with sand and sparsely scattered gravel. The uppermost part of the beach is steep and composed of gravel, pebbles and single debris. All sediments on the beach are schistose. The signs of sea ice push are present everywhere on the beach in the form of scour craters and gravel pileups. Here and there the driftwood and patches of gravel are spread

on bluff slopes up to 2-3 m above the beach upper limit. The mouths of water streams and ravines are damed up with beach sediments.

Figure 5.3.2-7. Stable north coast of the Maly Lyakhovsky Island, section 9.

Two shoreface profiles were measured in section 9. One of them is presented in Fig. 5.3.2-8. Evidently the hydrodynamics is not responsible for the shape of this profile, outside of 3-m isobath. A grab sampler never took a sample of sediments from the sea floor in the range of 3–5 m isobath. Apparently the bedrock, which underlies the ice complex on the shore, is exposed on this part of the sea bottom.

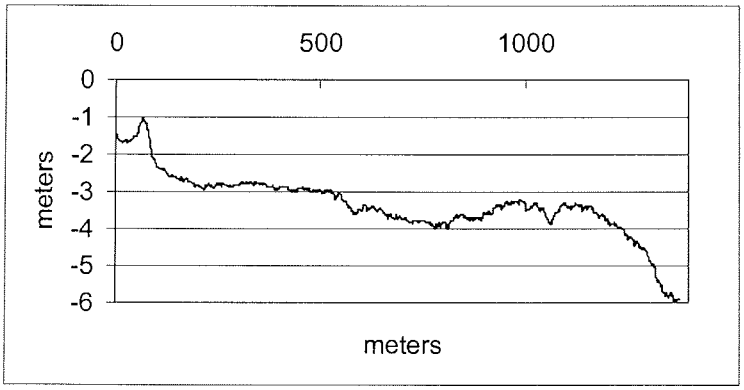

Figure 5.3.2- 8. Shoreface profile near north coast of the Maly Lyakhovsky Island, section 9.

The shoreface relief in the depth range of 1-2 m holds the signs of drift ice impact. It is indicated by the rough surface of the bottom, and asymmetric profile and sharp crest of the underwater long-shore bar, unusual for the sea floor relief created by waves (compare with the bars on the Bunge Land shoreface profile in Fig. 5.3.2-6). It is possible that the long-shore bar in Fig. 5.3.2-8 is formed without any wave impact, only due to the ice push onto the shore. The absence of a long-shore bar on the second shoreface profile, measured 2.7-km west from the first one in the same geological and geocryological conditions, testifies in favour of this assumption.

5.3.2.4 Discussion and conclusions

The shoreface of New Siberian Archipelago islands differs considerably from the shoreface of the Laptev Sea continental coast. The regular concave shape of the shoreface can not be distinguished along some coasts composed of hard bedrock (Stolbovoy and Belkovsky Islands). The shoreface along the coasts, where it can be recognized on profiles visually, is usually several hundred meters wide, and its outer boundary mostly do not reach below 4 m isobath. Along the Laptev Sea continental coasts the shoreface may be several kilometers wide and its outer boundary reaches 5-10 m isobaths.

Two factors may explain these differences: (1) bedrock is widespread below sea level around the New Siberian Islands, (2) decrease of sea roughness in the archipelago area, due to the next factors.

(1) The warming influence of river water in the archipelago area is lesser and correspondingly the open sea period is shorter in comparison with the continental coast areas.

(2) The drift ice remains near the islands during the whole summer and suppresses the waves.

(3) The dimensions of straits between the islands lessen the wave fetch, and vast shallows near the island coasts limit the wave height.

Apparently the decrease of wave energy is so large that even along the sandy coast of Bunge Land the outer boundary of the shoreface does not subside below 4 m isobath (Fig. 5.3.2-5).

Many signs of sea ice impact were observed on the island coasts.

- series of gravel-pebble long-shore ramparts as high as 3 m on the low coasts behind the beach,
- gravel, pebbles and driftwood pushed by the ice from the beach to the coastal slopes as high as 5 m above the beach,
- the mouths of water streams damed by beach material,
- the sediment piles on the beach, created by ice push,
- the pits on the beach scoured around the ice blocks pushed to the beach,
- the stripes of "stamukhi", grounded on the long-shore underwater bars.

All above phenomenon, created by drift ice, do not forward notably coastal erosion. Some of them have a protective impact.

There is no sign of drift ice impact on the sea floor outside of 2-m isobath on all three shoreface profiles presented in this report. The jagged outline of shoreface diagrams is caused probably by vertical movement of the boat with measurement equipment due to sea roughness. A shoreface profile segment 100-m long with measurement points, taken from Fig. 5.3.2-3, is shown on a large scale in Fig. 5.3.2-9 as an example. The distance between adjacent points is about 1.6 m. The standard deviation of measured depths from the mean value equals 4.5 cm. So the sea floor is very plain.

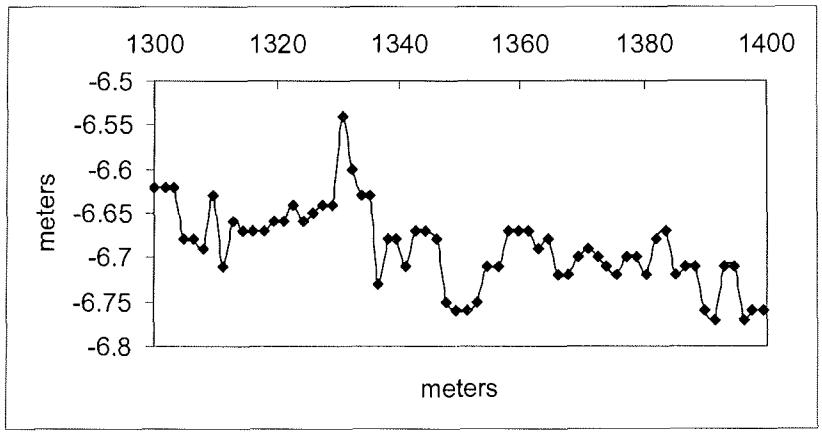

Figure 5.3.2-9. A seafloor profile segment near Cape Utyes Derewannykh Gor, Novaya Sibir Island, section 6.

5.3.3 Onshore coastal studies - coastal dynamics at key sites of the New Siberian Islands, Dmitry Laptev Strait, and Buor-Khaya Bay

Mikhail N. Grigoriev, Feliks E. Are, Hans-W., Hubberten, Volker Rachold, Sergey O. Razumov and Waldemar Schneider

5.3.3.1 Introduction

The main objective of the onshore coastal studies was to quantitatively assess coastal change rates (shoreline and cliff edge) focussing on erosive coasts. Twelve key sites along the coast of the Laptev and East-Siberian Seas were studied (Fig. 5.3.1-1):

New Siberian Archipelago:

1) north-eastern coast of Stolbovoy Island (Ice Complex and thermokarst deposits, ice-poor Pleistocene–Holocene coasts);
2) northern coast of Kotelny Island, Anisy Cape (Ice Complex and thermokarst deposits, ice-poor Pleistocene–Holocene coasts);
3) southern coast of Belkovsky Island, Skalisty Cape (rocky and other types of non-icy coasts);
4) south-eastern coast of Kotelny Island, Khomurgunnakh River mouth area (Ice Complex and thermokarst deposits, ice-poor Pleistocene–Holocene coasts);
5) south-western coast of Bunge Land, Bunge polar station ("high sand" area, marine terrace);
6) southern coast of Novoya Sibir Island, Wood Mountain Cape (rocky and other types of non-icy coasts, ice-poor Pleistocene coasts);
7) south-western coast of Novoya Sibir Island (Ice Complex and thermokarst deposits, ice-rich marine deposits, ice-poor Pleistocene–Holocene coasts);
8) southern coast of Bunge Land ("low sand" area, marine terrace);
9) north-western coast of Maly Lyakhovsky Island (Ice Complex and thermokarst deposits, ice-poor Pleistocene–Holocene coasts);

Dmitry Laptev Strait (mainland coast):

10) Svyatoy Nos Cape (ice-poor and ice-rich Pleistocene–Holocene coasts, rocky and other types of non-icy coasts);
11) Oyagossky Yar, mouth of Kondratev River area (Ice Complex and thermokarst deposits);

Buor-Khaya Bay:

12) north-western coast of Muostakh Island (Ice Complex).

5.3.3.2 Methods

A number of coastal segments, which are characterized by fast or slow retreat rate or almost stable dynamic regime, have been studied. Modern shoreline and cliff edge positions were measured using a laser theodolite and other methods.

Theodolite profiles and bench marks recorded in the field were identified on and compared with maps and aerial photographs taken in 1960th – 1980th. Detailed descriptions of the applied methods were published in the previous cruise reports (Rachold and Grigoriev, 2000, 2001; Pfeiffer and Grigoriev, 2002).

5.3.3.3 Results

The preliminary analysis of the field measurements at the selected coastal sites and other available data show that the average shore retreat rates of the New Siberian Islands are 0.1 - 3.5 m/yr for the long-term period (16-52 years), which is considerably less, than it was expected (Are, 1999; Grigorev and Kunitsky, 2000; Rachold and Grigoriev, 2000, 2001; Pfeiffer and Grigoriev, 2002). Most of the investigated continental coastal sections are characterized by significantly faster average shore retreat rates. The preliminary results are summarized in Table 5.3.3-1.

Table 5.3.3-1. Average retreat rates at the key sites (see Fig. 5.3.1-1).

key site (no.)	1	2	3	4	5	6	7	8	9	10	11	12
avg retreat. rate (m/yr)	0.1	0.4	0.5	0.7	0.3	0.4	1.9	-	0.9	0.3	3.0	13.0 (N); 5.0 (NE)

The fastest average coastal retreat rates were observed at the continental coast of Dmitry Laptev Strait west of the Kondratyeva River Mouth (key site 11, Oyagossky Yar,): 0.5-7 m/yr (Fig. 5.3.3-1 and Fig. 5.3.3-2). The average erosion rates at the western and eastern edges of the measured coastal profile (see Fig. 5.3.3-1) are 5 and 7 m/yr. In the central part of this profile, on the other hand, the recession is moderate: 1-2 m/yr. According to the preliminary analysis of the field data, highest erosion rates have to be expected for Muostakh Island (key site 12, central sector of the Laptev Sea): 13 m/yr on the northern cape and 4-6 m/yr on the north-eastern coast, which is approximately the same as we have determined during the last field seasons (Rachold and Grigoriev, 2000, 2001).

Figure 5.3.3-1. Complicated structure of the coastal relief at the Ice Complex coastal sections: a number of thermal terraces formed by thermal abrasive and thermal denudation processes. Oyagossky Yar, Dmitry Laptev Strait, East Siberian Sea, August 2002.

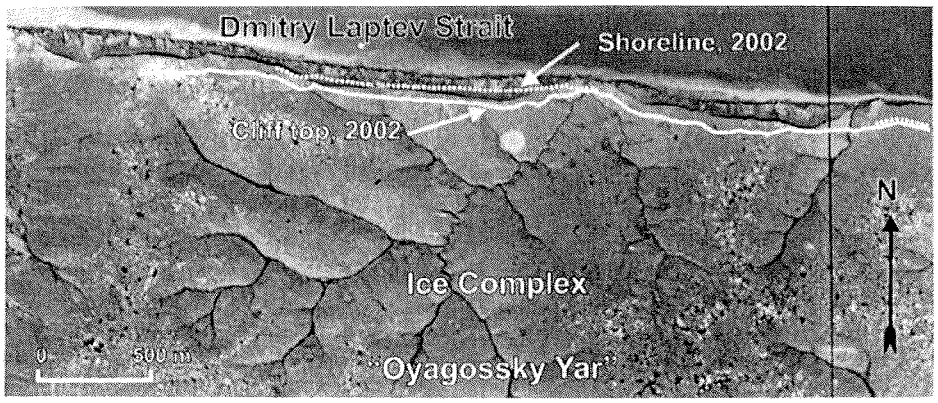

Figure 5.3.3-2. Aerial photograph taken in 1986 and modern positions of cliff top and shoreline. Oyagossky Yar, Dmitry Laptev Strait, East Siberian Sea, August 2002.

Comparably slow rates of coastal retreat were observed at most studied key sites along the coasts of the New Siberian Islands. A possible reason might be that there are many local sections consisting of rocks, which give rise to the formation of pebble beaches. These pebble beach formations are efficiently protecting the coast from wave erosion (Fig. 5.3.3-3). Even coasts consisting of the sensitive Ice Complex can be stable due to the blocking of a pebble beach.

We assume that this factor is one of the main reasons for the low retreat rates observed along the coastlines of the New Siberian Islands.

Figure 5.3.3-3. North-Eastern coastal section of Stolbovoy Island (ice-rich Pleistocene sediment). The non-active cliff is blocked by a pebble beach, which is reworked by ice-push. Laptev Sea, August 2002.

5.3.4 Water temperature and hydrometeorological characteristics along the coasts of the New Siberian Islands

Sergey O. Razumov and Mikhail N. Grigoriev

During the expedition "Lena-New Siberian Islands 2002" measurements of water temperature on vertical profiles at 11 stations were conducted. At two sites serial measurements during 1 and 3 days were carried out.

The measurements in the eastern Laptev Sea (west of the Sannikov Strait) have revealed a rather warm water layer (0-0.3 °C) in a water depth of 18-22 m (Fig. 5.3.4-1, Table 5.3.4-1). Apparently this layer was formed as a result of advection of a warmed up (0.1-0.4 °C) salt water mass (30-31 ‰) from the Yana Bay.

East of the Sannikov Strait (near Novoya Sibir Island) the temperature in the water column (0-15 m depth) changed from 2.7-3 °C at the surface to 1.6 °C at the bottom.

The hydrothermal profile along the Sannikov Strait (Fig. 5.3.4-2) shows that according to water temperature distribution cold water (down to –1.1 °C) can be supplied to the Sannikov strait from the Laptev Sea, and warmer water from the East Siberian Sea. During our observations the water temperature varied from –1.1 to 1.8 °C near the bottom and from 1.3 to 3.7 °C near the surface.

The direction of the water currents in the strait mainly depends on the wind regime. During western winds and calm conditions the current is directed from the Laptev to the East Siberian Sea. In this case the near-bottom water temperature decreases down to –0.6 to –1.1 °C (Table 5.3.4-1 and 5.3.4-2; Fig. 5.3.4-3). Under the influence of strong eastern winds a reverse and relatively warm current comes through the strait from the East Siberian Sea. In that case the temperature of the near-bottom water raises up to 1.5 to 1.8 °C.

The temperature measurements along vertical seawater profiles show that sea bottom temperatures below zero are a quite common phenomenon even within the coastal zone. This fact is very important for understanding the development of the off-shore sub-sea permafrost along the shallow shelf. The vast distribution of near bottom low summer temperatures (below zero) indicates that sub-sea permafrost can be preserved in the shallow shelf for a long time.

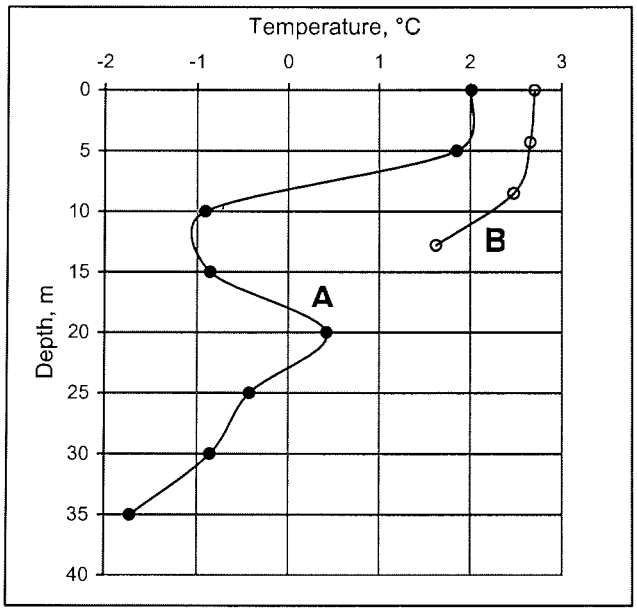

Figure 5.3.4-1. Water temperature profiles (A - station 2, north of Stolbovoy Island and B - station 7, south-west of Novoya Sibir Island).

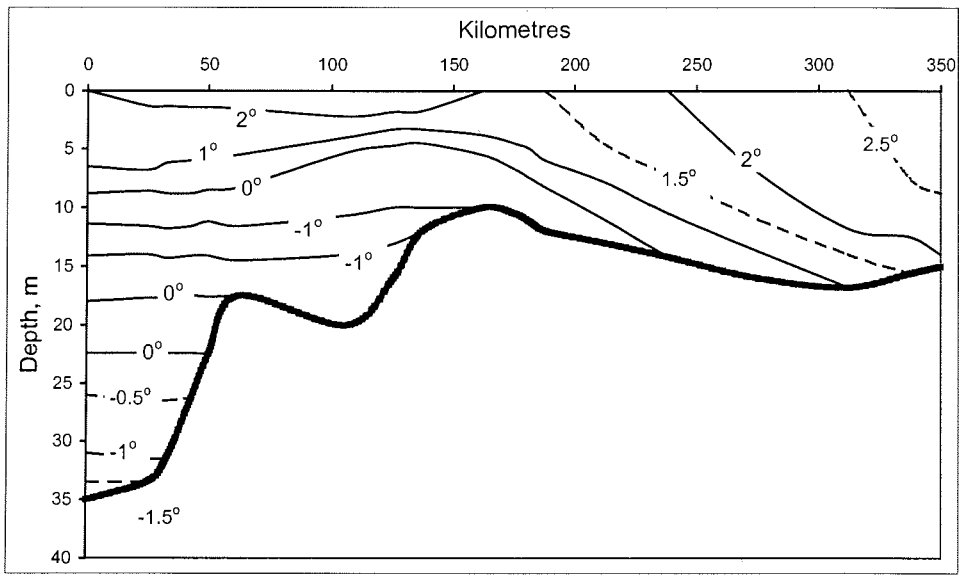

Figure 5.3.4-2. Hydrothermal profile along Sannikov Strait (from Stolbovoy Island to Novoya Sibir Island (August, 2002).

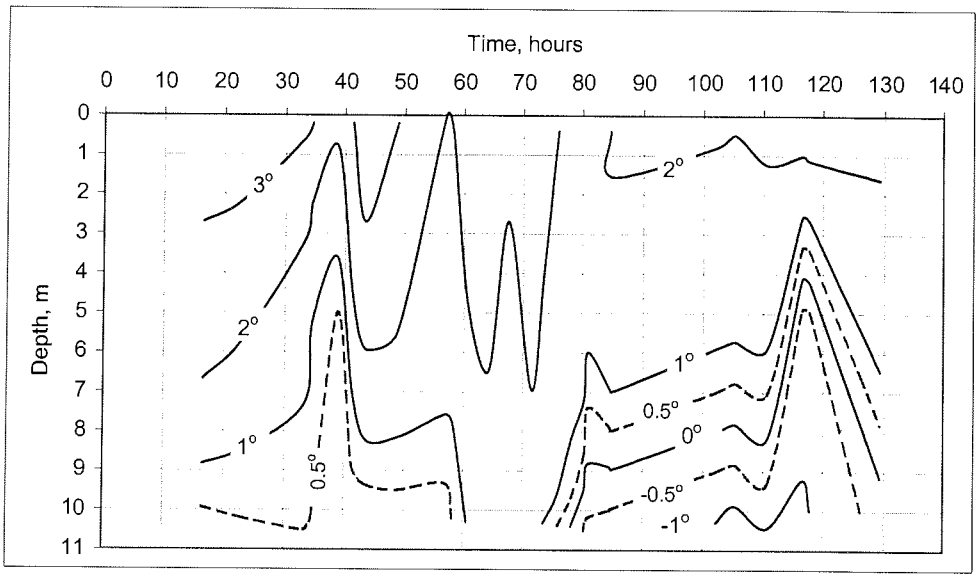

Figure 5.3.4-3. Variation of water temperature in the Sannikov strait (stations 8 and 9) from 22.08 to 27.08.02.

Table 5.3.4-1. Water temperature profiles along New Siberian Island coasts

№ St.	Date Time	Max. Depth, m	Horizon, m / Temperature, °C							
1bk	15.08 00^{30}	9	0 11.00	5 10.50	9 8.80					
2s	16.08 01^{00}	35	0 2.01	5 1.85	10 -0.91	15 -0.86	20 0.42	25 -0.43	30 -0.86	35 -1.72
3b	17.08 09^{00}	-	0 -1.20							
4k	18.08 9^{30}	11	1 0.04	6 -0.15	11 -1.05					
5zb	19.08 09^{30}	10	0 6.35	5 5.12	10 5.36					
6ns	20.08 09^{00}	7	0 3.10	2 2.90	7 2.68					
7ns	21.08 09^{10}	12.8	0 2.70	4.3 2.65	8.5 2.47	12.8 1.62				
8zb	22.08 16^{30}	10.2	0.2 3.27	5.2 2.68	10.2 0.38					
	23.08 09^{20}	10.2	0.2 3.15	5.2 1.22	10.2 0.70					
	23.08 14^{50}	10.3	0.3 2.18	5.3 0.40	10.3 0.05					
	23.08 19^{30}	10.2	0.2 3.71	5.2 2.32	10.2 0.14					
	24.08 09^{00}	10.2	0.2 1.95	5.2 1.68	10.2 0.25					
	24.08 16^{20}	10.5	0.5 2.49	5.5 2.06	10.5 1.75					
	24.08 19^{30}	10.3	0.3 2.11	5.3 1.88	10.3 1.52					
	24.08 23^{30}	10.3	0.3 2.60	5.3 2.27	10.3 1.45					
	25.08 09^{00}	10.5	0.5 1.33	5.5 1.18	10.5 -0.59					
	25.08 13^{00}	10.4	0.4 2.06	5.4 1.80	10.5 -0.72					
9k	26.08 09^{20}	10	0 2.07	5 1.35	10 -1.05					
	26.08 14^{40}	10	0 2.20	5 1.40	10 -0.80					
	26.08 20^{30}	10	0 2.65	5 -0.55	10 -1.08					
	27.08 09^{20}	10	0 2.22	5 1.54	10 -0.31					
10 ml	28.08 09^{00}	9.5	0 2.67							
11d l	29.08 23^{30}	12.5	0 4.50	2.5 4.57	7.5 4.30	12.5 4.29				

Indexes: **bk** – Buor-Khaya Peninsula, **s** – Stolbovoy Island, **b** – Belkovsky Island, **k** – Kotelny Island, **zb** – Zemlya Bunge, **ns** – Novaya Sibir Island, **ml** – Maly Lyakhovskiy Island, **dl** – Dmitry Laptev Strait.

Table 5.3.4-2. Hydrological-meteorological characteristics along New Siberian Island coasts (bottom water temperature – Tb, air temperature – Ta).

№ St.	Date Time	Lat N	Long E	Wind direc-tion	Wind velocity, m/s	Wave height, m	Wave length, m	Ta, °C	Depth, m	Tb, °C
1bk	15.08 00^{30}	71 58.080	133 06.154	WSW	3-6	0.5	10	6.40	9	8.80
2s	16.08 01^{00}	74 13.468	135 21.778	SE	3-5	0.4	9	3.82	35	-1.72
3b	17.08 09^{00}	75 21.660	135 49.845	SEE	1-2	0.2	1	2.70	-	-
4k	18.08 9^{30}	74 41.993	138 21.780		0	Swell	swell	4.18	11	-1.05
5zb	19.08 09^{30}	74 51.903	142 00.243	NE	4-6	0.3	6	6.55	10	5.36
6ns	20.08 09^{00}	74 59.823	146 56.852	E	2-3	swell 0.4	swell 10	3.85	7	2.68
7ns	21.08 09^{10}	75 05.862	146 25.455	SW	5-7	0.4	5	1.05	12.8	1.62
8zb	22.08 16^{30}	74 49.690	140 30.405	WSW	1-3	0.2	2	4.60	10.2	0.38
	23.08 09^{20}	-"-	- " -	WSW	5-7	0.8	9	6.55	10.2	0.70
	23.08 14^{50}	- " -	- " -	WSW	3-5	1.0	15	6.65	10.3	0.05
	23.08 19^{30}	- " -	- " -	WSW	0-1	swell 0.3	swell 15	6.12	10.2	0.14
	24.08 09^{00}	- " -	- " -	E	8-10	0.8	10	4.52	10.2	0.25
	24.08 16^{20}	- " -	- " -	E	7-10	0.7	7	4.33	10.5	1.75
	24.08 19^{30}	- " -	- " -	E	7-10	0.7	8	3.30	10.3	1.52
	24.08 23^{30}	- " -	- " -	E	7-9	0.7	7	3.60	10.3	1.45
	25.08 09^{00}	- " -	- " -	SE	5-7	0.6	6	3.70	10.5	-0.59
	25.08 13^{00}	- " -	- " -	SSE	4-6	0.4	5	6.49	10.4	-0.72
9k	26.08 09^{20}	74 38.363	139 20.806	SW	5-7	0.8	10	8.25	10	-1.05
	26.08 14^{40}	- " -	- " -	SSW	5-8	1.0	12	7.40	10	-0.80
	26.08 20^{30}	- " -	- " -	SW	3-5	swell 1.3	swell 18-20	6.07	10	-1.08
	27.08 09^{20}	- " -	- " -	SE	2-5	0.4	5	9.79	10	-0.31
10 ml	28.08 09^{00}	74 15.500	140 08.833	SE	8-12	1.3	15	5.48	9.5	-
11d l	29.08 23^{30}	72 48.653	142 23.202	SW	4-5	0.5	6	5.27	12.5	4.29

5.3.5 Calculations of the shore retreat rate using thermoterrace dimensions

Feliks E. Are, Mikhail N. Grigoriev, Hans-W. Hubberten and Volker Rachold

5.3.5.1 Introduction

Station 11 was chosen on the south coast of the Dmitry Laptev Strait (Fig. 5.3.5-1) were thermoterraces are wide spread. Geodetic measurements of shoreline and coastal bluff edges were carried out on this station. Three kilometers of the coast were measured. Well-developed singlestage and doublestage thermoterraces in ice complex are widespread along the section measured (Fig. 5.3.5-2). It was the first time during four seasons of fieldwork (1999-2002) that coastal group gained an opportunity to measure thermoterraces.

Thermoterraces in the ice complex represent a unique feature of coastal geomorphology, because their dimensions keep quantitative information on the time of their existence and may be used for calculation of the mean shore retreat rate during this time (Are, 1968, 1985, 1988).

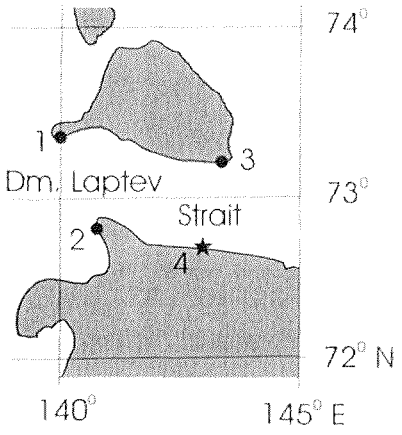

Figure 5.3.5-1. Location of Station 11. Polar Stations: 1 – Kigilyakh, 2 - Cape Svyatoy Nos, 3 – Cape Shalaurova; Station 11 – 4.

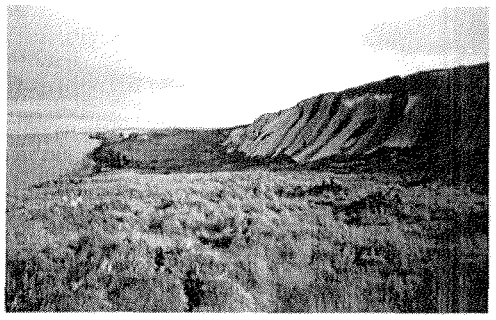

Figure 5.3.5-2. A singlestage thermoterrace on Station 11.

5.3.5.2 Measurements

Cross-profiles of four separate thermoterraces were measured on the Station 11 on August 30. In Fig. 5.3.5-3 a profile of a doublestage thermoterrace is shown as an example. Positions of points 1-5 measured with a laser theodolite as related to the origin of coordinates shown in Fig. 5.3.5-3 are given in Table 5.3.5-1. On the upper cliff surface (1-2 in Fig. 5.3.5-3) the ice wedges are exposed. Between points 3 and 4 the thermoterrace surface is flat, covered with meadowy vegetation and entirely stable. Between points 2 and 3 there is a transition zone between exposed ice surface and vegetated surface. The ice surface here is covered with tundra vegetation blocks sliding down. In the upper part there are single separated blocks. In the lower part the ice surface is entirely covered. Profile of the surface between points 2 and 3 is concave. Thawing of the underlying ice complex and corresponding thaw subsidence are taking place.

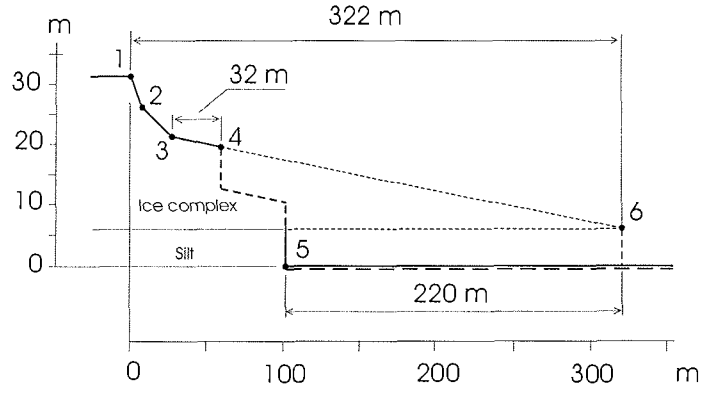

Figure 5.3.5-3. Profile of a doublestage thermoterrace on Station 11. 1 – upper cliff edge, 2 – upper cliff base, 3 – upper limit of thermoterrace stabilised surface, 4 – thermoterrace edge, 5 – lower cliff edge.

The thermoterrace profile between points 4 and 5 was not measured. Point 5 represents position of the lower cliff base. This cliff at the time of measurements was plumb with open wave niches at the base. Point 5 corresponds approximately with the highest sea level.

Table 5.3.5-1: Positions of points 1-5 measured with a laser theodolite as related to the origin of coordinates shown in Fig. 5.3.5-3.

Point number	Height	Distance
	m	
1	31.4	0
2	26.3	7.1
3	21.5	26.5
4	19.8	58.8
5	0	101.1

It is important that the ice complex base in the area of thermoterrace location is situated above the sea level. A thickness of silt with low ice content occurs below the ice complex. The edges of erosion cliffs composed of similar frozen sediments do not retreat far under the action of thermodenudation. Therefore the silt thickness does not take part in the thermoterrace formation, but its elevation above the sea level has to be taken into account by calculations of shore retreat rate using thermoterrace dimensions. Unfortunately the mark of the silt thickness top was not measured near the thermoterrace shown in Fig. 5.3.5-3. The measurements were carried out 540 m to the west (+8 m) and 1620 m to the east (0 m). The mark of the silt thickness top in the thermoterrace area +6 m was obtained using linear interpolation.

5.3.5.3 Calculations of the shore retreat rate

For calculation of the shore retreat rate the flat stable part (3-4) of the thermoterrace surface was used. The strait line 3-4 is extended offshore until the intersection with the ice complex base level in the point 6. It is the place, were the upper cliff 1-2 was created in the past by a storm. After that the erosion rate of the coast was less than thermodenudation rate of the cliff. Therefore the cliff retreated faster than the shoreline. Until now the upper cliff retreated for 322 m from the point 6 (Fig. 5.3.5-3). The shoreline during the same time retreated for 220 m.

The thermodenudation rate of an ice complex may be calculated using the mean annual sum of positive average daily air temperatures (Σt for brevity) (Are, 1985). The mean values of Σt, measured on polar stations, are available for the time before 1961 (Izyumenko, 1966). The polar stations nearest to the Station 11 are Cape Svyatoy Nos, Kigilyakh and Cape Shalaurova (Fig. 5.3.5-1). The last two are located on the B. Lyakhovsky Island. The Σt values measured on Laptev Sea islands are much less than that measured on the coast. Therefore we will use the sum for Svyatoy Nos p/s, which equals 345 °C·days (Izyumenko, 1966).

First we have to calculate the existence time of the upper cliff 1-2. During this time the cliff edge retreated for 322 m from point 6 to point 1 under the influence of thermodenudation (Fig. 5.3.5-3). The rate of thermodenudation (TDR, m/year) may be taken from the diagram presented in Fig. 5.3.5-4, or directly calculated by the empirical formula, which is based on the diagram (Are, 1985)

$$TDR = -3\times10^{-6}\cdot(\Sigma t)^2 + 98\cdot10^{-4}\cdot(\Sigma t) + 1.22 \qquad (1)$$

For Σt = 345 °C·days, TDR = 4.25 m ice per year.

TDR is the thickness of ice layer thawed during a year. It is equal with the annual rate of cliff edge retreat (CER) for a plumb cliff. But for an inclined cliff CER is larger than TDR. It can be easily seen in Fig. 5.3.5-5. The relation between CER and TDR is as follows

$$CER = TDR/\sin\varphi. \qquad (2)$$

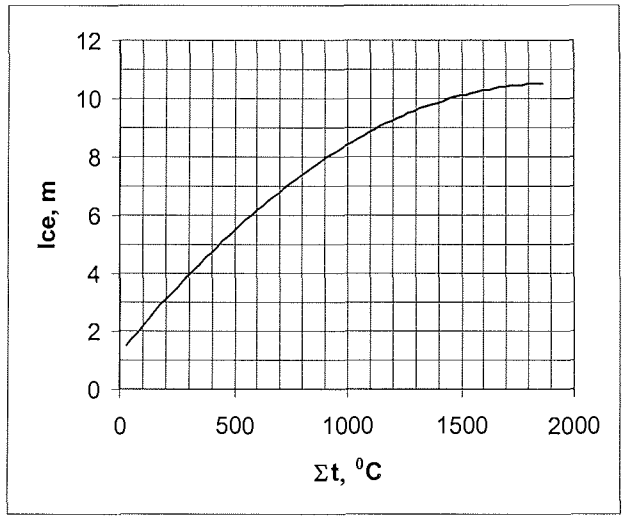

Figure 5.3.5-4. Thermodenudation rate of the vertical erosion cliffs, composed of ice complex, versus mean annual sum of positive average daily air temperatures (Are, 1985).

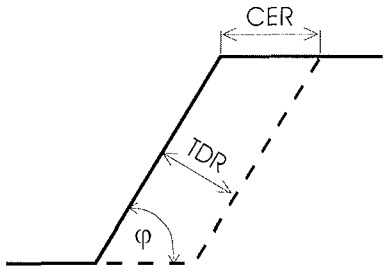

Figure 5.3.5-5. A schema showing retreat rate of inclined cliff edge (CER) and thermodenudation rate (TDR) of the same cliff.

According to the data presented in Fig. 5.3.5-3 and in Table 5.3.5-1, the upper cliff of the thermoterrace measured is inclined under the angle

$tg\varphi = 5.1m/7.1m = 0.7183 \Rightarrow \varphi = 35.7°$

In principle the primordial cliff in point 6 was plumb. Let us assume approximately that the cliff slope decreased with time linearly. Then the average $\varphi = (90 + 35.7)/2 = 62.85°$ and CER = 4.25/sin 62.85 = 4.78 m/year.

The time of existence of the upper cliff (EXT)

EXT = 322 m : 4.78 m/year = 67 years.

During this time the lower cliff (point 5 in Fig. 5.3.5-3) retreated for 220 m. The mean rate of retreat (shore erosion rate) during the same time was

SER = 220 m : 67 years = 3.3 m/year.

5.3.5.4 Discussion

The measurements and calculations described above prove that dimensions of thermoterraces may be used for calculations of shore retreat rate indeed. The rate values obtained using this technique are very probable. The next step to justify their reliability and to check the accuracy of calculations should be a comparison of calculated retreat rates with measured rates or with the rates obtained by means of comparison of aerial photographs or space images taken with possibly large time interval.

The working time of coastal group on Station 11 was limited by several hours. Measurements of thermoterraces were carried out on the side of the general geodetic survey of the coast. Therefore these measurements were insufficiently thorough. The constant inclination of thermoterrace surface is a crucial morphological feature for calculation of shore retreat rate. This feature may be clearly observed from a sufficient distance. But generally flat surface of the terrace shows itself on the background of a sometimes rather complicated microrelief. Therefore to obtain reliable results the points of geodetic measurements on the thermoterraces have to be chosen very carefully and several profiles across one and the same thermoterrace have to be measured. Especially important is the measurement of the upper cliff profile slope because thermodenudation rate strongly depends on it (Fig. 5.3.5-5).

5.4 References

Are, F.E. (1968): Development of the relief on thermoabrasion coasts. Transactions of AS USSR, Geography Series, No. 1, p. 92-100 (in Russian).

Are, F.E. (1985): Principles of shore thermoabrasion forecast. Novosibirsk: Nauka, 172 p.

Are, F.E. (1988): Thermal abrasion of sea coasts. Polar Geography and Geology, Vol. 12, No. 1-2, V.H. Winston & Sons, 157 p.

Are, F E. (1999): The role of coastal retreat for sedimentation of the Laptev Sea. In: Kassens H. et al. (ed.), Land-Ocean Systems in the Siberian Arctic. Dynamics and History. Springer-Verlag, pp. 287-295.

Are, F.E., Hubberten, H.-W., Rachold V., Reimnitz, E., and Solomon, S. (2002): Mathematical description of erosional shoreface profiles in the Arctic seas. Terra Nostra, Heft 2002/3. Climate drivers of the North. Selbstverlag der Alfred-Wegener-Stiftung, Berlin, p. 23-24.

Drachev, S.S.; Savostin, L.A.; Groshev, V.G. & Bruni, I.E. (1998): Structure and geology of the continental shelf of the Laptev Sea, Eastern Russian Arctic.- Tectonophysics, 298: 357-393.

Everdingen van, R.O. (ed.) (1998): Multi-Language Glossary of permafrost and related ground ice terms. International Permafrost Association, University of Calgary.

Franke, D.; Krüger, F. & Klinger, K. (2000): Tectonics of the Laptev Sea – Moma "Rift" Region: Investigations with seismologic broadband data.- journal of Seismology, 4: 99-116.

Gravis, G.F. (1978): Cyclicity of thermokarst at the coastal lowlands during the late Pleistocene and Holocene.- In: Publications of the 3rd International Permafrost Conference, July 10-13 1978, Edmonton, Alberta, Canada; Volume 1: 283-287.

Grigoriev, M.N., and V.V. Kunitsky (2000) Ice Complex of Yakutian Arctic Coast as a Sediment Source on the Shelf: Hydrometeorological and Biogeochemical Studies in the Arctic. Vladivostok: Arctic Regional Center, Far-Eastern Branch RAS, Vol. 2, pp. 109-116 (in Russian).

Inman, D.L., Elwany, M.H. and Jenkins, S.A. (1993): Shore rise and bar-berm on ocean beaches. Journal of Geophysical Research, 98, p. 18 181-18 199.

Ivanenko, G.V. (1998): State geological map of Russian Federation, New Siberian Islands, 1:1,00,000, map of Quaternary formations.- Ministry of Natural Resources of Russian Federation

Ivanov, O.A. (1972b): Stratigraphy and correlation of Neogene and Quaternary deposits of subarctic plains in Eastern Yakutia.- In: Problemes of the study of Quaternary Period.- Moscov, Nauka, pp. 202-211 (in Russian).

Izyumenko S.A. Ed. (1966) Handbook on USSR climate, Part 24, Leningrad, Hydrometeoizdat, 398 p.

Kaplina, T.N. & Lozhkin, A.V. (1985): Age and History of Accumulation of the "Ice Complex" of the Maritime Lowlands of Yakutiya. – In: Late Quaternary Environments of the Soviet Union. – Minneapolis: Univ. Minnesota Press, pp. 147-151.

Kayalainen, V.I. & Kulakov, Yu.N. (1966): To the questions of Paleogeography of the Yana-Indigirka coastal lowland during the Neogene-Quaternary period.- In: Quaternary Period in Siberia.-Moscow, Nauka, pp. 274-283 (in Russian).

Konishev, V.N.; Kolesnikov, S.F. (1981): Specialities of structure and composition of late Cenozoic deposits in the section of Oyogossky Yae.- In: Problems of cryolithology; Vil IX, Moscow, MGU Publishing, p. 107-117 (in Russian).

Kos'ko, M.K.; Lopatin, B.G. & Gamelin, V. G. (1990): Major geological features of the islands of the East Siberian and the Chukchi Seas and the nothern coast of Chukotka.- Mar. Geol. 93: 349-367.

Krasny, L. I. (ed.)(1981): Geology of Yakutian ASSR.- Moscow, Nedra, 300 pp. (In Russian).

Kunitsky, V.V. (1998): Ice Complex and cryoplanation terraces of Bol'shoy Lyakhovsky Island.- In: Kamensky, R.M., Kunitsky, V.V., Olovin, B.A. & Shepelev, V.V. (eds.): Problems of Geocryology – collected paper.- Russian Academy of Science, Siberian Branch, permafrost Institute Yakutsk, pp. 210.

Kunitsky, V.V. & Grigoriev, M.N. (2000): Boulders and cobble roundstones near the Svyatoy Nose Cape and on Big Lyakhovsky Island. – In: Fourth QUEEN Workshop, Lund, Sweden, 7-10 April 2000. – Abstracts, p. 62.

Kunitsky, V.V. (1996): Chemical content of ice wedges of the Ice complex. –In: Development of the Cryolithozone of Eurasia during the upper Cenozoic.- Yakutsk, Permafrostinstitut Publ., 93-117 (in Russian).

Lopatin, V.G. (ed.) (1998): State geological map of Russian Federation, New Siberian Islands, 1:1,00,000, map of Pre-Quaternary formations.- Ministry of Natural Resources of Russian Federation

Moriizumi, J., Iida, T. & M.Fukuda (1995): Radiocarbon dating of methane obtained from air in the ice complex (Edoma), in Arctic coast area of east Siberia.– In: Proceedings of the Third symposium on the joint Siberian Permafrost between Japan and Russia in 1994. – Sapporo: Hokkaido Univ. Press, pp. 14-21.

Meyer, H.; Dereviagin, A. Yu.; Siegert, C. & Hubberten, H.-W.: Paleoclimate studies on bykovsky peninsula, north Siberia – hydrogen and oxygen isotopes in ground ice.- Polarforschung.- 70: 37-51.

Nagaoka, D., Saijo, K. & M.Fukuda (1995): Sedimental environment of the Edoma in high Arctic eastern Siberia. – In: Proceedings of the Third Symposium on the Joint Siberian Permafrost between Japan and Russia in 1994. – Sapporo: Hokkaido Univ. Press, pp. 8-13.

Nikolaev, V.I., Genoni, L., Iacumin, P., Longinelli A., Nikolsky, P.A.& Sulerzhitsky, L.D. (2000): Isotopic studies of the Late Pleistocene megafauna in Northern Eurasia. – Moscow: Institute of Geography RAS. – 94 p. (in Russian).

Nikolsky, P.A.; Basilyan, A. Ye.; Simakova, A.N. (1999): New stratigraphical data of upper Cenozoic deposits in the area of Cape Svyatoy Nos (coast of the Laptev Sea).- In: Landscape-climate change, fauna and man during Late Pleistocene and Holocene.- Moscow, IGRAN, p. 51-60 (in Russian).

Parfenov, L., M. (ed.) (2001): Tectonics, Geodynamics and Metallogenesis of the area of the Republic Sakha (Yakutiya).- Moscow, "Nauka/Interperiodika", pp. 571.

Pfeiffer E.-M., Grigoriev, M. N. (Eds.) (2002): Russian-German Cooperation SYSTEM LAPTEV SEA 2000: The Expedition LENA 2001. Reports on Polar and Marine Research 426.

Prokhorova, S.M. & Ivanov, O.A. (1973): Tin-bearing granitoids of the Yana-Indigirka-Lowland and associated alluvial deposits.- Reports of NIIGA, volume 165. Leningrad, "Nedra", pp. 232.

Rachold, V., Grigoriev, M.N. (Eds.) (1999): Russian-German Cooperation System Laptev Sea 2000: The Lena Delta 1998 Expedition, Reports on Polar Research, 315.

Rachold V., Grigoriev, M.N. (Eds.) (2000): Russian-German Cooperation SYSTEM LAPTEV SEA 2000: The Expedition Lena Delta 1999. Report on Polar Research, 354.

Rachold, V., Grigoriev, M.N. (Eds.) (2001): Russian-German Cooperation SYSTEM LAPTEV SEA 2000: The Expedition LENA 2000. Reports on Polar and Marine Research 388.

Schirrmeister, L., Siegert, C., Kuznetsova, T., Kuzmina, S., Andreev, A.A., Kienast, F., Meyer, H., Bobrov, A.A. (2002). Paleoenvironmental and paleoclimatic records from permafrost deposits in the Arctic region of Northern Siberia, Quaternary International 89: 97-118.

Siegert, C., Schirrmeister, L., Babiy, O. (2002). The Sedimentological, Mineralogical and Geochemical Composition of Late Pleistocene Deposits from the Ice Complex on the Bykovsky Peninsula, Northern Siberia, Polarforschung, 70: 3-11.

Spektor, V.B. (1981): Tectonics of the New Siberian-Chukchi Fold Belt.- Sovetskaya Geologiya, 6: 102-105 (in Russian).

Tomirdiaro, S.V. (1980): Loess-glacial formation of east Siberia during Late Pleistocene and Holocene.- Moscow, Nauka, 184 pp. (in Russian).

Tormirdiaro, S.V. (1970): Eolian-cryogene origin of Yedoma-Complex deposits of North-east USSR. In: Abstracts of the allunion permafrost conference; Moscow, MGU Publishing, p. 106-107 (in Russian)

Vereshagin, V.N. (ed.) (1982): Stratigraphical dictionary USSR. Palaeogene, Neogene, Quaternary system.- Moscov, Nauk, 128 p. (in Russian)

"Berichte zur Polarforschung"

Eine Titelübersicht der Hefte 1 bis 376 (1981 - 2000) erschien zuletzt im Heft 413 der nachfolgenden Reihe "Berichte zur Polar- und Meeresforschung". Ein Verzeichnis aller Hefte beider Reihen sowie eine Zusammenstellung der Abstracts in englischer Sprache finden sich im Internet unter der Adresse:

http://www.awi-bremerhaven.de/Resources/publications.html

Ab dem Heft-Nr. 377 erscheint die Reihe unter dem Namen: "Berichte zur Polar- und Meeresforschung".

Heft-Nr. 377/2000 – „Rekrutierungsmuster ausgewählter Wattfauna nach unterschiedlich strengen Wintern" von Matthias Strasser.

Heft-Nr. 378/2001 – „Der Transport von Wärme, Wasser und Salz in den Arktischen Ozean", von Boris Cisewski.

Heft-Nr. 379/2001 – „Analyse hydrographischer Schnitte mit Satellitenaltimetrie", von Martin Losch.

Heft-Nr. 380/2001 – „Die Expeditionen ANTARKTIS XVI/1-2 des Forschungsschiffes POLARSTERN 1998/1999", herausgegeben von Eberhard Fahrbach und Saad El Naggar.

Heft-Nr. 381/2001 – „UV-Schutz- und Reparaturmechanismen bei antarktischen Diatomeen und *Phaeocystis antarctica*", von Lieselotte Riegger.

Heft-Nr. 382/2001 – "Age determination in polar Crustacea using the autofluorescent pigment lipofuscin", by Bodil Bluhm.

Heft-Nr. 383/2001 – „Zeitliche und räumliche Verteilung, Habitatspräferenzen und Populationsdynamik benthischer Copepoda Harpacticoida in der Potter Cove (King George Island, Antarktis)", von Gritta Veit-Köhler.

Heft-Nr. 384/2001 – „Beiträge aus geophysikalischen Messungen in Dronning Maud Land, Antarktis, zur Auffindung eines optimalen Bohrpunktes für eine Eiskerntiefbohrung", von Daniel Steinhage.

Heft-Nr. 385/2001 – „Actinium-227 als Tracer für Advektion und Mischung in der Tiefsee", von Walter Geibert.

Heft-Nr. 386/2001 – „Messung von optischen Eigenschaften troposphärischer Aerosole in der Arktis", von Rolf Schumacher.

Heft-Nr. 387/2001 – „Bestimmung des Ozonabbaus in der arktischen und subarktischen Stratosphäre", von Astrid Schulz.

Heft-Nr. 388/2001 – "Russian-German Cooperation SYSTEM LAPTEV SEA 2000: The Expedition LENA 2000", edited by Volker Rachold and Mikhail N. Grigoriev.

Heft-Nr. 389/2001 – "The Expeditions ARKTIS XVI/1 and ARKTIS XVI/2 of the Rearch Vessel ‚Polarstern' in 2000", edited by Gunther Krause and Ursula Schauer.

Heft-Nr. 390/2001 – "Late Quaternary climate variations recorded in North Atlantic deep-sea benthic ostracodes", by Claudia Didié.

Heft-Nr. 391/2001 – "The polar and subpolar North Atlantic during the last five glacial-interglacial cycles", by Jan P. Helmke.

Heft-Nr. 392/2001 – „Geochemische Untersuchungen an hydrothermal beeinflußten Sedimenten der Bransfield Straße (Antarktis)", von Anke Dählmann.

Heft-Nr. 393/2001 – "The German-Russian Project on Siberian River Run-off (SIRRO): Scientific Cruise Report of the Kara-Sea Expedition 'SIRRO 2000' of RV ‚Boris Petrov' and first results", edited by Ruediger Stein and Oleg Stepanets.

Heft-Nr. 394/2001 – „Untersuchungen der Photooxidantien Wasserstoffperoxid, Methylhydroperoxid und Formaldehyd in der Troposphäre der Antarktis ", von Katja Riedel.

Heft-Nr. 395/2001 – "Role of benthic cnidarians in the energy transfer processes in the Southern Ocean marine ecosystem (Antarctica)", by Covadonga Orejas Saco del Valle.

Heft-Nr. 396/2001 – "Biogeochemistry of Dissolved Carbohydrates in thew Arctic", by Ralph Engbrodt.

Heft-Nr. 397/2001 – "Seasonality of marine algae and grazers of an Antarctic rocky intertidal, with emphasis on the role of the limpet *Nacilla concinna* Strebel (Gastropoda: Patellidae)", by Dohong Kim.

Heft-Nr. 398/2001 – "Polare Stratosphärenwolken und mesoskalige Dynamik am Polarwirbelrand", von Marion Müller.

Heft-Nr. 399/2001 – "North Atlantic Deep Water and Antarctic Bottom Water: Their Interaction and Influence on Modes of the Global Ocean Circulation", by Holger Brix.

Heft-Nr. 400/2001 – "The Expeditions ANTARKTIS XVIII/1-2 of the Research Vessel 'Polarstern' in 2000", edited by Victor Smetacek, Ulrich Bathmann, Saad El Naggar.

Heft-Nr. 401/2001 – "Variabilität von CH_2O (Formaldehyd) - untersucht mit Hilfe der solaren Absorptionsspektroskopie und Modellen", von Torsten Albrecht.

Heft-Nr. 402/2001 – "The Expedition ANTARKTIS XVII/3 (EASIZ III) of RV 'Polarstern' in 2000", edited by Wolf E. Arntz and Thomas Brey.

Heft-Nr. 403/2001 – "Mikrohabitatansprüche benthischer Foraminiferen in Sedimenten des Südatlantiks", von Stefanie Schumacher.

Heft-Nr. 404/2002 – "Die Expedition ANTARKTIS XVII/2 des Forschungsschiffes 'Polarstern' 2000", herausgegeben von Jörn Thiede und Hans Oerter.

Heft-Nr. 405/2002 – "Feeding Ecology of the Arctic Ice-Amphipod *Gammarus wilkitzkii.* Physiological, Morphological and Ecological Studies", by Carolin E. Arndt.

Heft-Nr. 406/2002 – "Radiolarienfauna im Ochotskischen Meer - eine aktuopaläontologische Charakterisierung der Biozönose und Taphozönose", von Anja Nimmergut.

Heft-Nr. 407/2002 – "The Expedition ANTARKTIS XVIII/5b of the Research Vessel 'Polarstern' in 2001", edited by Ulrich Bathmann.

Heft-Nr. 408/2002 – "Siedlungsmuster und Wechselbeziehungen von Seepocken (Cirripedia) auf Muschelbänken (*Mytilus edulis* L.) im Wattenmeer", von Christian Buschbaum.

Heft-Nr. 409/2002 – "Zur Ökologie von Schmelzwassertümpeln auf arktischem Meereis - Charakteristika, saisonale Dynamik und Vergleich mit anderen aquatischen Lebensräumen polarer Regionen", von Marina Carstens.

Heft-Nr. 410/2002 – "Impuls- und Wärmeaustausch zwischen der Atmosphäre und dem eisbedeckten Ozean", von Thomas Garbrecht.

Heft-Nr. 411/2002 – "Messung und Charakterisierung laminarer Ozonstrukturen in der polaren Stratosphäre", von Petra Wahl.

Heft-Nr. 412/2002 – "Open Ocean Aquaculture und Offshore Windparks. Eine Machbarkeitsstudie über die multifunktionale Nutzung von Offshore-Windparks und Offshore-Marikultur im Raum Nordsee", von Bela Hieronymus Buck.

Heft-Nr. 413/2002 – "Arctic Coastal Dynamics. Report of an International Workshop. Potsdam (Germany) 26-30 November 2001", edited by Volker Rachold, Jerry Brown and Steve Solomon.

Heft-Nr. 414/2002 – "Entwicklung und Anwendung eines Laserablations-ICP-MS-Verfahrens zur Multielementanalyse von atmosphärischen Einträgen in Eisbohrkernen", von Heiko Reinhardt.

Heft-Nr. 415/2002 – "Gefrier- und Tauprozesse im sibirischen Permafrost – Untersuchungsmethoden und ökologische Bedeutung", von Wiebke Müller-Lupp.

Heft-Nr. 416/2002 – "Natürliche Klimavariationen der Arktis in einem regionalen hochauflösenden Atmosphärenmodell", von Wolfgang Dorn.

Heft-Nr. 417/2002 – "Ecological comparison of two sandy shores with different wave energy and morphodynamics in the North Sea", by Iris Menn.

Heft-Nr. 418/2002 – "Numerische Modellierung turbulenter Umströmungen von Gebäuden", von Simón Domingo López.

Heft-Nr. 419/2002 – "Scientific Cruise Report of the Kara-Sea Expedition 2001 of RV 'Academik Petrov': The German-Russian Project on Siberian River Run-off (SIRRO) and the EU Project 'ESTABLISH'", edited by Ruediger Stein and Oleg Stepanets.

Heft-Nr. 420/2002 – "Vulkanologie und Geochemie pliozäner bis rezenter Vukanite beiderseits der Bransfield-Straße / West-Antarktis", von Andreas Veit.

Heft-Nr. 421/2002 – "POLARSTERN ARKTIS XVII/2 Cruise Report: AMORE 2001 (Arctic Mid-Ocean Ridge Expedition)", by J. Thiede et al.

Heft-Nr. 422/2002 – "The Expedition 'AWI' of RV 'L'Atalante' in 2001", edited by Michael Klages, Benoit Mesnil, Thomas Soltwedel and Alain Christophe with contributions of the participants.

Heft-Nr. 423/2002 – "Über die Tiefenwasserausbreitung im Weddellmeer und in der Scotia-Sea: Numerische Untersuchungen der Transport- und Austauschprozesse in der Weddell-Scotia-Konfluenz-Zone", von Michael Schodlok.

Heft-Nr. 424/2002 – "Short- and Long-Term Environmental Changes in the Laptev Sea (Siberian Arctic) During the Holocene", von Thomas Müller-Lupp.

Heft-Nr. 425/2002 – "Characterisation of glacio-chemical and glacio-meteorological parameters of Amundsenisen, Dronning Maud Land, Antarctica", by Fidan Göktas.

Heft-Nr. 426/2002 – "Russian-German Cooperation SYSTEM LAPTEV SEA 2000: The Expedition LENA 2001", edited by Eva-Maria Pfeiffer and Mikhail N. Grigoriev.

Heft-Nr. 427/2002 – "From the Inner Shelf to the Deep Sea: Depositional Environments on the Antarctic Peninsula Margin - A Sedimentological and Seismostratigraphic Study (ODP Leg 178)", by Tobias Mörz.

Heft-Nr. 428/2002 – "Concentration and Size Distribution of Microparticles in the NGRIP Ice Core (Central Greenland) during the Last Glazial Period", by Urs Ruth.

Heft-Nr. 429/2002 – "Interpretation von FCKW-Daten im Weddellmeer", von Olaf Klatt.

Heft-Nr. 430/2002 – "Thermal History of the Middle and Late Miocene Southern Ocean - Diatom Evidence", by Bernd M. Censarek.

Heft-Nr. 431/2002 – "Radium-226 and Radium-228 in the Atlantic Sector of the Southern Ocean", by Claudia Hanfland.

Heft-Nr. 432/2002 – "Population dynamics and ecology of the surf clam *Donax serra* (Bivalvia, Donacidae) inhabiting beaches of the Benguela upwelling system", by Jürgen Laudien.

Heft-Nr. 433/2002 – "Die Expedition ARKTIS XVII/1 des Forschungsschiffes POLARSTERN 2001", herausgegeben von Eberhard Fahrbach.

Heft-Nr. 434/2002 – "The Rôle of Sponges in High-Antarctic Carbon and Silicon Cycling – a Modelling Approach", by Susanne Gatti.

Heft-Nr. 435/2002 – "Sedimente des Changeable-Sees, Oktoberrevolutions-Insel (Severnaja Zemlja), als Archive der Paläoumwelt Mittelsibiriens seit dem Frühweichsel", von Alexandra Raab.

Heft-Nr. 436/2003 – "The charnockite-anorthosite suite of rocks exposed in central Dronning Maud Land, East Antarctica: a study on fluid-rock interactions, and post-entrapment change of metamorphic fluid inclusions", by Bärbel Kleinefeld.

Heft-Nr. 437/2003 – "Variable C:N ratios of Particulate Organic Matter and Their Influence on the Marine Carbon Cycle", by Birgit Schneider.

Heft-Nr. 438/2003 – "Population ecology and genetics of the polychaete *Scoloplos armiger* (Orbiniidae)", by Inken Kruse.

Heft-Nr. 439/2003 – "Architecture and geodynamic evolution of the Svalbard Archipelago, the Yermak Plateau and the Fram Strait oceanic Province from deep seismic experiments", by Oliver Ritzmann.

Heft-Nr. 440/2003 – "Occurence, induction and physiological importance of UV-absorbing substances in polar macroalgae", by Kirsten Hoyer.

Heft-Nr. 441/2003 – "Sea ice conditions in the Transpolar Drift in August/September 2001. Observations during POLARSTERN cruise ARKTIS XVII/2", compiled by Christian Haas and Jan J. Lieser.

Heft-Nr. 442/2003 – "Süßwassereintrag und Festeis in der ostsibirischen Arktis – Ergebnisse aus Boden- und Satellitenbeobachtungen sowie Sensitivitätsstudien mit einem thermodynamischen Festeismodell", von Jörg Bareiss.

Heft-Nr. 443/2002 – "Arctic Coastal Dynamics. Report of the 3rd International Workshop. University of Oslo (Norway) 2-5 December 2002", edited by Volker Rachold, Jerry Brown, Steven Solomon and Johan Ludvig Sollid.

Heft-Nr. 444/2003 – "Ventilation der Grönlandsee – Variablilität und ihre Ursachen 1994-2001", von Stephanie Ronski.

Heft-Nr. 445/2003 – "Die Expedition ANTARKTIS XVIII/3-4 des Forschungsschiffes POLARSTERN 2000/2001 sowie die Aktivitäten an Land und bei der Neumayer-Station", herausgegeben von Eberhard Fahrbach, Dieter Fütterer, Saad El Naggar und Hans Oerter.

Heft-Nr. 446/2003 – "The Expedition ARKTIS XVIII/1 a, b of the Research Vessel "Polarstern" in 2002, edited by Peter Lemke.

Heft-Nr. 447/2003 – "Investigation of the Greenland Atmospheric Boundary Layer over Summit 2002 (IGLOS). Field Report", by Clemens Drüe and Günther Heinemann.

Heft-Nr. 448/2003 – "Die Expedition ANTARKTIS XIX mit FS "Polarstern" 2001/2002. Bericht von den Fahrtabschnitten 1 und 2", herausgegeben von Wilfried Jokat und Gunther Krause.

Heft-Nr. 449/2003 – "The Expedition ARKTIS XVIII/2 of RV "Polarstern" in 2002. Contributions of the Participants", edited by Wilfried Jokat.

Heft-Nr. 450/2003 – "Scientific Cruise Report of the joint Russian-German Kara Sea Expedition in 2002 with RV "Akademik Boris Petrov", edited by Frank Schoster and Michael Levitan.

Heft-Nr. 451/2003 – "Die Krustenstruktur der Fjordregion Ostgrönlands zwischen dem präkambrischen Schild und den rezenten mittelozeanischen Rücken: Ergebnisse seismischer und gravimetrischer Modellierungen", von Mechita Schmidt-Aursch.

Heft-Nr. 452/2003 – "Untersuchungen zur Biodiversität antarktischer benthischer Amphipoda (Malacostraca, Crustacea)", von Anne-Nina Lörz.

Heft-Nr. 453/2003 – "The Antarctic Circumpolar Current: Dynamics of a circumpolar channel with blocked geostrophic contours", by Daniel Borowski.

Heft-Nr. 454/2003 – "The effects of climate induced temperature changes on Cod (*Gadus morhua* L.): Linking ecological and physiological investigations", by Torsten Fischer.

Heft-Nr. 455/2003 – "Sediment Transport on Arctic Shelves – Seasonal Variations in Suspended Particulante Matter Dymamics on the Laptev Sea Shelf (Siberian Arctic)", by Carolyn Wegner.

Heft-Nr. 456/2003 – "Dynamics of the Ocean Surface in the Polar and Subpolar North Atlantic over the last 500 000 Years", by Evguenia S. Kandiano.

Heft-Nr. 457/2003 – "Structure and dynamics of a submarine continent: Tectonic-magmatic evolution of the Campbell Plateau (New Zealand). Report of the RV 'SONNE' cruise SO-169, Project CAMP, 17 January to 24 February 2003", edited by Karsten Gohl.

Heft-Nr. 458/2003 – "Antioxidative properties of marine macroalgae from the Arctic", by Angelika Dummermuth.

Heft-Nr. 459/2003 – "Analysing benthic communities in the Weddell Sea (Antarctica): a landscape approach", by Núria Teixidó Ullod.

Heft-Nr. 460/2003 – "The Expeditions Amery Oasis, East Antarctica, in 2001/02 and Taylor Valley, Southern Victoria Land, in 2002", by Bernd Wagner.

Heft-Nr. 461/2003 – "Late Quaternary climate history of Northern Siberia – evidence from ground ice", by Hanno Meyer.

Heft-Nr. 462/2003 – "The Expedition ANTARKTIS XIX/5 (LAMPOS) of RV 'Polarstern' in 2002", edited by Wolf E. Arntz and Thomas Brey.

Heft-Nr. 463/2003 – "Distribution, composition, flux and variability of organic carbon in Fram Strait/Yermak Plateau (Arctic Ocean) and (palaeo) environmental significance", by Daniel Birgel.

Heft-Nr. 464/2003 – "The influence of aerosols on the oceanic sedimentation and environmental conditions in the Arctic", by Vladimir Shevchenko.

Heft-Nr. 465/2003 – "Chemical ecology and palatability of marine invertebrates in the sub-Arctic Kongsfjord (Spitzbergen)", by Heike Lippert.

Heft-Nr. 466/2003 – "Russian-German Cooperation SYSTEM LAPTEV SEA. The Expedition LENA 2002", edited by Mikhail N. Grigoriev, Volker Rachold, Dmitry Yu. Bolshianov, Eva-Maria Pfeiffer, Lutz Schirrmeister, Dirk Wagner and Hans-Wolfgang Hubberten.